

An Investigation of Carbohydrate – Carbohydrate Interactions Using Glycopolymers and
Supramolecular Glycoconjugates as Multivalent Model Systems

By

Blaise W. Leeber III

B.S. Worcester Polytechnic Institute 2012

A Dissertation Submitted in Partial Fulfillment of the Requirements for the Degree of Doctor of
Philosophy in the Department of Chemistry at Brown University

Providence, Rhode Island

May 2018

© Copyright 2018 by Blaise W. Leeber III

This dissertation by Blaise W. Leeber III is accepted in its present form
by the Department of Chemistry as satisfying the
dissertation requirement for the degree of Doctor of Philosophy.

Date _____

Amit Basu, Ph.D., Advisor

Recommended to the Graduate Council

Date _____

Sarah Delaney, Ph.D., Reader

Date _____

Jason Sello, Ph.D., Reader

Approved by the Graduate Council

Date _____

Andrew G. Campbell, Ph.D.,
Dean of the Graduate School

Curriculum Vitae

Blaise Leeber was raised in Hull, Massachusetts and received his primary and secondary education at Hull public schools. He received his Bachelor of Sciences (with high distinction) degree from Worcester Polytechnic Institute WPI in 2012. While attending WPI Blaise performed undergraduate research in the laboratories of Professor José M. Argüello and Professor John C. MacDonald. In the fall of 2012 Blaise began his graduate studies at Brown University. Under the direction and guidance of Professor Amit Basu, he has investigated carbohydrate – carbohydrate Interactions (CCIs) using glycopolymers and supramolecular glycoconjugates as multivalent model systems. Blaise also frequently served as a teaching assistant for organic chemistry laboratory classes, serving as the head teaching assistant in the spring of 2017. For his efforts, he was awarded the W. J. King prize for outstanding performance as a teaching assistant in May of 2017. Blaise also received a dissertation fellowship from Brown University in May of 2017.

Publications:

Leeber, B., Kuhn, H., Caianiello, D., Dale, B., Lusi, R., Palaychuk, N., Weingarten, S., and Basu, A. "Supramolecular chirality of Yariv reagents dictates arabinogalactan binding" Manuscript in preperation.

Preface and Acknowledgements

In the writing of this dissertation I have depended on the support and guidance of my family, friends and colleagues. I owe each of you a debt of gratitude and I hope that I get the chance to repay you in kind.

Specifically, I would like to thank my advisor, Professor Amit Basu for all the time and energy he has spent helping me develop my skills as a chemist and for teaching me how to conduct research in a truly rigorous and thorough manner. I would also like to thank Professor Sarah Delaney and Professor Jason Sello for serving on my committee and for providing me with useful advice over the course of my graduate studies. I offer additional thanks to Professor Delaney for allowing me to use her lyophilizer. Thank you as well to Professor Shouheng Sun for allowing me to use his DLS instrument and to Professor Matthew Kieseewetter of the University of Rhode Island and his graduate student Oleg Kazakov for helping me run GPC analysis of my polymers. Thank you as well to all the members of the Basu Lab that I have worked with during my time at Brown.

I would like to thank my friends and family for always believing in me even when I was less than confident in myself. My parents, Paul and Ellen Leeber, have always provided me with unconditional love and support. Their confidence in me has driven me to strive to achieve lofty goals that would not have been attainable otherwise.

Finally, I would like to thank Dr. Katharina Bilotti. Through every trial and tribulation, I have faced during my life for the past five years she has been by my side and has supported me through it all. It would not have been possible to do this without her. She is truly an amazing woman and is the love of my life. Also, thank you to Mike (my cat / writing buddy).

I would like to dedicate this work to the memory of Blaise W. Leeber Jr., George T. Gildea, and Kathleen Gildea, all of whom helped shape me into the man I am today.

Table of Contents

1	SYNTHESIS AND CHARACTERIZATION OF GLYCOPOLYMER MODEL SYSTEMS OF CCIs	1
1.1	Introduction to cell-membrane CCIs.....	1
1.2	Introduction to multivalent model systems of CCIs	4
1.3	Glycopolymers	4
1.4	Glycopolymers as probes for CCIs.....	9
1.5	Facile synthesis of glycopolymers as probes for CCIs	11
1.5.1	Phase I: Terminating Agent Synthesis.....	11
1.5.2	Phase II: The synthesis of the alkyne-functionalized polymer backbone	13
1.5.2.1	Preparation of monomer	13
1.5.2.2	ROMP	13
1.5.2.2.1	Characterization of ROMP polymers by ¹ H NMR	15
1.5.2.2.2	Characterization of ROMP polymers by GPC.....	17
1.5.2.3	Preparation of alkyne functionalized polymer	18
1.5.2.3.1	MALDI-ToF Analysis of post-ROMP modified polymers	20
1.5.3	Phase III: Fluorescein labeling of the polymer backbone	23
1.5.4	Phase IV: Synthesis of azido sugars.....	25
1.5.5	Phase V: Synthesis of glycopolymer via CuCAAC of poly-alkyne and azido sugars	30
1.6	Conclusion.....	39
1.7	Supporting Information	39
2	PROBING MYELIN CCIs USING GLYCOPOLYMER MODEL SYSTEMS	67
2.1	Qualitative CCI binding studies using carbohydrate coated surfaces.....	67
2.1.1	Evidence of a SGal-Glc CCI	70
2.1.2	Effect of model system type on CCI specificity	72
2.2	Quantitative binding studies of CCIs.....	73
2.2.1	SPR studies of CCI.....	74
2.2.2	AFM studies of CCI	75
2.2.3	ITC studies of CCI.....	76
2.3	Qualitative and quantitative analysis of myelin CCIs using glycopolymers.....	77
2.4	Well-binding assays.....	78

2.4.1	Glycolipids	78
2.4.2	Preparation of the well-binding assay	78
2.4.3	Well-binding assays: normal method	79
2.4.3.1	Well-binding assays: normal method. Initial results.....	80
2.4.3.2	Well-binding assays: normal method. Results of changing lipid concentration. 81	
2.4.3.3	Well-binding assays: normal method. Results of changing polymer concentration.....	82
2.4.3.4	Well-binding assays: normal method. Results with 2% BSA in the glycopolymer solution	83
2.4.3.5	Well-binding assays: normal method. Results from performing experiments with calcium	84
2.4.4	Well-binding assays: methanol wash.....	85
2.4.5	Well-binding assays: Inverted method	86
2.4.6	Well-binding conclusions	88
2.5	Isothermal titration calorimetry	89
2.5.1	ITC experiments with 30-mer glycopolymers	93
2.5.2	ITC experiments with 90-mer glycopolymers	94
2.5.3	ITC Conclusions	97
2.6	Conclusions	98
2.7	Supporting information	98
3	YARIV REAGENT INTERACTIONS WITH ARABINOGALACTAN PROTEINS (AGPs)	104
3.1	Introduction	104
3.1.1	Supramolecular Glycoconjugates	105
3.1.2	Yariv reagents	108
3.1.3	Yariv – AGP interactions.....	110
3.1.4	Structural properties of Yariv aggregates	113
3.1.5	Hypothesis.....	114
3.2	Characterizing the helicity of the Yariv reagent aggregates.....	114
3.2.1	Absorbance and Circular Dichroism spectra of BGlc Yariv.....	114
3.2.2	Comparison of the UV-vis and Circular Dichroism spectra of Yariv reagents.....	117
3.2.2.1	NMR, UV-Vis, and CD spectra of a monovalent azo-linked galactoside 68	118
3.2.3	AGP titration experiments	119
3.2.4	Additional radial gel diffusion assays.....	123

3.2.4.1	Radial gel diffusion assays with gels containing DMF.....	123
3.2.4.2	Radial gel diffusion assays with the monovalent azo-linked galactoside 68 ...	124
3.3	Conclusions	125
3.4	Supporting information	126
4	YARIV – ALCOHOL AGGREGATION EFFECTS.....	136
4.1	Yariv reagent aggregation behavior.....	136
4.2	Background	136
4.2.1	Supramolecular polymers	136
4.2.2	Mechanisms of self-assembly for supramolecular polymers	141
4.2.3	C ₃ -Discotic supramolecular polymers and alcohol effects.....	143
4.3	Hypothesis.....	148
4.4	Experimental	148
4.4.1	Attempts to determine the mechanism of Yariv reagent self-assembly	148
4.4.2	First observations of alcohol effects	151
4.4.3	DLS experiments	153
4.4.3.1	Temperature dependent DLS experiments.....	153
4.4.4	Temperature-dependent CD experiments with alcohol.....	157
4.4.5	Additional hysteresis experiments.....	160
4.4.6	CD and UV-vis Experiments with varying alcohol concentrations	164
4.4.6.1	CD and UV-Vis experiments for βGlc in methanolic aqueous solutions	165
4.4.6.2	CD and UV-vis experiments for αGal in methanolic aqueous solutions	168
4.4.6.3	CD and UV-Vis experiments for αGal in ethanolic aqueous solutions.....	170
4.4.6.4	CD and UV-Vis experiments for αGal in isopropanolic aqueous solutions	172
4.4.7	Alcohol composition dependent DLS experiments.....	174
4.4.8	Additional temperature-dependent CD experiments.....	176
4.4.9	Yariv binding to AGP in the presence of alcohol.....	178
4.5	Conclusions	181
4.6	Supporting Information	182
5	APPENDIX.....	186
5.1	Appendix I: Gel Permeation Chromatography Traces	186
5.2	Appendix II: Click TLC Stains.....	189
5.3	Appendix III: Determination of fluorescence labeling (in PBS pH 7.4)	192
5.4	Appendix IV: NMR Spectra for glycopolymer synthesis.....	194

5.5	APPENDIX V – Raw ITC Data.....	231
5.6	APPENDIX VI: Yariv reagent ^1H and ^{13}C -NMR.....	237
5.7	APPENDIX VII – Dynamic light scattering intensity and correlogram reports	242

List of Figures

Figure 1.1: Glycan structures that participate in carbohydrate–carbohydrate interactions.....	1
Figure 1.2: The Basic Components of a Glycopolymer.	5
Figure 1.3: A general reaction mechanism for the ROMP reaction.....	6
Figure 1.4: Grubbs' 3rd generation ruthenium catalyst	6
Figure 1.5: Incorporation of a functional end group via ROMP termination	7
Figure 1.6: Copper catalyzed azide-alkyne cycloaddition (CuAAC).....	8
Figure 1.7: An example of a fluorescent glycopolymer used as a model system of myelin CCLs	9
Figure 1.8: Example of a new generation of glycopolymer prepared via a more facile synthetic route	10
Figure 1.9: Synthesis of the terminating agent.....	12
Figure 1.10: Synthesis of monomer	13
Figure 1.11: ROMP to give the alkene 20 and Teoc 21 terminated poly-NHS esters	14
Figure 1.12: ¹ H NMR of alkene terminated poly-NHS ester 20 (n ~ 30) taken in d ₆ -acetone.....	16
Figure 1.13: ¹ H NMR of alkene terminated poly-NHS ester 20 (n ~ 90) taken in d ₆ -acetone.....	16
Figure 1.14: ¹ H NMR of Teoc terminated poly-NHS ester 21 (n ~ 90) taken in d ₆ -acetone.....	17
Figure 1.15: Synthesis of poly-alkyne polymers	18
Figure 1.16: ¹ H-NMR of 20 (n ~ 90) and 22 (n ~ 90) taken in 1:1 (v/v) d ₆ -DMSO:CD ₃ OD	19
Figure 1.17: ¹ H NMR of alkene terminated poly-alkyne 22 (n ~ 90) taken in 1:1 (v/v) d ₆ -DMSO:CD ₃ OD	20
Figure 1.18: ¹ H-NMR of the Teoc protected poly-alkyne 23 (n ~ 90) taken in 1:1 (v/v) d ₆ -DMSO:CD ₃ OD	20
Figure 1.19: Synthesis of poly-PMB polymer	21
Figure 1.20: MALDI of poly-alkyne 22 (n ~ 30).....	22
Figure 1.21: Enlarged section of MALDI of poly-alkyne 22 (n ~ 30).....	23
Figure 1.22: MALDI of poly-PMB polymer	23
Figure 1.23: Synthesis of the fluorescein labeled poly-alkyne	24
Figure 1.24: ¹ H NMR spectra of 24, 25, and 26. The spectrum for 25 displays N-H peaks because it was acquired using aprotic NMR solvent (1:1 (v/v) d-acetone:d-DMSO). 24 and 26 were taken in 1:1 (v/v) d ₆ -DMSO:CD ₃ OD.	25
Figure 1.25: Synthesis of azido sugars	26
Figure 1.26: Deprotection of acetylated mannose	27
Figure 1.27: ¹ H NMR comparing sodium methoxide and potassium carbonate deprotections taken in D ₂ O	28
Figure 1.28: O3 regioselective sulfation of galactose azide.....	29
Figure 1.29: ¹ H NMR showing the sulfation of galactose azide taken in CD ₃ OD	29
Figure 1.30: COSY and HSQC spectra of 32	30
Figure 1.31: Proposed CuAAC mechanism.....	31
Figure 1.32: Synthesis of alkene terminated glycopolymers	32
Figure 1.33: Synthesis of fluorescein labeled glycopolymers	33
Figure 1.34: Fluorescent click responsive TLC stain.....	34
Figure 1.35: Monitoring the synthesis of poly-SGal using the click TLC stain.....	35
Figure 1.36: ¹ H NMR of glycopolymer 43, n ~ 30 in D ₂ O.....	36

Figure 1.37: ¹ H NMR comparison of the Gal glycopolymers (43 and 47)	36
Figure 1.38: ¹ H NMR comparison of the Man glycopolymers (44 and 48)	37
Figure 1.39: ¹ H NMR comparison of the Glc glycopolymers (45 and 49)	37
Figure 1.40: ¹ H NMR comparison of the SGal glycopolymers (46 and 50)	38
Figure 2.1: Synthesis of Glycolipids.....	69
Figure 2.2: Types of glycopolymers used in previous well binding studies 54-56.....	70
Figure 2.3: Myelin glycosphingolipids.....	71
Figure 2.4:Fluorescent polymer lipid well-binding assay.....	79
Figure 2.5: Results from binding assays using 10 mM glycolipid in well incubated with 2 μM fluorescein labeled glycopolymers (072917SGalGal0washpt2.2.xls)	80
Figure 2.6: Results from binding assays using 8, 6, and 4 mM Glc glycolipid in well incubated with 2 μM fluorescein labeled glycopolymers (080417glcmulticonc.xls).....	81
Figure 2.7: Results from binding assays using 10 mM glycolipid in well incubated with 1 μM fluorescein labeled glycopolymers (082017exp71mMglycopolymer.xls)	82
Figure 2.8: Results from binding assays using 10 mM glycolipid in well incubated with 1 μM fluorescein labeled glycopolymers. Three scans taken approximately 15 min apart. (082017exp71mMglycopolymer.xls)	83
Figure 2.9: Results from binding assays using 10 mM glycolipid in well incubated with 2 μM fluorescein labeled glycopolymers in 2% (w/v) BSA in PBS buffer (080917exp6.xls).....	84
Figure 2.10: Results from binding assays using 10 mM glycolipid in well incubated with 2 μM fluorescein labeled glycopolymers in 0.5 mM CaCl ₂ in PBS buffer (092617exp14calcium.xls)	84
Figure 2.11: Results from binding assays using 10 mM glycolipid in well incubated with 2 μM fluorescein labeled glycopolymers after washing with methanol (082917exp7meohwash.xls)...	85
Figure 2.12: Results from inverse binding assays using 10 mM glycolipid in well incubated with 0.5 μM fluorescein labeled glycopolymers (091117exp13inverseparafilmed.xls and 091117exp13inverseparafilmed48hrs.xls).....	87
Figure 2.13: Comparison of results from inverse binding assay wells containing lipid with negative control wells containing no lipid. (091117exp13inverseparafilmed.xls and 091117exp13inverseparafilmed48hrs.xls).....	87
Figure 2.14: Schematic of a typical isothermal titration calorimeter	90
Figure 2.15: ITC equations	91
Figure 2.16: Graphical representation of the ITC parameters.....	91
Figure 2.17: c-values calculation.....	92
Figure 2.18: Effect of c-values on ITC binding isotherms.....	93
Figure 2.19: Results from the 90-mer ITC Experiments (sgalgal.opj and sgalglc.opj).....	94
Figure 2.20: Results from the 90-mer ITC Experiments with fixed n value	95
Figure 3.1: Self-assembling carbohydrate functionalized discotic molecules	105
Figure 3.2: The bisignate cotton effect arising from excitonic coupling.....	106
Figure 3.3: Structure of Yariv reagents 60-67. 60-65 bind to AGPs while 66 and 67 do not.....	108
Figure 3.4: Schematic of a typical type II AGP	111
Figure 3.5: a. CD spectrum of 61 (300 μM); b. UV-Vis spectrum of 61 (300 μM) (1:1 Water:DMF spectra were acquired by H. Kuhn).....	116
Figure 3.6: a. CD spectra and b. UV-Vis spectra of Yariv reagents 59, 60, 65, and 66 (300 μM) (spectra for 59 and 66 were acquired by David Caianiello).....	118

Figure 3.7: single azo-linked galactoside 67	118
Figure 3.8: a. ¹ H-NMR spectrum of 68 in D ₂ O (acquired by Natalie Palaychuk); b. CD spectrum of 68; c. UV-vis spectrum of 68	119
Figure 3.9: CD spectra of 61 (300 μM) in the presence of gum arabic	121
Figure 3.10: UV-Vis spectra of 61 (300 μM) in the presence of gum arabic.....	121
Figure 3.11:a. CD spectra of 61 (300 μM) in the presence of AGP; b. CD spectra of 66 (300 μM) in the presence of AGP; c. UV-Vis spectra of 61 (300 μM) in the presence of AGP; d. UV-Vis spectra of 66 (300 μM) in the presence of AGP	122
Figure 3.12: Radial Gel Diffusion Assays with agarose gels containing 61 – left) agarose gels injected with 0.50 g/L gum arabic: clear halos are visible at the end of the incubation period; right) agarose gels injected with 1g/L frost grape AGP: no halos are visible. (Gels prepared by Brandon Dale)	123
Figure 3.13: Radial gel diffusion assays with agarose gels containing 61 and various concentrations of DMF. 0.8 μL of 1 g/L gum Arabic was injected in each well. (Gels prepared by Sarah Weingarten)	124
Figure 3.14: Radial gel diffusion assays with agarose gels containing 68. 0.8 μL of 5 g/L gum Arabic was injected in each well.....	124
Figure 4.1: Types of supramolecular polymers.....	137
Figure 4.2: Hierarchal self-assembly.....	138
Figure 4.3: Oligo(p-phenylenevinylene) monomer.....	139
Figure 4.4: Perylene bisimide derivative.....	140
Figure 4.5: Derivative of 3,3'-bis(acylamino)-2,2'-bipyridine-substituted benzene-1,3,5-tricarboxamide (BiPy-BTA).....	141
Figure 4.6: Isodesmic self-assembly mechanism of rigid discotic molecules	142
Figure 4.7: Isodesmic self-assembly mechanism of rigid discotic molecules. In this case the nucleus is a dimer.	143
Figure 4.8: Structure of PNiPAM.....	145
Figure 4.9: Excess enthalpy of mixing of alcohols with water	146
Figure 4.10: Temperature-dependent CD experiments using 0.3 mM αGal Yariv and aqueous solutions of DMF.....	150
Figure 4.11: CD spectra of 0.3 mM αGal Yariv reagent in alcoholic aqueous solutions	153
Figure 4.12: DLS experiments with αGal in water at 0.3 mM.....	154
Figure 4.13: DLS experiments with βGlc in water at 0.3 mM	155
Figure 4.14: DLS experiments with αGal.....	157
Figure 4.15: DLS experiments with βGlc in water at 0.3 mM	157
Figure 4.16: Temperature dependent CD experiments with 0.3 mM Yariv in methanolic aqueous solution	159
Figure 4.17: CD spectrum of the βGlc Yariv reagent in 25% (v/v) MeOH solution at 20 °C and 0.3 mM.....	160
Figure 4.18: Hysteresis CD experiment with αGal Yariv in 25% (v/v) methanolic aqueous solution. The first CD spectrum was acquired at 10 °C (run 1). The sample was then heated to 60 °C and a CD spectrum was acquired (run 2). The sample was then cooled to 10 °C and a CD spectrum was acquired (run 3). CD spectra were aquired for two more cycles of heating (runs 4 and 6) and cooling (runs 5 and 7).	161

Figure 4.19: Hysteresis CD experiment with β Glc Yariv in 25% (v/v) methanolic aqueous solution	162
Figure 4.20: Hysteresis UV/Vis experiment with α Gal Yariv in 25% (v/v) methanolic aqueous solution	163
Figure 4.21: Hysteresis UV/Vis experiment with β Glc Yariv in 25% (v/v) methanolic aqueous solution	163
Figure 4.22: Hysteresis UV/Vis experiment with α Gal and β Glc Yariv in 25% (v/v) methanolic aqueous solution (For DLS results with multiple peaks the larger sized peak is displayed).....	164
Figure 4.23: CD spectra of 0.3 mM β Glc Yariv reagent in methanolic aqueous solutions	166
Figure 4.24: UV-Vis spectra of 0.3 mM β Glc Yariv reagent in methanolic aqueous solutions	167
Figure 4.25: CD spectra of 0.3 mM α Gal Yariv reagent in methanolic aqueous solutions	169
Figure 4.26: CD spectra of 0.3 mM α Gal Yariv reagent in methanolic aqueous solutions	170
Figure 4.27: CD spectra of 0.3 mM α Gal Yariv reagent in ethanolic aqueous solutions	171
Figure 4.28: UV-Vis spectra of 0.3 mM α Gal Yariv reagent in ethanolic aqueous solutions	172
Figure 4.29: CD spectra of 0.3 mM α Gal Yariv reagent in isopropanolic aqueous solutions	173
Figure 4.30: UV/Vis spectra of 0.3 mM α Gal Yariv reagent in isopropanolic aqueous solutions	174
Figure 4.31: DLS experiments with Yariv reagents and various alcoholic aqueous solutions (For DLS results with multiple peaks the larger sized peak is displayed).....	176
Figure 4.32: Temperature dependent CD experiments with ethanolic solution.....	177
Figure 4.33: Temperature-dependent CD experiments performed with isopropanolic solution	178
Figure 4.34: The effects of gum Arabic AGP on the CD and UV/Vis spectra of 0.3 mM β Glc Yariv reagent in methanolic solution.....	179
Figure 4.35: The effects of gum Arabic AGP on the CD and UV/Vis spectra of 0.3 mM α Gal Yariv reagent in methanolic solution.....	180
Figure 4.36: Trends in CD and DLS measurements of α Gal Yariv samples in alcohol solutions of various compositions	182

List of Tables

Table 1.1: Molecular weight and polydispersity of polymers determined by GPC	18
Table 1.2: % Fluorescein labeling of glycopolymers	38
Table 2.1: Summary of the emission values obtained in the well-binding experiments.....	89

1 SYNTHESIS AND CHARACTERIZATION OF GLYCOPOLYMER MODEL SYSTEMS OF CCIs

1.1 Introduction to cell-membrane CCIs

Polysaccharides and other biological carbohydrates that are found on the surface of the cell membrane play an important role in cell signaling and recognition. Although such biological activity is most commonly the result of carbohydrate-protein binding interactions (CPIs), surface carbohydrates can also interact with other carbohydrates.¹ Carbohydrate-carbohydrate interactions (CCIs) (Fig. 1.1) take part in various important cell signaling and adhesion processes.

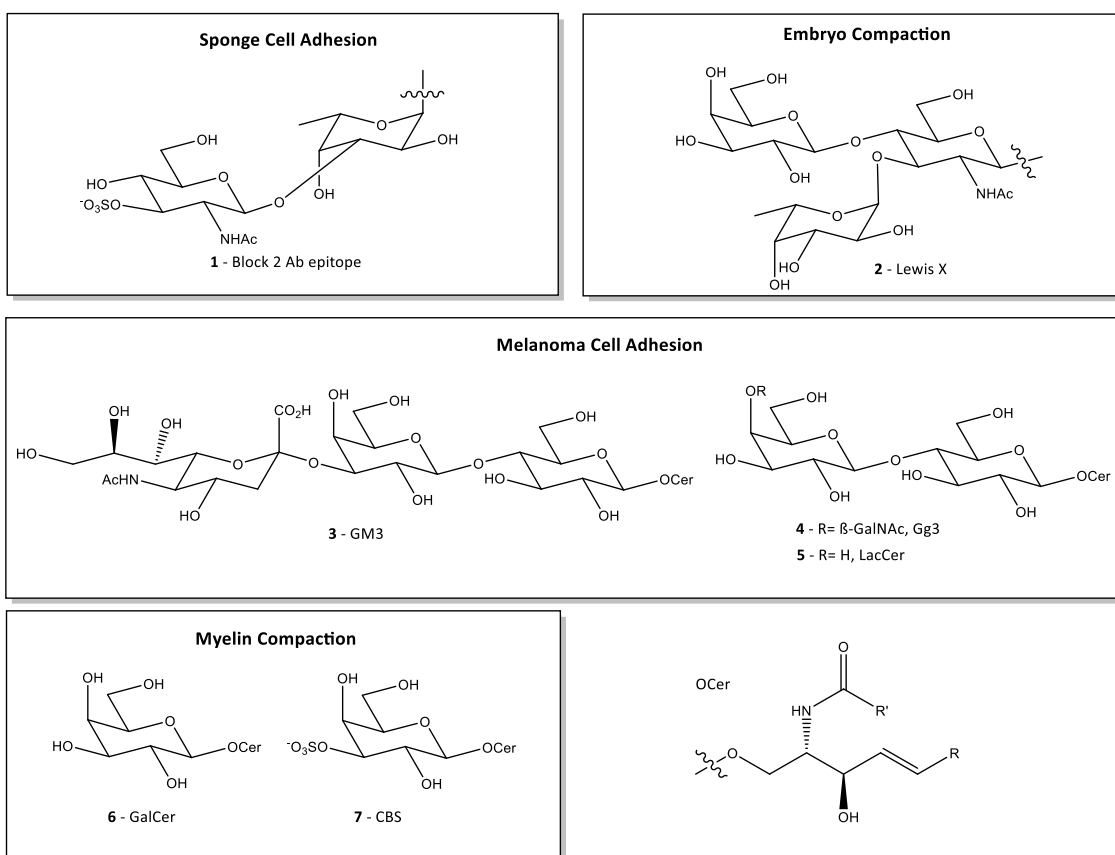


Figure 1.1: Glycan structures that participate in carbohydrate-carbohydrate interactions

One of the earliest CCIs observed was found to occur as part of the self-association process of sponge cells.² The cells of sea sponges are known to associate with other sponge cells of its specific

species if they have been separated. In a study of the self-aggregation of cells from the *Microciona prolifera* sponge, it was found that a proteoglycan known as MAF was responsible for the selective self-association.³ It was found that self-aggregation is inhibited when antibodies bind to two reactive epitopes on the carbohydrate portion of the proteoglycan. One of the epitopes is a sulfated disaccharide known as GlcNAc(3SO₃)β1–3Fuc **1**.³ Gold nanoparticles coated in the sulfated disaccharide were found to form aggregates in the presence of Ca²⁺, indicating that this epitope participates in a CCI.⁴

Another important CCI mediates the process of embryo cell adhesion. Cells that form aggregates during embryo compaction were found to possess large amounts of the Lewis X trisaccharide (Le^x) glycosphingolipid **2** on the surface of their cell membranes. Multivalent conjugates of the Le^x-containing oligosaccharide LNFP-III interact with Le^x on the cell membranes of embryonic cells, and disrupts the aggregation process, indicating a Le^x-Le^x CCI.⁵ Also, when Le^x-containing glycolipids are incorporated into the plasma membranes of the typically non-aggregating RBL cells, self-aggregation begins to occur, indicating that Le^x participates in a CCI.⁶

The previous two CCIs are examples of homotypic CCIs, meaning that the interaction occurs between identical epitopes. Heterotypic CCIs, in which the interaction occurs between different epitopes, exist as well. One such CCI occurs during the process of melanoma cell adhesion. B16 melanoma cells contain large amounts of the glycosphingolipid GM3 **3** in their cell membranes. These cells selectively adhere to mouse AA12 T-cell lymphomas that possess the Gg3 glycosphingolipid **4**.⁷ Experiments using GM3 and Gg3 binding antibodies have shown that adhesion is inhibited when either glycosphingolipid is bound by an antibody, indicating the presence of a specific CCI between Gg3 and GM3. It was also found that GM3 can interact with the glycosphingolipid LacCer **5** whose structure is similar to that of Gg3. Furthermore, GM3 is found in lipid-rich microdomains of the B16 cells known as lipid rafts which also contain signaling

proteins. When GM3 in the lipid rafts of a B16 cell adhere to plates coated with Gg3, the signaling proteins Rho and Ras are activated, indicating that the GM3-Gg3 CCI plays a role in cell signaling in addition to mediating cell adhesion.⁸

Another heterotypic CCI occurs in the myelin sheath, a multi-layered membrane found in the nervous system. The myelin sheath protects the axons from damage and aids in the process of transferring electric signals across the axon.⁹ Myelin cell membranes contain highly concentrated regions of glycosphingolipids positioned on the outer leaflet of the lipid bilayer. An estimated 40% of the outer leaflet of the myelin sheath is composed of the glycosphingolipids galactosylceramide (GalCer) **6** and 3-sulphogalactosylceramide (SGalCer) **7**.⁹ These glycosphingolipids play an important role in the post-natal compaction of the myelin sheath. In knockout studies conducted with mice, severe myelin related birth defects and early mortality were observed in mice lacking GalCer and SGalCer.¹⁰ Furthermore, it was shown that GalCer and SGalCer liposomes aggregate selectively in the presence of divalent cations, indicating the presence of a CCI.¹¹ Fluorescent binding assays were also performed using 96-well plates with glycolipid coated wells, and fluorescent glyconanoparticles. The strongest interactions were observed between nanoparticles functionalized with 3-sulfogalactose (SGal) and wells containing galactose (Gal) functionalized lipids. TEM microscopy showed aggregation of the glyconanoparticles, and fluorescence microscopy was used to visualize these nanoparticles binding to oligodendrocytes and myelin sheath fragments, providing direct evidence of this CCI.¹²

As described above, many different techniques have been utilized in an effort to discover and characterize biologically relevant CCIs. Moving forward it is necessary to develop new techniques and model systems to fill the gaps in our knowledge pertaining to CCIs. Synthetic model systems are especially attractive as they provide control over the presentation of the binding epitope, and simplify the environment in which binding will occur.

1.2 Introduction to multivalent model systems of CCI

Interactions between carbohydrate ligands and protein receptors are generally weak interactions (association constants weaker than 10^{-6} M^{-1}), and are too weak to mediate biological processes via monovalent interactions.¹³ To compensate for the weakness of these interactions, carbohydrates are presented as a multivalent ligand and many binding interactions occur simultaneously. The result of this increased avidity is a much stronger interaction that is capable of mediating biological processes.¹³⁻¹⁴ This concept can be applied to CCI as well, with many of the known interactions taking place between highly-concentrated microdomains of cell-surface glycosphingolipids referred to as glycosynapses.¹⁵

Characterization of the specificity and binding behavior of CCI in vivo can be problematic. The complex and dynamic nature of the cell makes it difficult to unambiguously correlate observed behavior with specific carbohydrate moieties. Therefore, CCI are often modeled using synthetic analogs containing only the sugar residues of interest.¹ Since biological CCI occur between regions of the cell surface where the binding carbohydrate moieties are presented in a multivalent array most CCI model systems are designed to be multivalent as well. Examples of multivalent model systems that have been used to study CCI include: vesicles of glycosphingolipids, surfaces coated with glycosphingolipids, glyconanoparticles and glycopolymers.¹ The use of glycopolymers as CCI model systems is attractive, because advances in polymer synthesis have allowed for good control over the degree of sugar multivalency and the spacing between sugars.¹⁶⁻¹⁹

1.3 Glycopolymers

The basic components of a glycopolymer model system consist of: a polymer backbone, linker groups,

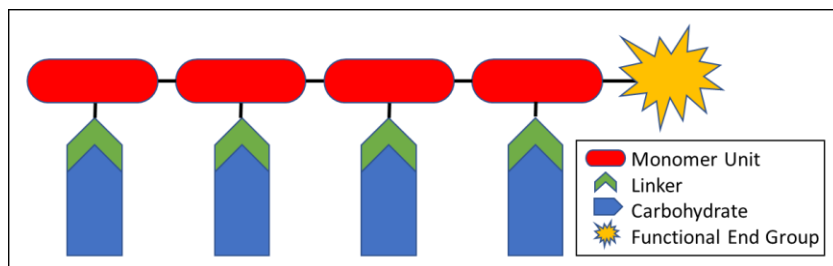


Figure 1.2: The Basic Components of a Glycopolymer.

carbohydrate pendant groups, and sometimes an end group functionality such as a fluorophore (Fig. 1.2). Living polymerization techniques such as controlled radical polymerization (CRP)¹⁸ and ring opening metathesis polymerization (ROMP)²⁰⁻²¹ allow for the synthesis of polymers with well-defined molecular weights and low polydispersity. Such backbones can be prepared as “telechelic” polymers, meaning that they contain reactive end groups that can be functionalized to serve as spectroscopic labels.¹⁹ Functionalization of the backbone with pendant sugar groups can be achieved pre or post polymerization. Various techniques exist for the post-polymerization functionalization of the backbone, but click reactions are especially useful due to their broad functional group tolerance and high yield.¹⁶

When designing glycopolymers to accurately model CCIs control over the degree of polymerization and polydispersity of the polymer backbone is important. Polymer backbones with higher degrees of polymerization have more monomer units, and thus increased sugar valency. The amplification of avidity that occurs in biological systems due to the multivalent sugar presentation is also observed in synthetic polymer model systems. For example, polymers functionalized with mannose inhibit cell agglutination mediated by concanavalin A, and the potency of the polymers as an inhibitor increases as the degree of polymerization increases.²² An ideal polymeric model system would consist of polymers of uniform length, so that the binding behavior is the same for each polymer in the system. Biopolymers such as proteins have virtually no polydispersity since they are assembled according to a complementary template, but there is

almost always some variance in length for synthetic polymers. Therefore, it is necessary to synthesize glycopolymers using a polymerization technique that gives a high degree of polymerization and minimal polydispersity.

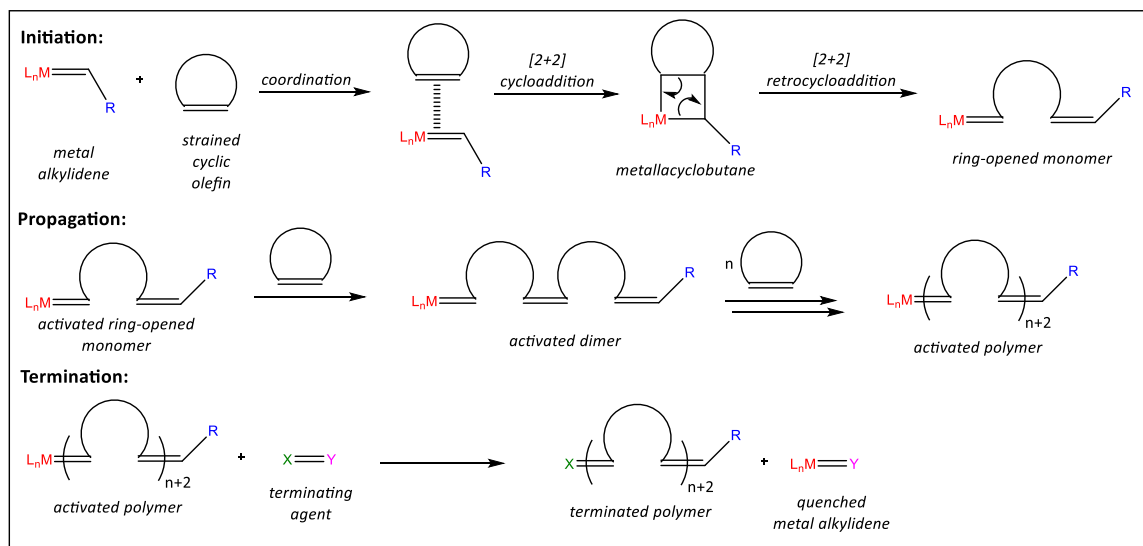


Figure 1.3: A general reaction mechanism for the ROMP reaction

Living polymerization techniques are commonly used to produce glycopolymers, because they offer excellent control over degree of polymerization and polydispersity.²⁰ Living ring opening metathesis polymerization (ROMP) (Fig 1.3) is particularly useful for glycopolymer synthesis, because useful end labels can be easily incorporated. In order to successfully perform ROMP it is important to use a cyclic

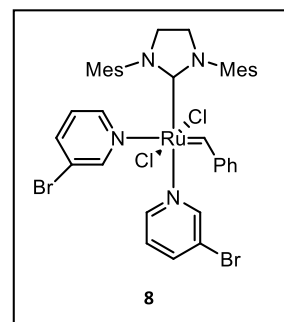


Figure 1.4: Grubbs' 3rd generation ruthenium catalyst

olefin monomer with a strained ring such as a norbornene. Since metathesis reactions are generally reversible, the release of ring strain can provide a strong enough enthalpic contribution to compensate for entropic penalty associated with polymerization and drive the polymerization forward.²³ The polymerization is initiated when the metal alkylidene catalyst coordinates to the alkene group of the monomer followed by a [2+2] cycloaddition to yield a metalocyclobutane intermediate. Ring opening occurs because of the subsequent [2+2] retrocycloaddition. The ring opened monomer will now possess a terminal reactive metal alkylidene functionality. After the

initial ring-opening the activated ring-opened monomer will react with an unreacted monomer and propagation and chain growth will occur (Fig 1.3). Highly polydisperse polymers will be produced if the rate of initiation is slower than the rate of propagation. Therefore, it is important to use a metathesis catalyst that is capable of fast and complete initiation as doing so will allow all chains to begin propagation virtually simultaneously and form polymers with low polydispersity. By using such a catalyst the degree of polymerization can be controlled by adjusting the mole ratio of monomer to catalyst.²³ Ruthenium catalysts (Fig. 1.4) such as Grubbs 3rd generation catalyst **8** are commonly used in ROMP due to their functional group tolerance, fast initiation rates, high activity and stability in air and organic solvents.²⁴

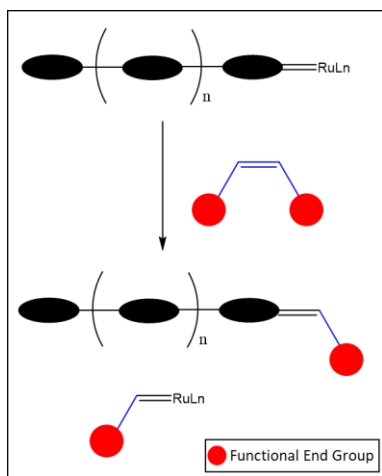


Figure 1.5: Incorporation of a functional end group via ROMP termination

An additional benefit of using a Grubbs ruthenium catalyst is that after all of the monomer has been consumed and incorporated into polymer chains there remains a reactive metal alkylidene at the terminus of each polymer. At this point if an acyclic alkene is added to the reaction mixture it can undergo metathesis and be incorporated into the polymer as an end group (Fig. 1.5).²⁵ Depending on what terminating group is

used, various spectroscopic handles and functionalities can be incorporated into the polymer. For example, a 3,6-disulfogalactose ROMP glycopolymer was synthesized and terminated with an end group capable of undergoing conjugation with a fluorescein derivative to yield fluorescently labeled glycopolymers. These polymers were then used to visualize glycopolymer binding to L-selectin.²⁶

The most important characteristic of glycopolymers is that they are functionalized with pendant sugar groups. It is possible to functionalize prior to polymerization by using sugar bearing monomers. This method can be useful for preparing glycopolymers because it ensures that each

repeat unit of the polymer will be functionalized.²⁰ However, it is important to use polymerization and end-group functionalization reagents that are compatible with the sugar moiety. Sometimes pre-functionalized monomers feature protected sugars that can be deprotected post-polymerization. Additionally, sugar-functionalized monomers often require several synthetic steps and can be tedious to prepare.²⁶ Furthermore, a new monomer must be synthesized for each new type of sugar. The chemical structure of the sugar can cause a change in the physical properties of the monomer and can result in different degrees of polymerization and polydispersities between polymers functionalized with different sugars.²⁷

The sugar pendant groups can also be added post-polymerization provided that the monomer contains the proper complementary functional group. If the desired functional group is not compatible with the polymerization reaction, then compatible groups can be further modified by linker groups post

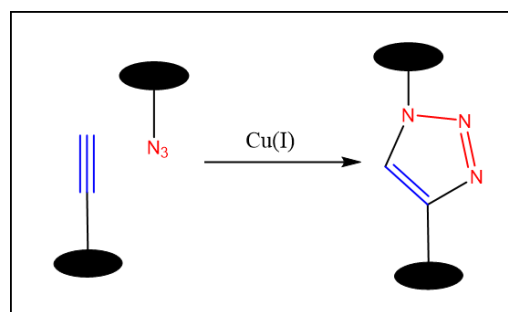


Figure 1.6: Copper catalyzed azide-alkyne cycloaddition (CuAAC)

polymerization to provide the desired product. Various techniques have been used to conjugate sugars to the polymer backbone.²⁰ However, steric hinderance can prevent complete conversion. Incomplete conversion will result in ill-defined polymers that may produce innaccurate data when used to model CCIs. In response to this issue “click chemistry” has been utilized to great effect to prepare completely functionalized glycopolymers.¹⁶

The term “click chemistry” was first used by Sharpless to describe a set of reactions that proceed rapidly to completion and are highly selective for a single product.²⁸ These reactions have been used to synthesize various molecules with complicated architecture. In particular, the copper catalyzed azide-alkyne cycloaddition (CuAAC) (Fig. 1.6) has been a widely used click reaction. In the absence of copper, alkynes and azides will undergo cycloaddition at elevated temperatures

over hours or days, but will yield a mixture of 1,4 and 1,5-substituted 1,2,3-triazoles. Use of a copper catalyst allows the reaction to proceed much faster at lower temperature, and produces only the 1,4-disubstituted-1,2,3-triazole product (Fig. 1.6).²⁹ Further, the functional group tolerance exhibited by the CuAAC makes it especially useful for functionalizing complicated molecules. Due to nearly complete conversions that are inherent to click reactions, many glycopolymers have been prepared using polymers containing alkyne or azide pendant groups and CuAAC to attach the corresponding azido or propargyl sugars.^{16, 21}

1.4 Glycopolymers as probes for CCI

As previously mentioned, the process of proper assembly and folding of the myelin sheath is mediated by a CCI that occurs between the glycosphingolipids GalCer and SGC, which possess galactose (Gal) and 3-sulfo-galactose (SGal) sugars, respectively. This CCI has been studied using liposomes composed of GalCer and SGalCer, and fluorescently labeled glyconanoparticles and fluorescent glycopolymers functionalized with the interacting sugar moieties.^{9, 12, 30}

The glycopolymer model system used to study this CCI were designed with several key characteristics in mind: 1) a well-defined polymer backbone with low polydispersity, 2) a

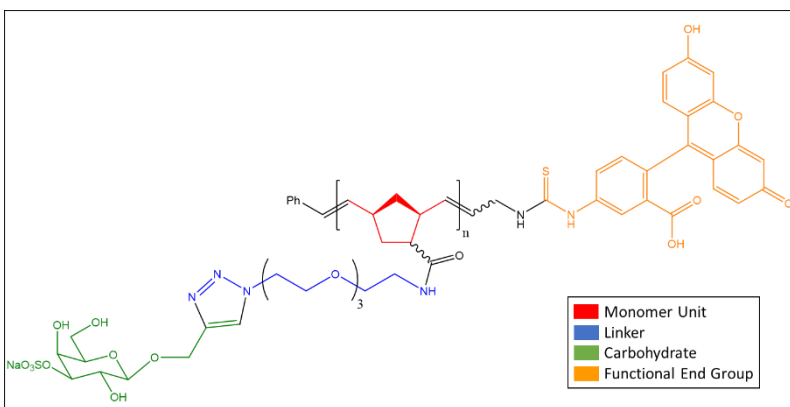


Figure 1.7: An example of a fluorescent glycopolymer used as a model system of myelin CCI

fluorescent end group functionality, and 3) complete sugar functionalization of the backbone. The polymer backbone was prepared using ROMP of a norbornene monomer functionalized with a N-hydroxysuccinimide (NHS) ester. The polymerization was terminated using a terminating agent

bearing a 2-(trimethylsilyl)ethoxycarbonyl (Teoc) functional group. The resulting poly-NHS ester contains a Teoc protected amino end group that can be further functionalized with a fluorophore molecule. The NHS ester pendant groups were displaced by α - ω -amino-azido linkers to impart the azide functionality to the polymer backbone. The addition of pendant sugar groups is achieved by CuAAC between propargyl sugars and the azido backbone.^{21, 30}

The previously described method for glycopolymer preparation was successfully used to prepare glycopolymers (Fig. 1.7), but there are several limitations of this synthetic route. This method requires the use of propargyl sugars, which must be synthesized and purified using silica gel column chromatography. Additionally, the linker groups that are used to impart azide functionality to the polymer backbone are not commercially available, and are must be synthesized in house. Also, the need for a fluorescent end group functionality requires several synthetic steps, including the synthesis of a custom terminating agent. Although fluorescently labeled glycopolymers are useful for studying CCI, it is not necessarily required depending on the method of analysis.

Since so many steps are required to prepare these glycopolymers the synthesis can be time consuming, and the overall yields of polymer can be quite low, which means that only experiments requiring very small amounts of polymer are feasible. Therefore, we set out to develop a more facile synthetic method to develop glycopolymer model systems that retained the key qualities of being a well-defined and completely functionalized polymer with optional end group functionalization. The sections that follow provide a detailed discussion of the synthesis of this new generation of

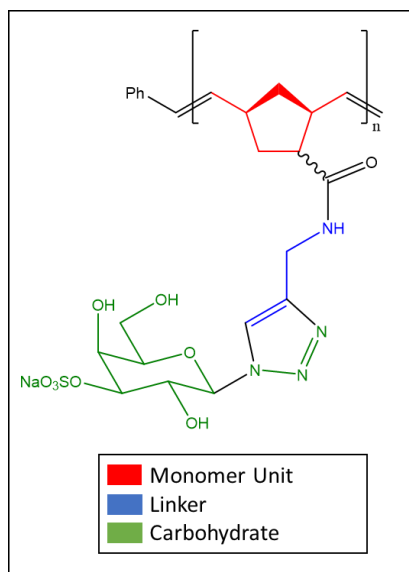


Figure 1.8: Example of a new generation of glycopolymer prepared via a more facile synthetic route

glycopolymers (Fig. 1.8). The key innovation here is that the polymer/sugar functionalization is switched, meaning that the polymer backbone will bear alkyne pendant groups and the sugars will be azide functionalized. This approach eliminates the need for complicated linker groups, since poly-alkyne can be prepared from the poly-NHS polymer using commercially available propargyl amine. Also, azido sugars can be rapidly prepared on a large scale, since most of the synthetic intermediates do not require chromatography for purification. Furthermore, non-fluorescent polymers are easily prepared using ethyl vinyl ether as a terminating agent. Fluorescent versions of this new generation of polymers were also prepared.

1.5 Facile synthesis of glycopolymers as probes for CCIs

The facile synthesis of glycopolymers as probes for CCIs can be broken down into several phases. Phase I involves the synthesis of a custom terminating agent, and is only required if fluorescently labeled glycopolymers are desired. Phase II involves the synthesis of the alkyne-functionalized polymer backbone. In Phase III the terminus of the polymer is functionalized using fluorescein to provide a fluorescently labeled backbone (only required for fluorescently labeled polymers). In Phase IV azido-functionalized 3-sulfo-galactose (SGal), galactose (Gal), glucose (Glc) and mannose (Man) are synthesized. It is important to note that Phase IV can be carried out in parallel to Phases I-III. Finally, the sugars are conjugated to the polymer backbone via a CuAAC reaction in Phase V to yield glycopolymers.

1.5.1 Phase I: Terminating Agent Synthesis

To obtain polymers with end-group functionality via ROMP it is necessary to utilize a suitable acyclic olefin as a terminating agent. The previous generation of polymers were prepared using terminating agent **15** (Fig. 1.9).²¹ This molecule is a symmetric *cis*-olefin in order to ensure that the desired end group is incorporated during the termination step regardless of the direction of coordination. After termination,

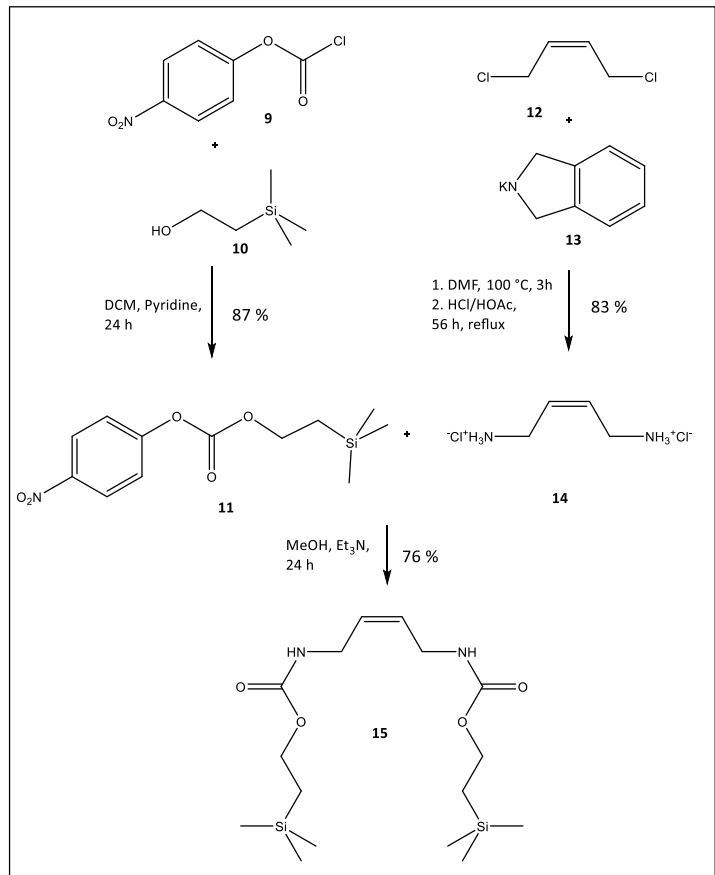


Figure 1.9: Synthesis of the terminating agent

the polymers will bear a primary amine functionality that is masked by a 2-trimethylsilylethyl carbamate (**Teoc**) protecting group that can later be removed to allow fluorescein labeling. Also, the trimethyl silyl (**TMS**) group present in the terminating agent serves as a useful NMR reference to help determine the success of the termination reaction.

In order to synthesize the terminating agent **15**, the precursors 4-nitrophenyl (2-trimethylsilyl)ethyl carbonate **11** and the bishydrochloride salt of *cis*-diamino-but-2-ene **14** must first be prepared. **11** is prepared by combining 4-nitrophenyl chloroformate **9** and 2-trimethylsilyl ethanol **10** in the presence of pyridine. **14** is prepared by reacting *cis*-1,4-dichloro-but-2-ene **12** and potassium phthalimide **13** to give the diphthalimide, which is then treated with strong acid at reflux to yield the desired product. **11** and **14** can then be combined in the presence of triethyl amine to yield the desired terminating agent **15**.³⁰

1.5.2 Phase II: The synthesis of the alkyne-functionalized polymer backbone

1.5.2.1 Preparation of monomer

As was the case for the previous generation of ROMP glycopolymers, bicyclo[2.2.1]hept-5-ene-2-carboxylic acid

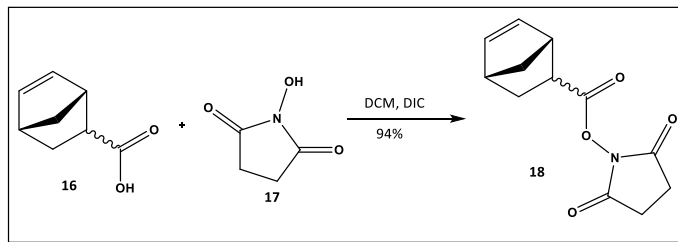


Figure 1.10: Synthesis of monomer

N-hydroxysuccinimide ester **18** was chosen as the strained ring olefin monomer to be used to construct the polymer backbone.²⁷ As previously mentioned, the strained norbornene ring is ideal for ROMP because the ring opening is favorable and contributes enough enthalpy to overcome the entropic cost of polymerization and thus will drive the polymerization forward. Also, the NHS-ester functionality is stable enough to withstand the polymerization conditions, but is labile enough to be displaced by primary amines.

18 was prepared by *N,N'*-diisopropylcarbodiimide (DIC) assisted coupling between 5-norbornene-2-carboxylic acid (97 % *endo* isomer) **16** and N-hydroxysuccinimide (NHS) **17** (Fig. 1.10). The resulting NHS-ester is isolated as a mixture of *exo* and *endo* isomers. Previous work has shown that ROMP of this mixed isomer monomer produces polymers with controlled lengths and these results are comparable to those obtained with isomerically pure monomer (Fig 1.10).³⁰

1.5.2.2 ROMP

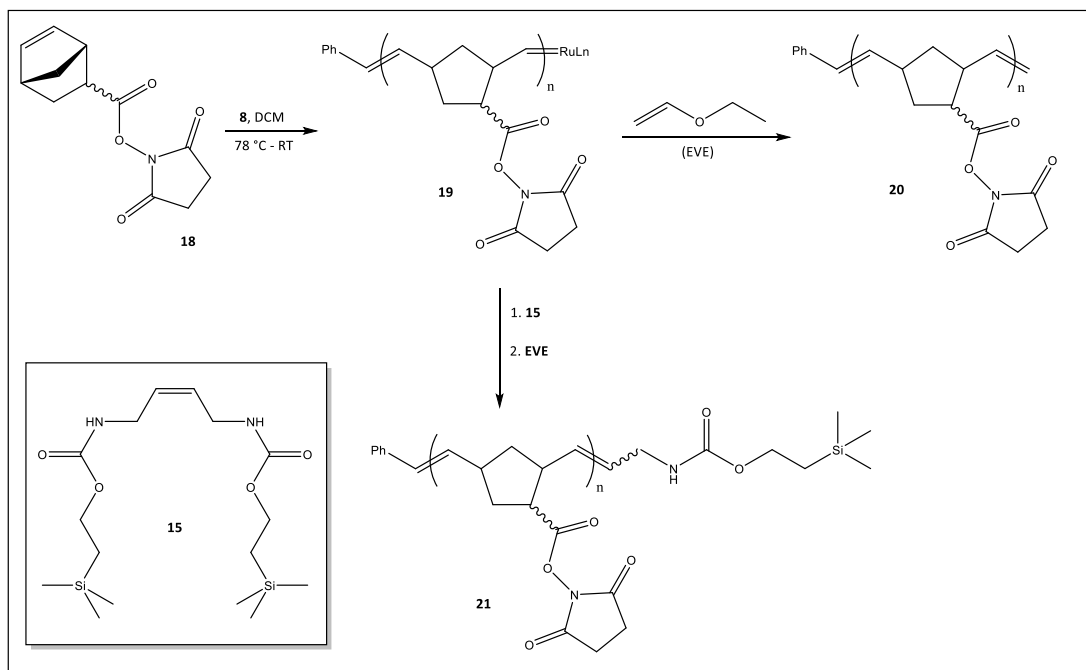


Figure 1.11: ROMP to give the alkene **20** and Teoc **21** terminated poly-NHS esters

As was the case for the previous generation of polymer, the ROMP (Fig. 1.11) of monomer **18** was catalyzed by Grubbs' 3rd generation ruthenium-carbene catalyst **8**.³⁰ Catalyst loading was adjusted based on the desired degree of polymerization (DP). For instance, if a polymer consisting of 30 monomer units is desired, then 1 mole of catalyst should be present for every 30 moles of monomer in the reaction. Also, to ensure uniform initiation, the solution of monomer must be cooled to -78 °C prior to addition of catalyst. Cooling the reaction drastically reduces the rate of initiation and allows the catalyst to be evenly dispersed throughout the reaction mixture prior to initiation.

Once the catalyst has been added to the reaction vessel and thoroughly mixed the reaction mixture is allowed to warm to room temperature. As the mixture warms the color of the mixture changes from bright green to brown indicating that the initiation step of the ROMP has occurred. Propagation proceeds until all monomer has been consumed (as determined by TLC).

At this point, ROMP is complete, but each polymer still has a catalytically active ruthenium carbene at the terminus **19**. Therefore, a terminating agent must be used to cap the polymer. If fluorescent polymers are being synthesized, then terminating agent **15** is added to the mixture. The resulting metathesis reaction will yield polymers bearing a Teoc protected primary amine end group **21** functionality and a ruthenium carbene byproduct. In a previous study no evidence of secondary cross metathesis was observed indicating that the ruthenium carbene byproduct is unreactive towards the internal alkenes present within the polymer.³⁰ To ensure complete deactivation of the ruthenium catalyst, the reaction is quenched by the addition of excess ethyl vinyl ether (EVE) to yield an electron rich carbene complex that is unreactive toward olefins.³¹ Also, EVE can be used as the terminating agent to yield an alkene terminated polymer **20**. No further end-group modifications are made to such polymers. After termination is complete the poly-NHS ester functionalized polymer is separated from any small molecule byproducts by precipitation in ether.

1.5.2.2.1 Characterization of ROMP polymers by ¹H NMR

The polymer that had been capped using the terminating agent **21** bears a terminal TMS group that provides a well resolved ¹H NMR peak that is easy to identify. The ¹H NMR spectra of these polymers shows a TMS singlet peak around 0 ppm (Fig. 1.14). The integral of the TMS peak was set to 9 H to calibrate the spectra. Then the average degree of polymerization (DP) be estimated by taking the integral of the olefinic proton multiplet (~5.5 ppm) and dividing the value by two. Also, the integral for the phenyl multiplet (~7.3 ppm) should be equal to 5 H when the TMS group is calibrated to 9 H (Fig. 1.14). The polymers that are terminated by EVE **20** do not contain a TMS group, so the DP is calculated by calibrating the spectra to the integral of the phenyl peaks which is set to 5 H (Fig. 1.12-13). Since the phenyl peaks are broad and close to the baseline some

inaccuracy in the integral value is expected. Any inaccuracy in the integral values of the phenyl peaks will result in inaccurate integral values for the olefinic peaks.

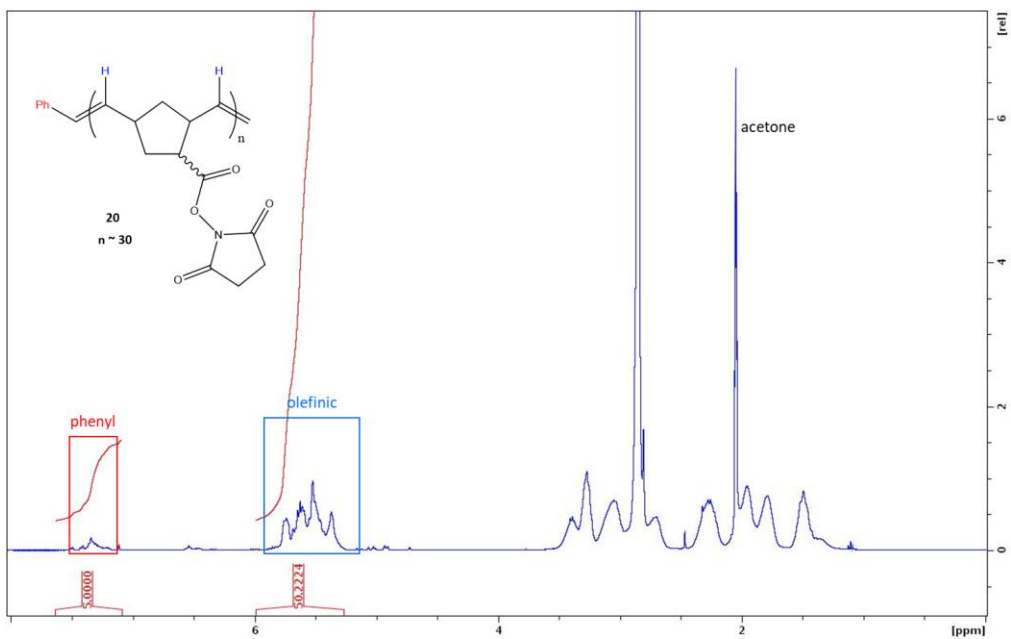


Figure 1.12: ¹H NMR of alkene terminated poly-NHS ester **20** (n ~ 30) taken in d₆-acetone

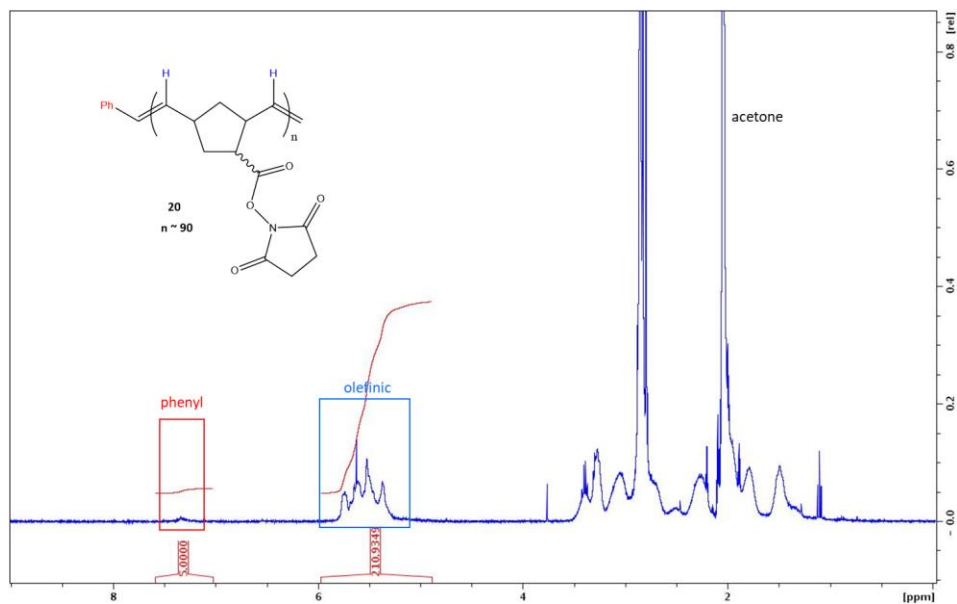


Figure 1.13: ¹H NMR of alkene terminated poly-NHS ester **20** (n ~ 90) taken in d₆-acetone

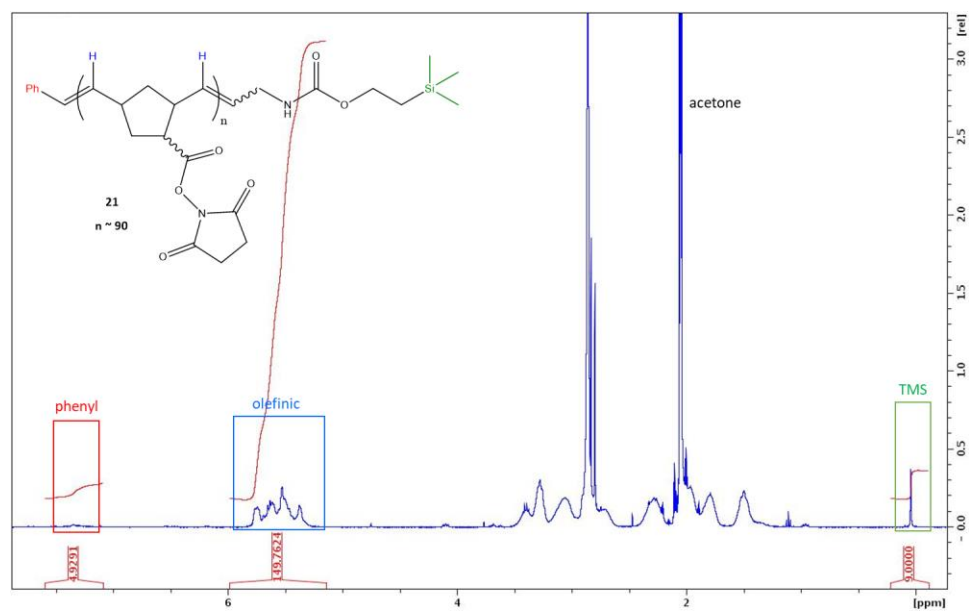


Figure 1.14: ¹H NMR of Teoc terminated poly-NHS ester **21** (n ~ 90) taken in d₆-acetone

1.5.2.2.2 Characterization of ROMP polymers by GPC

¹H NMR can provide useful estimates of average DPs and molecular weights. However, since synthetic polymers are not of uniform length it is important to understand how broad the range of chain lengths is for a given sample of polymer. This property is known as polydispersity (PD) and it cannot be determined using ¹H NMR. Gel permeation chromatography (GPC) is a useful technique for determining the polydispersity of a polymer sample. In GPC a sample of polymer is passed through a column packed with a porous gel. Higher molecular weight polymers will have shorter retention times than lower molecular weight polymers, because they are too large to pass through the smaller pores. At the end of the column is a detector that is used to determine the retention time and intensity of a polymer sample.

The weight average (M_w) and number average (M_n) molecular weights can then be calculated by comparing the experimental values to a calibration curve conducted using polymer standards.

Polydispersity is calculated by taking the ratio of M_n to M_w (Table 2.1). A large difference between M_n and M_w is indicative of a polymer sample with a broad range of polymer lengths,

and thus this sample will have a high PD. Polymers of uniform length such as proteins will have equal values for M_n and M_w , resulting in a PD of 1. Living ROMP polymers typically have a PD that is <1.5 .²³ The experimentally determined DPs of the polymers are slightly higher than expected, but the PDs are all <1.5 indicating successful ROMP (Table 2.1). An added benefit of calculating MW using GPC is that it does not require calibration based on the signal of an end-group, as is the case for ^1H NMR.

Table 1.1: Molecular weight and polydispersity of polymers determined by GPC

Sample	M_w	M_n	PD	DP_w	DP_n
20, $n \sim 30$	10350	9323	1.11	44	39
20, $n \sim 90$	29913	24988	1.20	127	106
21, $n \sim 90$	26508	24478	1.09	112	104

1.5.2.3 Preparation of alkyne functionalized polymer

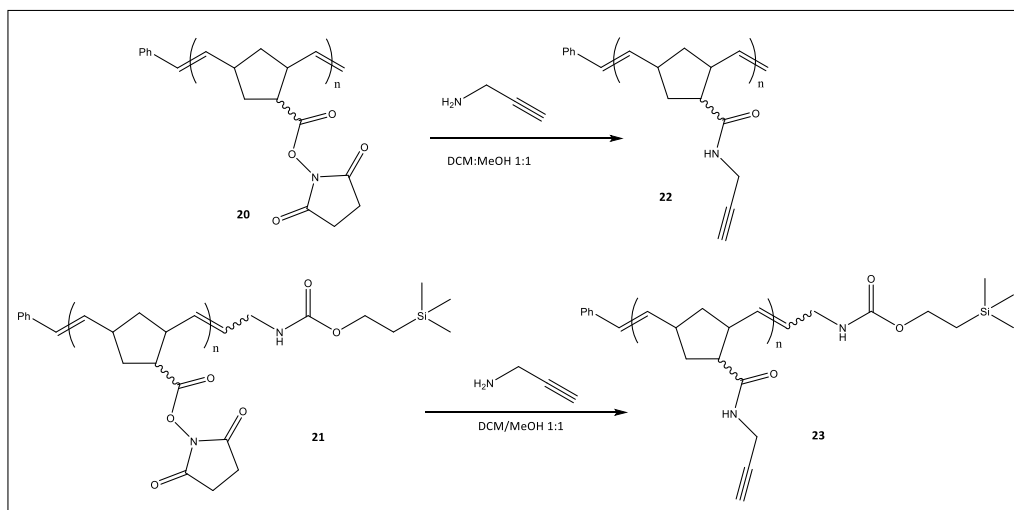


Figure 1.15: Synthesis of poly-alkyne polymers

The poly-alkyne polymers **22**, **23** were prepared via amide bond formation through reaction of excess propargyl amine with the activated NHS ester groups of the ROMP polymers **20**, **21** (Fig 1.15). To ensure complete displacement of the NHS esters, four equivalents of propargyl amine

per NHS ester were used and the reactions were stirred at room temperature for two days. The succinimide proton peak of the NHS esters appears in the same region as other aliphatic protons of the poly-alkyne polymers (Fig. 1.16). Therefore, the displacement of the NHS ester cannot be confirmed by the disappearance of the succinimide proton peak. Conversion of the polymer was confirmed by observing the appearance of a peak around 3.75 ppm (Fig. 1.17-18) from the propargyl protons which are present in approximately a 1:1 ratio with the alkene peaks. The poly-alkyne polymers were purified by dialysis in 1:1 DCM:MeOH.

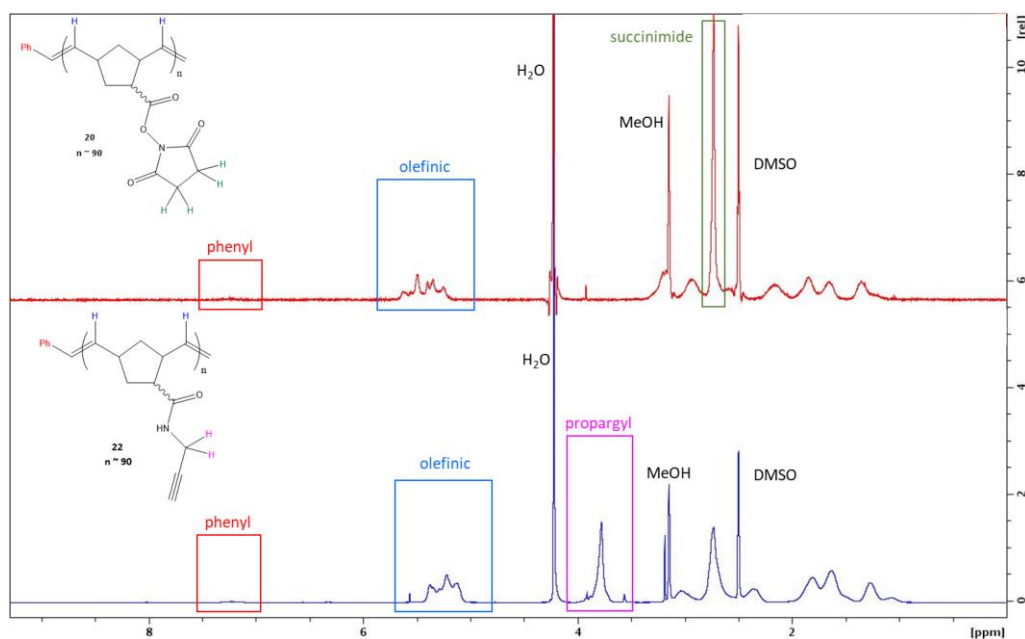


Figure 1.16: ¹H-NMR of **20** (n ~ 90) and **22** (n ~ 90) taken in 1:1 (v/v) d₆-DMSO:CD₃OD

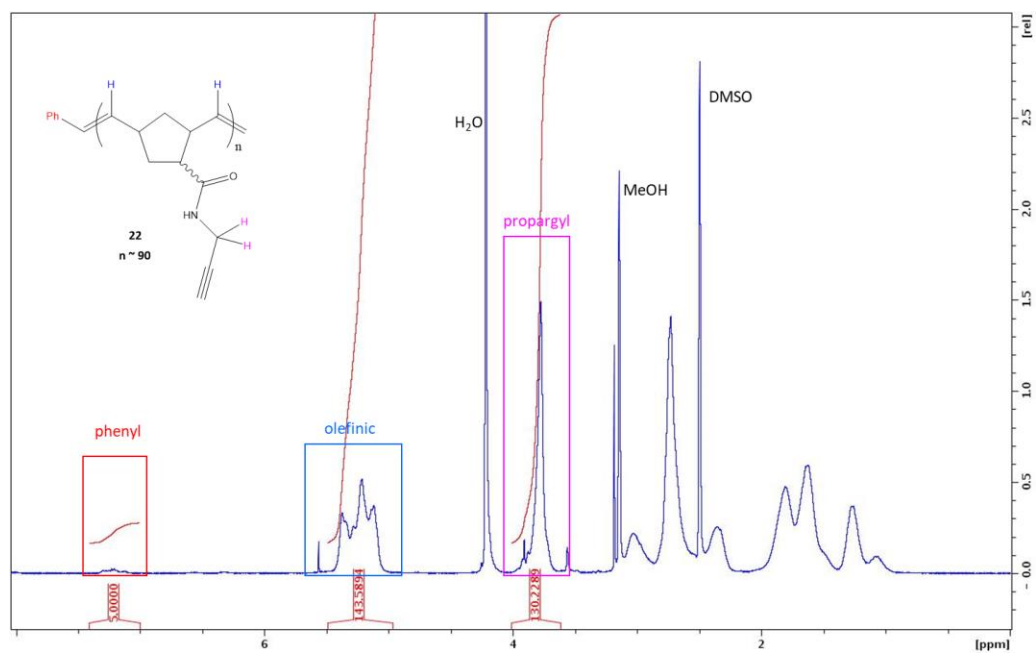


Figure 1.17: ^1H NMR of alkene terminated poly-alkyne **22** ($n \sim 90$) taken in 1:1 (v/v) d_6 -DMSO: CD_3OD

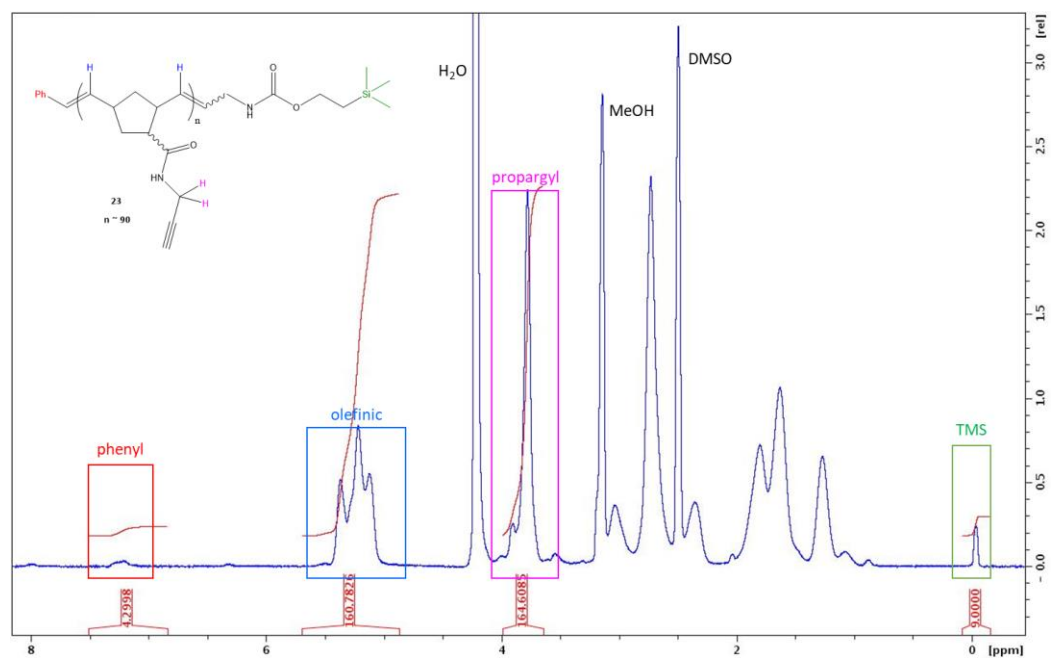


Figure 1.18: ^1H -NMR of the Teoc protected poly-alkyne **23** ($n \sim 90$) taken in 1:1 (v/v) d_6 -DMSO: CD_3OD

1.5.2.3.1 MALDI-ToF Analysis of post-ROMP modified polymers

Matrix assisted laser desorption ionization time of flight (MALDI-ToF) mass spectrometry was used as an additional technique for the determination of molecular weight and polydispersity of the poly-alkyne polymers. In

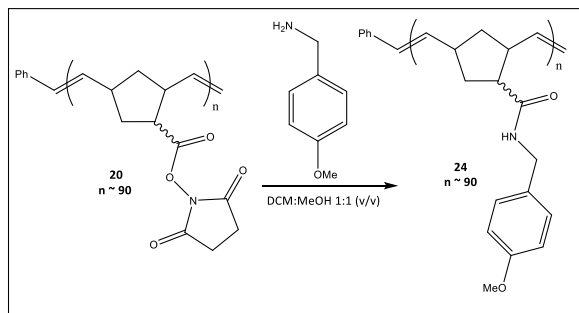


Figure 1.19: Synthesis of poly-PMB polymer

MALDI-ToF the analyte polymer is co-crystallized with a matrix molecule that allows for the formation of a stable polymer ion after the sample is struck by the laser beam. The 30-mer poly-alkyne co-crystallized well with the super-DHB matrix and a well-defined mass-spectra was obtained (Fig. 1.20). The peaks in this spectrum are of uniform distance and the mass (175 amu) in between peaks is equal to the MW of the monomer unit indicating that the alkyne functionalization was successful. There are also minor peaks present in the MALDI mass spectrum. The minor peaks are dispersed at the same intervals at the major peaks indicating that they represent polymers in which the end group has been degraded. The ends of some polymers have been found to undergo fragmentation due to the process of ionization required for MALDI analysis.³² The mass values of the minor peaks of this spectrum correlate to fragments of the monomer unit for **22** (Fig. 1.21).

The 90-mer poly-alkyne would not successfully co-crystallize with super-DHB or any other MALDI matrix. Therefore, a *p*-methoxybenzylamine derivative **24** was synthesized from **20**.³⁰ This polymer was successfully co-crystallized with α -Cyano-4-hydroxycinnamic acid (CCA) and a MALDI spectrum was obtained (Fig 1.22). However, this spectrum does not have well defined peaks, and while the average molecular weight was calculated to be 24101 amu, it is not possible to calculate polydispersity manually.

The DP values of **22** $n \sim 30$ and **22** $n \sim 90$ that were calculated by GPC ($DP_w = 44$ and $DP_n = 39$, and $DP_w = 127$ and $DP_n = 106$, respectively) are significantly higher than the values obtained by MALDI

($DP_w = 30$ and $DP_n = 29$, and $DP_{avg} = 93$, respectively). The higher DP values associated with GPC in comparison to MALDI have been observed for other polymers with polynorbornene backbones.^{30,}

³³ The GPC molecular weights are calculated using a calibration curve constructed using polystyrene molecular weight standards. Therefore, it is possible that there is an inherent discrepancy between the rate at which polynorbornene and polystyrene polymers travel through the gel. In fact, it has recently been demonstrated using small angle x-ray scattering (SAXS) that polynorbornene polymers do not adopt the typical globule conformation that is typically adopted by polymers in solution. Instead, polynorbornene adopts a conformation defined as a flexible cylinder, which is rigid and less densely packed than the typical globular conformation.³⁴

Therefore, it is possible that this difference in conformation causes the polynorbornene to travel through the GPC column faster than a polystyrene polymer of identical molecular weight. This would result in an overestimation of molecular weight for the polymer.

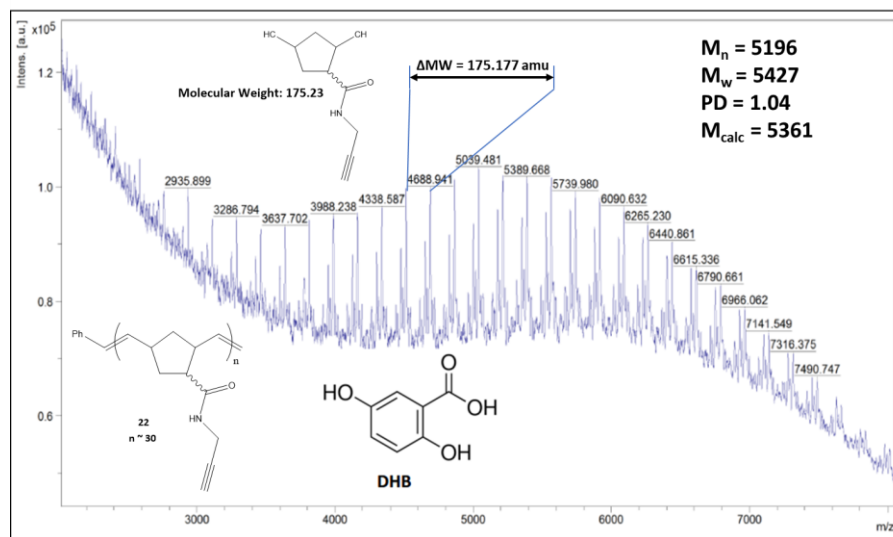


Figure 1.20: MALDI of poly-alkyne **22** ($n \sim 30$)

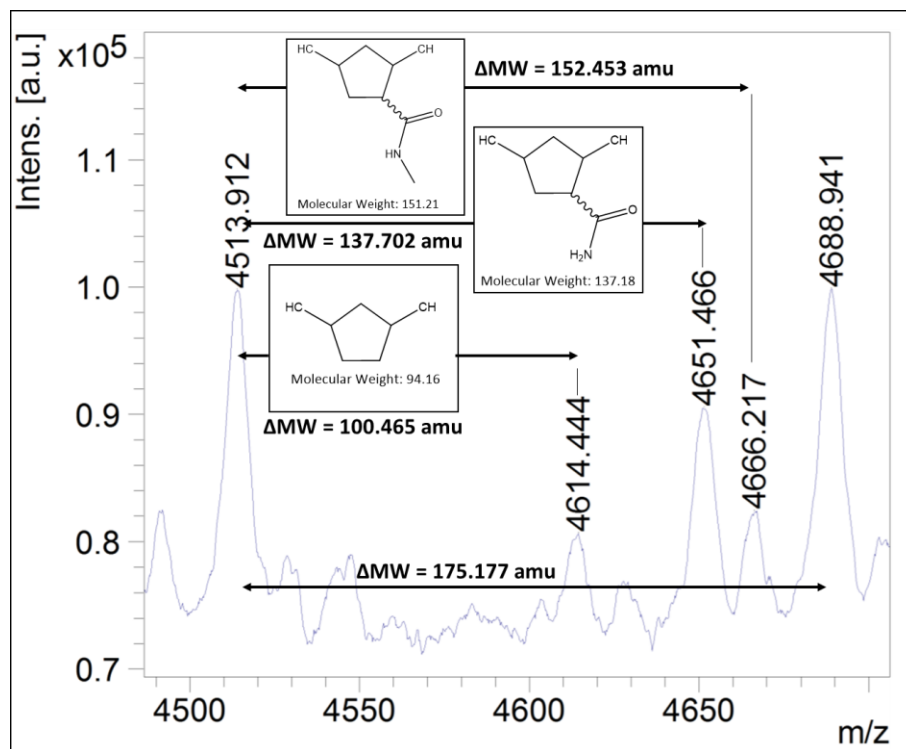


Figure 1.21: Enlarged section of MALDI of poly-alkyne **22** ($n \sim 30$)

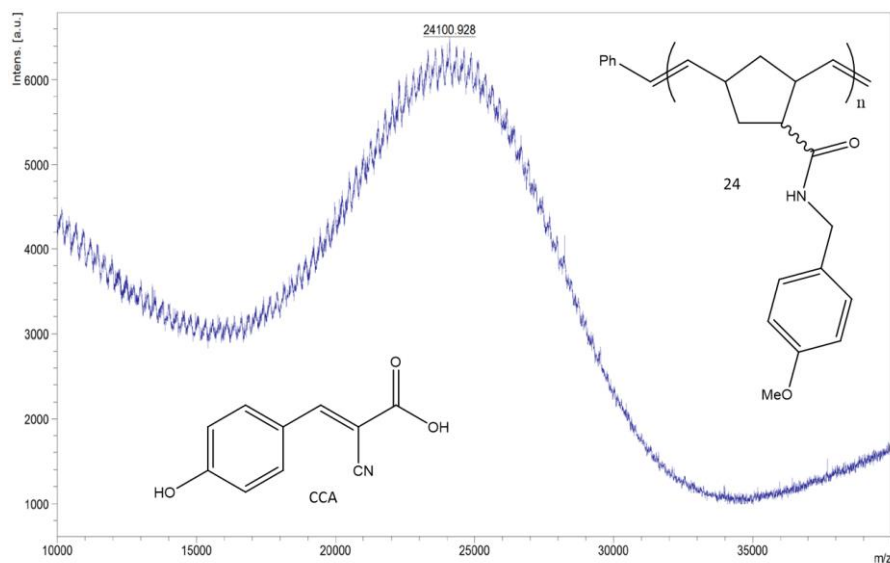


Figure 1.22: MALDI of poly-PMB polymer

1.5.3 Phase III: Fluorescein labeling of the polymer backbone

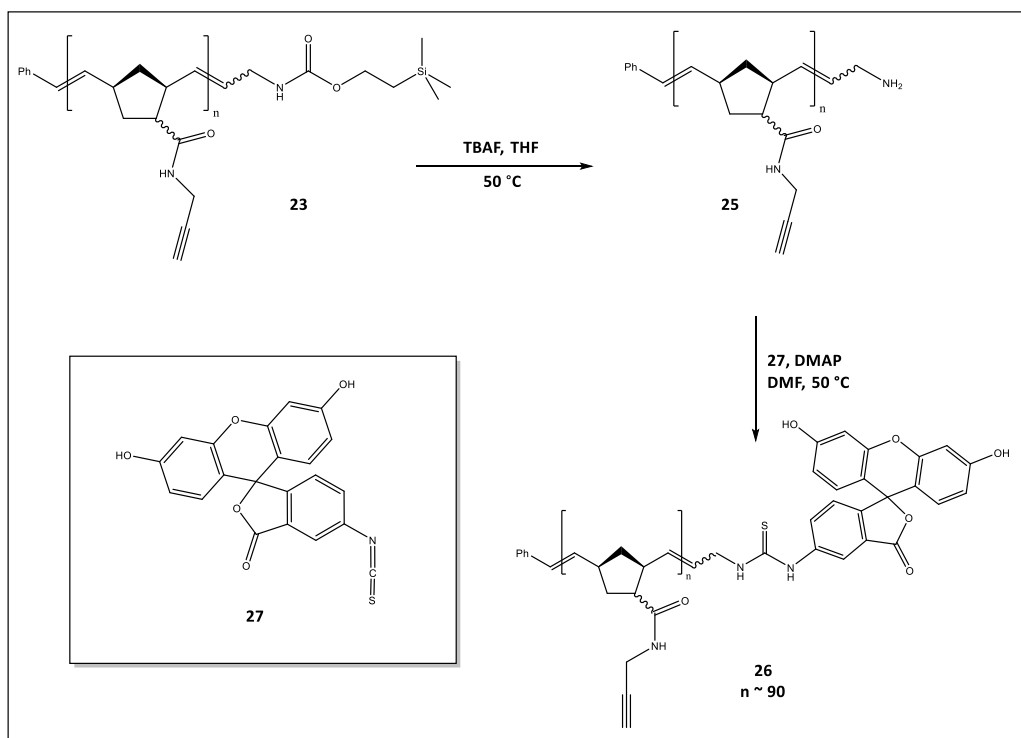


Figure 1.23: Synthesis of the fluorescein labeled poly-alkyne

The fluorescein end-group can be conjugated to the polymer either before or after the azido sugars have been added to the backbone. However, it was found that adding the fluorescein after the sugars had been attached resulted in polymers with vastly different % fluorescein labeling.³⁰ Therefore, when synthesizing the new generation of polymers the fluorescein was incorporated prior to the sugars (Fig 1.23). To accomplish this the Teoc protecting group was removed from the protected poly-alkyne by deprotection with tetra-*N*-butylammonium fluoride (TBAF). Complete deprotection was evaluated by observing the disappearance of the TMS peak in the ¹H NMR spectrum of the product (Fig 1.24). After the deprotection was complete the resulting poly-alkyne bears a primary amine end group functionality **25**. The primary amine end group reacted with fluorescein 5-isothiocyanate (FITC) **27** in the presence of 4-dimethylaminopyridine (DMAP) to yield the fluorescein labeled poly-alkyne backbone **26**.

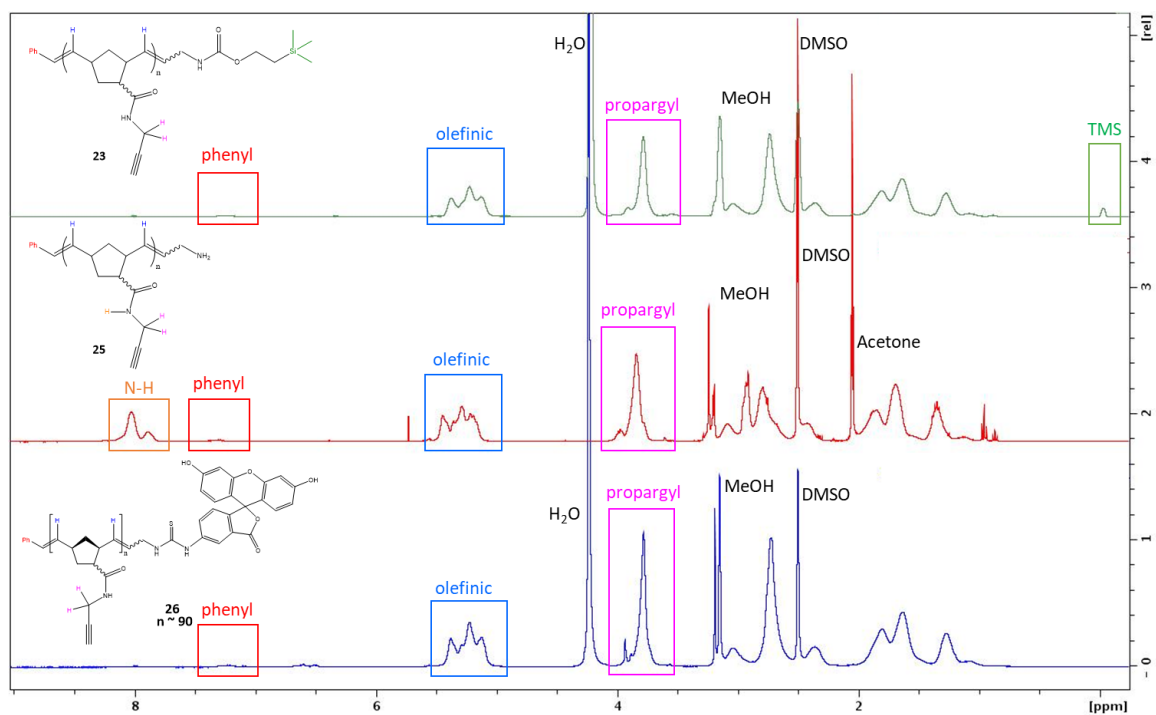


Figure 1.24: ^1H NMR spectra of 24, 25, and 26. The spectrum for 25 displays N-H peaks because it was acquired using aprotic NMR solvent (1:1 (v/v) *d*-acetone:*d*-DMSO). 24 and 26 were taken in 1:1 (v/v) d_6 -DMSO: CD_3OD .

1.5.4 Phase IV: Synthesis of azido sugars

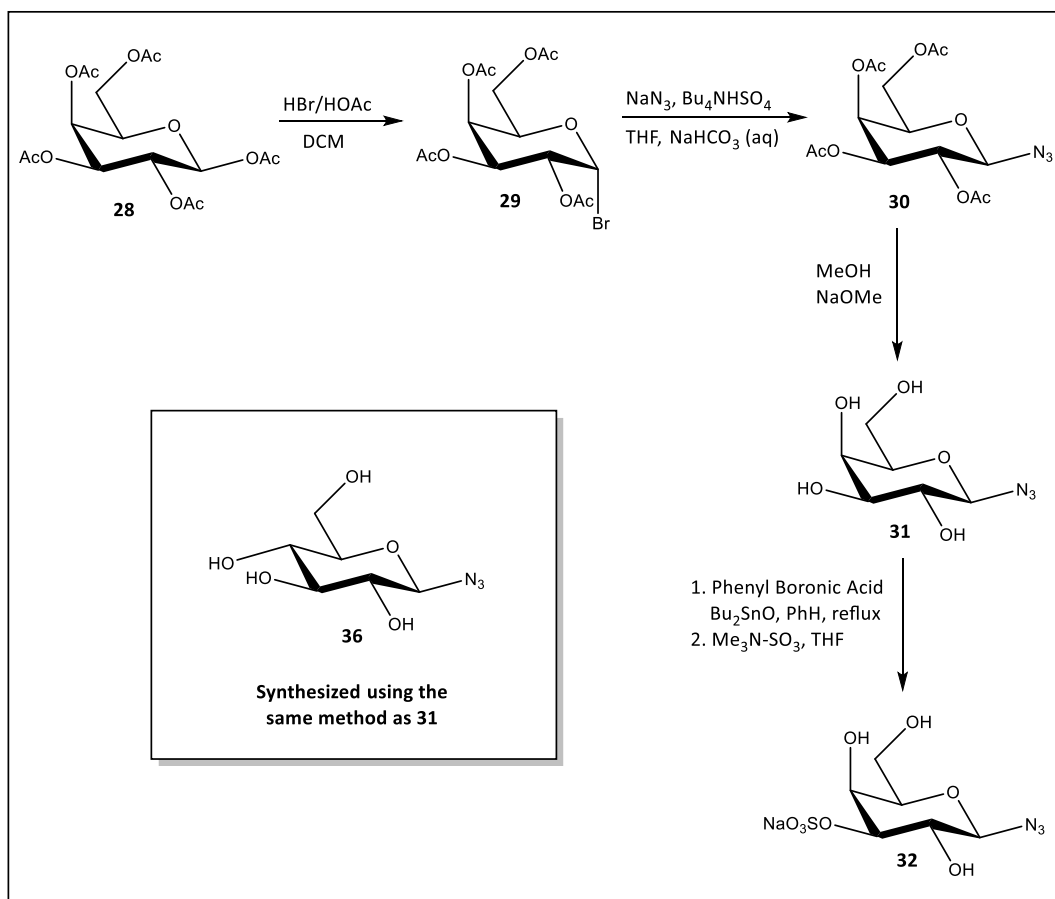


Figure 1.25: Synthesis of azido sugars

The synthesis of β -D-galactopyranosyl azide **31**, and β -D-glucopyranosyl azide **36** began using commercially available penta-O-acetyl- β -D-galactopyranose **28** and penta-O-acetyl- β -D-glucopyranose **33** respectively (Fig 1.25). The acetyl protected sugars were reacted with 33% HBr in acetic acid to yield 2,3,4,6-tetra-O-acetyl- α -D-galactopyranosyl bromide **29** and 2,3,4,6-tetra-O-acetyl- α -D-glucopyranosyl bromide **34**.³⁵ The α -anomeric bromides were then treated with sodium azide to initiate nucleophilic substitution by the azide resulting in the formation of the β -anomeric azides **30** and **35**.³⁶ Deprotection of the acetyl groups was achieved under Zémlen conditions in sodium methoxide in methanol to yield the desired azido sugar products **31** and **36**.³⁵ Pure products were obtained by liquid extraction and recrystallization.

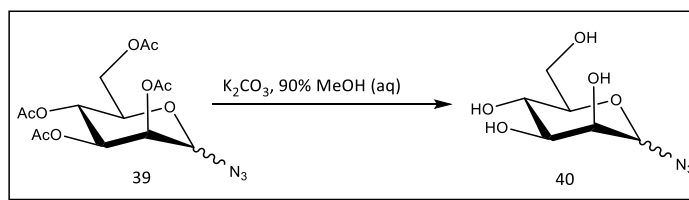


Figure 1.26: Deprotection of acetylated mannose

The synthesis of D-mannopyranosyl azide **40** (Fig 1.26) began by acetyl protection D-mannose hydroxyl groups by reacting the sugar with pyridine and acetic anhydride to yield penta-O-acetyl-D-mannopyranose (mixture of α/β anomers 33:67) **37**. Bromination and azide substitution were performed under similar conditions as those used for the other sugars to yield 2,3,4,6-tetra-O-acetyl- α -D-mannopyranosyl bromide **38** and tetraacetyl-D-mannopyranosyl azide (mixture of α/β anomers 1:10) **39** respectively. Anomeric composition was determined by comparing the ¹H NMR spectra of **39** to the literature ¹H NMR values for D-mannopyranosyl azide.³⁷ In our hands deprotection of the acetyl groups using sodium methoxide was unsuccessful. Although the product of this reaction was found to have a single spot observed by TLC ($R_f = 0.5$, 3:1 DCM:MeOH) and was recovered in quantitative yield, large contamination peaks were observed by ¹H NMR (Fig 1.27). The observation of this issue with sodium methoxide deprotection of mannose azides was previously reported in the literature.³⁸ Therefore, we decided to use milder deprotection conditions.³⁹ Deprotection was successfully achieved by combining the protected sugar with potassium carbonate in 90% methanol (v/v, aq) (Fig 1.27).

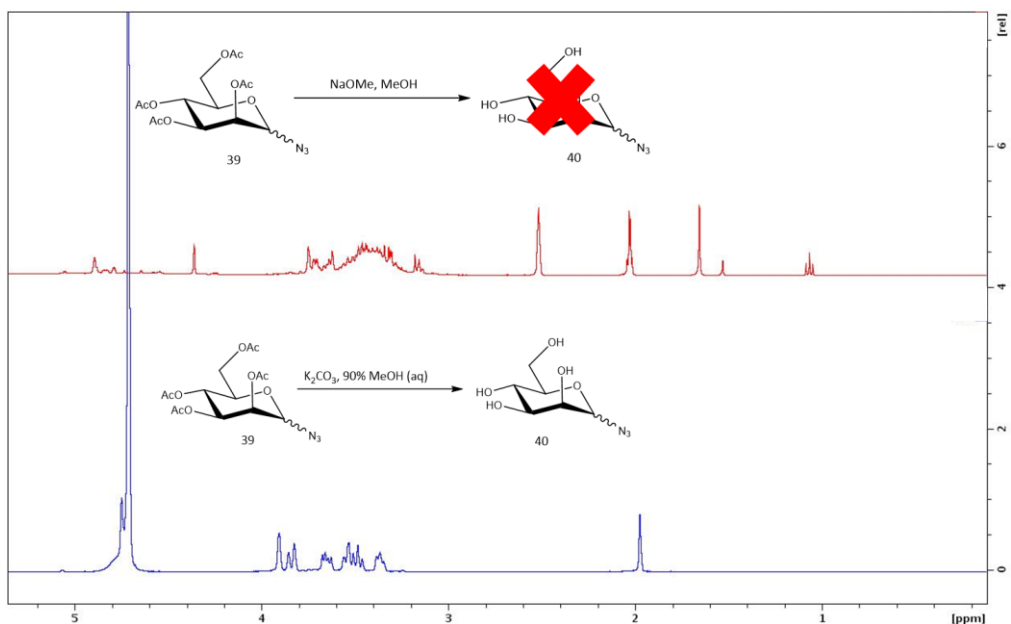


Figure 1.27: ¹H NMR comparing sodium methoxide and potassium carbonate deprotections taken in D₂O

The 3'-O-sulfo-β-D-galactopyranosyl azide **32** was prepared using the previously prepared β-D-galactopyranosyl azide **31** (Fig 1.28). The 4- and 6-hydroxyl groups were first protected as a cyclic phenyl boronate **41** using phenyl boronic acid (PBA), to ensure that the sulfation would occur only at the O3 position. Treatment of **41** with dibutyltin oxide results in the formation of an intermediate with a stannylene acetal between the O3 and O2 positions (**42**). Treatment of **42** with trimethylamine sulfur trioxide complex results in a regioselective sulfation at the O3 position. Upon quenching with methanol and Na⁺ ion exchange the desired 3'-O-sulfo-β-D-galactopyranosyl azide **32** is obtained.⁴⁰⁻⁴¹ The COSY spectrum (Fig 1.30) of this compound shows cross-peaks along the line of 3.7 ppm that intersect at 4.3 and 4.6 ppm. Since the anomeric peak shows up at 4.6 ppm this means that the cross peak at 4.3 ppm is from the H₃ proton. In the HSQC spectrum (Fig 1.30) of this compound a cross peak is observed at 4.3 ppm in the ¹H domain and 80 ppm in the ¹³C domain and is the most downfield of the non-anomeric carbon shifts. The strong downfield shift of the H₃ proton in the ¹H NMR spectrum (Fig 1.29) and the C₃ proton in the ¹³C NMR is indicative of sulfation at the O3 position.

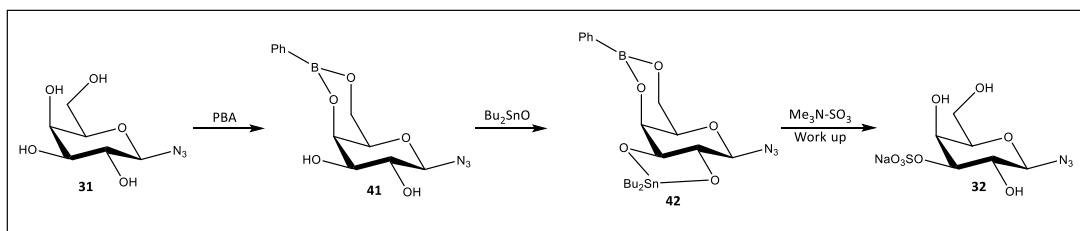


Figure 1.28: O3 regioselective sulfation of galactose azide

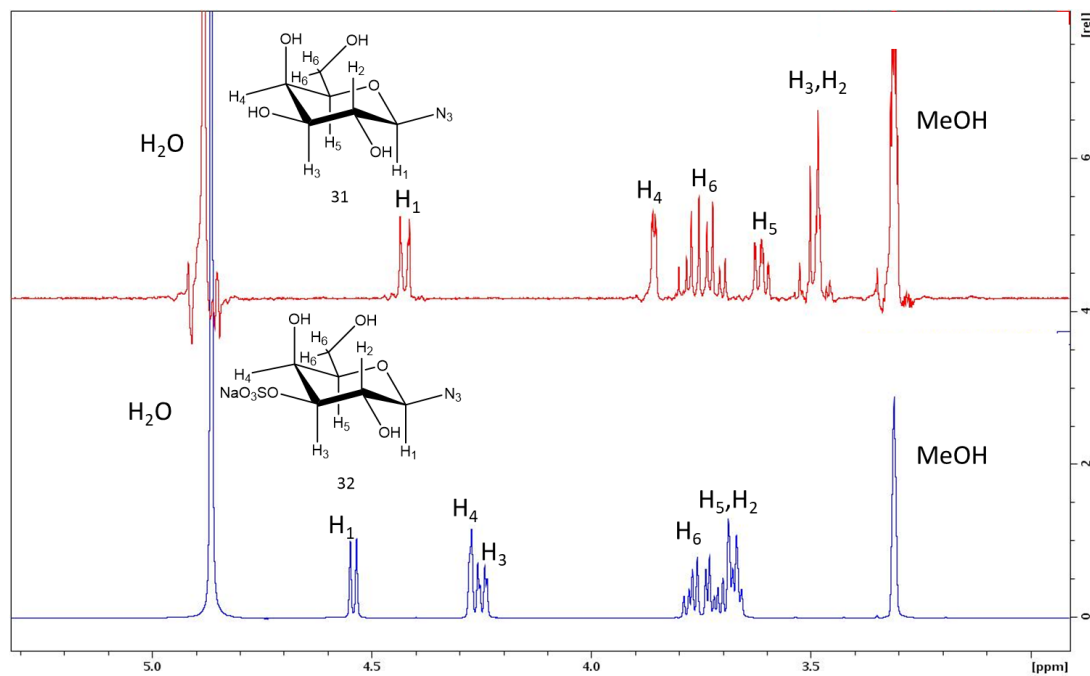


Figure 1.29: ^1H NMR showing the sulfation of galactose azide taken in CD_3OD

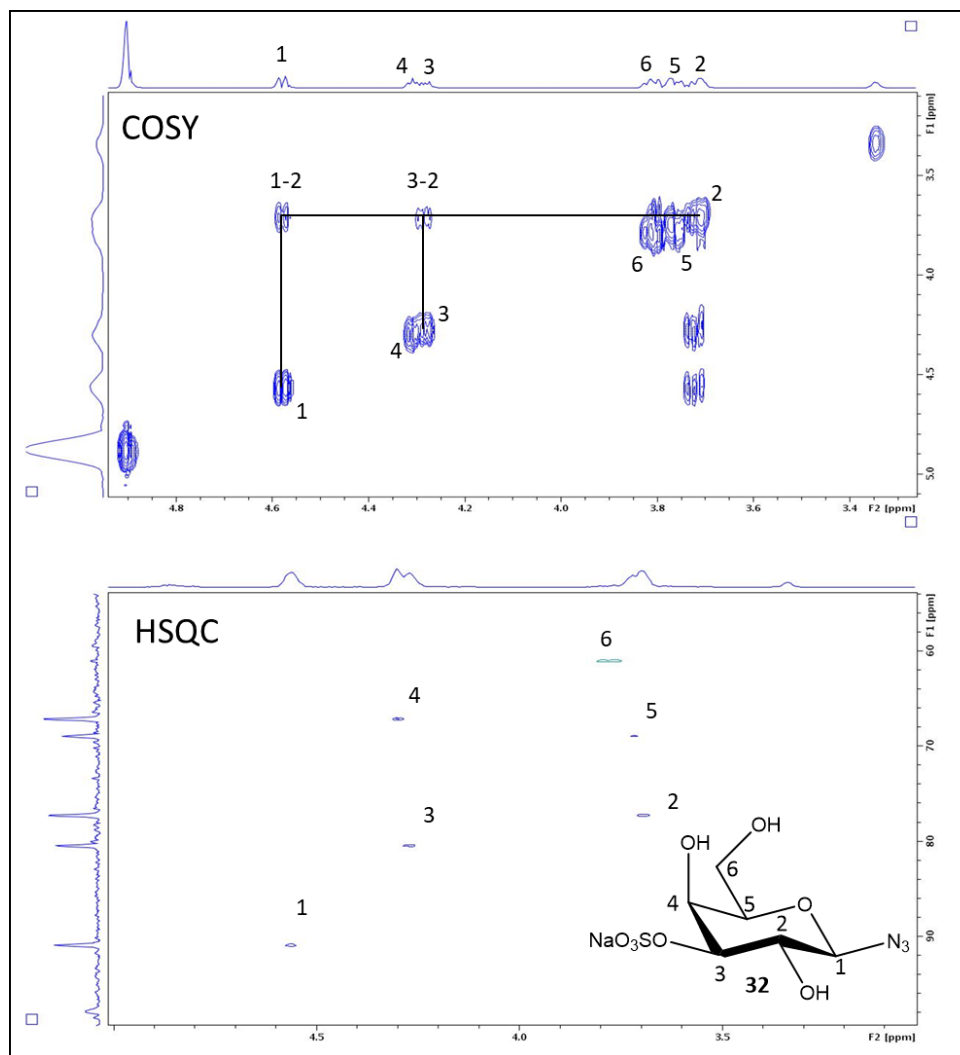


Figure 1.30: COSY and HSQC spectra of **32**

1.5.5 Phase V: Synthesis of glycopolymer via CuCAAC of poly-alkyne and azido sugars

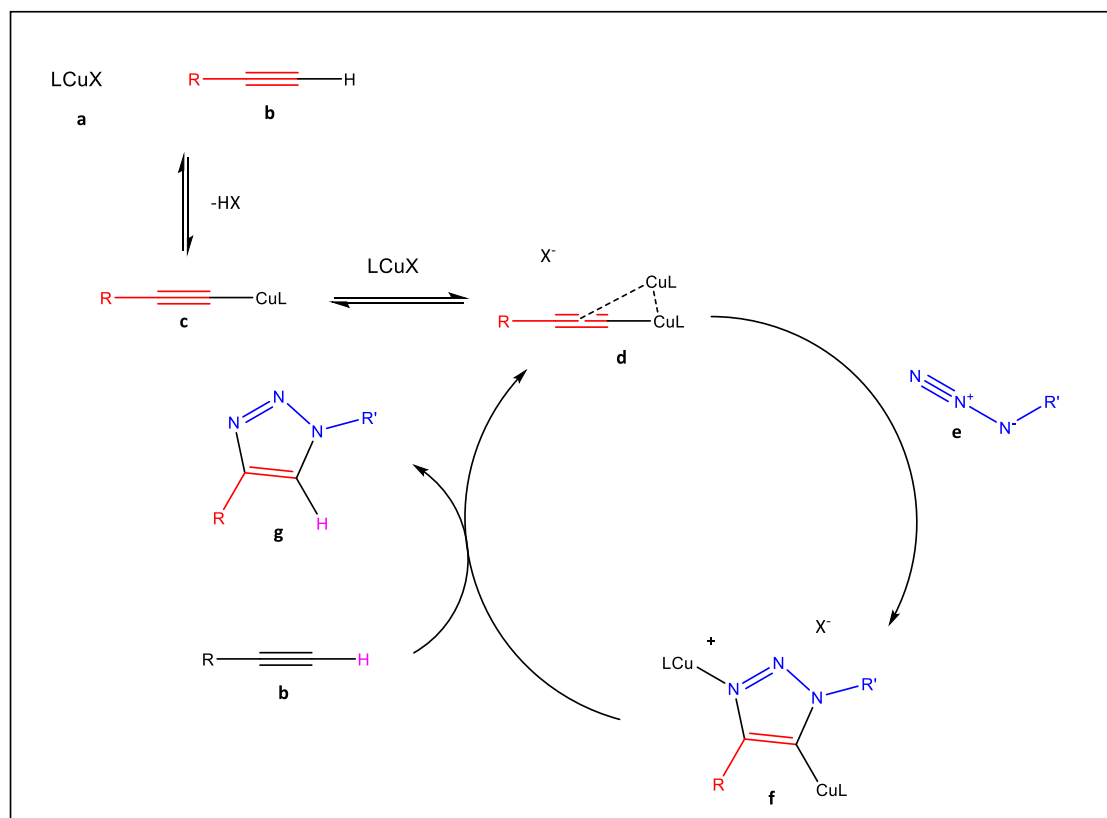


Figure 1.31: Proposed CuAAC mechanism

As previously discussed, the CuCAAC reaction is a useful technique for functionalizing a polymer backbone with pendant groups such as sugars. The widely accepted mechanism for CuAAC⁴² (Fig 1.31) is initiated by deprotonation of the acidic terminal alkyne proton (**b**) by the catalyst (**a**) resulting in the formation of a monomeric copper-acetylide complex (**c**). Next, an additional equivalent of the catalyst coordinates to the alkyne of **c** to yield a π,σ -bis(copper) acetylide complex (**d**). Next, **d** undergoes a cycloaddition with the azide (**e**) to give the 3,5-bis(copper) triazole (**f**). This species is still catalytically active, and will react with an equivalent of **b** to yield the 1,4 triazole product (**g**) and regenerating the π,σ -bis(copper) acetylide complex (**d**).

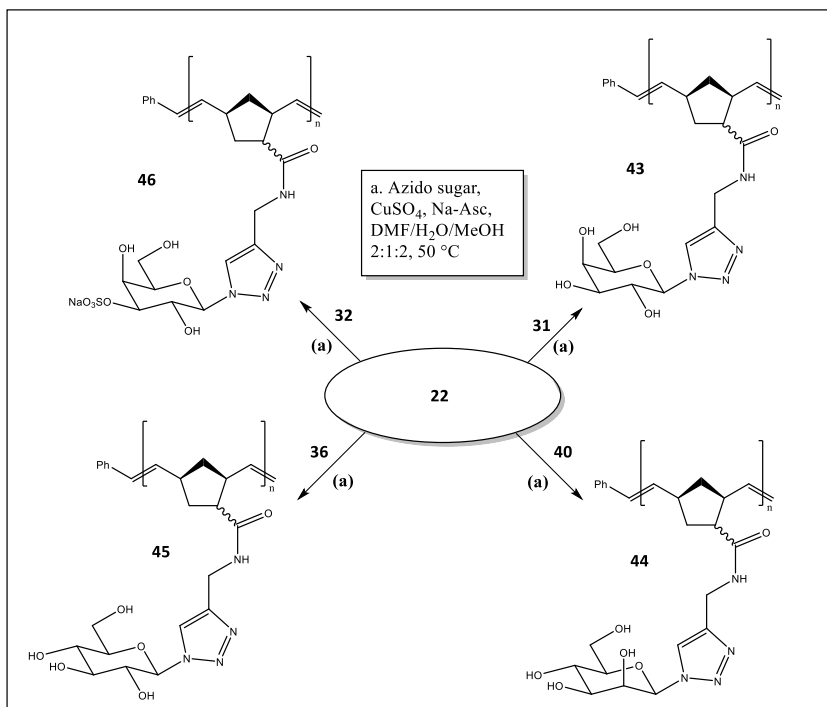


Figure 1.32: Synthesis of alkene terminated glycopolymers

To prepare the desired glycopolymers **43-50** (Figures 1.32 and 1.33) the necessary poly-alkyne (**22** or **23**) is dissolved in DMF and mixed with an excess of azido sugar (**31**, **32**, **36**, or **40**) dissolved in methanol. Next, an aqueous solution of copper (II) sulfate and sodium ascorbate is added to the reaction mixture and the mixture is heated to 50 °C. After completion of the reaction, as determined by click TLC stain, Cuprisorb™ is added to the reaction mixture and adsorbs the copper. After treatment with Cuprisorb™ the glycopolymers are purified by dialysis in water. Mannose functionalized alkene terminated polymers **44** with $n \sim 90$ were found to be insoluble in water and were not isolated. Mannose functionalized fluorescein labeled polymers **48** with $n \sim 90$ were found to be partially insoluble in water but were isolated and characterized.

After purification, ¹H NMR spectroscopy can be performed to confirm the completion of the reaction by monitoring the appearance of the triazole resonance (~8 ppm). However, dialysis requires several days to complete and if NMR shows that the conversion of alkyne to triazole is

incomplete then the reaction must be repeated. To ensure complete conversion of alkyne to triazole it is useful to have some way to monitor the progress of the CuAAC reaction prior to purification. With the previous generation of poly-azide polymer backbones the reaction progress could be monitored by observing the disappearance of the azide asymmetric stretch signal in the FTIR spectrum of the sample.³⁰ It is less trivial to monitor the disappearance of the alkyne FTIR signal, because the OH stretch signal obscures the *sp* C-H IR signal and the C≡C stretch IR signal is weaker than the azide signal making it difficult to observe. Therefore, an alternate method must be used.

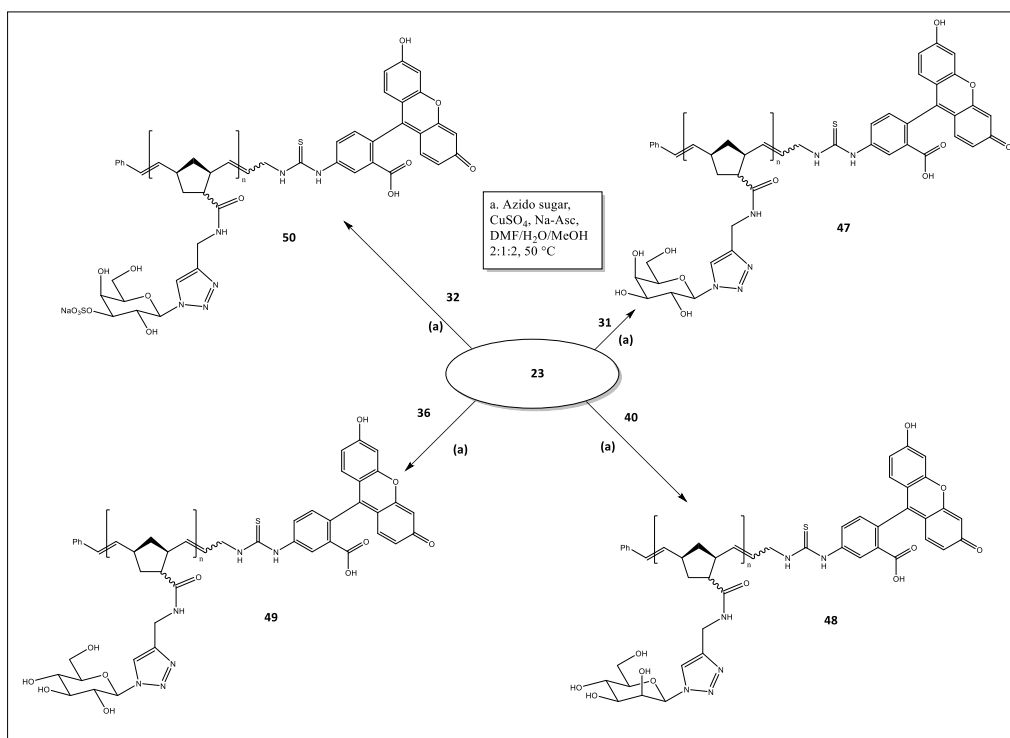


Figure 1.33: Synthesis of fluorescein labeled glycopolymers

A click responsive TLC stain is an attractive option for monitoring the progress of the CuAAC reaction. 3-azido-7-hydroxycoumarin is a dye molecule that bears an azide functional group. This

molecule is not fluorogenic, but once the azide functionality has been converted to a triazole by a click reaction with an alkyne the dye has been found to exhibit strong fluorescence emission when excited at 360 nm (Fig. 1.34).⁴³ This allows for the success of a click reaction to be evaluated using

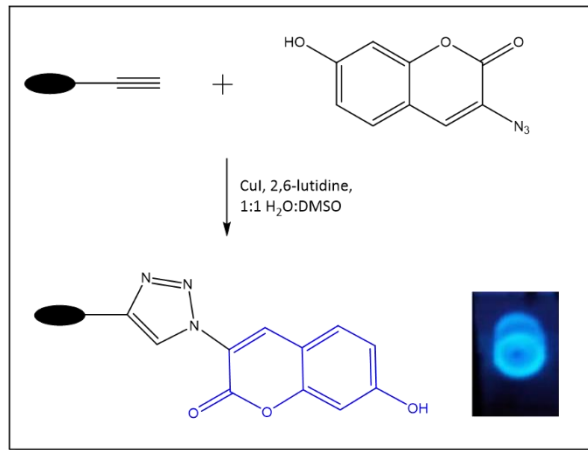


Figure 1.34: Fluorescent click responsive TLC stain

standard UV TLC detectors set to the long wavelength mode. Also, a brominated analog of the coumarin azide dye was recently used as a tag to enable detection of triazole products via fluorescence/ mass spectrometry.⁴⁴

With this utility in mind a click TLC stain was developed to allow for monitoring of click reactions by TLC.⁴⁵ The optimized stain contains the 3-azido-7-hydroxycoumarin dye, copper (I) iodide as a copper source and 2,6-lutidine as a stabilizing agent dissolved in a 1:1 (v/v) H₂O:DMSO solvent mixture. To use the stain, some of the reaction mixture is spotted onto a TLC plate, dried, and dipped into the click stain. The slide is then placed into an oven at 80 °C for 15 minutes. When the TLC plate is placed under a UV lamp, the presence of a bright blue fluorescent spot indicates that unreacted alkyne is still present in the sample (Fig 1.34). Therefore, the reaction is complete once fluorescence is no longer observed using the click stain. This technique was used to monitor the progress of the CuAAC reaction used to synthesize the non-fluorescent glycopolymers.

Typically, when preparing glycopolymers by adding azido sugars to an alkyne functionalized backbone the reaction is run for multiple days to ensure that it has gone to completion.⁴⁶ However, using the click stain to monitor these reactions has revealed that in some cases only 30 minutes are needed to consume the alkyne (Fig 1.35). Therefore, the click

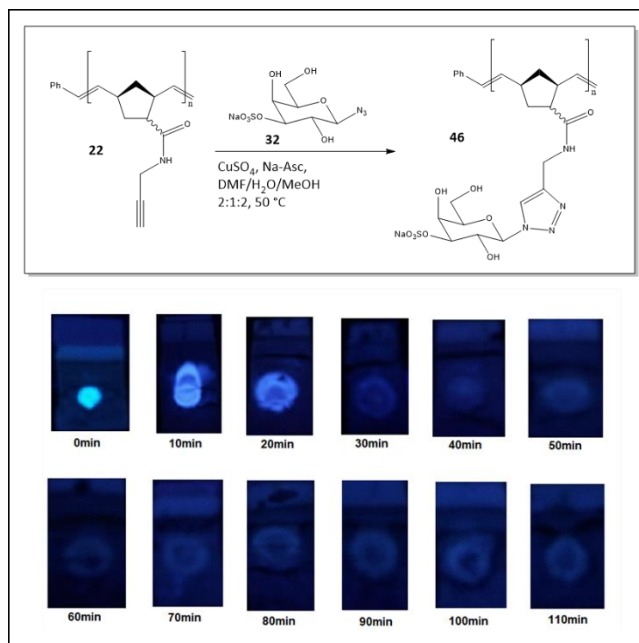


Figure 1.35: Monitoring the synthesis of poly-SGal using the click TLC stain

stain allows for a more time efficient synthesis of glycopolymers. Using the click stain to monitor the progress of the fluorescently labeled polymers is problematic since the fluorescence of the fluorescein interferes with that of the coumarin. However, since none of the other reactions required more than a few hours to go to completion, allowing the click reactions to run for 24 hours was deemed appropriate to ensure completion of the reaction.

As previously mentioned, success of the click reaction is also evaluated by observing the appearance of the triazole peak in the ¹H-NMR of the purified product (Fig 1.36). The integration of the triazole peak is compared to the integration of the peaks arising from alkene hydrogens and H₁ sugar hydrogens. The ratio of these integrals (triazole: alkene and H₁) should be roughly 1:3. Sometimes, we observe that the integration of the alkene and H₁ peaks is lower than expected, suggesting that there is more than one triazole H per alkene H, which is unlikely. This phenomenon is more likely a consequence of the proximity of the alkene peaks to the water peak which tend to overlap slightly and obscure the integral values. Furthermore, each glycopolymer displays a unique and characteristic pattern of peaks corresponding to the sugar hydrogens. This

pattern is the same regardless of the length or end group functionality of the polymer and can be used to confirm that the desired sugar functionalization has been achieved (Fig 1.37-40).

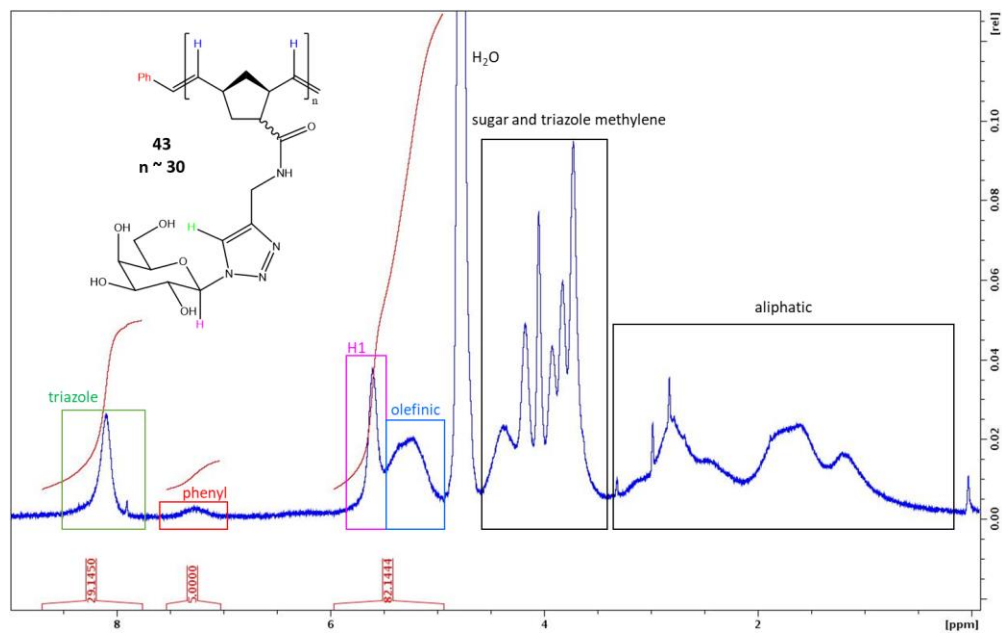


Figure 1.36: ¹H NMR of glycopolymer **43**, $n \sim 30$ in D₂O

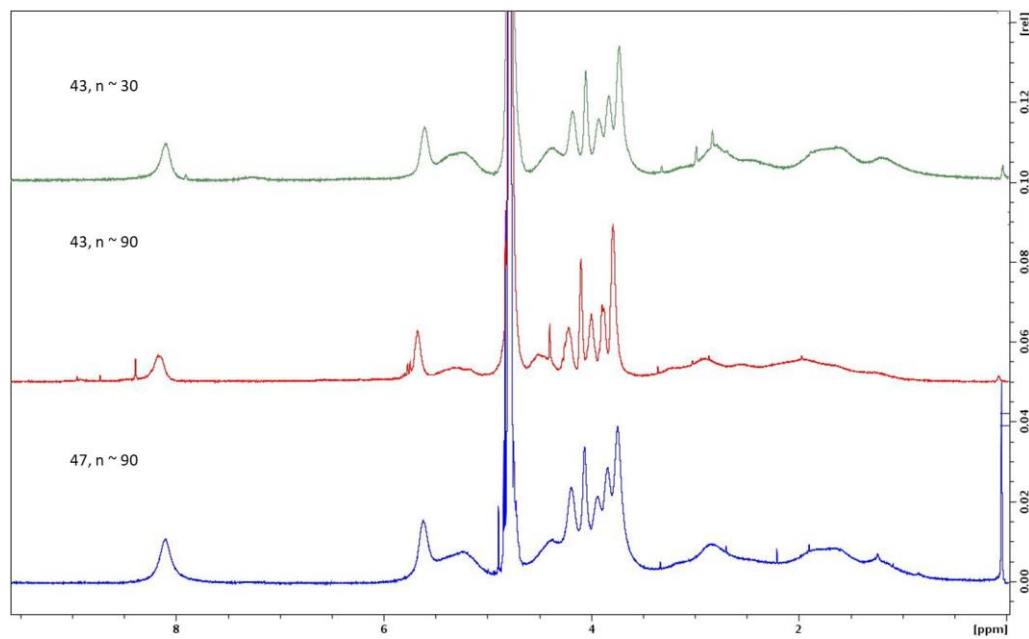


Figure 1.37: ¹H NMR comparison of the Gal glycopolymers (**43** and **47**)

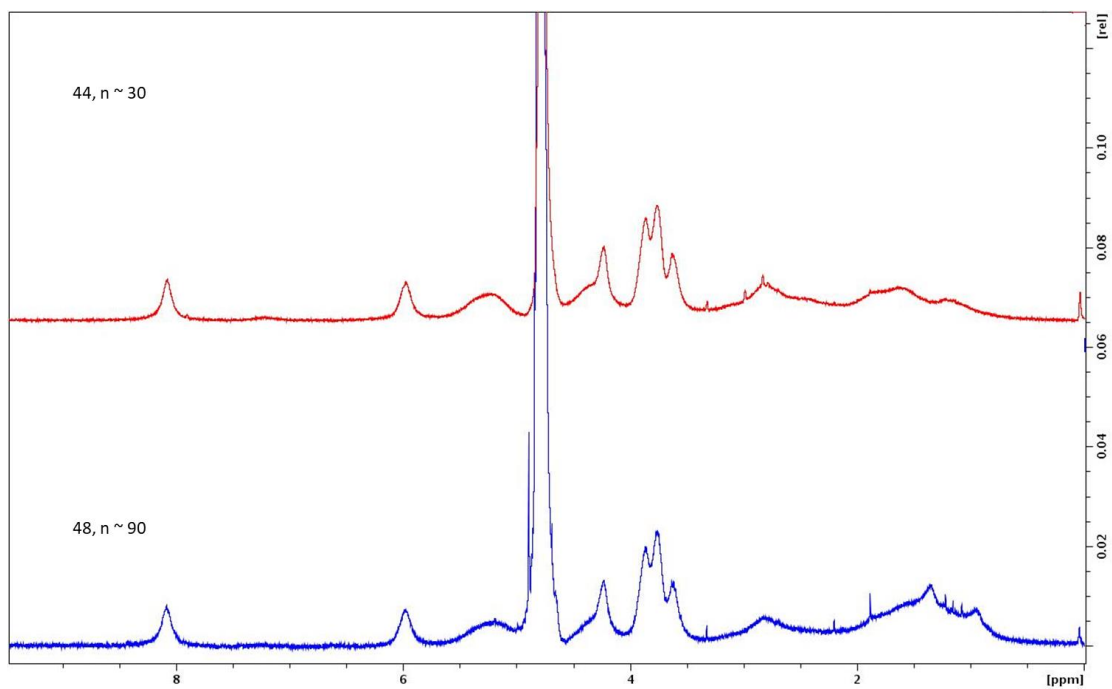


Figure 1.38: ^1H NMR comparison of the Man glycopolymers (**44** and **48**)

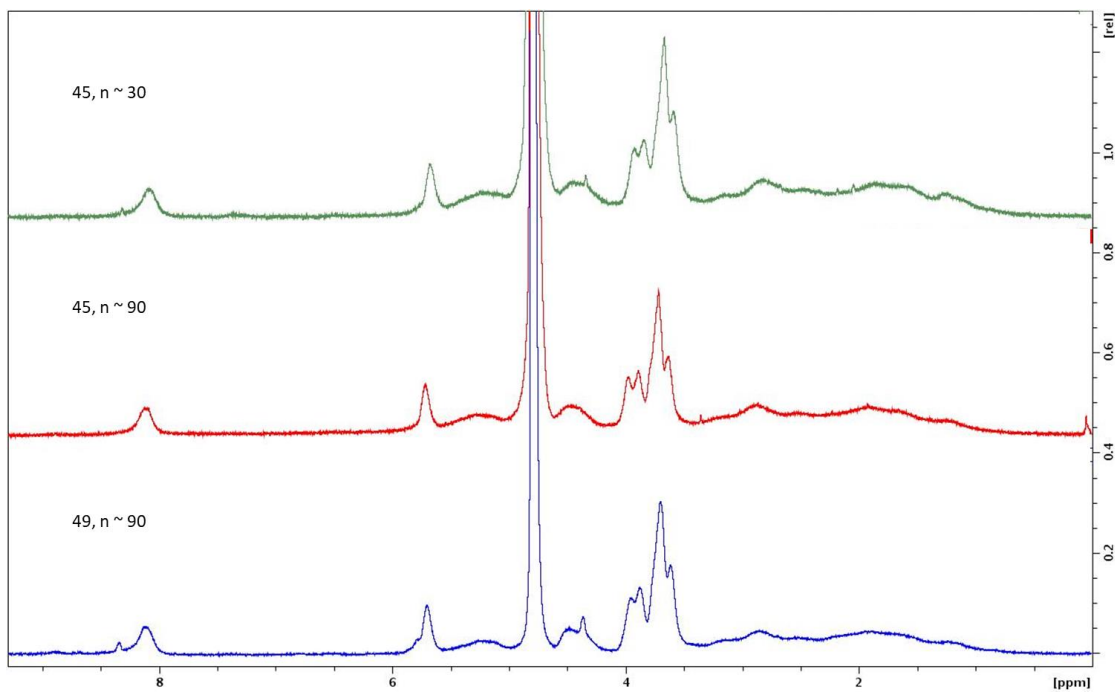


Figure 1.39: ^1H NMR comparison of the Glc glycopolymers (**45** and **49**)

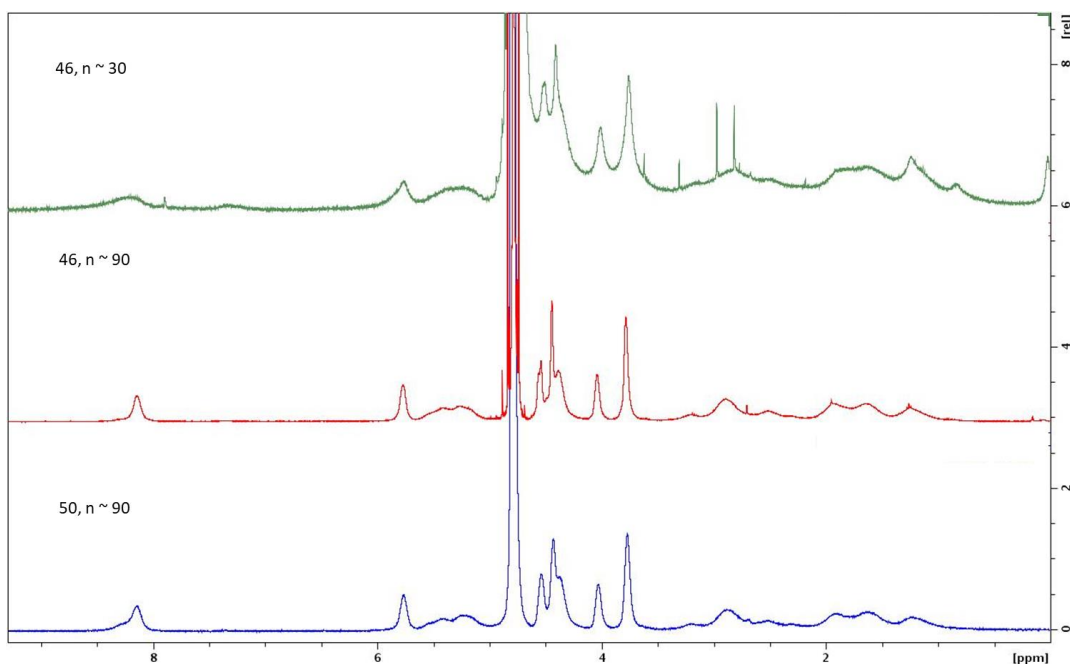


Figure 1.40: ^1H NMR comparison of the SGal glycopolymers (**46** and **50**)

For the fluorescently labeled glycopolymers percent (%) fluorescein labeling was determined using solutions of glycopolymers dissolved in phosphate buffered saline (PBS, pH 7.4). Values were obtained using Beer's law with the extinction coefficient of FITC **27**

Table 1.2: % Fluorescein labeling of glycopolymers

Product	% Labeling
47 (Gal)	88.7
48 (Man)	36.3
49 (Glc)	62.6
50 (SGal)	79.7

as a standard (Table 1.2). This work used the extinction coefficient reported by Okoth.³⁰ As previously reported³⁰ an accurate calculation of the % fluorescein labeling can be difficult to achieve since the fluorescence properties of the fluorescein end label, may be different than those of free fluorescein. Also, the uncertainty associated with the calculation of the theoretical molecular weight of the polymer, can contribute to inaccurate values. Furthermore, the presence of any water in the sample will lead to inaccurate mass calculations, and thus incorrect % labeling values. Although the % labeling determined here may be somewhat inaccurate, these values do allow for comparison of the intensity of fluorescence observed among the glycopolymers, which can be potentially important when interpreting the results of fluorescence assays.

1.6 Conclusion

In this work, we have reported the synthesis and characterization of glycopolymers synthesized via ring-opening metathesis polymerization (ROMP) of a norbornene NHS-ester monomer, followed by alkyne functionalization of the polymer and finally addition of azido sugars via a click reaction. The poly-alkyne does not require a custom synthesized linker and the neutral azido sugars can be prepared and purified without the use of column chromatography, allowing for a more facile route to glycopolymers than the previously described method. The click reaction was monitored by a fluorogenic TLC stain, to ensure complete functionalization of the alkyne moieties and allow for more efficient reaction times. The route to glycopolymers described in this research allows for the rapid synthesis of polymers that can be functionalized with any azido sugar, or other biologically relevant small molecule with an azide functionality. This set of glycopolymers can potentially be used as multivalent model systems to investigate CCIs, such as the SGal-Gal CCI that mediates myelin compaction, PCIs, or other biologically relevant interactions.

1.7 Supporting Information

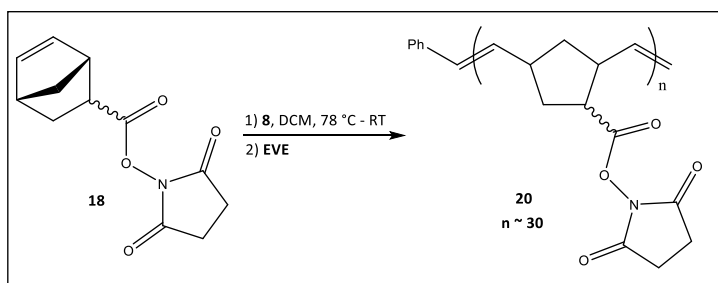
Experimental Procedures

General procedures and materials. Dry solvents were obtained from a commercially available solvent purification system based on protocols reported by Grubbs.⁴⁷ All reactions were carried out under nitrogen atmosphere unless otherwise stated. Automated flash chromatography was performed using Teledyne ISCO COMBI Flash Rf instrument using Redi Sep Rf silica columns (24 g and 40 g) and self-packed silica cartridges. Dialysis was performed using 6 Spectra/Por regenerated cellulose dialysis membrane 1000 MWCO from Spectrum. Centrifugation of the precipitated polymers **20** and **21** was done using an Adams physician's compact centrifuge. NMR spectra were recorded on BRUKER 600 MHz or 400 MHz instruments for ¹H NMR, 151 MHz, 100

MHz or 75 MHz for ^{13}C NMR and referenced at 2.05 ppm for d_6 -acetone, 4.79 ppm for D_2O , 7.26 ppm for CDCl_3 , 2.50 ppm for d_6 -DMSO and 3.31 ppm for CD_3OD in ^1H NMR and 41.0 ppm for CD_3OD in ^{13}C NMR.⁴⁸ ^1H NMR for all polymer products were obtained with delay time (D[1]) of 5 seconds. MALDI-ToF spectra were obtained using a Bruker MALDI-ToF mass spectrometer, and super DHB matrix (2,5-dihydroxybenzoic acid doped with 2-hydroxy-5-methoxybenzoic acid) or α -cyano-4-hydroxycinnamic acid (CCA) matrix. MALDI - ToF samples were prepared as follows; Polymers (ca. 6 mg of **20**, $n \sim 30$ or 3 mg of **24**, $n \sim 90$) were dissolved in 80 μL of THF. 70 μL water containing 0.1% (v/v) TFA, and 30 μL acetonitrile were added to about 6 mg of matrix and the mixture was vortexed to a clear solution. 10 μL of the polymer solution and 10 μL of the matrix solution were mixed. 1 μL of the matrix/polymer mixture applied directly to the MALDI target plate and allowed to dry completely before acquisition. Gel Permeation Chromatography (GPC) was performed at 40 $^\circ\text{C}$ using HPLC grade dichloromethane eluent on an Agilent Infinity GPC system equipped with three Agilent PLGel columns 7.5 mm \times 300 mm (5 μm , pore sizes: 10^3 , 10^4 , 50 \AA). M_n and M_w/M_n were determined versus polystyrene standards (500 g/mol-3150 kg/mol, Polymer Laboratories). 10 μL of polymer solution (2 mg in 1 mL DCM, DCM was filtered through a 20 μm PTFE syringe filter) was injected and eluted using HPLC grade DCM flowing at 1 mL/min at room temperature. Presence of polymers was detected using a refractive index (RI) detector. Agilent 8453 UV-visible spectrometer was used to obtain UV-VIS spectra of end labeled glycopolymers solutions in a 1 cm quartz cell. TLC stains were prepared as follows; KMnO_4 (3g KMnO_4 , 20g K_2CO_3 , 5 mL of 5% NaOH , 300 mL H_2O); Anisaldehyde (9.2 mL anisaldehyde, 3.75 mL AcOH , 338 mL 95% EtOH , 12.5 mL conc. H_2SO_4); click stain (5 mg azido-coumarin, 4 μL 2,6-lutidine, 9 mL DMSO , 40 mg copper (I) iodide, 9 mL H_2O) TLC Silica Gel 60 F254 plates from EMD Chemicals were used. The ROMP terminating agent **15** and the bicyclo-[2.2.1]-hept-5-ene-2-carboxylic acid *N*-hydroxysuccinimide ester **18** were prepared as reported by Okoth.²¹ Catalyst **8** was prepared as reported by Grubbs.⁴⁹ Bromides

(**29**, **34**, **38**) and azides (**30**, **31**, **35**, **36**, **39**, and **40**) were prepared by procedures adapted from Kuhn.⁵⁰ **SPECIAL CAUTION** was taken when performing reactions with **sodium azide** due to potential for explosion.⁵¹ Only plastic spatulas were used to weigh **NaN₃**, and no chlorinated solvent were present in the starting material (confirmed by ¹H-NMR) or the reaction mixture. Also, waste was disposed of in a designated azide waste container. All azide reactions were set up behind a plexiglass blast shield.

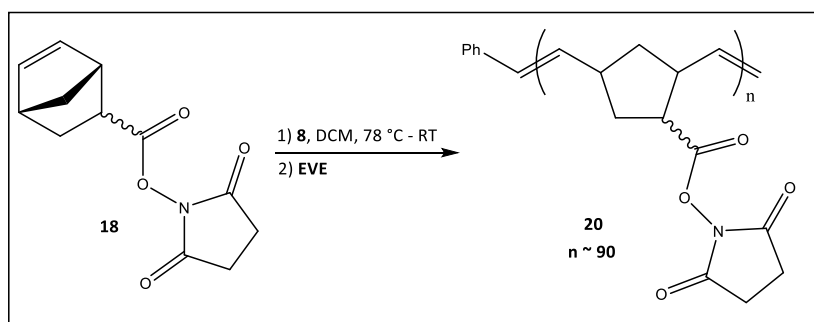
Polymerization to give **20**, **n=30** (¹H-NMR u/artemis/bl/2-32)



To a septum capped vial was added bicyclo[2.2.1]hept-5-ene-2-carboxylic acid N-succinimide ester **18** (0.48 g, 2.05 mmol, 1 equiv) and anhydrous DCM (10 mL). The solution was placed in a dry ice-acetone bath and cooled to -78 °C. To the cooled solution was added a solution of Grubbs' 3rd generation catalyst **8** (0.06 g, 0.07 mmol, 30 equiv) in anhydrous DCM (2.5 mL) quickly via a syringe. Anhydrous DCM (2.5 mL) was added to the flask that had originally contained **8** and then transferred to the reaction mixture to ensure that all catalyst was transferred to the reaction flask. The reaction mixture was removed from the cooling bath and was allowed to warm to room temperature upon which the solution turned from bright green to brown after about 2 minutes. After 40 minutes ethyl vinyl ether (5.2 mmol, 0.5 ml) was added via a syringe. After 20 minutes, the reaction solution was transferred using a Pasteur pipette to 4 different test tubes each containing about 10 mL of ether, forming a light brown precipitate. The test tubes were centrifuged and the ether decanted, and the precipitate was washed by adding 10 mL of ether

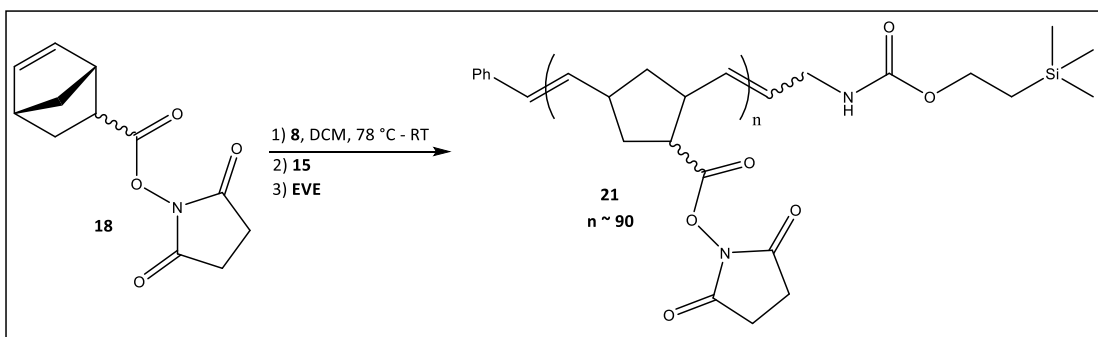
into the test tubes and agitating the mixture with a Pasteur pipette then centrifuging and decanting the ether. Washing was repeated until the ether was clear. The grey precipitate was collected and dried under vacuum to give **20**, $n \sim 30$ (0.45 g, 0.063 mmol, 92% yield) as a grey solid. Partial ^1H NMR (400 MHz, d_6 -acetone) δ 7.5–7.0 (m, 5 H, H-Ph) 5.8–5.2 (m, 64 H, H-olefinic) 3.6–1.2 (m, 344 H, H-aliphatic) DP = 32. M_w 10350, M_n 9323, PDI 1.11 (GPC).

Polymerization to give **20**, $n \sim 90$ (^1H -NMR u/artemis/bl/2-27)



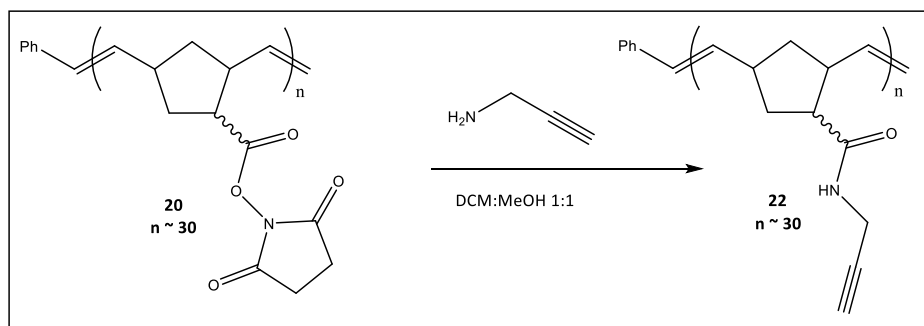
Polymer **20**, $n \sim 90$ was prepared using the same procedure reported for polymer **28**, $n \sim 30$ with the appropriate molar ratio of **8:18** i.e. (1:90). 0.92 g of polymer was recovered after using 0.96 g of monomer corresponding to 96 % yield. Partial ^1H NMR (400 MHz, d_6 -acetone) δ 7.6–7.05 (m, 5 H, H-Ph) 5.9–5.0 (m, 210 H, H-olefinic) 3.6–1.2 (m, 1535 H, H-aliphatic) DP = 105. M_w 29913, M_n 24988, PDI 1.197 (GPC).

Polymerization to give **21**, $n=90$ (^1H -NMR u/artemis/bl/3-7)



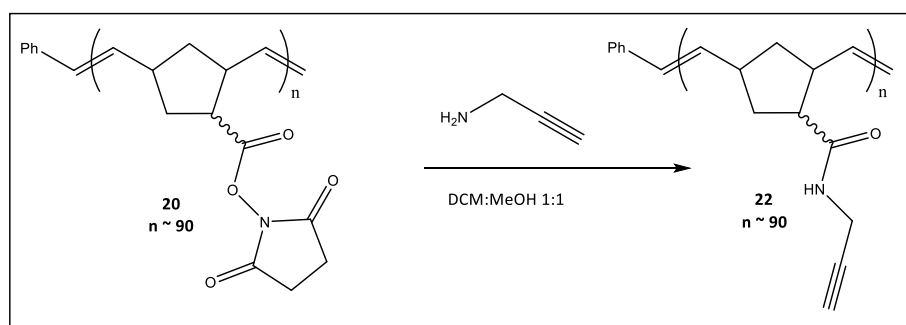
To a two-necked round bottom flask was added bicyclo-[2.2.1]-hept-5-ene-2-carboxylic acid N-succinimide ester **18** (3 g, 12.75 mmol). The flask was sealed with a septum and placed in a dry ice-acetone bath and cooled to $-78\text{ }^{\circ}\text{C}$. Anhydrous DCM (60 mL) was added to the flask. To a round bottom flask was added Grubbs' 3rd generation catalyst **8** (0.126 g, 0.142 mmol) and anhydrous DCM (20 mL). The flask was sealed with a septum and placed in a dry ice-acetone bath and cooled to $-78\text{ }^{\circ}\text{C}$ under nitrogen. The catalyst solution was transferred to flask of monomer solution via cannula transfer. The catalyst flask was washed with anhydrous DCM (5 mL x2) and after allowing ~ 5 minutes for cooling, the wash was transferred to the reaction mixture. The reaction was allowed to warm to room temperature upon which the solution turned from bright green to brown after about 2 minutes. After 1 hour a solution of **15** (0.3 g, 0.712 mmol) in 5 mL dry DCM was added to the reaction via a syringe. After 20 minutes ethyl vinyl ether (31.2 mmol, 3 ml) was added via a syringe. After 20 minutes the reaction solution was transferred using a Pasteur pipette into test tubes each containing about 10 mL of ether, forming a light brown precipitate. The test tubes were centrifuged and the ether decanted, and the precipitate was washed by adding 10 mL of ether into the test tubes and agitating the mixture with a Pasture pipette then centrifuging and decanting the ether. Washing was repeated until the ether was clear. The grey precipitate was collected and dried under vacuum to give **21**, $n \sim 90$ (2.68 g, 0.125 mmol, 89% yield) as a grey solid. Partial ^1H NMR (400 MHz, d_6 -acetone) δ 7.6–7.1 (m, 5H, H-Ph) 5.8–5.2 (m, 150H, H-olefinic) 3.6–1.2 (m, 860 H, H-aliphatic) 0.04 (s, 9H, H-TMS) DP = 75. M_w 26508, M_n 24478, PDI 1.083 (GPC).

Alkene terminated poly-alkyne **22**, $n \sim 30$ (^1H -NMR u/artemis/bl/2-33)



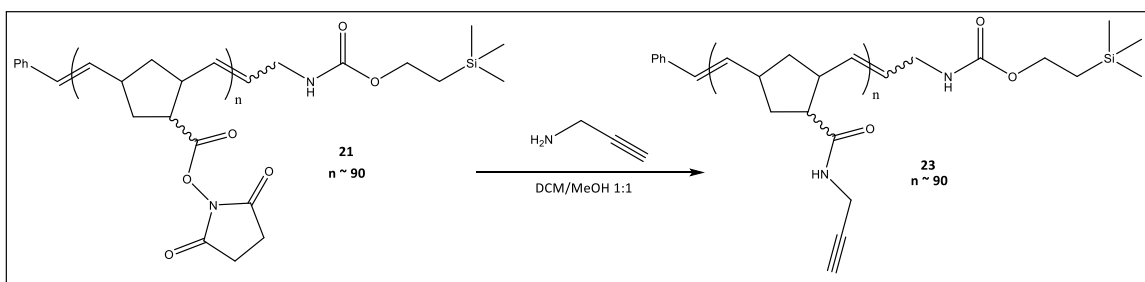
To a solution of **20**, $n \sim 30$ (260 mg, 0.036 mmol, 1 equiv) in 40 mL dry DCM:MeOH (1:1) in a vial was added propargyl amine (142 μ L, 120 mg, 2.16 mmol, 60 equiv) and the mixture stirred at room temperature. After 24 h more propargyl amine (142 μ L, 120 mg, 2.18 mmol, 60 equiv) was added and the mixture stirred at room temperature for another 24 h. The contents in the vial were transferred to a dialysis tube (Spectra/Por[®] Dialysis Membrane MWCO: 1000) and dialyzed against DCM: MeOH (1: 1) (400 mL) for 2 days with the solvent reservoir changed every 12 h. After dialysis, solvent was removed under reduced pressure and the residue dried under high-vac overnight to give the poly-alkyne ester **22**, $n \sim 30$ (121 mg, 23 μ mol, 63% yield) as a brown film. Partial ¹H NMR (400 MHz, 1:1 CD₃OD: *d*₆-DMSO) δ 7.3-7.1 (m, 5 H, H-Ph) 5.4–5.1 (m, 45 H, H-olefinic) 4.0-3.7 (m, 43 H, H-propargyl) 3.1-1.9 (m, 200 H, H-aliphatic). M_w 5427, M_n 5196, PDI 1.04 (MALDI-ToF using Super-DHB matrix).

Alkene terminated poly-alkyne **22**, $n \sim 90$ (¹H-NMR u/artemis/bl/2-28)



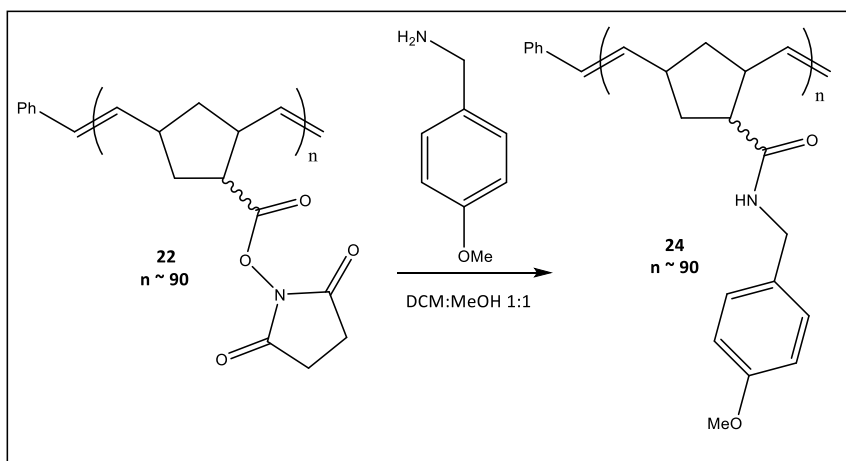
Poly-alkyne **22**, $n \sim 90$ was obtained using the same procedure reported for preparation of Poly-alkyne **22**, $n \sim 30$ using the polymer **20**, $n \sim 90$. 0.26 g of product was isolated after using 0.52 g of polymer **22**, $n \sim 90$ and 568 μL (360 equiv) of propargyl amine corresponding to 68 % yield. Partial ^1H NMR (400 MHz, 1:1 CD_3OD : d_6 -DMSO) δ 7.4-7.1 (m, 5H, H-Ph) 5.5–4.9 (m, 143 H, H-olefinic) 4.0-3.6 (m, 130 H, H-propargyl) 3.1-1.9 (m, 582 H, H-aliphatic).

Teoc terminated poly-alkyne **23**, $n \sim 90$ (^1H -NMR u/artemis/bl/BL-3-8))



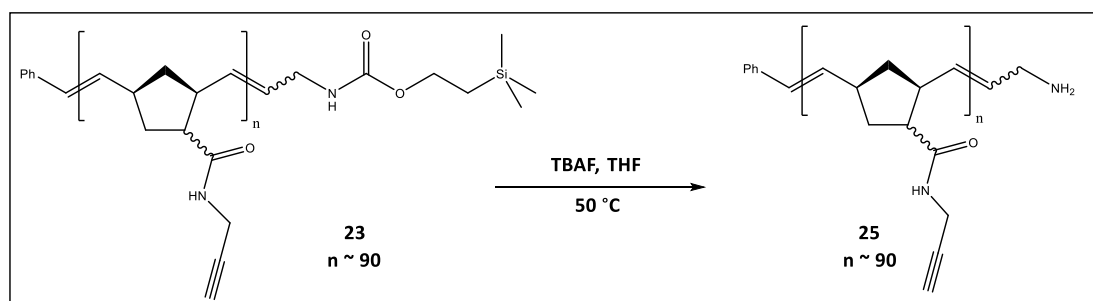
Poly-alkyne **23**, $n \sim 90$ was obtained using the same procedure reported for preparation of Poly-alkyne **22**, $n \sim 30$ using the polymer **21**, $n \sim 90$. 1.73 g of product was isolated after using 2.5 g of polymer **22**, $n \sim 90$ and 2.74 mL (366 equiv) corresponding to 91 % yield. Partial ^1H NMR (400 MHz, 1:1 CD_3OD : d_6 -DMSO) δ 7.3-7.1 (m, 5 H, H-Ph) 5.4–4.9 (m, 161 H, H-olefinic) 4.0-3.7 (m, 165 H, H-propargyl) 3.1-1.9 (m, 752 H, H-aliphatic) 0.03 (s, 10 H, H-TMS).

Preparation of poly-PMB **24**, $n \sim 90$ (^1H -NMR u/artemis/bl/2-03)



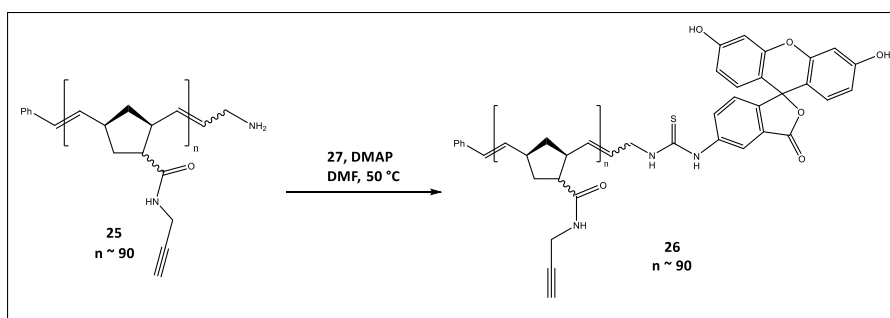
To a solution of **24**, $n \sim 90$ (0.045 g, 0.002 mmol, 1 equiv) in 5 mL dry DCM was added 4-methoxybenzyl amine (0.13 g, 0.47 mmol, 235 equiv), and the mixture was stirred for 24 h. The solvent was evaporated, the residue was dissolved in 20 mL THF and filtered through a plug of cotton, and then the cotton was washed with 10 mL THF. The filtrate was then transferred to a dialysis tube (Spectra/Por® Dialysis Membrane MWCO: 1000) and dialyzed in a 400 mL THF reservoir (12 h \times 3). The solution in the tube was collected, and the solvent was evaporated and dried to give **24**, $n \sim 90$ (0.06 g, 0.012 mmol, 56% yield) as a white film partial ^1H NMR (400 MHz, CDCl_3) δ 7.15 (bs, 2 H, H-aromatic) 6.79 (bs, 2 H, H-aromatic) 5.5–5.0 (m, 2 H, H-olefinic) 2.27 (s, 3 H, H-OMe). M_{obs} : 24101 (MALDI-ToF using CCA matrix).

Amino terminated poly-alkyne **25**, $n \sim 90$ (^1H -NMR u/artemis/bl/BL-3-10)



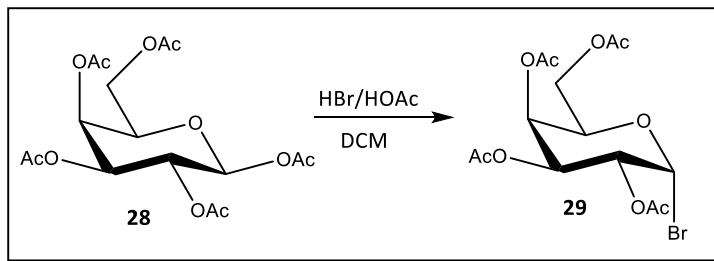
To a solution of **23**, $n=90$ (1.73 g, 0.107 mmol) in 30 mL dry THF was added 6 mL of TBAF (ca. 1 mol/L in THF) and the mixture heated to 50 °C. To aid dissolution 25 mL of dry DMF was added and the mixture was left at 50 °C overnight. The filtrate was then transferred to a dialysis tube (Spectra/Por® Dialysis Membrane MWCO: 1000) and dialyzed in a 500 mL 1:1 DCM:MeOH reservoir (12 h \times 3). The solution in the dialysis tube was collected, evaporated and dried under vacuum to give **25**, $n=90$ (1.39 g, 0.087 mmol, 82% yield) as a light brown film. Partial ^1H NMR (400 MHz, 1:1 d_6 -acetone: d_6 -DMSO) δ 8.3-7.7 (m, 106 H, H-N) 6.5-6.3 (m, 5 H, H-Ph) 5.6–4.9 (m, 221 H, H-olefinic) 4.1-3.7 (m, 218 H, H-propargyl).

Preparation of fluorescein labeled poly-alkyne **26** (^1H -NMR u/artemis/bl/BL-3-11)



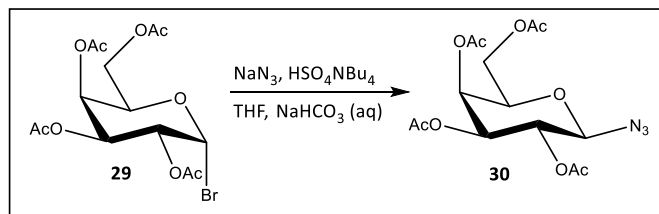
To a solution of **25**, $n \sim 90$ (1.31 g, 0.082 mmol) in 60 mL DMF in a round bottom flask was added a solution of **27** (0.236 g, 0.606 mmol) in 10 mL DMF and the flask containing **27** washed with an additional 5 mL DMF. DMAP (0.012 g, 0.098 mmol) was added to the reaction mixture. The flask and apparatus was covered with foil and the reaction stirred at 50 °C for 48 h under nitrogen. The solution was transferred into a dialysis tube (MWCO 1000) and dialyzed against 500 mL 1:1 DCM:MeOH until the reservoir was clear (5 days with reservoir exchanged every 12 h). The dialysis apparatus was wrapped in foil throughout the entire process to keep out light. The solution in the tube was collected and the solvent evaporated to give **26**, $n \sim 90$ as a yellow film (1.15 g, 0.071 mmol, 83% yield).

Synthesis α -bromo-galactosylpyranoside tetraacetate **29** (¹H-NMR u/artemis/bl/1-41dry)



Galactose pentaacetate (7.69 mmol, 3 g) **28** was dissolved in DCM (15 mL). A 33% (w/v) solution of HBr/HOAc (8 mL) was then added at 0 °C via syringe. The reaction was monitored by TLC (1:1; toluene: ethyl acetate) until complete. The solution was then diluted with DCM (30 mL) and washed with water (3x), saturated sodium bicarbonate (2x), and brine. The organic layer was dried with sodium sulfate and concentrated in vacuo. The residue was dissolved in toluene. The toluene was removed under reduced pressure and the sample was placed under high vacuum overnight to give **29** (7.3 mmol, 3 g, 95% yield) as a white solid. Spectral properties matched those found in the literature (NMR in CDCl₃).⁵⁰ **CAUTION:** It was confirmed via ¹H-NMR that all DCM was removed from **29** before using **29** to prepare **30**. Chlorinated solvents have been found to violently react with sodium azide.⁵¹

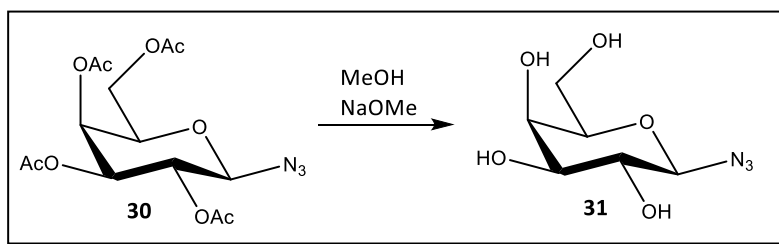
Synthesis of Azido- β -D-galactopyranoside tetraacetate **30** (¹H-NMR u/artemis/bl/1-42)



The tetraacetyl galactosyl bromide **29** (7.3 mmol, 3 g) was dissolved in THF (14 mL). Tetrabutyl ammonium hydrogen sulfate (6.99 mmol, 2.37 g) and sodium azide (34.95 mmol, 2.27 g) was added. Saturated aqueous sodium bicarbonate (7 mL) was added and the solution was vigorously

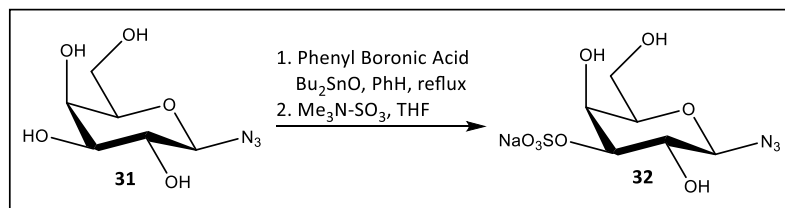
stirred at room temperature. Upon completion as shown by TLC, the mixture was diluted with ethyl acetate (28 mL). The organic layer was separated and washed with saturated sodium bicarbonate (2x), water (2x), and brine. The organic layer was then dried with sodium sulfate, filtered, and concentrated. The crude product was recrystallized in ethanol to yield **30** (5.80 mmol, 2.17 g, 80% yield) as fine white needle-like crystals. Spectral properties matched those found in the literature (NMR in CDCl₃).⁵⁰

Synthesis of Azido-β-D-galactopyranoside **31** (¹H-NMR u/artemis/bl/1-47cosy-1)



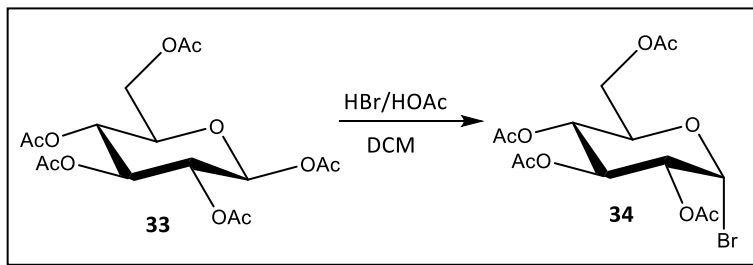
Azido-β-D-galactopyranoside tetraacetate **30** (1.5 g, 4 mmol) was dissolved in 15 mL of methanol in a clean dry round bottom flask. Sodium methoxide (0.3 mL, 0.3 M) solution was added until the solution was basic as judged by pH paper. The reaction was stirred at room temperature until the reaction was complete as shown by TLC (10:1 DCM/MeOH). The reaction was quenched by neutralization with Amberlite IR-120 resin (H⁺ form, prewashed with methanol), followed by filtration and evaporation of the solvent under reduced pressure to provide **31** (0.9 g, 4 mmol, quantitative yield) as a white solid. Spectral properties matched those found in the literature (NMR in CD₃OD).⁵²

Synthesis of Sodium 1-azido-3-sulfonato-β-D-galactopyranoside **32** (¹H-NMR u/cronus/bl/1-48-3, ¹³H-NMR u/cronus/bl/1-48-1, COSY u/cronus/bl/1-48-7, HSQC u/cronus/bl/1-48-6)



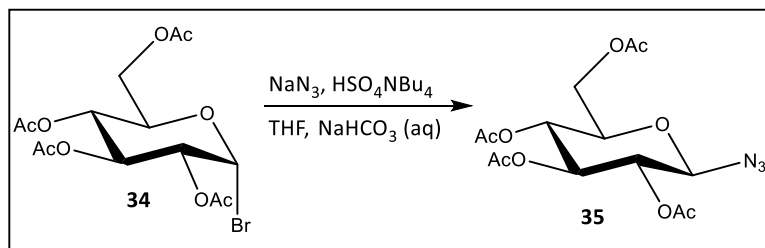
To a solution of phenyl boronic acid (0.53 g, 4.36 mmol) and galactose azide **31** (0.9 g, 4 mmol) in dry MeOH (2 mL) was added benzene (50 mL) and the reaction vessel fitted with a Dean-Stark apparatus. The solvent was evaporated to about 2 mL. More benzene (50 mL) was added to the reaction and the solvent evaporated to about 2 mL. Dibutyltin oxide (1.09 g, 4.36 mmol) and benzene (100 mL) were added and the Dean-Stark apparatus reattached. The reaction was heated at reflux for 2 h then concentrated to about 2 mL. Solvent was removed under reduced pressure and residue was dried under vacuum for 1 h to provide the tin acetal derivative. To a solution of the tin acetal in anhydrous THF (60 mL) was added trimethylamine sulfur trioxide (0.7 g, 5.03 mmol) and the solution stirred overnight. The reaction was quenched with methanol (5 mL) and concentrated under vacuum. A slurry of silica in methanol was added to the vessel and swirled to dissolve the concentrated residue. The solvent was evaporated under reduced pressure and the residue added to the top of a silica gel column. The residue was then purified by column chromatography (DCM/ MeOH, 1:0 to 3:1. R_f 0.2 – anisaldehyde stain 3:1 DCM: MeOH). The solvent was evaporated on a rotary evaporator and the product dried under vacuum. The clear oil was dissolved in water (2 mL) and passed through a cation exchange resin (Amberlite IR-120H, Na⁺ form, washed with MeOH) and the water removed under reduced pressure to give **32** (1.02 g, 3.31 mmol, 82 % yield) as a white solid. ¹H NMR (600 MHz; CD₃OD): δ 4.54 (1H, d, *J*=8.6 Hz, H-1), 4.27 (1H, m, H-4), 4.25 (1H, m, H-3), 3.75 (2H, m, H-6), 3.67 (2H, m, H-5, H-2). ¹³C NMR (600 MHz; CD₃OD): δ 92.3 (C-1), 81.8 (C-3), 78.6 (C-2), 70.2 (C-5), 68.4 (C-4), 62.3 (C-6). HRMS (FAB) calculated for C₆H₁₀N₃NaO₈S [M+Na]⁺ 329.9986 found 329.9980.

Synthesis α -Bromo-glucosylpyranoside tetraacetate **34** ($^1\text{H-NMR}$ u/artemis/bl/1-43)



Glucose pentaacetate (7.69 mmol, 3 g) **33** was dissolved in DCM (15 mL). A solution of 33% (w/v) HBr/HOAc (8 mL) was then added via syringe at 0 °C. The reaction was monitored by TLC (1:1; toluene: ethyl acetate) until complete. The solution was then diluted with DCM (30 mL) and washed with water (3x), saturated sodium bicarbonate (2x), and brine. The organic layer was dried with sodium sulfate and concentrated in vacuo. The residue was dissolved in toluene. The toluene was removed under reduced pressure and the sample was placed under high vacuum overnight to give **34** (7.3 mmol, 3 g, 95% yield) as a white solid. Spectral properties matched those found in the literature (NMR in CDCl_3).⁵³ **CAUTION:** It was confirmed via $^1\text{H-NMR}$ that all DCM was removed from **33** before using **33** to prepare **34**. Chlorinated solvents have been found to violently react with sodium azide.⁵¹

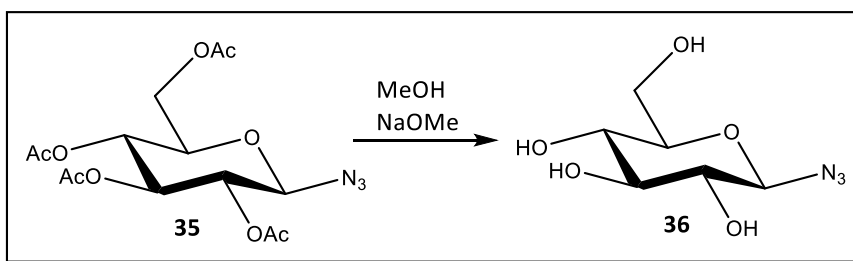
Synthesis of Azido- β -D-glucosylpyranoside tetraacetate **35** ($^1\text{H-NMR}$ u/artemis/bl/1-54)



The tetraacetyl glucosyl bromide **34** (7.3 mmol, 3 g) was dissolved in THF (14 mL). Tetrabutyl ammonium hydrogen sulfate (6.99 mmol, 2.37 g) and sodium azide (34.95 mmol, 2.27 g) was

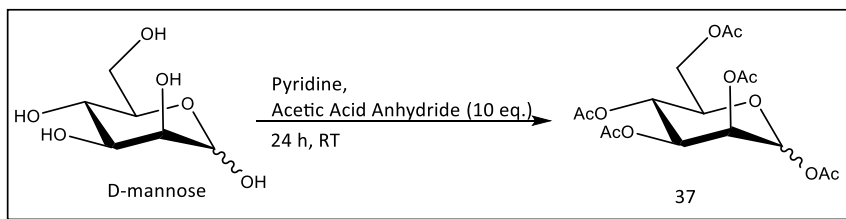
added. Saturated aqueous sodium bicarbonate (7 mL) was added and the solution was vigorously stirred at room temperature. Upon completion as shown by TLC, the mixture was diluted with ethyl acetate (28 mL). The organic layer was separated and washed with saturated sodium bicarbonate (2x), water (2x), and brine. The organic layer was then dried with sodium sulfate, filtered, and concentrated. The crude product was recrystallized in ethanol to yield **35** (6.46 mmol, 2.41 g, 88% yield) as fine white needle-like crystals. Spectral properties matched those found in the literature (NMR in CDCl₃).⁵⁴

Synthesis of Azido-β-D-glucosylpyranoside **36** (¹H-NMR. CD₃OD: u/artemis/bl/1-55, D₂O: u/cronus/bl/1-55-d2o)



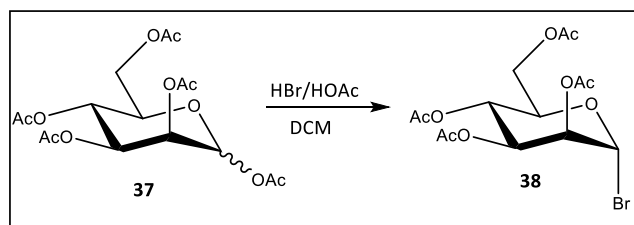
Azido-β-D-glucosylpyranoside tetraacetate **35** (1.5 g, 4 mmol) was dissolved in 15 mL of methanol in a clean dry round bottom flask. Sodium methoxide (.300 mL 0.3 M) solution was added until the solution was basic as judged by pH paper. The reaction was stirred at room temperature until the reaction was complete as shown by TLC (10:1 DCM/MeOH). The reaction was quenched by neutralization with Amberlite IR-120 resin (H⁺ form, prewashed with methanol), followed by filtration and evaporation of the solvent under reduced pressure to provide **36** (0.8 g, 4 mmol, quantitative yield) as a white solid. ¹H NMR⁵⁵ (400 MHz; CD₃OD): δ 4.47 (1H, d, *J*=8.6 Hz, H-1), 3.86 (1H, dd, *J*=12.0, 2.0 Hz, H-6), 3.66 (1H, dd, *J*=12.1, 5.5 Hz, H-6), 3.40-3.25 (3H, m, H-3, H-5, H-4), 3.12 (1H, t, *J*=8.8 Hz, H-2).

Synthesis of Mannose Pentaacetate **37** (¹H-NMR u/artemis/bl/1-57)



To a round-bottom flask was added D-mannose (5 g, 0.03 mol), anhydrous pyridine (50 ml), and acetic anhydride (26 mL, 0.277mol). The mixture was left to stir at room temperature overnight. After TLC confirmed complete transformation of starting materials DCM (50 ml) was added to the reaction vessel. The organic phase was washed with 1M HCl (x8), water (x1) and brine (x3). The organic phase was dried over sodium sulfate and solvent was removed via reduced pressure. Sample was placed under high vac overnight to give **37** (11.4 g, 0.03 mol, mixture of both anomers α/β 33:67, quantitative yield) as a clear syrup. Spectral properties matched those found in the literature (NMR in CDCl_3).⁵⁶

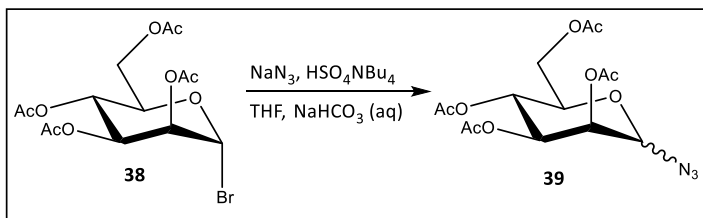
Synthesis of α -Bromo-mannosylpyranoside tetraacetate **38** (¹H-NMR u/artemis/bl/1-58)



Mannose pentaacetate (0.03 mmol, 11.4 g) **37** was dissolved in DCM (30 mL). A 33% HBr/HOAc (16.2 mL) was then added via syringe at 0 °C. The reaction was monitored by TLC (1:1; toluene: ethyl acetate) until complete. The solution was then diluted with DCM (30 mL) and washed with water (3x), saturated sodium bicarbonate (2x), and brine. The organic layer was dried with sodium sulfate and concentrated in vacuo then dissolved in toluene. The toluene was removed under reduced pressure and the sample was placed under high vac overnight to give **38** (25 mmol, 10.3

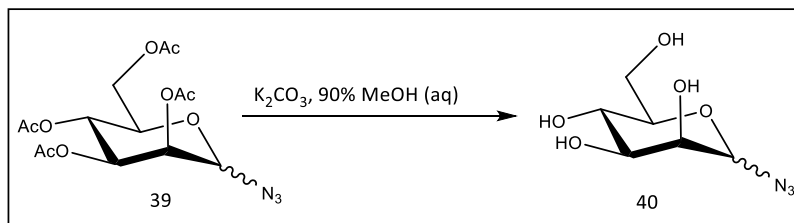
g, 83% yield) as a yellow syrup. Spectral properties matched those found in the literature (NMR in CDCl₃).⁵⁷

Synthesis of Azido-D-mannosylpyranoside tetraacetate **39** (¹H-NMR u/artemis/bl/1-59rexal)



The tetraacetyl mannose bromide (10.3 g, 25.0 mmol) was dissolved in THF (48 mL). Tetrabutyl ammonium hydrogen sulfate (8.14 g, 24.0 mmol) and sodium azide (7.79g, 120 mmol) was added. Saturated aqueous sodium bicarbonate (24 mL) was added and the solution was vigorously stirred at room temperature. Upon completion as shown by TLC, the mixture was diluted with ethyl acetate (96 mL). The organic layer was separated and washed with saturated sodium bicarbonate (2x), water (2x), and brine. The organic layer was then dried with sodium sulfate, filtered, and concentrated. The crude product was recrystallized in ethanol (2x) to yield **39** (mixture of both anomers α/β 1:10, 0.4 g, 1.1 mmol, 5% yield) as fine white needle-like crystals. Spectral properties matched those found in the literature (NMR in CDCl₃).⁵⁸

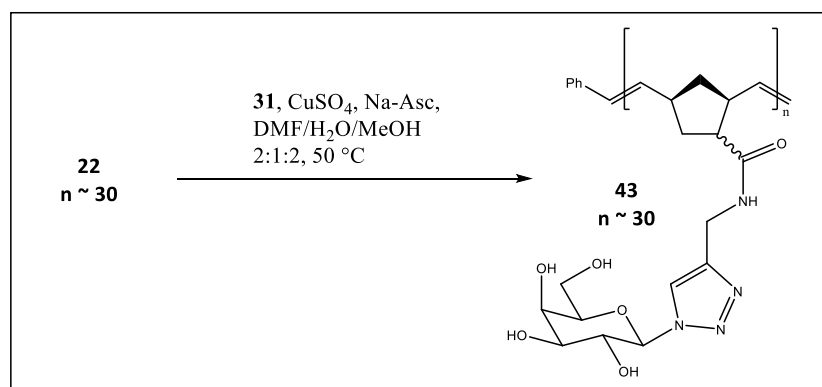
Synthesis of Azido-D-mannosylpyranoside (¹H-NMR u/artemis/bl/1-82)



Protected mannose azide **39** (50 mg, 0.14 mmol) and potassium carbonate (74 mg, 0.54 mmol) was dissolved in 90% methanol (v/v, aq) (2 mL) in a vial. The reaction was stirred overnight. The

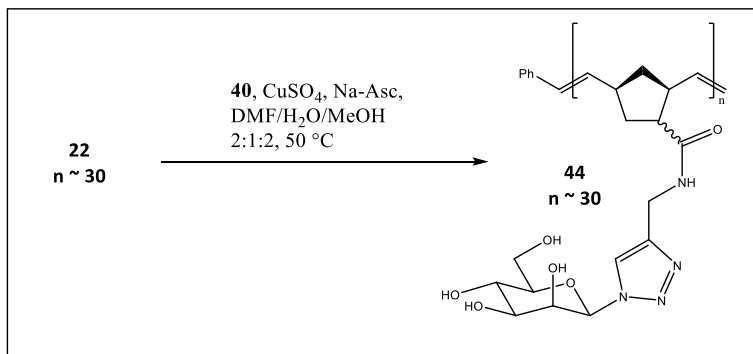
reaction was quenched by neutralization with Amberlite IR-120 resin (H⁺ form, prewashed with methanol), followed by filtration and evaporation of the solvent under reduced pressure to provide compound **40** as a yellow syrup (30 mg, 0.14 mmol, quantitative yield). Spectral properties matched those found in the literature (NMR in D₂O).^{38, 59} HRMS (FAB) calculated for C₆H₁₁N₃O₅ [M+Na]⁺ 228.0598 found 228.0591.

Synthesis of the alkene terminated Gal Glycopolymer **43 n ~ 30** (¹H-NMR u/artemis/bl/2-39)



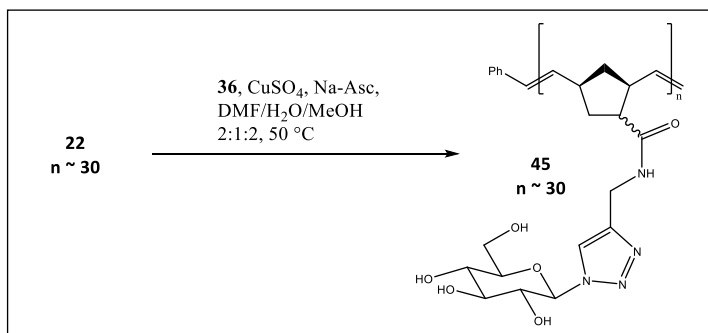
To a solution of poly-alkyne **22 n ~ 30** (25 mg, 4.8 μmol) in DMF (2 mL) in a vial was added solutions of **31** (40 mg, 0.2 mmol) in MeOH (2 mL), CuSO₄•5H₂O (8 mg, 0.03 mmol) in H₂O (0.5 mL), sodium-ascorbate (12 mg, 0.01 mmol) in H₂O (0.5 mL) and the mixture stirred at 50 °C. 1 hr after completion of the reaction (as judged by TLC with the click stain) 1 g of CupriSorb[®] was added and the mixture stirred overnight at 50 °C. The CupriSorb[®] was filtered off and the filtrate transferred to a dialysis tube (Spectra/Por[®] Dialysis Membrane MWCO: 1000) and dialyzed against H₂O (500 mL) for 3 days with the solvent reservoir changed every 12 h. After dialysis, the solution was transferred to a scintillation vial and frozen in liquid nitrogen. The water was then removed by lyophilization to give **43 n ~ 30** (42 mg, 3.6 μmol, 77 % yield) as a puffy white solid. Partial ¹H NMR (400 MHz, D₂O) δ 8.0 (br s, 29 H, H-Triazole) 7.5-7.0 (br s, 5H, H-Ph) 5.9-4.9 (m, 82 H, H-olefinic and H-1) 4.5-3.5 (m, 210 H, H-triazole methylene and H-sugar) 3.3-0.3 (m, 246 H, H-aliphatic).

Synthesis of the alkene terminated Man Glycopolymer **44** $n \sim 30$ ($^1\text{H-NMR}$ u/artemis/bl/2-38)



Mannosylated glycopolymer **44**, $n \sim 30$ was obtained using the same procedure reported for galactosylated glycopolymer **43**, $n \sim 30$. Use of 25 mg of polymer **22** $n \sim 30$ and 40 mg of sugar **40** provided the product **44**, $n \sim 30$ (28 mg, $2.4 \mu\text{mol}$, 51 % yield) as a puffy white solid. Partial ^1H NMR (400 MHz, D_2O) δ 8.0 (br s, 25 H, H-Triazole) 7.2-7.0 (br s, 5H, H-Ph). 5.9-4.9 (m, 70 H, H-olefinic and H-1) 4.5-3.5 (m, 191 H, H-triazole methylene and H-sugar) 3.3-0.5 (m, 213 H, H-aliphatic).

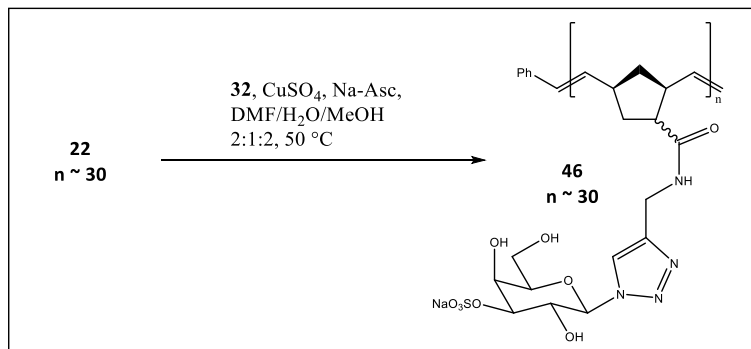
Synthesis of the alkene terminated Glc Glycopolymer **45** $n \sim 30$ ($^1\text{H-NMR}$ u/artemis/bl/2-35)



Glucosylated glycopolymer **45**, $n \sim 30$ was obtained using the same procedure reported for galactosylated glycopolymer **43**, $n \sim 30$. Use of 25 mg of polymer **22** $n \sim 30$ and 40 mg of sugar **36** provided the product **45**, $n \sim 30$ (32 mg, $2.8 \mu\text{mol}$, 58 % yield) as a puffy white solid. Partial ^1H NMR (400 MHz, D_2O) δ 8.0 (br s, 31 H, H-Triazole) 7.2-7.0 (br s, 5H, H-Ph) 5.9-4.9 (m, 90 H, H-

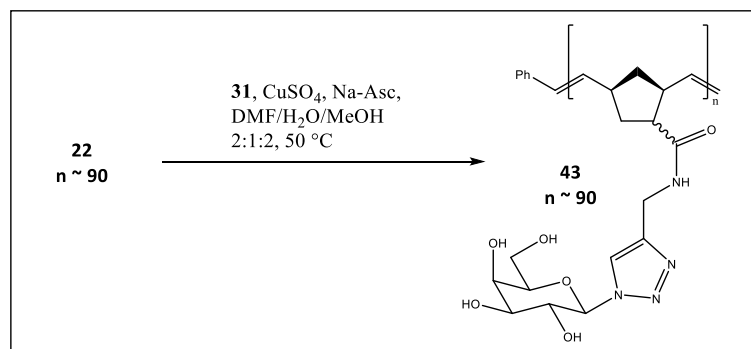
olefinic and H-1) 4.6-3.4 (m, 216 H, H-triazole methylene and H-sugar) 3.2-0.6 (m, 246 H, H-aliphatic).

Synthesis of the alkene terminated SGal Glycopolymer **46** $n \sim 30$ ($^1\text{H-NMR}$ u/artemis/bl/2-34-he)



3-Sulfogalactosylated glycopolymer **46**, $n \sim 30$ was obtained using the same procedure reported for galactosylated glycopolymer **43**, $n \sim 30$. Use of 25 mg of polymer **22** $n \sim 30$ and 63 mg of sugar **32** provided the product **46**, $n \sim 30$ (51 mg, $3.5 \mu\text{mol}$, 73 % yield). Partial ^1H NMR (400 MHz, D_2O) δ 8.2 (br s, 13 H, H-Triazole) 7.5-7.0 (br s, 5H, H-Ph) 6.0-5.0 (m, 36 H, H-olefinic and H-1) 4.6-3.4 (m, 142 H, H-triazole methylene and H-sugar) 3.4-0.4 (m, 179 H, H-aliphatic).

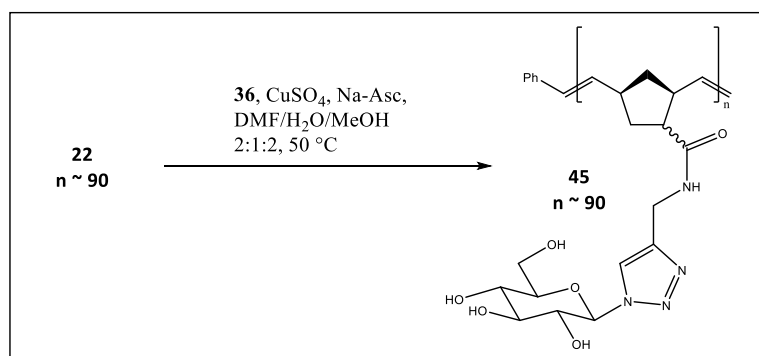
Synthesis of the alkyne terminated Gal Glycopolymer **43** $n \sim 90$ ($^1\text{H-NMR}$ u/artemis/bl/2-22)



Galactosylated glycopolymer **43**, $n \sim 90$ was obtained using the same procedure reported for galactosylated glycopolymer **43**, $n \sim 30$. Use of 25 mg of polymer **22** $n \sim 90$ and 40 mg of sugar **32**

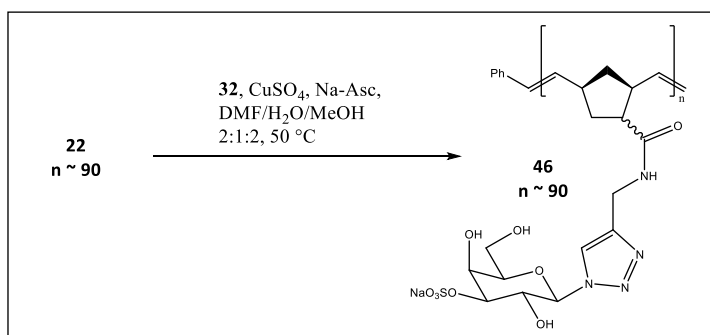
provided the product **43**, $n \sim 90$ (43 mg, 1.3 μmol , 80 % yield) as a puffy white solid. Volume of solvent DMF (4 mL), MeOH (4 mL), H₂O (2 mL). Partial ¹H NMR (400 MHz, D₂O) δ 8.0 (br s, 65 H, H-Triazole) 7.2-7.0 (br s, 5H, H-Ph) 6.0-5.0 (m, 181 H, H-olefinic and H-1) 4.6-3.6 (H-triazole methylene and H-sugar) 3.6-0.7 (m, 614 H, H-aliphatic).

Synthesis of the alkyne terminated Glc Glycopolymer **45** $n \sim 90$ (¹H-NMR u/artemis/bl/2-20)



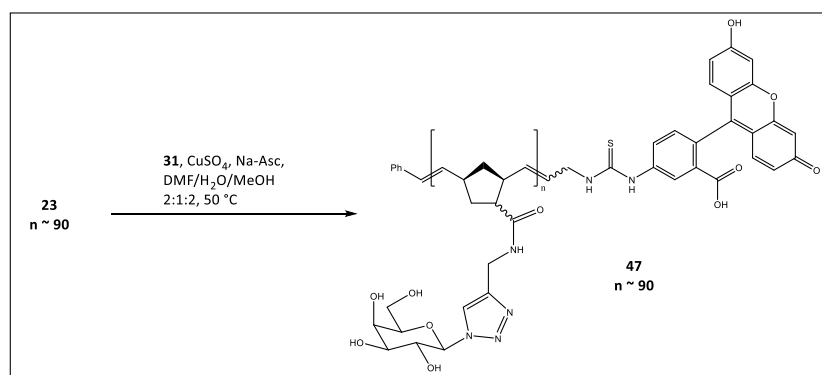
Glucosylated glycopolymer **45**, $n \sim 90$ was obtained using the same procedure reported for galactosylated glycopolymer **43**, $n \sim 30$. Use of 25 mg of polymer **22** $n \sim 90$ and 40 mg of sugar **36** provided the product **45**, $n \sim 90$ (47 mg, 1.4 μmol , 88 % yield) as a puffy white solid. Volume of solvent DMF (4 mL), MeOH (4 mL), H₂O (2 mL). Partial ¹H NMR (400 MHz, D₂O) δ 8.1 (br s, 20 H, H-Triazole) 6.8-6.5 (br s, 5H, H-Ph) 5.9-4.9 (m, 58 H, H-olefinic and H-1) 4.6-3.6 (m, 148 H, H-triazole methylene and H-sugar) 3.4-0.7 (m, 177 H, H-aliphatic).

Synthesis of the alkyne terminated SGal Glycopolymer **46** $n \sim 90$ (¹H-NMR u/artemis/bl/BL-3-2)



3-Sulfogalactosylated glycopolymer **46**, $n \sim 90$ was obtained using the same procedure reported for galactosylated glycopolymer **43**, $n \sim 30$. Use of 25 mg of polymer **22** $n \sim 90$ and 63 mg of sugar **32** provided the product **46**, $n \sim 90$ (46 mg, 1.1 μmol , 67 % yield) as a puffy white solid. Partial ^1H NMR (400 MHz, D_2O) δ 8.1 (br s, 70 H, H-Triazole) 7.5-7.1 (br s, 5H, H-Ph) 5.8-5.0 (m, 217 H, H-olefinic and H-1) 4.6-3.6 (m, 530 H, H-triazole methylene and H-sugar) 3.4-0.6 (m, 583 H, H-aliphatic).

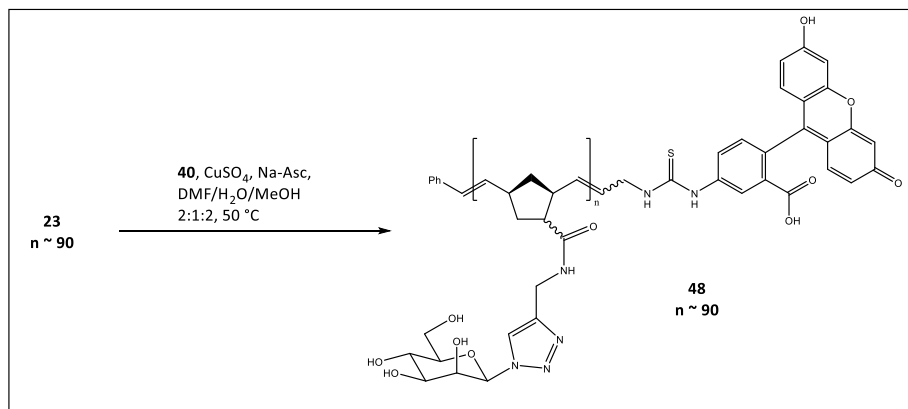
Synthesis of the fluorescently labeled Gal Glycopolymer **47** $n \sim 90$ (^1H -NMR u/artemis/bl/BL-3-12)



Fluorescently labeled galactosylated glycopolymer **47**, $n \sim 90$ was obtained using the same procedure reported for galactosylated glycopolymer **43**, $n \sim 30$. All work was done under low light conditions, and reaction vessels and dialysis beakers were wrapped in foil. Use of 26 mg of polymer **26** $n \sim 90$ and 50 mg of sugar **31** provided the product **47**, $n \sim 90$ (25 mg, 0.7 μmol , 44 % yield) as a puffy orange solid. Volume of solvent DMF (5 mL), MeOH (5 mL), H_2O (2.5 mL). Partial ^1H NMR (400 MHz, D_2O) δ 8.1 (br s, 114 H, H-Triazole) 7.4-7.1 (br s, 5H, H-Ph) 6.0-4.9 (m, 321 H, H-olefinic and H-1) 4.6-3.6 (m, 977 H, H-triazole methylene and H-sugar) 3.4-0.6 (m, 924 H, H-aliphatic).

Synthesis of the fluorescently labeled Man Glycopolymer **48** $n \sim 90$ ($^1\text{H-NMR}$ u/artemis/bl/BL-3-

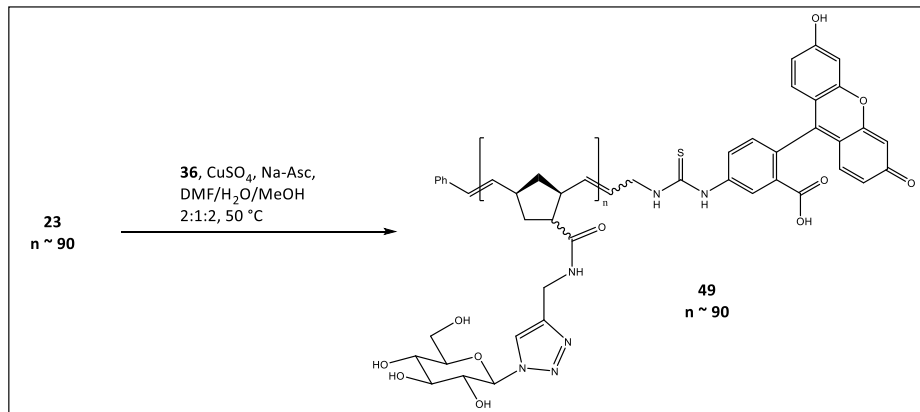
15)



Fluorescently labeled mannosylated glycopolymer **48**, $n \sim 90$ was obtained using the same procedure reported for galactosylated glycopolymer **43**, $n \sim 30$. All work was done under low light conditions, and reaction vessels and dialysis beakers were wrapped in foil. Product (18 mg, $0.5\text{ }\mu\text{mol}$, 32 % yield) was recovered from Use of 26 mg of polymer **26** $n \sim 90$ and 45 mg of sugar **40** provided the product **48**, $n \sim 90$ (18 mg, $0.5\text{ }\mu\text{mol}$, 30 % yield) as a puffy orange solid. Volume of solvent DMF (5 mL), MeOH (5 mL), H_2O (2.5 mL). Partial $^1\text{H NMR}$ (400 MHz, D_2O) δ 8.0 (br s, 39 H, H-Triazole) 7.4-7.2 (br s, 5H, H-Ph) 6.2-4.9 (m, 106 H, H-olefinic and H-1) 4.6-3.4 (m, 262 H, H-triazole methylene and H-sugar) 3.2-0.4 (m, 400 H, H-aliphatic).

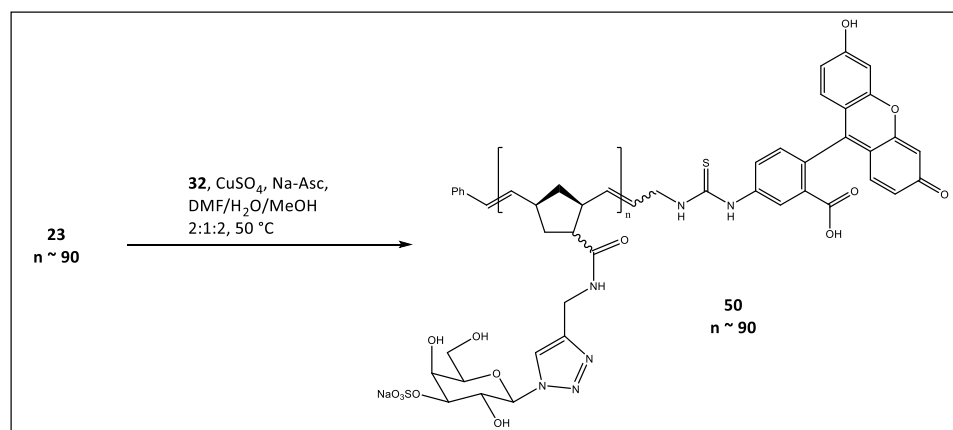
Synthesis of the fluorescently labeled Glc glycopolymer **49** $n \sim 90$ ($^1\text{H-NMR}$ u/artemis/bl/BL-3-

14)



Fluorescently labeled glucosylated glycopolymer **49**, $n \sim 90$ was obtained using the same procedure reported for galactosylated glycopolymer **43**, $n \sim 30$. All work was done under low light conditions, and reaction vessels and dialysis beakers were wrapped in foil. Use of 26 mg of polymer **26** $n \sim 90$ and 45 mg of sugar **36** provided the product **49**, $n \sim 90$ (26 mg, 0.7 μmol , 46 % yield) as a puffy orange solid. Volume of solvent DMF (5 mL), MeOH (5 mL), H_2O (2.5 mL). Partial ^1H NMR (400 MHz, D_2O) δ 8.1 (br s, 156 H, H-Triazole) 7.4-7.2 (br s, 5H, H-Ph) 5.9-4.9 (m, 345 H, H-olefinic and H-1) 4.6-3.4 (m, 1,261 H, H-triazole methylene and H-sugar) 3.3-0.5 (m, 1,174 H, H-aliphatic).

Synthesis of the fluorescently labeled SGal glycopolymer **50** $n \sim 90$ (^1H -NMR u/artemis/bl/BL-3-13)



Fluorescently labeled 3-sulfogalactosylated glycopolymer **50**, $n \sim 90$ was obtained using the same procedure reported for galactosylated glycopolymer **43**, $n \sim 30$. All work was done under low light conditions, and reaction vessels and dialysis beakers were wrapped in foil. Use of 26 mg of polymer **26** $n \sim 90$ and 64 mg of sugar **32** provided the product (59 mg, 1.3 μmol , 83 % yield) as a puffy orange solid. Volume of solvent DMF (5 mL), MeOH (5 mL), H_2O (2.5 mL). Partial ^1H NMR (400 MHz, D_2O) δ 8.1 (br s, 126 H, H-Triazole) 7.5-7.3 (br s, 5H, H-Ph) 6.0-5.0 (m, 346 H, H-olefinic and H-1) 4.6-3.6 (m, 848 H, H-triazole methylene and H-sugar) 3.4-0.6 (m, 930 H, H-aliphatic).

References:

1. Seah, N.; Basu, A., Carbohydrate– Carbohydrate Interactions. In *Wiley Encyclopedia of Chemical Biology*, John Wiley & Sons, Inc.: 2007.
2. Spillmann, D.; Burger, M. M., Carbohydrate-carbohydrate interactions in adhesion. *Journal of Cellular Biochemistry* **1996**, *61* (4), 562-568.
3. Misevic, G.; Burger, M. M., The species-specific cell-binding site of the aggregation factor from the sponge *Microciona prolifera* is a highly repetitive novel glycan containing glucuronic acid, fucose, and mannose. *Journal of Biological Chemistry* **1990**, *265* (33), 20577-20584.
4. Carvalho de Souza, A.; Halkes, K. M.; Meeldijk, J. D.; Verkleij, A. J.; Vliegthart, J. F.; Kamerling, J. P., Gold glyconanoparticles as probes to explore the carbohydrate-mediated self-recognition of marine sponge cells. *ChemBioChem* **2005**, *6* (5), 828-831.
5. Fenderson, B. A.; Zehavi, U.; Hakomori, S. I., A multivalent lacto-N-fucopentaose III-lyssyllysine conjugate decompacts preimplantation mouse embryos, while the free oligosaccharide is ineffective. *Journal of Experimental Medicine* **1984**, *160* (5), 1591-1596.
6. Eggens, I.; Fenderson, B.; Toyokuni, T.; Dean, B.; Stroud, M.; Hakomori, S.-I., Specific interaction between Lex and Lex determinants. A possible basis for cell recognition in

- preimplantation embryos and in embryonal carcinoma cells. *Journal of Biological Chemistry* **1989**, *264* (16), 9476-9484.
7. Kojima, N.; Hakomori, S. I., Specific interaction between gangliosylceramide (Gg3) and sialosylgalactosylceramide (GM3) as a basis for specific cellular recognition between lymphoma and melanoma cells. *Journal of Biological Chemistry* **1989**, *264* (34), 20159-20162.
 8. Iwabuchi, K.; Yamamura, S.; Prinetti, A.; Handa, K.; Hakomori, S. I., GM3-enriched microdomain involved in cell adhesion and signal transduction through carbohydrate-carbohydrate interaction in mouse melanoma B16 cells. *Journal of Biological Chemistry* **1998**, *273* (15), 9130-9138.
 9. Boggs, J. M.; Gao, W.; Zhao, J.; Park, H.-J.; Liu, Y.; Basu, A., Participation of galactosylceramide and sulfatide in glycosynapses between oligodendrocyte or myelin membranes. *FEBS Letters* **2010**, *584* (9), 1771-1778.
 10. Coet, T.; Suzuki, K.; Popko, B., New perspectives on the function of myelin galactolipids. *Trends in neurosciences* **1998**, *21* (3), 126-130.
 11. Stewart, R. J.; Boggs, J. M., A carbohydrate-carbohydrate interaction between galactosylceramide-containing liposomes and cerebroside sulfate-containing liposomes: Dependence on the glycolipid ceramide composition. *Biochemistry* **1993**, *32* (40), 10666-10674.
 12. Zhao, J.; Liu, Y.; Park, H.-J.; Boggs, J. M.; Basu, A., Carbohydrate-coated fluorescent silica nanoparticles as probes for the galactose/3-sulfogalactose carbohydrate-carbohydrate interaction using model systems and cellular binding studies. *Bioconjugate Chemistry* **2012**, *23* (6), 1166-1173.
 13. Ladmiral, V.; Melia, E.; Haddleton, D. M., Synthetic glycopolymers: an overview. *European Polymer Journal* **2004**, *40* (3), 431-449.
 14. Lee, Y. C.; Lee, R. T., Carbohydrate-protein interactions: basis of glycobiology. *Accounts of Chemical Research* **1995**, *28* (8), 321-327.
 15. Hakomori, S., Carbohydrate-to-carbohydrate interaction, through glycosynapse, as a basis of cell recognition and membrane organization. *Glycoconjugate Journal* **2004**, *21* (3-4), 125-137.
 16. Slavin, S.; Burns, J.; Haddleton, D. M.; Becer, C. R., Synthesis of glycopolymers via click reactions. *European Polymer Journal* **2011**, *47* (4), 435-446.
 17. Becer, C. R., The glycopolymer code: synthesis of glycopolymers and multivalent carbohydrate-lectin interactions. *Macromolecular Rapid Communications* **2012**, *33* (9), 742-752.
 18. Vázquez-Dorbatt, V.; Lee, J.; Lin, E. W.; Maynard, H. D., Synthesis of glycopolymers by controlled radical polymerization techniques and their applications. *ChemBioChem* **2012**, *13* (17), 2478-2487.
 19. Tasdelen, M. A.; Kahveci, M. U.; Yagci, Y., Telechelic polymers by living and controlled/living polymerization methods. *Progress in Polymer Science* **2011**, *36* (4), 455-567.
 20. Okada, M., Molecular design and syntheses of glycopolymers. *Progress in Polymer Science* **2001**, *26* (1), 67-104.
 21. Okoth, R.; Basu, A., End-labeled amino terminated monotelechelic glycopolymers generated by ROMP and Cu (I)-catalyzed azide-alkyne cycloaddition. *Beilstein journal of organic chemistry* **2013**, *9*, 608.

22. Kanai, M.; Mortell, K. H.; Kiessling, L. L., Varying the Size of Multivalent Ligands: The Dependence of Concanavalin A Binding on Neoglycopolymer Length. *Journal of the American Chemical Society* **1997**, *119* (41), 9931-9932.
23. Bielawski, C. W.; Grubbs, R. H., Living ring-opening metathesis polymerization. *Progress in Polymer Science* **2007**, *32* (1), 1-29.
24. Love, J. A.; Sanford, M. S.; Day, M. W.; Grubbs, R. H., Synthesis, Structure, and Activity of Enhanced Initiators for Olefin Metathesis. *Journal of the American Chemical Society* **2003**, *125* (33), 10103-10109.
25. Gibson, V. C.; Okada, T., Synthesis of End-Functionalized Polynorbornenes and Polynorbornanes via Metathesis: Novel Macromonomers for Polycondensation Reactions. *Macromolecules* **2000**, *33* (3), 655-656.
26. Gordon, E. J.; Gestwicki, J. E.; Strong, L. E.; Kiessling, L. L., Synthesis of end-labeled multivalent ligands for exploring cell-surface-receptor–ligand interactions. *Chemistry & biology* **2000**, *7* (1), 9-16.
27. Strong, L. E.; Kiessling, L. L., A General Synthetic Route to Defined, Biologically Active Multivalent Arrays. *Journal of the American Chemical Society* **1999**, *121* (26), 6193-6196.
28. Kolb, H. C.; Finn, M.; Sharpless, K. B., Click chemistry: diverse chemical function from a few good reactions. *Angewandte Chemie International Edition* **2001**, *40* (11), 2004-2021.
29. Hein, J. E.; Fokin, V. V., Copper-catalyzed azide–alkyne cycloaddition (CuAAC) and beyond: new reactivity of copper (I) acetylides. *Chemical Society Reviews* **2010**, *39* (4), 1302-1315.
30. Okoth, R. S. O., "Probing Carbohydrate - Carbohydrate Interactions (CCIs) Using End-Labeled Glycopolymers and the Determination of Deuterium Isotope Shifts (DIS) of Selected Methyl D-Glycosides in Methanol". *Chemistry Theses and Dissertations. Brown Digital Repository. Brown University Library*. **2015**.
<https://repository.library.brown.edu/studio/item/bdr:419377/>
31. Louie, J.; Grubbs, R. H., Metathesis of electron-rich olefins: structure and reactivity of electron-rich carbene complexes. *Organometallics* **2002**, *21* (11), 2153-2164.
32. Charles, L., MALDI of synthetic polymers with labile end-groups. *Mass Spectrometry Reviews* **2014**, *33* (6), 523-543.
33. Lienkamp, K.; Madkour, A. E.; Musante, A.; Nelson, C. F.; Nusslein, K.; Tew, G. N., Antimicrobial polymers prepared by ROMP with unprecedented selectivity: a molecular construction kit approach. *Journal of the American Chemical Society* **2008**, *130* (30), 9836-9843.
34. Huang, H.; Rodolis, M. T.; Bhatia, S. R.; Sampson, N. S., Sugars require rigid multivalent displays for activation of mouse sperm acrosomal exocytosis. *Biochemistry* **2017**.
35. Lindhorst, T. K., *Essential of Carbohydrate Chemistry and Biochemistry*, 2nd ed. *WILEY-VCH Verlag GmbH & Co. KGaA: Weinheim* **2003**.
36. Rossi, L. L. *Synthesis and Evaluation of α -Glycosyl-1, 2, 3-Triazole Derivatives as-Glycosidase Inhibitors*. Brown University, 2007.
37. Sabesan, S.; Neira, S., Synthesis of glycosyl phosphates and azides. *Carbohydrate Research* **1992**, *223*, 169-185.
38. Bojarová, P.; Petrásková, L.; Ferrandi, E. E.; Monti, D.; Pelantova, H.; Kuzma, M.; Simerská, P.; Křen, V., Glycosyl azides—an alternative way to disaccharides. *Advanced Synthesis & Catalysis* **2007**, *349* (8-9), 1514-1520.
39. Araujo, N.; Banos, M.; Gil, M. V.; Caceres, L. E.; Roman, E.; Serrano, J. A., New C-aryl alditols from Diels-Alder adducts of sugar nitroalkenes. *ARKIVOC* **2008**, 175-186.

40. Manning, D. D.; Hu, X.; Beck, P.; Kiessling, L. L., Synthesis of Sulfated Neoglycopolymers: Selective P-Selectin Inhibitors. *Journal of the American Chemical Society* **1997**, *119* (13), 3161-3162.
41. Langston, S.; Bernet, B.; Vasella, A., Temporary Protection and Activation in the Regioselective Synthesis of Saccharide Sulfates. *Helvetica Chimica Acta* **1994**, *77* (8), 2341-2353.
42. Jin, L.; Tolentino, D. R.; Melaimi, M.; Bertrand, G., Isolation of bis (copper) key intermediates in Cu-catalyzed azide-alkyne "click reaction". *Science advances* **2015**, *1* (5), e1500304.
43. Sivakumar, K.; Xie, F.; Cash, B. M.; Long, S.; Barnhill, H. N.; Wang, Q., A fluorogenic 1, 3-dipolar cycloaddition reaction of 3-azidocoumarins and acetylenes. *Organic Letters* **2004**, *6* (24), 4603-4606.
44. Yang, L.; Chumsae, C.; Kaplan, J. B.; Moulton, K. R.; Wang, D.; Lee, D. H.; Zhou, Z. S., Detection of Alkynes via Click Chemistry with a Brominated Coumarin Azide by Simultaneous Fluorescence and Isotopic Signatures in Mass Spectrometry. *Bioconjugate Chemistry* **2017**, *28* (9), 2302-2309.
45. Dräger, M.; Lusi, R.; Okoth, R.; Basu, A., Specific TLC detection of terminal alkynes using the copper promoted triazole formation of a fluorogenic azido-coumarin dye. *Unpublished*.
46. Ladmiral, V.; Mantovani, G.; Clarkson, G. J.; Cauet, S.; Irwin, J. L.; Haddleton, D. M., Synthesis of neoglycopolymers by a combination of "click chemistry" and living radical polymerization. *Journal of the American Chemical Society* **2006**, *128* (14), 4823-4830.
47. Pangborn, A. B.; Giardello, M. A.; Grubbs, R. H.; Rosen, R. K.; Timmers, F. J., Safe and convenient procedure for solvent purification. *Organometallics* **1996**, *15* (5), 1518-1520.
48. Gottlieb, H. E.; Kotlyar, V.; Nudelman, A., NMR chemical shifts of common laboratory solvents as trace impurities. *The Journal of organic chemistry* **1997**, *62* (21), 7512-7515.
49. Love, J. A.; Morgan, J. P.; Trnka, T. M.; Grubbs, R. H., A practical and highly active ruthenium-based catalyst that effects the cross metathesis of acrylonitrile. *Angewandte Chemie International Edition* **2002**, *41* (21), 4035-4037.
50. Kuhn, H., Synthesis of N-Acetylglucosamine-Triazoles As Antimicrobial Compounds and Galactose Analogues to Study Plant Cell Wall Development in Arabidopsis Thaliana. *Thesis (Ph.D. -- Brown University)* **2016**.
<https://repository.library.brown.edu/studio/item/bdr:674279/>
51. Conrow, R. E.; Dean, W. D., Diazidomethane explosion. *Organic Process Research & Development* **2008**, *12* (6), 1285-1286.
52. Harmand, L.; Cadet, S.; Kauffmann, B.; Scarpantonio, L.; Batat, P.; Jonusauskas, G.; McClenaghan, N. D.; Lastécouères, D.; Vincent, J. M., Copper catalyst activation driven by photoinduced electron transfer: a prototype photolatent click catalyst. *Angewandte Chemie International Edition* **2012**, *51* (29), 7137-7141.
53. Floyd, N.; Vijaykrishnan, B.; Koeppe, J.; Davis, B., Thiyl glycosylation of olefinic proteins: S-linked glycoconjugate synthesis. *Angewandte Chemie (International ed. in English)* **2009**, *48* (42), 7798.
54. Sirion, U.; Kim, H. J.; Lee, J. H.; Seo, J. W.; Lee, B. S.; Lee, S. J.; Oh, S. J.; Chi, D. Y., An efficient F-18 labeling method for PET study: Huisgen 1, 3-dipolar cycloaddition of bioactive substances and F-18-labeled compounds. *Tetrahedron Letters* **2007**, *48* (23), 3953-3957.

55. Vinson, N.; Gou, Y.; Becer, C. R.; Haddleton, D. M.; Gibson, M. I., Optimised 'click' synthesis of glycopolymers with mono/di-and trisaccharides. *Polymer Chemistry* **2011**, *2* (1), 107-113.
56. Šardžik, R.; Noble, G. T.; Weissenborn, M. J.; Martin, A.; Webb, S. J.; Flitsch, S. L., Preparation of aminoethyl glycosides for glycoconjugation. *Beilstein journal of organic chemistry* **2010**, *6*, 699.
57. Nóbrega, C.; Vázquez, J. T., Conformational Study of the Hydroxymethyl Group in α -D-mannose Derivatives. *Tetrahedron: Asymmetry* **2003**, *14* (18), 2793-2801.
58. Sabesan, S.; Neira, S., Synthesis of glycosyl phosphates and azides. *Carbohydrate Research* **1992**, *223* (Supplement C), 169-185.
59. Abronina, P. I.; Kachala, V. V.; Kononov, L. O., A novel synthesis of β -d-mannopyranosyl azide by phase transfer catalysis. *Carbohydrate Research* **2009**, *344* (2), 240-244.

2 PROBING MYELIN CCIs USING GLYCOPOLYMER MODEL SYSTEMS

As previously discussed, CCIs are biologically relevant interactions that occur between cell surface domains that are multivalent in carbohydrates.¹ The multivalent presentation increases the avidity of the interaction and is critical to the ability of the carbohydrates to mediate biological processes.²⁻³ These carbohydrates are present at the cell surface and coexist with many other complex macromolecules. The inherent complexity and fluidity of the cell surface can make it difficult to study the binding behavior of carbohydrate epitopes on a molecular level *in vivo* or using cultured cells. Multivalent synthetic model systems have been prepared to simulate CCIs in a simplified and controlled environment. This allows for CCI binding studies to be performed in an environment in which the only carbohydrate epitopes of interest are present. Qualitative binding studies of CCIs, such as determination of specificity, are achieved using such carbohydrate model systems.⁴

2.1 Qualitative CCI binding studies using carbohydrate coated surfaces

Commonly, protein-carbohydrate interaction (PCI) and CCI binding studies are performed using carbohydrate coated surfaces as a multivalent model system to which proteins or other multivalent carbohydrate model systems, such as liposomes, BSA-glycoconjugates, glyconanoparticles or glycopolymers, may bind.⁴⁻⁶ Polystyrene microtiter plates are routinely used as surfaces for carbohydrate functionalization. Native carbohydrates can be covalently attached to modified polystyrene surfaces that contain amines via reductive amination of the reducing end of the sugar.⁴ Also, synthetic carbohydrates that have been chemically modified to allow for conjugation to a variety of functional groups such as amines or NHS-esters can be used to functionalize the surface of polystyrene microtiter plates that have been modified to contain such

functional groups.⁴ Covalent linkages make these surfaces quite robust under a variety of conditions, and amine modified polystyrene plates are commercially available.

Non-covalent attachment of carbohydrates to a surface is also possible and relies on the hydrophobic interaction between polystyrene microtiter plates and hydrophobic carbohydrate substituents, such as the polyacrylamide backbone of a glycopolymer, or the long alkyl chain of a synthetic glycolipid.^{4,7} Such surfaces are simple to produce when compared to covalently coated surface, but offer less control over the orientation of the presentation of the carbohydrates and are more prone to degradation. Also, different carbohydrates may affect the binding affinity of the hydrophobic substituent to the surface resulting in inconsistent carbohydrate surface concentrations. Furthermore, the possibility of non-specific binding between the probe system and the surface is a concern regardless of whether non-covalent or covalent linkages are used. Nevertheless, non-covalently coated glyco-surfaces have been successfully used to study CCI.⁵⁻⁷

The SGal-Gal CCI that has been found to play a role in myelin sheath compaction has been investigated using 96-well microtiter plates with glycolipid coated wells. In these studies, neoglycolipids were synthesized⁶ by using the CuAAC reaction to connect acetylated propargyl sugars to 1-azidohexadecane alkyl chains followed by Zemplén deacetylation to yield neoglycolipids bearing galactose, glucose, and mannose functionalities (Fig. 2.1).⁵ The neoglycolipids were then dissolved in methanol and the solution added to the polystyrene wells. Upon drying, the neoglycolipids are non-covalently adsorbed to the well via hydrophobic interaction between the alkyl chain and the polystyrene surface.⁵

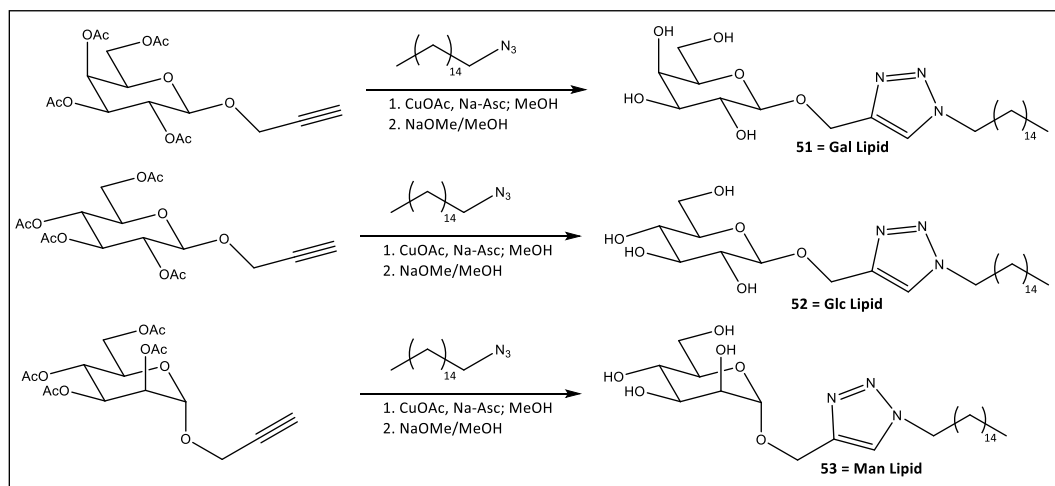


Figure 2.1: Synthesis of Glycolipids

In previous studies, fluorescent glyconanoparticles⁶ and glycopolymers⁵ have been used to characterize the specificity of the SGal-Gal CCI. Fluorescently doped glyconanoparticles bearing galactose, glucose, mannose, and 3-sulfogalactose residues were suspended in phosphate buffered saline (PBS) (pH 7.4), added to lipid coated wells, and incubated. After washing with PBS to remove non-interacting nanoparticles the fluorescence emissions of each well were determined using a plate reader. It was found that the wells containing SGal functionalized nanoparticles and Gal functionalized lipids displayed a much stronger fluorescence signal than any other nanoparticle-well combination.⁵ These results suggest a specific SGal-Gal interaction.

Additional studies were performed using fluorescently labeled glycopolymers (Fig 2.2 **54-56**) instead of nanoparticles, and using plates prepared by a similar procedure as used for the nanoparticles.⁵ However, it was found that when these experiments were performed using fluorescent glycopolymers the wells displaying the strongest emissions after washing were those with SGal containing polymers, and Glc functionalized lipids, suggesting a specific SGal-Glc CCI.⁵ Conditions such as polymer and lipid concentration, blocking solution concentration, linker type (long hydrophilic **54**, short hydrophilic **55**, and short hydrophobic **56**), fluorophore type, buffer

type and calcium concentration were varied. Under some conditions, such as low lipid concentration, low glycopolymer concentration, low concentration of BSA blocking solution, short hydrophobic linker type (**56**), and Tris buffer type, SGal-Glc binding specificity was lost. However, no clear SGal-Gal specificity was observed under any conditions.⁵

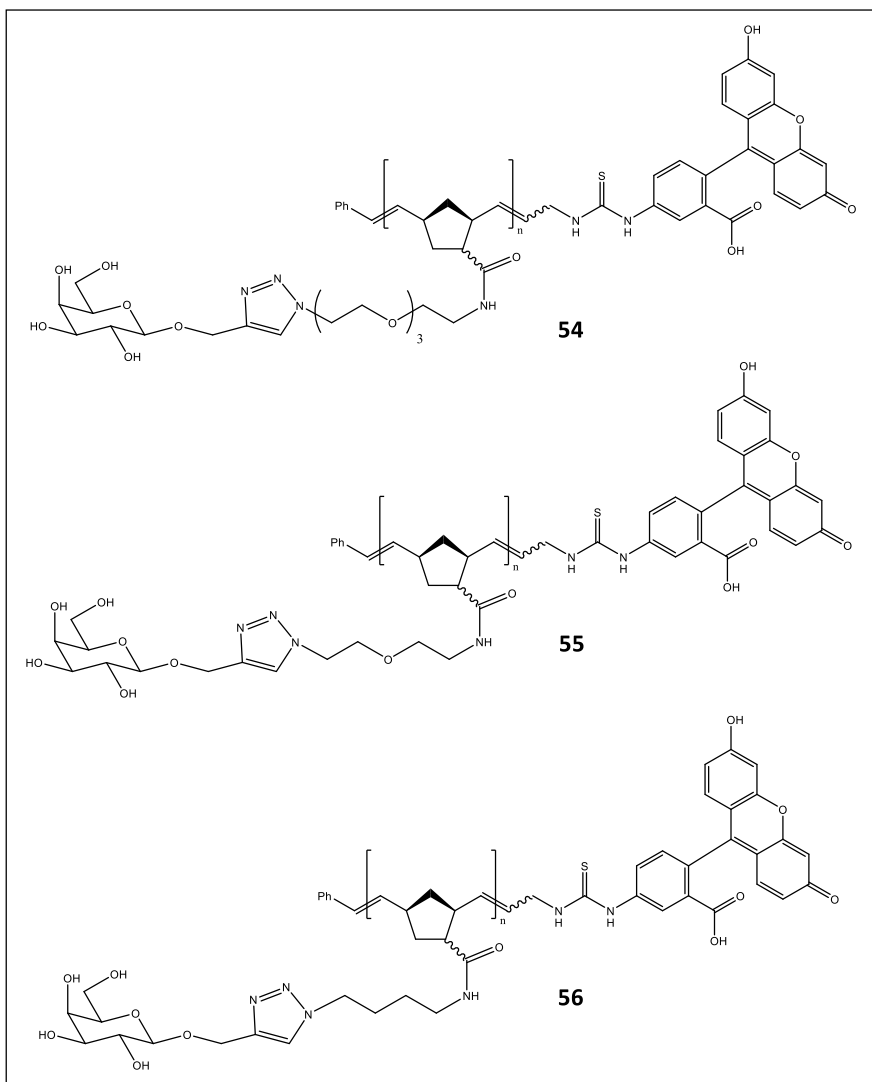


Figure 2.2: Types of glycopolymers used in previous well binding studies **54-56**

2.1.1 Evidence of a SGal-Glc CCI

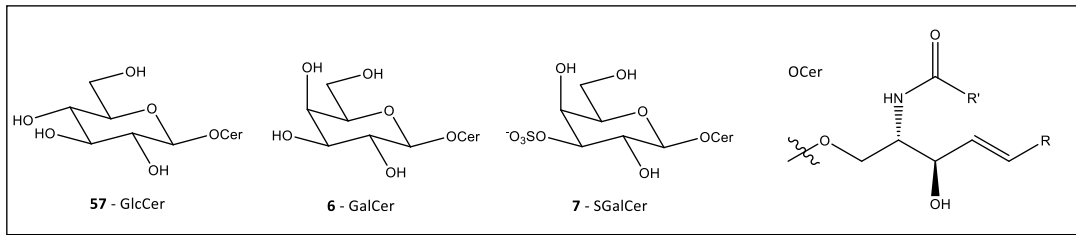


Figure 2.3: Myelin glycosphingolipids

Although the process of myelin sheath compaction is believed to be mediated by a SGal-Gal CCI there is some evidence that compaction of some degree can be achieved in myelin containing GlcCer glycosphingolipids (Fig. 2.3). Mutant mouse models lacking the GalCer **6** and SGalCer **7** glycosphingolipids have been prepared by disrupting the gene that encodes ceramide galactosyltransferase (CGT).⁸ However, thin-layer chromatography experiments (TLC) demonstrated that these mice possessed GlcCer **57** lipids in the myelin instead of **6**.⁹ Also, TLC experiments indicated that sulfated derivatives of **57** were present in the PNS myelin.¹⁰ Compaction was observed in the mutant mouse myelin, but abnormalities were observed in the CNS myelin, and it deteriorated after six weeks leading to mortality in the mice.¹¹ The PNS myelin was observed to be more stable suggesting that glucose can interact with sulfo-glucose in a similar manner to the SGal-Gal CCI.¹⁰

SGal-Glc interactions have been observed using other types of model systems. In experiments performed using liposomes composed **6**, **7**, and **57** it was found that the absorbance of a sample of **6** and **57** liposomes increased when liposomes of **7** were added, and that this absorbance was higher than the sum of the absorbances of the unmixed liposomes. The values of the sum of the absorbances of the unmixed liposomes represents a control measurement as it provides the expected absorbance value for a liposome mixture in which no interaction has occurred. The observed increase in absorbance values for liposome mixtures was interpreted by the authors as evidence that aggregation had occurred. The combination of **57** and **7** liposomes were found to

aggregate to a lesser extent when compared to the combination of **6** and **7** liposomes, but nonetheless this is evidence of an SGal-Glc CCI.¹²

Furthermore, SGal-Glc CCIs were observed in bilayers and vesicles composed of **57** and **7**.¹³ Transmission electron microscopy (TEM) images and Fourier Transform infrared spectroscopy (FT-IR) were used to demonstrate that an interaction between **57** and **7** alters the microstructural features of vesicles formed from a mixture of the lipids when compared to vesicles consisting of only one lipid. For instance, vesicles composed of **57** typically form ribbons when incubated under stable state conditions, but only small vesicles are observed for mixtures of **57** and **7**. The inhibition of ribbon formation is presumed to be a result of the SGal-Glc CCI. Also, FTIR data shows an increase in hydrogen bonding interactions in mixtures of **57** and **7** that is likely due to a SGal-Glc CCI.¹³ Furthermore, positive electrospray ionization mass spectrometry was used to demonstrate that **57** and **6** both form heterotypic complexes with **7**, although it is important to note that the **57-7** complexes were found to be somewhat less stable than the **6-7** complex.¹⁴ Furthermore, glucose-BSA glycoconjugates were found to cause clustering of myelin basic protein (MBP) and depolymerization of microtubules in oligodendrocyte cells.¹⁵ These phenomena are believed to occur as a result of extracellular signaling initiated by a binding interaction involving the **7** present at the cell surface. Therefore, this is another example of the existence of a SGal-Glc CCI. However, it is important to note that these phenomena were observed to a higher degree in cells treated with galactose-BSA.¹⁵

2.1.2 Effect of model system type on CCI specificity

There is evidence that a SGal-Glc CCI exists, but that does not explain why a different specificity is observed when using different types of model systems. Since these studies were performed using model systems it is possible that the change in presentation of the sugar molecules can result in

a change in specificity. Changes in CCI behavior resulting from changes in model systems have been observed for model systems used to study the Le^x - Le^x CCI. Le^x functionalized nanoparticles were found to aggregate in the presence of calcium ions while lactose functionalized nanoparticles did not aggregate under identical conditions indicating a specific calcium mediated CCI.¹⁶ However, a fluorescent glycopolymer model system bearing lactose pendant groups was found to aggregate in the presence of calcium ions. This aggregation behavior suggests the presence of a CCI that was not observed when nanoparticles were used.¹⁷ Also, a different type of lactose-functionalized glyconanoparticle was prepared by adding a thiolated lactose derivative to a solution of previously prepared gold nanoparticles. These nanoparticles were found to aggregate in the presence of calcium ions.¹⁸ In the preparation of the previously discussed nanoparticles, disulfide lactose derivative were added to the reaction mixture before nanoparticles were formed.¹⁶ This demonstrates that different preparations of similar model systems can result in different aggregation behavior.

Furthermore, another study found that glycopolymers with poly-norbornene backbones were more effective inducers of mouse sperm acrosomal exocytosis (AE) than glycopolymers with polycyclooctene backbones. Using SAXS experiments it was shown that the polycyclooctene glycopolymers adopt a globular conformation in solution that is typical for solvated polymers, while the poly-norbornene polymers adopt a flexible cylinder conformation.¹⁹ These results indicate that changes to the structure of the model system can have a profound effect on the specificity of the CCI and is possibly is the reason for the switch in specificity observed in the previously described polymer systems.

2.2 Quantitative binding studies of CCIs

Although qualitative information regarding CCI, such as specificity, can be collected with relative ease using fluorescence well-binding experiments, it has been considerably more difficult to obtain accurate quantitative information such as the values of thermodynamic and binding constants for these interactions. However, there has been limited success in obtaining quantitative information using multivalent model systems and analytical techniques such as surface plasmon resonance (SPR), atomic force microscopy (AFM), and isothermal titration calorimetry (ITC).

2.2.1 SPR studies of CCI

To investigate the binding affinity of the GM3-Gg3 CCI, a model system was prepared in which GM3 glycosphingolipids were non-covalently attached to a thiol-coated gold plate to form an immobilized glycosphingolipid monolayer. Gg3-polystyrene glycopolymers were prepared and surface plasmon resonance (SPR) was used to monitor the adsorption of the Gg3 polymers to the GM3 monolayer. The SPR data was used to calculate a binding association constant (K_a) of $2.5 \times 10^6 \text{ M}^{-1}$ per sugar unit. The specificity of the GM3-Gg3 interaction evaluated by performing SPR experiments with lipids and polymers functionalized with different sugar moieties. The K_a values for these combinations were never above $6.5 \times 10^5 \text{ M}^{-1}$ per sugar unit and most were below $1 \times 10^5 \text{ M}^{-1}$ per sugar unit, indicating that the GM3-Gg3 CCI occurs with a high degree of specificity.²⁰

A similar experiment again used SPR to investigate the Le^x-Le^x CCI by monitoring the adsorption of Le^x-coated gold nanoparticles onto a Le^x-coated monolayer.²¹ The data was used to calculate an energy of binding (ΔG) of -8.5 kcal/mol and a K_a of $1.9 \times 10^6 \text{ M}^{-1}$ for the Le^x-Le^x CCI. SPR experiments performed using monovalent moieties, lactose functionalized nanoparticles and lactose coated surfaces resulted in K_a values that were all below $1.8 \times 10^2 \text{ M}^{-1}$, several orders of

magnitude weaker than the K_a observed for the Le^x-nanoparticle-Le^x-monolayer interaction. These results demonstrate the existence of a specific Le^x-Le^x CCI.²¹

SPR was also used to investigate the binding affinity of the MAF-MAF sponge cell adhesion CCI. In this study BSA glycoconjugates of the GlcNAc(3SO₃)β1–3Fuc disaccharide were immobilized on a surface and a solution of the same BSA conjugates was allowed to flow over the surface. The adsorption was monitored by SPR and the resulting data was used to calculate a K_a of 10⁵ M⁻¹ for the interaction. No evidence of an interaction between unfunctionalized BSA and the conjugate coated surface was observed indicating that a specific interaction was occurring between the GlcNAc(3SO₃)β1–3Fuc disaccharide BSA conjugates.²²

2.2.2 AFM studies of CCI

Atomic force microscopy (AFM) was also used to measure adhesion forces between carbohydrate moieties that participate in CCIs. In these experiments thiol functionalized carbohydrate moieties were attached to a stationary gold surface, and a gold coated tip attached to a cantilever.²³ The tip was moved onto the surface and then pulled away to measure the adhesion force. An AFM study of the Le^x-Le^x CCI was performed and found that the force needed to separate the individual interacting moieties was 20 +/- 4 pN. No interactions were observed in AFM experiments in which Le^x was substituted with lactose on the tip, or the surface, or both. This data demonstrated that the force measured by AFM is the adhesion force of a specific Le^x-Le^x CCI.²³

AFM experiments were also performed using the g200 glycan portion of MAF proteins gauge the adhesion force of the MAF-MAF CCI. AFM experiments determined that the force binding individual MAF molecules is about 200-300 pN. Experiments performed in which g200 was substituted with an unrelated sulfur glycan of similar size (CSB) on the tip, or the surface, or both yielded only weak unspecific force measurements comparable to those obtained for experiments

performed using g200 and an unfunctionalized gold surface. This data demonstrates that the adhesion forces measured are those of the specific MAF-MAF CCI.²⁴

2.2.3 ITC studies of CCI

Isothermal titration chromatography (ITC) was used to obtain further thermodynamic data on the Le^x-Le^x CCI.²⁵ ITC is a technique that is commonly used to investigate the thermodynamic properties of the interactions between various chemical and biological entities. A typical ITC experiment involves the addition of substrate into a sample cell containing a receptor that binds to the substrate. The instrument detects the change in temperature of the sample cell that results from the binding of the substrate. The instrument then applies power to the sample cell to bring the temperature back to equilibrium with the reference cell. The values for applied power are integrated with respect to time to give the total heat exchanged for the injection. The values for heats of injections are plotted as a function of the molar ratio of ligand to substrate. A binding model can be fitted to this plot and used to calculate the entropy, enthalpy, Gibbs' free energy, and binding constants of the interaction.²⁶ In the Le^x-Le^x CCI, Le^x functions as both receptor and substrate. Since the Le^x-Le^x CCI does not occur in the absence of Ca⁺², the interaction was observed via ITC by adding aliquots of a solution of Le^x coated gold nanoparticles to a solution of Ca⁺² and observing the temperature change as the interaction occurred. For this set of experiments the authors reported the slowness of the association of the gold nanoparticles limited the number of injections to three per each experiment due to limits imposed by the size of the experimental-data collecting files.²⁵ Therefore, there were not enough data points to calculate any thermodynamic properties except for the heat of enthalpy (ΔH) (which only requires two injections) of the interaction from the ITC data.²⁶ The calculated value for the ΔH of the interaction was determined to be about -160(+/-30) kcal/mol, indicating that the interaction is enthalpically favored. Data for the ΔG of the interaction between Le^x glyconanoparticles and a Le^x coated

surface was obtained from SPR studies. Although the value of ΔG was obtained using a different model system, it can probably be inferred that the interaction between the Le^x-Le^x glyconanoparticles interaction has a similar value of ΔG . Therefore, the interaction probably proceeds with an unfavorable decrease of entropy (ΔS).^{16, 27}

2.3 Qualitative and quantitative analysis of myelin CCI using glycopolymers

As previously discussed, there has been some inconsistency regarding the specificity of the CCI that mediates myelin sheath compaction. Well binding experiments using fluorescent nanoparticle model systems of the CCI have demonstrated SGal-Gal binding specificity, while similar experiments using fluorescent glycopolymer systems have shown SGal-Glc binding specificity.⁵⁻⁶ One possible explanation for this change in specificity is that the long linkers used in the glycopolymers **54-56** cause the sugar moieties to be presented in such a manner that makes SGal-Glc CCI favored while at the same time prevents the SGal-Gal interaction from occurring. In the glycopolymer well binding study it was found that switching from a long hydrophilic linker **56** to a short hydrophobic linker **56** resulted in a loss of specificity, and resulted in Poly-SGal, Poly-Gal, and Poly-Glc polymers binding to Gal and Glc lipids. This result suggests that the specificity is dependent on linker identity.⁵ Although the hydrophobic linker **56** is shorter there are still four carbons in the linker chain, and an additional carbon separating the sugar from the triazole. The linker length is even more drastically reduced using the new generation of glycopolymers described in chapter 1 (**43-50**). This further reduction of linker length may result in a more rigid presentation of the carbohydrate moieties and alter the binding specificity of the polymers in well-binding experiments. Also, it is possible that these glycopolymers can be used to obtain the values of thermodynamic and binding constants for these interactions using ITC for quantitative analysis.

The following sections describe efforts to qualitatively and quantitatively characterize myelin CCl_s using a novel glycopolymer model system. In this work, fluorescent well-binding assays and isothermal titration calorimetry (ITC) were used.

2.4 Well-binding assays

Fluorescent well-binding assays were performed to determine if the change to a short propargyl amine linker has had any effect on the binding specificity of the glycopolymer model system.

2.4.1 Glycolipids

Glycolipids bearing galactose **51**, glucose **52**, and mannose **53** functionalities were used to prepare the carbohydrate microtiter plates used in these experiments. The glycolipids were prepared via CuAAC between 1-propargyl peracetylated pyranosides and 1-azidohexadecane followed by deprotection under Zemplen conditions (glycolipids were prepared by Ronald Okoth).⁵

2.4.2 Preparation of the well-binding assay

The carbohydrate coated surfaces that were used in CCl binding experiments were prepared by non-covalently immobilizing glycolipids (**51-53**) on the polystyrene wells of a microtiter plate.⁵⁻⁶ Fluorescent glycopolymers (**47-50**) were added to each well and allowed to interact with the glycolipid coated surfaces. The strength of binding between the glycopolymers and lipids were evaluated by determining which well-polymer combination provided the highest fluorescence emissions after several rounds of washing with buffer. Since the lipids are non-covalently attached to the plate it is important to confirm that the lipids are not being washed away by the buffer. In a previous study a phenol-sulfuric acid assay was performed.⁵ It was determined that after three washes, wells containing the three glycolipids contain comparable amounts of glycolipids, although the value remaining was about 35-45% less than the initial amount loaded.⁵

The microtiter plates were prepared according to procedures reported by Okoth (Fig. 2.4).⁵ The polystyrene plates were first soaked in a methanol bath for one hour to remove any mold release agents left over from the manufacturing process. After the methanol soak the plates were inverted and shaken to remove the remaining methanol and the plates were left to air dry for 30 minutes. After drying, a methanolic solution of the glycolipids were added to each well using a micropipette, and the plates were left on the bench top for several hours to allow the methanol to evaporate and the lipids to adhere to the polystyrene in the wells. Once the plates were completely dry, a 10% (w/v) solution of bovine serum albumin (BSA) in PBS buffer (pH 7.4) was added to each well and left to incubate overnight to block non-specific interactions between the polymer and the polystyrene plate. After blocking was complete excess BSA solution was removed by inverting and shaking the plates and then washing them twice with PBS buffer. After washing the plates are ready for immediate addition of solutions of glycopolymers in PBS buffer solution.

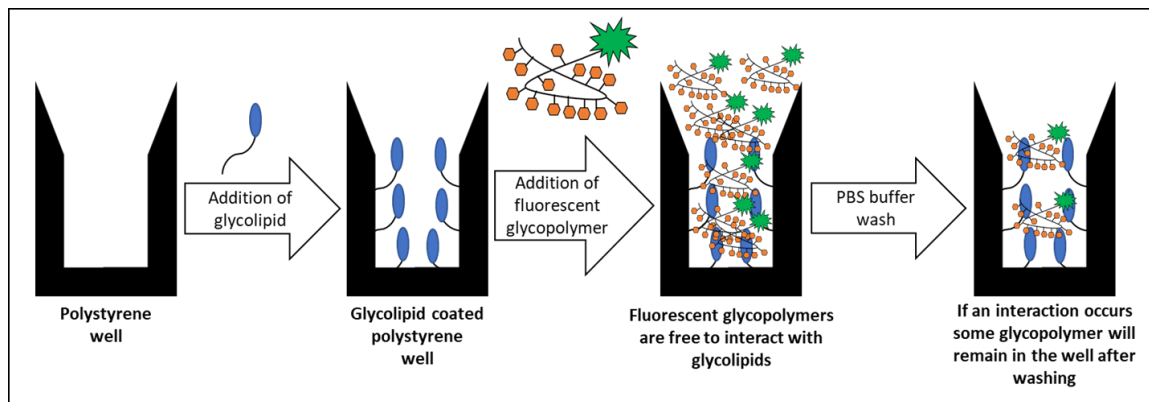


Figure 2.4:Fluorescent polymer lipid well-binding assay

2.4.3 Well-binding assays: normal method

Well-binding assays performed according to the typical method described by Okoth.⁵ were run under various conditions, but always using the same procedure (Fig. 2.4). After the plates were prepared, solutions of fluorescent glycopolymers in PBS buffer were added to each well and

allowed to incubate for several hours. The plates were prepared in such a way to allow for there to be three replicate wells for each unique polymer-lipid combination. After the incubation was complete the emission from each well was recorded. The wells were then emptied as previously described, and PBS buffer was added to each well. Emissions were again recorded, and the washing process was repeated.

2.4.3.1 Well-binding assays: normal method. Initial results.

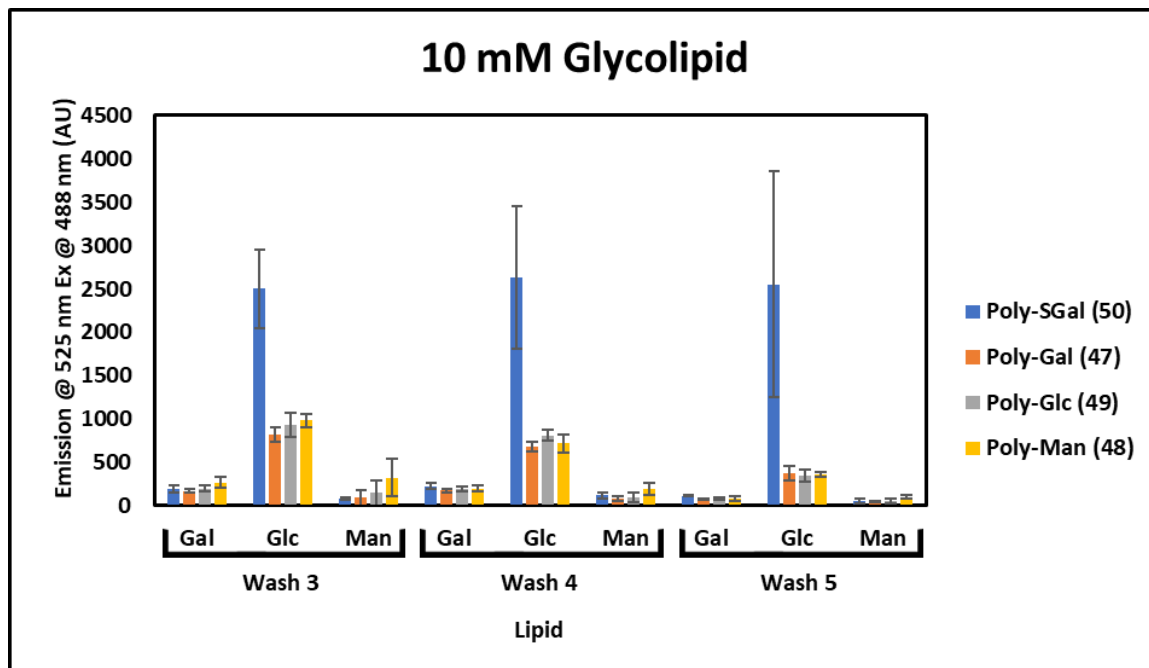


Figure 2.5: Results from binding assays using 10 mM glycolipid in well incubated with 2 μ M fluorescein labeled glycopolymers (072917SGalGal0washpt2.2.xls)

The first round of well binding experiments was performed under conditions that yielded the strongest fluorescence results and most clearly demonstrated SGal-Glc specificity using the previous generation of fluorescent glycopolymers (54).⁵ For these experiments plates were prepared using 10 mM solutions of glycolipids, 10% (w/v) BSA in PBS buffer, and 2 μ M solutions of glycopolymers. Under these conditions the highest emissions were observed in the wells containing Glc lipids and SGal polymers after three washes (Fig. 2.5). This specificity is identical to

that observed in the previous well-binding glycopolymer study.⁵ Additionally, significant emission was observed in wells containing neutral polymers and glucose lipids. Although these values are much lower than those observed in the SGal-Glc wells the values are higher than those observed in the mannose or galactose coated wells suggesting that there may be some non-specific interaction between the polymers and the glucose wells. This result was also observed in the previous study to a lesser degree. Additional washes resulted in an eventual decrease in emissions from glucose wells containing neutral polymers and those containing SGal polymers.

2.4.3.2 Well-binding assays: normal method. Results of changing lipid concentration.

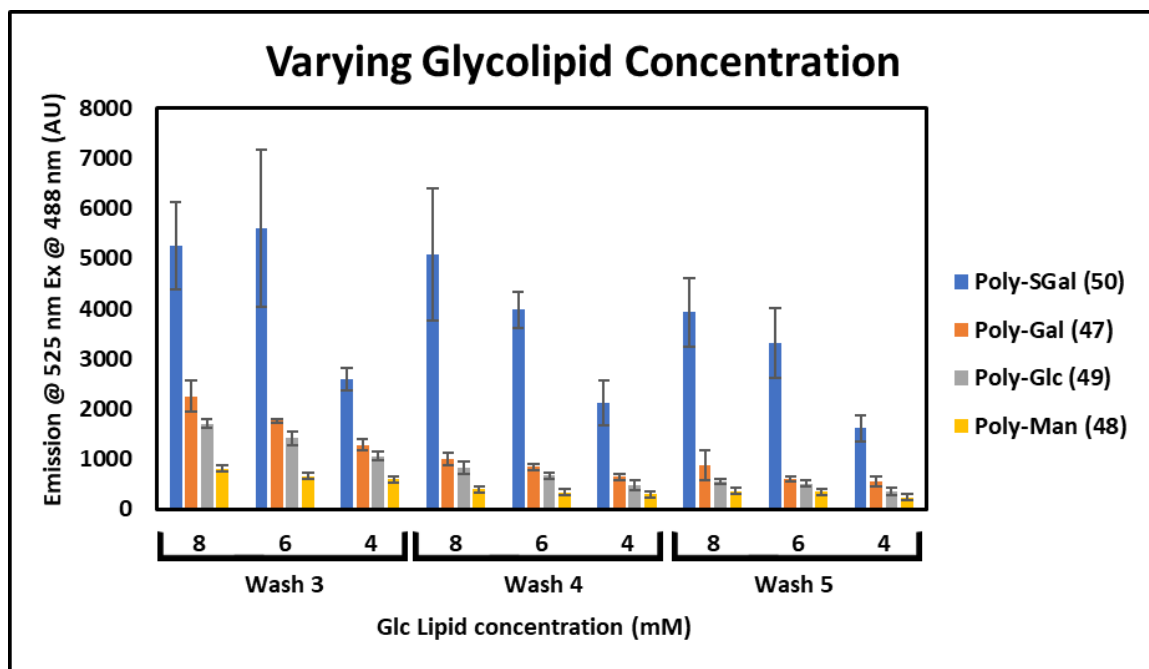


Figure 2.6: Results from binding assays using 8, 6, and 4 mM Glc glycolipid in well incubated with 2 μ M fluorescein labeled glycopolymers (080417glcmlitconc.xls)

An experiment was performed using wells containing glucose lipid concentrations of 8, 6, and 4 mM to attempt to reduce the non-specific interactions between the neutral polymers and the wells containing glucose lipids (Fig 2.6). In the wells containing 8 and 6 mM Glc lipid concentrations the strongest emissions were again observed in the SGal-Glc wells while lesser,

but still significant emissions were observed for wells containing neutral polymers. At 4 mM lipid, the emissions of the SGal-Glc wells are significantly reduced suggesting a loss of specificity. Additional washes resulted in an eventual decrease in emissions from glucose wells containing neutral polymers and those containing SGal polymers.

2.4.3.3 Well-binding assays: normal method. Results of changing polymer concentration.

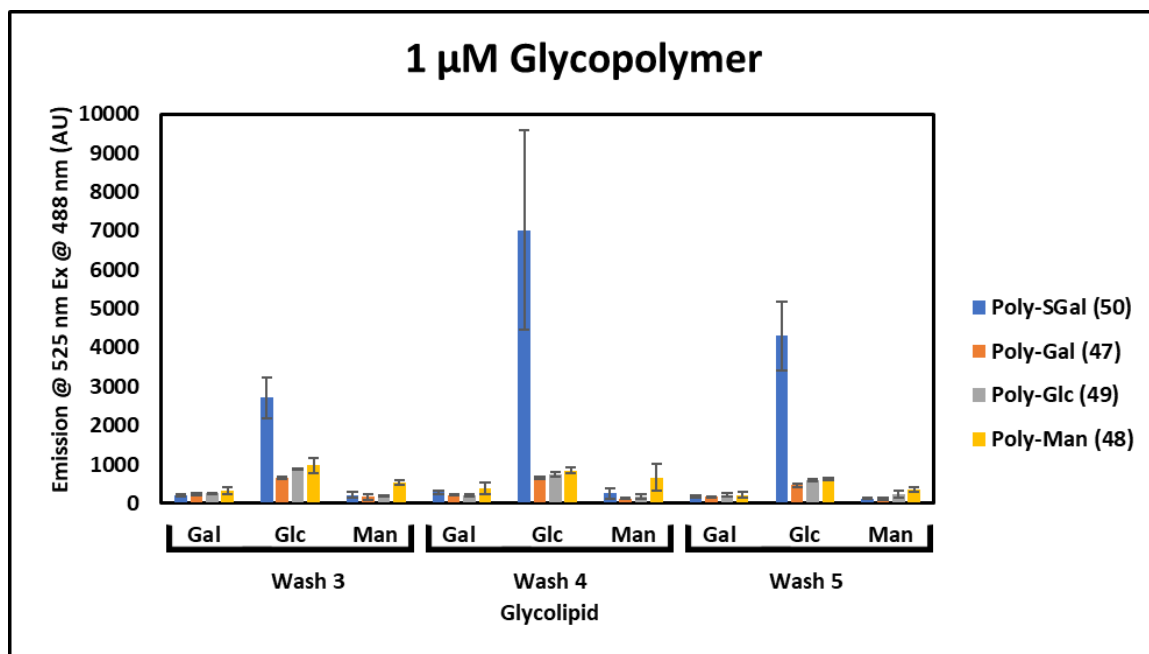


Figure 2.7: Results from binding assays using 10 mM glycolipid in well incubated with 1 μM fluorescein labeled glycopolymers (082017exp71mGlycopolymer.xls)

Continuing the effort to reduce the non-specific interactions between the neutral polymers and the wells containing glucose lipids an experiment was performed using 1 μM solutions of glycopolymers (Fig. 2.7). The strongest emissions were again observed in the SGal-Glc wells while lesser, but still significant emissions were observed for wells containing neutral polymers. Surprisingly, the intensity of the emission from the SGal-Glc wells for the 3rd wash was much lower than those observed in the 4th wash. This may be due to some lag-time in the release of polymer that is bound to the plate into buffer solution for the 3rd wash, thus attenuating the fluorescence

signal. When multiple scans of the 3rd wash are taken (approximately 15 min apart) the strength of the emission signal increases indicating that more polymer has been released into the buffer over time (Fig 2.8).

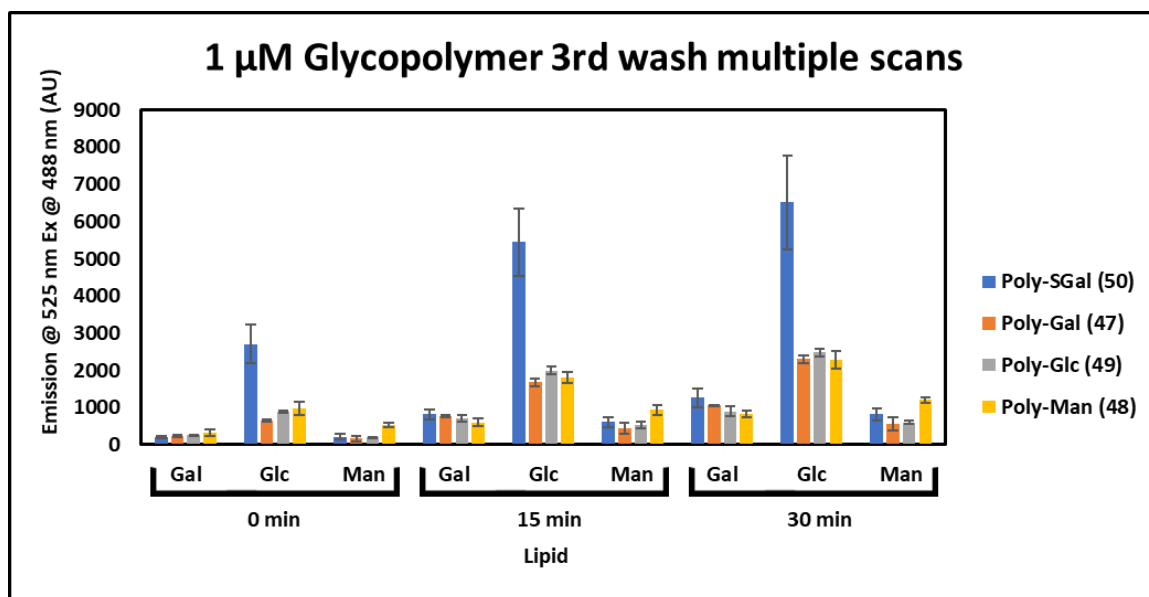


Figure 2.8: Results from binding assays using 10 mM glycolipid in well incubated with 1 μM fluorescein labeled glycopolymers. Three scans taken approximately 15 min apart. (082017exp71mMglycopolymer.xls)

2.4.3.4 Well-binding assays: normal method. Results with 2% BSA in the glycopolymer solution

In the well binding experiments performed using nanoparticles, BSA was included in the nanoparticle solution to prevent non-specific interactions between the nanoparticles and the plate.⁶ Therefore, we prepared polymer solutions with 2% BSA (w/v) solution in PBS to use in this experiment (Fig. 2.9) in an attempt to reduce non-specific binding. The strongest emissions were again observed in the SGal-Glc wells while lesser, but still significant emissions were observed for wells containing neutral polymers. Additional washes resulted in an eventual decrease in emissions from glucose wells containing neutral polymers and those containing SGal polymers.

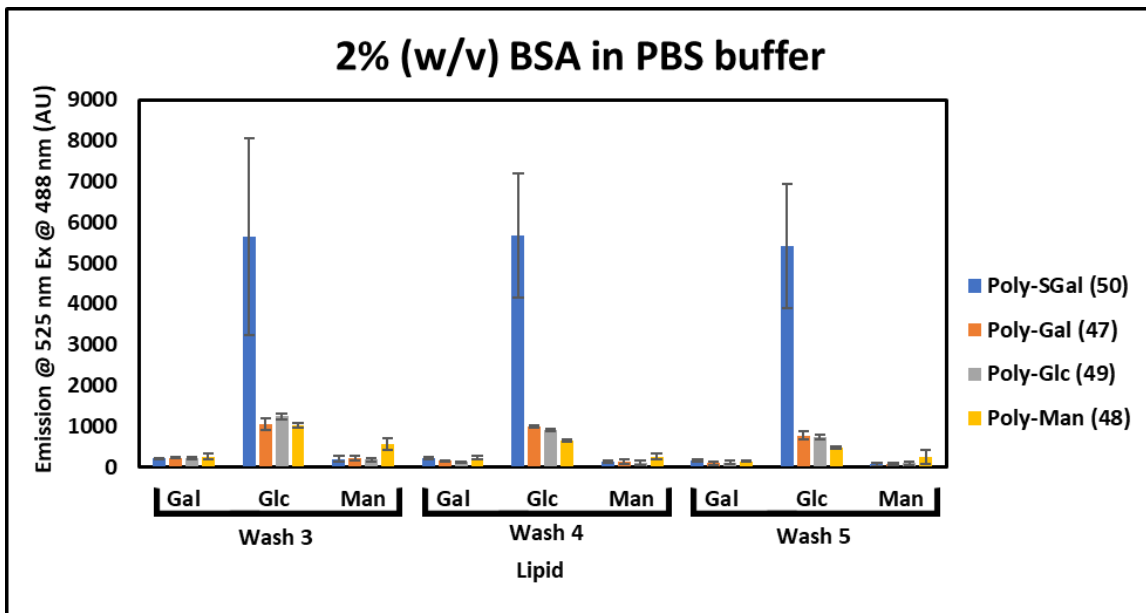


Figure 2.9: Results from binding assays using 10 mM glycolipid in well incubated with 2 μ M fluorescein labeled glycopolymers in 2% (w/v) BSA in PBS buffer (080917exp6.xls)

2.4.3.5 Well-binding assays: normal method. Results from performing experiments with calcium

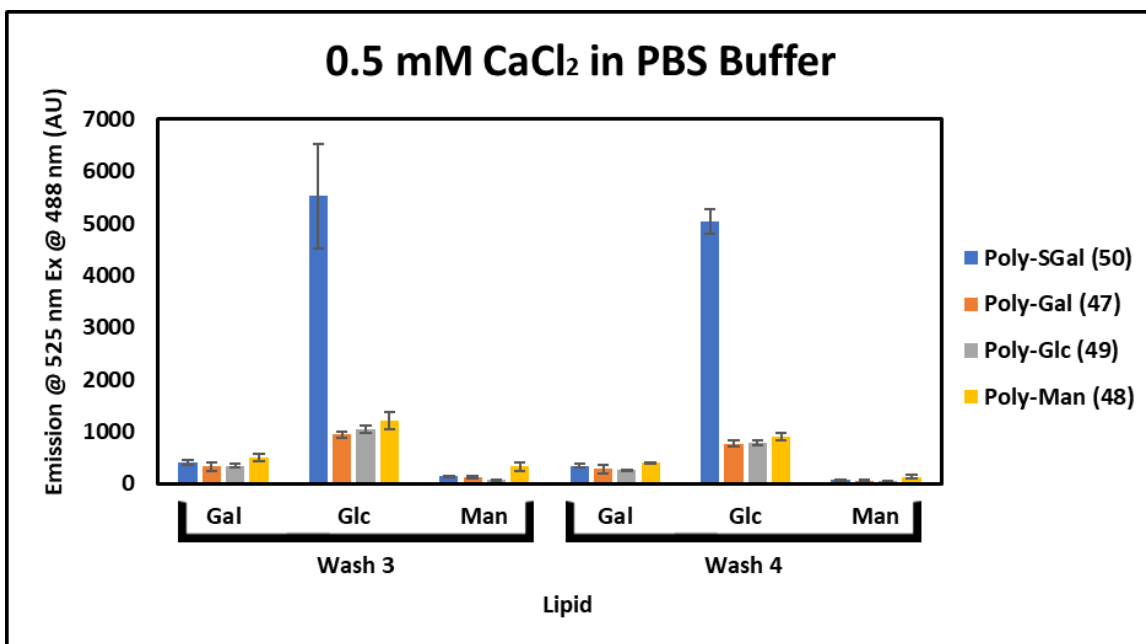


Figure 2.10: Results from binding assays using 10 mM glycolipid in well incubated with 2 μ M fluorescein labeled glycopolymers in 0.5 mM CaCl₂ in PBS buffer (092617exp14calcium.xls)

While the role of calcium in the myelin CCl₁s is not very well understood some studies suggest that the Ca²⁺ ion may play a role in mediating interaction between SGal-Gal or SGal-Glc¹⁴ while others suggest it is not important.⁵⁻⁶ Therefore, an experiment was performed using a solution of PBS buffer containing 0.5 mM calcium chloride to determine if the presence of calcium will affect the binding specificity of the glycopolymers (Fig 2.10). The strongest emissions were again observed in the SGal-Glc wells, while much less intense emissions were observed for wells containing neutral polymers.

2.4.4 Well-binding assays: methanol wash.

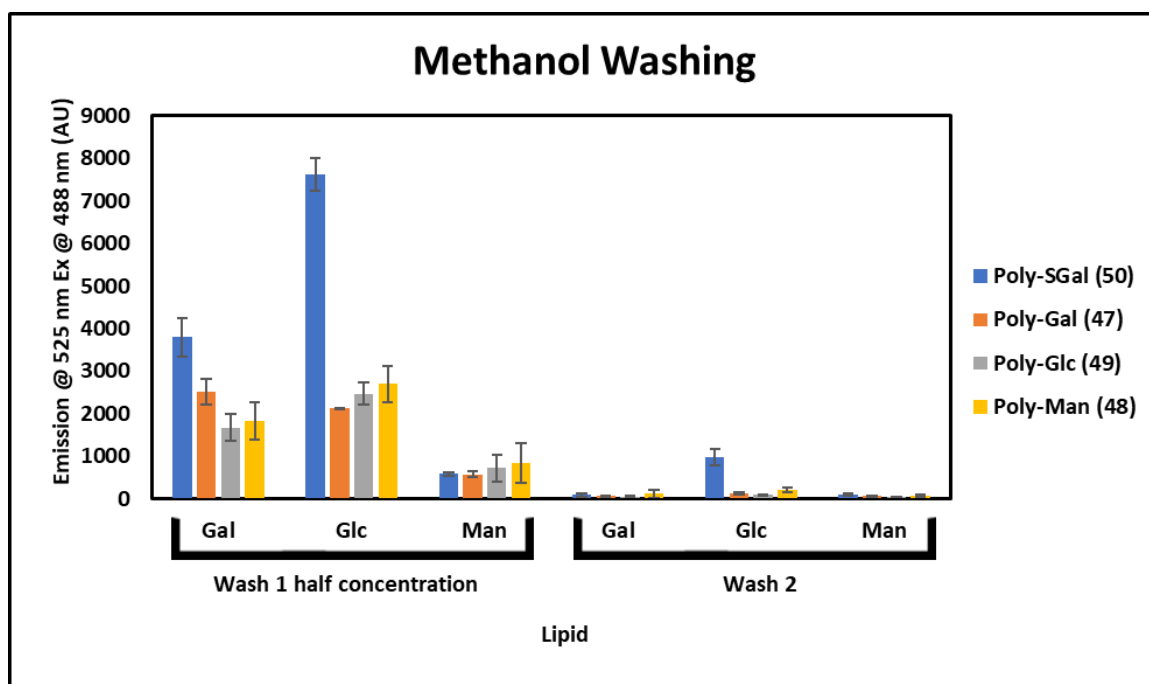


Figure 2.11: Results from binding assays using 10 mM glycolipid in well incubated with 2 μ M fluorescein labeled glycopolymers after washing with methanol (082917exp7meohwash.xls)

Based on the SGal-Glc specificity observed in our well-binding experiments it appears that moving from a nanoparticle to a polymer model system has influenced the specificity of the interaction. To further confirm the specificity of the interaction, we decided to evaluate some technical aspects of the well-binding experiments. Since this is a binding assay, the strength of interaction

is determined by the amount of polymer that adheres to the lipid coated well. However, the quantification of polymer remaining is obtained by detection of fluorescence in solution. It is possible that the binding interactions of other polymers in other wells is stronger than that observed for SGal-Glc, but the polymers become insoluble when interacting with the plate and do not go back into solution after the buffer wash. This would result in no fluorescence response for these bound polymers, and an inaccurate representation of binding specificity.

One technique that was used to address this issue was the use of a methanol wash on plates that had already been used to evaluate well-binding via the normal method. The expected result was that methanol would cause the lipids to become released from the plate, thus freeing all bound polymer.

To perform the methanol wash experiments methanol was added to the wells of a plate that had already undergone five rounds of washing with PBS buffer. Upon scanning the plate, a global increase in fluorescence was observed indicating that a large amount of polymer had been released from all the wells (Fig 2.11). Since some of the readings were over the detection limits of the instrument, the samples were diluted by half and the plate was scanned again. The fluorescence readings from wells containing Gal lipids were comparable to the values for the neutral polymers in the wells containing the Glc lipids. There is perhaps even a slight SGal-Gal specificity observed in the Gal wells when compared to fluorescence for neutral polymers and the Gal wells. A second methanol wash resulted in emissions readings that showed only appreciable fluorescence in wells containing SGal-Glc although the values are much lower than had been observed in other experiments.

2.4.5 Well-binding assays: Inverted method

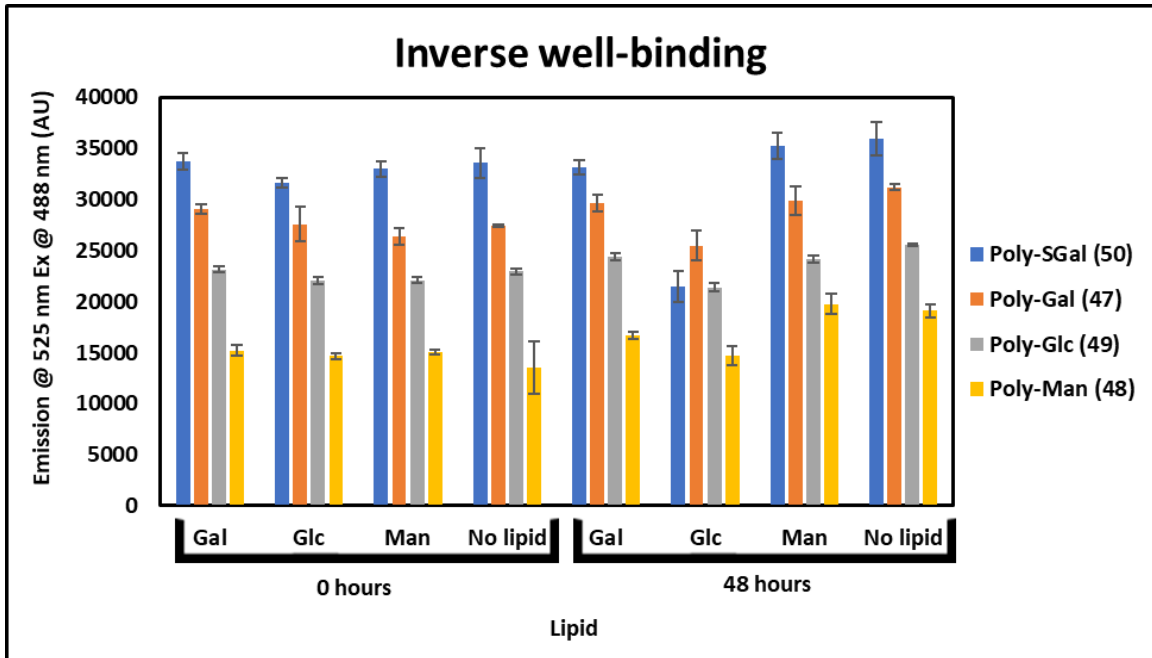


Figure 2.12: Results from inverse binding assays using 10 mM glycolipid in well incubated with 0.5 μ M fluorescein labeled glycopolymers (091117exp13inverseparafilmed.xls and 091117exp13inverseparafilmed48hrs.xls)

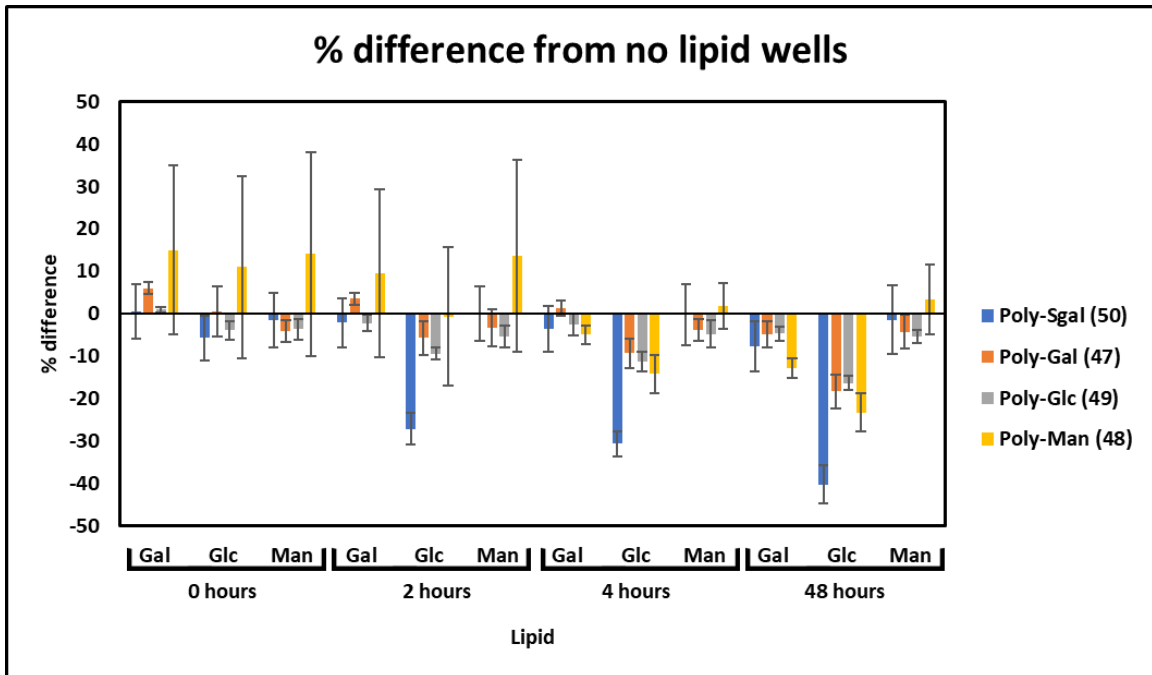


Figure 2.13: Comparison of results from inverse binding assay wells containing lipid with negative control wells containing no lipid. (091117exp13inverseparafilmed.xls and 091117exp13inverseparafilmed48hrs.xls)

Based on the results of the methanol wash experiment it seemed that some glycopolymer had clearly been adhered to the wells containing each glycolipid. To gain a better understating of the

quantity of polymer that is being bound to the wells we performed “inverted” well binding experiments. In these experiments, the plates were prepared as previously discussed with the exception that one set of wells were prepared without any lipid. Then, polymer was added and a scan was taken. The plate was then allowed to incubate for 2 hours, and another scan was taken. Additional scans were taken at 4 and 48 hours (Fig. 2.12). All wells displayed fluorescence, but it was clear that the emissions values for the SGal-Glc wells decreased over time. When emissions values for the polymers in the lipid wells were compared to emissions in the lipid free control wells it was clear that the largest decrease in fluorescence was observed in wells containing SGal-Glc (Fig. 2.13). Significant decreases were also observed for wells containing neutral polymers and wells containing Glc lipid at 2 and 4 hours. The fluorescence readings for the plate at 48 hours show an even more pronounced decrease in fluorescence from wells containing Glc lipid. There is also a small decrease in fluorescence observed in wells containing Gal lipids. This data indicates that the strongest interaction is again occurring between SGal polymers and Glc lipid coated wells since the strongest decrease in emissions is related to the most polymer coming out of solution as it adheres to the lipid coated well.

2.4.6 Well-binding conclusions

The well-binding experiments described here indicate that the strongest interaction occurs between wells containing Glc lipid and the SGal functionalized polymers. There is some apparent interaction taking place between the neutral polymers and the Glc lipid wells, but emissions are lower than are observed for the SGal-Glc wells, and decrease with additional washing. Changing variables such as lipid concentration, glycopolymer concentration, or the inclusion of BSA or calcium in the buffer has some effect on the observed emissions intensities, but does not result in a change in the SGal-Glc binding specificity observed while using glycopolymer model systems. Upon washing with methanol, a release of bound polymer was observed in all wells, but the most

intense emissions were again observed in the SGal-Glc wells. Inverted well-binding experiments also demonstrated that the decrease in emissions was strongest for the SGal-Glc wells indicating SGal-Glc specificity.

Table 2.1: Summary of the emission values obtained in the well-binding experiments

Conditions Lipids	Polymer	Wash 3			Wash 4			Wash 5		
		Gal	Glc	Man	Gal	Glc	Man	Gal	Glc	Man
10 mM lipid, 2 μ M polymer	SGal (50)	220	5109	513	147	5109	133	371	3041	166
	Gal (47)	242	1358	227	133	1358	100	92	602	118
	Glc (49)	370	1945	463	256	1945	152	157	873	158
	Man (48)	236	1653	318	192	1653	160	119	590	111
8 mM lipid, 2 μ M polymer	SGal (50)		5251			5075			3926	
	Gal (47)		2254			1002			878	
	Glc (49)		1709			838			545	
	Man (48)		810			399			367	
6 mM lipid, 2 μ M polymer	SGal (50)		5602			3983			3318	
	Gal (47)		1763			842			596	
	Glc (49)		1416			672			516	
	Man (48)		664			335			350	
4 mM lipid, 2 μ M polymer	SGal (50)		2601			2119			1622	
	Gal (47)		1280			649			546	
	Glc (49)		1058			473			348	
	Man (48)		600			301			239	
10 mM lipid, 1 μ M polymer	SGal (50)	195	2709	213	284	7020	258	179	4294	125
	Gal (47)	241	660	167	217	655	121	179	461	114
	Glc (49)	265	887	197	207	740	170	209	592	234
	Man (48)	328	978	522	391	844	664	215	616	351
10 mM lipid, 2 μ M polymer, 2% BSA	SGal (50)	218	5639	193	212	5669	119	166	5417	75
	Gal (47)	222	1059	218	158	995	125	92	776	81
	Glc (49)	226	1245	179	127	912	109	111	738	94
	Man (48)	261	1034	566	228	638	262	134	488	239
10 mM lipid, 2 μ M polymer, 0.5 mM CaCl ₂	SGal (50)	405	5523	135	343	5032	72			
	Gal (47)	333	938	120	285	765	47			
	Glc (49)	343	1049	71	253	782	42			
	Man (48)	504	1210	328	401	894	131			
		Wash 3	0 min		Wash 3	15 min		Wash 3	30 min	
		Gal	Glc	Man	Gal	Glc	Man	Gal	Glc	Man
10 mM lipid, 1 μ M polymer Additional scans of wash 3	SGal (50)	195	2709	213	823	5454	608	1261	6516	824
	Gal (47)	241	660	167	771	1684	449	1066	2306	561
	Glc (49)	265	887	197	717	1999	542	894	2488	603
	Man (48)	328	978	522	606	1813	946	826	2282	1203
		Wash 1	Half-conc.		Wash 2				Key	
		Gal	Glc	Man	Gal	Glc	Man			
10 mM lipid, 1 μ M polymer	SGal (50)	3792	7618	585	90	974	92		High	
Post wash 5 methanol wash	Gal (47)	2512	2117	567	55	118	55		Medium	
	Glc (49)	1665	2460	724	38	98	29		Low	
	Man (48)	1824	2691	835	113	194	66			

These results (Table 3.1) suggest that a specific SGal-Glc CCI occurs for systems containing glycopolymers and glycolipid coated wells. As previously discussed there is evidence for the existence of a SGal-Glc CCI, but these glycopolymer model systems and those prepared by Okoth et al. represent the first instance of a system that is specific for SGal-Glc and displays little or no binding affinity for SGal-Gal.

2.5 Isothermal titration calorimetry

Isothermal titration calorimetry (ITC) is a technique that has been used to determine thermodynamic parameters and binding constants for various ligand-receptor interactions. As previously mentioned this technique was used with some

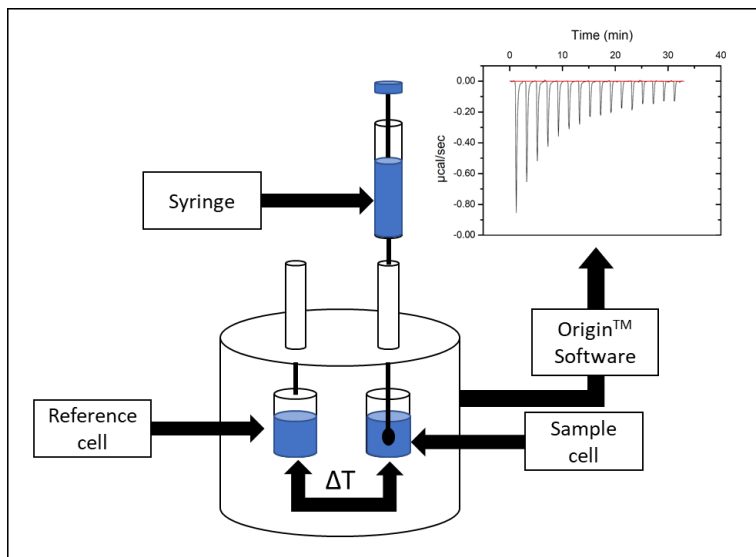


Figure 2.14: Schematic of a typical isothermal titration calorimeter

degree of success to characterize the Le^x - Le^x CCl.¹⁶ The ITC instrument (Fig 2.14) consists of two insulated cells in which the temperature is monitored by a very sensitive thermostat.²⁶ In a typical ITC experiment, one cell is loaded with buffer to serve as a reference cell and the other is loaded with the receptor molecule dissolved in buffer. A solution of ligand is then loaded into a syringe. The concentration of the ligand is usually 10-20 times greater than the concentration of the receptor to ensure that the receptor will be completely saturated with ligand at the end of the experiment. Aliquots of the ligand solution are then injected into the cell containing the receptor. If there is an interaction between the receptor and the ligand, heat will be either released or absorbed and the temperature of the cell will change. This change will be detected as a difference in temperature between the sample cell and the reference cell. The thermostat will eventually equilibrate the temperatures between the cells and another injection will occur. As more injections occur, more ligand is bound to receptor, and eventually the receptor starts to become saturated with ligand. This results in a decrease in the magnitude of change in heat with each injection until the receptor is completely saturated and no more binding can occur. A titration is also performed with ligand being injected into a well containing only buffer. The heats obtained

from these injections arise from the heat of dissolution of the ligand and are subtracted from the values obtained in the experiment performed with ligand and receptor.^{26, 28}

$$A + B \rightleftharpoons AB \quad \text{Eq. 3.1} \quad \Delta H = \frac{q_1}{v_{\text{cell}} * \Delta[A]_{\text{bound}}} \quad \text{Eq. 3.2}$$

$$Q = \frac{n * [B]_{\text{total}} * \Delta H * v_{\text{cell}}}{2} * \left[1 + \frac{[A]_{\text{total}}}{n * [B]_{\text{total}}} + \frac{1}{n * [B]_{\text{total}} * K_A} - \left(\left(1 + \frac{[A]_{\text{total}}}{n * [B]_{\text{total}}} + \frac{1}{n * [B]_{\text{total}} * K_A} \right)^2 - \frac{4[A]_{\text{total}}}{n * [B]_{\text{total}}} \right)^{1/2} \right] \quad \text{Eq. 3.3}$$

$$K_D = \frac{1}{K_A} \quad \text{Eq. 3.4} \quad \Delta G = -RT \ln(K_D) \quad \text{Eq. 3.5} \quad \Delta S = \frac{-(\Delta G - \Delta H)}{T} \quad \text{Eq. 3.6}$$

Figure 2.15: ITC equations

The heat released or absorbed for each interaction is then calculated by the instrument's software, and this data is used to calculate the enthalpy (ΔH) and association constant (K_a) for the equilibrium depicted in eq. 3.1 (Fig 2.15). The value of ΔH can be calculated using the values for the heat of the first injection (q_1), the volume of the cell (v_{cell}), and the change in concentration of bound ligand

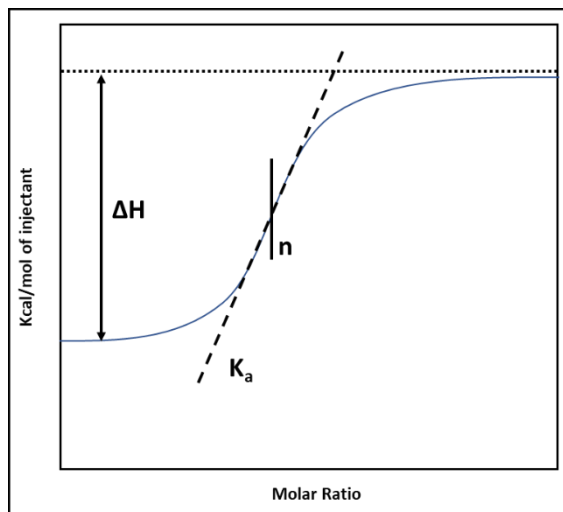


Figure 2.16: Graphical representation of the ITC parameters

($\Delta[A]_{\text{bound}}$) using equation 3.2 (Fig 2.15). This value can only be accurately calculated if all of the ligand from the first injection is bound, i.e. if $\Delta[A]_{\text{bound}} = \Delta[A]_{\text{total}}$.²⁸ The value of K_a is calculated by fitting the binding model described by equation 3.3 (Fig 2.15) to the isotherm constructed by plotting the heat measurements obtained for each injection against the molar ratio of ligand to receptor for each injection. In this equation Q is the total heat of the titration, $[B]_{\text{total}}$ is the total

concentration of receptor and n is the number of binding sites.²⁹ This binding model is for a one-to-one receptor-ligand binding interaction, more complicated binding situations require more complex binding models.²⁸ These parameters are represented graphically in figure 2.16. Additionally, the number of binding sites (n) is represented as the molar ratio at which inflection occurs. Once ΔH and K_a values are determined they can be used to calculate dissociation constant (K_d), Gibbs' free energy (ΔG), and entropy (ΔS) using equations 3.4-3.6 (Fig 2.15).²⁸

The binding isotherm must be properly sigmoidal shaped (Fig 2.18b) to allow for proper calculation of n ,

$$c = K_a * [A]_{total} * n \quad \text{Eq. 3.7}$$

Figure 2.17: c -values calculation

ΔH , and K_a . A weak binding interaction can give rise to an isotherm that immediately changes after the initial injection (Fig. 2.18c). This type of isotherm cannot be used to calculate ΔH , because the assumption that $\Delta[A]_{bound} = \Delta[A]_{total}$ cannot be made since the affinity of the receptor is too weak to form complex with all the injected ligand over the first couple of injections at the given concentration. However, reasonably accurate values for K_a can still be obtained if the binding model can still be fit to the data.²⁶ If the binding interaction is too strong, then the slope of the curve will be too steep (Fig. 2.18a) to apply the binding model thus preventing calculation of K_a . However, ΔH and n can still be calculated using such an isotherm. The shape of the binding isotherm is determined by the unitless parameter c which is defined by equation 3.7 (Fig 2.17).²⁶ Usually, isotherms with c -values between 10 and 100 are ideal for determination of ΔH and K_a . The concentration of the ligand and receptor can be changed to obtain a desirable c -value, however the degree to which concentration can be increased may be limited by the solubility of the ligand and receptor.

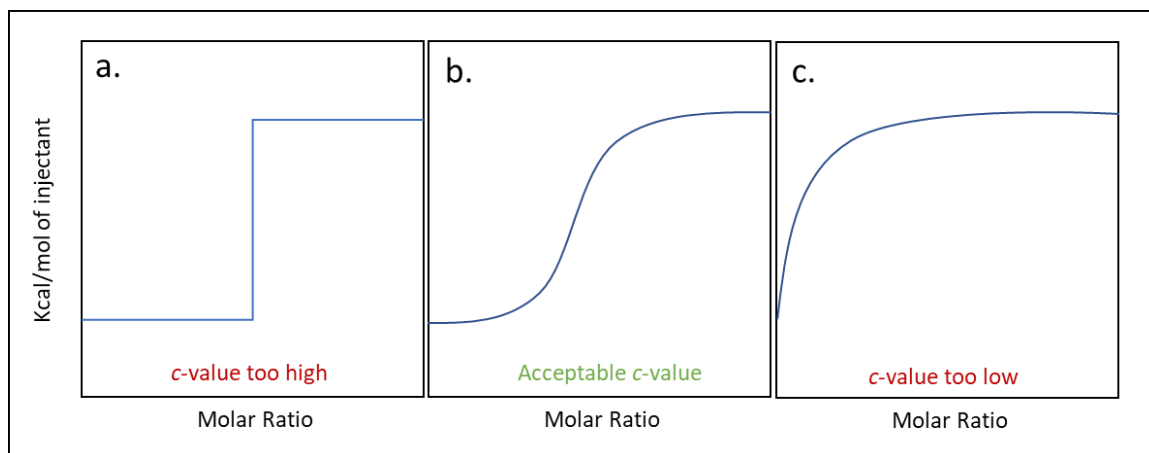


Figure 2.18: Effect of c-values on ITC binding isotherms

2.5.1 ITC experiments with 30-mer glycopolymers

Initial ITC experiments were performed using 30-mer glycopolymers (**43, 45, and 46** $n \sim 30$) to characterize the interaction of SGal polymers with the neutral polymers. Since the SGal polymer is a negatively charged polymer it has a higher water solubility than the neutral polymers. Therefore poly-SGal was selected to serve as the ligand and the neutral polymers were selected to serve as the receptors. Since it is typical for ITC experiments to be performed at millimolar concentrations when a low heat of interaction is expected²⁶ the SGal-polymer was loaded into the syringe at a concentration of 3.33 mM (100 mM in sugar residues) in PBS buffer and the neutral polymer was loaded into the sample cell at a concentration of 0.33 mM (10 mM in sugar residues) in PBS buffer. Each titration was run with 16 injections of a 2 μ L volume of SGal into a sample cell containing 200 μ L of neutral polymer solution. The results from the ITC experiments indicate that a binding interaction is occurring because of the observation that heat change decreases with additional injections indicating that saturation is occurring. However, the isotherms resulting from these experiments were not sigmoidal shaped and were characteristic of an isotherm with low c-values, so ΔH could not be calculated. Also, large uncertainty values were associated with the K_a

values. This data suggests that the binding interaction is too weak to be characterized using the 30-mer glycopolymers.

2.5.2 ITC experiments with 90-mer glycopolymers

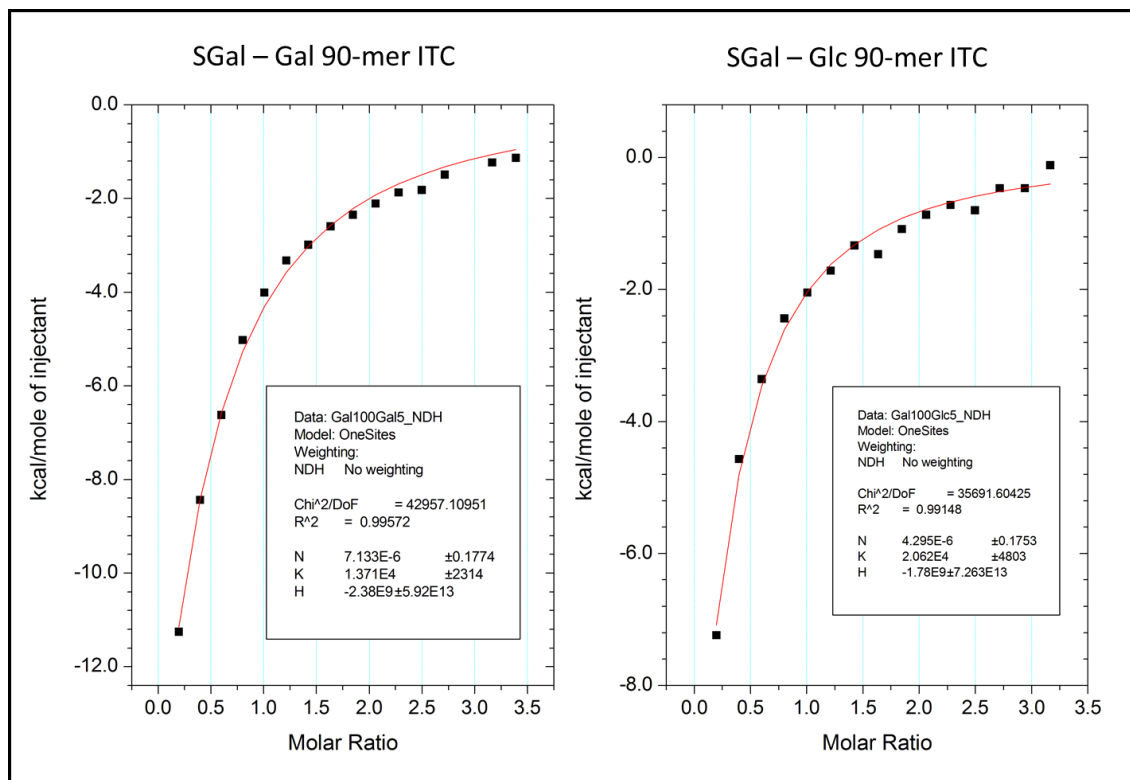


Figure 2.19: Results from the 90-mer ITC Experiments (sgalgal.opj and sgalglc.opj)

ITC experiments were performed using longer glycopolymers (**43, 45, and 46** $n \sim 90$) in an attempt to increase the strength of the interaction by increasing the valency of the model system, and produce ITC data with a more ideal c -value. SGal-polymer was loaded into the syringe at a concentration of 1.11 mM (100 mM in sugar residues) in PBS buffer and the neutral polymer was loaded into the sample cell at a concentration of 0.06 mM (5 mM in sugar residues) in PBS buffer. Results from these ITC experiments again indicate that binding was occurring when SGal was injected into Gal and Glc polymer solutions (Fig 2.19). The shapes of these isotherms are still characteristic of low c -values, so n and ΔH could not be accurately calculated. However, K_d values

are calculated by fitting the binding model to the data. The K_a value obtained for the SGal-Glc experiment ($2.06 \cdot 10^4 \text{ M}^{-1}$) is higher than the value obtained for SGal-Gal ($1.37 \cdot 10^4 \text{ M}^{-1}$), suggesting that the SGal-Glc interaction is the stronger of the two. However, control experiments are still needed to confirm that the interactions observed by ITC are resulting from CCI and not some other nonspecific binding interaction that occurring between the polymers. Such experiments could be performed using neutral polymers functionalized with non-interacting carbohydrates, or some other type of non-sugar functionality that does not interact with SGal.

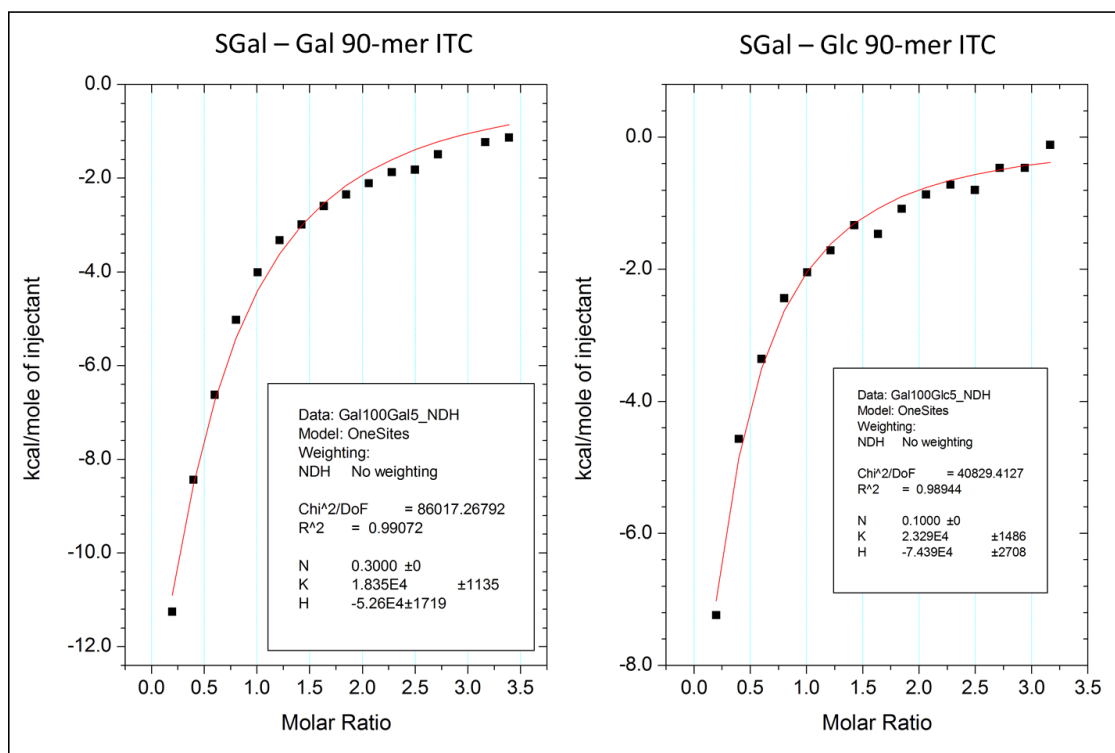


Figure 2.20: Results from the 90-mer ITC Experiments with fixed n value

The values for n and ΔH given by the curve fit are clearly not accurate. Values for n are extremely low ($\sim 10^{-6}$) and ΔH values are unreasonably high ($\sim 10^6$ kcal/mol, biological interactions rarely exceed 30 kcal/mol) and the uncertainties are several orders of magnitude above the reported values. However, n can be fixed to a more reasonable value, such as 0.3 or 0.1 and provide a

reasonable fit of the binding model with $R^2 \sim 0.99$. For the SGal-Gal experiment when the value of n is changed from 7.133×10^{-6} to 0.3 the value of K_a changes from $1.37 \times 10^4 \text{ M}^{-1}$ to $1.84 \times 10^4 \text{ M}^{-1}$ a 34% increase. For the SGal-Glc experiment when the value of n is changed from 4.295×10^{-6} to 0.1 the value of K_a changes from $2.06 \times 10^4 \text{ M}^{-1}$ to $2.33 \times 10^4 \text{ M}^{-1}$ a 13% increase. These results show that increasing the value of n by several orders of magnitude has only slightly increased the values of K_a in comparison indicating that the observed K_a are reasonable for a wide range of n values. Fixing the value of n also provides a more reasonable value for ΔH . Although the values for n and ΔH have been altered by many orders of magnitude the values for K_a have remained relatively the same. This shows that the values of K_a are not affected much by large variations in n and ΔH , and therefore the range of values obtained for K_a from n values of 0.1 (for SGal-Glc) or 0.3 (for SGal-Gal) to values of n that are near zero are essentially an accurate representation of the K_a for the interaction.³⁰

The values for K_a of the 90-mer glycopolymers are in the range of 10^4 M^{-1} . K_a values in the range of 10^5 - 10^6 M^{-1} were reported for other CCIs by SPR experiments performed using nanoparticle²⁷ and BSA glycoconjugate²² model systems. Since the K_a values reported for the ITC experiments are within 1-2 orders of magnitude of those observed using similar model systems it can be reasonably assumed that the glycopolymer model systems used in this study are simulating CCI in a manner similar to what was observed for other synthetic model systems.

The experimental values obtained for K_a were used in a simulation (ITCsim, MicroCal) to calculate c -values for these isotherms. The estimated c -values for the SGal-Gal and SGal-Glc ITC isotherms are 0.7 and 1.2 respectively. Therefore, a concentration increase of at least ten-fold would be required to yield acceptable c -values for these interactions. Since the neutral glycopolymers already experience solubility issues above 0.55 mM increasing this value to a minimum of 1.11 mM is unlikely to be achieved using the current system. Also, the SGal-PBS buffer blank titrations

show endothermic peaks which are likely due to a buffer mismatch that can be caused by slight differences in the salt concentrations between the sample containing buffer and the pure buffer. Buffer matching can be problematic when preparing samples by dissolving solid material in buffer, but can be avoided by dialyzing sample solutions in buffer and then saving that buffer for later use in experiments.²⁶

2.5.3 ITC Conclusions

An effort was made to characterize myelin CCI by performing ITC experiments using glycopolymers as model systems. Experiments performed using 30-mer glycopolymers showed some evidence of a CCI, but the weak association constants of the interactions resulted in c -values that were too low for accurate determination of ΔH . Increasing the length of the glycopolymers improved the strength of the interaction, but still the K_a was too low to provide a properly sigmoidal shaped isotherm at the given concentrations. A ten-fold increase in polymer concentration would likely be necessary to achieve an acceptable c -value and allow for proper determination of ΔH .

Higher concentrations could be achieved by redesigning the polymer systems to allow for a more water-soluble model system. The backbone of the polymer is hydrophobic, so introducing additional heteroatoms into the backbone, or using more hydrophilic linkers could provide a more water-soluble polymer. Also, designing a linker that would allow multiple carbohydrate moieties to be attached to each monomer could result in glycopolymers that are not only more water soluble, but also have increased avidity.

There are also several additional factors to consider when moving forward with ITC experiments. There should be a negative control polymer developed for these experiments to confirm that the interaction is truly a CCI and not a non-specific interaction occurring between the polymer

backbones. Such a negative control would likely consist of a PEG, or polyol functionalized polymer. Also, a limitation of this technique is that we assume one-to-one binding between the carbohydrate moieties of the glycopolymers which is unlikely given that most it would require all polymers to be the same length, and have all the sugars interacting at the same time.

2.6 Conclusions

In conclusion, we have investigated the CCl_s that are believed to mediate myelin compaction using glycopolymer model systems in conjunction with well-binding fluorescence assays, isothermal titration calorimetry, and UV-Vis spectroscopy. Well-binding experiments demonstrate that glycopolymer model systems display a strong SGal-Glc specificity, even when a very short linker is used. ITC experiments demonstrated that an interaction between polymers is observed, however weak association constants and the solubility limitations of the glycopolymers prevented the full characterization potential of this technique from being realized. The results are encouraging and suggest that a more water soluble glycopolymer may be utilized to provide a quantitative characterization of CCl_s.

2.7 Supporting information

PBS Buffer

1 L of 1x phosphate buffered saline (pH 7.4) buffer was prepared by first combining NaCl (8.0 g, 0.137 mol), KCl (0.2 g, 0.0027 mol), Na₂HPO₄ (1.44 g, 0.010 mol), KH₂PO₄ (0.24 g, 0.0018 mol), and Millipore water (800 mL). The pH was then adjusted to 7.4 using HCl and the volume of the solution was raised to 1 L by adding additional Millipore water (200 mL). The pH was measured again and further adjusted if a value different than 7.4 was observed.

Well binding: plate preparation

A black 96 well plate (OptiPlate-96F Black, Flat-bottomed, PerkinsElmer) was soaked in a MeOH bath. After 1 hr. the plates were removed and rinsed with MeOH and air dried for 30 minutes. 50 μ L of a 10, 8, 6 or 4 mM solution of glycolipid **51**, **52** or **53** in MeOH (warmed at 50 °C to dissolve) was pipetted into the wells and the solvent allowed to evaporate for 4 h on the bench top. 160 μ L of blocking solution (10% w/v BSA in PBS pH 7.4) was added to the wells and incubated overnight. The BSA used in these experiments was obtained from Sigma-Aldrich as a lyophilized powder (96%, agarose gel electrophoresis). The wells were then washed with 160 μ L PBS buffer twice. All experiments were performed using a Tecan Safire microplate reader. Fluorescence readings were obtained using 488 nm as the excitation wavelength and 525 as the emission wavelength. Excitation and emission bandwidths were both set to 2.5 nm. Number of flashes was set to 10. Lag time was set to 0 μ s. Integration time was set to 40 μ s. There were 9 reads per well taken in a 3 x 3 square pattern. Z-position was automatically calculated from well A1 (SGal polymer-Gal lipid). Gain was set automatically using well A1 (SGal polymer-Gal lipid) as a reference. This resulted in gain being set to 200 for the washes 3-5 in each experiment. The gain values set for washes 0-2 are different and therefore emissions reading cannot be compared to those obtained for wells 3-5. In the future, it might be better to manually set gain to ensure consistency in emissions reading for every experiment.

Well-binding assays: normal method

80 μ L of buffer (PBS, 2% BSA (w/v) in PBS, or 1 mM CaCl₂ in PBS) was added to the wells followed by 80 μ L of 2 μ M or 4 μ M fluorescein labeled glycopolymers **47-50** in PBS. The plate was wrapped tightly in aluminum foil and incubated for 4 hrs. on the bench top in the hood. After incubation, the emission from each well was recorded (0 wash) then the wells were washed as followed; the binding solution in the well was removed by quickly turning the plates upside down and shaking to pour out the solution followed by adding 160 μ L of PBS or Tris buffer or 0.5 mM CaCl₂ in PBS

and the emission from each well recorded (1st wash). The washing was repeated to give 2nd, 3rd, 4th and 5th wash emissions. The binding experiments were carried out in three different wells on each plate and the bar graphs below are averages of the absorbance from the wells with the standard deviation depicted as the error bar.

Well-binding assays: methanol wash

The binding solution was removed from the plate used to perform the well-binding experiments with 1 μM glycopolymer, and 160 μL of methanol was added to each of the wells. Initial emissions readings were too high for detection, so 80 μL of solution were removed from each well and the remaining solution was diluted with an additional 80 μL of methanol and the plate was scanned. The solution was then washed again with 160 μL of methanol and another scan was taken.

Well-binding assays: inverse method

The plates were prepared as previously described with the exception that one set of wells were prepared without any glycolipid. 80 μL of buffer (in PBS) was added to the wells followed by 80 μL of 1 μM fluorescein labeled glycopolymers **47-50** in PBS. An emissions scan was taken immediately. The plate was wrapped tightly in parafilm then was wrapped in aluminum foil. Additional scans were taken at 2, 4, and 48 h.

ITC experiments

All experiments were performed using a MicroCal iTC200 isothermal titration calorimeter using Origin ITC analysis software. The sample cell, reference cell, and syringe were all washed three times using PBS buffer (pH 7.4). For each experiment 40 μL of Poly-SGal (**46**) solution (1.11 mM for 90-mer and 3.33 mM for 30-mer, to give sugar concentration of 100 mM for both) was loaded into the syringe. 200 μL of Poly-Gal (**43**) and Poly-Glc (**45**) (0.06 mM for 90-mer to give sugar

concentration of 5 mM and 0.33 mM for 30-mer, to give sugar concentration of 10 mM) were added to the sample cell using a 500 μ L Hamilton syringe. 200 μ L of PBS buffer was added to the reference cell using a 500 μ L Hamilton syringe. Experiments were run at 25 °C and with a reference power of 10. Each run consisted of 16, 2 μ L injections with each injection taking 4 s and a 120 s delay between injections and a 5 s filter time. There was also an initial 60 s delay at the beginning of the run. A blank run was also performed in which the Poly-SGal solution was injected into PBS buffer to account for the heat of dilution of the polymer. The heats of the blank run were subtracted from the heats of the binding experiments using the Origin ITC analysis software.

References:

1. Seah, N.; Basu, A., Carbohydrate– Carbohydrate Interactions. In *Wiley Encyclopedia of Chemical Biology*, John Wiley & Sons, Inc.: 2007.
2. Kiessling, L. L.; Pohl, N. L., Strength in numbers: non-natural polyvalent carbohydrate derivatives. *Chemistry & biology* **1996**, *3* (2), 71-77.
3. Hakomori, S., Carbohydrate-to-carbohydrate interaction, through glycosynapse, as a basis of cell recognition and membrane organization. *Glycoconjugate Journal* **2004**, *21* (3-4), 125-137.
4. Larsen, K.; Thygesen, M. B.; Guillaumie, F.; Willats, W. G.; Jensen, K. J., Solid-phase chemical tools for glycobiology. *Carbohydrate Research* **2006**, *341* (10), 1209-1234.
5. Okoth, R. S. O., "Probing Carbohydrate - Carbohydrate Interactions (CCIs) Using End-Labeled Glycopolymers and the Determination of Deuterium Isotope Shifts (DIS) of Selected Methyl D-Glycosides in Methanol". *Chemistry Theses and Dissertations. Brown Digital Repository. Brown University Library*. **2015**.
<https://repository.library.brown.edu/studio/item/bdr:419377/>
6. Zhao, J.; Liu, Y.; Park, H.-J.; Boggs, J. M.; Basu, A., Carbohydrate-coated fluorescent silica nanoparticles as probes for the galactose/3-sulfogalactose carbohydrate–carbohydrate interaction using model systems and cellular binding studies. *Bioconjugate Chemistry* **2012**, *23* (6), 1166-1173.
7. Fazio, F.; Bryan, M. C.; Blixt, O.; Paulson, J. C.; Wong, C.-H., Synthesis of sugar arrays in microtiter plate. *Journal of the American Chemical Society* **2002**, *124* (48), 14397-14402.
8. Bosio, A.; Binczek, E.; Stoffel, W., Functional breakdown of the lipid bilayer of the myelin membrane in central and peripheral nervous system by disrupted galactocerebroside synthesis. *Proceedings of the National Academy of Sciences* **1996**, *93* (23), 13280-13285.
9. Coetzee, T.; Fujita, N.; Dupree, J.; Shi, R.; Blight, A.; Suzuki, K.; Suzuki, K.; Popko, B., Myelination in the Absence of Galactocerebroside and Sulfatide: Normal Structure with Abnormal Function and Regional Instability. *Cell* **1996**, *86* (2), 209-219.
10. Bosio, A.; Binczek, E.; Haupt, W. F.; Stoffel, W., Composition and Biophysical Properties of Myelin Lipid Define the Neurological Defects in Galactocerebroside-and Sulfatide-Deficient Mice. *Journal of Neurochemistry* **1998**, *70* (1), 308-315.

11. Dupree, J. L.; Coetzee, T.; Blight, A.; Suzuki, K.; Popko, B., Myelin galactolipids are essential for proper node of Ranvier formation in the CNS. *Journal of Neuroscience* **1998**, *18* (5), 1642-1649.
12. Stewart, R. J.; Boggs, J. M., A carbohydrate-carbohydrate interaction between galactosylceramide-containing liposomes and cerebroside sulfate-containing liposomes: Dependence on the glycolipid ceramide composition. *Biochemistry* **1993**, *32* (40), 10666-10674.
13. Dicko, A.; Heng, Y. M.; Boggs, J. M., Interactions between glucosylceramide and galactosylceramide I3 sulfate and microstructures formed. *Biochimica et Biophysica Acta (BBA) - Biomembranes* **2003**, *1613* (1–2), 87-100.
14. Koshy, K. M.; Wang, J.; Boggs, J. M., Divalent Cation-Mediated Interaction Between Cerebroside Sulfate and Cerebroside: An Investigation of the Effect of Structural Variations of Lipids by Electrospray Ionization Mass Spectrometry. *Biophysical Journal* **1999**, *77* (1), 306-318.
15. Boggs, J. M.; Wang, H., Co-clustering of galactosylceramide and membrane proteins in oligodendrocyte membranes on interaction with polyvalent carbohydrate and prevention by an intact cytoskeleton. *Journal of Neuroscience Research* **2004**, *76* (3), 342-355.
16. de la Fuente, J. M.; Barrientos, A. G.; Rojas, T. C.; Rojo, J.; Cañada, J.; Fernández, A.; Penadés, S., Gold Glyconanoparticles as Water-Soluble Polyvalent Models To Study Carbohydrate Interactions. *Angewandte Chemie* **2001**, *113* (12), 2317-2321.
17. Chen, Q.; Cui, Y.; Zhang, T.-L.; Cao, J.; Han, B.-H., Fluorescent Conjugated Polyfluorene with Pendant Lactopyranosyl Ligands for Studies of Ca²⁺-Mediated Carbohydrate–Carbohydrate Interaction. *Biomacromolecules* **2009**, *11* (1), 13-19.
18. Reynolds, A. J.; Haines, A. H.; Russell, D. A., Gold glyconanoparticles for mimics and measurement of metal ion-mediated carbohydrate– carbohydrate interactions. *Langmuir* **2006**, *22* (3), 1156-1163.
19. Huang, H.; Rodolis, M. T.; Bhatia, S. R.; Sampson, N. S., Sugars require rigid multivalent displays for activation of mouse sperm acrosomal exocytosis. *Biochemistry* **2017**.
20. Matsuura, K.; Oda, R.; Kitakouji, H.; Kiso, M.; Kitajima, K.; Kobayashi, K., Surface Plasmon Resonance Study of Carbohydrate– Carbohydrate Interaction between Various Gangliosides and Gg3-Carrying Polystyrene. *Biomacromolecules* **2004**, *5* (3), 937-941.
21. Hernáiz, M.; de la Fuente, J.; Barrientos, A.; Penadés, S., A model system mimicking glycosphingolipid clusters to quantify carbohydrate self-interactions by surface plasmon resonance. *Angewandte Chemie (International ed. in English)* **2002**, *41* (9), 1554.
22. Haseley, S. R.; Vermeer, H. J.; Kamerling, J. P.; Vliegthart, J. F., Carbohydrate self-recognition mediates marine sponge cellular adhesion. *Proceedings of the National Academy of Sciences* **2001**, *98* (16), 9419-9424.
23. Tromas, C.; Rojo, J.; de la Fuente, J. M.; Barrientos, A. G.; García, R.; Penadés, S., Adhesion forces between Lewis x determinant antigens as measured by atomic force microscopy. *Angewandte Chemie International Edition* **2001**, *40* (16), 3052-3055.
24. Garcia-Manyes, S.; Bucior, I.; Ros, R.; Anselmetti, D.; Sanz, F.; Burger, M. M.; Fernandez-Busquets, X., Proteoglycan mechanics studied by single-molecule force spectroscopy of allotypic cell adhesion glycans. *Journal of Biological Chemistry* **2006**, *281* (9), 5992-5999.
25. de la Fuente, J. M.; Eaton, P.; Barrientos, A. G.; Menéndez, M.; Penadés, S., Thermodynamic evidence for Ca²⁺-mediated self-aggregation of lewis X gold glyconanoparticles. A model for cell adhesion via carbohydrate– carbohydrate Interaction. *Journal of the American Chemical Society* **2005**, *127* (17), 6192-6197.

26. Velázquez-Campoy, A.; Ohtaka, H.; Nezami, A.; Muzammil, S.; Freire, E., Isothermal titration calorimetry. *Current protocols in cell biology* **2004**, 17.8. 1-17.8. 24.
27. Hernáiz, M. J.; de la Fuente, J. M.; Barrientos, Á. G.; Penadés, S., A model system mimicking glycosphingolipid clusters to quantify carbohydrate self-interactions by surface plasmon resonance. *Angewandte Chemie* **2002**, 114 (9), 1624-1627.
28. Freire, E.; Mayorga, O. L.; Straume, M., Isothermal titration calorimetry. *Analytical Chemistry* **1990**, 62 (18), 950A-959A.
29. Instruments, M., MicroCal iTC200 system user manual. **2014**, (MAN0560-01-EN-00).
30. Milev, S., Don't throw away your "bad" N-value ITC data. *Malvern Materials Talks* **2015**.

3 YARIV REAGENT INTERACTIONS WITH ARABINOGALACTAN PROTEINS (AGPs)

Note: Much of this chapter is adapted from a manuscript¹ in preparation for publication. Some of the data presented in this chapter was produced by authors of the manuscript other than myself. Therefore, throughout this chapter I have indicated which data is attributed to these authors.

3.1 Introduction

The previous sections have discussed the use of glycopolymers as model systems that can be used to perform CCI binding studies. The multivalent presentation of the carbohydrates in these systems provides the avidity required for binding that is not observed in monovalent systems. Although conventional covalently bonded polymers have been useful tools for studying CCIs, supramolecular polymers are also used as powerful tools for studying carbohydrate recognition processes. In these supramolecular glycoconjugate systems, the monomers are easily prepared and self-assembly into larger multivalent forms provides the avidity required for receptor binding and subsequent functions.² Yariv reagents are a class of supramolecular glycoconjugates that have been found to participate in binding interactions with arabinogalactan protein (AGP), a proteoglycan found in plant cell walls that plays a role in various biological processes. The mechanism of this binding interaction is not well understood. A better understanding of the Yariv-AGP binding mechanism could provide insights into the nature of the role of AGP as a biological macromolecule.

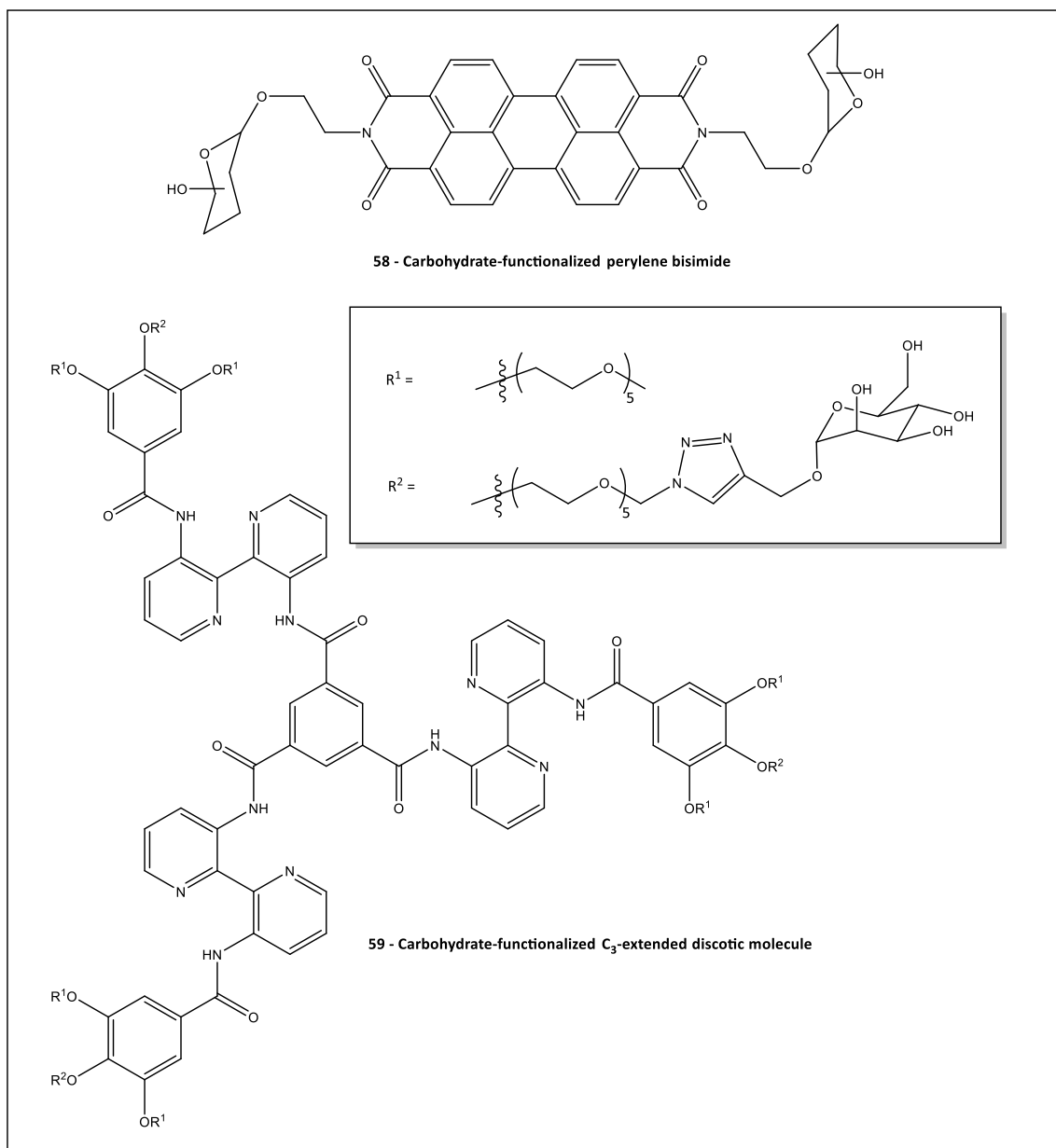


Figure 3.1: Self-assembling carbohydrate functionalized discotic molecules

3.1.1 Supramolecular Glycoconjugates

Supramolecular glycopolymers are often composed of discotic molecules with polyaromatic cores that self-assemble into one-dimensional stacks in solution via π -bonding interactions. Such discotic molecules can be decorated with carbohydrate moieties (Fig 3.1), and these molecules are known to interact via π -bonding interactions between the polyaromatic cores and hydrogen

bonding between the carbohydrate groups.² Since aggregation is driven by stacking of the aromatic cores and by hydrogen bonding between stacked monomers, the core can adopt a propeller-like conformation and self-assemble into homochiral helical aggregates if the peripheral substituent contains a stereocenter.³ Since carbohydrates are chiral it is often the case that supramolecular glycoconjugates assemble into uniformly helical stacks, with the handedness of the helix being largely dependent on the identity of the carbohydrate moiety. Circular dichroism (CD) spectroscopy is commonly used to confirm the presence of helical supramolecular aggregates.

A CD spectrum is generated by passing left and right-handed polarized light through a solution of a given chromophore that absorbs light in the UV-Vis range. If the chromophore is chiral one type of polarized light will be absorbed more strongly than the other. The difference in the ability of polarized light to pass through the sample is known as ellipticity and is measured over a range of wavelengths to provide the CD spectrum.⁴

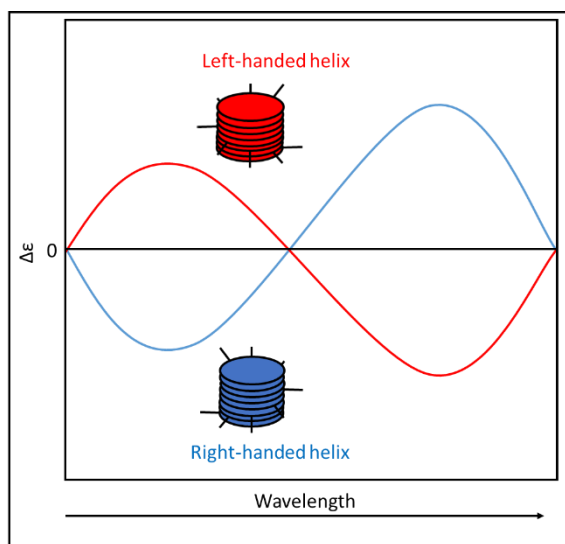


Figure 3.2: The bisignate cotton effect arising from excitonic coupling

Typically, if two or more chromophores are in close proximity and their transition dipoles are oriented in a helical fashion, a CD spectra with a bisignate pattern is observed (Fig 3.2). This pattern is referred to as the Cotton effect. For supramolecular polymers with polyaromatic cores this Cotton effect is observed, and is the result of excitonic interactions between helically stacked dyes.⁵ If the stack possesses right-handed helicity, then a positive cotton effect is observed meaning that the sign of the CD spectrum is positive at long wavelength and becomes negative at

shorter wavelengths. The opposite sign spectrum is observed for stacks with left-handed helicity.⁵ Therefore, if the Yariv reagents aggregate to form helical stacks then a Cotton effect will be observed in the CD spectrum, and the sense of helicity can be determined from the sign of the Cotton effect.

Circular dichroism (CD) spectroscopy experiments demonstrated that the helicity of the supramolecular glycopolymers formed from stacks of perylene bisimide **57** is determined by the identity of the carbohydrate functional group. Perylene bisimides functionalized with D-lactose and D-maltose at the imide positions show right-handed helicity, while those functionalized with D-mannose or D-galactose give rise to left-handed helices.⁶ Changing the non-carbohydrate portion of the discotic monomer can affect helicity as well. This was demonstrated in CD studies of glycosylated perylene bisimide derivatives functionalized with alkyl chains of various lengths. In these studies the handedness of the aggregate was found to be dependent on the length of the alkyl chain substituent.⁷

Supramolecular glycoconjugates have also been found to serve as useful tools for studying the carbohydrate recognition processes of biological macromolecules. CD experiments demonstrated that D-lactose functionalized perylene bisimides aggregated into right-handed helical stacks in water. In DMSO the supramolecular glycoconjugates become completely disaggregated and no CD signal is observed. Turbidity assays demonstrated that the supramolecular glycoconjugates exhibit specific binding with peanut agglutinin (PNA) lectin. This study demonstrates the potential for supramolecular glycoconjugates to serve as sensors to detect carbohydrate-lectin interactions.⁸ C₃-symmetrical discotic molecules with expanded polyaromatic cores and mannose functionality **58** were observed to become fluorescent upon aggregation. Fluorescence microscopy was used to observe binding between the fluorescent supramolecular polymers and *E. coli* bacteria cells which display the mannose binding FimH lectin

on the cell surface. This study demonstrates the utility of supramolecular glycoconjugates as tools for detection of bacteria.⁹

3.1.2 Yariv reagents

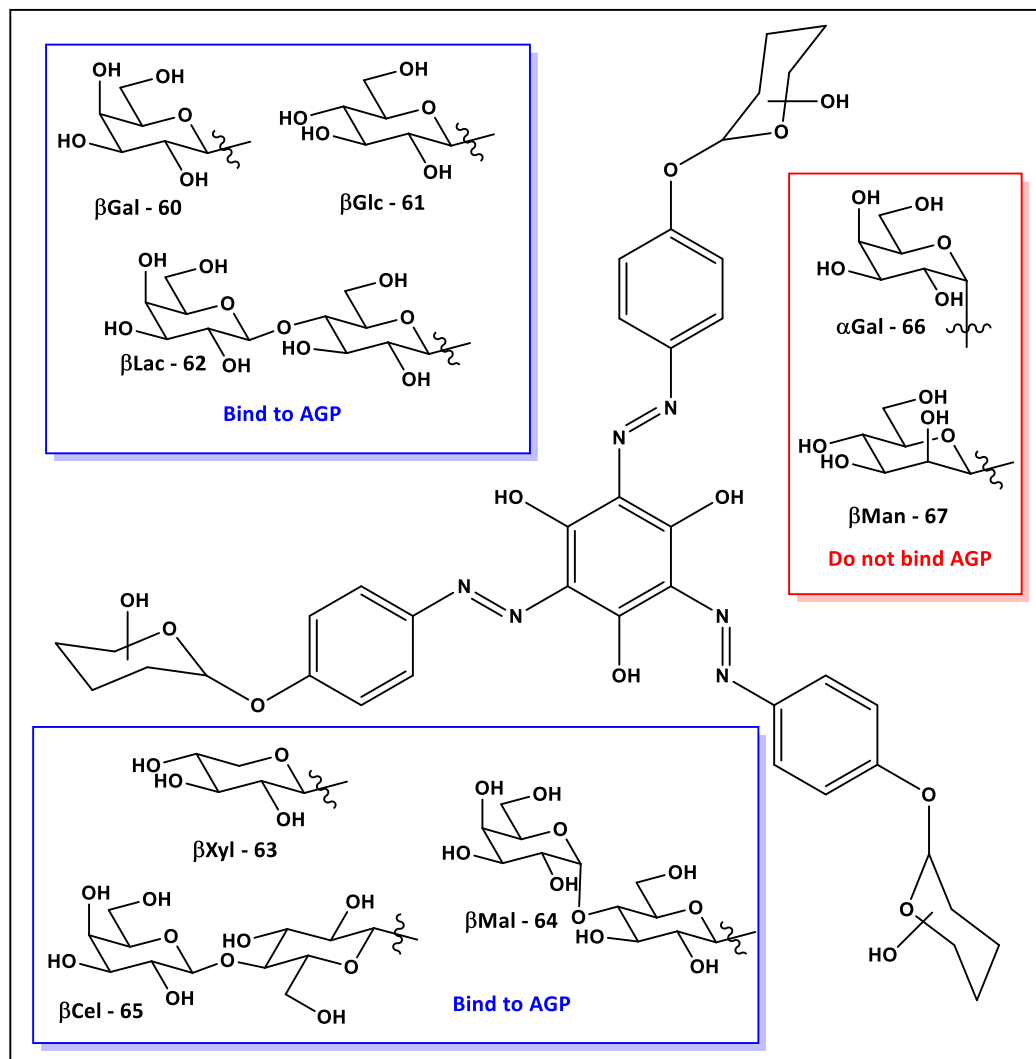


Figure 3.3: Structure of Yariv reagents 60-67. 60-65 bind to AGPs while 66 and 67 do not.

A class of supramolecular glycoconjugates are the glycosylated tri-azo dyes commonly referred to as Yariv reagents (Figure 3.3). These compounds are C_3 -symmetric molecules, with a hydrophobic aromatic core decorated with hydrophilic groups on the periphery. ^{13}C -NMR spin-lattice relaxation measurements taken in DMF show that disaggregated Yariv molecules behave as rigid

discs in solution.¹⁰ Therefore, Yariv reagents are discotic molecules that are similar to those discussed in the previous section.

Yariv reagents were originally synthesized to identify carbohydrate-binding antibodies. It was found that Yariv reagents functionalized with β -D-galactose (β Gal **59**), β -D-glucose (β Glc **60**), and β -D-lactose (β Lac **61**) were able to form a precipitate the complementary carbohydrate binding antibody while no precipitation was observed between Yariv reagents and non-complementary antibodies.¹¹ Since this initial study was performed in 1962, Yariv reagents serve as one of the earliest examples of the importance of multivalent glycoconjugates in carbohydrate recognition.¹²⁻¹³

Later, The Yariv research group prepared an α -L-fucosyl (α Fuc) Yariv reagent for use in the precipitation of an L-fucose binding protein from the seed of *Lotus tetragonolobus*.¹⁴ Upon examination of the material precipitated using α Fuc it was discovered that some polysaccharide components were isolated from the seeds.¹⁴ These polysaccharides were also precipitated from the *Lotus tetragonolobus* and various other flours using **61**. The polysaccharides were isolated from the Yariv reagent by column chromatography. After acid hydrolysis, TLC experiments demonstrated that these polysaccharides are composed of mainly of galactose and arabinose sugars. Further studies demonstrated that this polysaccharide could be isolated from the seeds of numerous (91 out of 104 families tested) angiosperms and gymnosperms using a variety of Yariv reagents including β -D-galacto- **60**, -D-gluco- **61**, -lacto- **62**, -D-xylo- **63**, -malto- **64**, and -cellobiosyl **65** Yariv reagents.¹⁵ Analysis of the isolated polysaccharides revealed that they typically contained a hydroxyproline-rich protein core accounting for 2-10% of the composition of these macromolecules which are typically referred to as arabinogalactan proteins (AGPs).¹⁶⁻¹⁷ Yariv reagents decorated with α -D-configured sugars, such α -D-galactose **66** were found to lack the AGP binding capability of the β -Yarivs (**60-65**).¹⁸

3.1.3 Yariv – AGP interactions

Typically, Yariv-AGP binding is observed using radial gel-diffusion assays. In these experiments solutions of AGP are added to wells cut or molded into Yariv impregnated gels. As the AGP diffuses through the gel, complexation occurs with the Yariv reagent resulting in the appearance of a brownish ring of precipitate around the well. Higher affinity interactions give rise to precipitate rings with wider diameters.¹⁹⁻²⁰

AGPs are involved in a wide range of cellular and physiological processes including fertilization, growth and development, signal transduction, and plant-microbe interactions.²¹⁻²⁸ AGPs are present at the surface of the stigma of *Gladiolus gandavensis* and likely function as an adhesive base that helps pollen bind to the stigma surface.²⁹ AGPs were also found to play a role in controlling plant growth, as cucumber plant mutants that overexpress a certain type of AGP are much taller than the wild types.³⁰ Also, an AGP found in *Arabidopsis* roots was found to be required for root regeneration.³¹ AGPs are abundantly synthesized in the roots of plant cells and have been found to play a role in mediating interactions between root cells and microbes allowing for the colonization of beneficial microbes and inhibition or repulsion of pathogenic ones.²² Overexpression of a type of AGP found in *Lycopersicon esculentum* resulted in plants that were shorter, more highly branched, had more flower buds and smaller than normal seeds, indicating that the AGP plays an important role in the plant's reproduction and growth.³² The examples given here provide only a small sample of the wide range of physiological and cellular processes which are believed to be mediated by AGPs. AGPs are also widely used commercially as food emulsifiers.²⁸

The type II AGP polysaccharide (Fig 3.4) is comprised of a β -1,3-galactan main chain with branching β -1,6-galactan side chains, which can be elaborated further with α -L-arabinofuranosyl and β -D-

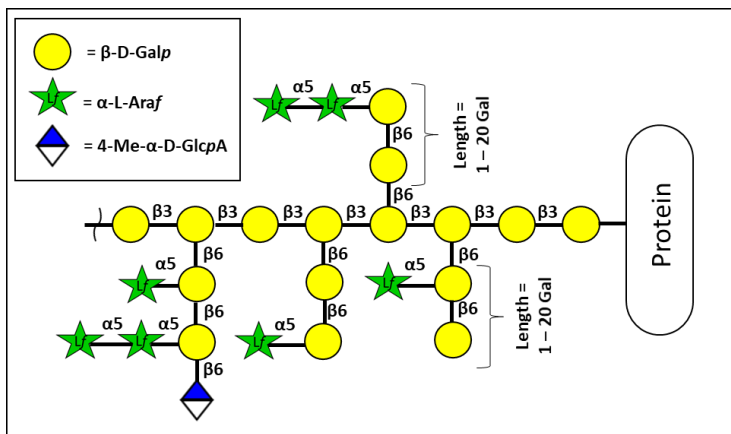


Figure 3.4: Schematic of a typical type II AGP

glucuronosyl residues.²³ AGPs also contain a protein component that is usually rich in hydroxyproline. When the side chains are removed from radish root AGP via enzymatic degradation, the AGP is still precipitated by 59 indicating that these side chains do not play a role in Yariv binding.²⁰ However, when the main chain undergoes enzymatic cleavage no precipitation occurs indicating that the main chain (and not the protein) is the Yariv binding epitope.²⁰ In further experiments the β -1,6-galactan side chains of Gum Arabic AGP were removed by Smith degradation. Removal of the side chains was found to enhance Yariv reactivity, again implicating the main chain as the Yariv binding epitope.²⁰

β -1,3-galactan oligosaccharides ranging from 4-9 sugars in length were prepared by acid hydrolysis of the β -1,3-galactan AGP backbone and fractionation by gel permeation chromatography. Gel diffusion assays demonstrated that Yariv binding only occurs for oligosaccharides that are seven or more sugars long indicating that the minimal epitope required for binding to Yariv reagents is a β -1,3-heptagalactan.²⁰

Molecular dynamics (MD) simulations were performed to determine the conformation of the β -1,3-galactan AGP backbone. The simulations were performed using a β -1,3-oligogalactan that is 16 sugars in length that was placed in a virtual water box. The simulation suggests that the oligosaccharide adopts a right-handed helical conformation in water with 7-8 sugar residues per

turn.²⁰ The interior of the helix is relatively hydrophobic with all of the hydroxyl groups of the galactosyl residues facing outward toward water with the exception of the C2 hydroxyl group. The fact that the minimal binding epitope for Yariv-AGP binding (heptagalactan) has the same number of residues as one turn of the β -1,3-galactan helix suggests that the right-handed helical shape is required for Yariv-AGP binding. Also, the hydrophobic character of the helix core may allow for hydrophobic interactions between the β -1,3-galactan and the polyaromatic cores of the Yariv reagents.²⁰ However, this observation still does not explain why some Yariv reagents bind to AGP while others do not.

The Yariv reagent's ability to bind and precipitate AGPs depends on the identity of the sugar residue on the dye. As previously mentioned many Yariv reagents containing β -D-configured sugar residues (**60-65**) precipitate AGPs while Yariv reagents with α -D-configured residues **66** do not.^{15, 18, 33} Also, β -D-mannosyl **67** Yariv was found to be ineffective in precipitating AGP.^{15, 18} Methylation or removal of the C-3,4, or 6 position hydroxyl groups of the β Glc Yariv reagent does not affect Yariv-AGP precipitation, but methylation or removal of the C-2 hydroxyl group abolishes AGP binding activity.¹⁸ This data suggests that β -configuration and the presence of an unsubstituted equatorial C-2 hydroxyl group are required for AGP binding. The structure of the aromatic core of the Yariv reagents is also important for Yariv-AGP binding as Yariv analogs with N-, methylene-, methoxy-, and phenoxy- linked glycosides have all do not bind AGPs. Yariv reagents with thiol-linked glycosides bind to some AGPs, but not to others.^{18, 34}

Yariv reagents are one of the primary tools used to identify, isolate, and investigate AGP structure and function and are routinely used to precipitate AGP from plant matter.²³ Despite the wide use of Yariv reagents in plant biology, the molecular basis for the Yariv-AGP interaction and the origin of specificity is unclear. Some structural components of the Yariv reagents have been identified as important factors for AGP binding, but the reason for this importance is not well understood.

However, the amplification of avidity of CCl₃s that arise from the multivalent presentation of carbohydrates,¹²⁻¹³ coupled with the observation that the minimal Yariv binding epitope is a right-handed oligosaccharide helix,²⁰ suggests that the origin of specificity may be related to the macromolecular structural properties of the Yariv aggregates.

3.1.4 Structural properties of Yariv aggregates

The supramolecular assembly of Yariv reagents has previously been examined using a variety of techniques. Ultra-centrifugation experiments demonstrated that **60**, **61**, **66**, and **67** each self-assemble in aqueous solution to form aggregates at concentrations as low as 5 μ M; aggregates up to 80-mers were observed at higher concentrations. Also, association constants were calculated for **60** ($9 \times 10^6 \text{ M}^{-1}$), **61** ($2.5 \times 10^7 \text{ M}^{-1}$), **66** ($3 \times 10^6 \text{ M}^{-1}$), and **67** ($2 \times 10^6 \text{ M}^{-1}$) from the centrifugation data indicating that **60** and **61** show the strongest association behavior.³⁵ Dynamic light scattering (DLS) experiments determined the hydrodynamic radii of aggregates of **61** and **66** in water to be 122 nm and 82 nm respectively.¹⁰ **60** was found to be aggregated at the lowest concentration where it can be detected spectroscopically ($< 10 \mu\text{M}$), and AGP binding was observed at concentrations as low as 500 nM, indicating that the associative forces of the aggregates are strong enough to allow for persistence of aggregates at low concentrations.³⁶

Yariv aggregates were found to disaggregate upon exposure to organic solvents, high temperatures, or denaturing agents such as sodium dodecyl sulfate (SDS), urea, and guanidinium hydrochloride.^{10, 35} ¹H-NMR spectra of Yariv reagents in D₂O display extremely broad peaks in the aromatic and aliphatic spectral regions. These broad peaks indicate that Yariv reagents are aggregated. NMR spectra taken in DMF and DMSO display well resolved peaks indicating that the Yariv reagents are completely disaggregated in these solvents.¹⁰ In 1:1 DMF:D₂O NMR peaks are broad at 300 K, but begin to resolve as the temperature increases. At 330 K the peaks are well-

resolved indicating that an increase in temperature causes the Yariv reagents to disaggregate.¹⁰ Dynamic light scattering (DLS) experiments found that in 8 M urea the Yariv aggregates are much less aggregated (hydrodynamic radius (r) = 52 nm) than those observed in pure water (r = 122 nm). In 100% DMF the Yariv aggregates are even less aggregated (r = 0.4 nm).¹⁰

Yariv reagents are much more effective at binding to AGP than monomeric sugars. Glucose at concentrations three orders of magnitude higher than that of **61** was unable to inhibit AGP precipitation.³⁶ Also, phenylglucosides are capable of inhibiting Yariv-AGP binding, but only at concentrations 2-10 times higher than that of the Yariv reagent.³⁶ This suggests that the aggregated state of Yariv reagents leads to an increase in avidity related to multivalent presentation of carbohydrates, similar to what is observed for other CCIs.¹²⁻¹³ Although the multivalent presentation of carbohydrates is likely important for Yariv-AGP binding, this does not explain why some Yariv reagents do not bind AGP even though they form aggregates.

3.1.5 Hypothesis

Based on the prior observations of Yariv reagent aggregation coupled with the fact that similar discotic molecules form helical assemblies, we hypothesized that the aggregates of the Yariv reagent are supramolecular helices. Furthermore, due to the observation that the β -1,3-galactan AGP backbone likely adopts a right-handed helical conformation in solution,²⁰ we hypothesized that the helicity of a Yariv aggregate is correlated to its AGP binding capabilities.

3.2 Characterizing the helicity of the Yariv reagent aggregates

3.2.1 Absorbance and Circular Dichroism spectra of BGlc Yariv

The o-azo-phenol chromophore provides a convenient spectroscopic signature for probing the supramolecular chirality of Yariv reagents. We first obtained the absorption spectrum of an

aqueous solution of **61**. The spectrum exhibits two maxima at 397 and 483 nm (Fig 3.5b), consistent with previously reported spectral data.^{10-11, 15} Studies of related phenylazo-phenols, phenylazo-naphthols, and phenylazo-phloroglucinols have shown that the shorter wavelength absorbance corresponds to the azo form of the Yariv reagent, while the longer wavelength absorbance corresponds to the hydrazone tautomer.³⁷⁻³⁹ We next obtained the circular dichroism (CD) spectrum of **61**, which exhibits a bisignate pattern (Fig. 3.5a) with extrema corresponding to each of these absorbances. The CD spectrum displays maxima at $\lambda = 521$ and 432 nm ($\Delta\epsilon = 31.70$ and $8.87 \text{ L}\cdot\text{mol}^{-1}\text{cm}^{-1}$ respectively) and minima at $\lambda = 467$ and 378 nm ($\Delta\epsilon = 0.14$ and $-54.88 \text{ L}\cdot\text{mol}^{-1}\text{cm}^{-1}$ respectively), which is representative of a positive Cotton effect. When coupled with previous analytical ultracentrifugation, NMR and DLS studies that provided evidence for aggregation,^{10, 35} our observation of a positive Cotton effect indicates that the stacked aggregates of **60** possess right-handed helicity.

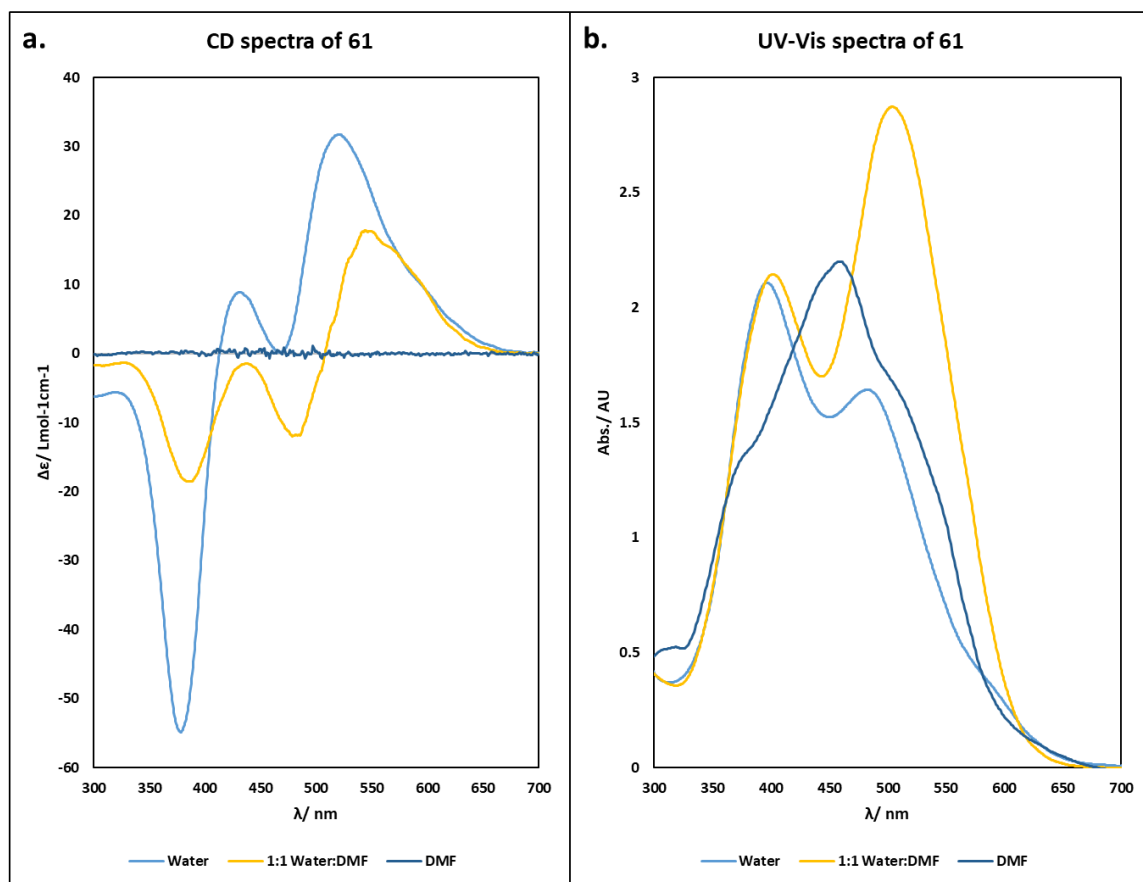


Figure 3.5: a. CD spectrum of **61** (300 μM); b. UV-Vis spectrum of **61** (300 μM) (1:1 Water:DMF spectra were acquired by H. Kuhn)

To confirm that the observed CD signals are derived from the supramolecular chirality of aggregates of **61** and not from the monomeric species, CD and absorbance spectra were acquired in the presence of DMF (Fig. 3.5a and b). The Yariv reagent exhibits decreasing aggregation in the presence of increasing amounts of organic solvent, as previously shown by NMR and DLS.¹⁰ The UV-vis spectrum of **61** in 1:1 DMF:H₂O exhibits a change in the relative ratios of the azo and hydrazone tautomers of the Yariv reagent, as seen previously (Fig. 3.5b).^{10, 35} This change in the absorption spectrum is accompanied by a concomitant reduction in the absolute intensities of the extrema in the CD spectra (Fig. 3.5a). In pure DMF, where the reagent is completely dissociated according to DLS and NMR,¹⁰ the individual absorbance maxima of each tautomer coalesce into a single broad peak with underlying shoulders, and the CD spectrum is flat (Fig. 3.5a and b). The

lack of a CD signal in DMF confirms that the helicity observed in aqueous solutions is derived from the aggregated form of **61** and not from the monomer.

3.2.2 Comparison of the UV-vis and Circular Dichroism spectra of Yariv reagents

Since the identity of the sugar in a Yariv reagent dictates whether or not they bind to AGP, we sought to determine whether there is any correlation between the structure of the sugar on the dye and the helicity of the Yariv aggregates. We acquired the absorption (Fig. 3.6b) and CD (Fig. 3.6a) spectra of several additional Yariv reagents: β -Gal-Yariv (**60**), β -Man-Yariv (**67**) and α -Gal-Yariv (**66**). The absorption spectra for these species are very similar to that of **61**, consistent with their known aggregation in aqueous solution.^{10, 35} The CD spectrum of **60** ($\lambda = 521$ nm, $\Delta\epsilon = 24.93$ L•mol⁻¹cm⁻¹) has an identical profile to **61**, with similar wavelength maxima and minima, albeit somewhat less intense. This similarity indicates that **60** also forms right-handed helical aggregates. Although, a very weak positive Cotton effect is observed for **67** ($\lambda = 521$ nm, $\Delta\epsilon = 2.50$ L•mol⁻¹cm⁻¹), the spectrum is much flatter than that for **60** or **61**. Since UV-vis and ultracentrifugation studies indicate that **67** is also aggregated in solution,³⁵ the weak CD signal may arise from an almost racemic mixture of helices or from aggregates that are only slightly helical. The CD spectrum for **66** ($\lambda = 521$ nm, $\Delta\epsilon = -24.30$ L•mol⁻¹cm⁻¹) displays a negative Cotton effect, indicating that α -Gal-Yariv aggregates adopt a left-handed helical orientation. Since **60** and **61** bind AGP while **66** and **67** do not, the results shown in figure 3.6 indicate a correlation between Yariv reagents that form aggregates with strong net right-handed helicity and the ability of these reagents to bind AGP.

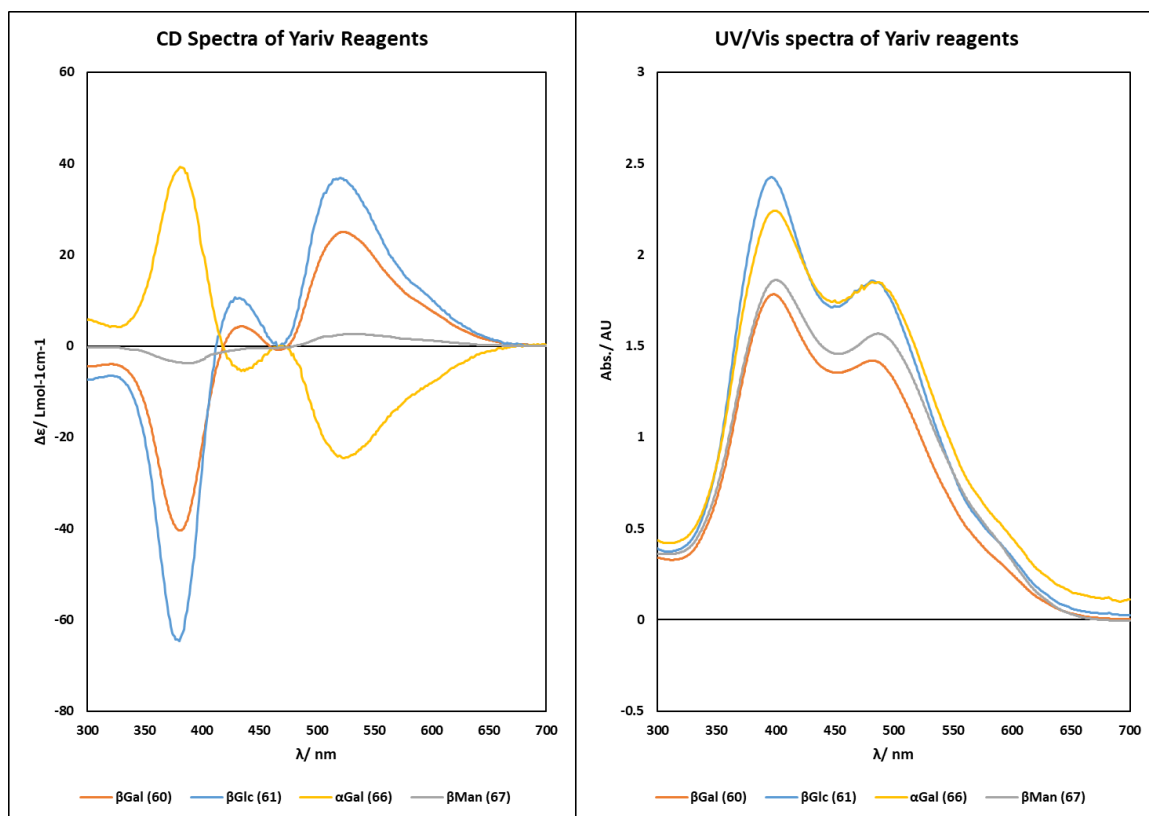


Figure 3.6: a. CD spectra and b. UV-Vis spectra of Yariv reagents **59**, **60**, **65**, and **66** (300 μ M) (spectra for **59** and **66** were acquired by David Caianiello)

3.2.2.1 NMR, UV-Vis, and CD spectra of a monovalent azo-linked galactoside **68**

We have prepared an analog of **60** containing a single azo-linked galactoside (Fig 3.7) **68**, and its CD spectrum is essentially flat (Fig.

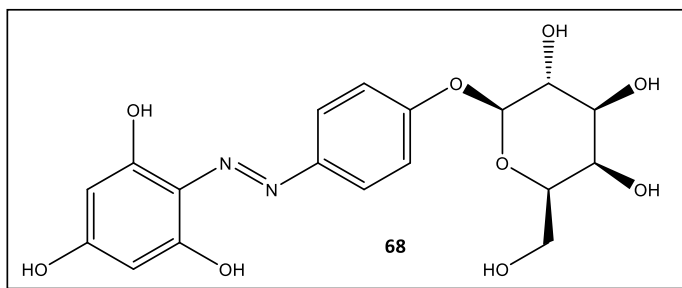


Figure 3.7: single azo-linked galactoside **67**

3.8b), although a very weak positive Cotton effect ($\lambda = 450$ nm, $\Delta\epsilon = 1.00$ L \cdot mol $^{-1}$ cm $^{-1}$) is observed. More significantly, the NMR spectrum of this compound in D₂O does not show the aggregation-induced large line broadening observed for the Yariv reagents (Fig. 3.8a).¹⁰ Previous reports indicate that more than one azo-linked glycoside is required for GA binding.¹⁸ Therefore, the fact that these molecules do not form helical aggregates provides more evidence of the necessity of helical aggregates for Yariv-AGP

binding. This data also indicates that a strong Cotton effect is not observed for disaggregated glycosylated phenyl-azo dyes and provides further evidence that aggregation gives rise to the Cotton effects observed for **60**, **61**, **66**, and **67**.

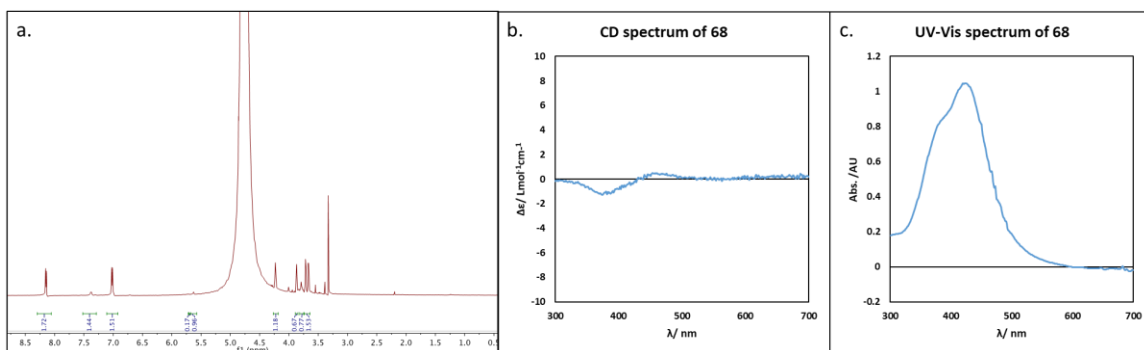


Figure 3.8: a. ¹H-NMR spectrum of **68** in D₂O (acquired by Natalie Palaychuk); b. CD spectrum of **68**; c. UV-vis spectrum of **68**

3.2.3 AGP titration experiments

To further evaluate the AGP binding of the Yariv reagents we acquired CD spectra of mixtures of **61** and gum arabic (GA), an AGP isolated from the acacia tree (Fig. 3.9). Initially, we had planned on using solutions prepared with 1% NaCl so that conditions would be similar to those used in the radial-gel diffusion assays. However, it was found that precipitate formed after 16 h in AGP-Yariv solutions prepared with 1% NaCl. Fortunately, we found that precipitation can be avoided if Yariv-GA binding experiments are carried out in pure water.⁴⁰

In these experiments, concentration-dependent increases in the CD extrema are observed. The change in CD signal upon GA binding may arise from a perturbation of the chromophore that strengthens the absorption, or from a binding-induced increase in the size distribution of the Yariv aggregate. No significant increase in CD intensity is observed at GA concentrations above 0.5 mg/mL (Fig. 3.9 inset). We were unable to determine an association constant from this binding experiment, likely due to the broad MW distribution of GA⁴¹ and the potential for multi-site

binding on both the Yariv reagent and GA. AGP from gum Arabic is composed of three major fractions. The major fraction (88.4 % wt. of the total) has a weight average molecular weight (M_w) of 2.86×10^5 g/mol, the second major fraction (10.4 % wt. of the total) has a M_w of 1.86×10^6 g/mol, and the minor fraction (1.2 % wt. of the total) has a M_w of 2.5×10^5 g/mol. All three fractions are polydisperse and bind Yariv reagent. Since we cannot determine the active concentration of binding sites for a given sample using the experiments presented in this work we cannot accurately calculate an association constant. Nonetheless, the saturation of the CD signal at fairly low GA concentrations suggests a high affinity interaction between **61** and GA. The intensity of the UV-Vis spectra of **61** also displays a GA concentration-dependent increase (Fig. 3.10). Several control experiments were performed to validate the specificity of these spectral changes. The CD and UV-Vis spectra of **66**, which does not bind AGP, in the presence of 0.63 mg/mL GA was identical to the spectrum of **4** without GA (Fig. 3.11b and d).

To confirm the presence of a specific interaction between **61** and the GA AGP we conducted experiments using an AGP that does not bind Yariv reagents. The ability of frost grape AGP⁴² (FG) to bind **61** was evaluated using a gel diffusion assay. Agarose gels containing **61** were prepared in a petri dish. GA or FG were injected into pre-molded wells and incubated overnight. Upon visualization, there is no evidence of any precipitate in the FG gel, confirming that there is no interaction between **61** and FGP (Fig. 3.12).

The presence of FG does not alter the CD or UV-Vis spectra of either **61** or **66** at a concentration of 0.63 mg/mL (Fig. 3.11). These control spectra indicate that the spectral changes seen in figure 3.9 are due to specific interactions between **61** and GA, and do not arise from non-specific interactions of polysaccharides with Yariv aggregates.

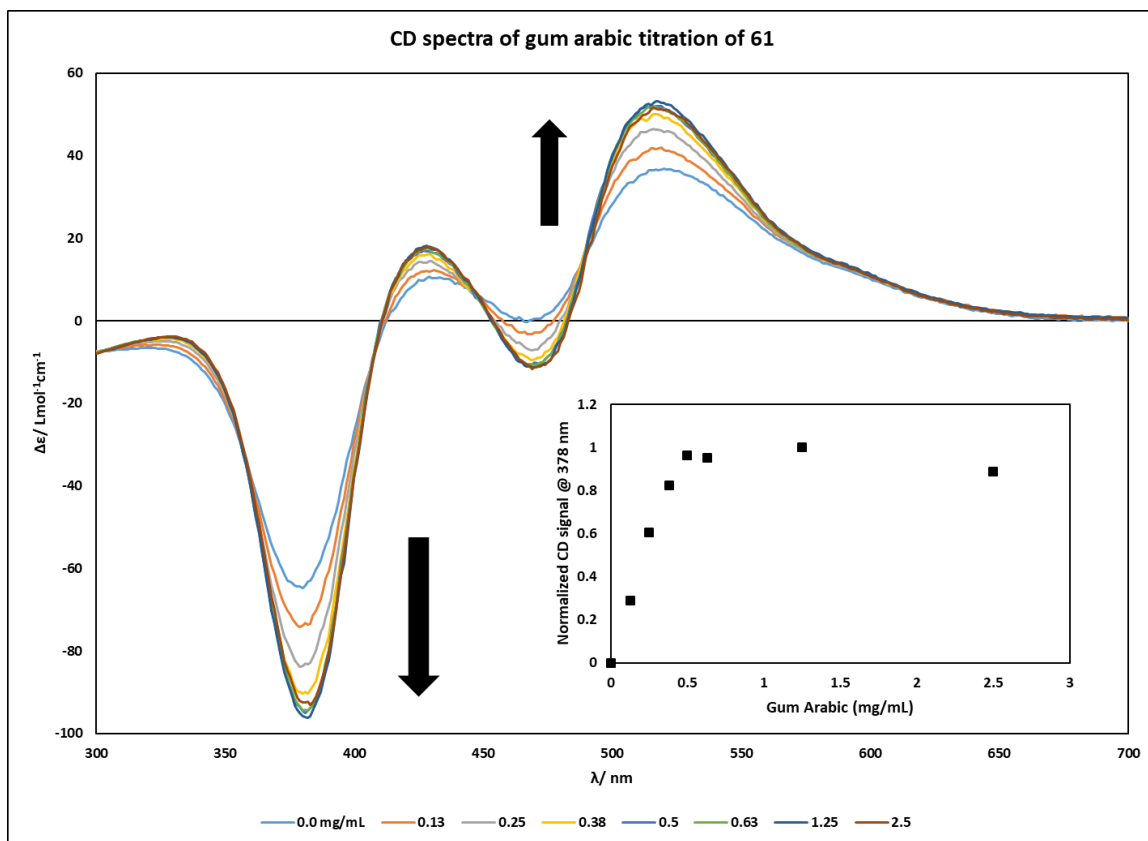


Figure 3.9: CD spectra of **61** (300 μM) in the presence of gum arabic

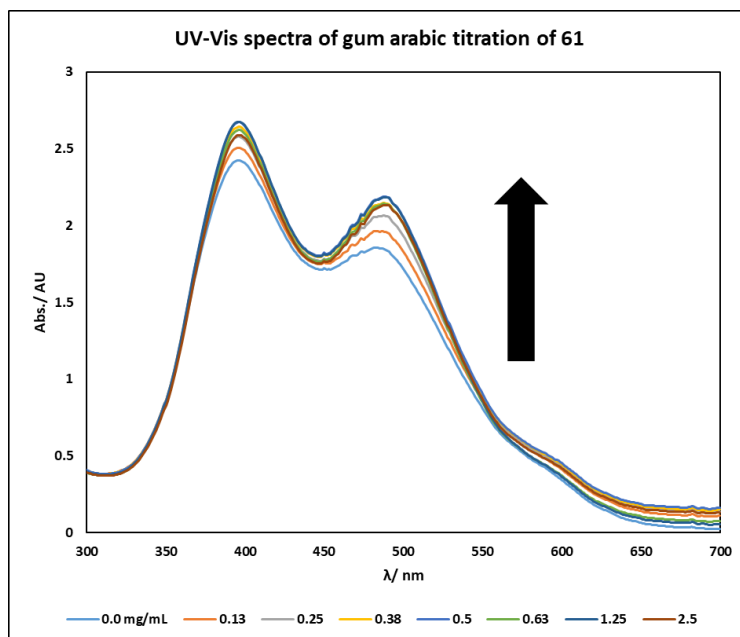


Figure 3.10: UV-Vis spectra of **61** (300 μM) in the presence of gum arabic

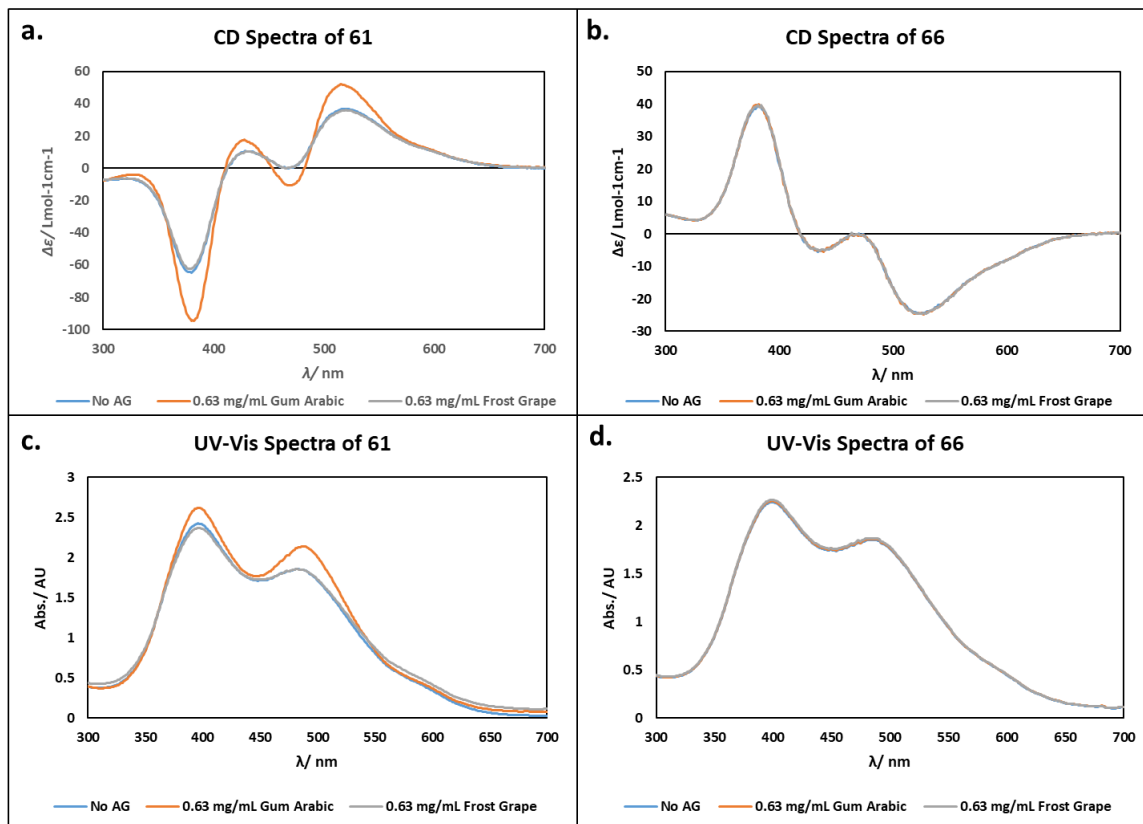


Figure 3.11: a. CD spectra of **61** (300 μ M) in the presence of AGP; b. CD spectra of **66** (300 μ M) in the presence of AGP; c. UV-Vis spectra of **61** (300 μ M) in the presence of AGP; d. UV-Vis spectra of **66** (300 μ M) in the presence of AGP

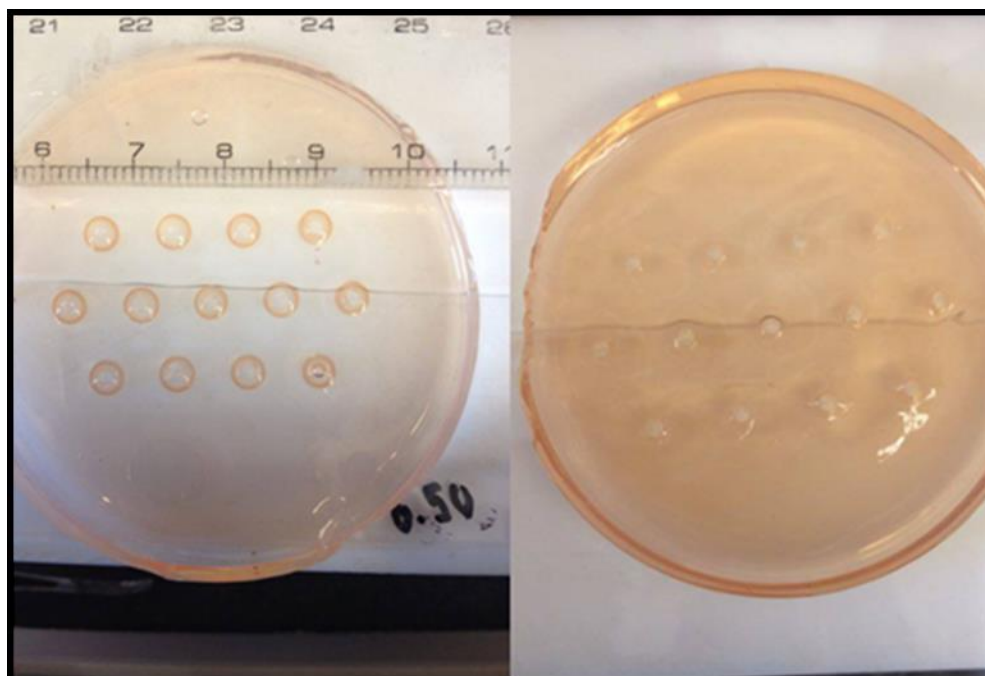


Figure 3.12: Radial Gel Diffusion Assays with agarose gels containing **61** – left) agarose gels injected with 0.50 g/L gum arabic: clear halos are visible at the end of the incubation period; right) agarose gels injected with 1g/L frost grape AGP: no halos are visible. (Gels prepared by Brandon Dale)

3.2.4 Additional radial gel diffusion assays

3.2.4.1 Radial gel diffusion assays with gels containing DMF

To provide further evidence of the importance of Yariv aggregation in AGP binding, radial gel diffusion assays were performed in which Yariv gels of **61** were prepared with 0, 20, 30, 40 and 50% DMF (Fig 3.13).⁴³ It is known from previously discussed CD and NMR¹⁰ experiments that DMF causes the disaggregation of Yariv reagents. Therefore, if aggregation and thus the multivalent presentation of sugars, is important for AGP binding, then the presence of DMF should prevent Yariv-AGP binding. In the Yariv gel assays only light precipitate is seen in gels prepared

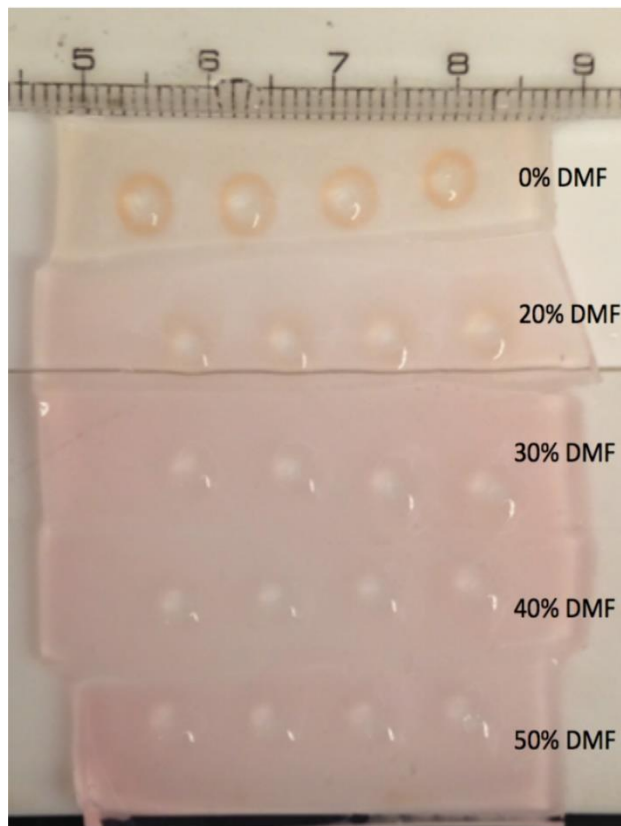


Figure 3.13: Radial gel diffusion assays with agarose gels containing **61** and various concentrations of DMF. 0.8 μ L of 1 g/L gum Arabic was injected in each well. (Gels prepared by Sarah Weingarten)

with 20% DMF, and no precipitate in gels prepared with 30-50% DMF, indicating that the AGP binding ability of **61** is abolished by DMF, possibly due to disaggregation and decrease of multivalency.

3.2.4.2 Radial gel diffusion assays with the monovalent azo-linked galactoside **68**

Radial gel diffusion assays were performed using gels prepared with **68** to demonstrate that the monovalent non-aggregating analog of **60** does not bind GA. No evidence of AGP precipitation was



Figure 3.14: Radial gel diffusion assays with agarose gels containing **68**. 0.8 μ L of 5 g/L gum Arabic was injected in each well.

observed in gels prepared with **68** suggesting that multivalent presentation of sugars is required

for Yariv-AGP binding to occur. Also, this result is consistent with previous reports that indicate that more than one azo-linked glycoside is required for GA binding.¹⁸

3.3 Conclusions

While it has long been known that Yariv reagents form aggregates in solution, the current work provides the first evidence that these aggregates are helical. Furthermore, it is also well established that while some changes to the carbohydrate structure of the Yariv reagent don't affect AGP binding (e.g. epimerization at C-4, **60** vs. **61**), other changes abrogate binding (e.g. epimerization at C-1 or C-2, **61** vs. **67** and **61** vs. **67**). Our observations that these deleterious changes result in loss of a strong net right-handed helicity in the aggregates suggest that Yariv-AGP interactions are sensitive to the supramolecular chirality of the Yariv reagents.

The CD titration method for testing Yariv-AGP binding is in some ways an improvement over the radial gel diffusion assay method. The CD experiments reported here require less than 15 minutes per sample, whereas gel experiments must be incubated overnight. Also, CD experiments are performed in solution, so sample preparation is simplified, and the Yariv/AG interactions can be observed free of any interference that may be caused by the gel environment. The CD method also allows for binding experiments to be easily performed at variable temperatures and/or in the presence of organic solvents. The quantitative nature of CD spectroscopy also provides much more reliable data for potential mechanistic or kinetics experiments than can be obtained using radial gel diffusion assays which are semi-quantitative at best. In summary, the CD method allows for rapid and quantitative analysis of Yariv/AG binding in solution.

Yariv reagents are not unique in being the only glycoconjugates with supramolecular chirality that bind to receptors,⁸⁻⁹ but the Yariv-AGP interaction presents several novel features. First, prior examples involve the binding of glycoconjugates to proteins, while the Yariv-AGP interaction is a

carbohydrate-carbohydrate interaction. More significantly, it is generally presumed that binding specificity in supramolecular glycoconjugate-protein interactions is driven by the identity of the sugar, with aggregation primarily providing the multivalency required for high avidity. In contrast, specificity in Yariv-AGP interactions appears to be driven by the supramolecular chirality of the Yariv aggregate. Since the target of the Yariv reagent, the oligogalactan epitope in AGP, is postulated to be a right-handed helix,²⁰ our observations suggest that shape complementarity to form intertwined helices may play a role in Yariv-AGP binding. Other helical polysaccharides such as carrageenan, gellan, and curdlan self-assemble to form double or triple helical structures, and can provide a model for Yariv - AGP binding.⁴⁴⁻⁴⁶ Yariv reagent self-assembly can be driven by stacking interactions between the aromatic core, carbohydrate-carbohydrate interactions between adjacent sugars, and C-H/ π interactions. The use of well-defined AGPs and AGP fragments,⁴⁷⁻⁴⁹ along with additional derivatives of the Yariv reagents,¹⁸ may provide opportunities to better characterize these interactions. Future studies will further explore the role of the sugar in dictating supramolecular chirality as well as the relationship between helicity and AGP binding.

3.4 Supporting information

Thin layer chromatography was carried out on Merck silica gel 60 F₂₅₄ precoated glass plates. Spots were visualized under a UV lamp and/or by immersion in p-anisaldehyde stain. All NMR spectra were recorded on Bruker Advance III HD Ascend 600 MHz. ¹H-NMR and ¹³C-NMR spectra were referenced to residual solvent peaks. Coupling constants are given in [Hz] and chemical shifts in [ppm]. Electrospray ionization (ESI) mass spectra were obtained using a Thermo LCQ Deca XP Max ion trap mass spectrometer. Purified water was obtained from a EMD Millipore Direct-Q™ 3 Tap to Pure and Ultrapure Water Purification System. Acacia gum arabic was purchased from Sigma-

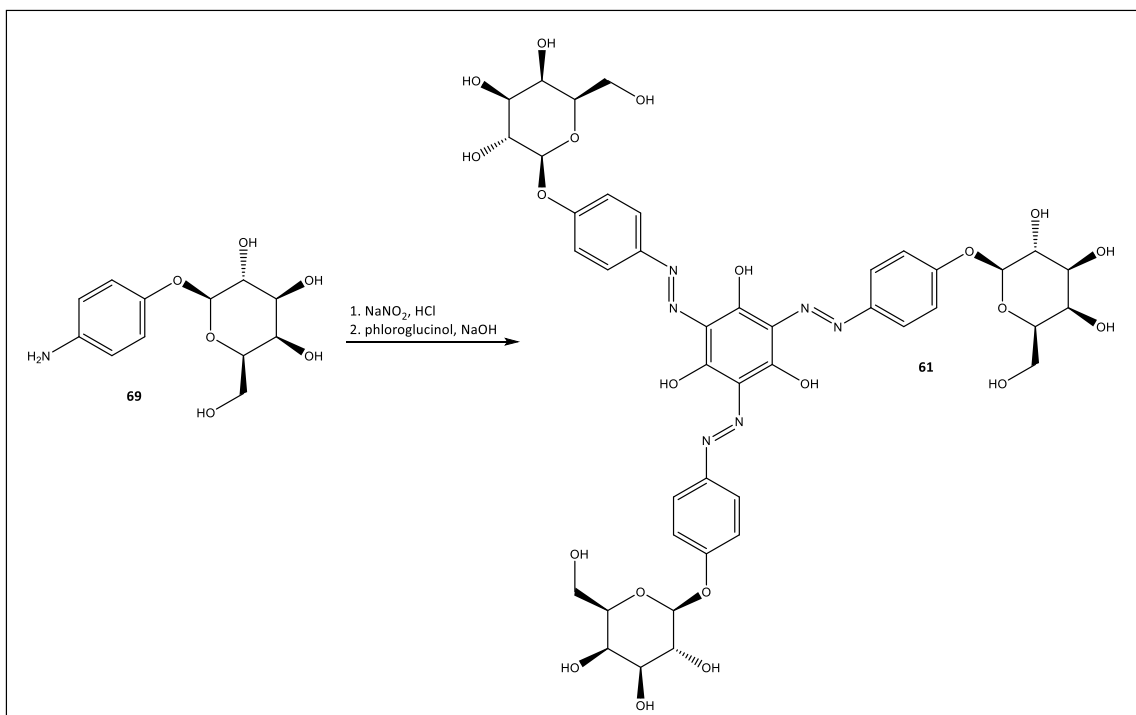
Aldrich. Frost grape polysaccharide (FGP) was generously provided by Dr. Neil Price (USDA, Peoria). Yariv reagents **60**, **61**, and **66** were prepared from the corresponding para-aminophenyl glycosides using minor modifications of reported protocols.⁵⁰ The β -mannosyl Yariv reagent **67** was purchased from Biosupplies Australia Pty. Limited (www.biosupplies.com.au) and used as is.

CD and UV-vis Experiments

Circular dichroism measurements were performed using a Jasco J-815 spectropolarimeter. Each spectrum is presented as the average of three scans. Temperature was controlled by a JASCO Peltier temperature control unit. Unless otherwise noted the concentration and volume of the Yariv reagent samples was 0.3 mM and 600 μ L, respectively. The sample cell was kept at 20 °C for all experiments. CD/UV-vis spectroscopy measurements were obtained in a Hellma analytics 2mm pathlength stoppered cuvette and corrected against a purified water standard. Wavelength readings ranged from 300 to 700 nm and were obtained at a speed of 100 nm/minute. The measured ellipticity θ was converted to molar circular dichroism $\Delta\epsilon = \theta / 32980 \cdot c \cdot l$, where ellipticity is given in mdeg, c is the concentration in $\text{mol} \cdot \text{L}^{-1}$ and l is the optical path length in cm.

Radial gel diffusion assays

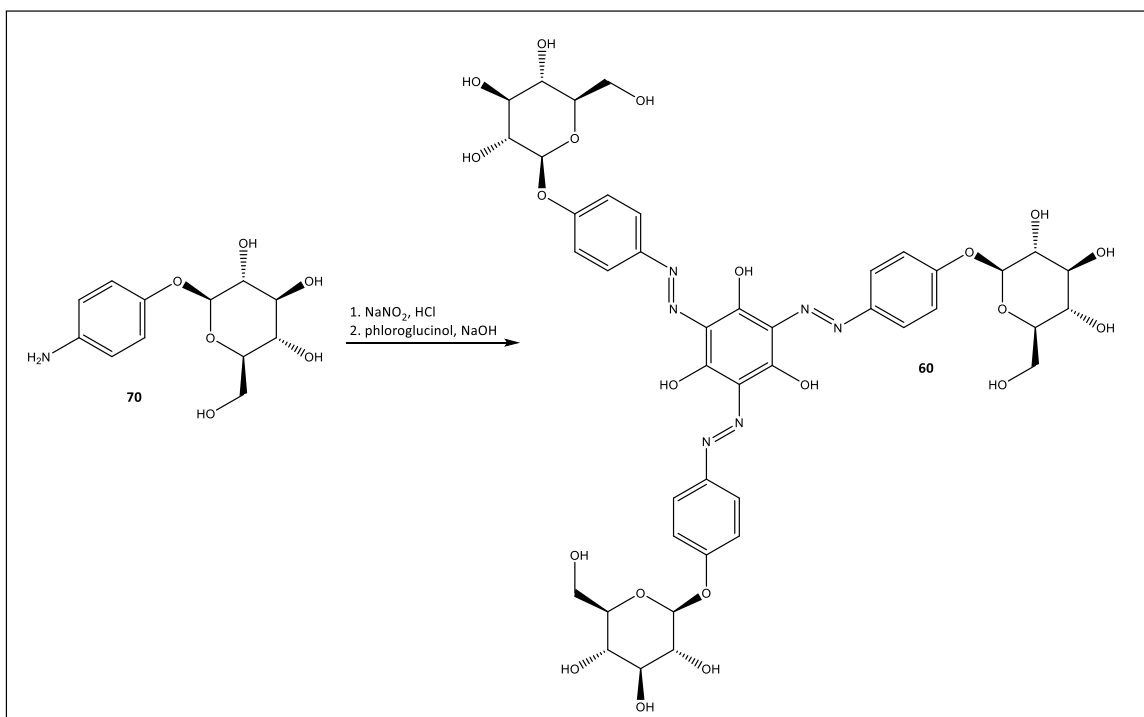
Gel diffusion assays of **61** and **68** with AGP and FGP were carried out using reported protocols.¹⁹ Briefly, gels containing 1% w/v agarose, 0.15 M NaCl, 0.02% w/v NaN_3 , and 10 $\mu\text{g/ml}$ of Yariv reagent were prepared in a petri dish. 0.8 μL of AGP or FGP solution were injected into the wells and the petri dishes were placed in an enclosed chamber that contained an open beaker of water (to maintain humidity) and incubated for 16 hours prior to visualization.



β -D-glucosyl-Yariv reagent (**61**) (Prepared by Helene Kuhn)

p-aminophenyl- β -D-glucopyranoside **69** (218 mg, 0.81 mmol) was dissolved in 0.5 M HCl (4.7 mL) and cooled to 0 °C. A freshly prepared cold aqueous solution of 0.3 M NaNO₂ (2.7 mL) was added with an addition funnel over a period of 15 min, and the solution was stirred for 2.5 h. The reaction mixture was cooled to 0 °C and a solution of phloroglucinol (31 mg, 0.25 mmol, 0.3 eq.) in cold water (9.5 mL), was added dropwise with an addition funnel over a period of 30 min. The pH of the reaction mixture was adjusted to 9 with 0.5M NaOH. The reaction mixture was stirred for an additional 3 h, while readjusting the pH to 9 if necessary. After 3 h EtOH (25 mL) was added to the reaction mixture and the pH was adjusted to neutral with 1 M HCl. The neutralized reaction mixture was placed in a freezer overnight. The formed precipitate was collected using a Hirsch-funnel and rinsed with cold ethanol. The precipitate was dried under high vacuum, but the ¹H NMR spectrum showed considerable residual ethanol, so the product was dissolved in methanol and the solvent was removed on a rotary evaporator. The product was dried under high vacuum

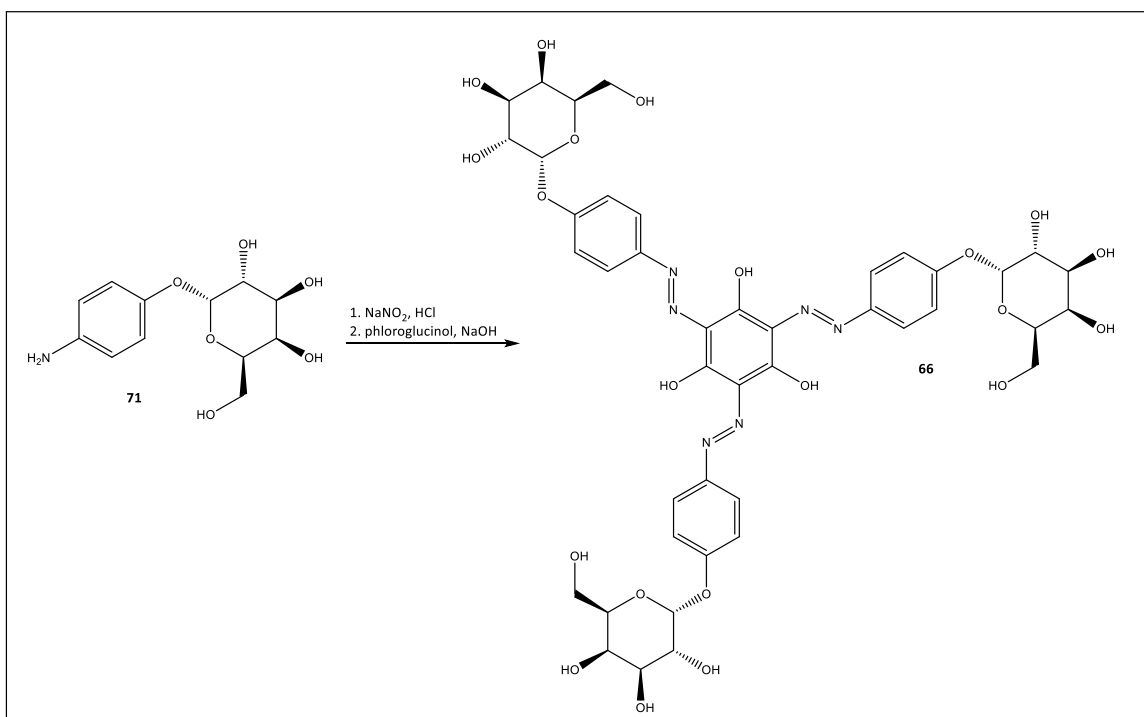
to provide the product as a deep red powder (57 mg 60 μ mol, 24%). Additional precipitate was collected from the mother liquor (43 mg, 44 μ mol, 18%). ^1H NMR (600 MHz, $\text{DMSO-}d_6$) δ 15.90 & 15.07 (br s, 3H); 7.65 (d, $J = 9.2$, 6H), 7.17 (d, $J = 8.6$, 6H); 5.35 (d, $J = 5$, 3H); 5.11 (d, $J = 5$, 3H); 5.04 (d, $J = 5$, 3H); 4.92 (d, $J = 7.4$, 3H); 4.60 (t, $J = 5$, 3H); 3.72 (m, 3H); 3.49 (m, 3H), 3.37 (m, 3H); 3.27 (m, 6H); 3.18 (m, 6H). ^{13}C NMR (150 MHz, $\text{DMSO-}d_6$) δ 171.7, 156.4, 136.1, 128.4, 118.5, 117.5, 100.5, 77.1, 76.6, 73.2, 69.7, 60.7. HRMS Calc. for $\text{C}_{42}\text{H}_{49}\text{N}_6\text{O}_{21}[\text{M}+\text{H}]$: 973.2951, Obsd. 973.2933



β -D-galactosyl-Yariv reagent (**60**) (Prepared by Robert Lusi and David Caianiello)

p -aminophenyl- β -D-galactopyranoside **70** (461 mg, 1.7 mmol) was dissolved in 0.5 M HCl (9.9 mL) and cooled to 0 $^\circ\text{C}$. A freshly prepared cold aqueous solution of 0.3 M NaNO_2 (5.7 mL) was added with an addition funnel over a period of 5 min, and the solution was stirred for 2 h. The reaction mixture was cooled to 0 $^\circ\text{C}$ and a solution of phloroglucinol (67 mg, 0.53 mmol, 0.3 eq.) in cold water (21 mL), was added dropwise with an addition funnel over a period of 30 min. The pH of

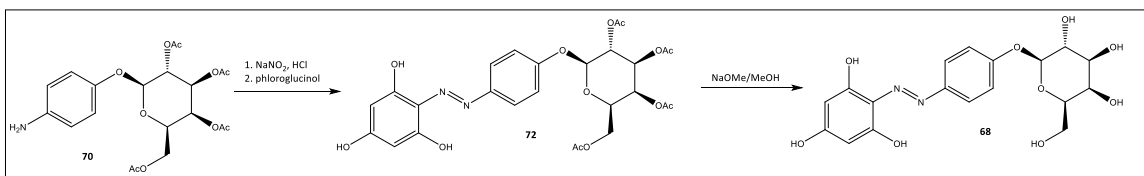
the reaction mixture was adjusted to 9 with 0.5 M NaOH. The reaction mixture was stirred for an additional 2 h, while readjusting the pH to 9 if necessary. After 3 h EtOH (50 mL) was added to the reaction mixture and reaction mixture was placed in a freezer overnight. The formed precipitate was collected using a Hirsch-funnel and rinsed with cold ethanol to yield **60** as a deep red powder (292 mg, .300 mmol, 53 % yield). $^1\text{H-NMR}$ (600 MHz, $\text{DMSO-}d_6$ with 5% D_2O) δ 7.44 (s, 6H,) 7.11 (d, $J = 8.6$, 6H,) 5.19 (s, 3H), 4.86 (m, 6H), 4.69 (s, 3H), 4.52 (3H), 3.70 (m, 3H), 3.61 – 3.41 (m, 15H). HRMS Calc. for $\text{C}_{42}\text{H}_{49}\text{N}_6\text{O}_{21}$ [M+H]: 973.2951, Obsd. 973.2932.



α -D-galactosyl-Yariv (**66**) (Prepared by Helene Kuhn)

p-aminophenyl- α -D-galactopyranoside **71** (218 mg, 0.81 mmol) was dissolved in 0.5 M HCl (4.7 mL) and cooled to 0 °C. A freshly prepared cold aqueous solution of 0.3 M NaNO_2 (2.7 mL) was added with an addition funnel over a period of 5 min, and the solution was stirred for 2 h. The reaction mixture was cooled to 0 °C and a solution of phloroglucinol (31 mg, 0.25 mmol, 0.3 eq.) in cold water (10 mL), was added dropwise with an addition funnel over a period of 15 min. The

pH of the reaction mixture was adjusted to 9 with 0.5M NaOH. The reaction mixture was stirred for an additional 2 h, while readjusting the pH to 9 if necessary. After 2 h MeOH (25 mL) was added to the reaction mixture and the reaction mixture was placed in a freezer overnight. The pH was adjusted to neutral with 1 M HCl and the reaction mixture was placed in a freezer overnight. The formed precipitate was collected using a Hirsch-funnel and rinsed with cold methanol, and dried under high vacuum overnight to provide **66** as a deep red powder (186 mg 0.19 mmol, 76 % yield). ^1H NMR (600 MHz, DMSO- d_6) δ = 15.93 (s, 3H), 7.64 (d, $J=8.9$, 6H), 7.22 (d, $J=8.5$, 6H), 5.46 (d, $J=3.2$, 3H), 4.94 (d, $J=6.0$, 3H), 4.77 (d, $J=5.2$, 3H), 4.58 (d, $J=3.4$, 3H), 4.55 (t, $J=5.9$, 3H), 3.79 (m, 9H), 3.72 (t, $J=6.3$, 3H), 3.50 (m, 3H), 3.42 (m, 3H). ^{13}C NMR (151 MHz, DMSO- d_6) δ 178.0, 156.8, 136.1, 128.5 118.9, 118.6, 98.8, 72.8, 69.8, 69.1, 68.4, 60.9. HRMS Calc. for $\text{C}_{42}\text{H}_{49}\text{N}_6\text{O}_{21}$ [M+H]: 973.2951, Obsd 973.2925



Single azo-linked β -D-galactoside (**68**) (Prepared by Natalie Palaychuk)

2,3,4,6-Tetraacetyl-*p*-aminophenyl- β -D-galactopyranoside **70** (1.52 g, 3.5 mmol) was dissolved in acetic acid (20.8 ml). and cooled to 0 °C. Hydrochloric acid (0.89 ml) was added, followed by a freshly prepared cold aqueous solution of 0.3 M NaNO_2 (18 mL) was added, and the solution was stirred for 70 min. A cold aqueous solution of phloroglucinol (4.54 g, 36 mmol, 10 eq) was prepared in approximately 350 mL water. The diazo compound was then rapidly added to the phloroglucinol, with vigorous stirring. Stirring was continued for 10 min, at which point potassium iodide (0.90g, 5.4 mmol) was added, and the reaction was stirred for an additional 10 minutes.

The reaction mixture was diluted with dichloromethane and washed with water. The aqueous layer was re-extracted with dichloromethane. The combined organic layers were washed 4 times with water, once with saturated sodium bicarbonate, and once with brine. The organic layer was dried (sodium sulfate) and concentrated in vacuo. The product was obtained after silica gel chromatography (7:3 ethyl acetate:hexane) to provide **72** as a yellow solid (274 mg, 0.48 mmol, 14 %). ^1H NMR (600MHz, CDCl_3) δ 13.75 (br s), 7.60 (m, 2H), 7.02 (m, 2H), 5.99 (br s, 2H), 5.48 (m, 2H), 5.15 (m, 2H), 4.23 (m 1H), 4.10 (m, 1H), 2.18, 2.08, 2.05, 2.02 (s, 12H). ^{13}C NMR (125 MHz, CDCl_3) δ 170.9, 170.6, 169.9, 164.8, 158.1, 157.8, 145.0, 122.5, 122.3, 117.4, 99.0, 96.1, 94.5, 71.1, 70.9, 68.7, 67.0, 61.5, 20.8, 20.71, 20.65, 20.63.

72 (15 mg, 0.026 mmol) was dissolved in methanol (0.15 mL). Freshly prepared 1 M NaOMe was added (2.0 μL) and the solution was stirred at room temperature. The reaction mixture was monitored by TLC (5:1 DCM/methanol). After 6 h no conversion was seen, 4 μL NaOMe and 0.15 mL methanol were added. At 22 h there was still no conversion, so NaOMe was added until the pH of the solution was 10. The solution was stirred for 2 more hours, at which TLC showed full conversion. The solution was diluted with methanol (10 mL) and neutralized with Amberlite IR-120 ion exchange resin. The mixture was filtered and washed with methanol. Concentration in vacuo provided **68** quantitatively (11 mg, 0.026 mmol). ^1H NMR (600MHz, CDCl_3) δ 12.0 (br s, 3H), 7.91 (d, $J = 10.2$, 2H), 7.14 (d, $J = 8.9$, 2H), 5.86 (s, 2H), 5.22 (d, $J = 4.9$, 1H), 4.93 (d, $J = 7.1$, 1H), 4.91 (d, $J = 5.2$, 1H), 4.69 (t, $J = 4.8$, 1H), 4.54 (d, $J = 4.1$, 1H), 3.71 (m, 1H), 3.65 – 3.42 (m, 5H). HRMS Calc. for $\text{C}_{18}\text{H}_{21}\text{N}_2\text{O}_9$ [M+H]: 409.1247, Obsd. 409.1246.

References

1. Leeber, B. W. III.; Kuhn, H.; Caianiello, D.; Dale, B.; Lusi, R.; Palaychuk, N.; Weingarten, S.; Basu, A., Supramolecular chirality of Yariv reagents dictates arabinogalactan binding. **2017**.
2. Delbianco, M.; Bharate, P.; Varela-Aramburu, S.; Seeberger, P. H., Carbohydrates in Supramolecular Chemistry. *Chemical Reviews* **2016**, *116* (4), 1693-1752.
3. Palmans, A. R.; Meijer, E. e. W., Amplification of chirality in dynamic supramolecular aggregates. *Angewandte Chemie International Edition* **2007**, *46* (47), 8948-8968.
4. Woody, R. W., [4] Circular dichroism. *Methods in Enzymology* **1995**, *246*, 34-71.
5. Thalacker, C.; Würthner, F., Chiral Perylene Bisimide–Melamine Assemblies: Hydrogen Bond-Directed Growth of Helically Stacked Dyes with Chiroptical Properties. *Advanced Functional Materials* **2002**, *12* (3), 209-218.
6. Wang, K.-R.; Han, D.; Cao, G.-J.; Li, X.-L., Synthesis and Predetermined Supramolecular Chirality of Carbohydrate-Functionalized Perylene Bisimide Derivatives. *Chemistry – An Asian Journal* **2015**, *10* (5), 1204-1214.
7. Huang, Y.; Wang, J.; Wei, Z., Modulating supramolecular helicity and electrical conductivity of perylene dyes through an achiral alkyl chain. *Chemical Communications* **2014**, *50* (61), 8343-8345.
8. Wang, K.-R.; An, H.-W.; Wu, L.; Zhang, J.-C.; Li, X.-L., Chiral self-assembly of lactose functionalized perylene bisimides as multivalent glycoclusters. *Chemical Communications* **2012**, *48* (45), 5644-5646.
9. Müller, M. K.; Brunsveld, L., A Supramolecular Polymer as a Self-Assembling Polyvalent Scaffold. *Angewandte Chemie International Edition* **2009**, *48* (16), 2921-2924.
10. Paulsen, B. S.; Craik, D. J.; Dunstan, D. E.; Stone, B. A.; Bacic, A., The Yariv reagent: Behaviour in different solvents and interaction with a gum arabic arabinogalactanprotein. *Carbohydrate Polymers* **2014**, *106*, 460-468.
11. Yariv, J.; Rapport, M.; Graf, L., The interaction of glycosides and saccharides with antibody to the corresponding phenylazo glycosides. *Biochemical Journal* **1962**, *85* (2), 383.
12. Lee, Y. C.; Lee, R. T., Carbohydrate-protein interactions: basis of glycobiology. *Accounts of Chemical Research* **1995**, *28* (8), 321-327.
13. Lundquist, J. J.; Toone, E. J., The cluster glycoside effect. *Chemical Reviews* **2002**, *102* (2), 555-578.
14. Yariv, J.; Kalb, A. J.; Katchalski, E., Isolation of an L-fucose binding protein from Lotus tetragonolobus seed. *Nature* **1967**, *215* (5103), 890-891.
15. Jermyn, M.; Yeow, Y.; Woods, E., A Class of Lectins Present in the Tissues of Seed Plants. *Functional Plant Biology* **1975**, *2* (4), 501-531.
16. Anderson, D.; Farquhar, J., The composition of eight Acacia gum exudates from the series Gummiferae and Vulgares. *Phytochemistry* **1979**, *18* (4), 609-610.
17. Fincher, G. B.; Stone, B. A.; Clarke, A. E., Arabinogalactan-proteins: structure, biosynthesis, and function. *Annual Review of Plant Physiology* **1983**, *34* (1), 47-70.
18. Jermyn, M., Comparative specificity of concanavalin A and the beta lectins. **1978**.
19. van Holst, G.-J.; Clarke, A. E., Quantification of arabinogalactan-protein in plant extracts by single radial gel diffusion. *Analytical Biochemistry* **1985**, *148* (2), 446-450.

20. Kitazawa, K.; Tryfona, T.; Yoshimi, Y.; Hayashi, Y.; Kawauchi, S.; Antonov, L.; Tanaka, H.; Takahashi, T.; Kaneko, S.; Dupree, P., β -Galactosyl Yariv reagent binds to the β -1, 3-galactan of arabinogalactan proteins. *Plant Physiology* **2013**, *161* (3), 1117-1126.
21. Seifert, G. J.; Roberts, K., The biology of arabinogalactan proteins. *Annu. Rev. Plant Biol.* **2007**, *58*, 137-161.
22. Nguema-Ona, E.; Vicré-Gibouin, M.; Cannesan, M.-A.; Driouich, A., Arabinogalactan proteins in root–microbe interactions. *Trends in Plant Science* **2013**, *18* (8), 440-449.
23. Tan, L.; Showalter, A. M.; Egelund, J.; Hernandez-Sanchez, A.; Doblin, M. S.; Bacic, A., Arabinogalactan-proteins and the research challenges for these enigmatic plant cell surface proteoglycans. *Frontiers in Plant Science* **2012**, *3*.
24. Perera, N.; Yang, F.-L.; Chang, C.-M.; Lu, Y.-T.; Zhan, S.-H.; Tsai, Y.-T.; Hsieh, J.-F.; Li, L.-H.; Hua, K.-F.; Wu, S.-H., Galactomannan from *Antrodia cinnamomea* Enhances the Phagocytic Activity of Macrophages. *Organic Letters* **2017**, *19* (13), 3486-3489.
25. Nguema-Ona, E.; Coimbra, S.; Vicré-Gibouin, M.; Mollet, J.-C.; Driouich, A., Arabinogalactan proteins in root and pollen-tube cells: distribution and functional aspects. *Annals of Botany* **2012**, *110* (2), 383-404.
26. Majewska-Sawka, A.; Nothnagel, E. A., The multiple roles of arabinogalactan proteins in plant development. *Plant Physiology* **2000**, *122* (1), 3-10.
27. Verbeke, D.; Dierckx, S.; Dewettinck, K., Exudate gums: occurrence, production, and applications. *Applied Microbiology and Biotechnology* **2003**, *63* (1), 10-21.
28. Saeed, F.; Pasha, I.; Anjum, F. M.; Sultan, M. T., Arabinoxylans and arabinogalactans: a comprehensive treatise. *Critical reviews in food science and nutrition* **2011**, *51* (5), 467-476.
29. Clarke, A.; Gleeson, P.; Harrison, S.; Knox, R. B., Pollen—stigma interactions: Identification and characterization of surface components with recognition potential. *Proceedings of the National Academy of Sciences* **1979**, *76* (7), 3358-3362.
30. Park, M. H.; Suzuki, Y.; Chono, M.; Knox, J. P.; Yamaguchi, I., CsAGP1, a gibberellin-responsive gene from cucumber hypocotyls, encodes a classical arabinogalactan protein and is involved in stem elongation. *Plant physiology* **2003**, *131* (3), 1450-1459.
31. Van Hengel, A. J.; Roberts, K., AtAGP30, an arabinogalactan-protein in the cell walls of the primary root, plays a role in root regeneration and seed germination. *The Plant Journal* **2003**, *36* (2), 256-270.
32. Sun, W.; Kieliszewski, M. J.; Showalter, A. M., Overexpression of tomato LeAGP-1 arabinogalactan-protein promotes lateral branching and hampers reproductive development. *The Plant Journal* **2004**, *40* (6), 870-881.
33. Vicré, M.; Santaella, C.; Blanchet, S.; Gateau, A.; Driouich, A., Root border-like cells of *Arabidopsis*. Microscopical characterization and role in the interaction with rhizobacteria. *Plant physiology* **2005**, *138* (2), 998-1008.
34. Nothnagel, E. A.; Lyon, J., Structural requirements for the binding of phenylglycosides to the surface of protoplasts. *Plant physiology* **1986**, *80* (1), 91-98.
35. Woods, E.; Lilley, G.; Jermyn, M., The self-association of glycosyl phenylazo dyes (Yariv antigens). *Australian Journal of Chemistry* **1978**, *31* (10), 2225-2238.
36. Larkin, P., Plant protoplast agglutination and membrane-bound beta-lectins. *Journal of Cell Science* **1977**, *26* (1), 31-46.
37. Kuhn, R.; Bär, F., Über die Konstitution der Oxy-azo-verbindungen. *European Journal of Organic Chemistry* **1935**, *516* (1), 143-155.
38. Chen, X.-C.; Tao, T.; Wang, Y.-G.; Peng, Y.-X.; Huang, W.; Qian, H.-F., Azo-hydrazone tautomerism observed from UV-vis spectra by pH control and metal-ion complexation

- for two heterocyclic disperse yellow dyes. *Dalton transactions* **2012**, 41 (36), 11107-11115.
39. Lee, H. Y.; Song, X.; Park, H.; Baik, M.-H.; Lee, D., Torsionally Responsive C₃-Symmetric Azo Dyes: Azo–Hydrazone Tautomerism, Conformational Switching, and Application for Chemical Sensing. *Journal of the American Chemical Society* **2010**, 132 (34), 12133-12144.
 40. Dale, B., Elucidating the Binding Mechanism of Arabinogalactan and Yariv Phenylglycosides through Radial Diffusion Assays and Circular Dichroism Spectroscopy. *Brown University* **2017**.
 41. Renard, D.; Garnier, C.; Lapp, A.; Schmitt, C.; Sanchez, C., Structure of arabinogalactan-protein from Acacia gum: From porous ellipsoids to supramolecular architectures. *Carbohydrate Polymers* **2012**, 90 (1), 322-332.
 42. Price, N. P.; Vermillion, K. E.; Eller, F. J.; Vaughn, S. F., Frost Grape Polysaccharide (FGP), an Emulsion-Forming Arabinogalactan Gum from the Stems of Native North American Grape Species *Vitis riparia* Michx. *Journal of Agricultural and Food Chemistry* **2015**, 63 (32), 7286-7293.
 43. Weingarten, S., Use of radial diffusion gel assays to characterize interactions between gum arabic arabinogalactan proteins and Yariv reagents. *Brown University* **2015**.
 44. Piculell, L.; Borgström, J.; Chronakis, I. S.; Quist, P.-O.; Viebke, C., Organisation and association of κ -carrageenan helices under different salt conditions. *International Journal of Biological Macromolecules* **1997**, 21 (1), 141-153.
 45. Prajapati, V. D.; Jani, G. K.; Zala, B. S.; Khutliwala, T. A., An insight into the emerging exopolysaccharide gellan gum as a novel polymer. *Carbohydrate Polymers* **2013**, 93 (2), 670-678.
 46. McIntosh, M.; Stone, B.; Stanisich, V., Curdlan and other bacterial (1 \rightarrow 3)- β -D-glucans. *Applied Microbiology and Biotechnology* **2005**, 68 (2), 163-173.
 47. Tryfona, T.; Liang, H.-C.; Kotake, T.; Tsumuraya, Y.; Stephens, E.; Dupree, P., Structural characterization of Arabidopsis leaf arabinogalactan polysaccharides. *Plant physiology* **2012**, 160 (2), 653-666.
 48. Bartetzko, M. P.; Schuhmacher, F.; Hahm, H. S.; Seeberger, P. H.; Pfrengle, F., Automated Glycan Assembly of Oligosaccharides Related to Arabinogalactan Proteins. *Organic Letters* **2015**, 17 (17), 4344-4347.
 49. Kinnaert, C.; Daugaard, M.; Nami, F.; Clausen, M. H., Chemical Synthesis of Oligosaccharides Related to the Cell Walls of Plants and Algae. *Chemical Reviews* **2017**, 117 (17), 11337-11405.
 50. Basile, D. V.; Ganjian, I., β -D-glucosyl and α -D-galactosyl Yariv reagents: syntheses from p-nitrophenyl-D-glycosides by transfer reduction using ammonium formate. *Journal of Agricultural and Food Chemistry* **2004**, 52 (25), 7453-7456.

4 YARIV – ALCOHOL AGGREGATION EFFECTS

4.1 Yariv reagent aggregation behavior

As discussed in the previous chapter, the glycosylated phenyl-azo dyes known as Yariv reagents aggregate in aqueous solution to form helical stacked supramolecular polymers. The helical stacked arrangement of the polyaromatic cores of the Yariv reagents results in intermolecular excitonic interactions. These interactions give rise to a bisignate Cotton effect in the circular dichroism (CD) spectra of these compounds. The sign of this Cotton effect can be used to determine the helical sense of the Yariv aggregates (i.e. left or right-handed). Also, only Yariv aggregates that form right handed helices are capable of binding to arabinogalactan protein (AGP). This is likely due to the Yariv binding epitope being the β -1,3-galactan backbone of the AGP, which adopts a helical conformation in solution.

This chapter will focus on developing the understanding of the aggregation behavior of Yariv reagents and investigating how the presence of alcohol affects Yariv aggregation.

4.2 Background

4.2.1 Supramolecular polymers

Supramolecular polymers are macromolecules composed of smaller molecules that are connected by non-covalent linkages such as hydrogen bonds or electrostatic interactions.¹ There are various examples of supramolecular polymers in living systems. Clathrin proteins self-assemble during endocytosis to form clathrin coated vesicles.² Also, the cell cytoskeleton is composed of long filaments of ordered protein monomers that assemble and disassemble to regulate important biological functions.¹ Furthermore, fibrous collagen proteins self-assemble to

form triple helices, and then further assemble into quasi hexagonal staggered structures known as collagen fibrils, which themselves can further assemble to produce fibers and gels.³ Self-assembly of these biological supramolecular polymers is highly controlled and is directed by information contained within the monomeric units, such as hydrogen bonding patterns, electrostatic and steric features.⁴ This characteristic allows for vast and complex architectures to be assembled from relatively simple monomeric units.

Applying the concepts of biological supramolecular assembly to synthetically prepared systems enables the design of complex self-assembled architectures through synthesis custom monomers.¹ Some supramolecular polymers are random coils with no internal order, and are similar to covalently bonded polymers. However, other supramolecular polymers are highly

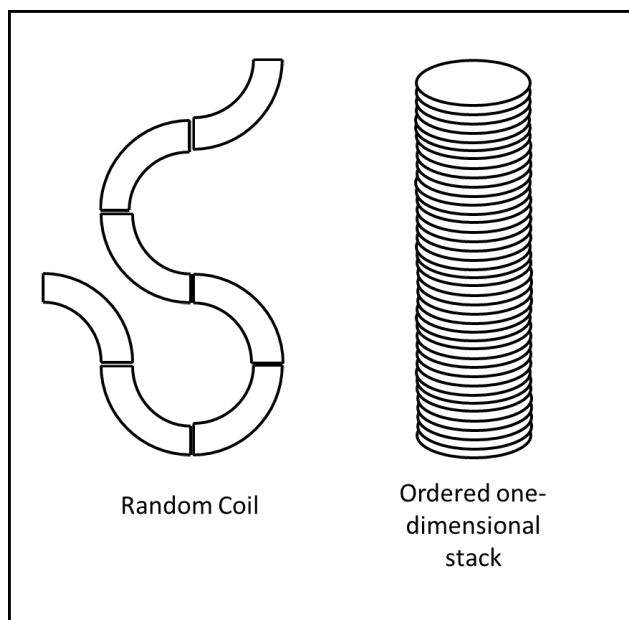


Figure 4.1: Types of supramolecular polymers

ordered one-dimensional shape-persistent nanostructures (Fig. 4.1).¹ Examples of the latter type of supramolecular polymer includes nanotubes prepared from cyclic peptide monomers that self-assemble via hydrogen bonding⁵ and nanofibers prepared from discotic molecules with polyaromatic cores that assemble via hydrogen bonding and π - π stacking interactions.⁶

In addition to ordered structure, the monomeric units of these supramolecular polymers can be designed to impart functionality to the assembly. Supramolecular nanofibers that are formed by the self-assembly of cyclic peptide amphiphile molecules were designed to promote regeneration of axons in damaged spinal cords,⁷ stimulate the growth of blood vessels,⁸ and regenerate bone

and cartilage.⁹ Peptide amphiphile supramolecular polymers have also been used to prepare networks to encapsulate cells and enable their growth. This nanofiber scaffold can also be degraded by enzymatic-mediated degradation of the peptides. This system essentially mimics several key features of the extracellular matrix.¹⁰ Also, supramolecular nanofibers that are formed by the self-assembly of discotic molecules with extended polyaromatic cores have been found to conduct electricity and have been used as nanowires in electronic devices.¹¹⁻¹² Such nanofibers are able to conduct electricity due to the π - π stacking interactions that enable the polymers to self-assemble.¹¹⁻¹²

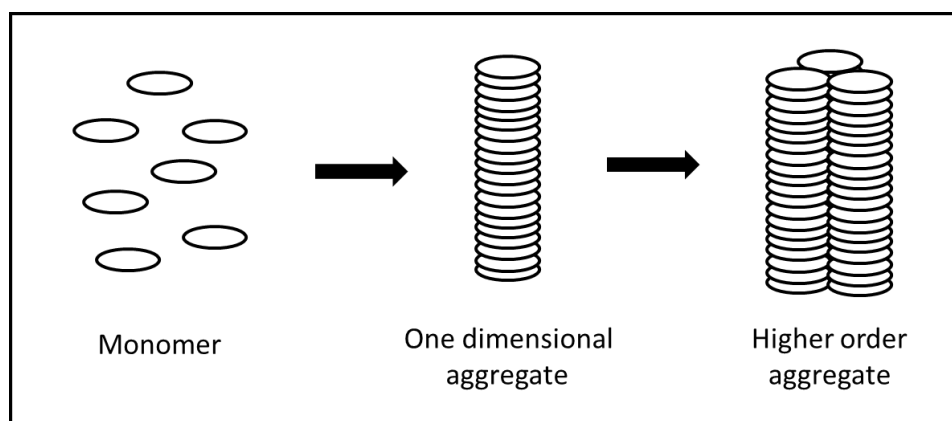


Figure 4.2: Hierarchical self-assembly

The ability of supramolecular polymers to provide functional and controlled architectures from self-assembly of simple monomers makes them very attractive materials. However, in order to mimic biological supramolecular polymers like collagen, it is important that these polymers can be designed to go beyond just one-dimensional nanotubes and fibers and form higher-order two and three-dimensional architectures (Fig 4.2). Synthetic peptide chains have been prepared that self-assemble in a way that mimics the self-assembly of collagen by first forming triple helices, then nanofibers before forming a hydrogel network.³ Also, charged amphiphilic peptides self-assemble into cylindrical nanofibers¹³ which further aggregate into bundles of fibers that form a

liquid crystal solution.¹⁴ This solution of supramolecular polymers can be manually manipulated and when mixed with cells can be used to form microdomain gels of aligned cells and filaments.¹⁴ Another example of a supramolecular polymer that can assemble into higher order aggregates are those composed of the oligo(*p*-phenylenevinylene) monomer **73** (Fig. 4.3). These monomers first form dimers via hydrogen-bonding and then the dimers stack to form 1-D fibers. Chiral derivatives of the monomers form helical fibers. The length of the fibers increases with a decrease in temperature. As temperature decreases, the helical stacks begin to interact with one another to form bundles of stacks and/or gel networks.¹⁵

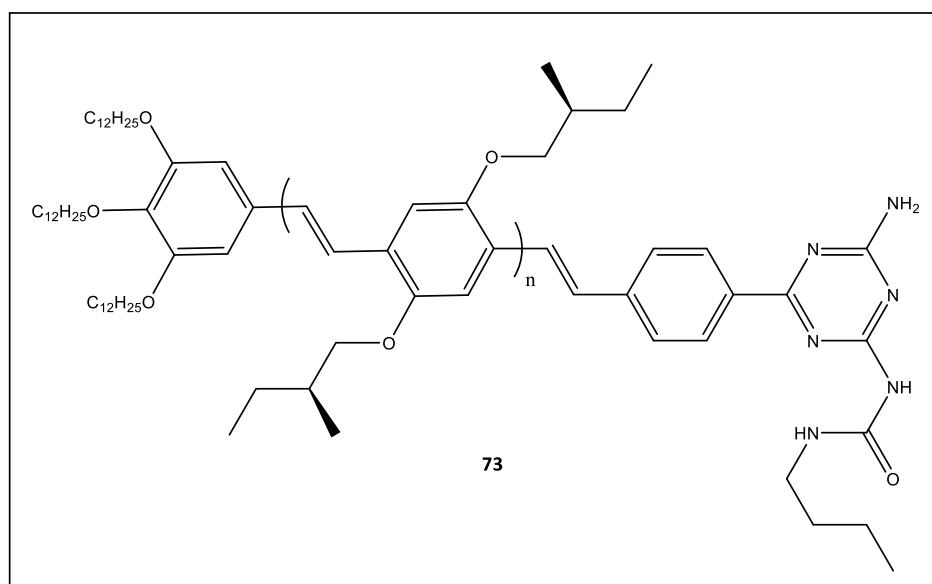


Figure 4.3: Oligo(*p*-phenylenevinylene) monomer

The ability of synthetic supramolecular polymers to form hierarchical ordered structures is an important feature when it comes to mimicking biological supramolecular assemblies. However, the ability to control or trigger this self-assembly is equally important when it comes to the utility of these assemblies as dynamic materials. The self-assembly behavior of the previously mentioned oligo(*p*-phenylenevinylene) supramolecular polymers is temperature controlled. As the temperature decreases, aggregation is increased.¹⁵ This behavior is indicative of aggregation that

is enthalpically driven, and thus polymerization occurs upon cooling.¹⁶ Supramolecular polymers are dynamic materials that can be polymerized or depolymerized by changing the temperature or other thermodynamic parameters such as concentration and pressure.¹⁶

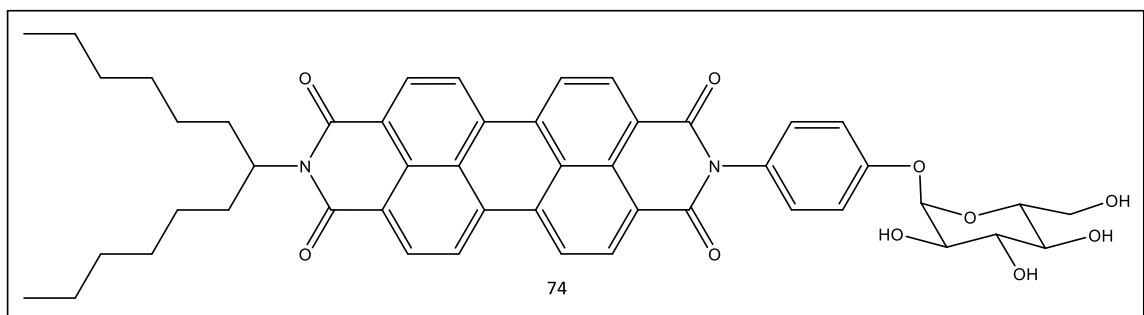


Figure 4.4: Perylene bisimide derivative

The identity of the solvent can also affect the self-assembly of supramolecular aggregates. For example, supramolecular polymers composed of perylene bisimide derivatives (Fig. 4.4) functionalized with hydrophobic alkyl chains on one end and a hydrophilic carbohydrate on the other undergo a change in helicity depending on the composition of the solvent. When solutions of **74** are prepared in hydrophilic solvent mixtures such as 40:60 THF:H₂O (v/v) the carbohydrates of the monomers are exposed to solvent and a right-handed helix is observed. When solutions of **74** are prepared in more hydrophobic solvent mixtures, such as 80:20 CHCl₃:C₈H₁₈ (v/v) the alkyl chains are exposed to solvent and give rise to left-handed helices.¹⁷ In another example, a chiral derivative of a C₃-symmetrical discotic monomer, 3,3'-bis(acylamino)-2,2'-bipyridine-substituted benzene-1,3,5-tricarboxamide (BiPy-BTA) **75** (Fig. 4.5), containing an extended polyaromatic core elaborated with hydrophilic PEG chains is observed to undergo a transition from a single stranded 1-D helical aggregate in pure isopropanol to a triple stranded helical aggregate when the monomer is dissolved in aqueous alcoholic solutions with larger fractions of water.¹⁸ It is important to understand how stimuli such as temperature and solvent composition affect the architectures of supramolecular polymers if they are to be applied as useful materials.

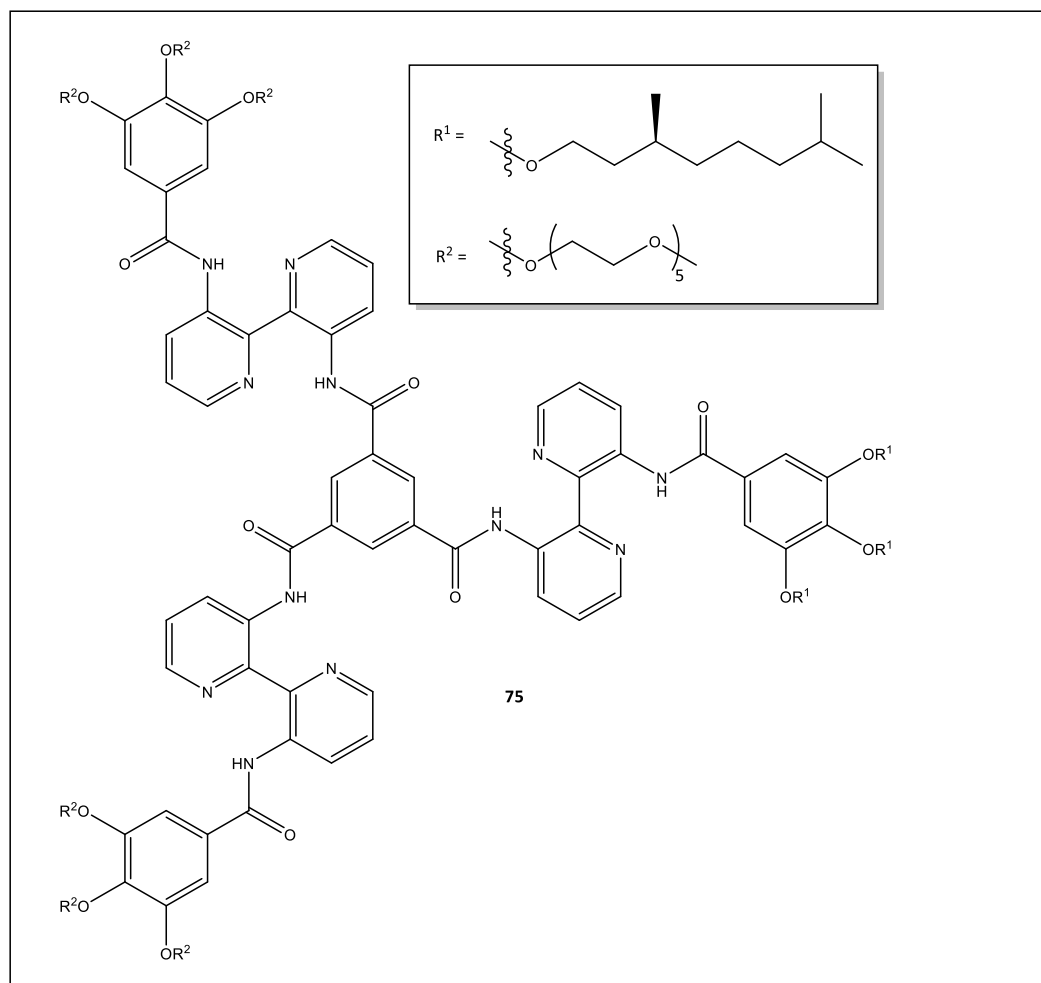


Figure 4.5: Derivative of 3,3'-bis(acylamino)-2,2'-bipyridine-substituted benzene-1,3,5-tricarboxamide (BiPy-BTA)

4.2.2 Mechanisms of self-assembly for supramolecular polymers

Polymerization through the formation of covalent bonds usually proceeds under kinetic control since there is usually a high barrier to reversibility,¹⁶ except in the case of condensation polymers such as polyimines for which polymerization is reversible.¹⁹ Since supramolecular polymers are not formed through covalent bond formation their self-assembly is much more dependent on thermodynamic factors such as temperature, concentration and pressure.¹⁶ As, previously noted, supramolecular polymers can undergo hierarchal aggregation to form complex 2-D and 3-D

architectures, but ordered supramolecular polymers initially form some type of 1-D stack. These 1-D aggregates typically self-assemble via either isodesmic or cooperative self-assembly.¹⁶

In isodesmic self-assembly (Fig 4.6) each addition of a monomer occurs in an identical manner at all steps of polymerization and thus the association constant (K) is not dependent on the size of the aggregate. Therefore, the degree of self-assembly of these type of supramolecular polymers is entirely dependent on thermodynamic factors such as temperature and concentration.¹⁶

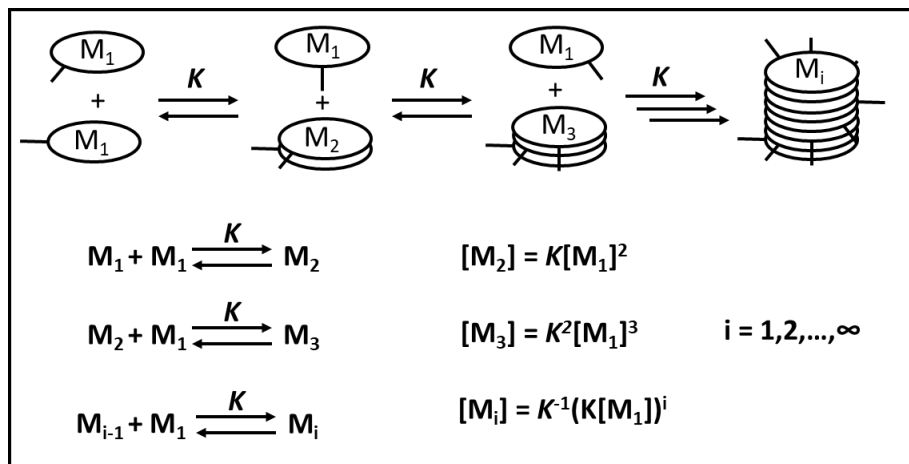


Figure 4.6: Isodesmic self-assembly mechanism of rigid discotic molecules

In cooperative self-assembly (Fig. 4.7) there is first a nucleation phase where the monomers associate via an isodesmic mechanism with a weak association constant (K_n).¹⁶ At some critical point in temperature, concentration, or pressure; thermodynamic conditions allow for the formation of a stable nucleus. Once the nucleus is formed further aggregation becomes much more favorable, and the elongation phase begins in which the self-assembly occurs via an isodesmic mechanism with a much stronger association constant (K_e) than the nucleation phase.¹⁶ While the mechanisms of 1-D self-assembly of supramolecular polymers can be easily characterized, higher order aggregates assemble by mechanisms that are more complex.

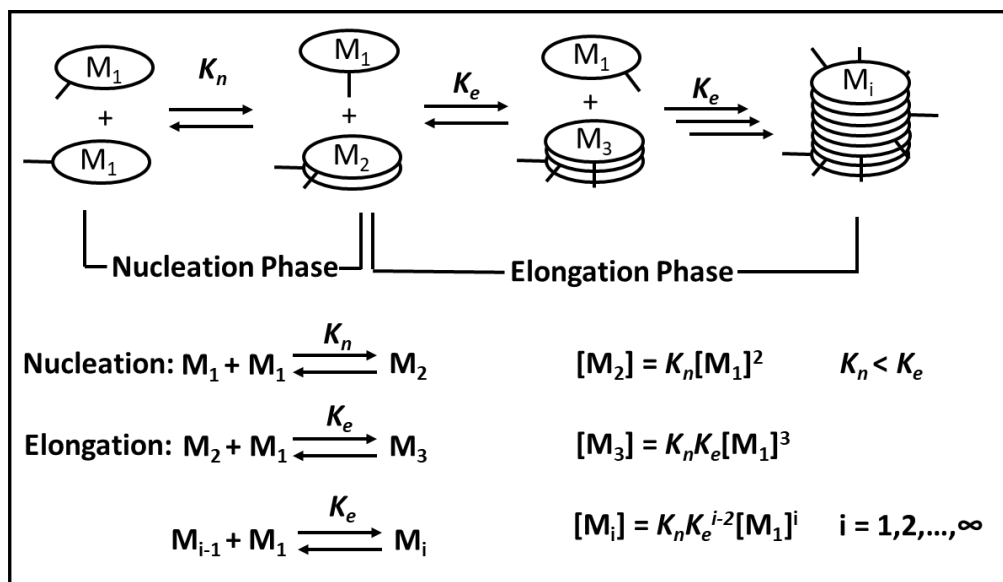


Figure 4.7: Isodesmic self-assembly mechanism of rigid discotic molecules. In this case the nucleus is a dimer.

4.2.3 C_3 -Discotic supramolecular polymers and alcohol effects

The BiPy-BTA molecules described in a previous section are interesting because they are analogous to the Yariv reagent in that they possess an extended aromatic core, C_3 -symmetry, and are soluble in aqueous solutions.^{18,20} This last feature is quite important, as some of the previously described hierarchal assembling supramolecular systems are too non-polar to remain soluble in aqueous solution.²¹ In order to develop these systems for biomedical use, it must be possible for supramolecular polymers to assemble in aqueous media. However, design rules that apply to systems that assemble in organic media do not necessarily apply when designing systems for application in aqueous media. Unpredictable behavior can result. For example, nanoparticles decorated with hydrophobic patches form larger aggregates in aqueous solutions that are more dilute, seemingly contradicting the law of mass action.²² Also, 1,4,5,8-naphthalene-tetracarboxylic acid diimide-lysine amphiphiles functionalized with methoxy groups unexpectedly formed multilamellar 1-D nanotubes in water while other derivatives formed simple 1-D

nanotubes.²³ It is important to understand the reason for such phenomena at a molecular level, to enable the future development of useful supramolecular polymeric materials.

BiPy-BTA self-assembles into 1-D helical stacks in isopropanol (iPrOH) via π - π stacking of the polyaromatic cores.¹⁸ When PEG chains are added onto the BiPy-BTA core the molecules are more amphiphilic, and are water soluble. The amphiphilic 1-D helical stacks of BiPy-BTA further aggregate to form triple-helices in H₂O:iPrOH solutions for which the molar fraction of water is higher than 0.05. It is more favorable, due to the hydrophobic effect, for the stacks to aggregate and shield some of their hydrophobic surfaces from the aqueous solvent.¹⁸ The ability to control aggregation of the stacks using by forces orthogonal to the π - π stacking interaction, could be useful in designing functional supramolecular polymeric materials.¹⁸

The higher order aggregation of BiPy-BTA results in a transition from a single helical stack in pure isopropanol (regime III) to a short triple helix (regime II) to an elongated triple helical fiber (regime I), as the fraction of water in the solution is increased.¹⁸ This transition was first observed in circular dichroism (CD) experiments in which three distinctly different spectra (corresponding to the three regimes of aggregation) of BiPy-BTA were observed as the H₂O:iPrOH ratio is varied. Cryo-TEM and small angle X-ray scattering (SAXS) experiments confirmed that triple-helical fibers in were present in more aqueous solutions while only single helical fibers were present in iPrOH.¹⁸ CD experiments were also used to show that the transition is temperature-dependent as well. However at higher concentrations of water a lower critical solution temperature (LCST) is observed causing the aggregates to precipitate when temperatures are raised above 340 K.¹⁸

The LCST aggregation behavior of BiPy-BTA in water-alcohol solutions is similar to behavior observed in aqueous-alcoholic solutions of poly-N-isopropyl acrylamide (PNiPAM) **76** (Fig 4.8). In pure water PNiPAM is completely soluble at low temperatures, but precipitates when the

temperature of the water is raised above the LCST.²⁴ The amphiphilic polymer becomes solubilized at lower temperature due to the enthalpically favored process of hydrophobic hydration.²⁴

Hydrophobic hydration occurs when a hydrophobe is added to water resulting in the formation of a hydration shell of water molecules that solubilize the hydrophobe in a process that is enthalpically favored at the cost of being unfavorable to entropy.²⁵ The hydration is enthalpically favorable to water, because the water molecules in the hydration shell form stronger hydrogen bonds than the bulk water.²⁵ Increasing the temperature results in an entropy gain and a disintegration of the hydration shell as a result of the release of water molecules. This causes the hydrophobe to precipitate.²⁵

The LCST of the PNIPAM polymers was found to decrease with the addition of alcohol until at some point the polymer is insoluble at all temperatures measured in the experiment.²⁴ The degree to which the LCST decreases as the fraction of alcohol increases is dependent on the identity of the alcohol, with lower fractions of isopropanol being required to lower the LCST than

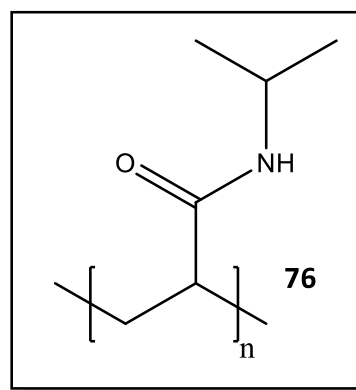


Figure 4.8: Structure of PNIPAM

methanol (isopropanol (iPrOH) < ethanol (EtOH) < methanol (MeOH)). The LCST is not dependent on the molecular weight of the PNIPAM polymers or the polymer concentration. These observations suggest that a physical property of the water-alcohol solutions is responsible for the variations in the LCST.²⁴ It has been proposed that this physical property is the excess enthalpy of mixing (ΔH_E) of the alcohol-water solutions.²⁴

Excess enthalpy, or the enthalpy of mixing, is defined as the change in enthalpy per mole of mixture when the pure components are mixed at constant temperature and pressure.²⁶ When values for ΔH_E are plotted against the mole fraction of alcohol (χ) for alcohol-water

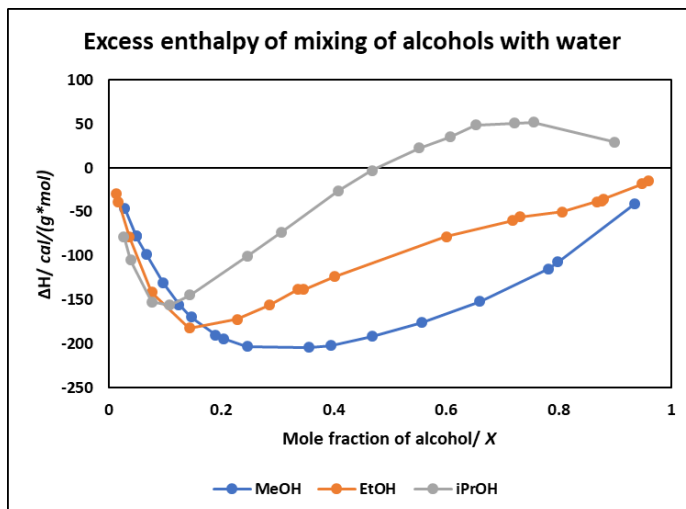


Figure 4.9: Excess enthalpy of mixing of alcohols with water

mixtures (iPrOH, EtOH, and MeOH) a minimum is observed at $\chi < 0.4$ for all alcohols (Fig 4.9).²⁶ The value for χ at which the minima is observed is lowest for iPrOH and highest for MeOH (iPrOH < EtOH < MeOH).²⁴ This trend correlates well with the trend at which the value of the LCST decreased based on alcohol identity. Also, the χ values at which the LCST is at a minimum (or becomes lower than the range of measured temperatures) correlates very well with the χ values at which ΔH_E is at a minimum suggesting a link between the thermodynamic behavior of the solvent mixtures and the aggregation behavior of the PNIPAM polymers.²⁴

When mixed with water these alcohols behave as kosmotropes, which are chemical agents that increase the strength of hydrogen bonding between water molecules without disrupting the water network. These solutes likely do not form direct hydrogen bonds with water and instead remain solvated by inducing a structuring of the bulk water by hydrophobic hydration of their hydrophilic groups.²⁴ The decrease in enthalpy observed for the alcohol-water mixtures at $\chi < 0.4$ are likely the result of this hydrophobic hydration of the alcohol molecules. Thus, the presence of alcohol molecules causes a decrease in the enthalpy of the bulk water and an increase in the strength of the hydrogen bonding among water molecules in the water network. As a result, the gain in enthalpy for water acquired by forming the hydration shell around the PNIPAM polymers

is decreased since there is less of a difference in the strength of the hydrogen bonds in the hydration shell and those in the bulk water, and thus the formation of the hydration shell becomes less favorable. Therefore, there is a decrease in the LCST since lower temperatures are required to keep the formation of the hydration shell favorable.²⁴ This phenomena is known as the kosmotropic effect²⁷ and is likely the reason for the observed phase behavior of the PNIPAM polymers.

The phase change behavior observed for the BiPy-BTA supramolecular polymers are also correlated to the values for χ where ΔH_E is at a minimum (and maximum)¹⁸ The phase behavior of the BiPy-BTA supramolecular polymers are more complicated than that of the PNIPAM polymers. At 300 K, there is a phase change from the long triple-helix to the short triple helix when χ is > 0.3 and from short triple-helix to the single-helix when χ is > 0.9 . These transitions occur at the χ values where ΔH_E of isopropanol-water is near a minimum and maximum, respectively.¹⁸ This data suggests that the behavior of the BiPy-BTA supramolecular polymers correlate with the solvent thermodynamics of the alcohol-water mixtures.

The phase behavior of the BiPy-BTA supramolecular polymers is complex, and explanation of this behavior is not trivial. One possible explanation for this behavior is that at high concentrations of water hydrophobic hydration of the triple-helical aggregates are more favorable since less surface area is exposed to water, while at high concentrations of alcohol the single helical aggregates are more favorable since the aggregates are readily soluble in alcohol.¹⁸ Another factor that may explain the aggregation behavior of the BiPy-BTA supramolecular polymers is the microheterogeneity of water-alcohol solutions. Such mixtures are not truly homogeneous due to microaggregates that form between H-bonded alcohol molecules.²⁸ It is possible that the small molecule monomers of a supramolecular polymer interact with the microaggregates in a way that

a macromolecule like a covalently bonded polymer would not. This could result in the changes in the supramolecular structure of the polymers to accommodate these interactions.

4.3 Hypothesis

Yariv reagents are similar to the BiPy-BTA molecules in that they are discotic molecules with polyaromatic cores. These molecules also self-assemble to form 1-D stacked aggregates via non-covalent π - π interactions and H-bonding. Since Yariv reagents also form stacked aggregates in solution it is possible that the addition of alcohol could trigger some higher order aggregation in these systems. Also, the extent of this aggregation behavior may be correlated to the extremity of the value of ΔH_E for a given χ value, as is the case for BiPy-BTA systems.

4.4 Experimental

4.4.1 Attempts to determine the mechanism of Yariv reagent self-assembly

Initially, our goal was to better understand the mechanism of self-assembly of Yariv reagents by determining if the mechanism was isodesmic or cooperative, and to determine what the binding coefficients for the mechanisms were. Previous ultracentrifugation²⁹ studies have already identified the Yariv self-assembly mechanism as isodesmic, and have calculated the association constants for several different Yariv reagents, but we wanted to confirm these findings using temperature-dependent CD experiments.

The mechanism of self-assembly for a 1-D supramolecular polymers can be evaluated using temperature-dependent CD spectroscopy if the system meets certain conditions. First, the aggregate must be helical so that a CD signal can be observed. Also, the aggregate must completely disassociate at some temperature so that the starting point of the self-assembly can

be identified.³⁰ This is required to differentiate whether or not the mechanism is isodesmic or cooperative.

Aggregates that assemble isodesmically will provide temperature-dependent CD traces that are sigmoidal shaped with intensity increasing as temperature decreases making the equilibrium shift towards the assembled state until the maximum aggregate length is reached. Cooperative self-assembly mechanisms will display little to no CD signal until the nucleation critical temperature is reached, at which point the nucleus is formed and the aggregates adopt an ordered helical configuration. At this point aggregation becomes more favorable, and the presence of an ordered helical aggregate gives rise to an observable CD signal. This results in a rapid increase in CD signal as the temperature continues to decrease below the critical nucleation temperature. As the temperature continues to decrease the aggregates will eventually reach some maximum length and the CD signal will stop increasing. Furthermore, if aggregation is driven by more than one attractive force, it is possible that the mechanism will be more complex than simply isodesmic or cooperative, and if higher order aggregation occurs the temperature-dependent CD spectra may be impossible to fit to these mechanisms since they assume only 1-D aggregation.¹⁵⁻¹⁶

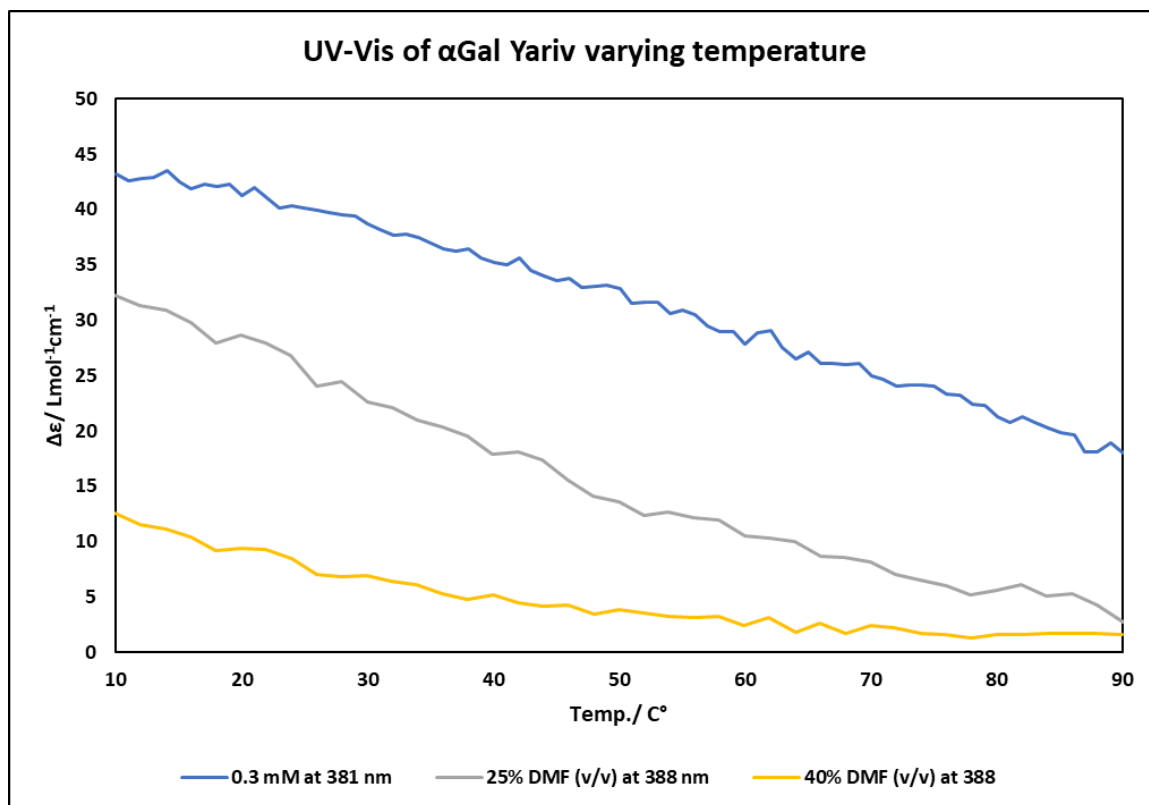


Figure 4.10: Temperature-dependent CD experiments using 0.3 mM α Gal Yariv and aqueous solutions of DMF

To investigate the mechanism of self-assembly for the Yariv reagents we first chose to perform temperature-dependent CD experiments of α Gal Yariv reagent (Fig 4.10). In these experiments, a 0.3 mM sample of Yariv reagent was heated at a rate of 1 °C/min from 10 °C to 90 °C. The intensity of the CD signal was recorded at 381 nm. This wavelength was selected since it was the signal of greatest intensity in the CD spectrum of α Gal Yariv. As expected the temperature dependent trace shows a decrease in signal (Fig 4.10). This observation is consistent with decreases in aggregate size with increasing temperature. However, even at 90 °C the value of $\Delta\epsilon$ has not decreased to zero, indicating that the Yariv reagent has not completely disaggregated.

We conducted a CD screen of α Gal Yariv in aqueous solution using several different organic co-solvents (25% (v/v) MeOH, EtOH, iPrOH, THF, MeCN, and DMF) at 60 °C (90 °C for DMF) (Fig 4.11b) to find a co-solvent that would completely disaggregate the Yariv reagent molecules at elevated

temperatures. We found that samples dissolved in 25% (v/v) DMF provided a CD spectrum that was mostly flat ($\Delta\epsilon_{390\text{nm}} = \sim 3.1 \text{ L}\cdot\text{mol}^{-1}\text{cm}^{-1}$) at 90 °C. To favor total disaggregation, we prepared samples in 25% and 40% (v/v) DMF. Temperature-dependent CD experiments show that the addition of DMF has resulted in the near total attenuation of the CD signal. However, since neither a sigmoidal shaped curve or a rapid increase in CD signal is observed, the nature of the mechanism of the self-assembly is not immediately clear. The trace of the temperature-dependent CD experiments appears to be somewhat linear. The linear shape of these traces may be the result of the self-assembly of Yariv reagents into 1-D stacks being more complex than those observed for other types of supramolecular polymers.

4.4.2 First observations of alcohol effects

The temperature-dependent CD experiments display how the CD signal is affected by temperature at a single wavelength. To better understand how the entire CD spectrum is affected by temperature we acquired CD spectra for samples of α Gal Yariv in aqueous solution using several different organic co-solvents (25% (v/v) MeOH, EtOH, iPrOH, THF, MeCN, and DMF) at 60 °C (90 °C for DMF) and 10 °C (Fig 4.11). As previously mentioned, at 60 °C (90 °C for DMF) the CD spectra all appear attenuated when compared to the sample in pure water. As expected, at 10 °C the samples containing THF, MeCN, and DMF all give spectra that are attenuated when compared to that of the sample in pure water, but have absolute values of $\Delta\epsilon$ greater than those observed for the same solvent compositions at 60 or 90 °C. However, for samples containing MeOH, EtOH, and iPrOH at 10 °C an unexpected effect is observed. The CD spectra for the samples containing methanol and ethanol are inverted when compared to the spectrum of the sample with pure water. Also, the CD spectrum for the isopropyl alcohol sample exhibits a large increase in absolute $\Delta\epsilon$ with values extending beyond the detection limits of the instrument. This deviation from the aqueous CD behavior of the Yariv aggregates suggests that a change in the self-assembly

mechanism of the Yariv aggregates has occurred in response to the presence of alcohol in the sample solution.

Similar inversion of CD spectra of supramolecular polymers was observed for the previously discussed BiPy-BTA supramolecular polymers when CD spectra were obtained in different compositions of an iPrOH:H₂O solvent mixture. In this case the changes in the CD spectra were found to be a result of a transition from a single-helical aggregate to a triple-helical aggregate.¹⁸ Therefore, it is possible that the inversion of the Cotton effect observed for the Yariv samples containing methanol and ethanol is a result of individual helical stacks of Yariv reagents associating to form a higher order aggregate with an opposite helical sense, similar to the single to triple helix transition observed for the BiPy-BTA supramolecular polymers.¹⁸ This inversion behavior was also observed for β Glc Yariv samples prepared with a 25% (v/v) aqueous solution of methanol (see Fig 4.18).

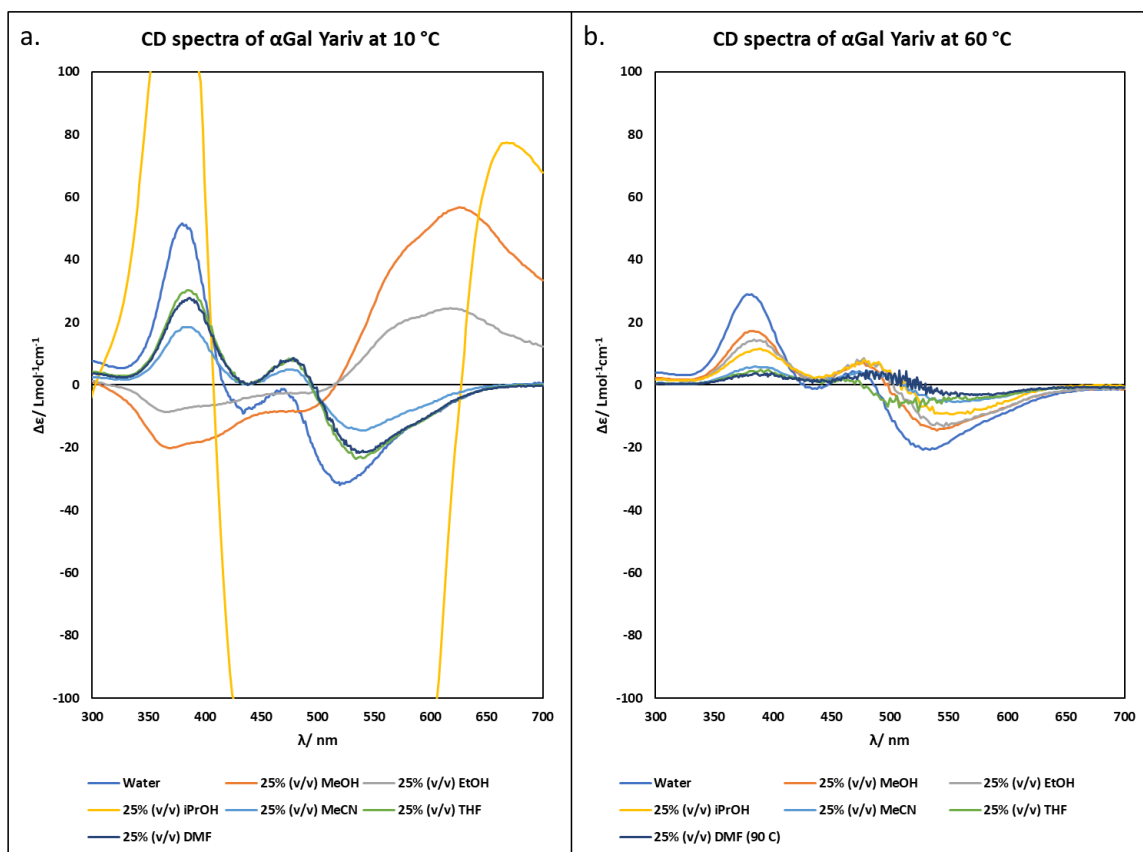


Figure 4.11: CD spectra of 0.3 mM α Gal Yariv reagent in alcoholic aqueous solutions

4.4.3 DLS experiments

Although the CD spectra of Yariv reagents can provide an understanding of the helical ordering of an aggregate and show if the aggregation is increasing or decreasing, it cannot give any information on the actual size of the aggregates. If the phenomena observed in the CD experiments are the result of a transition from a single helical aggregate to a higher order aggregate then there should also be an observed increase in the size of the aggregates. Dynamic light scattering (DLS) experiments can be used to measure the size of supramolecular polymer aggregates. Therefore, it should be possible to observe an increase in size when Yariv reagents are subjected to conditions that result in the inversion of the CD spectra.

4.4.3.1 Temperature dependent DLS experiments

Temperature dependent DLS experiments were performed to confirm that the spectrum inversion observed in the CD experiments is consistent with a transition to higher order aggregates. First, DLS size measurements of α Gal (Fig. 4.12) and β Glc (Fig. 4.13) Yariv in pure water were obtained. Samples were prepared with a concentration of 0.3 mM and experiments were run at 10 °C and 60 °C. At 10 °C aggregates with hydrodynamic diameters of 209 nm for α Gal and 335 nm for β Glc were observed which are roughly in agreement with the reported literature values of 164 nm and 244 nm for α Gal and β Glc Yariv reagents respectively.³¹ At higher temperatures the aggregates are smaller, which is expected as the Yariv reagents were shown to decrease in molecular weight at higher temperatures via centrifugation experiments.²⁹

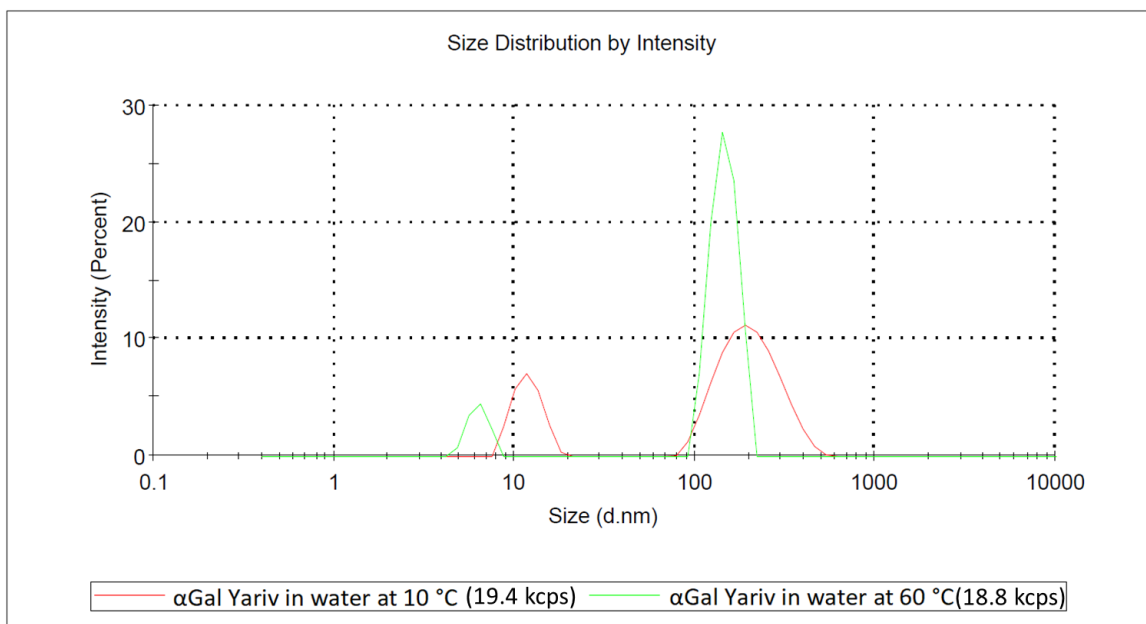


Figure 4.12: DLS experiments with α Gal in water at 0.3 mM

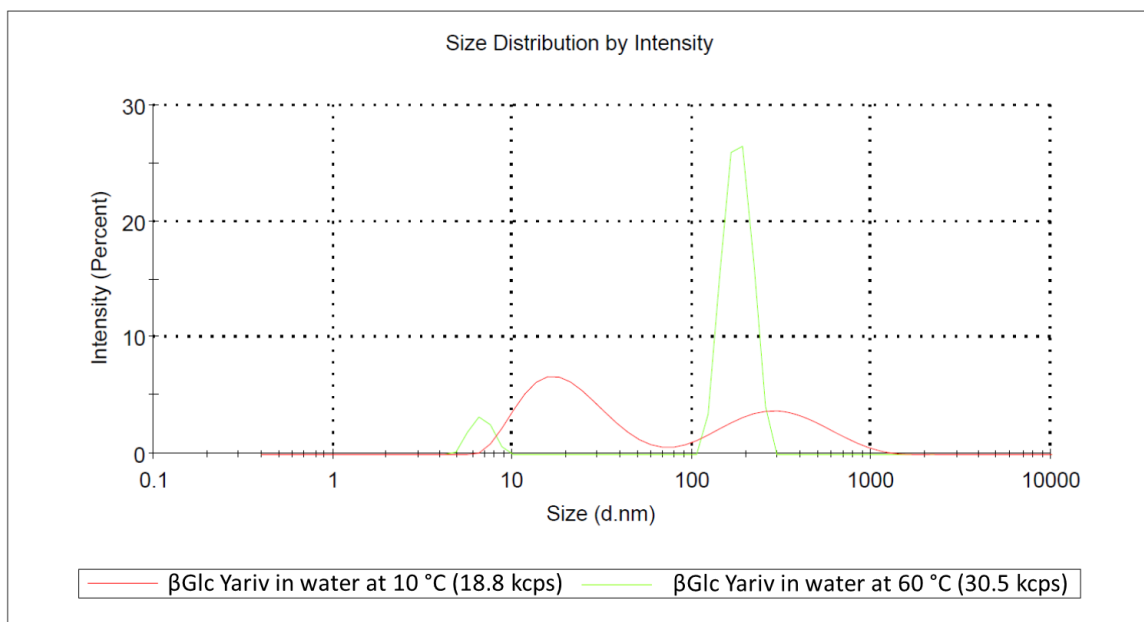


Figure 4.13: DLS experiments with β Glc in water at 0.3 mM

At both temperatures, a bimodal distribution is observed for both α Gal and β Glc Yariv reagents. One possible explanation for this distribution may be related to the fact that Yariv reagents form rigid rod-like aggregates. DLS is used to determine size by calculating diffusion coefficients of particles in solution. If a particle is globular shaped, then only the translational diffusion coefficient is observed due to light scattering, but if the particle has some aspect ratio other than 1:1 the rotational diffusion constant will affect the light scattering as well. This results in a larger sized peak calculated from the translational diffusion coefficient, and a smaller sized peak is calculated from the rotational diffusion coefficient.³² Another consequence of using DLS to determine the size of rod-like aggregates is that the calculated value for hydrodynamic diameter will be somewhat inaccurate due to the fact that the motion of rod-shaped aggregates through solution is different than that of spherical particles.³² Although these values of size do not accurately describe the physical measurements of the rod-like aggregates they can be used to monitor size increases due to aggregation and therefore are still useful for our purposes.

Also, the low count rate observed for these Yariv samples (<50 kcps) can result in unreliable data that is a result of the software attempting to fit the correlation data to noise.³³ Typically, count rates greater than 100 kcps are required for accurate determination of size. Low count rates can be attributed to samples in which the concentration is too low for enough scattering to occur.³³ However, an increase in the size of the aggregates can allow for more scattering to occur.³³ Therefore, if higher count rates are observed in response to the increase in the amount of alcohol present in solutions of the same concentration, then the increase in count rate can be attributed to formation of higher order aggregates.

Temperature-dependent DLS experiments were also performed with α Gal (Fig. 4.14) and β Glc (Fig. 4.15) Yariv reagents in 25 % (v/v) aqueous methanol solution at 10 °C and 60 °C to determine if a size increase occurs at low temperatures compared to higher temperatures. The results of the experiments show a large increase in size of the aggregates observed at 10 °C when compared with the values observed in pure water. Also observed is the disappearance of the smaller sized peak, perhaps due to the higher order aggregate being more globular shaped than rod-shaped. At higher temperature, a marked decrease in particle size is observed and the smaller sized peak reappears, suggesting a reversion to the original rod-shaped aggregate. This observation strongly suggests that that the temperature dependent inversion of the CD spectra observed in the presence of alcohol occurs in conjunction with an increase in particle size of the Yariv aggregates, suggesting the formation of higher order aggregates. Also, the count rates for the samples at 10 °C are much higher (> 100 kcps) than those for the samples at 60 °C (< 50 kcps) or those prepared in pure water. The increase in count rate is consistent with an increase in aggregate size and thus higher order aggregates.

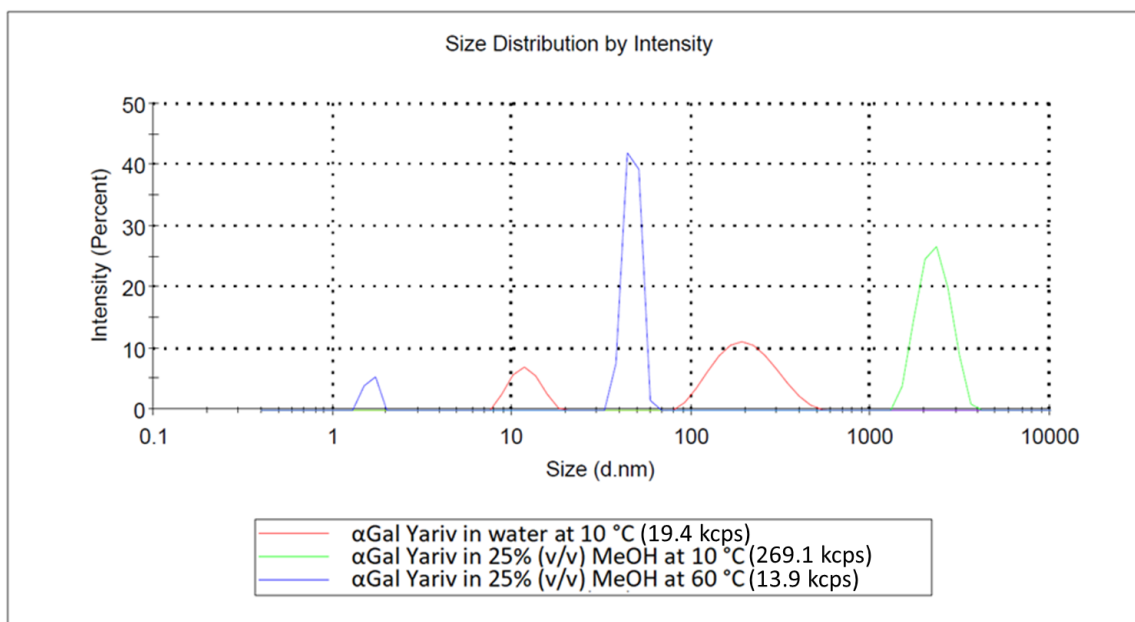


Figure 4.14: DLS experiments with α Gal

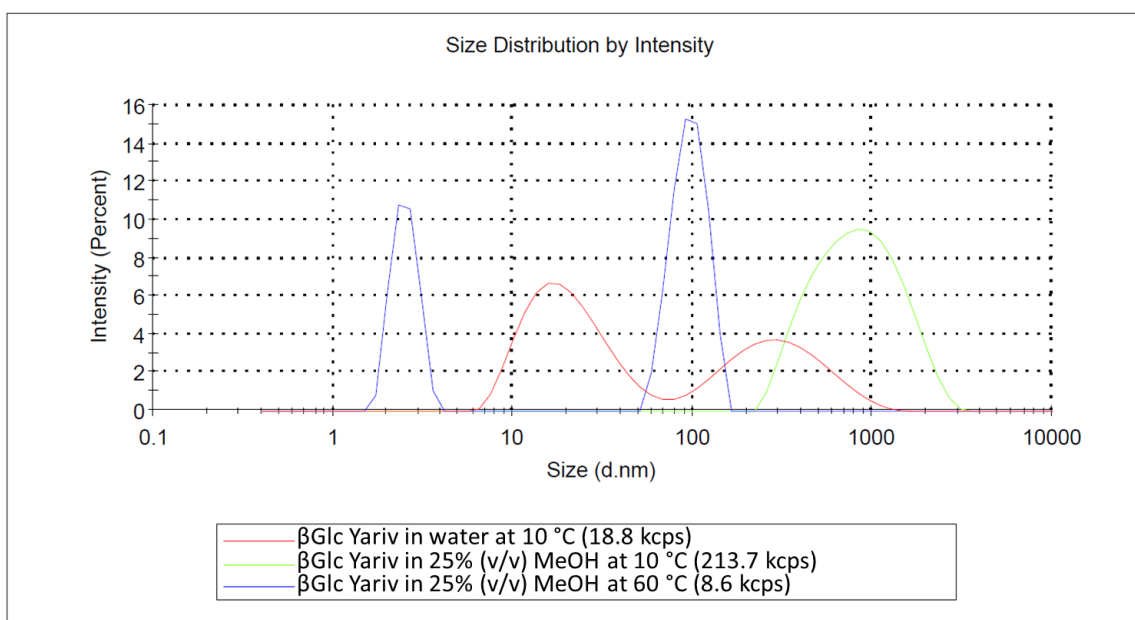


Figure 4.15: DLS experiments with β Glc in water at 0.3 mM

4.4.4 Temperature-dependent CD experiments with alcohol

Temperature-dependent CD experiments were performed to better understand the temperature-dependent transition that Yariv reagents undergo in the presence of alcohol. CD experiments

were performed in which samples of β Glc and α Gal Yariv reagents in 25% (v/v) methanol solution were heated from 10 up to 60 °C and then cooled from 60 down to 10 °C. The results were compared to identical experiments performed in pure water (Fig. 4.16). For the α Gal samples, $\Delta\epsilon$ was monitored at 388 nm since it is the wavelength where the CD spectra reaches a maximum. For the β Glc samples, spectra were taken at 432 nm. This is the wavelength where the CD spectra reaches a maximum, but it is not the global maxima which occurs at 520 nm. This was done to avoid running into complications due to the values of $\Delta\epsilon$ exceeding the detection limits of the instrument (see Figure 4.17).

When heating β Glc samples from 10-60 °C (Fig 4.16a grey line) the $\Delta\epsilon$ values are initially negative, but as the temperature increases a rapid increase in $\Delta\epsilon$ occurs crossing over into the positive region around 20 °C and increasing rapidly before eventually decreasing rapidly at around 40 °C. Eventually, at around 40 °C $\Delta\epsilon$ begins to decrease at a rate that is similar to that observed for the sample in pure water (Fig 4.16a blue line). When cooling β Glc Yariv samples from 60-10 °C (Fig 4.16a yellow line) a much smoother sigmoidal shaped transition occurs at around 25 °C resulting in $\Delta\epsilon$ values that are negative, but much less intense than observed at the beginning of the experiment. The heating experiment for α Gal proceeded by a similar, but much less dramatic, pattern as was observed for the β Glc samples. The α Gal Yariv cooling experiment (Fig 4.16b orange line) resulted in an initial increase in $\Delta\epsilon$ before a decrease of $\Delta\epsilon$ began at around 20 °C, but did not cross over into negative values once cooling was complete. These results demonstrate hysteresis, since the aggregates do not return to their original state after cooling. To better understand the observed hysteresis full spectra were taken at 10 and 60 °C, and will be discussed in the upcoming section.

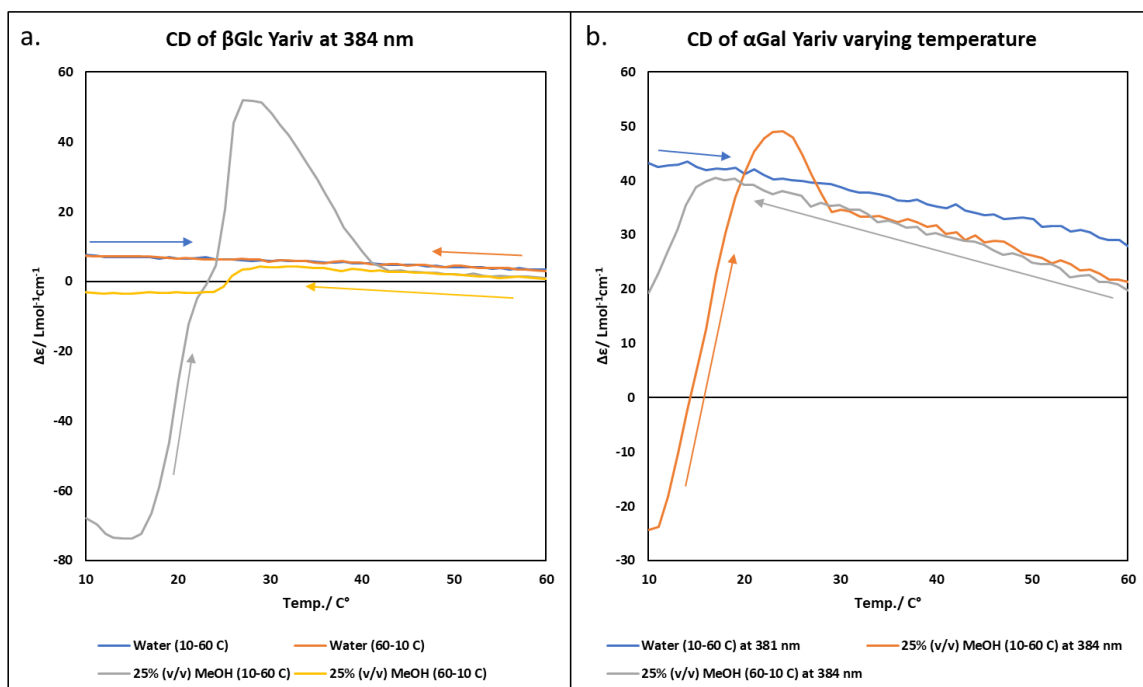


Figure 4.16: Temperature-dependent CD experiments with 0.3 mM Yariv in methanolic aqueous solution

Hysteresis is observed in other supramolecular systems as well. The supramolecular polymerization of a C_3 -symmetric trisurea discotic molecule displays hysteresis that is likely the result of a cooperative process in which the discs first form a disordered stack which then slowly is ordered to provide the final chiral aggregate.⁶ Also, hysteresis was observed in the self-assembly of triple-stranded nucleic acid structures that likely results from a very slow duplex to triplex transition rate.³⁴ Hysteresis is the result of a large kinetic barrier to assembly or disassembly.¹⁶ Thus it is possible that the higher-order self-assembly of Yariv aggregates is more difficult once the 1-D assemblies have undergone some significant degree of disaggregation by heating. This observation is important as it demonstrates that the Yariv aggregate is not a system at equilibrium in 25% (v/v) MeOH at 10 °C.

A CD spectrum of the β Glc Yariv reagent in 25% (v/v) MeOH solution at 20 °C was also taken to determine what the shape of the spectrum was near the point at which the temperature-dependent transition occurs (Fig 4.17). This CD spectrum is rather attenuated compared to the

spectra taken at 10 °C and 60 °C suggesting that at 20 °C the sample is undergoing a transition between the two aggregation states.

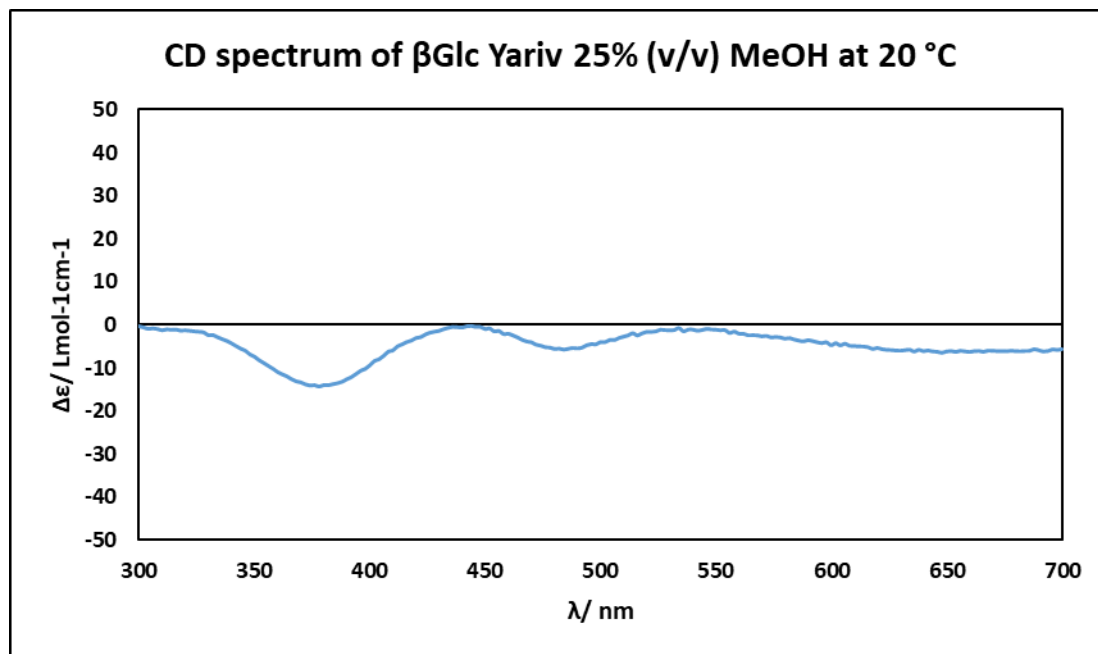


Figure 4.17: CD spectrum of the β Glc Yariv reagent in 25% (v/v) MeOH solution at 20 °C and 0.3 mM

4.4.5 Additional hysteresis experiments

To further investigate the thermal hysteresis observed for the self-assembly of the Yariv reagents, CD and UV-vis spectra were acquired for samples of β Glc and α Gal Yariv reagents dissolved in 25% (v/v) methanolic aqueous solution for three rounds of heating and cooling. Initial measurements were taken at 10 °C and then the sample was rapidly heated to 60 °C and measurements were taken again. The sample was then rapidly cooled to 10 °C and another measurement was taken. Two more cycles of heating and cooling were performed. Results of the β Glc heating and cooling experiments shows essentially no change in the CD spectra at 60 °C as heating and cooling occurs, but there is clear hysteresis observed at 10 °C as the absolute values of $\Delta\epsilon$ for the spectra become larger with each cycle of heating and cooling (Fig 4.19). For α Gal Yariv very little variation in the CD spectra is observed at 60 °C, but at 10 °C the spectrum becomes attenuated after one cycle,

and then becomes inverted and there is an increase in the absolute values of $\Delta\epsilon$ at the extrema of the spectrum with additional cycles of heating and cooling (Fig. 4.18). This data is consistent with previously observed experiments in that the hysteresis is not observed at 60 °C, but is observed at 10 °C.

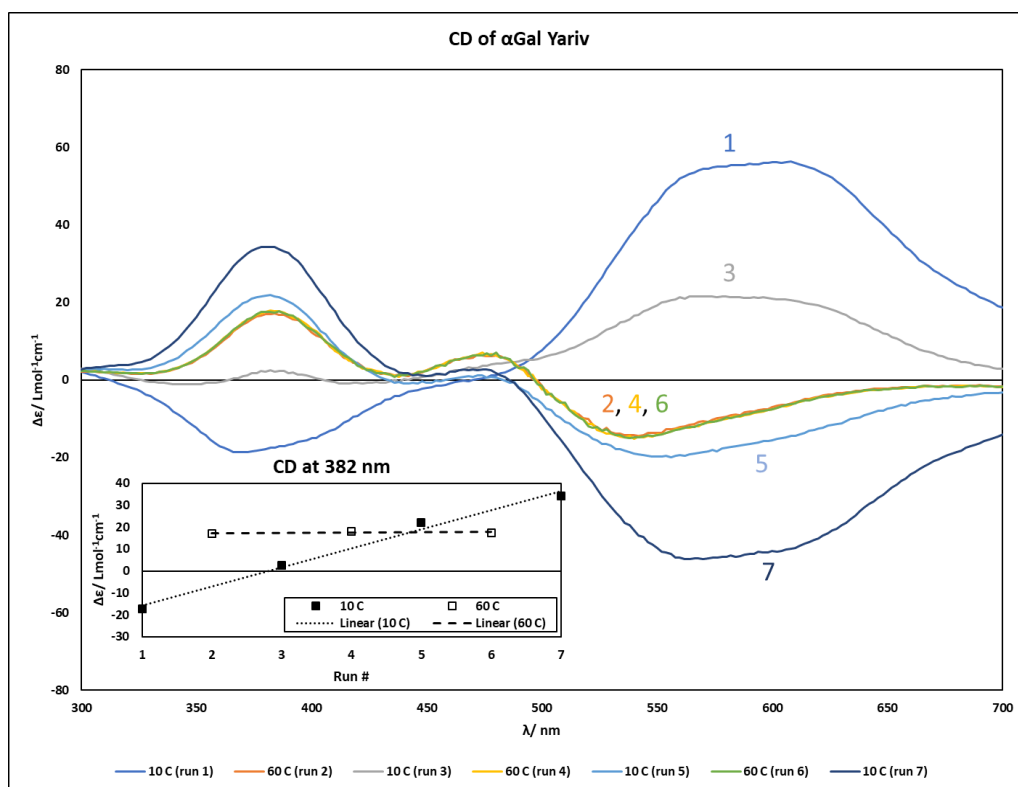


Figure 4.18: Hysteresis CD experiment with α Gal Yariv in 25% (v/v) methanolic aqueous solution. The first CD spectrum was acquired at 10 °C (run 1). The sample was then heated to 60 °C and a CD spectrum was acquired (run 2). The sample was then cooled to 10 °C and a CD spectrum was acquired (run 3). CD spectra were acquired for two more cycles of heating (runs 4 and 6) and cooling (runs 5 and 7).

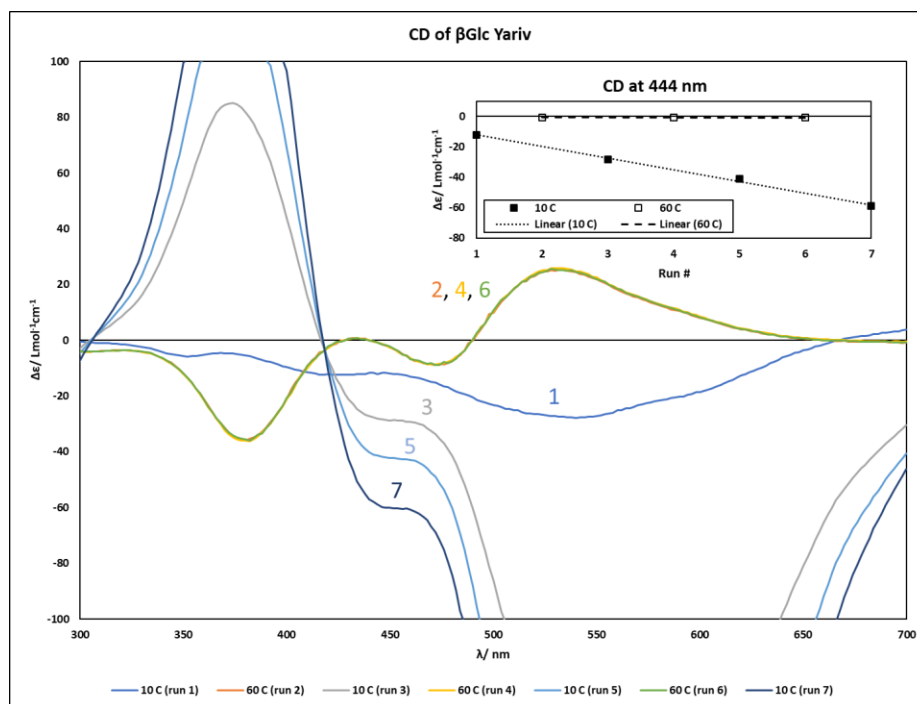


Figure 4.19: Hysteresis CD experiment with β Glc Yariv in 25% (v/v) methanolic aqueous solution

In the β Glc temperature dependent experiment (Fig 4.16a) the CD signal after cooling to 10 °C is less intense than the initially observed signal at 10 °C which is opposite of what was observed in these hysteresis experiments (Fig. 4.19). It is possible that this discrepancy is a result of the rapid heating and cooling used in these experiments compared to the slow heating and cooling used in the temperature dependent experiments.

UV-Vis spectra were acquired simultaneously with the CD spectra. Results of the β Glc heating and cooling experiments shows essentially no change in the spectra at 60 °C as heating and cooling occurs, but there is some hysteresis observed at 10 °C as the absorbance values of the spectra increase with each cycle of heating and cooling (Fig. 4.21). For α Gal Yariv very little variation in the spectra is observed at 60 °C, but at 10 °C the absorbance values of the spectra increase after one cycle, and then only slightly increase with additional cycles of heating and cooling (Fig. 4.20). Again, hysteresis is observed.

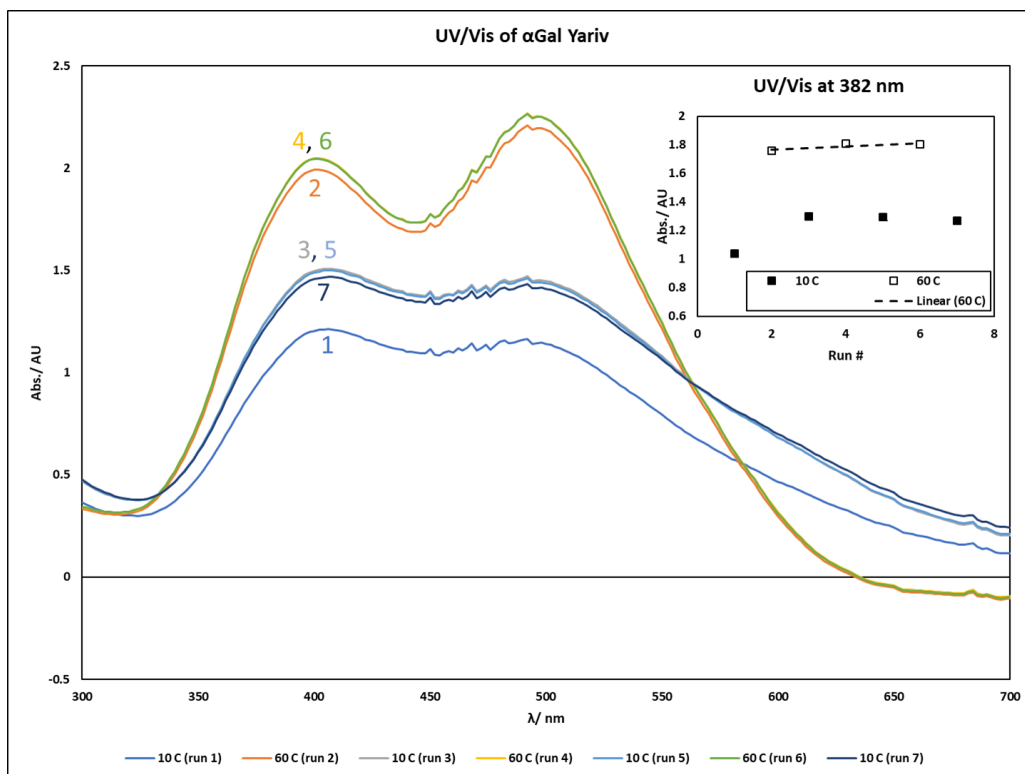


Figure 4.20: Hysteresis UV/Vis experiment with α Gal Yariv in 25% (v/v) methanolic aqueous solution

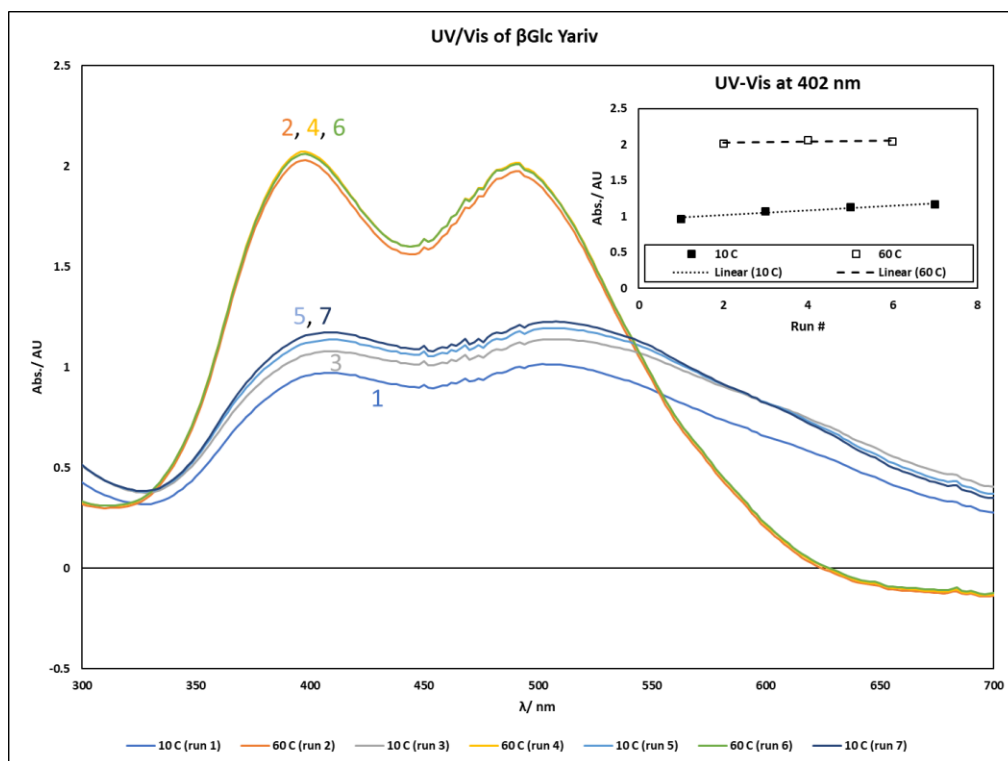


Figure 4.21: Hysteresis UV/Vis experiment with β Glc Yariv in 25% (v/v) methanolic aqueous solution

DLS measurements were acquired for samples of β Glc and α Gal Yariv reagents dissolved in 25% (v/v) methanolic aqueous solution for two rounds of heating and cooling (Fig 4.22). These experiments demonstrated that the size of the aggregates increases as a result of cooling for both β Glc and α Gal. For the α Gal samples the size of the aggregates at 10 °C is relatively constant after two rounds of heating and cooling. For the β Glc Yariv samples the size of the aggregates after one round of heating and cooling is nearly double what is observed initially, after two rounds of heating and cooling the size of the aggregates decrease to a size more consistent with the initial value for size 10 °C. This data demonstrates that the α Gal Yariv reagent remains in its higher-order aggregate form after two cycles of heating and cooling even though the α Gal Yariv CD spectrum displays negative cotton effect. This observation suggests that the formation of the higher-order aggregates and the helical ordering of these aggregates are separate processes.

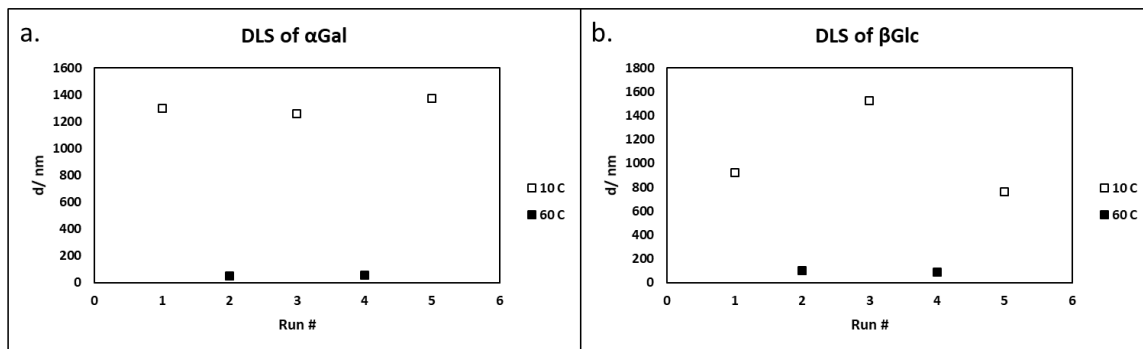


Figure 4.22: Hysteresis UV/Vis experiment with α Gal and β Glc Yariv in 25% (v/v) methanolic aqueous solution (For DLS results with multiple peaks the larger sized peak is displayed)

4.4.6 CD and UV-vis Experiments with varying alcohol concentrations

The aggregation effects observed for samples of Yariv reagents in aqueous solutions of alcohol is similar to behavior observed in PNIPAM²⁴ and BiPy-BTA¹⁸ systems, in that typical temperature dependent aggregation behavior is altered. In these previously described systems the extent of the atypical behavior was linked to the molar fraction of alcohol present in the solution (χ), and

the phase change behavior was correlated to the values for χ in which the excess enthalpy of mixing (ΔH_E) is at a minimum or maximum.

CD and UV-Vis spectra of the Yariv reagents were taken in solutions with varying alcohol compositions in an attempt to explain the aggregation behavior of Yariv reagents in alcoholic aqueous solutions by linking the inversion behavior observed in CD experiments to the intensity of values for excess enthalpy of mixing (ΔH_E). All CD and UV-Vis experiments were performed at 10 °C and with Yariv concentration of 0.3 mM.

4.4.6.1 CD and UV-Vis experiments for β Glc in methanolic aqueous solutions

CD and UV-Vis experiments were performed at various molar compositions of methanol in water ($\chi = 0, 0.02, 0.07, 0.13, 0.16, 0.19, \text{ and } 0.31$). CD experiments show that initially the absolute $\Delta\epsilon$ values of the extrema increase as χ increases from 0 - 0.07. At $\chi = 0.07$ the CD spectrum displays a broad peak with a maxima at ~ 550 nm with a shoulder peak at ~ 600 . As the χ value increases from 0.07 - 0.13 an inversion of the CD spectrum occurs, suggesting that a transition to a higher order aggregate has occurred. From χ values from 0.13 – 0.16 the absolute $\Delta\epsilon$ values decrease and then increase from 0.16 – 0.19. Finally, the absolute $\Delta\epsilon$ values of the spectrum decrease drastically from 0.19 – 0.31.

The CD spectrum at $\chi = 0.31$ displays a broad peak with a maxima at ~ 550 nm with a shoulder peak at ~ 600 similar to the peak observed at $\chi = 0.07$. These peaks may indicate that there is a combination of 1-D and higher-order aggregates at these values of χ . The peak 550 nm may correspond to the maxima found for spectra of 1-D aggregates at $\chi = 0.00$ and 0.02 at ~ 525 nm while the peak at 600 nm may correspond to the maxima found for spectra of higher-order aggregates at $\chi = 0.13, 0.16$ and 0.19 at ~ 650 nm (Fig. 4.23).

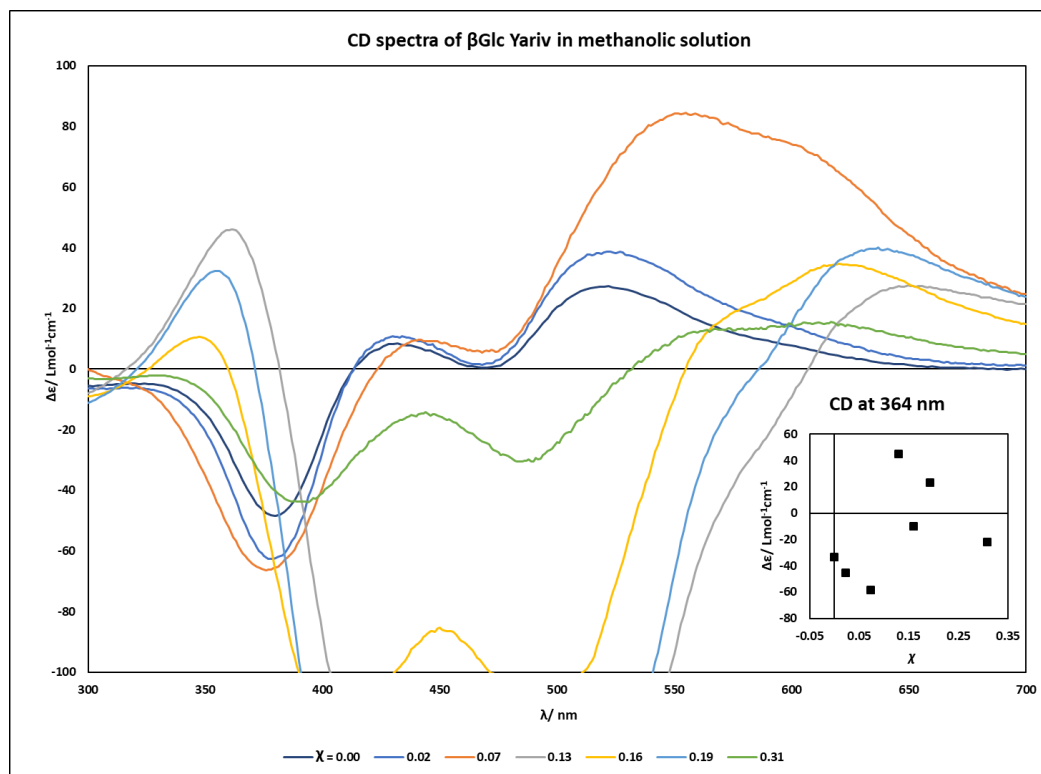


Figure 4.23: CD spectra of 0.3 mM β Glc Yariv reagent in methanolic aqueous solutions

UV-Vis experiments show that the intensity of the spectra generally increases as χ increases from 0 - 0.19 before decreasing significantly from 0.19 – 0.31 (Fig. 4.24).

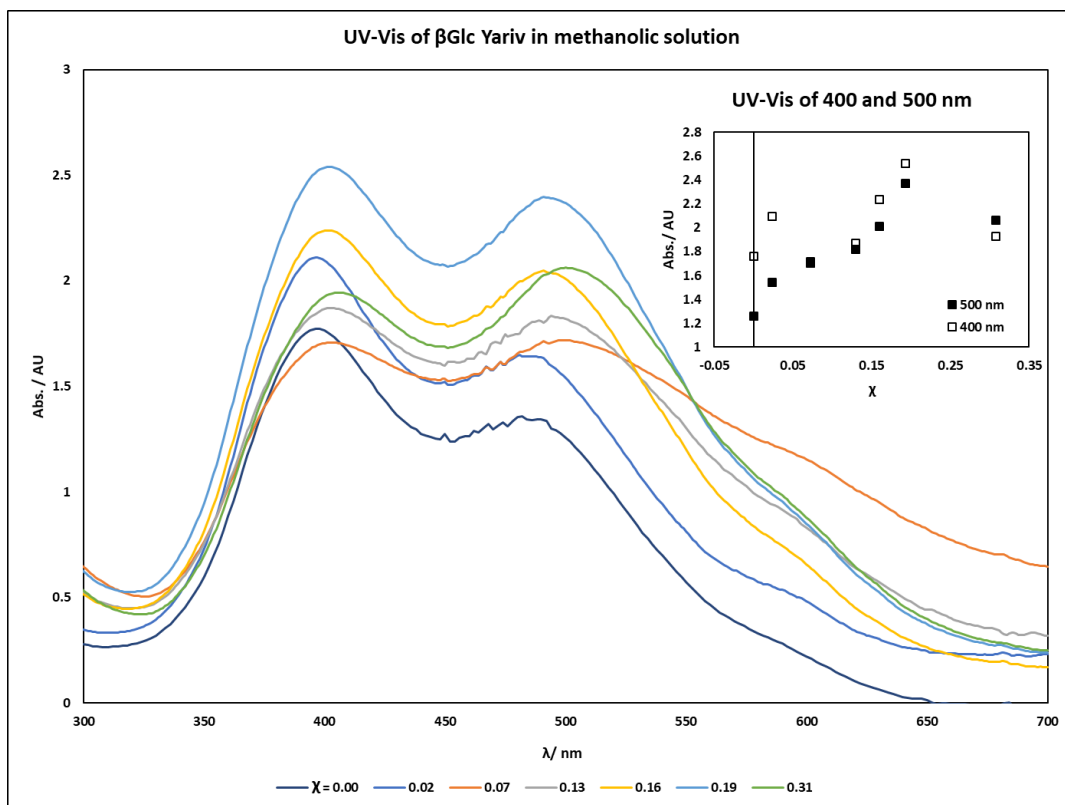


Figure 4.24: UV-Vis spectra of 0.3 mM β Glc Yariv reagent in methanolic aqueous solutions

According to the literature²⁶ ΔH_E reaches a minimum at $\chi = 0.32$ for a water – methanol mixture. Therefore, if the transition of Yariv aggregates to higher order aggregates is affected by ΔH_E in the same way that the transitions of BiPy-BTA supramolecular polymers and the PNIPAM polymers are, then we would have expected the most intense inverted CD spectra at χ values close to 0.32 instead of the observed value of 0.13. However, the progress of the phase change may not be represented simply by the intensity of the inverted spectrum. In fact, the changes in shape of the spectra are not so simple as just inversion of the normal spectra. In the CD spectrum for the sample at 0.07 the positive peak at ~ 550 nm has $\Delta\epsilon$ values that are much larger than those observed at other values of χ , and appears to develop a shoulder peak at higher wavelength (~ 625 nm) (Fig. 4.23). At higher χ values after inversion of the main positive peak has occurred, the shoulder peak appears to remain as a separate high wavelength peak. The CD data here clearly

demonstrates that some change in aggregation behavior has occurred due to the presence of methanol. Since the change in the shape of the spectra becomes more drastic with the increase in χ it is possible that this behavior is linked to changes in the values of ΔH_E , but it is not immediately clear how these phenomena are related.

4.4.6.2 CD and UV-vis experiments for α Gal in methanolic aqueous solutions

CD and UV-vis experiments were performed at various compositions of methanol in water ($\chi = 0, 0.02, 0.07, 0.13, 0.16, 0.19, \text{ and } 0.31$). CD experiments (Fig. 4. 25) show that initially the absolute values of $\Delta\epsilon$ of the spectra increases as χ increases from 0 - 0.13. As the χ value increases from 0.13 - 0.16 an inversion of the CD spectrum occurs, suggesting that a transition to a higher order aggregate has occurred. From χ values from 0.16 – 0.19 the absolute values of $\Delta\epsilon$ decreased drastically and the lower wavelength (~ 400 nm) peak reverts to its original sign. At $\chi = 0.31$, the spectrum is reverted to its original shape, but with much higher intensity, and a higher wavelength peak (~ 550 nm) that is quite broad and appears to be a combination of two peaks.

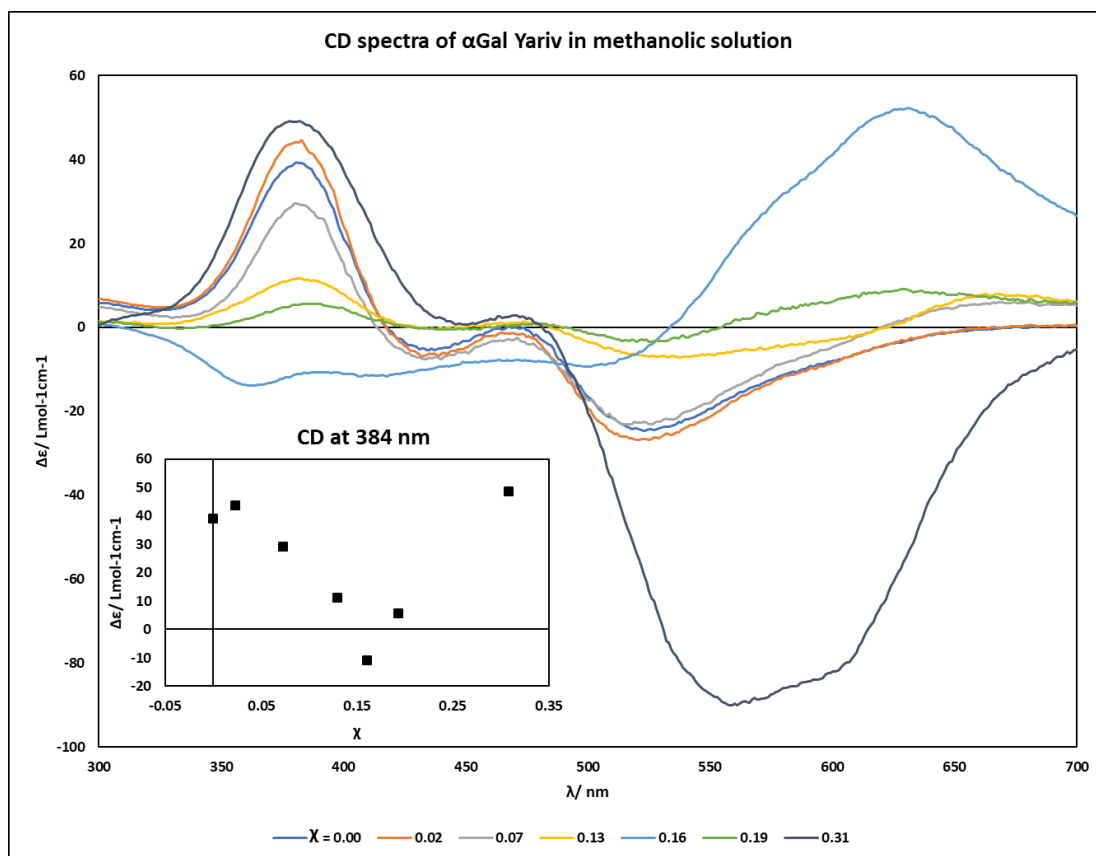


Figure 4.25: CD spectra of 0.3 mM α Gal Yariv reagent in methanolic aqueous solutions

UV-vis experiments (Fig. 4.26) show that the absorbance values of the spectra decrease as χ increases from 0 - 0.16 and then the absorbance values increase as χ increases from 0.16 – 0.31. Interestingly, this behavior is opposite to what is observed for the β Glc Yariv under the same conditions. Although the assembly mechanism that would cause this behavior is not clear, the decrease in absorbance exhibited in the α Gal UV-vis spectra suggests that the interaction between the aggregates is preventing the polyaromatic cores of the Yariv reagents from absorbing light in such a way that is not observed for the β Glc Yariv aggregates.

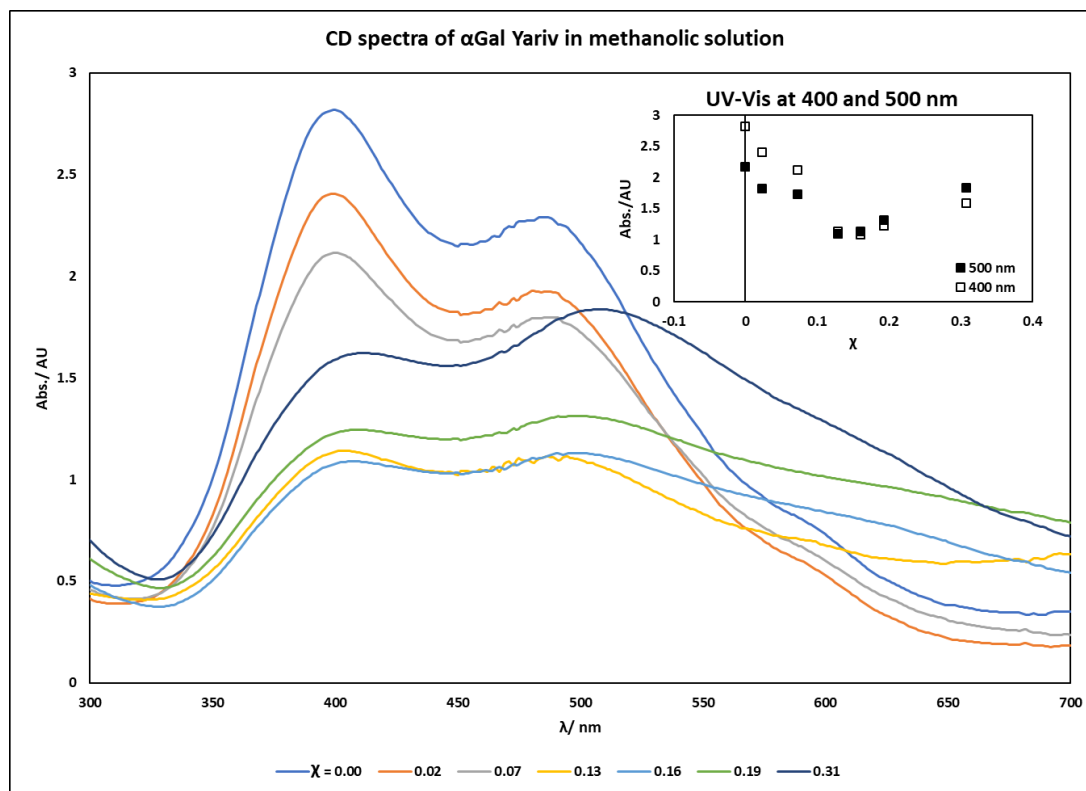


Figure 4.26: CD spectra of 0.3 mM α Gal Yariv reagent in methanolic aqueous solutions

Again, the CD data here clearly demonstrates that some change in the self-assembly mechanism has occurred due to the presence of methanol. Since the change in the shape of the spectra becomes more drastic with the increase in χ it is possible that this mechanism change is linked to changes in the values of ΔH_E , but it is not immediately clear how these phenomena are related.

4.4.6.3 CD and UV-Vis experiments for α Gal in ethanolic aqueous solutions

CD and UV-Vis experiments were performed at various compositions of ethanol in water ($\chi = 0, 0.02, 0.03, 0.05, 0.07, 0.09, \text{ and } 0.24$). CD experiments (Fig. 4.27) show that initially the absolute values of $\Delta\epsilon$ of the spectra do not change as χ increases from 0 - 0.03. As the χ value increases from 0.03 - 0.05 an inversion of the CD spectrum occurs, suggesting that a transition to a higher order aggregate has occurred. From χ values from 0.05 – 0.07 the intensity of the CD spectrum increased, before decreasing from 0.07 – 0.09. At $\chi = 0.24$, the spectrum is reverted to its original

sign, but the shape is quite deformed compared to the original pure water spectrum, and the absolute values of $\Delta\epsilon$ are drastically reduced. Again, the CD data here clearly demonstrates that some change in aggregation behavior has occurred due to the presence of ethanol.

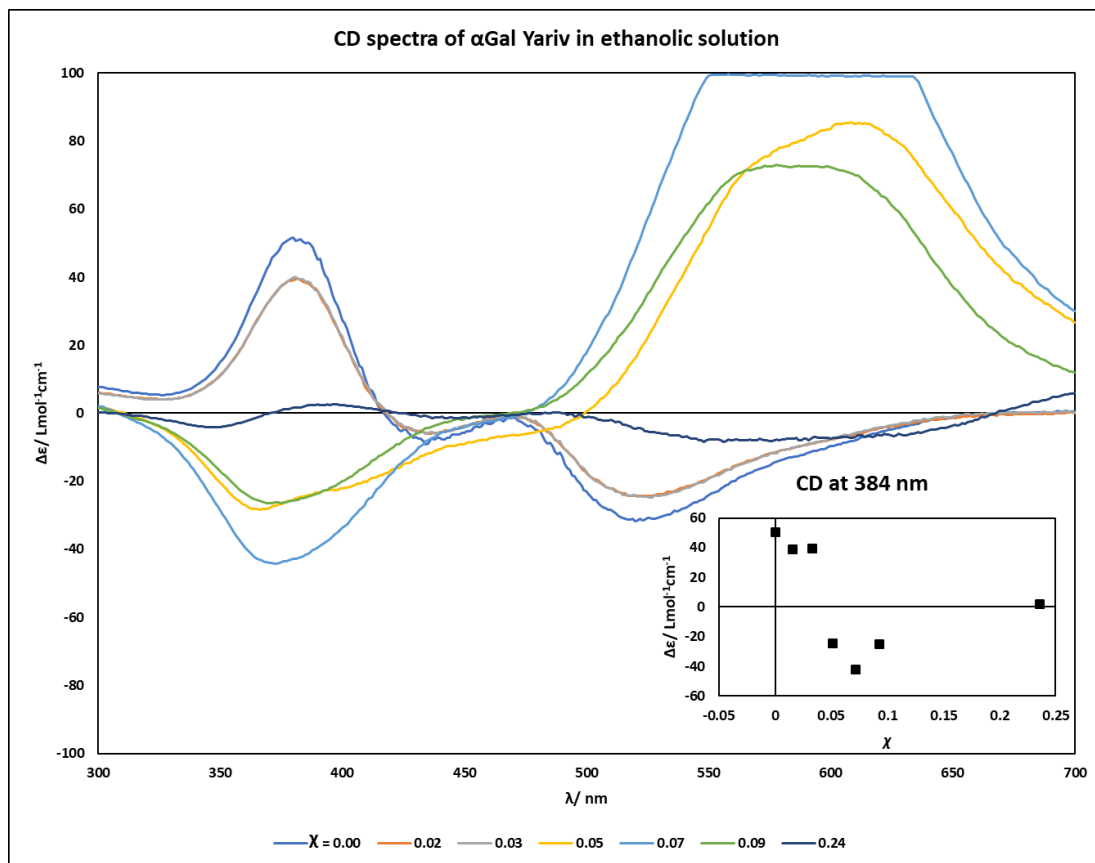


Figure 4.27: CD spectra of 0.3 mM α Gal Yariv reagent in ethanolic aqueous solutions

UV-Vis experiments (Fig. 4.28) show that the absorbance values of the spectra generally decrease as χ increases from 0 - 0.09, then the absorbance values increase slightly from 0.09 – 0.24. In this experiment, the same pattern of change in the absorbance is observed as was seen in the α Gal Yariv in methanolic solution experiments, suggesting that the mechanism of assembly is the same regardless of the identity of the alcohol.

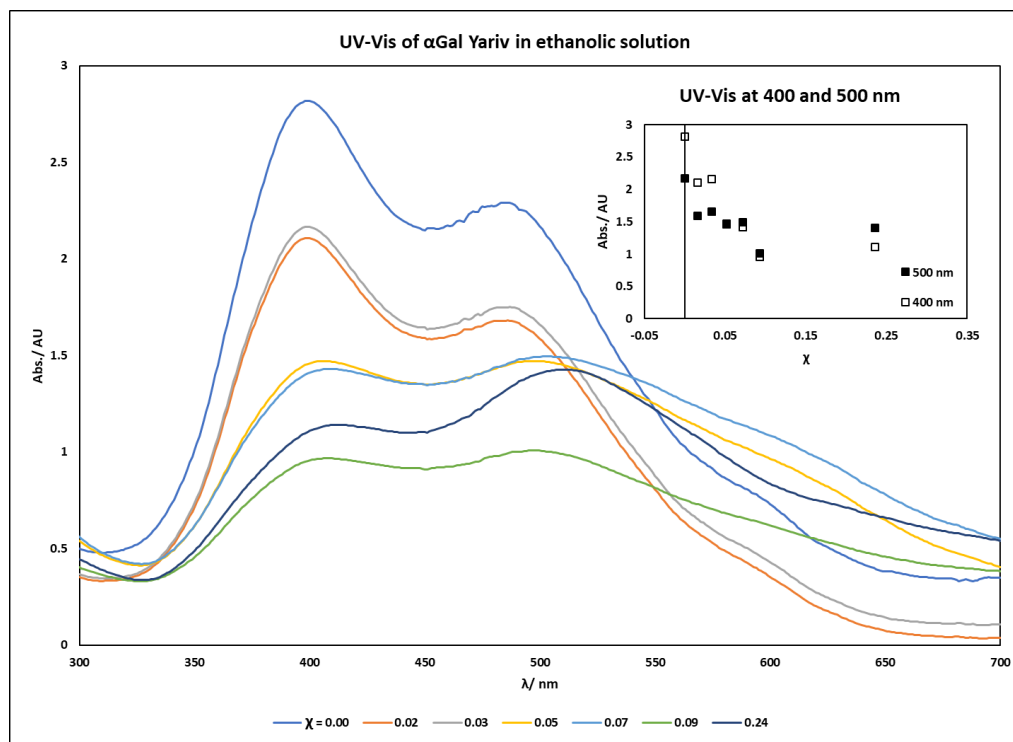


Figure 4.28: UV-Vis spectra of 0.3 mM α Gal Yariv reagent in ethanolic aqueous solutions

According to the literature²⁶ ΔH_E reaches a minimum at $\chi = 0.15$ for a water – ethanol mixture. Therefore, we would have expected the most intense inverted CD spectra at χ values close to 0.15 instead of the observed value of 0.07. However, it is clear that the ethanol causes the CD spectrum to invert at lower χ values than were seen for methanol which is expected given the more rapid decrease in ΔH_E . Again, this data suggests some relationship between the aggregation behavior of the Yariv reagent, and the values of ΔH_E , but it is obvious that this relationship is much more complex than was observed in the previously discussed systems such as the PNIPAM polymers.

4.4.6.4 CD and UV-Vis experiments for α Gal in isopropanolic aqueous solutions

CD and UV-Vis experiments were performed at various compositions of isopropanol in water ($\chi = 0, 0.01, 0.02, 0.03, 0.04, 0.07, 0.26$ and 0.41). CD experiments (Fig. 4.29) show that initially the the absolute values of $\Delta\epsilon$ of the spectra do not change much as χ increases from 0 - 0.02. As the χ value increases from 0.02 - 0.03 an inversion of the CD spectrum occurs, suggesting that a

transition to a higher order aggregate has occurred. At χ values from 0.03 – 0.07 the intensity of the CD spectrum increases, eventually becoming so intense that large portions of the spectra appear outside of the observable range. At $\chi = 0.26$ and 0.41 the intensity of the spectra appears to continuously increase, but it is difficult to discern what is happening since so much of the spectra are above the detection limit of the instrument.

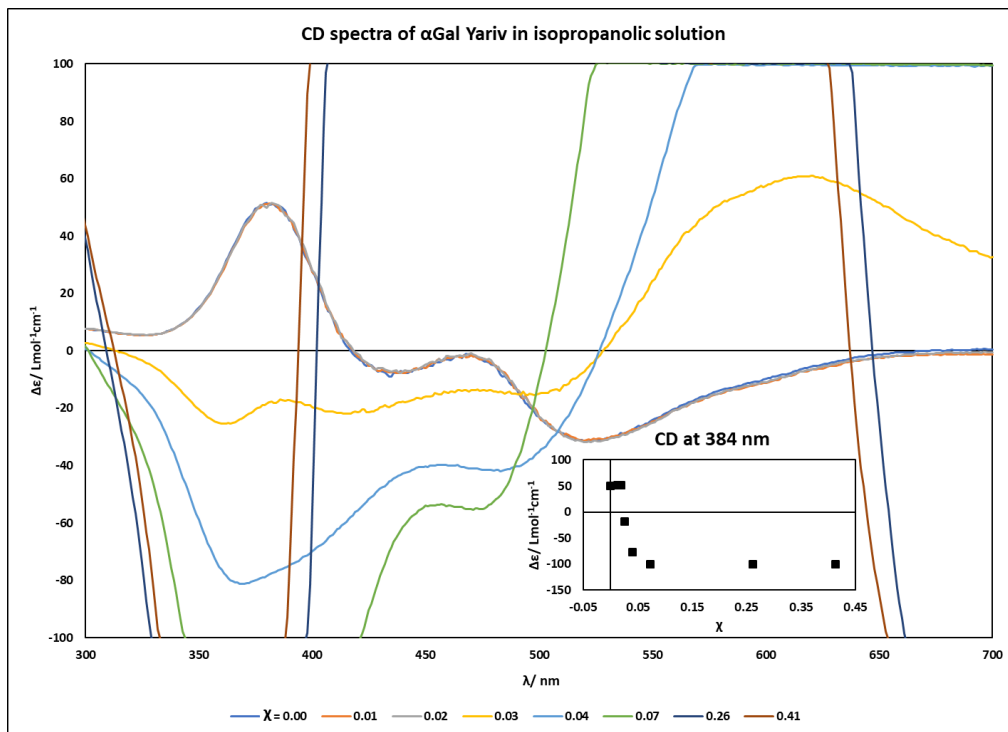


Figure 4.29: CD spectra of 0.3 mM α Gal Yariv reagent in isopropanolic aqueous solutions

UV-vis experiments (Fig. 4.30) show that the absorbance values of the spectra generally decrease as χ increases from 0 - 0.07. Then the absorbance values of the spectra increase significantly from 0.07 – 0.41. In this experiment, the same decrease in absorbance is observed as was seen in the α Gal in methanolic and ethanolic solution experiments, suggesting that the mechanism of assembly is the same regardless of the identity of the alcohol.

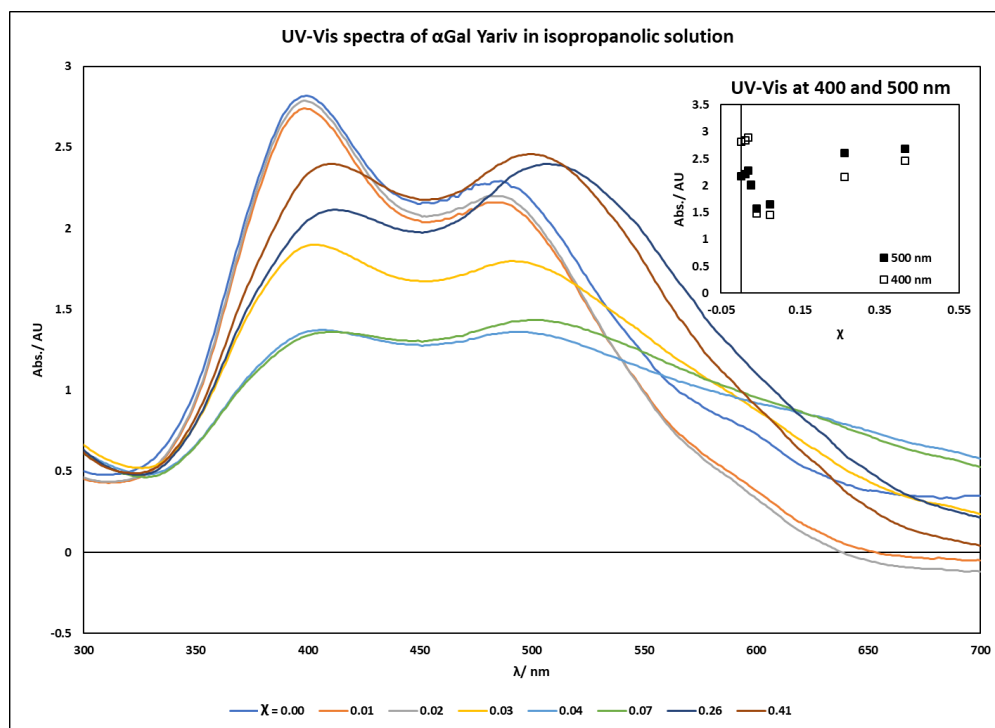


Figure 4.30: UV/Vis spectra of 0.3 mM α Gal Yariv reagent in isopropanolic aqueous solutions

According to the literature²⁶ ΔH_E reaches a minimum at $\chi = 0.10$ for a water – isopropanol mixture. Therefore, we would have expected the most intense inverted CD spectra at χ values close to 0.10 instead of the observed value of 0.03. However, it is clear that the isopropanol causes the spectrum to invert at lower χ values than were seen for ethanol which is expected given the more rapid decrease in ΔH_E . Again, this data suggests some relationship between the aggregation behavior of the Yariv reagent, and the values of ΔH_E , but it is obvious that this relationship is much more complex than was observed in the previously discussed systems.

4.4.7 Alcohol composition dependent DLS experiments

DLS experiments were also performed using varying compositions of alcohol-water solutions to examine the effect alcohol composition will have upon the aggregation behavior of the Yariv reagents (Fig. 4.31). These experiments were conducted at 10 °C with the same samples and concentrations (0.3 mM) used to perform the CD and UV-Vis experiments.

For β Glc in methanolic solutions (Fig. 4.31b) the initial increase in aggregate size was observed from χ values 0.02 – 0.07. The size continued to increase (except for one lower value at $\chi = 0.16$) before finally decreasing drastically from χ values 0.20 – 0.30. This correlated with the changes observed in the CD experiments over the same χ range.

For α Gal in methanolic solutions (Fig. 4.31a) the initial increase in aggregate size was observed from χ values 0.02 – 0.07. The increase in aggregate size continues until it decreases drastically from χ values 0.20 – 0.30. This correlated with the changes observed in the CD experiments over the same χ range.

For α Gal in ethanolic solutions (Fig. 4.31c) the initial increase in aggregate size was observed from χ values 0.03 – 0.05. The increase in aggregate size continues from χ values increase. The increase in aggregate size correlates with the changes observed in the CD experiments over the same χ range except for the fact that the size increases from χ values 0.09 – 0.24 whereas the intensity of the CD spectrum decreases over the same range.

For α Gal in isopropanolic solutions (Fig. 4.31d) the initial increase in aggregate size was observed from χ values 0.02 – 0.03. The size of the aggregates continues to increase until it decreases from χ values 0.07 – 0.26 before increasing again from χ values 0.26 – 0.41. This correlated with the changes observed in the CD experiments from χ values 0.00 – 0.07, but cannot really be compared to the CD experiments at higher χ values due to the CD spectra being largely uninterpretable due to the high intensity values of the CD spectra.

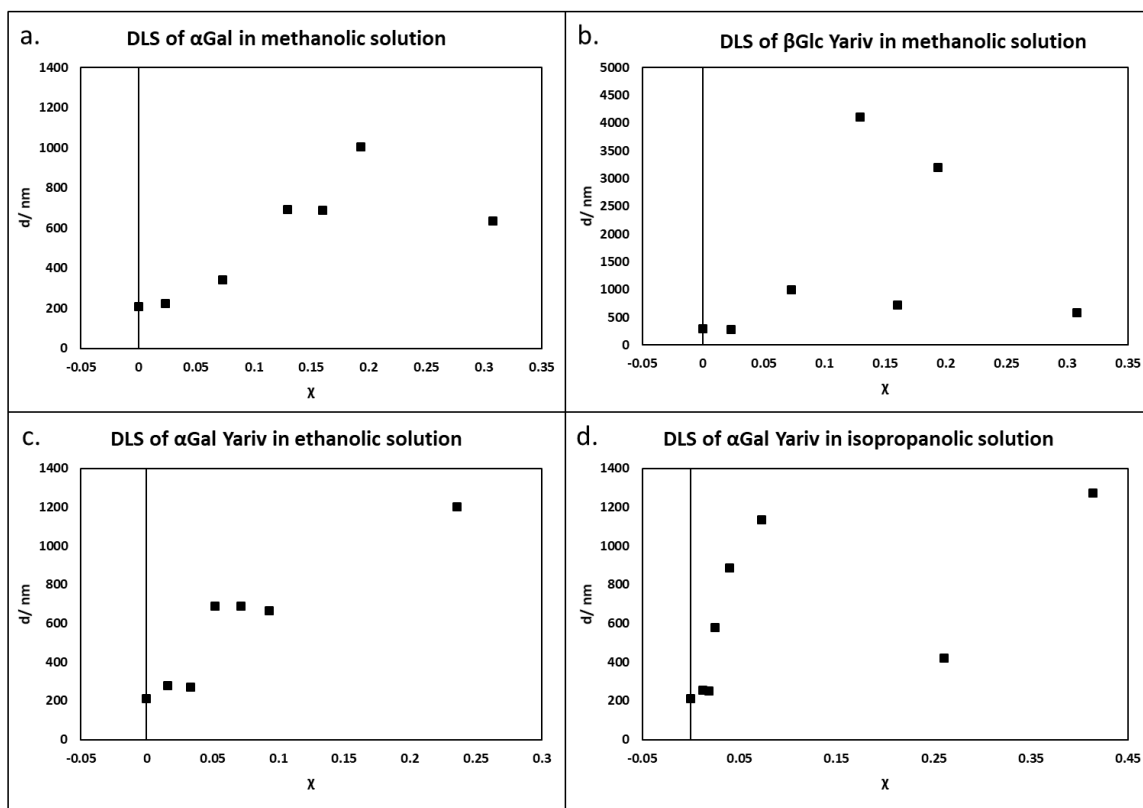


Figure 4.31: DLS experiments with Yariv reagents and various alcoholic aqueous solutions (For DLS results with multiple peaks the larger sized peak is displayed)

The general correlations between the CD data and the DLS results suggest that the change in aggregation behavior that results in the inversion of the CD spectra is related to an increase in aggregate size indicative of the formation of higher order aggregates.

4.4.8 Additional temperature-dependent CD experiments

We decided to conduct additional temperature-dependent CD experiments with αGal dissolved in aqueous solutions of ethanol and isopropanol. These experiments were performed to determine if hysteresis is observed in these aggregates. Experiments were performed using samples dissolved in 15% (v/v) EtOH ($\chi = 0.05$) and 10% (v/v) iPrOH ($\chi = 0.03$). These values were selected since they were the lowest values at which the inversion of the CD spectra and larger

sized DLS peaks were observed, making it likely that increasing the temperature will result in a transition back to 1-D aggregates.

For these experiments, a CD spectrum (Fig 4.32a and 4.33a) was acquired at 10 °C and then a temperature-dependent experiment (Fig 4.32b and 4.33b) was performed by heating the sample from 10-50 °C. The sample was then held at 50 °C and another CD spectrum was acquired. Another temperature-dependent experiment was performed by cooling the sample from 50-10 °C and a final CD spectra was acquired at 10 °C. Hysteresis was observed in experiments performed using the sample containing ethanol and the sample containing isopropanol. This demonstrates that the similar hysteresis behavior is observed in aqueous alcohol solutions of α Gal Yariv regardless of the identity of the alcohol.

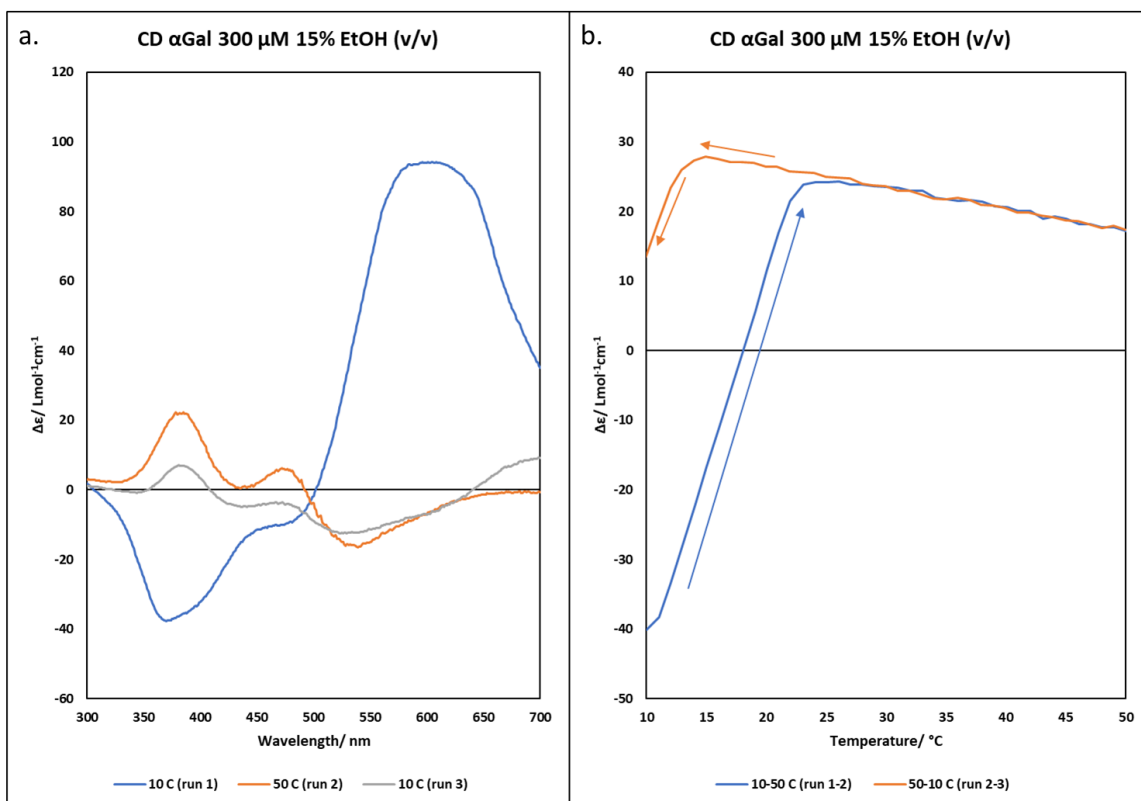


Figure 4.32: Temperature dependent CD experiments with ethanolic solution

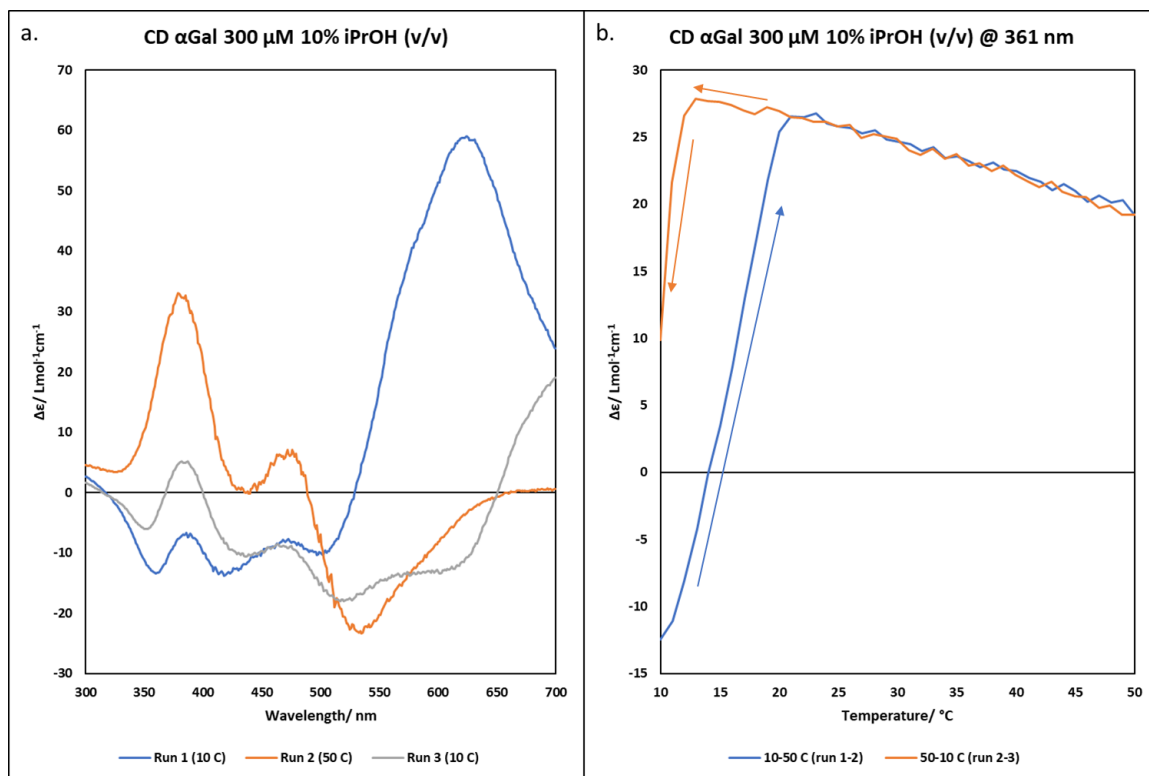


Figure 4.33: Temperature-dependent CD experiments performed with isopropanolic solution

4.4.9 Yariv binding to AGP in the presence of alcohol

If the higher order aggregates observed in alcoholic solutions are indeed multi-helices formed by an aggregation of the single helical aggregates it is possible that that the individual helices could still interact with and bind to AGP. The CD spectra (Fig. 4.34) of solutions of β Glc in 25% (v/v) methanolic aqueous solution prepared with 0.63 g/L gum Arabic AGP do not show any inversion of the spectrum at 10 °C. Also, when AGP is added directly the cuvette containing the sample of β Glc in 25% (v/v) methanolic aqueous solution the inverted CD reverts from to the typical spectrum with a positive Cotton effect. This data indicates that the β Glc Yariv reagent is still able to bind to AGP in its aggregated state, and that this binding results in a breakup of the higher order aggregate suggesting that the Yariv-AGP binding is strong enough to overcome the forces that drive higher order aggregation. However, since this is not a covalently bound system, the

higher order Yariv aggregate is in equilibrium with the 1-D Yariv aggregates, and monomeric Yariv molecules. Therefore, it is possible that when the AGP is added the equilibrium is shifted toward 1-D Yariv aggregates as they bind to AGP. This results in the disappearance of the higher order structures. The UV-vis spectra (Fig 4.34) also show that the presence of gum Arabic AGP causes the spectra of the Yariv reagents to revert to a state that is more like the spectra obtained in pure water. When Frost Grape AGP is present in a β Glc Yariv sample containing 25% (v/v) MeOH a negative CD spectrum and attenuated UV-Vis spectrum are still observed indicating that higher order aggregates are still present.

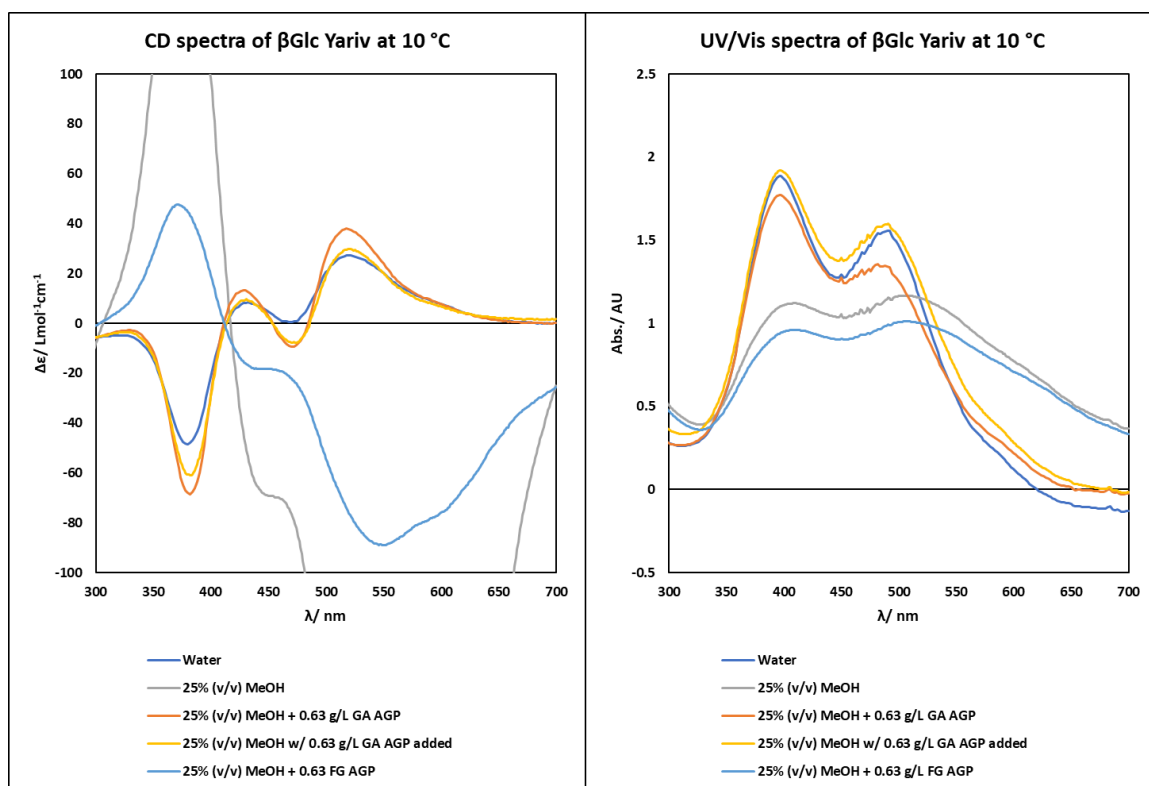


Figure 4.34: The effects of gum Arabic AGP on the CD and UV/Vis spectra of 0.3 mM β Glc Yariv reagent in methanolic solution

The CD spectra (Fig. 4.35) of solutions of α Gal in 25% (v/v) methanolic aqueous solution prepared with 0.63 g/L GA still shows an inverted spectrum at 10 °C indicating that the higher order aggregates are still intact. While this spectrum is still inverted, it is less intense than the spectrum

for the sample in methanolic solution without any AGP. This data suggests that the mere presence of AGP may have some effect on the stability of the higher order aggregates, but the effect is clearly not nearly as drastic as the effect observed for β Glc suggesting that binding has not occurred. The UV/Vis spectra (Fig. 4.35) for these samples also show that the presence of gum Arabic AGP does not cause the spectrum of α Gal in methanolic solution to revert to the shape of the spectra taken in pure water. In samples of α Gal Yariv in 25% (v/v) MeOH and Frost Grape AGP a weakly negative CD spectrum is observed suggesting that the higher order aggregates have become broken up, however the UV-Vis spectrum shows a spectrum that is more characteristic of the higher order Yariv aggregates. In the hysteresis experiments it was observed that α Gal Yariv can display a negative CD spectra while still existing as higher order aggregates (as shown by DLS), so it is possible that this is the case for the Frost Grape AGP containing samples.

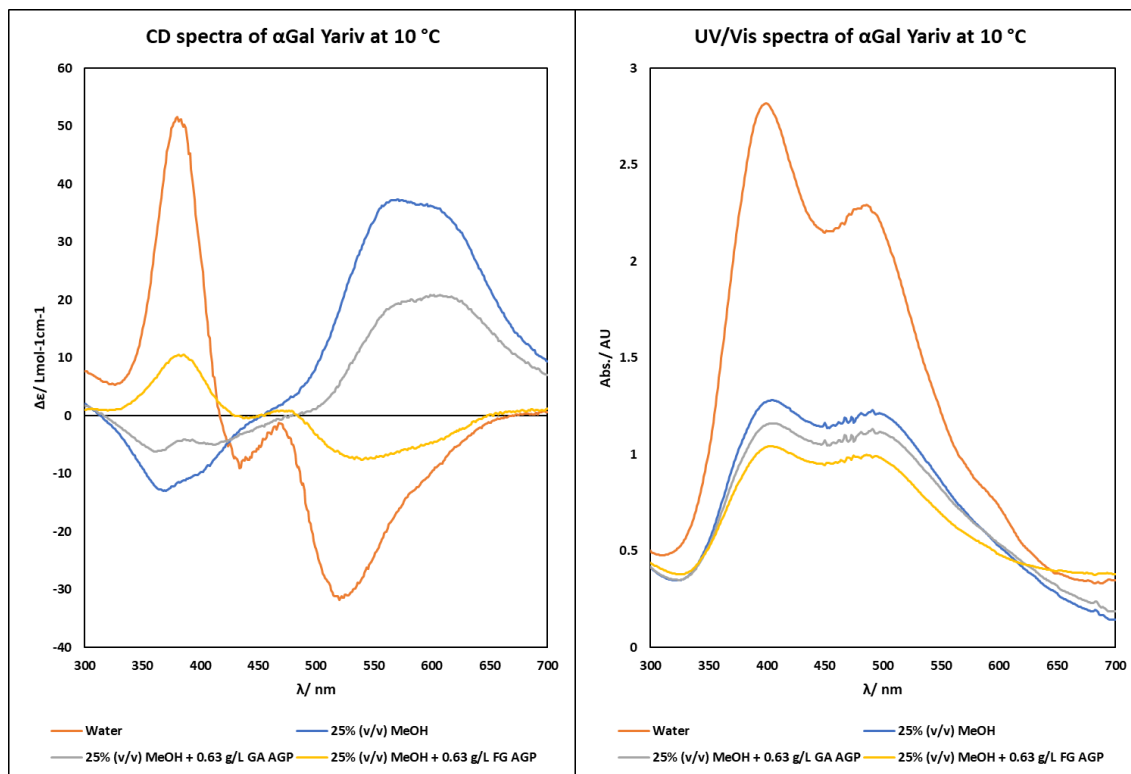


Figure 4.35: The effects of gum Arabic AGP on the CD and UV/Vis spectra of 0.3 mM α Gal Yariv reagent in methanolic solution

4.5 Conclusions

In this study, we observed an inversion of the CD spectra for samples of Yariv reagents dissolved in aqueous alcoholic solutions at 10 °C. This behavior is temperature-dependent and displays hysteresis after heating and cooling cycles. This behavior is also dependent on the alcohol composition of the solvent and shows some relation to the value of ΔH_E for the solvent mixture. The inversion behavior of the CD spectra is correlated to an increase in aggregate size observed in DLS measurements. This data indicates that 1-D Yariv aggregates undergo a transition to higher order aggregates in the presence of aqueous solutions of alcohol at 10 °C. Higher order β Glc Yariv aggregates are still able to interact with AGP and revert to their original state because of this interaction.

Although the χ value at which the Yariv reagents transition from 1-D aggregates to higher-order aggregates (χ_{trans}) is not directly correlated to the χ value for which the minimum ΔH_E is observed (as is the case for the PNIPAM²⁴ polymers and the BiPy-BTA¹⁸ supramolecular polymers) solvent dependent changes in χ_{trans} are observed. For isopropanolic mixtures the χ value at which ΔH_E is minimal is lower than is found for methanol (Fig 4.36). The same trend is observed for values of χ_{trans} in the two solvents, suggesting a link between χ_{trans} and ΔH_E and that there is a critical value of ΔH_E at which the transition to higher order aggregates occurs.

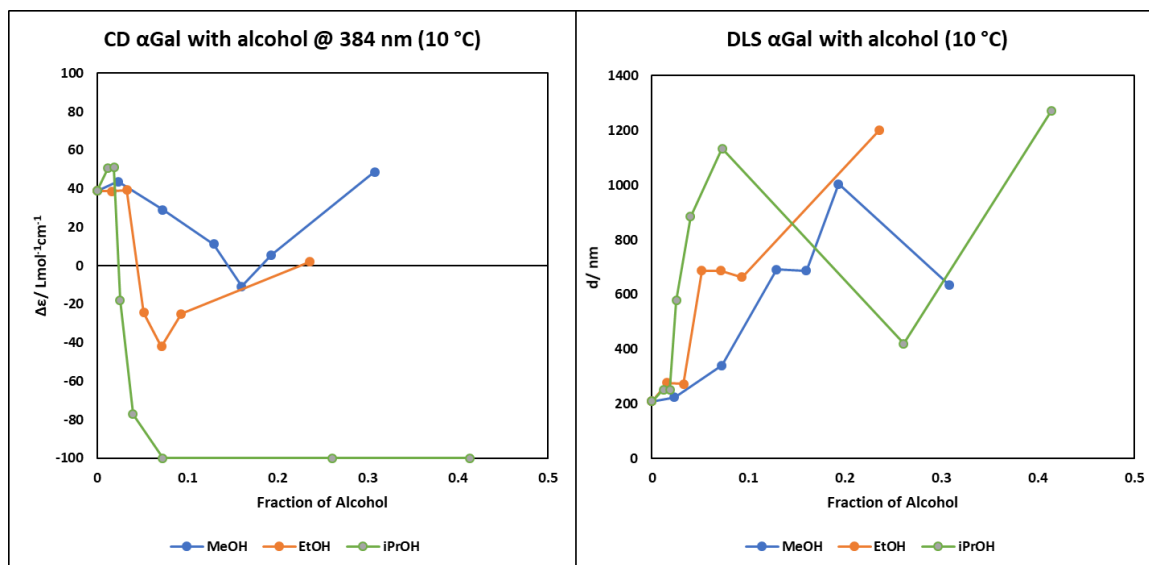


Figure 4.36: Trends in CD and DLS measurements of α Gal Yariv samples in alcohol solutions of various compositions. Additional experiments should be performed to examine the effects of n-propanol on α Gal Yariv, and methanol, ethanol, and n-propanol on β Glc Yariv. Also, it would be interesting to observe how the self-assembly of other Yariv reagents are affected by the presence of alcohol. Furthermore, analysis by cryo-TEM or SAXS may provide additional information on the shape of the aggregates and lead to a better understanding of the mechanism of self-assembly that results in the formation of higher-order aggregates. A better understanding of the mechanism that drives the alcohol induced aggregation observed in Yariv reagents may provide information that will be valuable for the design of similar systems to serve as functional supramolecular polymers.

While these preliminary results demonstrate that Yariv reagents are capable of alcohol mediated hierarchical self-assembly, the nature of the mechanism for this process and the structure of the higher order aggregate are not known. It is possible that the driving force for aggregation is the decrease in ΔH_E that results from the increase in χ and that the change in the energetics of the bulk solvent causes the Yariv reagents to form multi-helical aggregates.

4.6 Supporting Information

CD and UV-Vis Experiments

Circular dichroism and UV-Vis measurements were performed using a Jasco J-815 spectropolarimeter. Each spectrum is the average of three replicates. Temperature was controlled by a JASCO Peltier temperature control unit. Concentration and volume of the Yariv reagent samples were 0.3 mM and 0.6 mL, respectively. Samples containing alcohol were prepared by adding 0.09 mL of a 2 mM Yariv stock solution to an Eppendorf tube followed by the necessary amount of alcohol (pre-filtered through a Whatman 0.22 μm PTFE syringe filter) and then the volume was brought to 0.6 mL with Millipore water. The sample cell was kept at either 10 $^{\circ}\text{C}$ or 60 $^{\circ}\text{C}$ for all experiments. CD/UV-vis spectroscopy measurements were obtained in a Hellma analytics 2mm path length stoppered cuvette and corrected against a purified water standard, or blanks prepared with purified water and filtered alcohol. Wavelength readings ranged from 300 to 700 nm and were obtained at a speed of 100 nm/min. The measured ellipticity θ was converted to molar circular dichroism $\Delta\epsilon = \theta / 32980 \cdot c \cdot l$, where ellipticity is given in mdeg, c is the concentration in $\text{mol} \cdot \text{L}^{-1}$ and l is the optical path length in cm. For temperature-dependent experiments heating and cooling was performed at a rate of 1 $^{\circ}\text{C}/\text{min}$. For hysteresis experiments samples were rapidly heated and cooled using the temperature controller.

DLS Experiments

To a 3 mL 10 mm quartz cuvette was added 0.4 mL of the desired Yariv sample. The samples were prepared in the same manner as those used for the CD experiments. The cuvette was then placed into the cell of a Zetasizer Nano dynamic light scattering instrument. All experiments were run using the preset standard operating procedure for dynamic light scattering measurements to give results for size distribution by intensity. Measurements were taken at 10 and 60 $^{\circ}\text{C}$ with a scattering angle of 90 $^{\circ}$.

References:

1. Aida, T.; Meijer, E.; Stupp, S., Functional supramolecular polymers. *Science* **2012**, *335* (6070), 813-817.
2. Brodsky, F. M.; Chen, C.-Y.; Knuehl, C.; Towler, M. C.; Wakeham, D. E., Biological basket weaving: formation and function of clathrin-coated vesicles. *Annual Review of Cell and Developmental Biology* **2001**, *17* (1), 517-568.
3. O'leary, L. E.; Fallas, J. A.; Bakota, E. L.; Kang, M. K.; Hartgerink, J. D., Multi-hierarchical self-assembly of a collagen mimetic peptide from triple helix to nanofibre and hydrogel. *Nature chemistry* **2011**, *3* (10), 821-828.
4. Lehn, J. M., Perspectives in supramolecular chemistry—from molecular recognition towards molecular information processing and self-organization. *Angewandte Chemie International Edition* **1990**, *29* (11), 1304-1319.
5. Hartgerink, J. D.; Granja, J. R.; Milligan, R. A.; Ghadiri, M. R., Self-assembling peptide nanotubes. *Journal of the American Chemical Society* **1996**, *118* (1), 43-50.
6. van Gorp, J. J.; Vekemans, J. A.; Meijer, E., C₃-symmetrical supramolecular architectures: Fibers and organic gels from discotic trisamides and trisureas. *Journal of the American Chemical Society* **2002**, *124* (49), 14759-14769.
7. Tysseling-Mattiace, V. M.; Sahni, V.; Niece, K. L.; Birch, D.; Czeisler, C.; Fehlings, M. G.; Stupp, S. I.; Kessler, J. A., Self-assembling nanofibers inhibit glial scar formation and promote axon elongation after spinal cord injury. *Journal of Neuroscience* **2008**, *28* (14), 3814-3823.
8. Rajangam, K.; Behanna, H. A.; Hui, M. J.; Han, X.; Hulvat, J. F.; Lomasney, J. W.; Stupp, S. I., Heparin binding nanostructures to promote growth of blood vessels. *Nano Letters* **2006**, *6* (9), 2086-2090.
9. Mata, A.; Geng, Y.; Henrikson, K. J.; Aparicio, C.; Stock, S. R.; Satcher, R. L.; Stupp, S. I., Bone regeneration mediated by biomimetic mineralization of a nanofiber matrix. *Biomaterials* **2010**, *31* (23), 6004-6012.
10. Jun, H. W.; Yuwono, V.; Paramonov, S. E.; Hartgerink, J. D., Enzyme-Mediated Degradation of Peptide-Amphiphile Nanofiber Networks. *Advanced Materials* **2005**, *17* (21), 2612-2617.
11. El Hamaoui, B.; Zhi, L.; Pisula, W.; Kolb, U.; Wu, J.; Müllen, K., Self-assembly of amphiphilic imidazolium-based hexa-peri-hexabenzocoronenes into fibrous aggregates. *Chemical Communications* **2007**, (23), 2384-2386.
12. Xiao, S.; Tang, J.; Beetz, T.; Guo, X.; Tremblay, N.; Siegrist, T.; Zhu, Y.; Steigerwald, M.; Nuckolls, C., Transferring self-assembled, nanoscale cables into electrical devices. *Journal of the American Chemical Society* **2006**, *128* (33), 10700-10701.
13. Hartgerink, J. D.; Beniash, E.; Stupp, S. I., Self-assembly and mineralization of peptide-amphiphile nanofibers. *Science* **2001**, *294* (5547), 1684-1688.
14. Zhang, S.; Greenfield, M. A.; Mata, A.; Palmer, L. C.; Bitton, R.; Mantei, J. R.; Aparicio, C.; De La Cruz, M. O.; Stupp, S. I., A self-assembly pathway to aligned monodomain gels. *Nature materials* **2010**, *9* (7), 594-601.
15. Jonkheijm, P.; van der Schoot, P.; Schenning, A. P.; Meijer, E., Probing the solvent-assisted nucleation pathway in chemical self-assembly. *Science* **2006**, *313* (5783), 80-83.
16. De Greef, T. F.; Smulders, M. M.; Wolfs, M.; Schenning, A. P.; Sijbesma, R. P.; Meijer, E., Supramolecular polymerization. *Chemical Reviews* **2009**, *109* (11), 5687-5754.

17. Huang, Y.; Hu, J.; Kuang, W.; Wei, Z.; Faul, C. F. J., Modulating helicity through amphiphilicity-tuning supramolecular interactions for the controlled assembly of perylenes. *Chemical Communications* **2011**, *47* (19), 5554-5556.
18. Gillissen, M. A. J.; Koenigs, M. M. E.; Spiering, J. J. H.; Vekemans, J. A. J. M.; Palmans, A. R. A.; Voets, I. K.; Meijer, E. W., Triple Helix Formation in Amphiphilic Discotics: Demystifying Solvent Effects in Supramolecular Self-Assembly. *Journal of the American Chemical Society* **2014**, *136* (1), 336-343.
19. Lehn, J.-M., Dynamers: dynamic molecular and supramolecular polymers. *Progress in Polymer Science* **2005**, *30* (8), 814-831.
20. Brunsveld, L.; Zhang, H.; Glasbeek, M.; Vekemans, J. A. J. M.; Meijer, E. W., Hierarchical Growth of Chiral Self-Assembled Structures in Protic Media. *Journal of the American Chemical Society* **2000**, *122* (26), 6175-6182.
21. Brunsveld, L.; Folmer, B. J. B.; Meijer, E. W.; Sijbesma, R. P., Supramolecular Polymers. *Chemical Reviews* **2001**, *101* (12), 4071-4098.
22. Hermans, T. M.; Broeren, M. A.; Gomopoulos, N.; Van Der Schoot, P.; Van Genderen, M. H.; Sommerdijk, N. A.; Fytas, G.; Meijer, E., Self-assembly of soft nanoparticles with tunable patchiness. *Nature nanotechnology* **2009**, *4* (11), 721-726.
23. Shao, H.; Gao, M.; Kim, S. H.; Jaroniec, C. P.; Parquette, J. R., Aqueous Self-Assembly of L-Lysine-Based Amphiphiles into 1D n-Type Nanotubes. *Chemistry-A European Journal* **2011**, *17* (46), 12882-12885.
24. Bischofberger, I.; Calzolari, D.; De Los Rios, P.; Jelezarov, I.; Trappe, V., Hydrophobic hydration of poly-N-isopropyl acrylamide: a matter of the mean energetic state of water. *Scientific reports* **2014**, *4*, 4377.
25. Southall, N. T.; Dill, K. A.; Haymet, A., A view of the hydrophobic effect. ACS Publications: 2002.
26. Lama, R.; Lu, B. C.-Y., Excess Thermodynamic Properties of Aqueous Alcohol Solutions. *Journal of Chemical and Engineering Data* **1965**, *10* (3), 216-219.
27. Galinski, E. A.; Stein, M.; Amendt, B.; Kinder, M., The kosmotropic (structure-forming) effect of compensatory solutes. *Comparative Biochemistry and Physiology Part A: Physiology* **1997**, *117* (3), 357-365.
28. Dixit, S.; Crain, J.; Poon, W.; Finney, J.; Soper, A., Molecular segregation observed in a concentrated alcohol-water solution. *Nature* **2002**, *416* (6883), 829-832.
29. Woods, E.; Lilley, G.; Jermyn, M., The self-association of glycosyl phenylazo dyes (Yariv antigens). *Australian Journal of Chemistry* **1978**, *31* (10), 2225-2238.
30. Smulders, M. M. J.; Nieuwenhuizen, M. M. L.; de Greef, T. F. A.; van der Schoot, P.; Schenning, A. P. H. J.; Meijer, E. W., How to Distinguish Isodesmic from Cooperative Supramolecular Polymerisation. *Chemistry – A European Journal* **2010**, *16* (1), 362-367.
31. Paulsen, B. S.; Craik, D. J.; Dunstan, D. E.; Stone, B. A.; Bacic, A., The Yariv reagent: Behaviour in different solvents and interaction with a gum arabic arabinogalactanprotein. *Carbohydrate Polymers* **2014**, *106*, 460-468.
32. Liu, H.; Pierre-Pierre, N.; Huo, Q., Dynamic light scattering for gold nanorod size characterization and study of nanorod-protein interactions. *Gold Bulletin* **2012**, *45* (4), 187-195.
33. Instruments, M., Zetasizer nano series user manual. *MAN0317* **2004**, *1*.
34. Rougée, M.; Faucon, B.; Mergny, J.; Barcelo, F.; Giovannangeli, C.; Garestier, T.; Hélène, C., Kinetics and thermodynamics of triple-helix formation: Effects of ionic strength and mismatched. *Biochemistry* **1992**, *31* (38), 9269-9278.

5 APPENDIX

5.1 Appendix I: Gel Permeation Chromatography Traces

20, n ~ 30

GPC/SEC Software Sample GPC Analysis Report

Generated by Kiesewetter at 4:19 PM on Friday, August 04, 2017



Results

Analysed by

Kiesewetter at 4:19:16 PM on Friday, August 04, 2017

Comments

Molecular Weight Averages

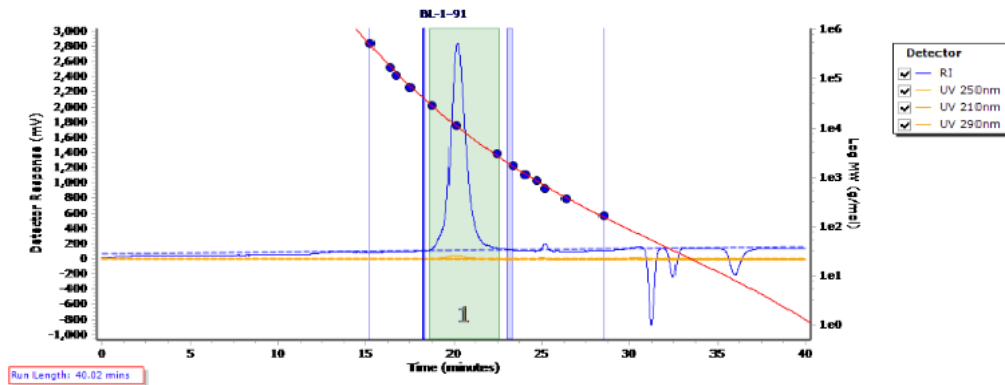
Peak	Mp	Mn	Mw	Mz	Mz+1	Mv	PD
Peak 1	10426	9323	10350	11394	12558	11232	1.11

Peak information

	Start (mins)	End (mins)
Baseline region 1	18.23	18.42
Baseline region 2	23.03	23.39
Peak 1	18.61	22.65

Peak	Trace	Peak Max RT (mins)	Peak Area (mV.s)	Peak Height (mV)
Peak 1	RI	20.20	171056.295	2731.009
Peak 1	UV 250nm	20.06	2957.513	44.209
Peak 1	UV 210nm	20.10	527.120	8.139
Peak 1	UV 290nm	20.03	173.147	2.389

Chromatogram



20, n ~ 90

GPC/SEC Software Sample GPC Analysis Report



Generated by Kiesewetter at 4:20 PM on Friday, August 04, 2017

Results

Analysed by
Comments

Kiesewetter at 4:20:13 PM on Friday, August 04, 2017

Molecular Weight Averages

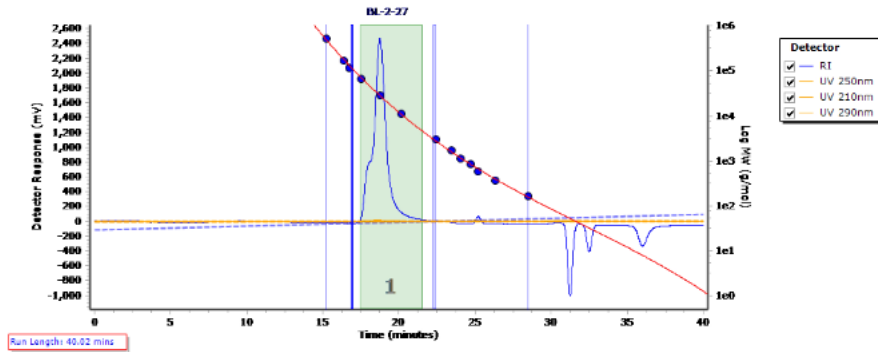
Peak	Mp	Mn	Mw	Mz	Mz+1	Mv	PD
Peak 1	27943	24988	29613	34414	36864	33757	1.197

Peak Information

	Start (mins)	End (mins)
Baseline region 1	16.87	17.06
Baseline region 2	22.26	22.52
Peak 1	17.43	21.58

Peak	Trace	Peak Max RT (mins)	Peak Area (mV.s)	Peak Height (mV)
Peak 1	RI	18.76	153231.576	2480.314
Peak 1	UV 250nm	18.58	1277.070	19.604
Peak 1	UV 210nm	18.55	275.582	4.915
Peak 1	UV 290nm	18.58	85.566	1.146

Chromatogram



21, n ~ 90

GPC/SEC Software Sample GPC Analysis Report



Generated by Kieseletter at 4:18 PM on Friday, August 24, 2017

Results

Analysed by
Comments

Kieseletter at 12:31 49 PM on Wednesday, August 02, 2017

Molecular Weight Averages

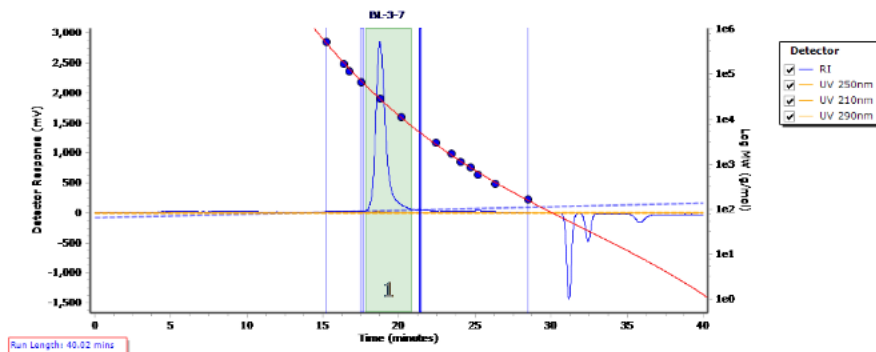
Peak	Mp	Min	Mw	Mz	Mz+1	Mv	PD
Peak 1	27943	24478	26508	28145	29574	27923	1.063

Peak Information

	Start (mins)	End (mins)
Baseline region 1	17.43	17.75
Baseline region 2	21.83	21.5
Peak 1	17.81	20.88

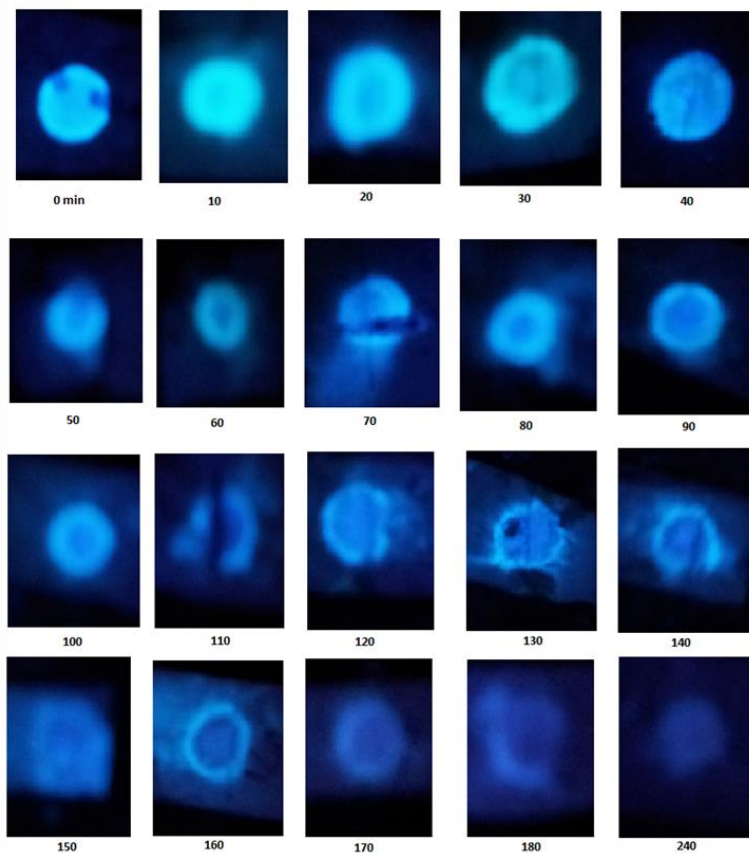
Peak	Trace	Peak Max RT (mins)	Peak Area (mV.s)	Peak Height (mV)
Peak 1	RI	18.78	127466.037	2819.133
Peak 1	UV 250nm	18.57	1085.203	22.704
Peak 1	UV 210nm	18.38	211.701	5.386
Peak 1	UV 290nm	18.58	88.078	1.624

Chromatogram

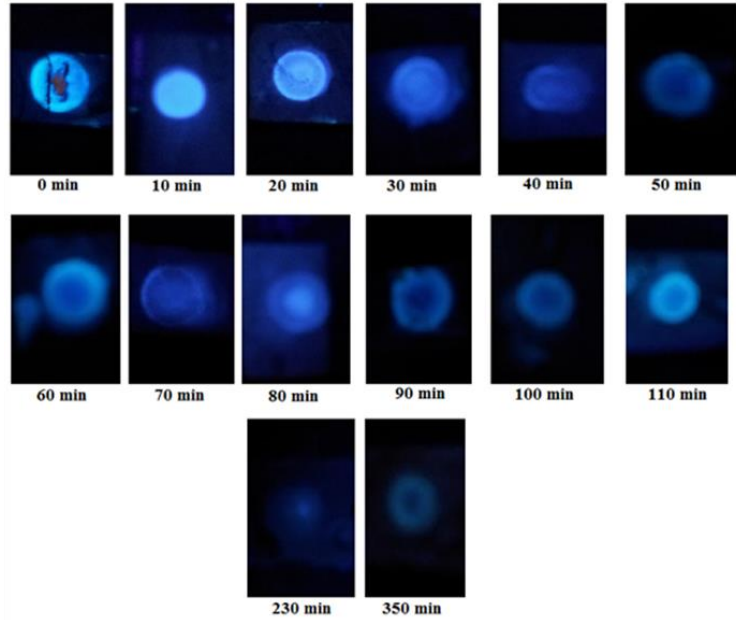


5.2 Appendix II: Click TLC Stains

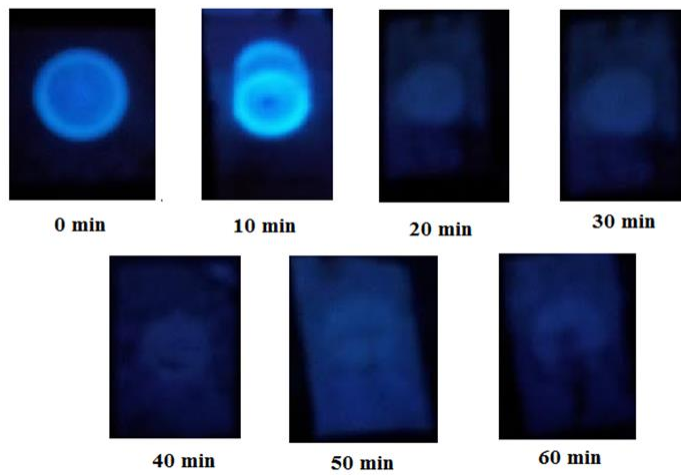
Click stain monitoring of **43**, $n \sim 30$ synthesis



Click stain monitoring of **44**, $n \sim 30$ synthesis



Click stain monitoring of **45**, $n \sim 30$ synthesis



Click stain monitoring
of 47, n ~ 90 synthesis



0 min After completion

Click stain monitoring
of 49, n ~ 90 synthesis



0 min After completion

Click stain monitoring of 50, n ~ 90 synthesis



0 min



10 min



20 min



30 min



40 min



50 min



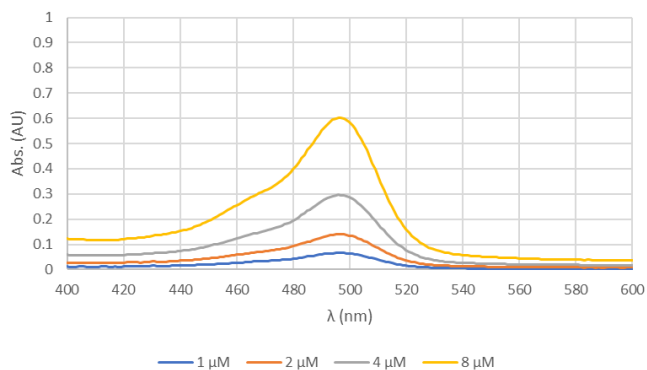
60 min



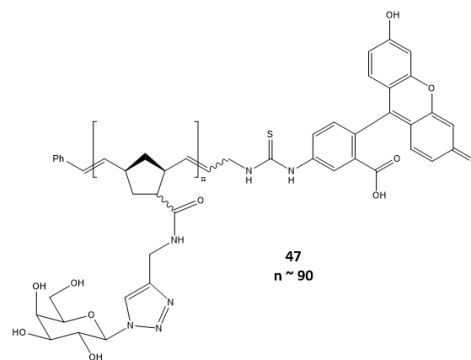
70 min

5.3 Appendix III: Determination of fluorescence labeling (in PBS pH 7.4)

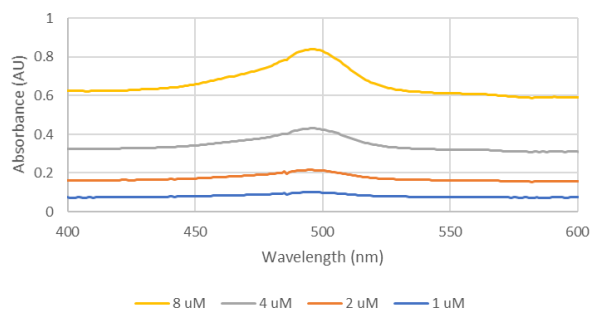
47 UV-Vis



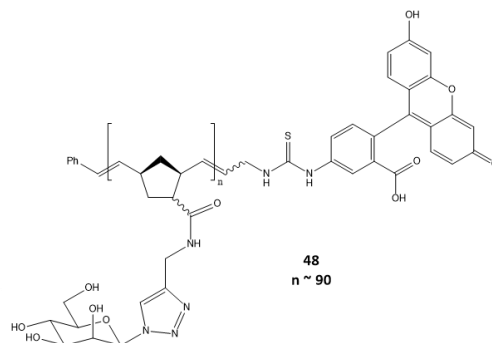
μM Poly-Gal	ABS @ 494 nm	μM FITC	% FITC Labeled
1	0.065057	0.82	82%
2	0.137954	1.74	86%
4	0.291757	3.68	92%
8	0.593672	7.49	93%
		average	88%



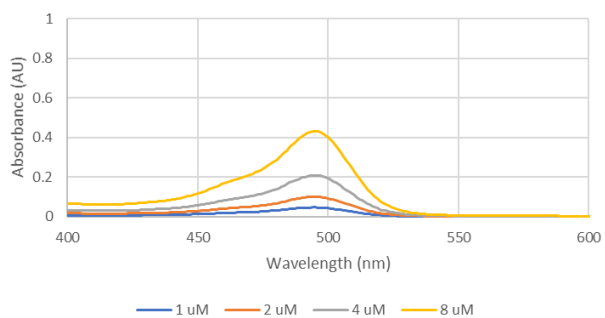
48 UV-Vis



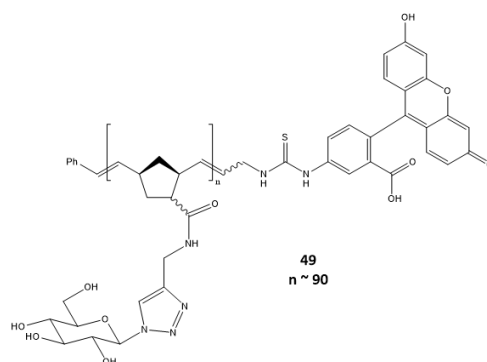
μM Poly-Man nm	ABS @ 497 nm	ABS @ 600 nm	difference	corrected μM FITC	% FITC labeled
1	0.099858	0.07355	0.026308	0.327215	32.72147
2	0.214898	0.156838	0.058059	0.72213	36.10648
4	0.430145	0.309671	0.120474	1.498437	37.46093
8	0.840449	0.590254	0.250196	3.111884	38.89855
			Avg.		36.29686



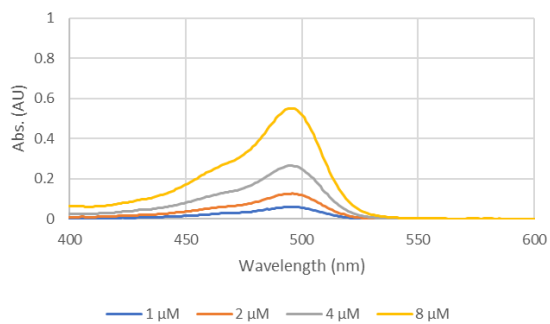
49 UV-Vis



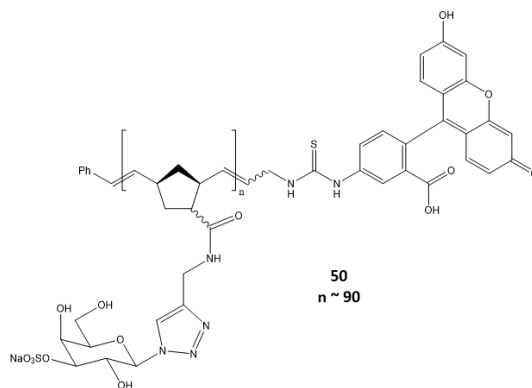
μM Poly-Glc	ABS @ 494 nm	μM FITC	% FITC labeled
1	0.046062	0.572916	57.29163
2	0.099523	1.237849	61.89245
4	0.207712	2.583485	64.58712
8	0.429149	5.337676	66.72095
		average	62.62304



50 UV-Vis



μM Poly-SGal	ABS @ 494 nm	μM FITC	% FITC Labeled
1	0.059238	0.736796	73.67964
2	0.125296	1.558409	77.92047
4	0.26396	3.283083	82.07708
8	0.548302	6.819679	85.24598
		Avg	79.73079



5.4 Appendix IV: NMR Spectra for glycopolymer synthesis

Polymer	MW _{calc}	DP _{calc}	H _{phenyl}	H _{olefinic}	H _{aliphatic}	DP _{obs}
20, n ~ 30	7162	30	5	64	344	32
20, n ~ 90	21324	90	5	210	1535	105
21, n ~ 90	21449	90	5	150	859	75

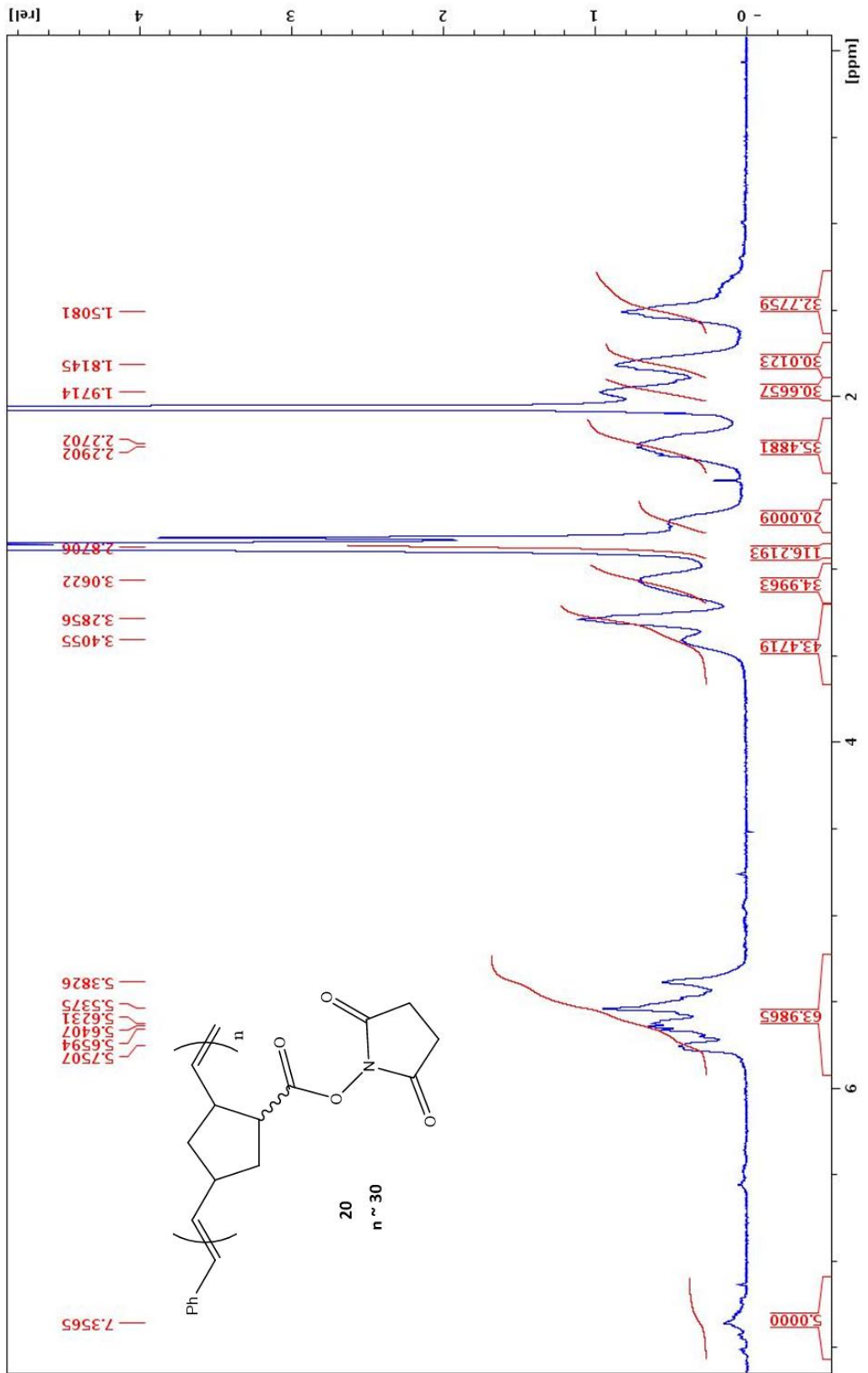
Polymer	H _{phenyl}	Expected H _{olefinic}	Observed H _{olefinic}	Expected H _{propargyl}	Observed H _{propargyl}	Expected H _{olefinic} /H _{propargyl}	Observed H _{olefinic} /H _{propargyl}
22, n ~ 30	5	60	45	60	43	1	1.04
22, n ~ 90	5	180	143	180	130	1	1.10
23, n ~ 90	5	180	161	180	165	1	0.98

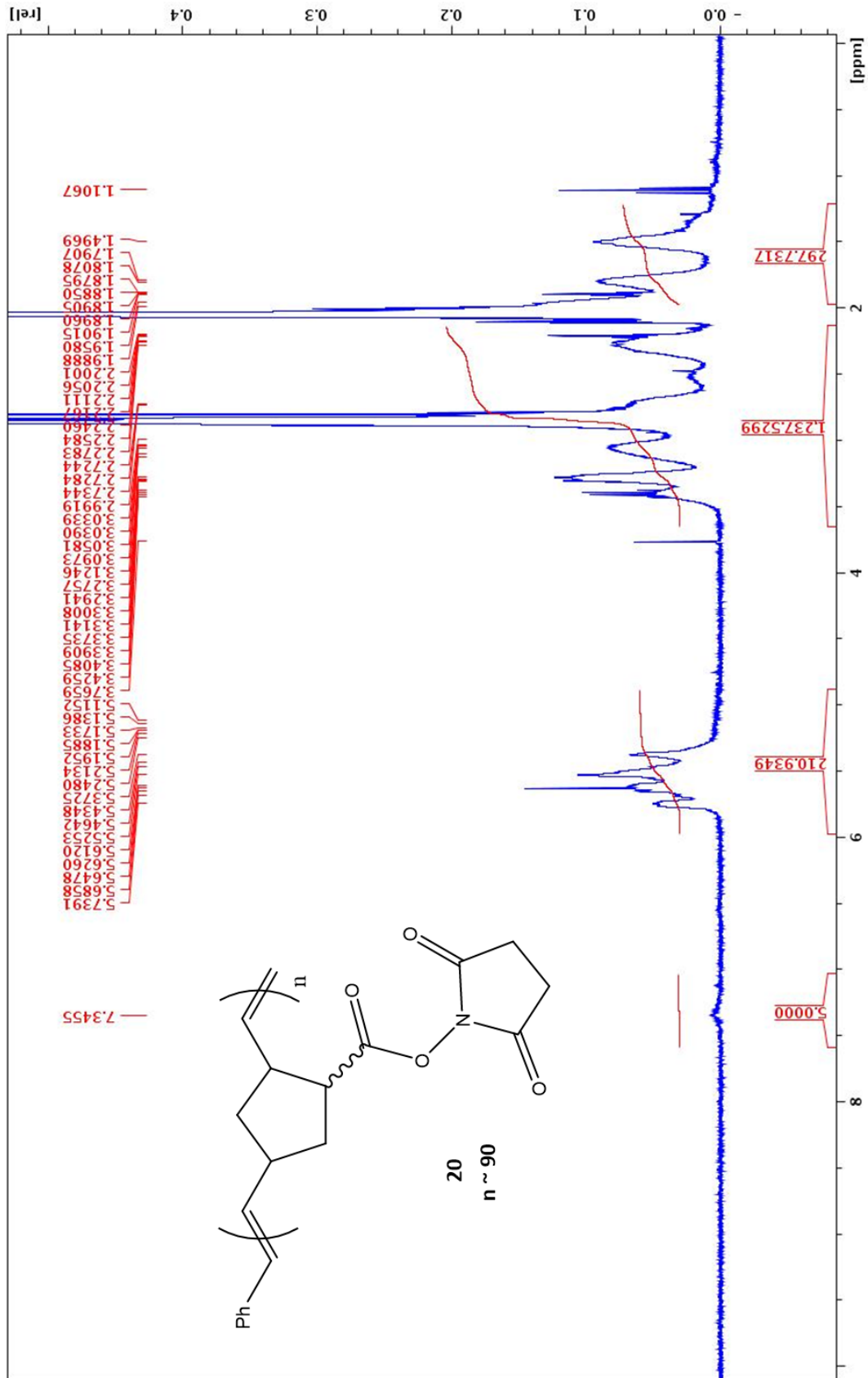
Polymer	MW _{calc}	Expected H _{aliphatic}	Observed H _{aliphatic}	Expected H _{aliphatic} /H _{olefinic}	Observed H _{aliphatic} /H _{olefinic}
22, n ~ 30	5257	240	200	4	4.44
22, n ~ 90	15874	720	582	4	4.07
23, n ~ 90	16046	720	752	4	4.67

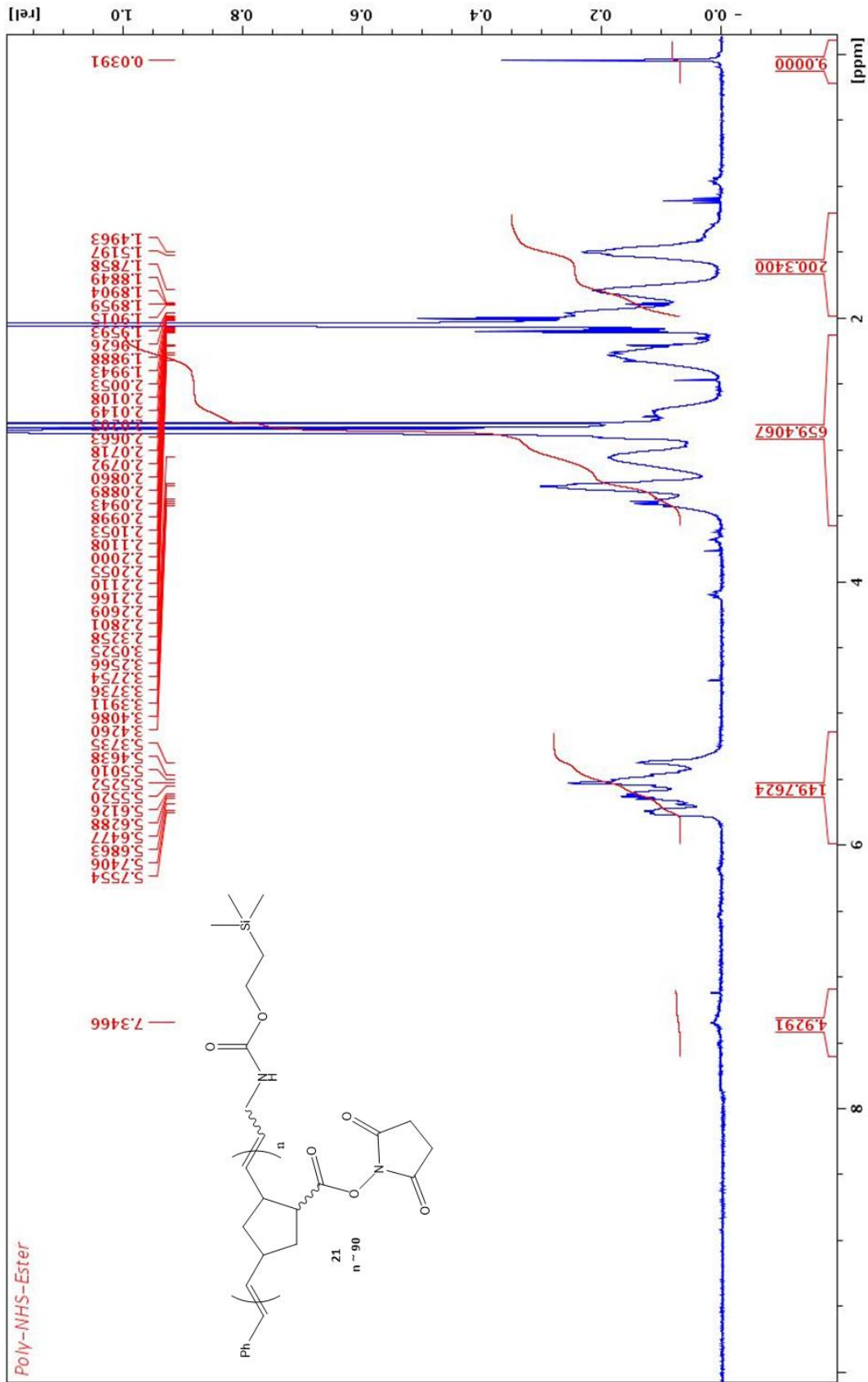
Polymer	H _{phenyl}	Expected H _{triazole}	Observed H _{triazole}	Expected H _{olefinic} + H ₁	Observed H _{olefinic} + H ₁	Expected (H _{olefinic} + H ₁)/H _{triazole}	Observed (H _{olefinic} + H ₁)/H _{triazole}
43, n ~ 30	5	30	29	90	82	3	2.83
44, n ~ 30	5	30	25	90	70	3	2.80
45, n ~ 30	5	30	31	90	90	3	2.90
46, n ~ 30	5	30	13	90	36	3	2.77
43, n ~ 90	5	90	65	270	181	3	2.78

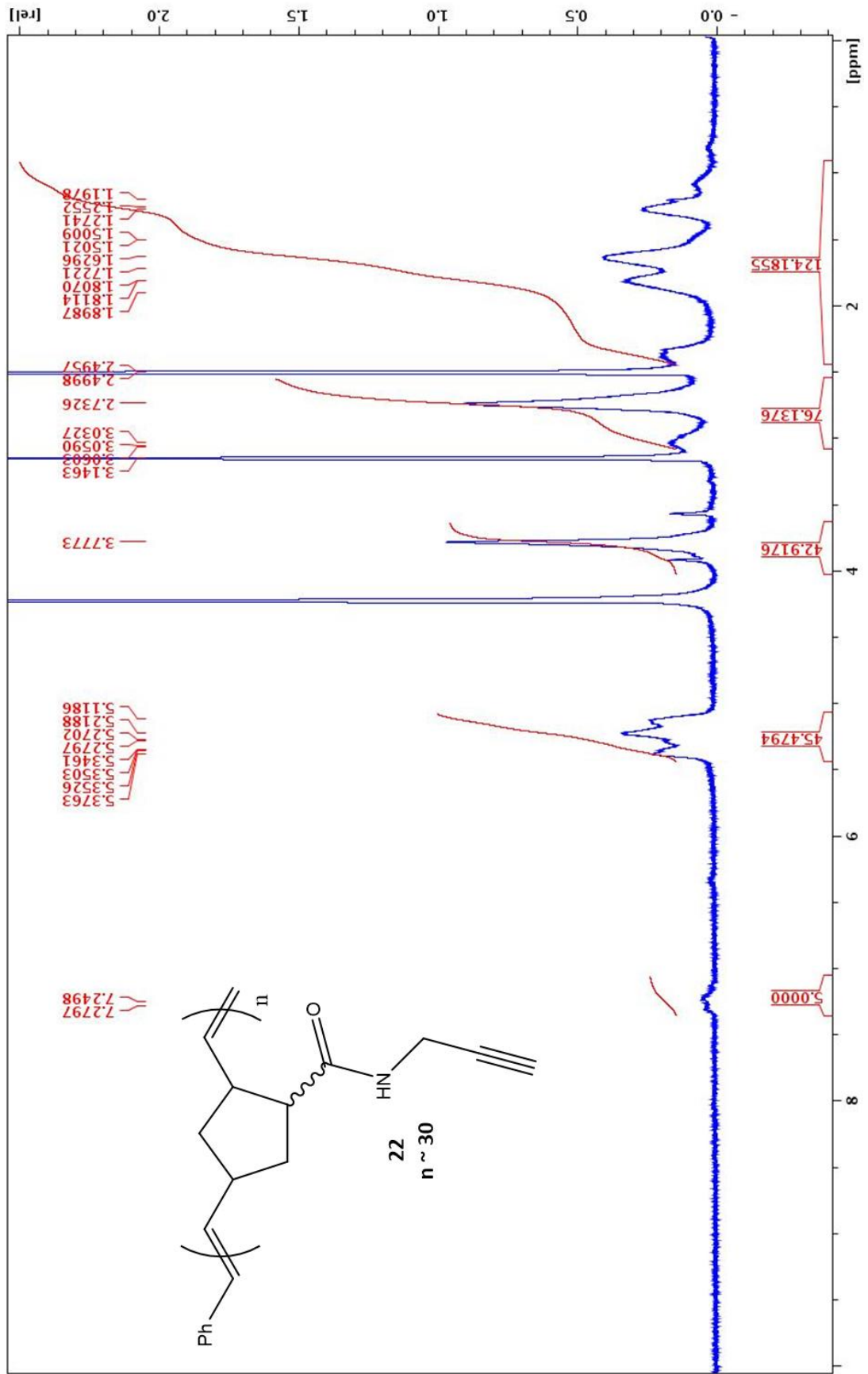
45, n ~ 90	5	90	20	270	58	3	2.90
46, n ~ 90	5	90	70	270	217	3	3.10
47, n ~ 90	5	90	114	270	321	3	2.82
48, n ~ 90	5	90	39	270	106	3	2.72
49, n ~ 90	5	90	156	270	345	3	2.21
50, n ~ 90	5	90	126	270	346	3	2.74

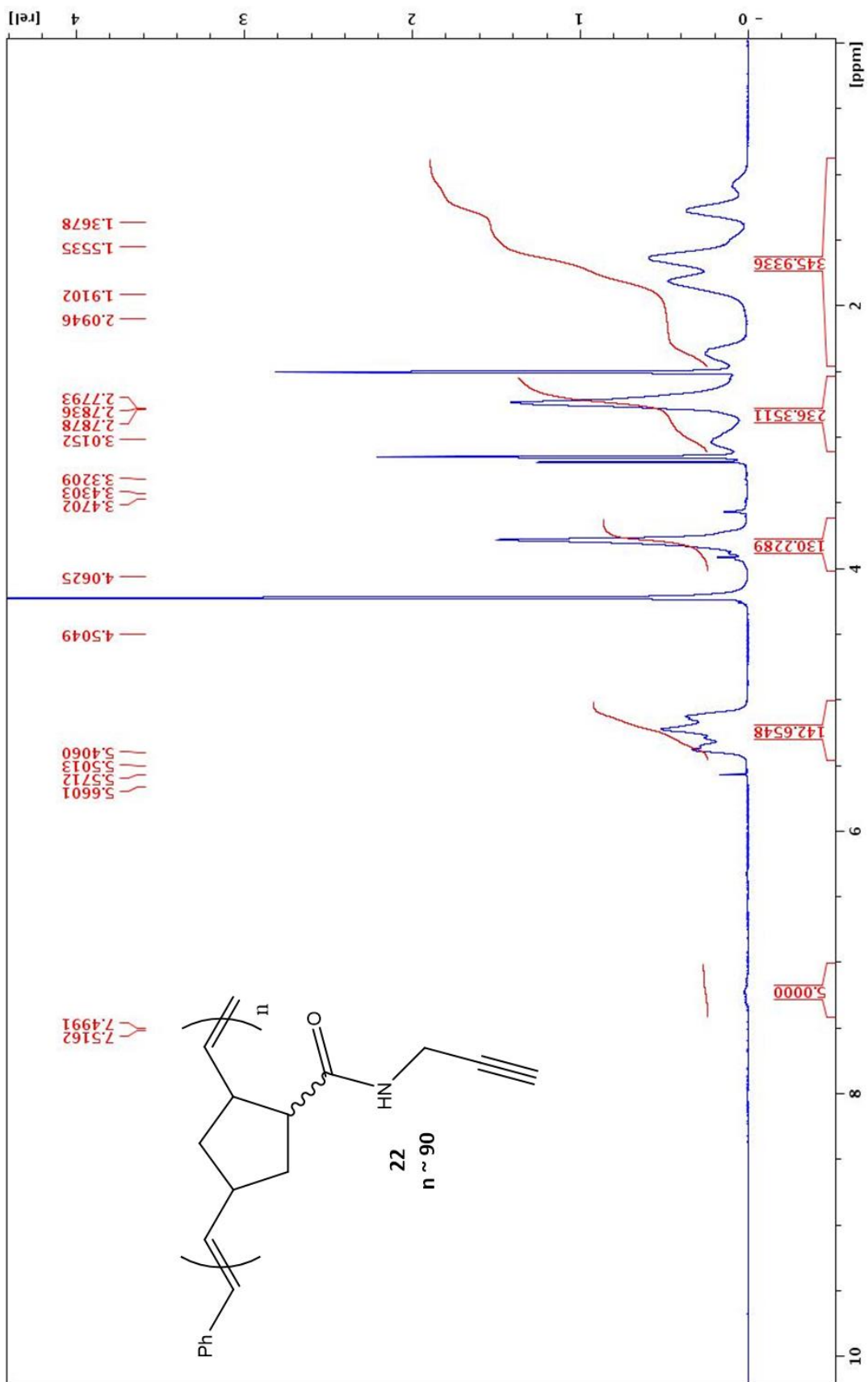
Polymer	MW_{calc}	Expected H_{propargyl} + H_{sugar}	Observed H_{propargyl} + H_{sugar}	Expected H_{aliphatic}	Observed H_{aliphatic}
43, n ~ 30	11516	240	210	210	246
44, n ~ 30	11516	240	191	210	213
45, n ~ 30	11516	240	217	210	243
46, n ~ 30	14577	240	142	210	179
43, n ~ 90	34340	720	599	630	613
45, n ~ 90	34340	720	148	630	177
46, n ~ 90	43523	720	530	630	583
47, n ~ 90	34759	720	977	630	924
48, n ~ 90	34759	720	262	630	400
49, n ~ 90	34759	720	1262	630	1174
50, n ~ 90	43941	720	849	630	930

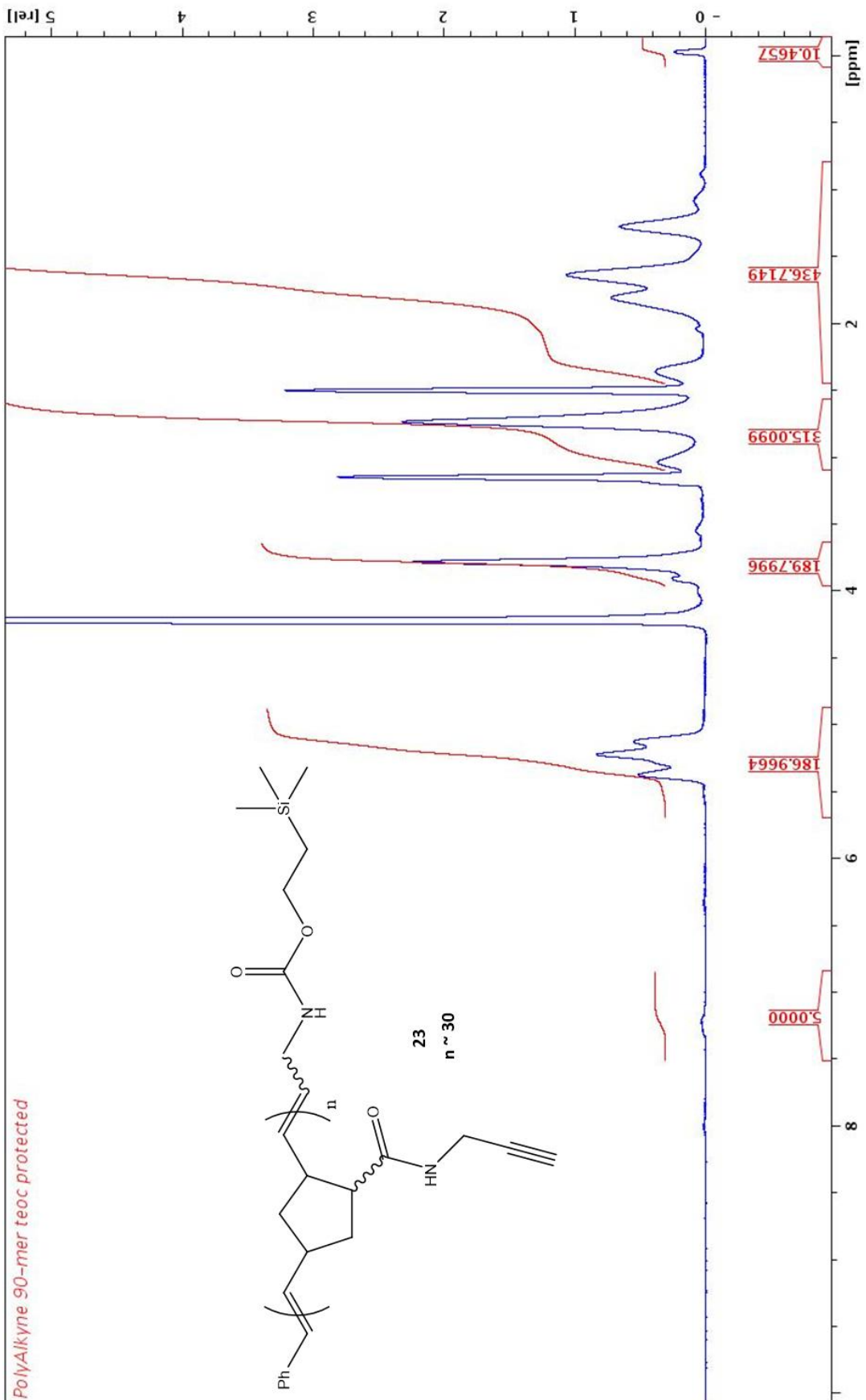




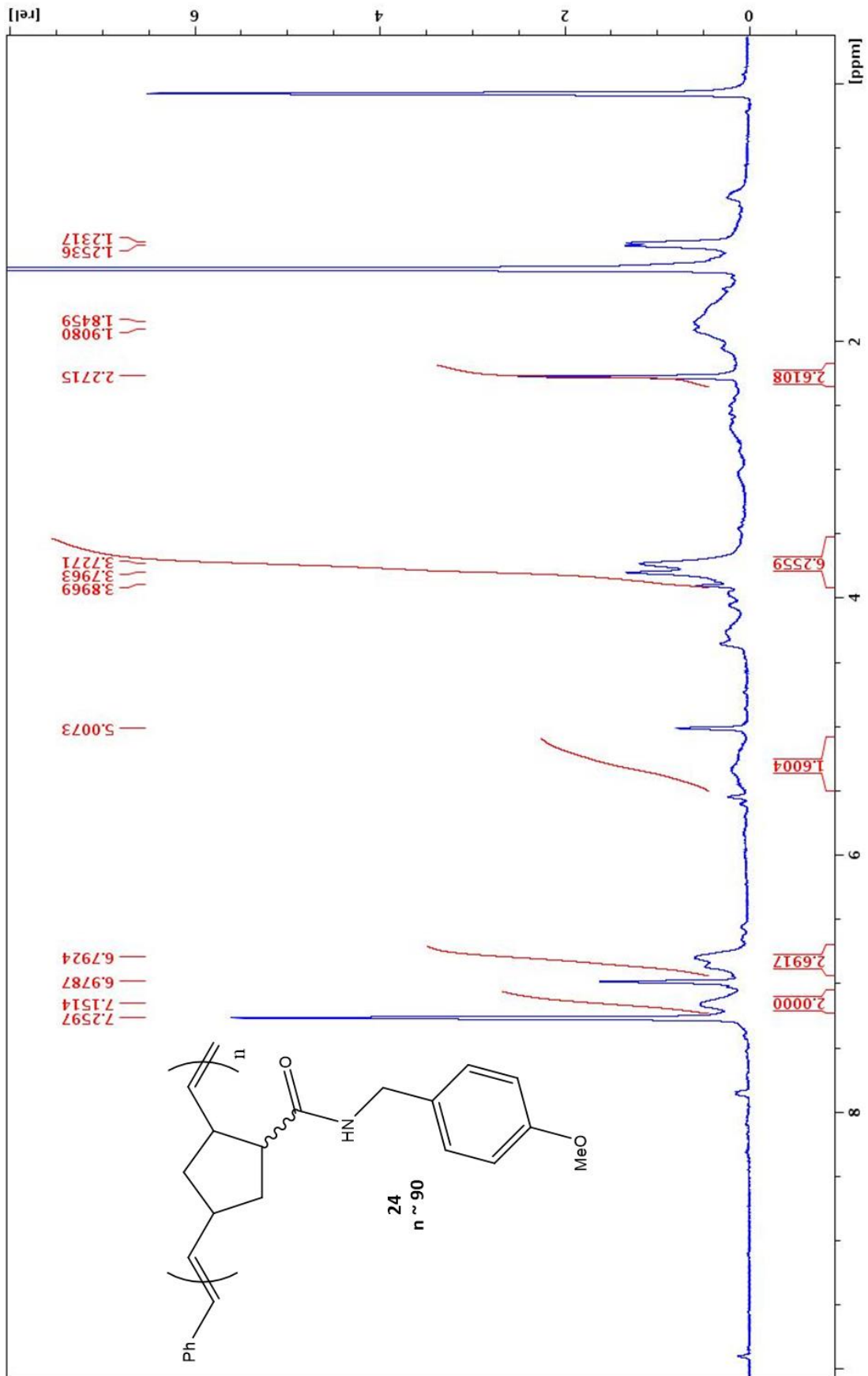


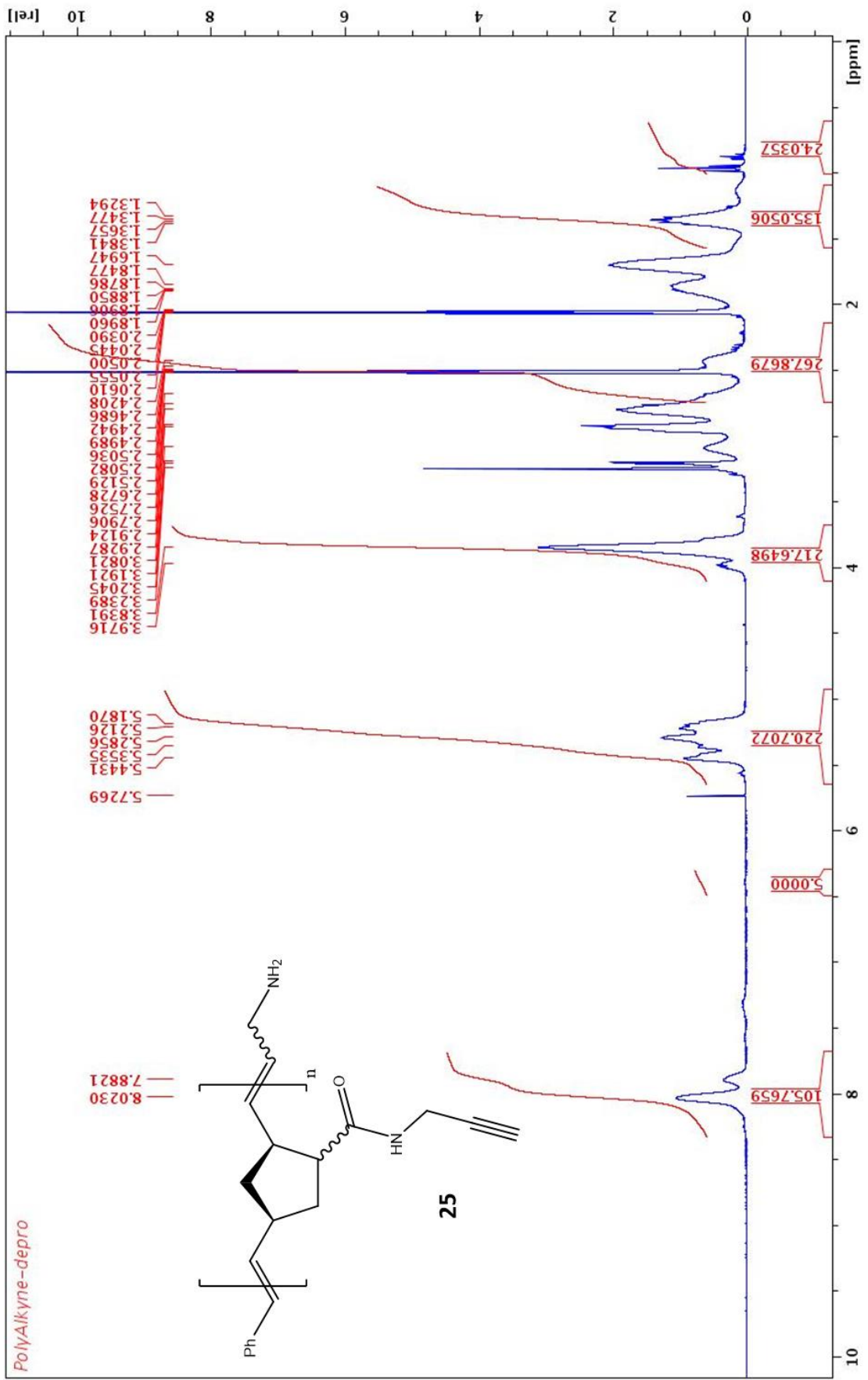


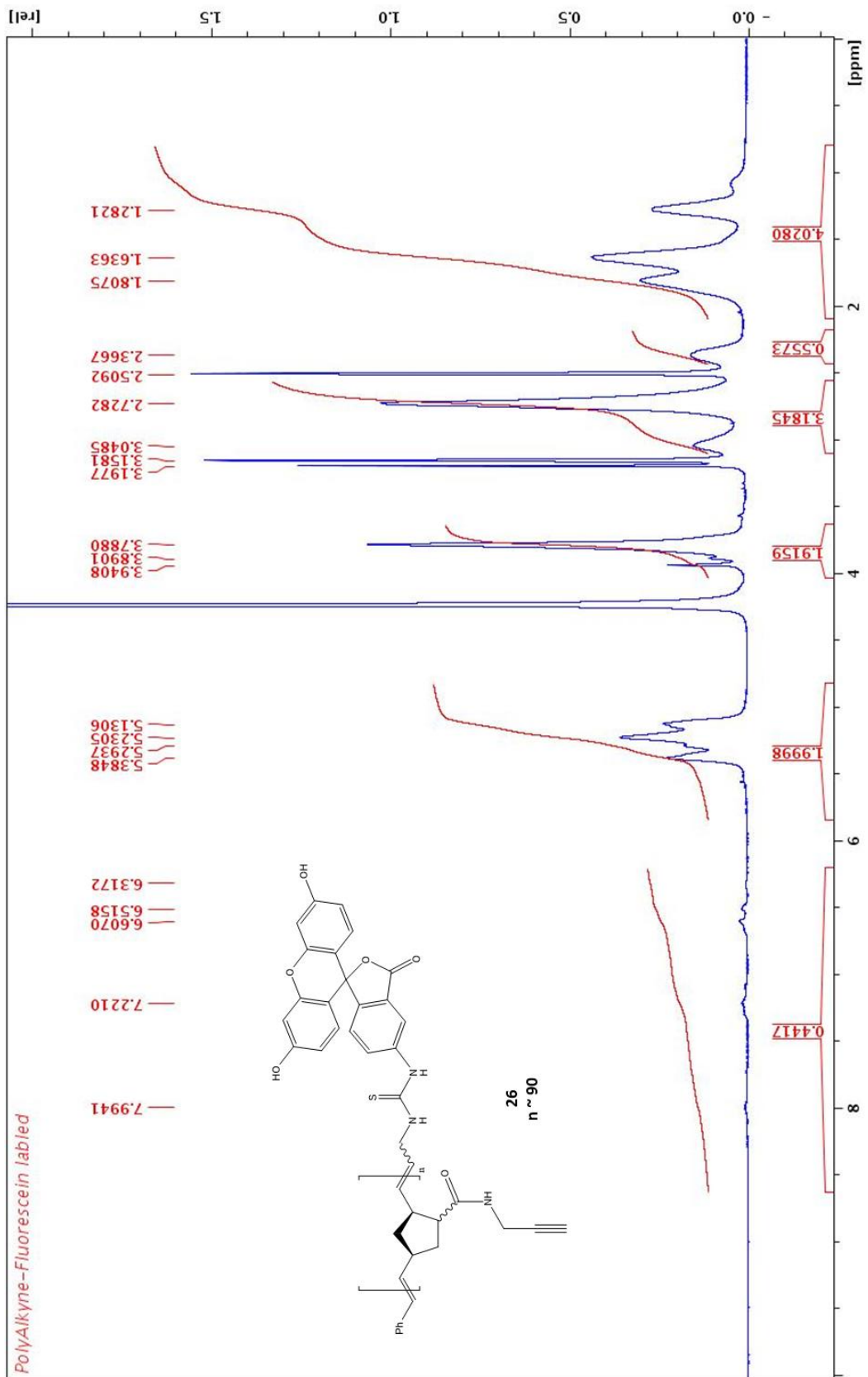


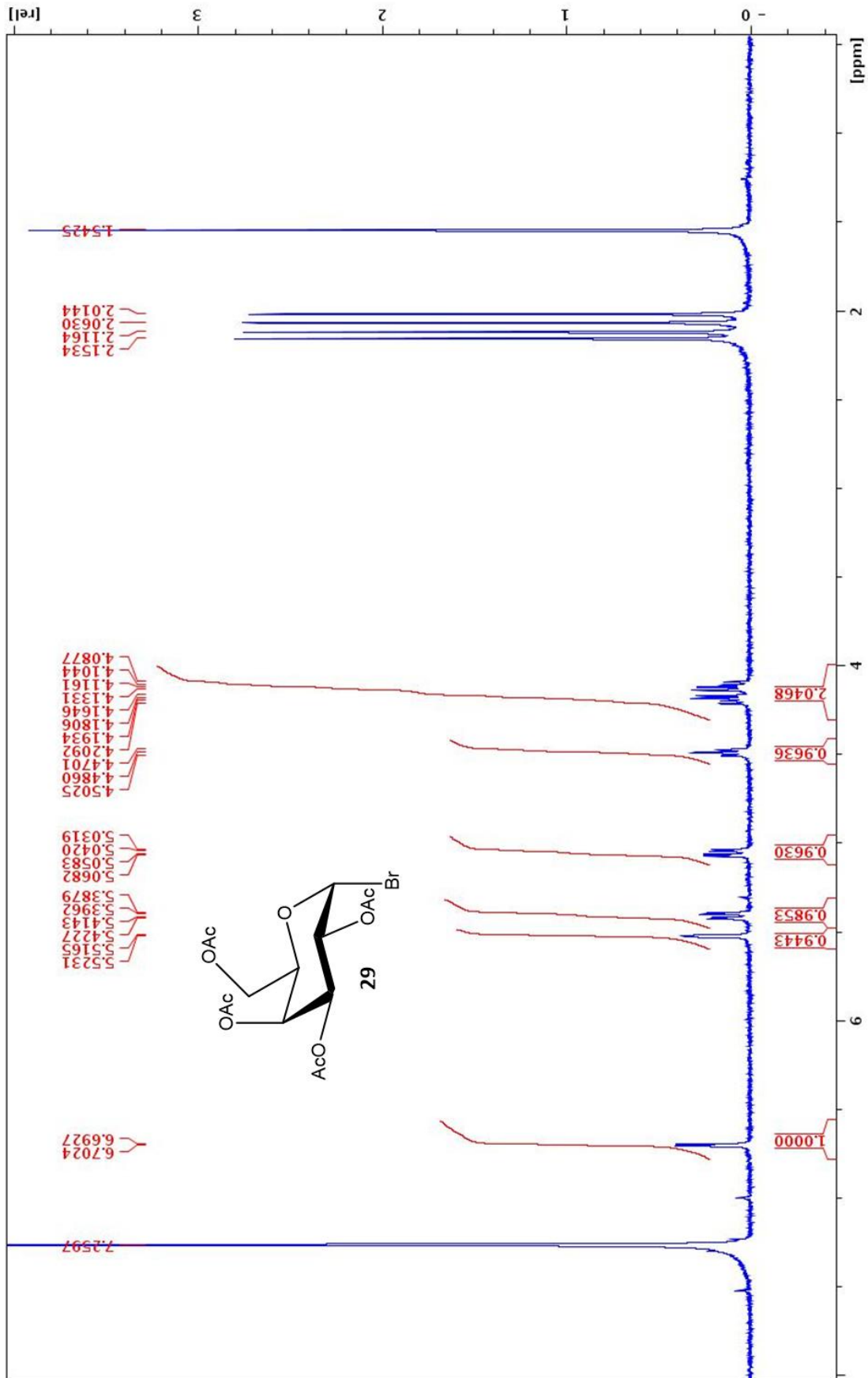


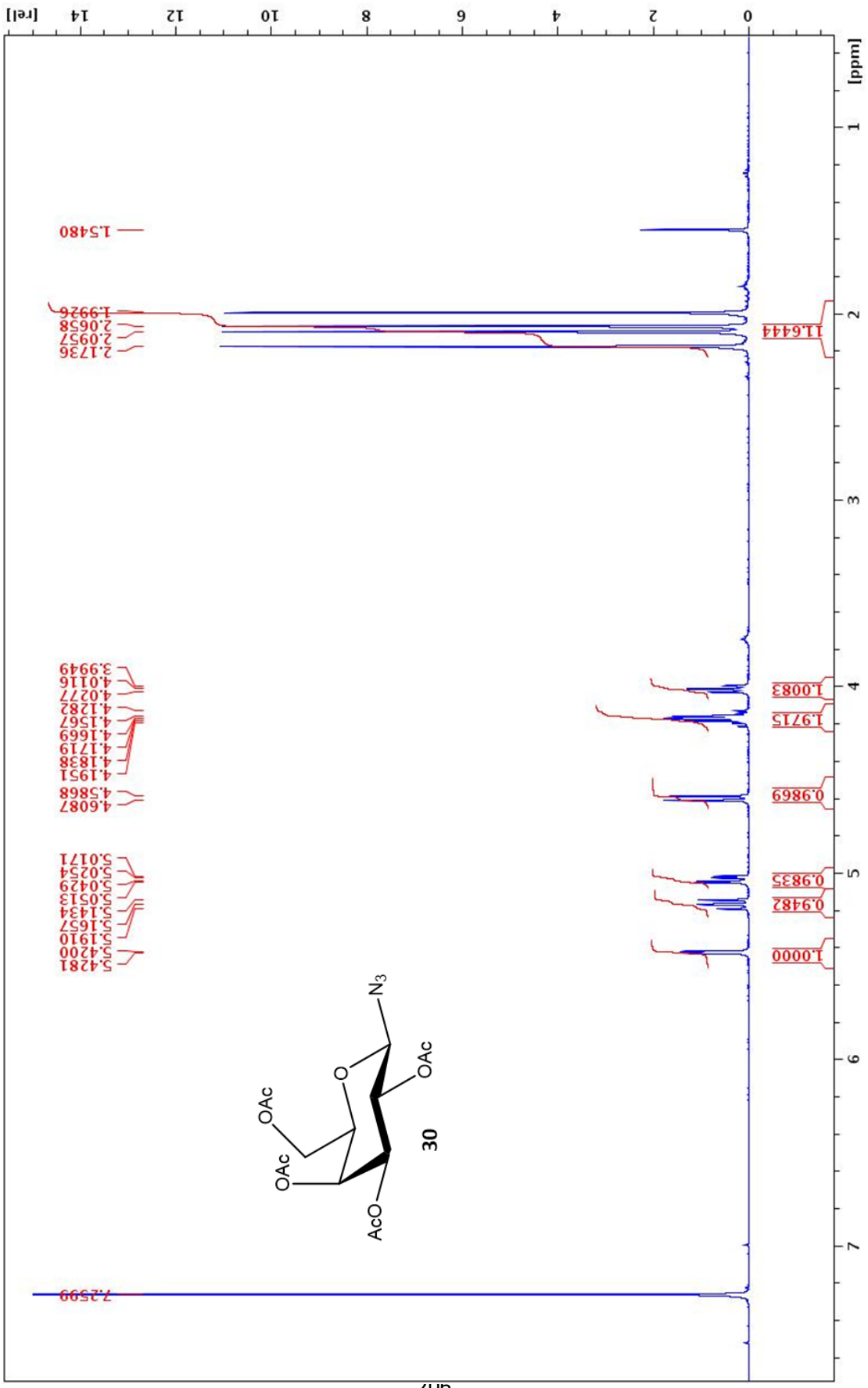
PolyAlkyne 90-mer teoc protected



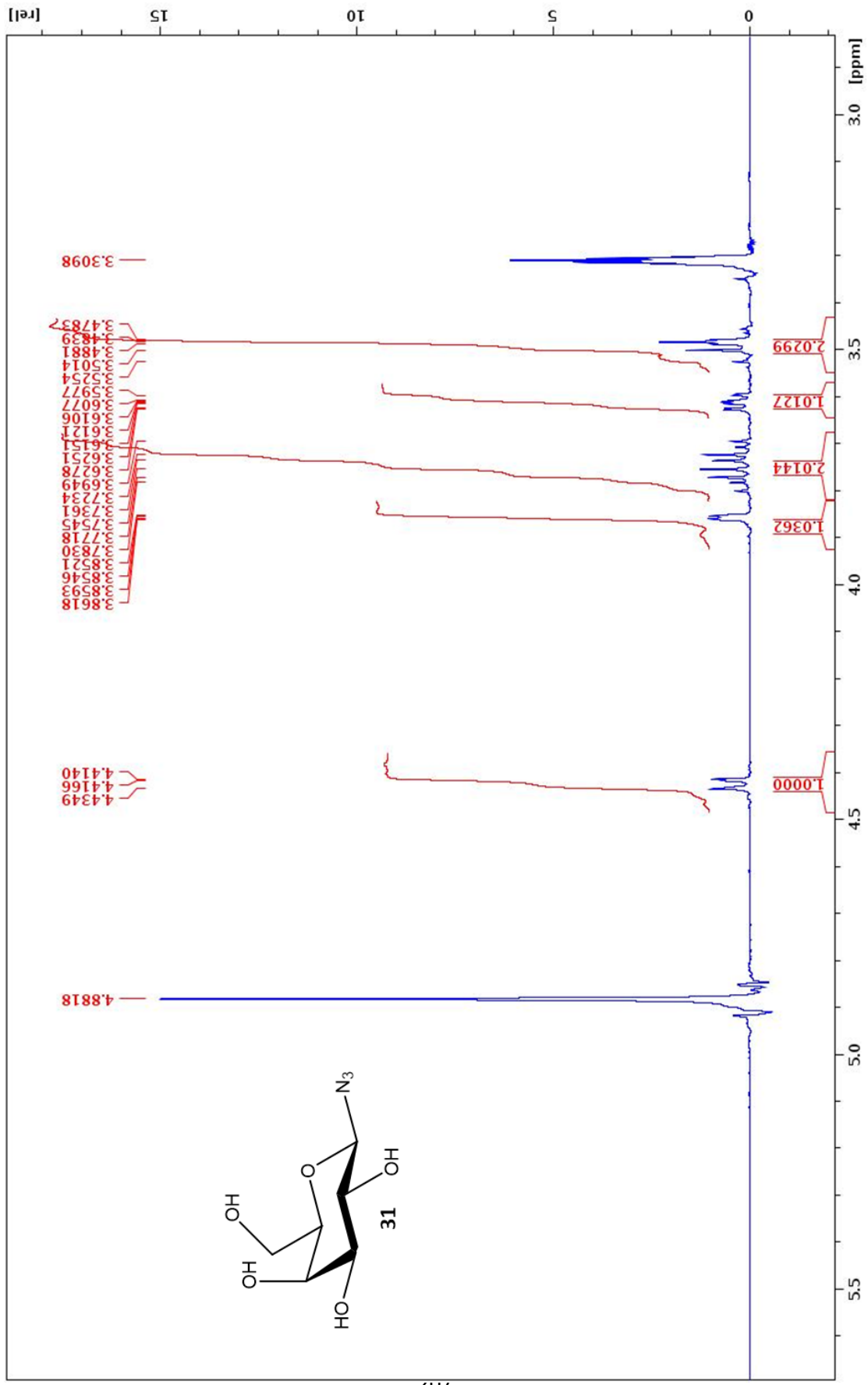


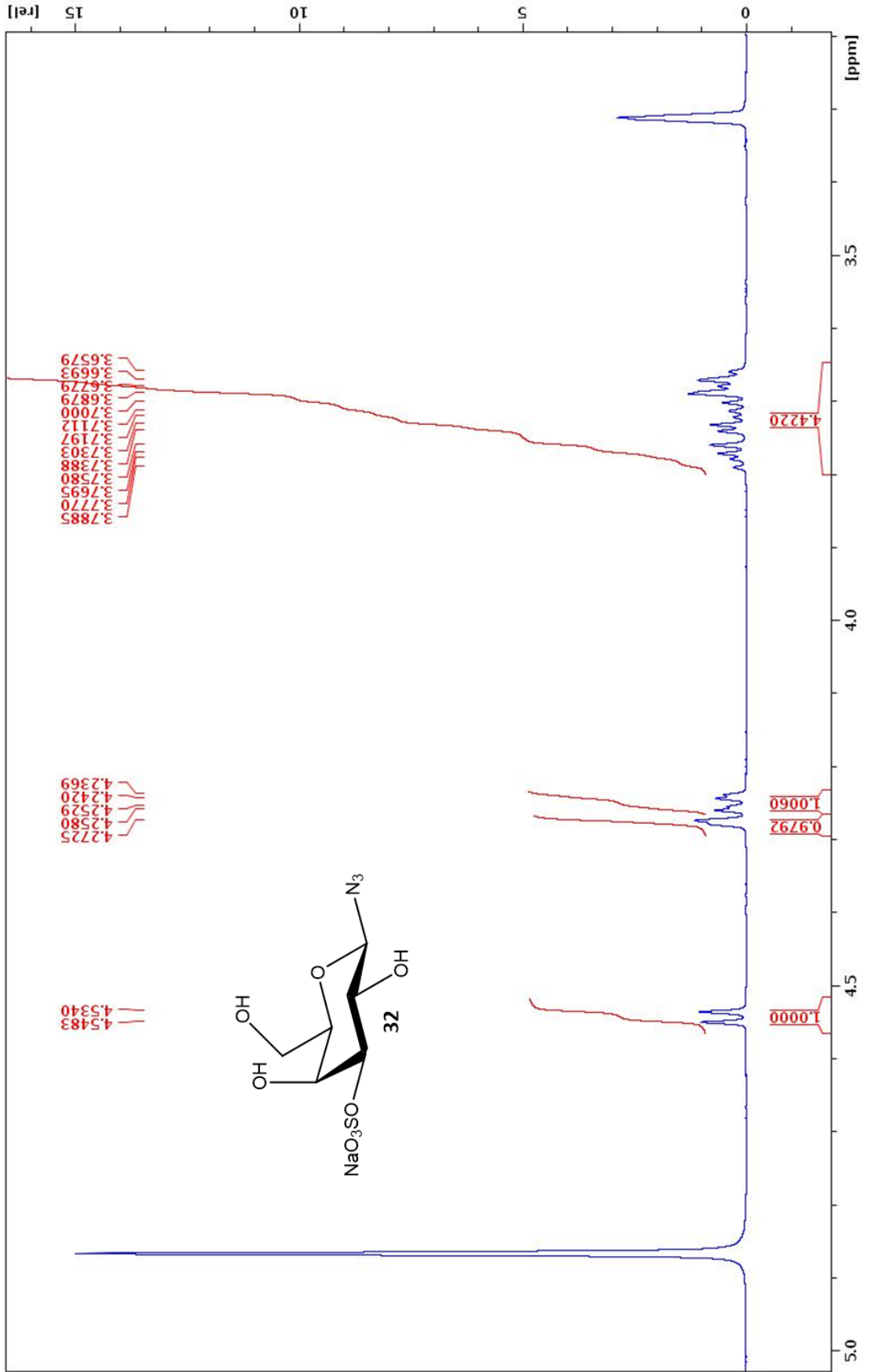


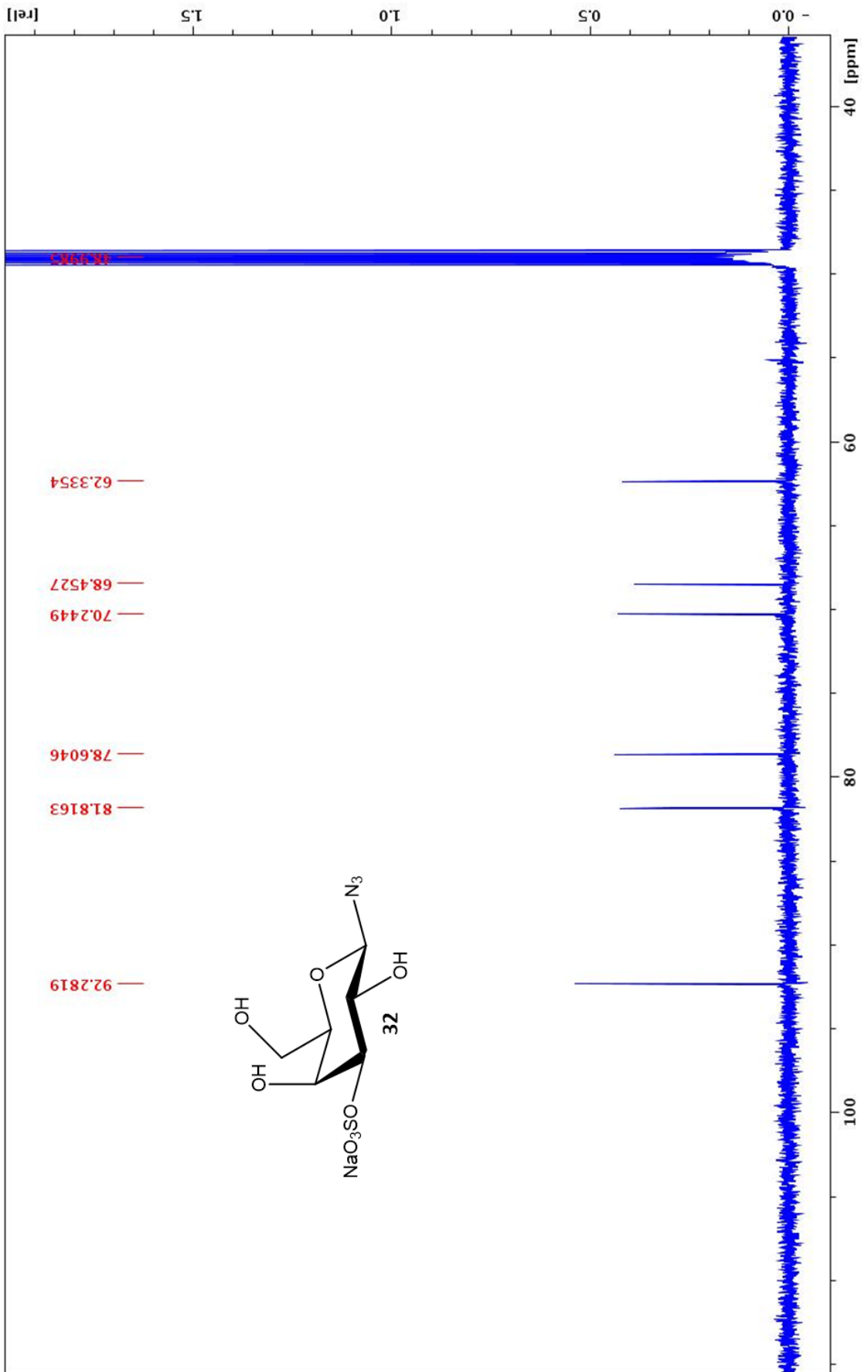


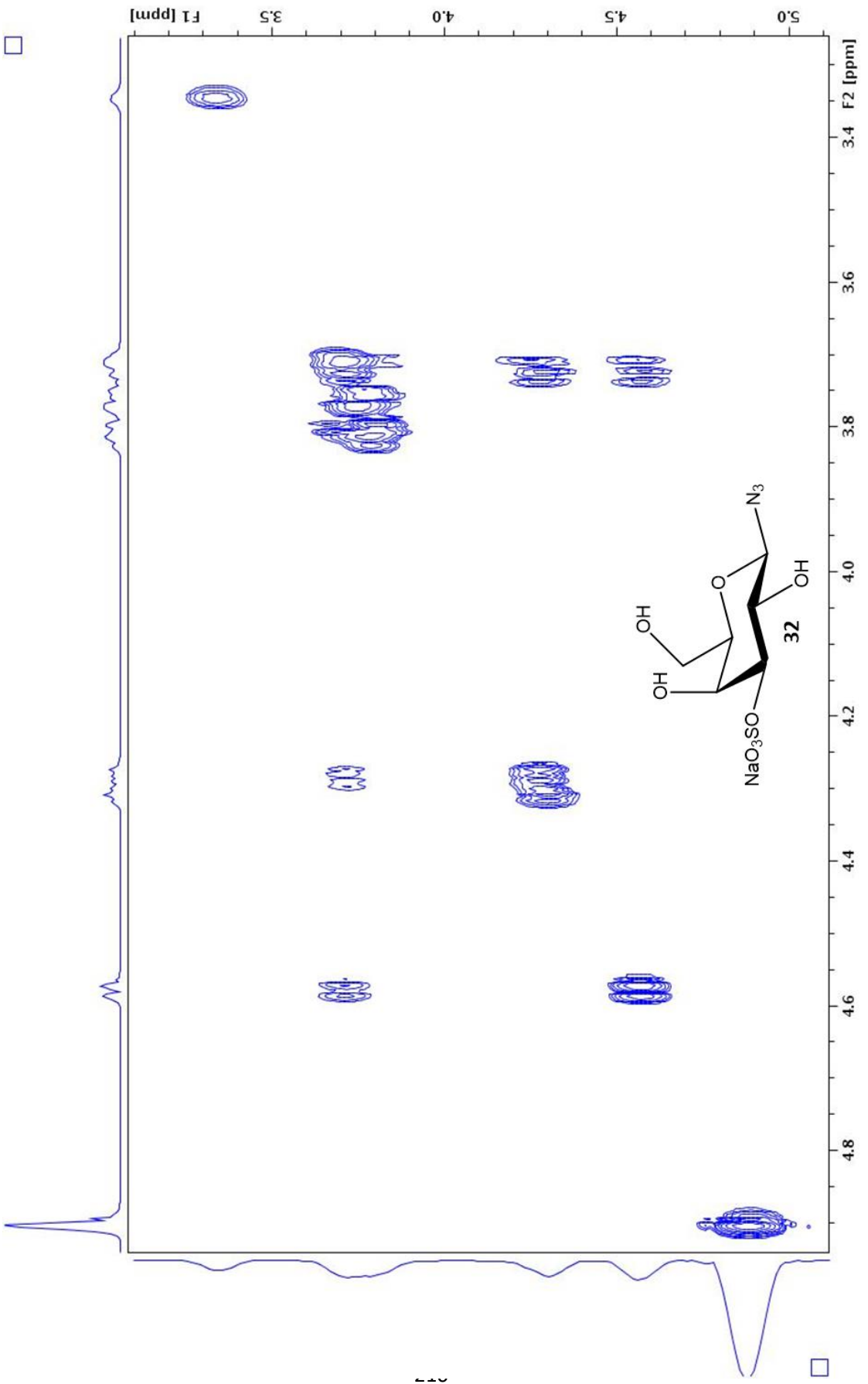


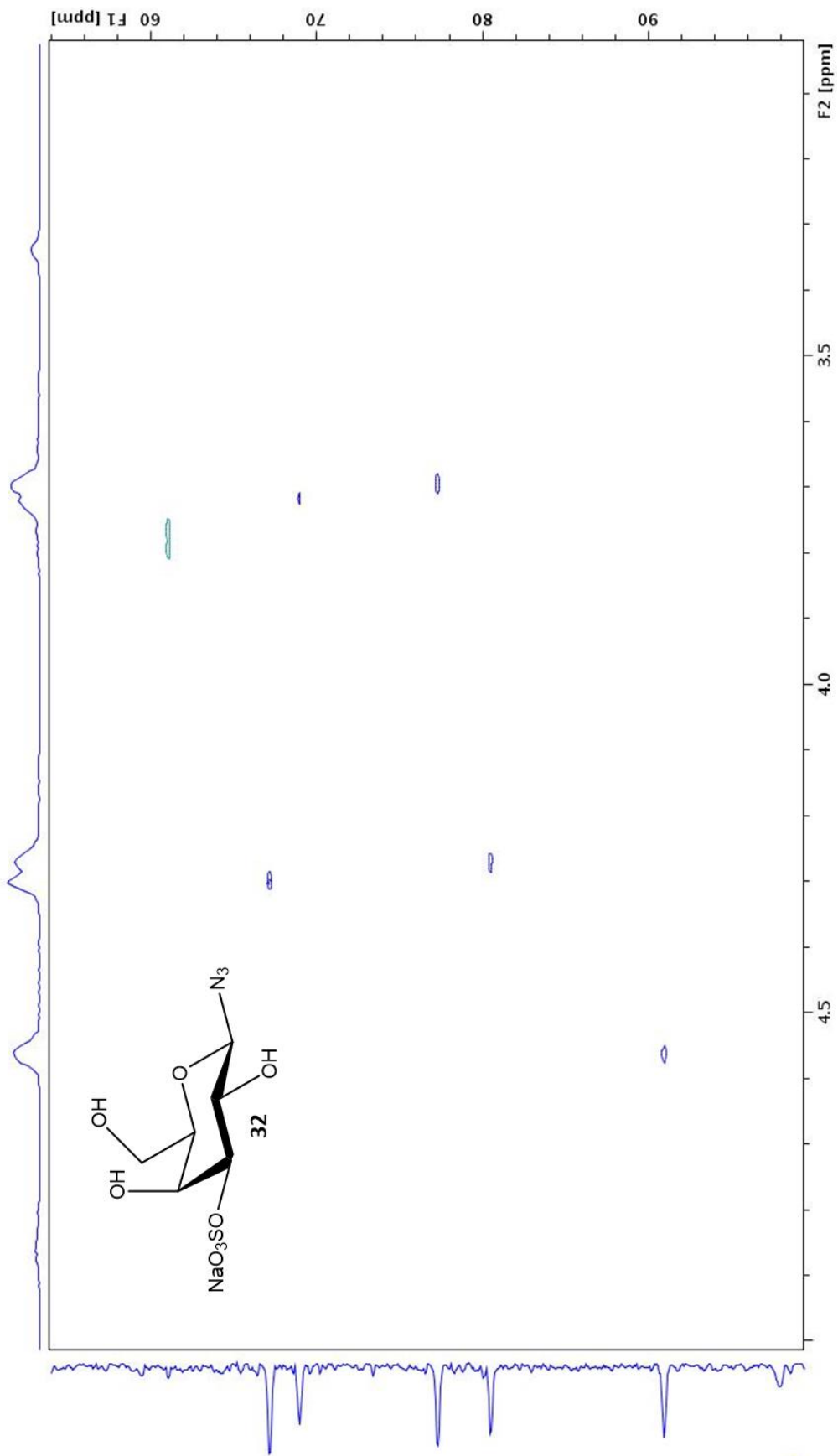
Q17

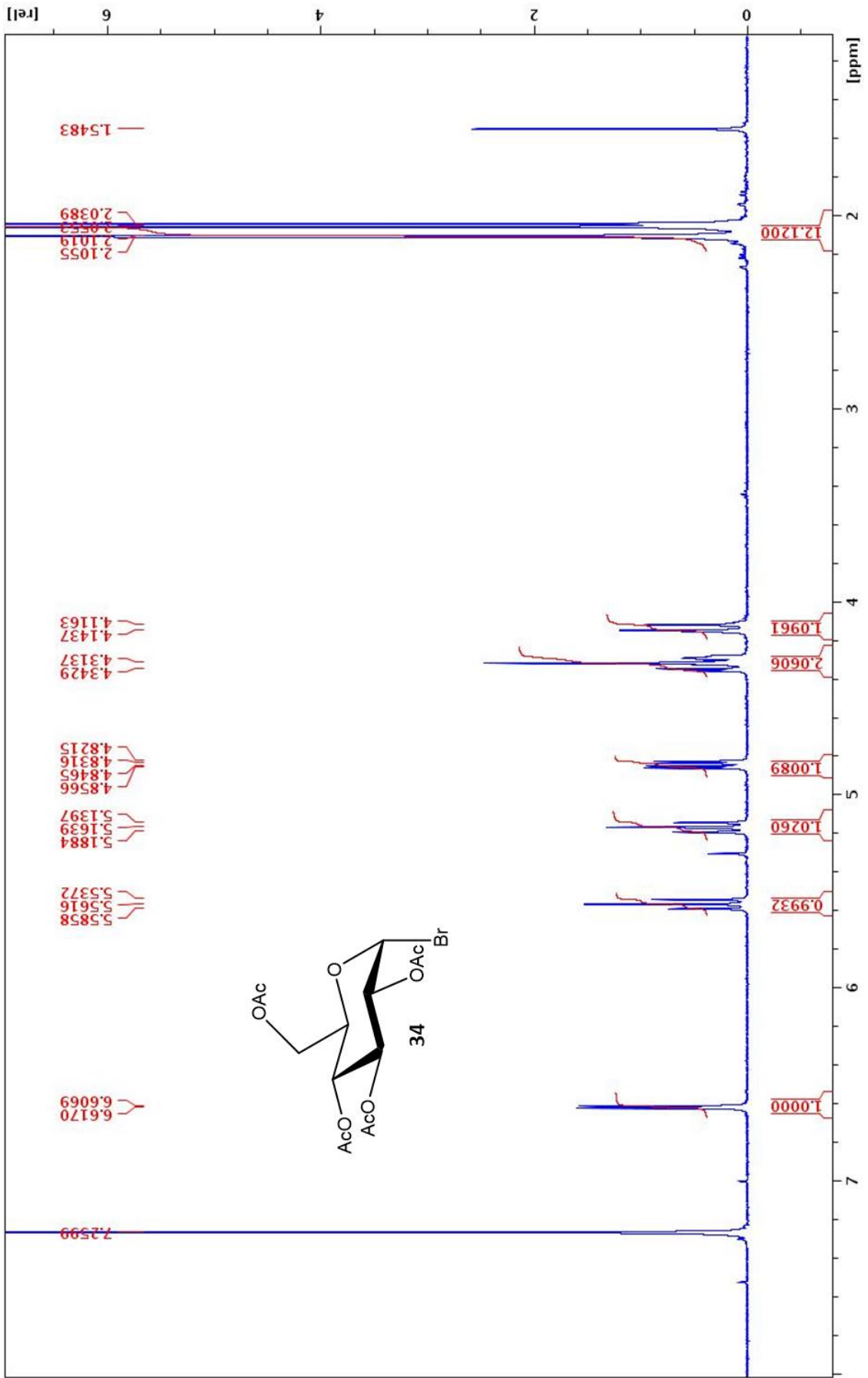


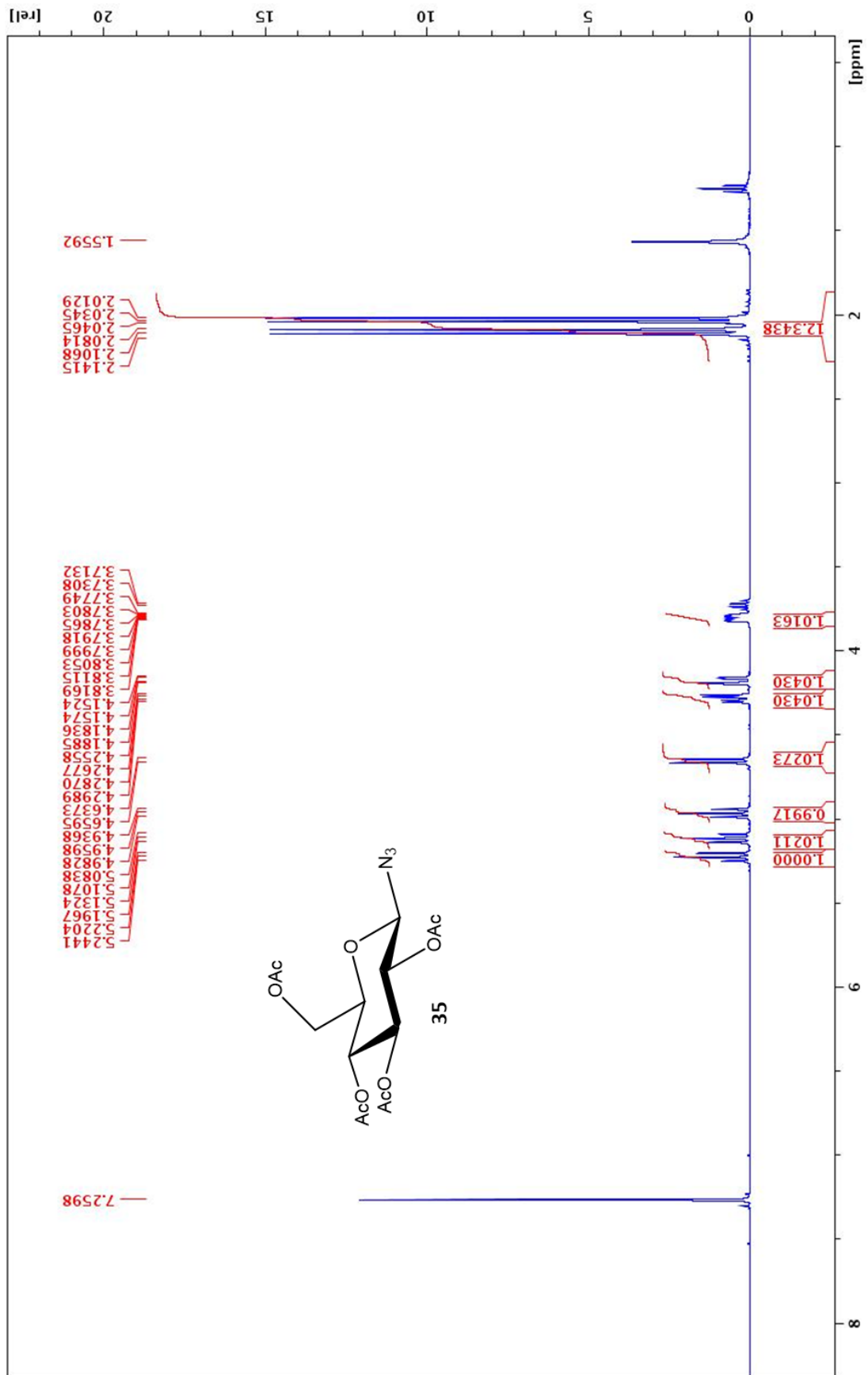


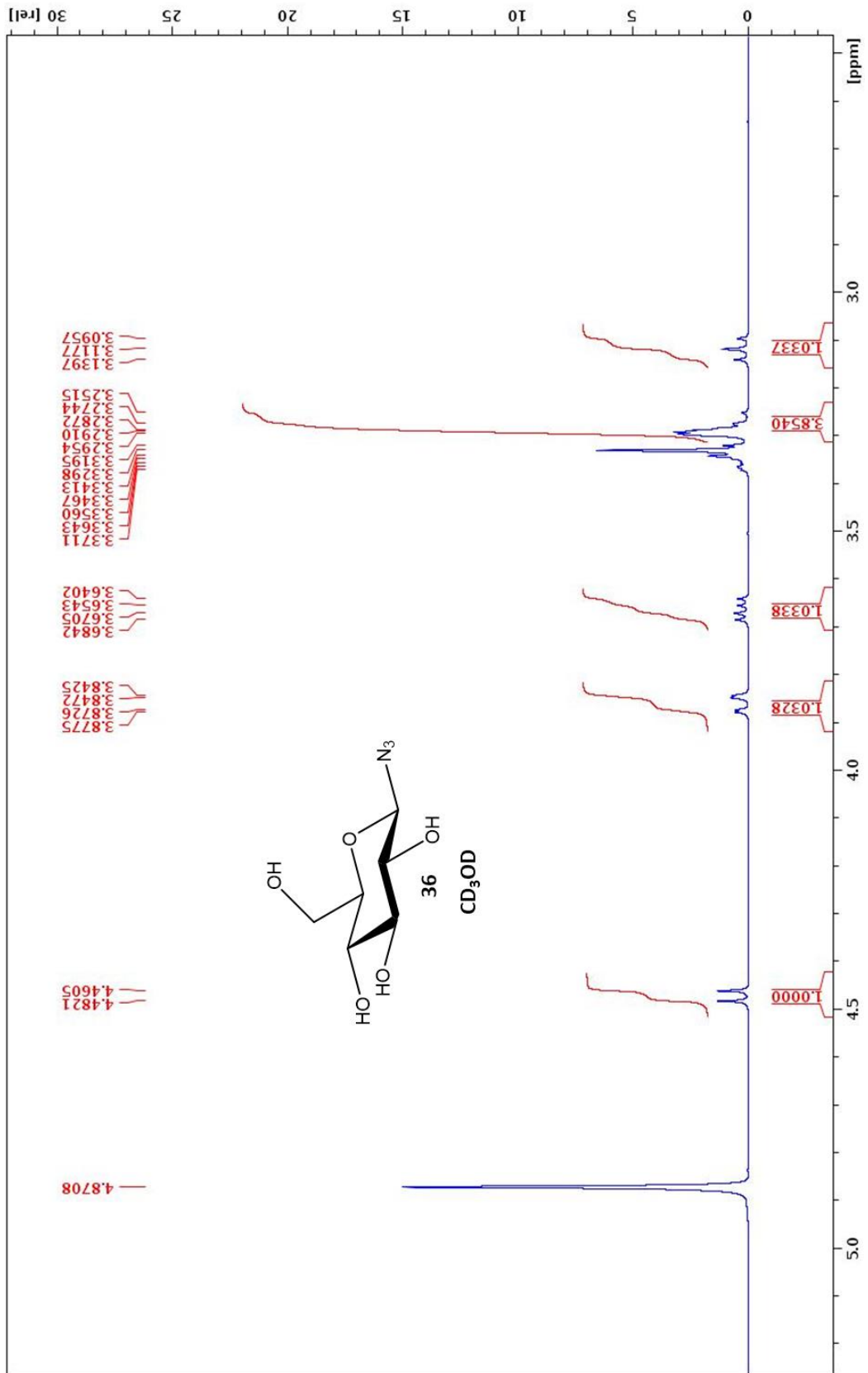


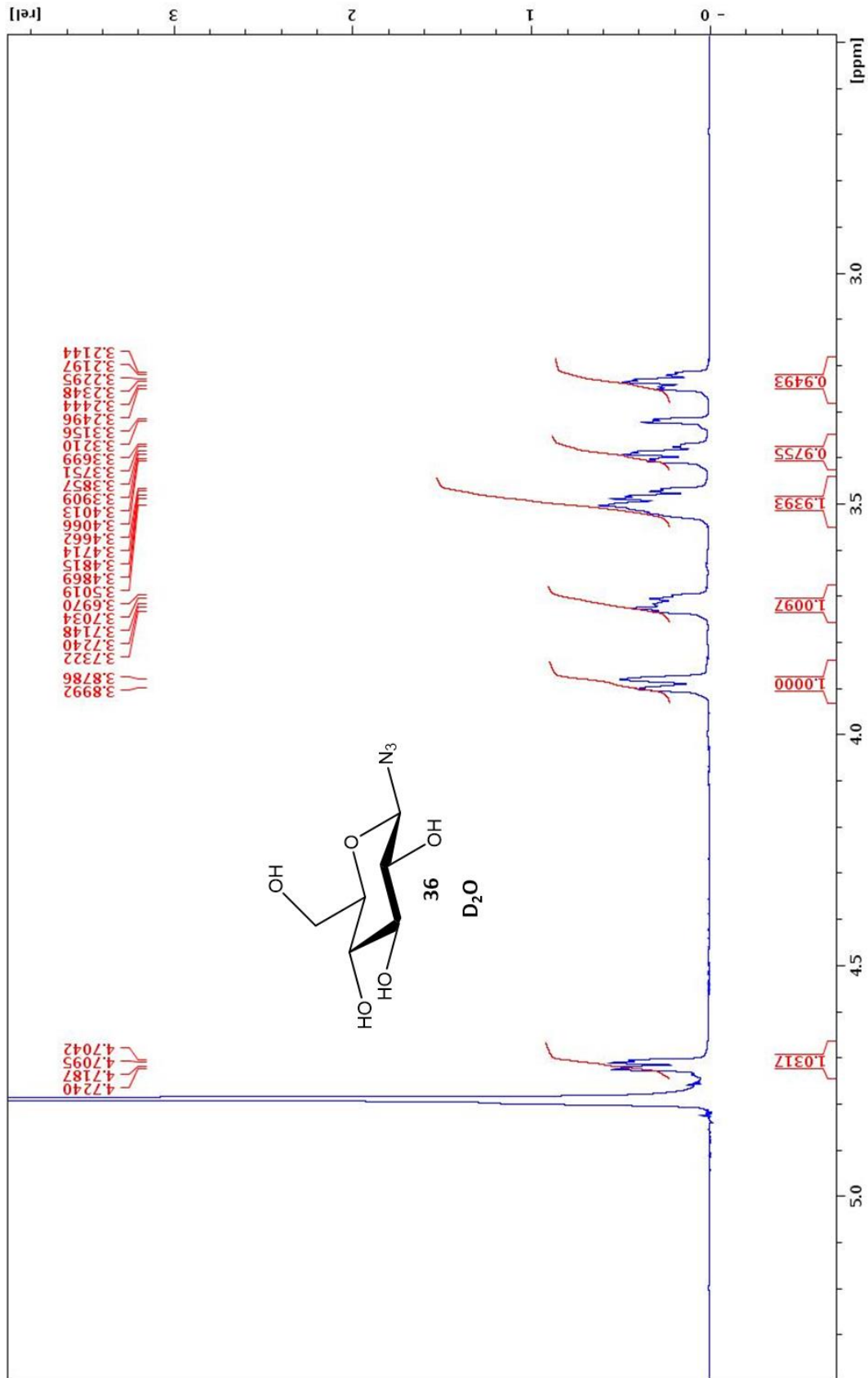


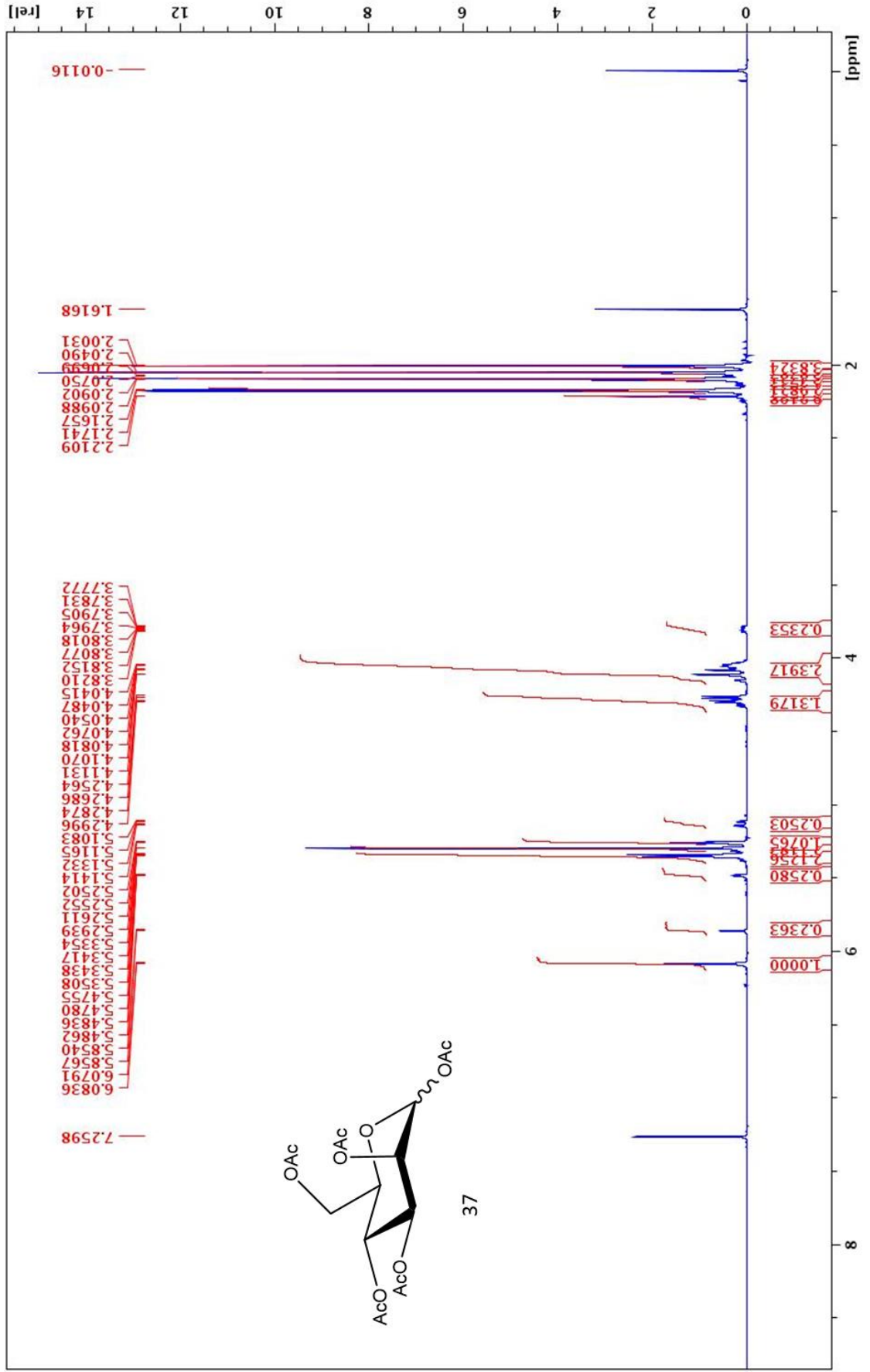


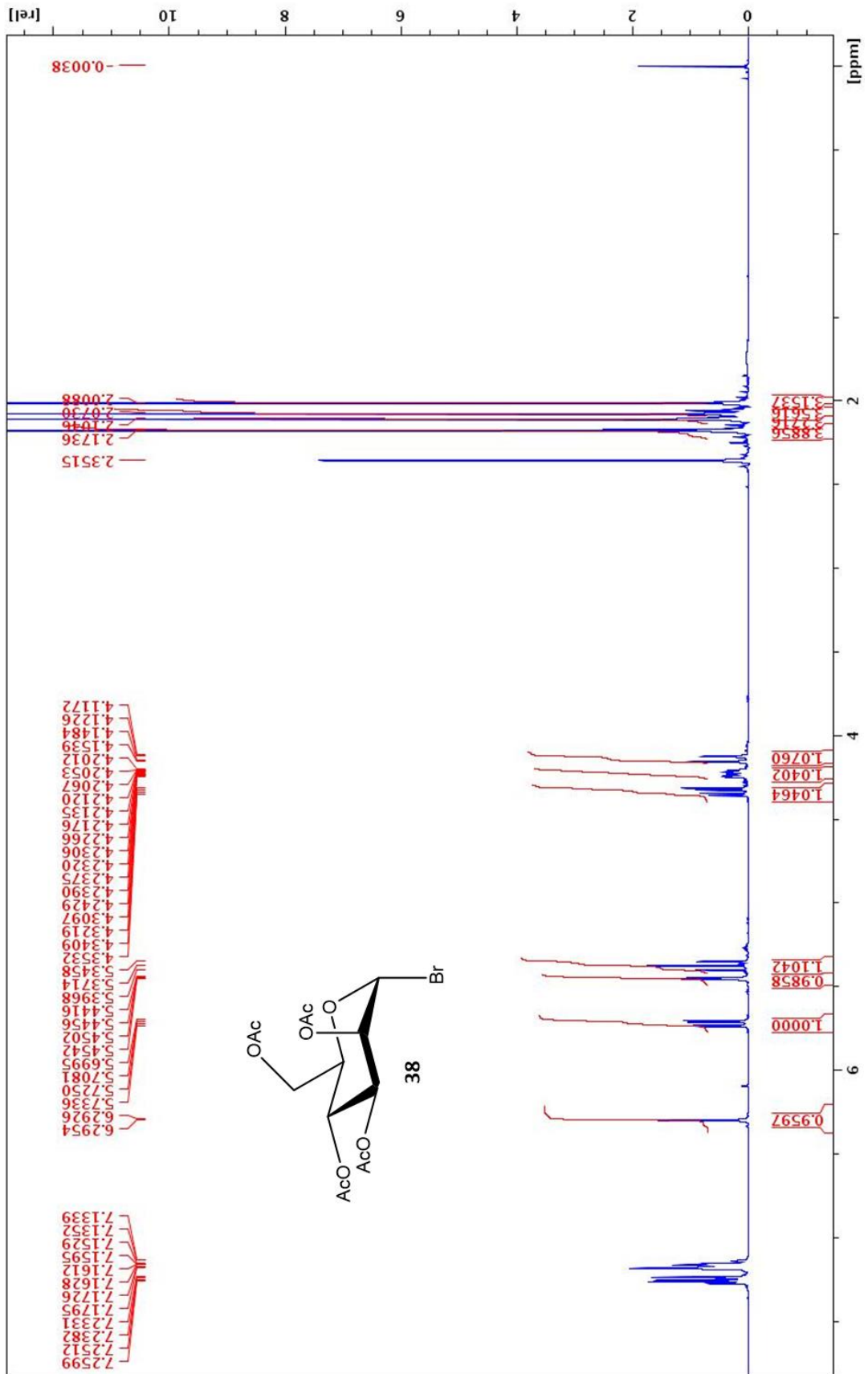


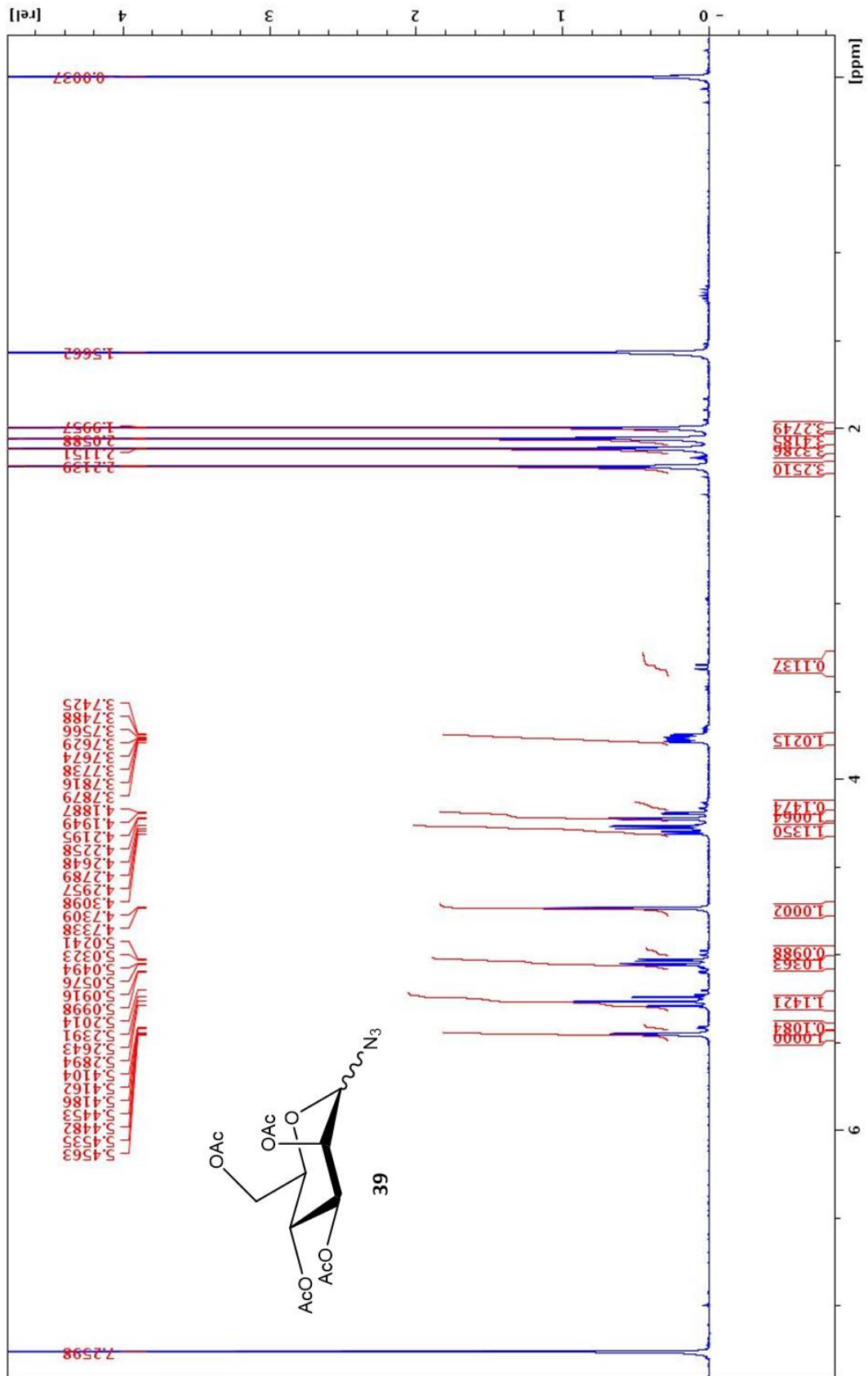


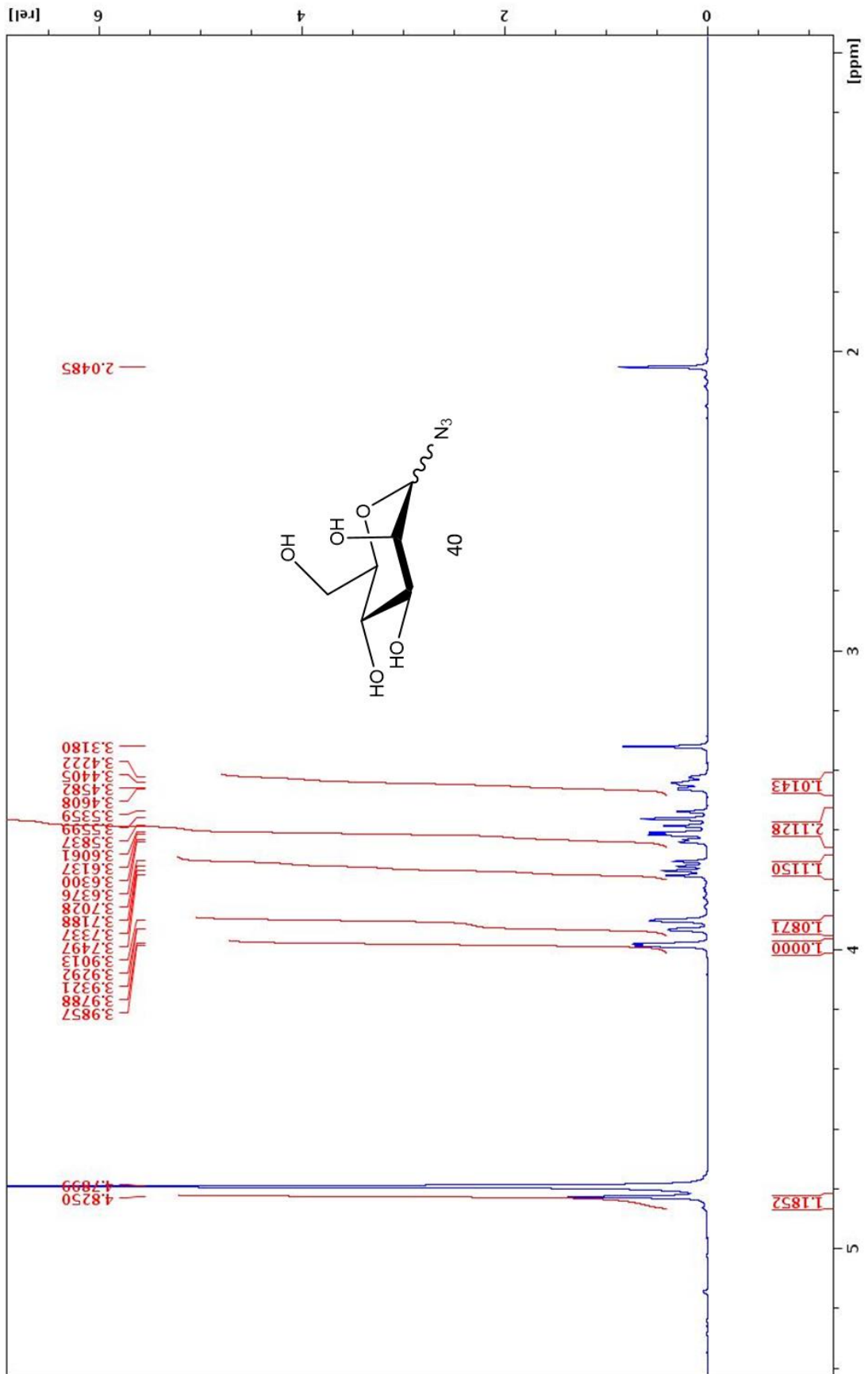


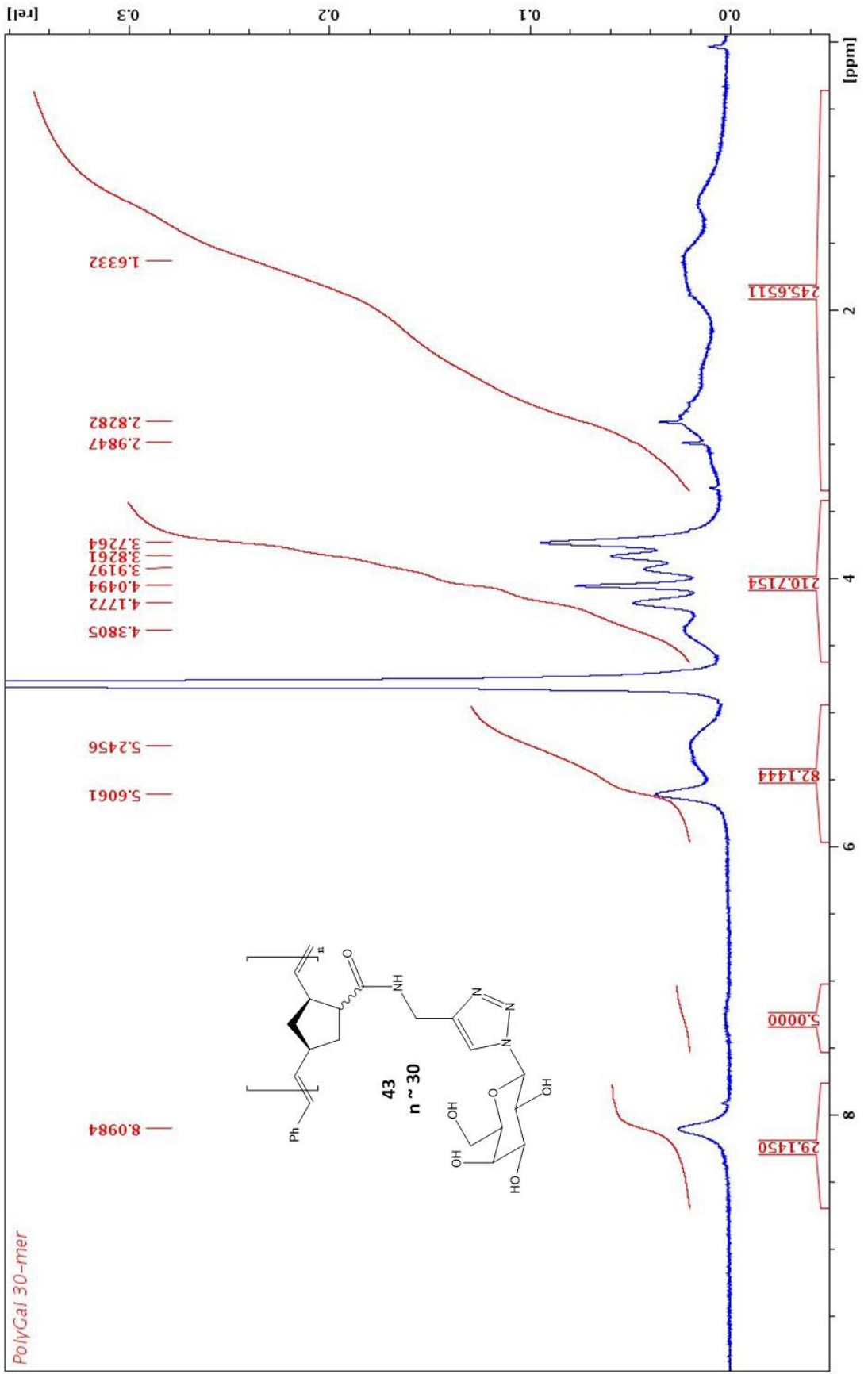


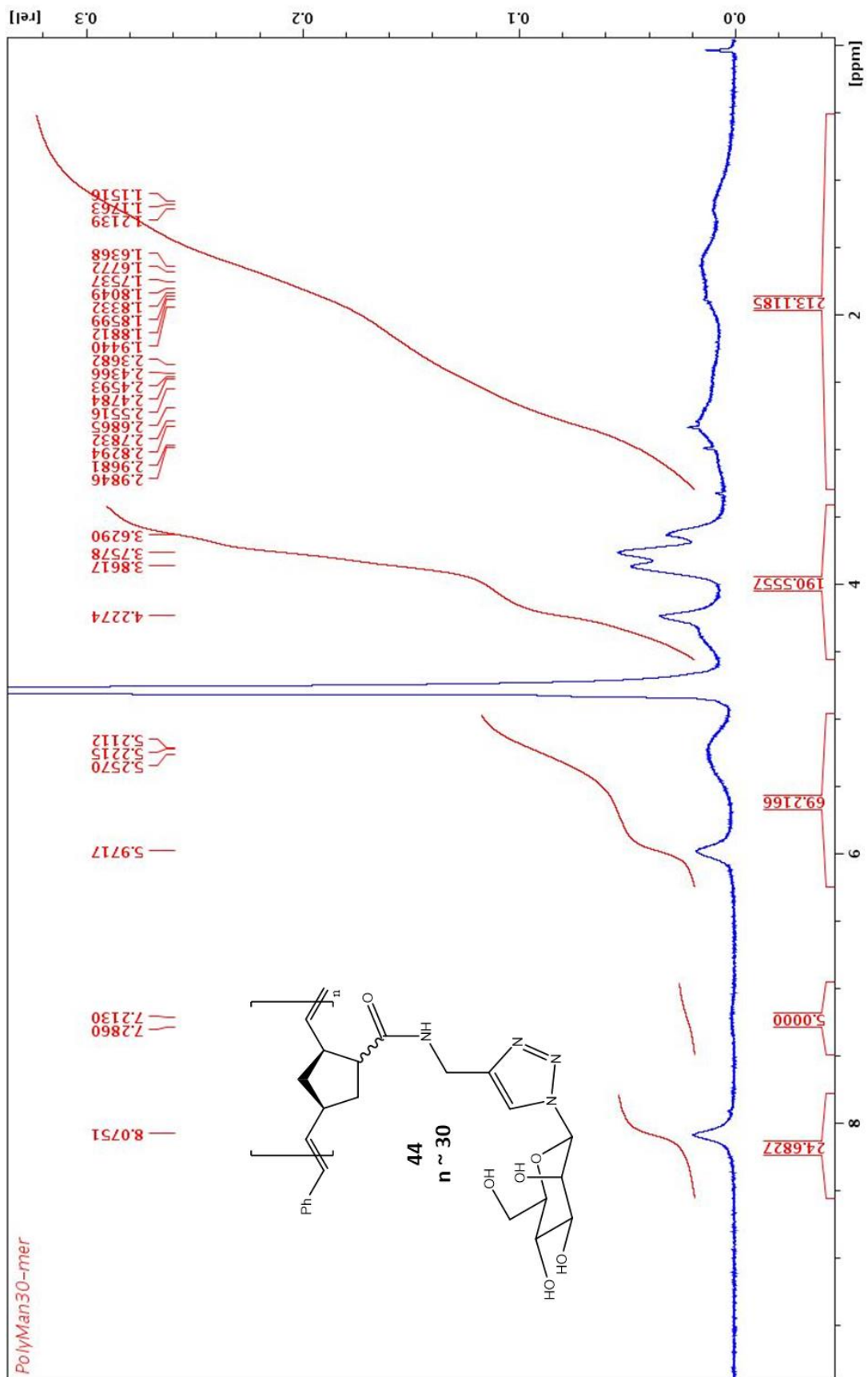


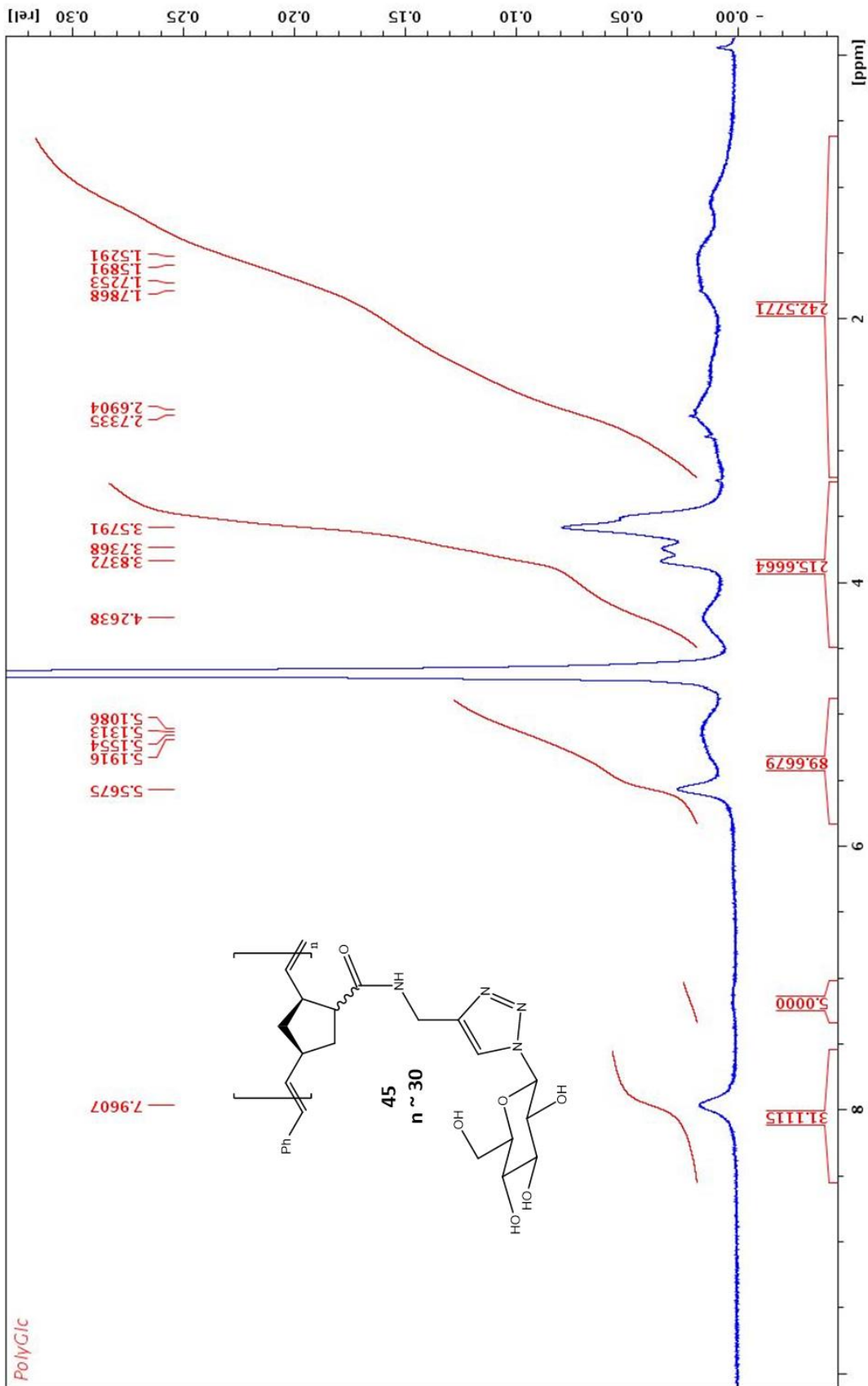


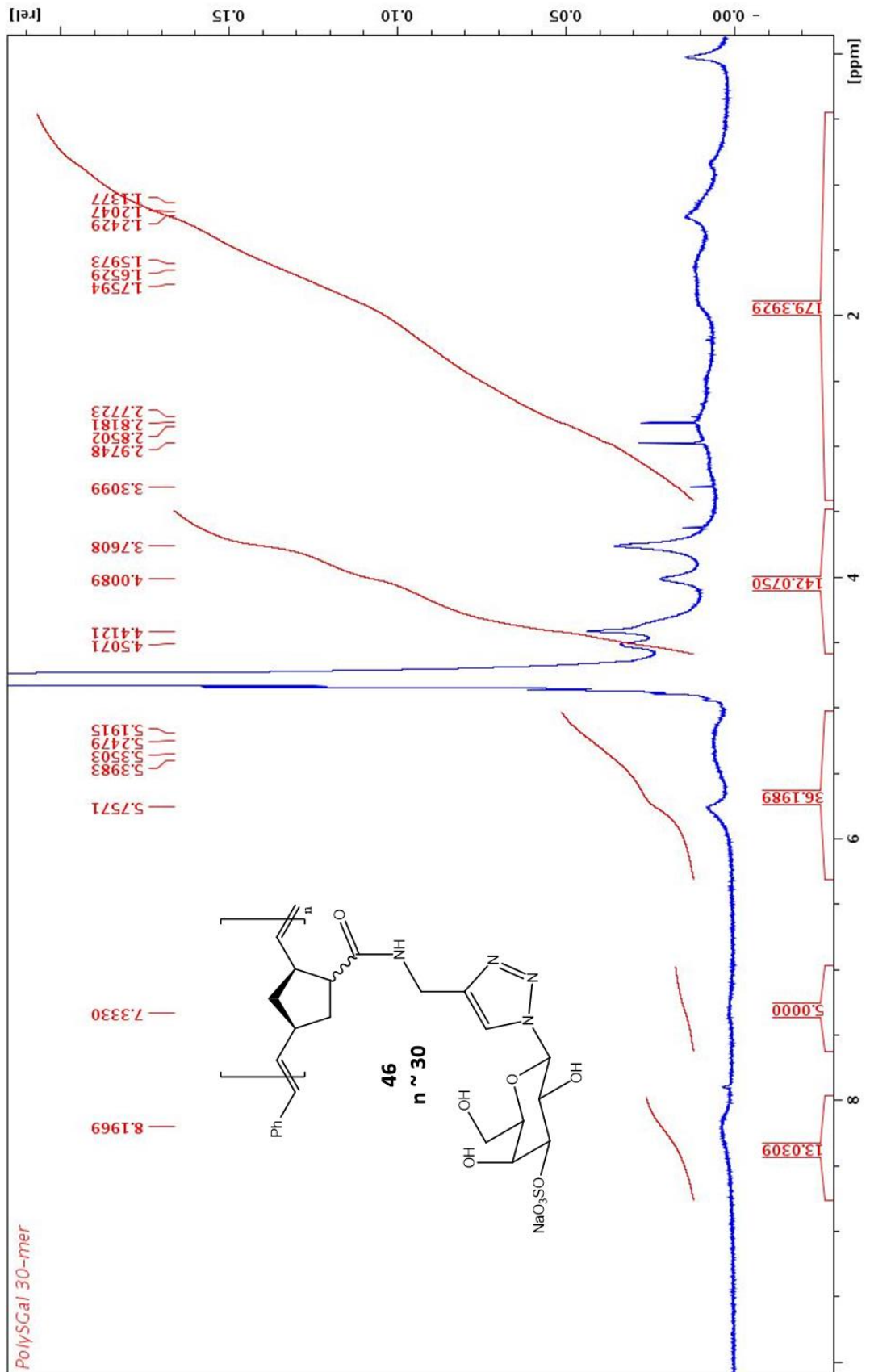


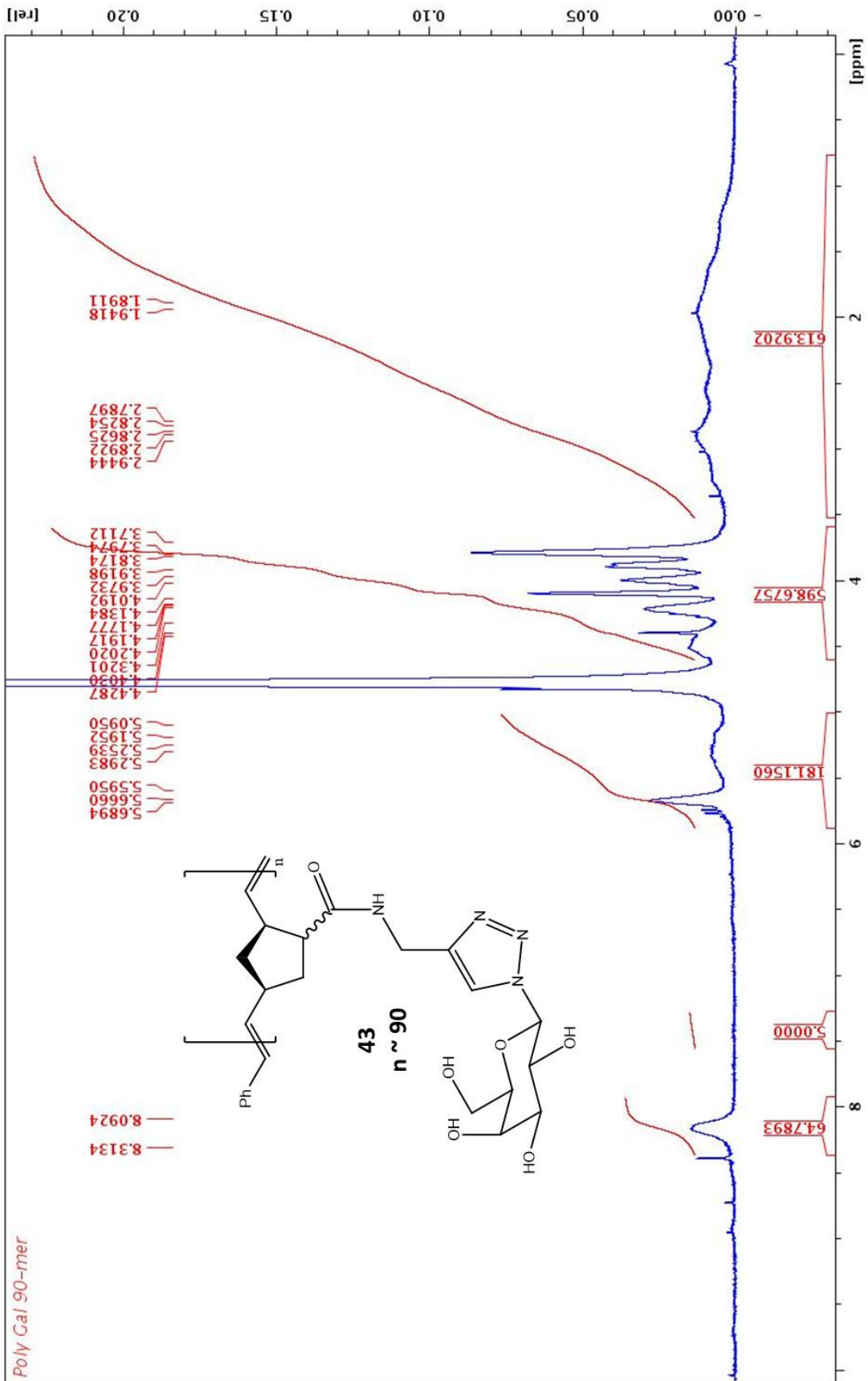


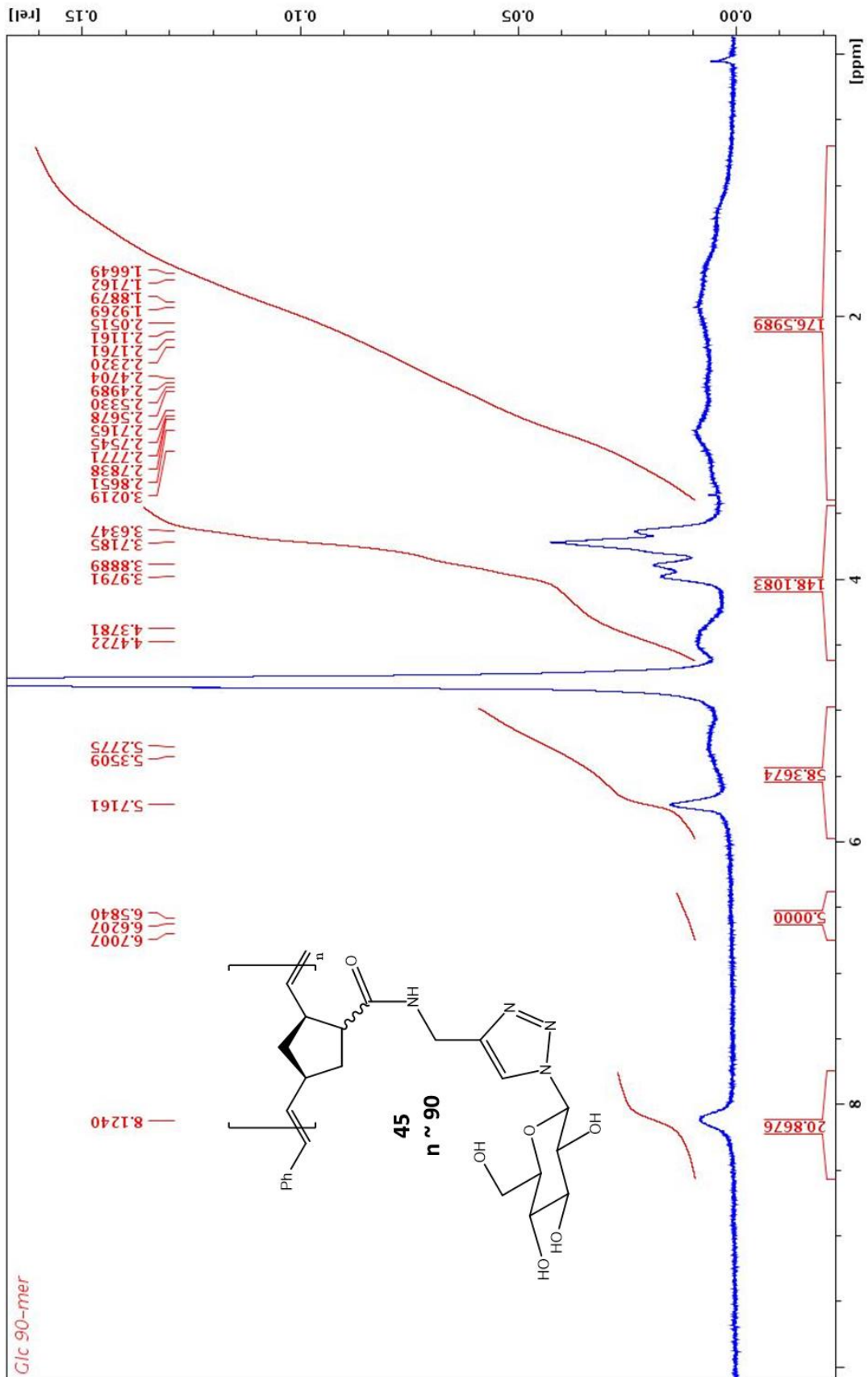


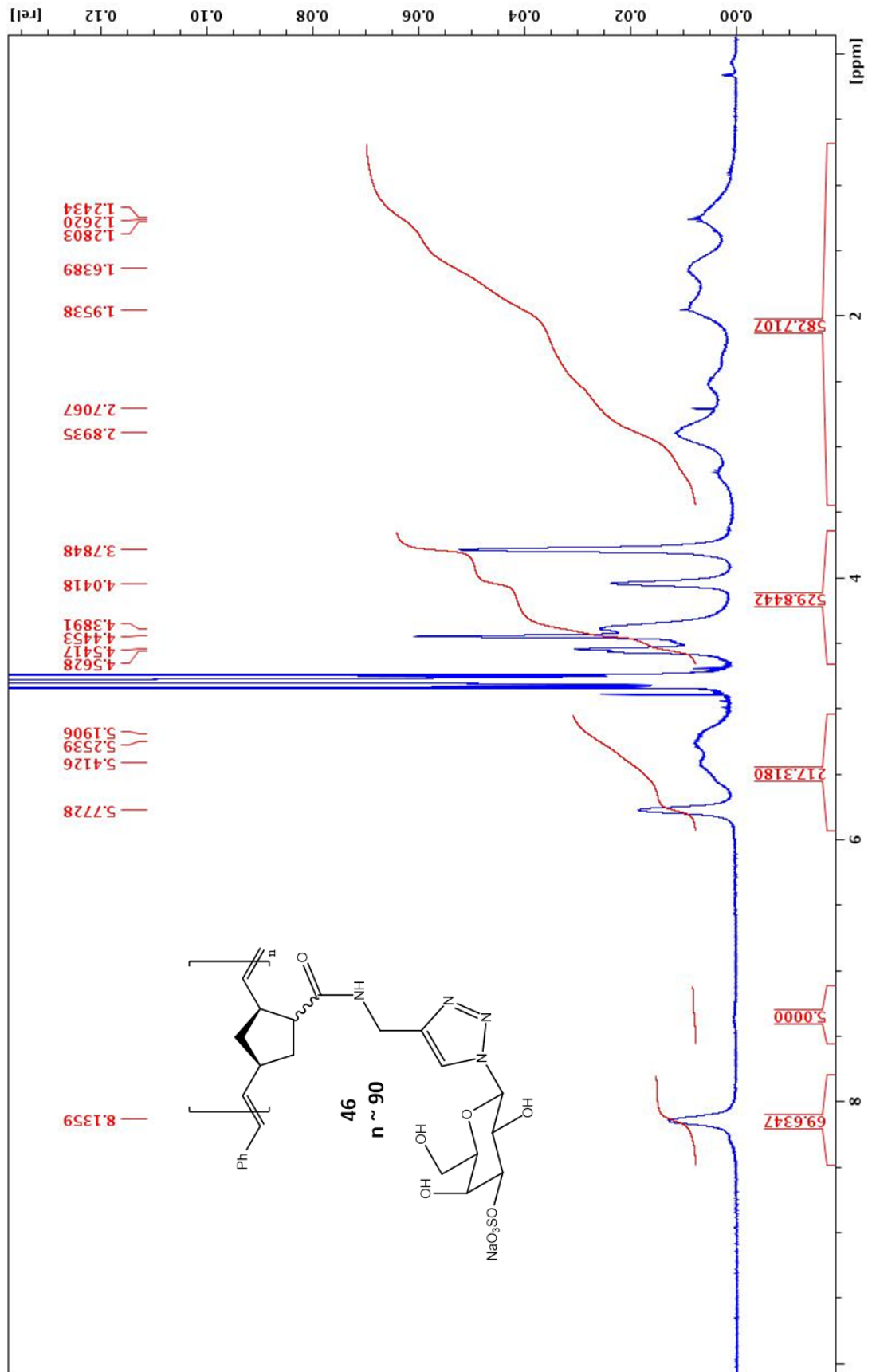


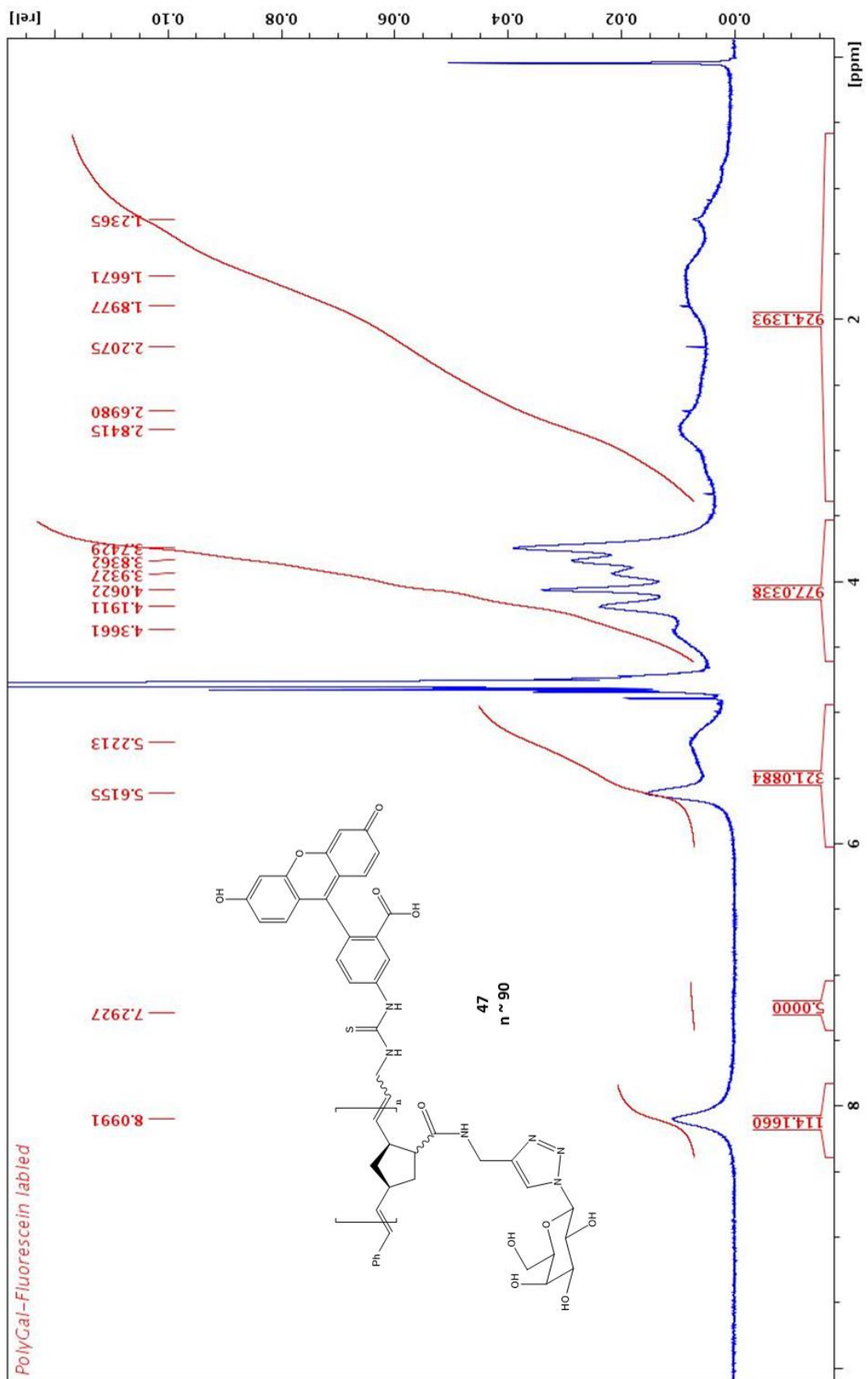


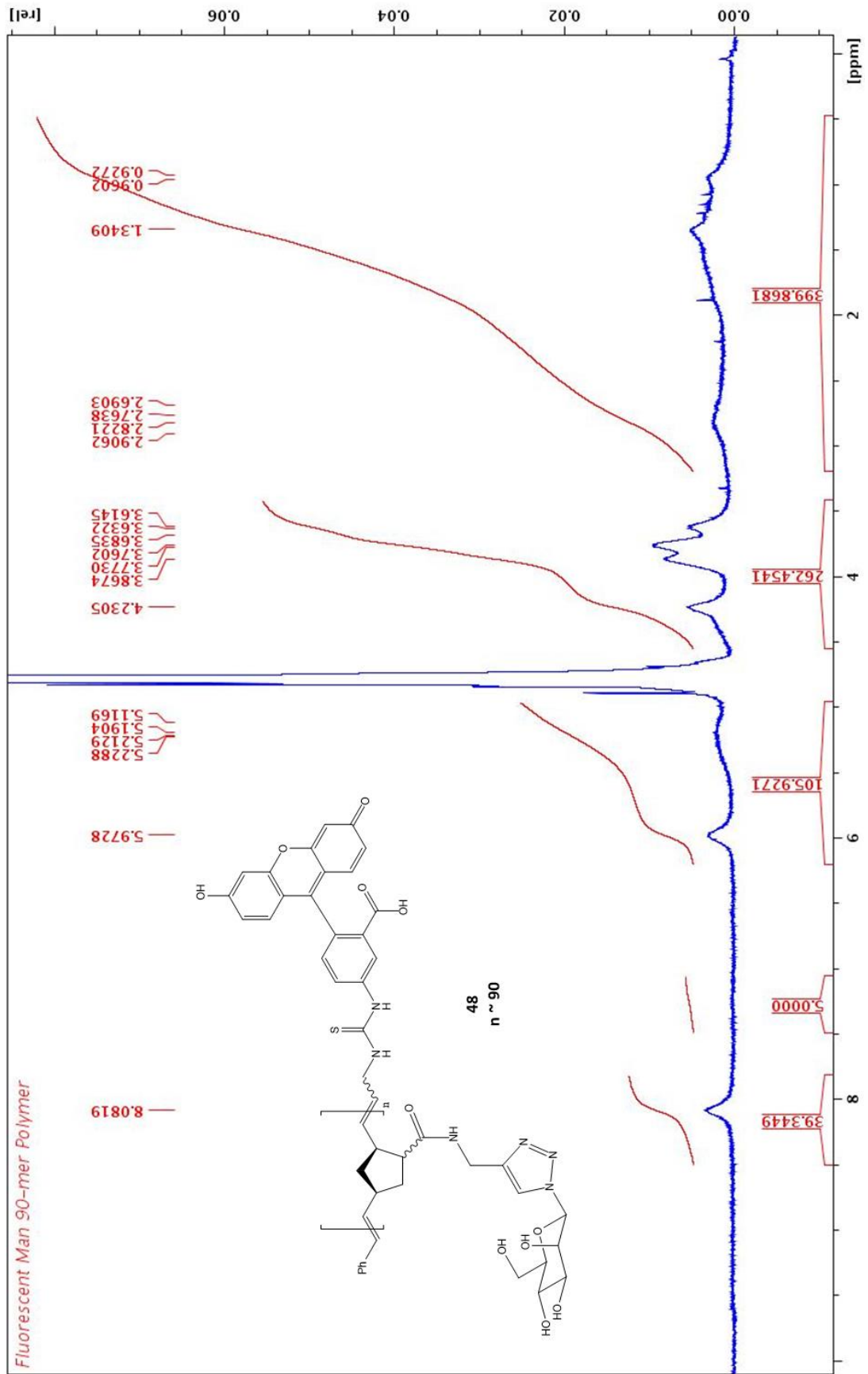


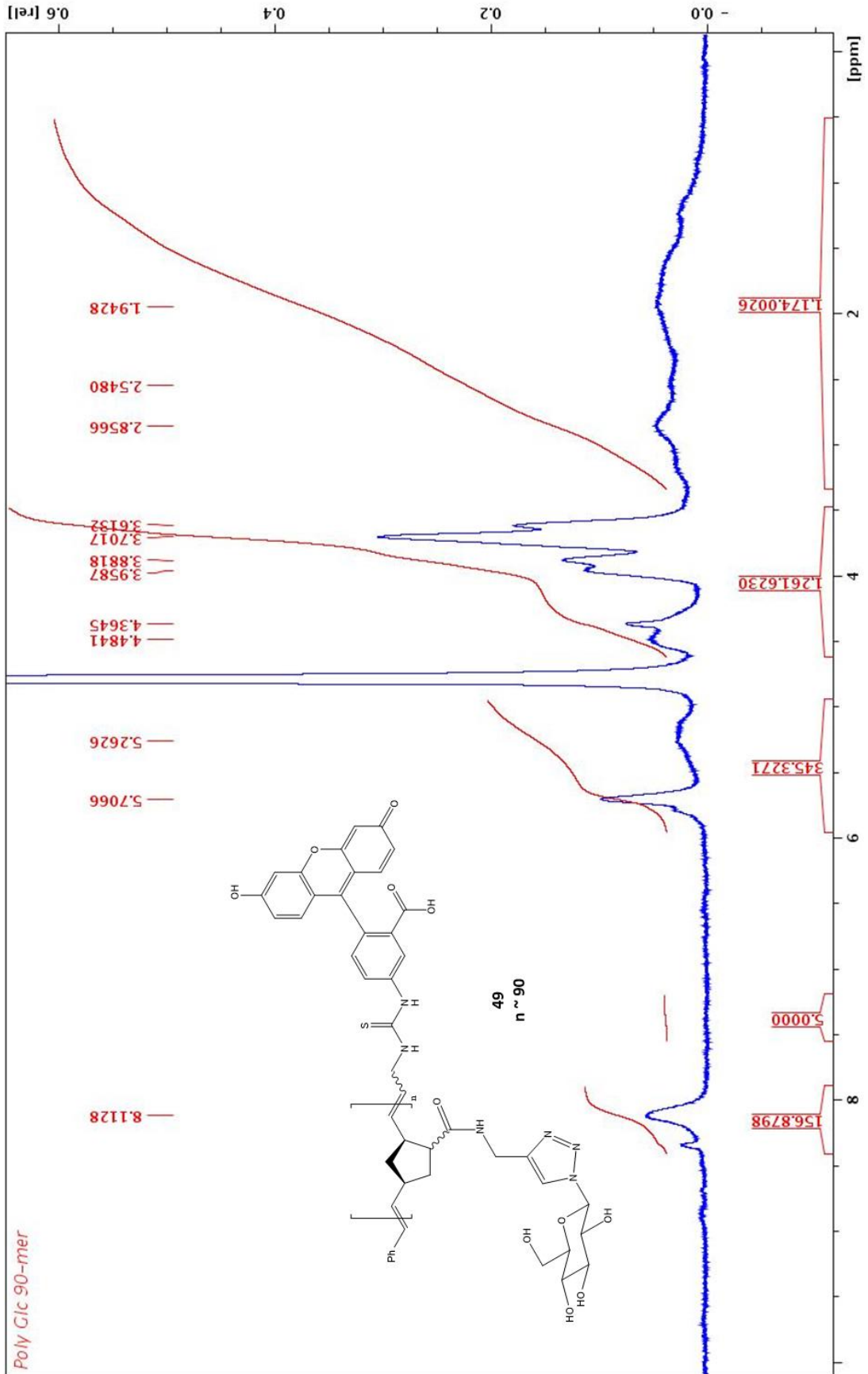


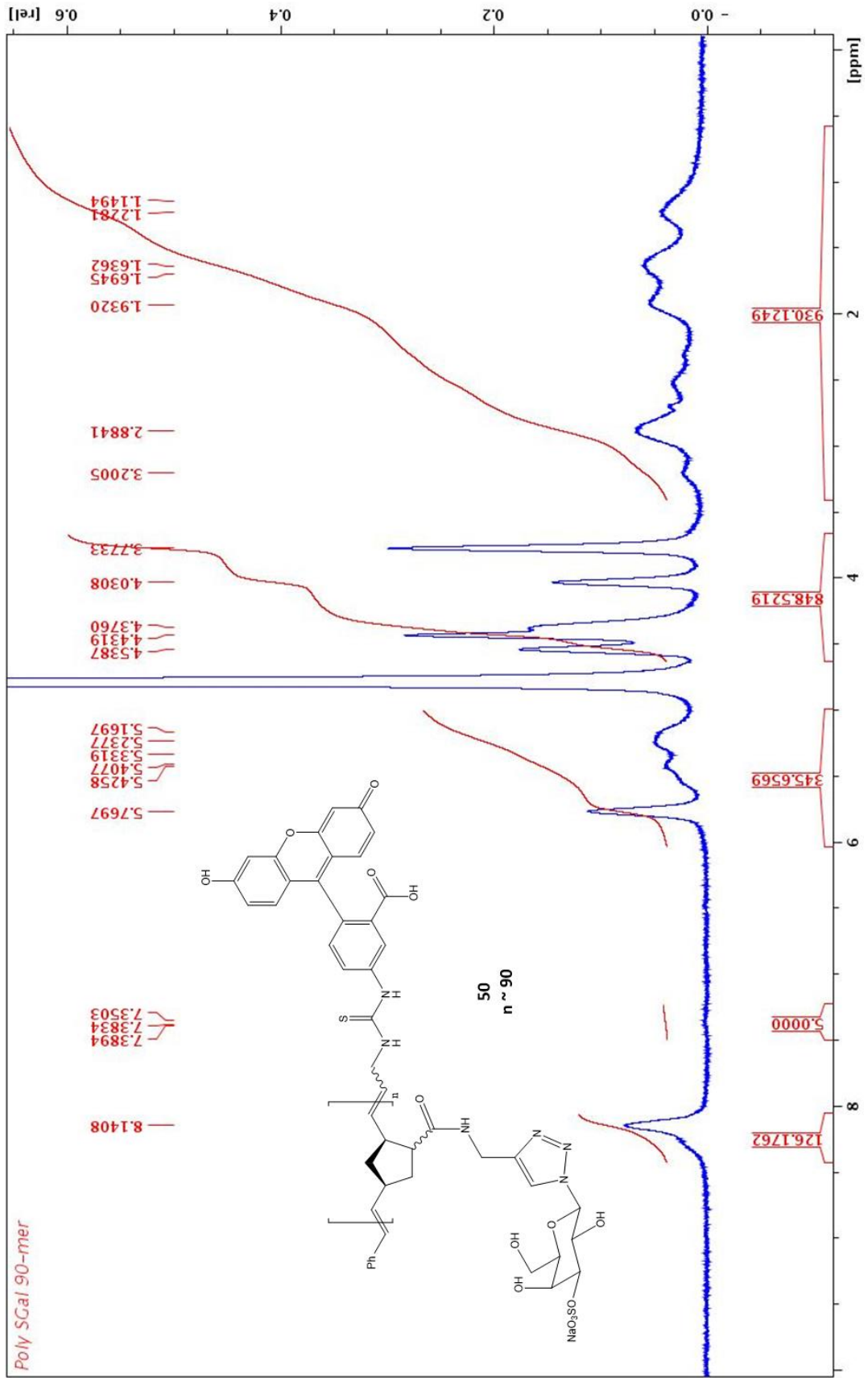






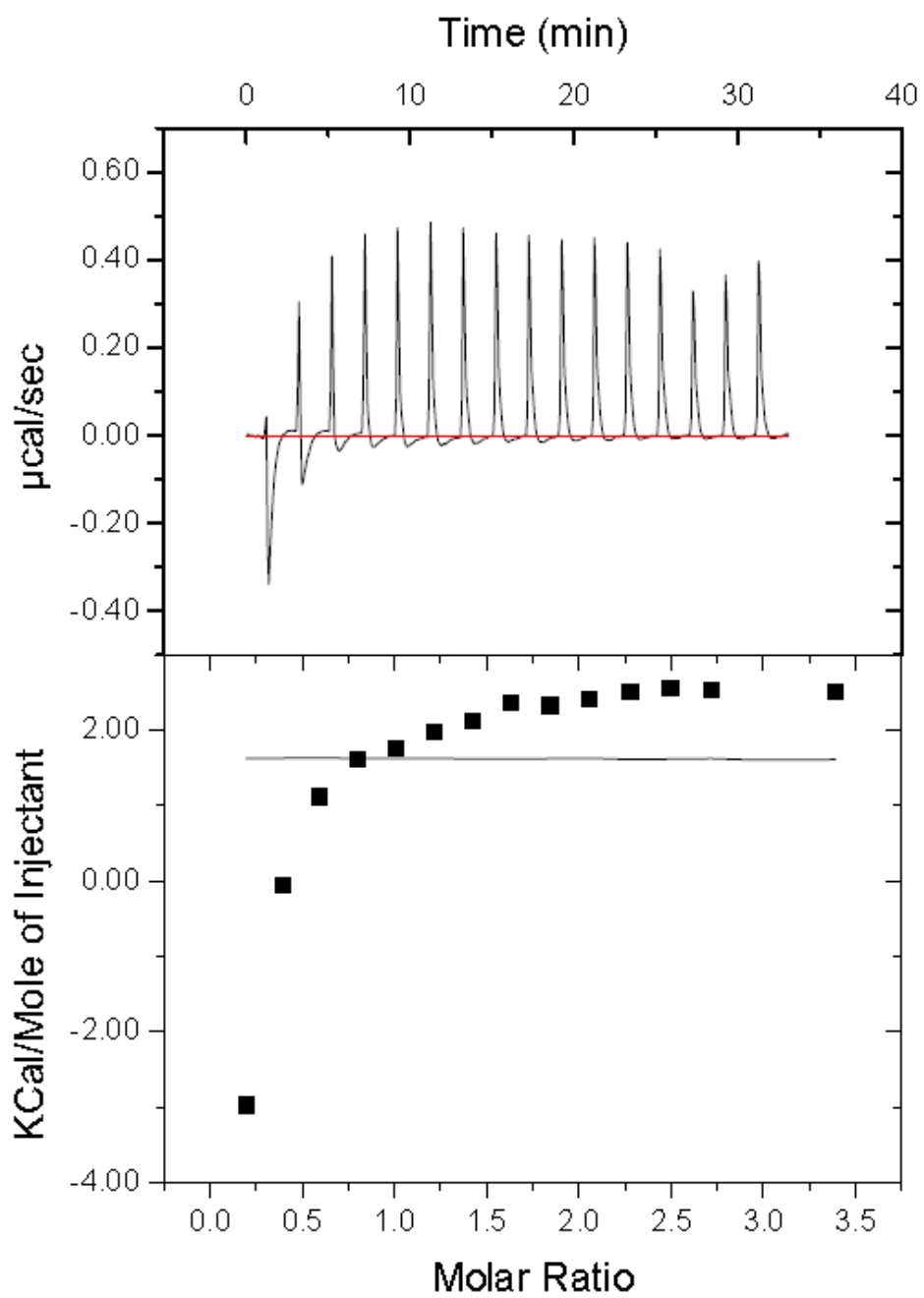




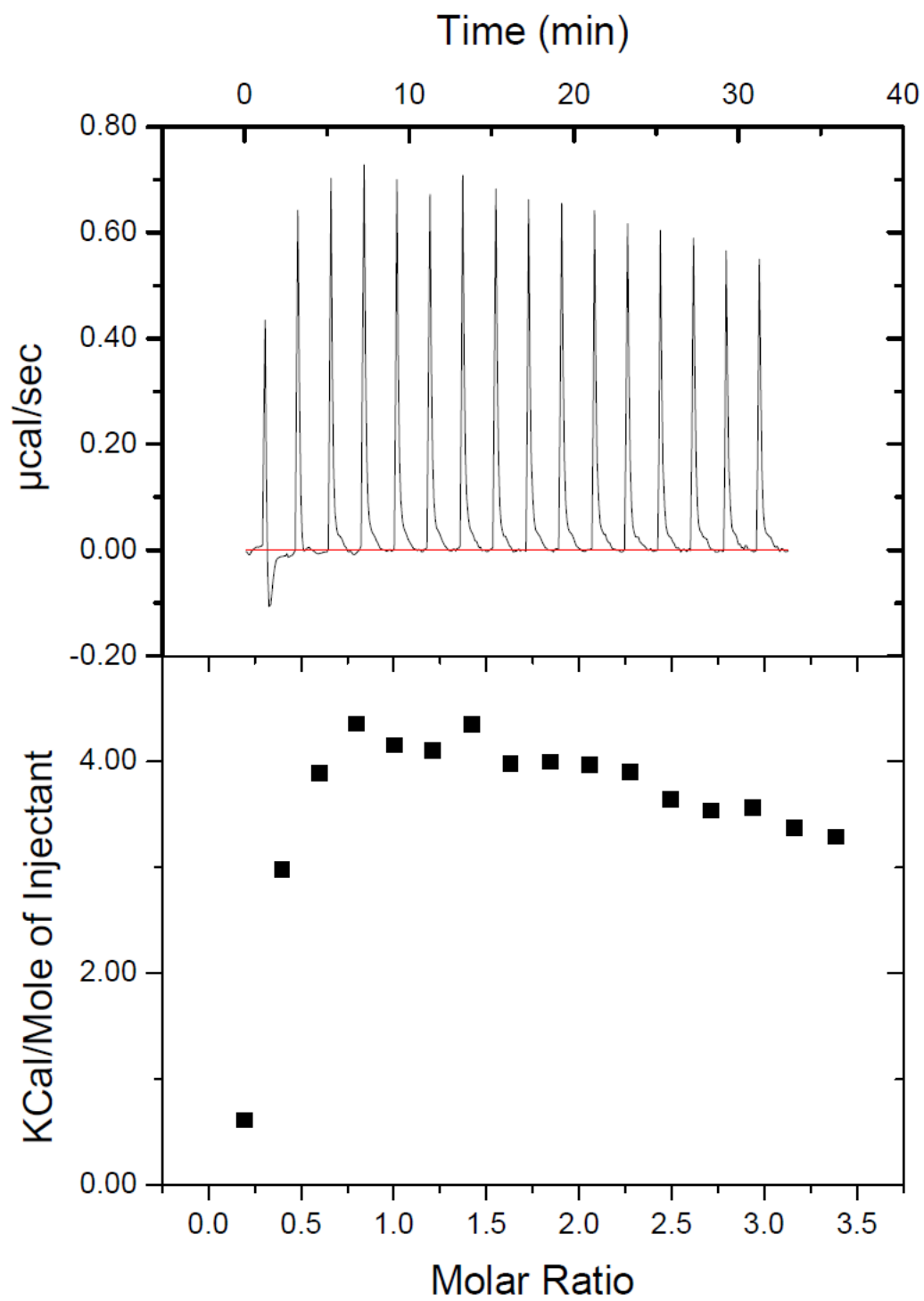


5.5 APPENDIX V – Raw ITC Data

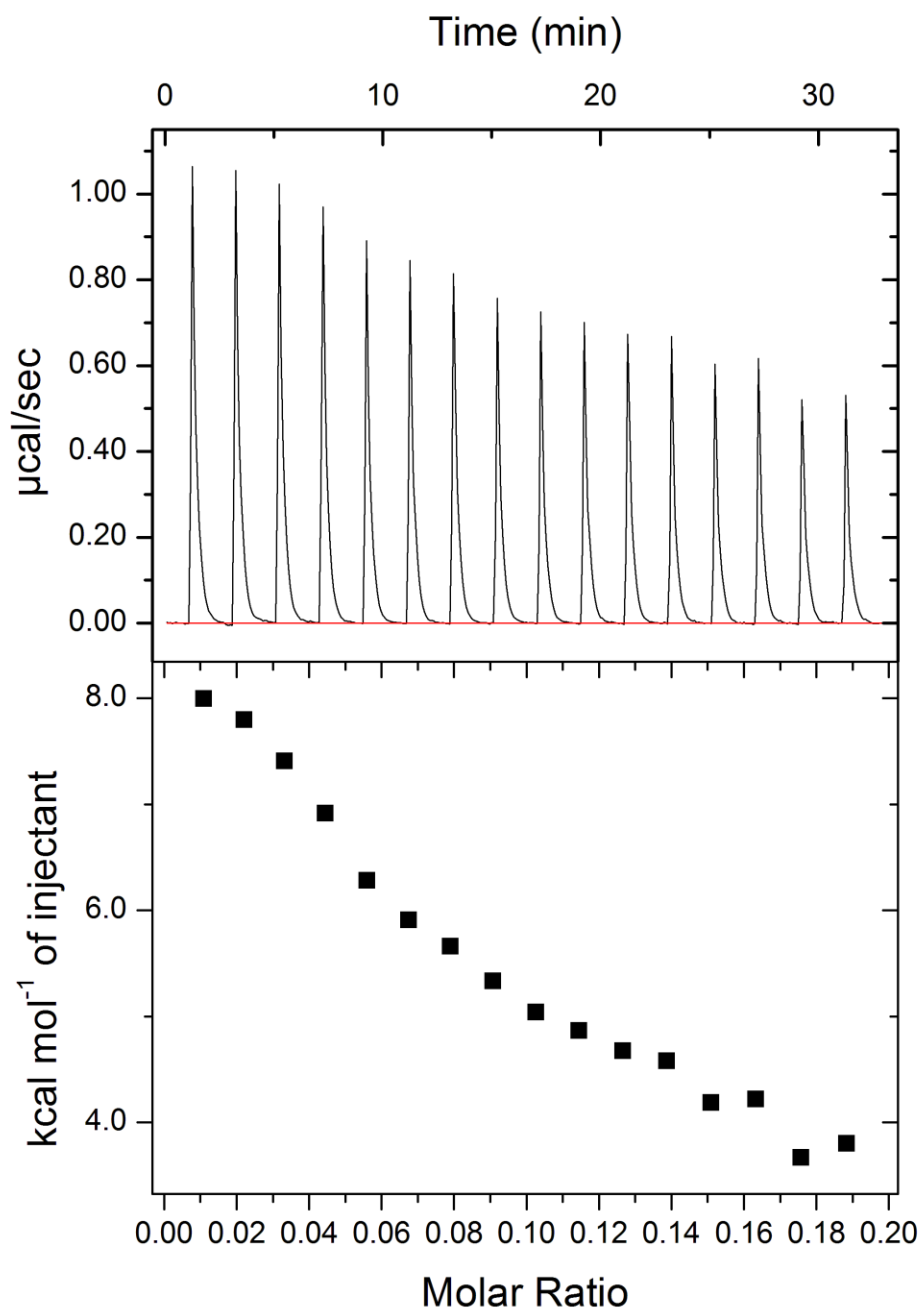
90-mer SGal 1.11 mM – Gal 0.06mM (072115SGal100Gal. ITC)



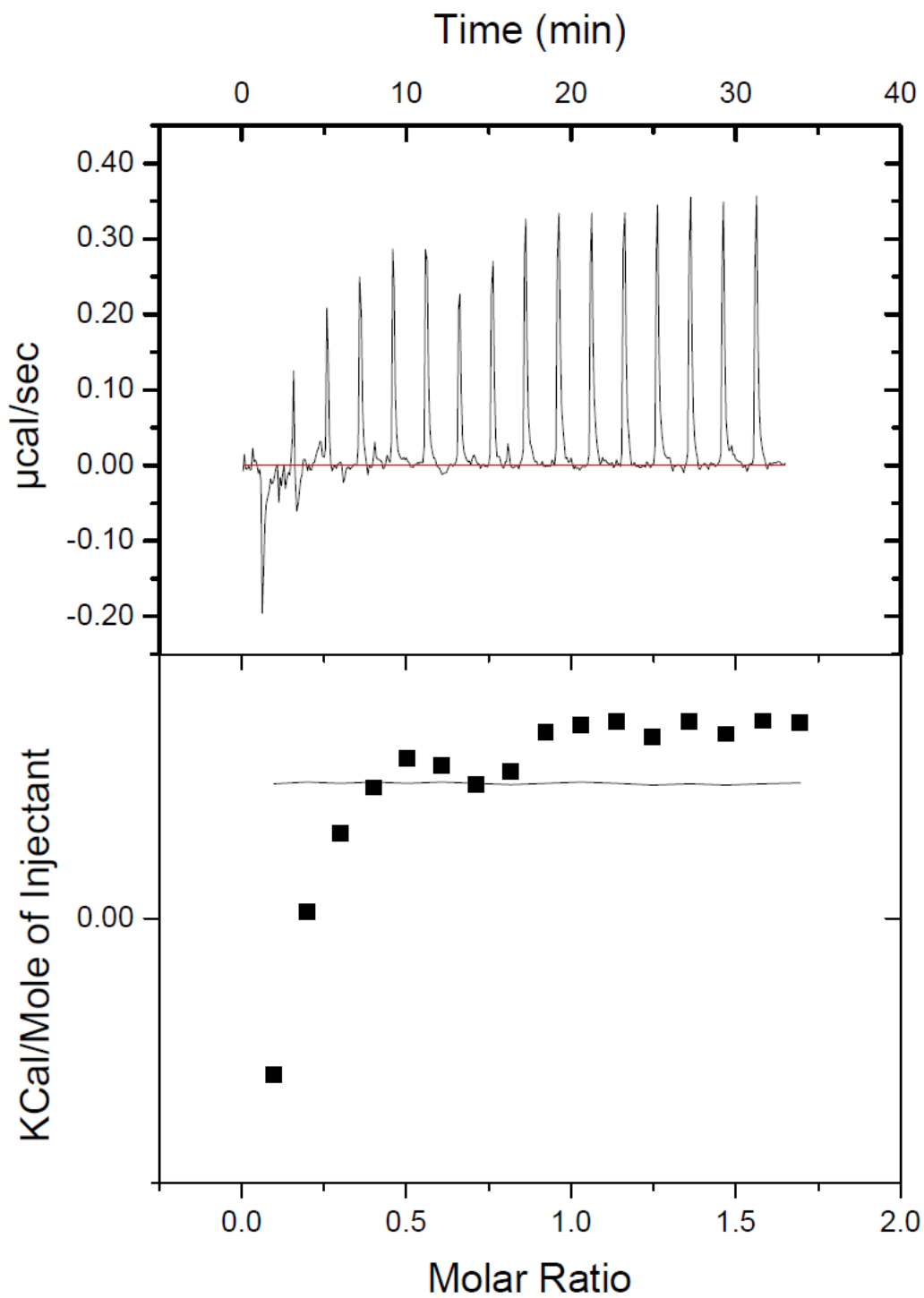
90-mer SGal 1.11 mM – Glc 0.06mM (073015SGal100Glc5.ITC)



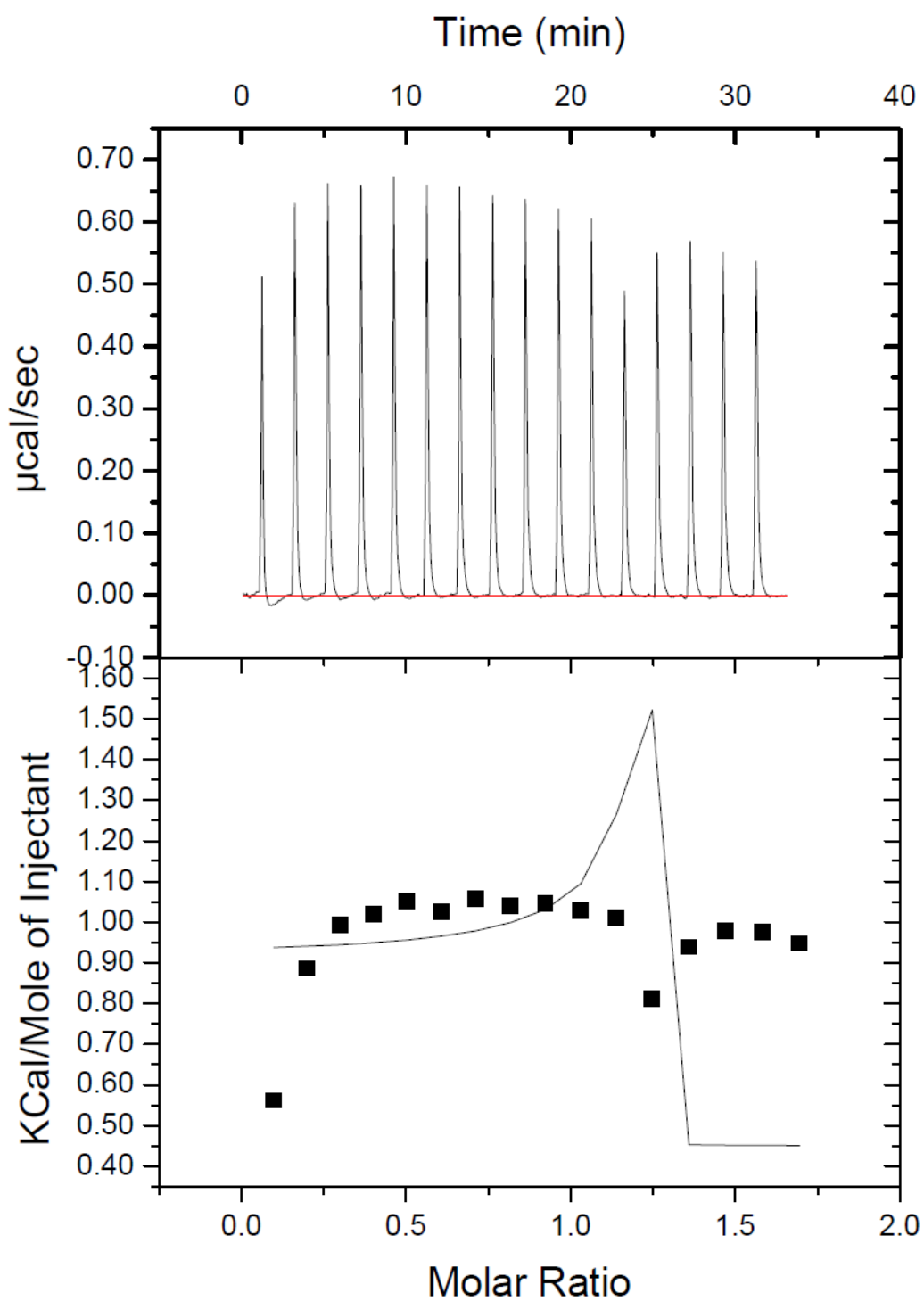
90-mer SGal 1.11 mM – PBS 7.4 pH (072115SGal100PBS.itc)



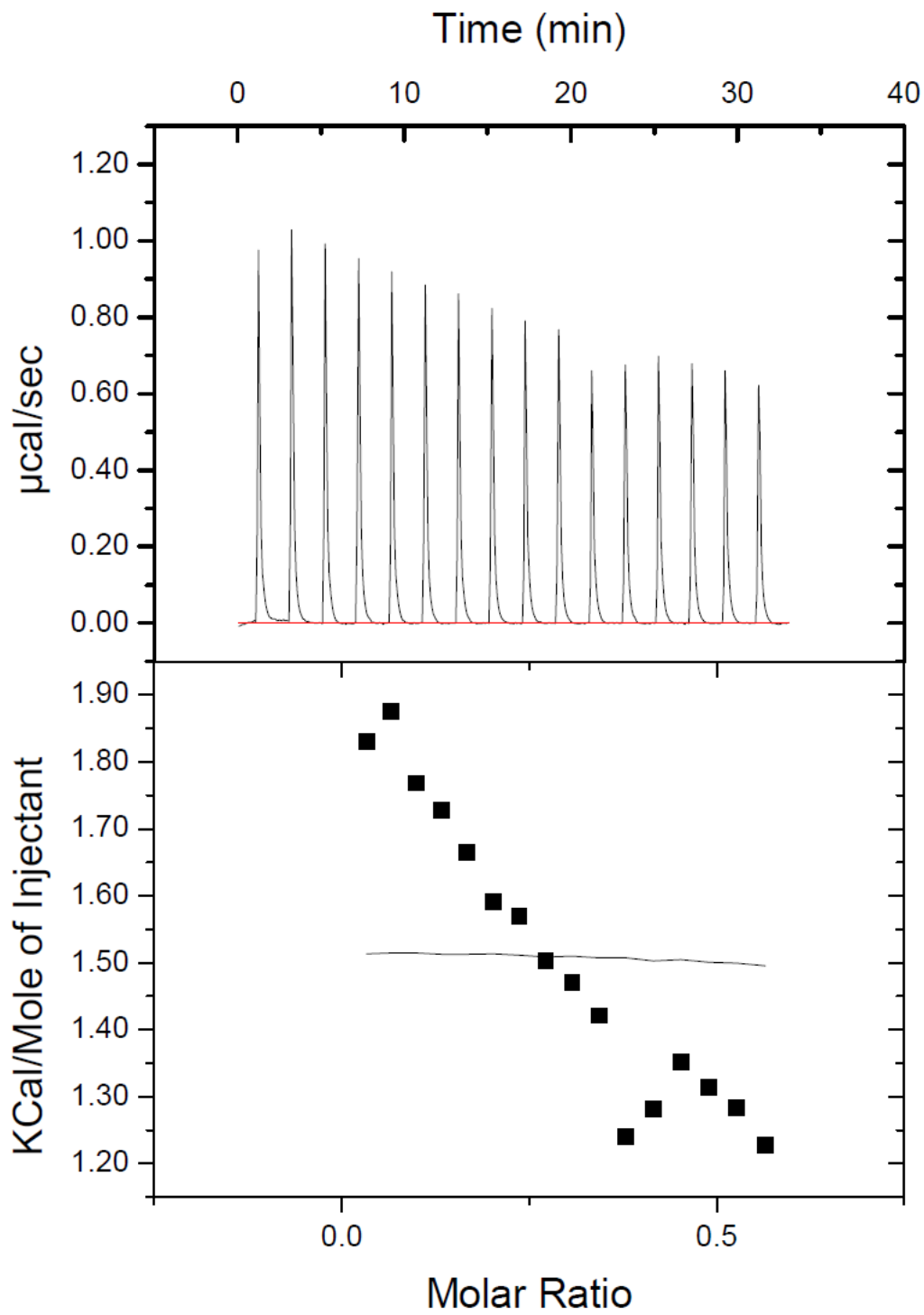
30-mer SGal 1.11 mM – Gal 0.11mM (SGALGLC100914. ITC)



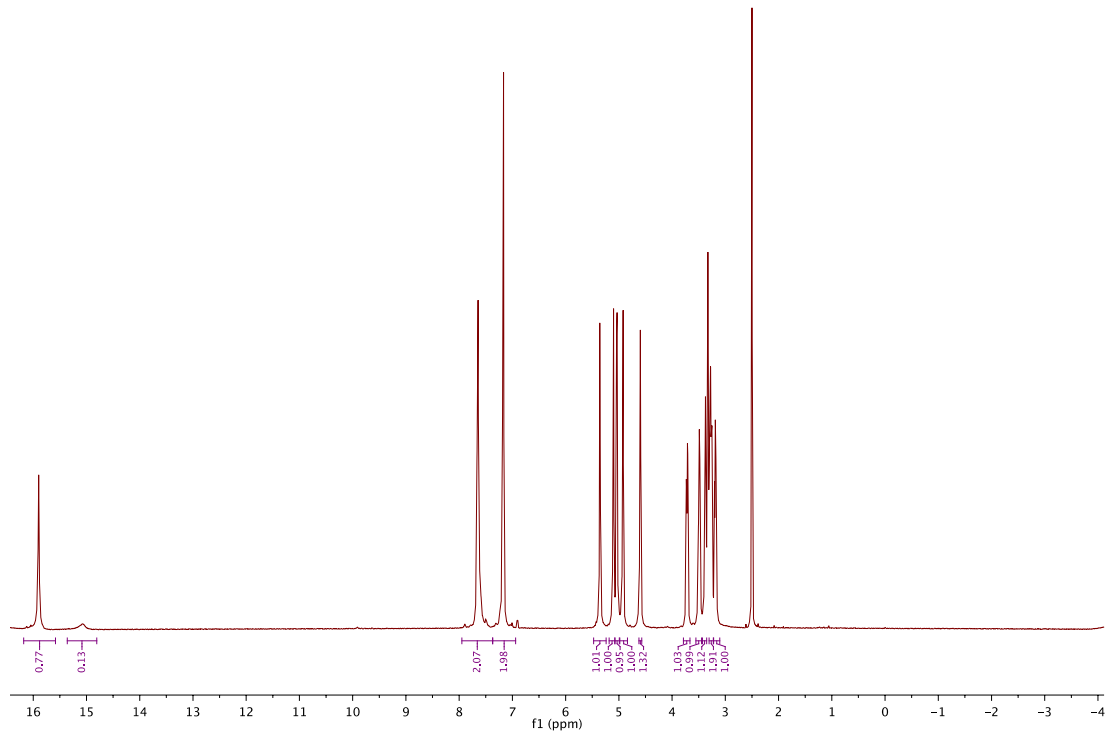
30-mer SGal 1.11 mM – Gal 0.11mM (SGALGAL100914.ITC)



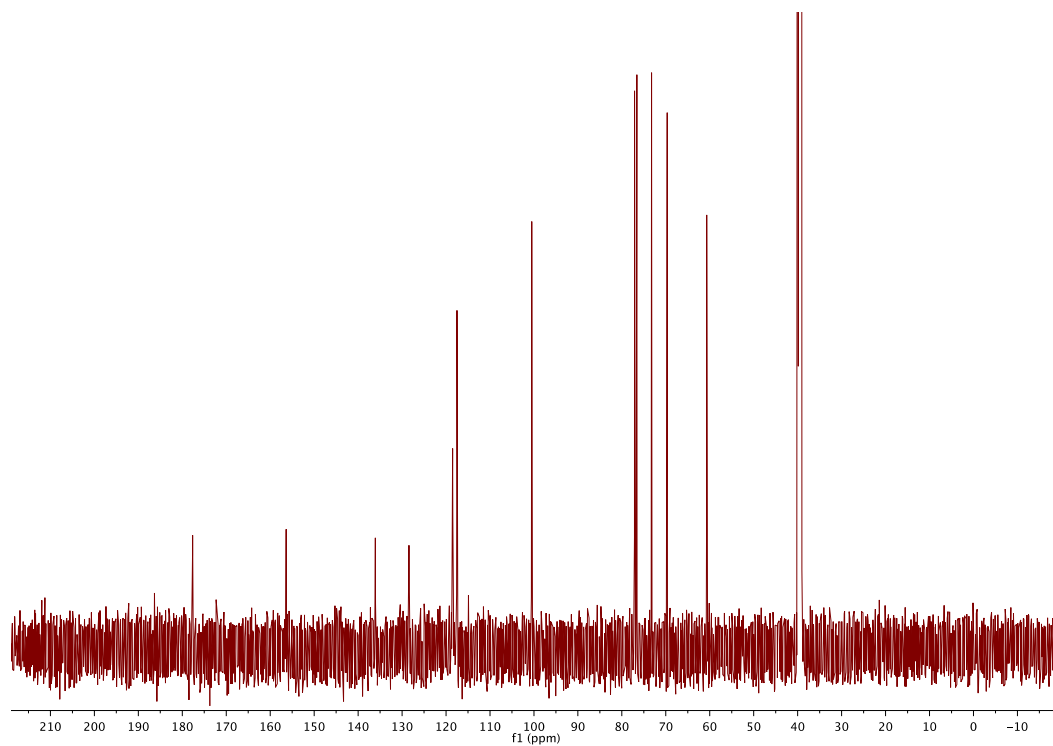
30-mer SGal 1.11 mM – PBS 7.4 pH (SGALPBS100914.itc)



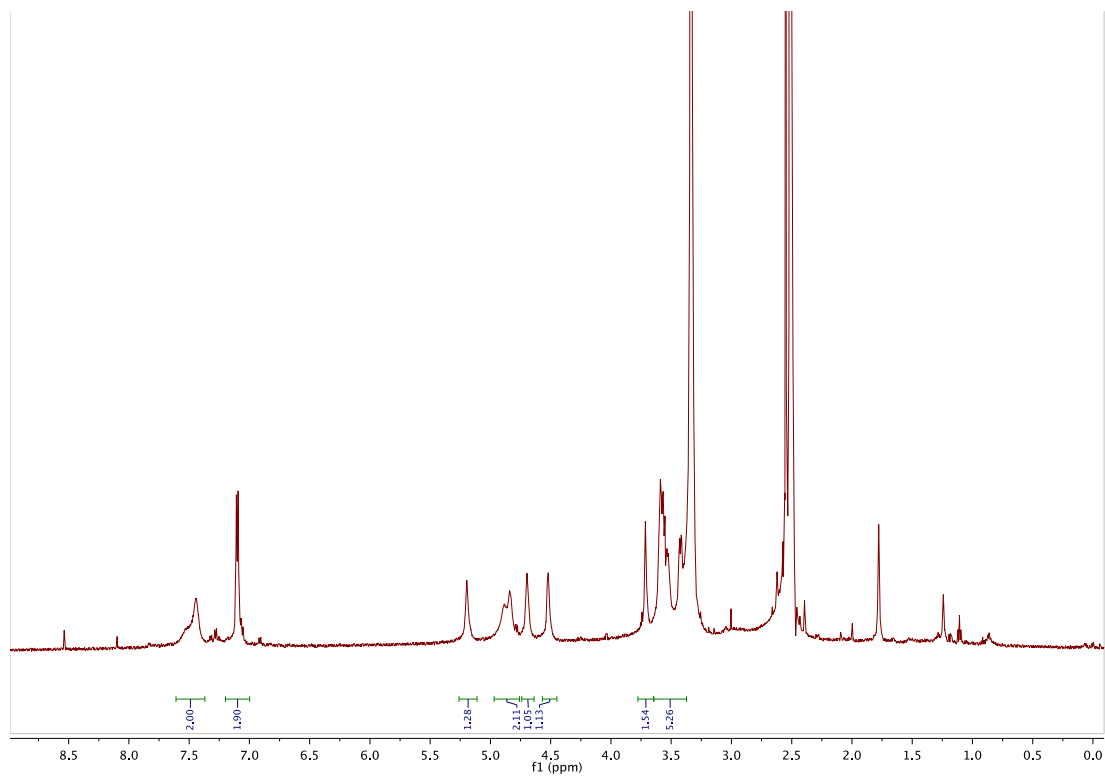
5.6 APPENDIX VI: Yariv reagent ^1H and ^{13}C -NMR



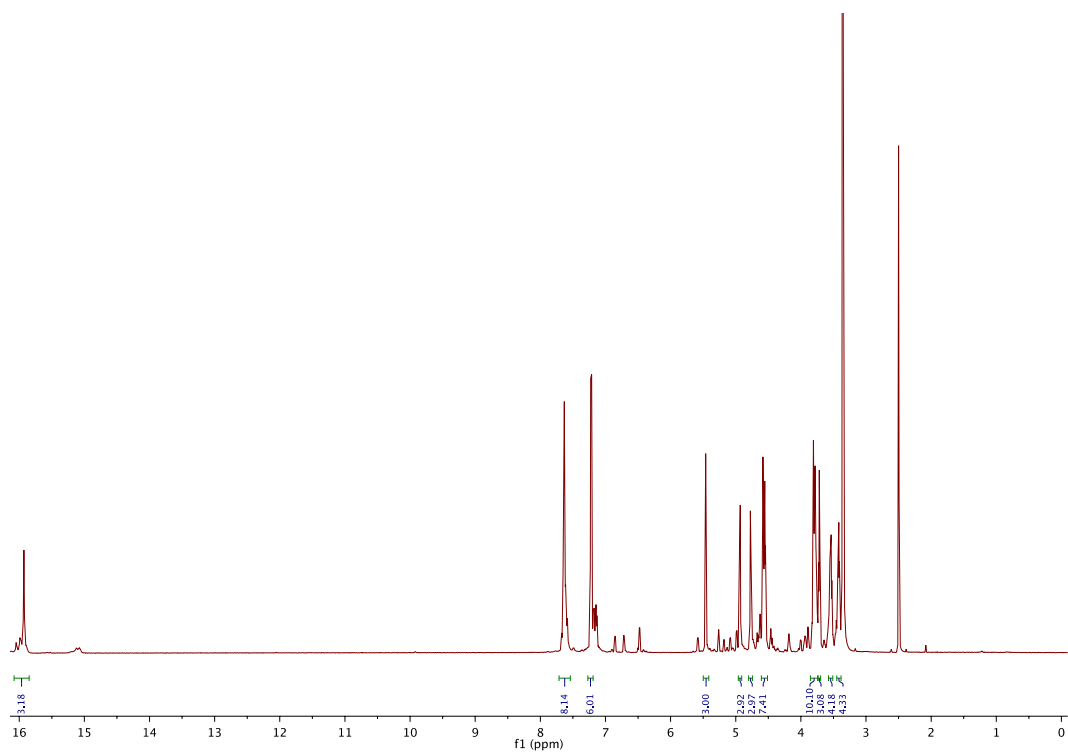
β -Glc Yariv **61** – ^1H NMR



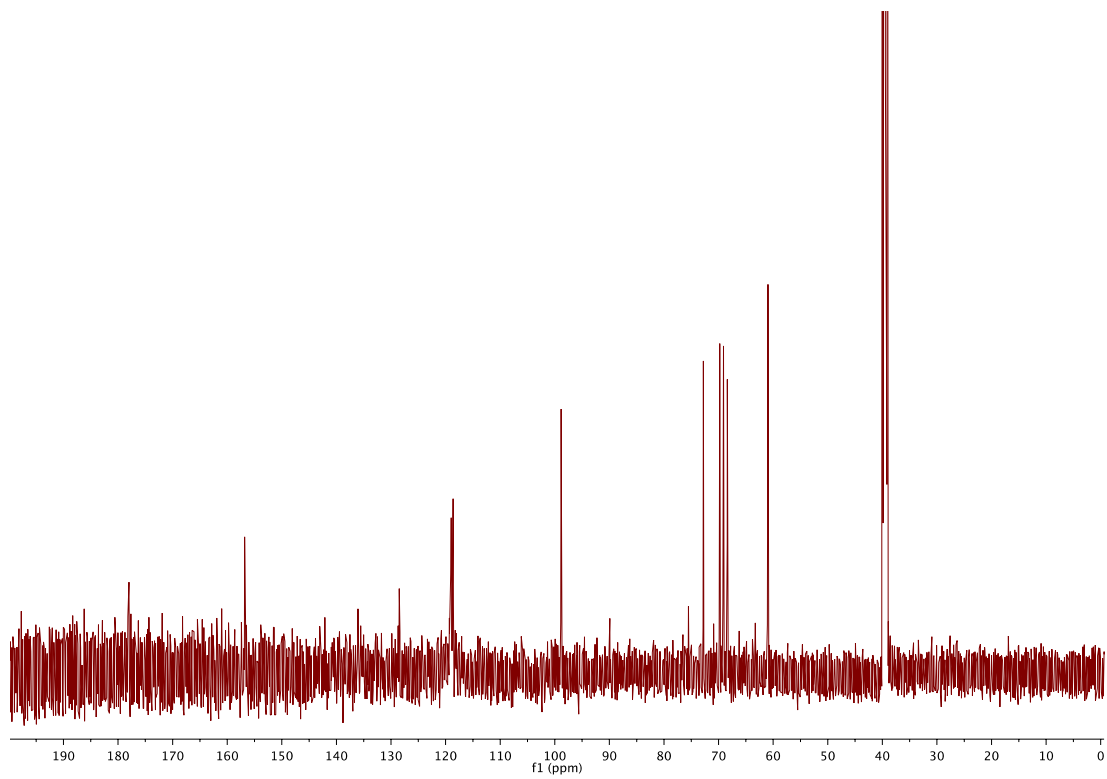
β -Glc Yariv **61** – ^{13}C NMR



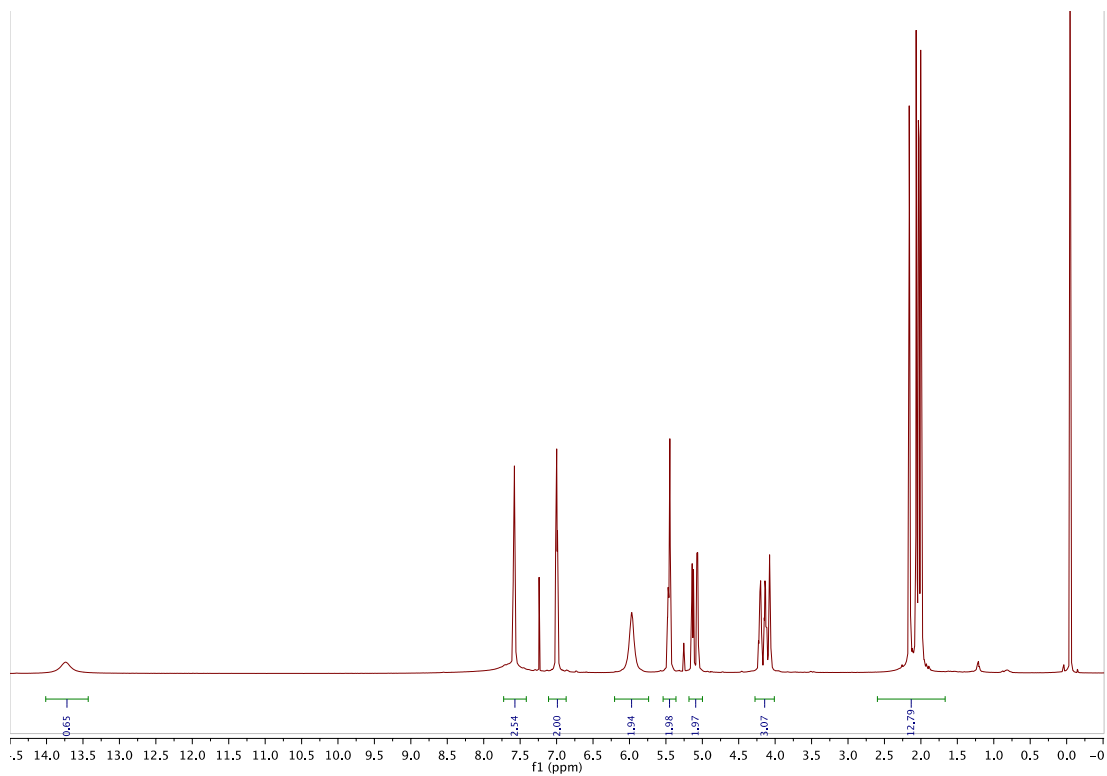
β -Gal Yariv 60 – ^1H NMR



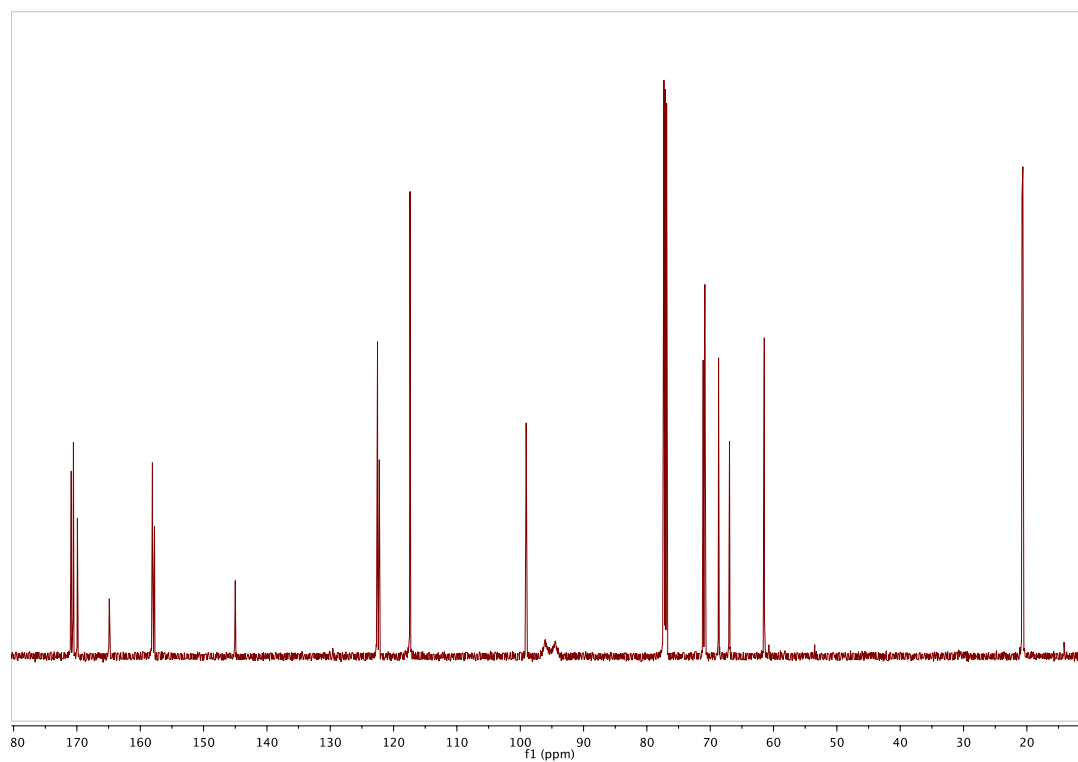
α -Gal Yariv **66** – ^1H NMR



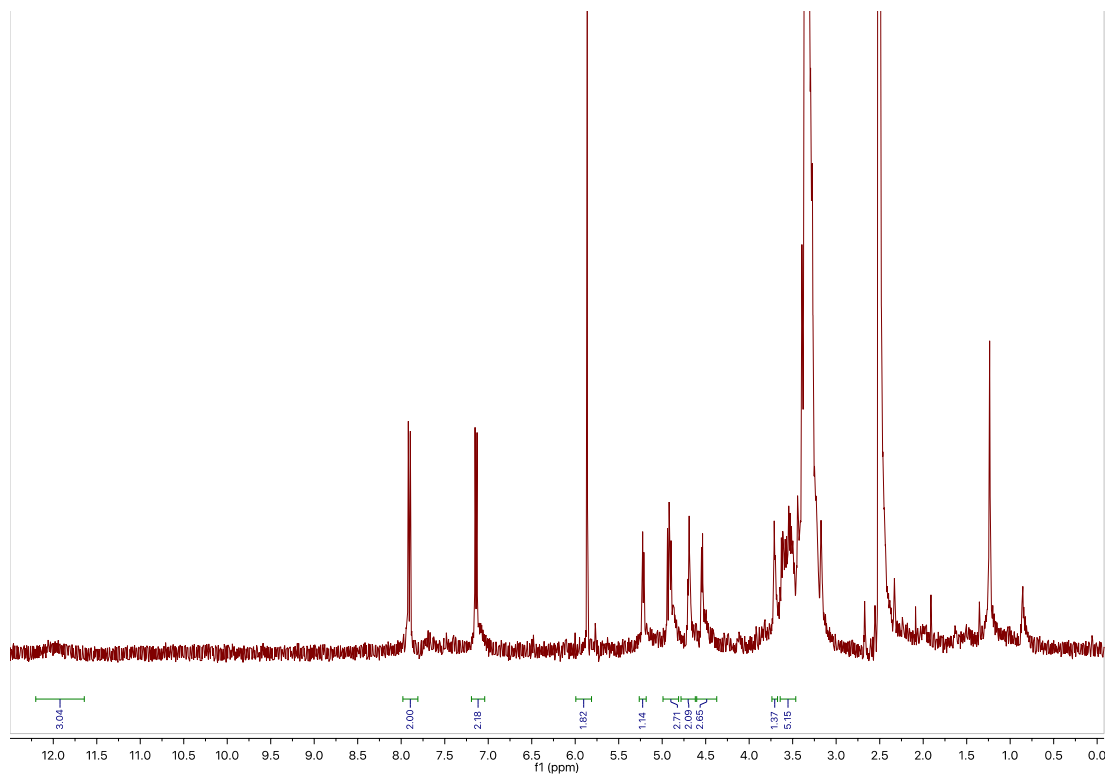
α -Gal Yariv **66** – ^{13}C NMR



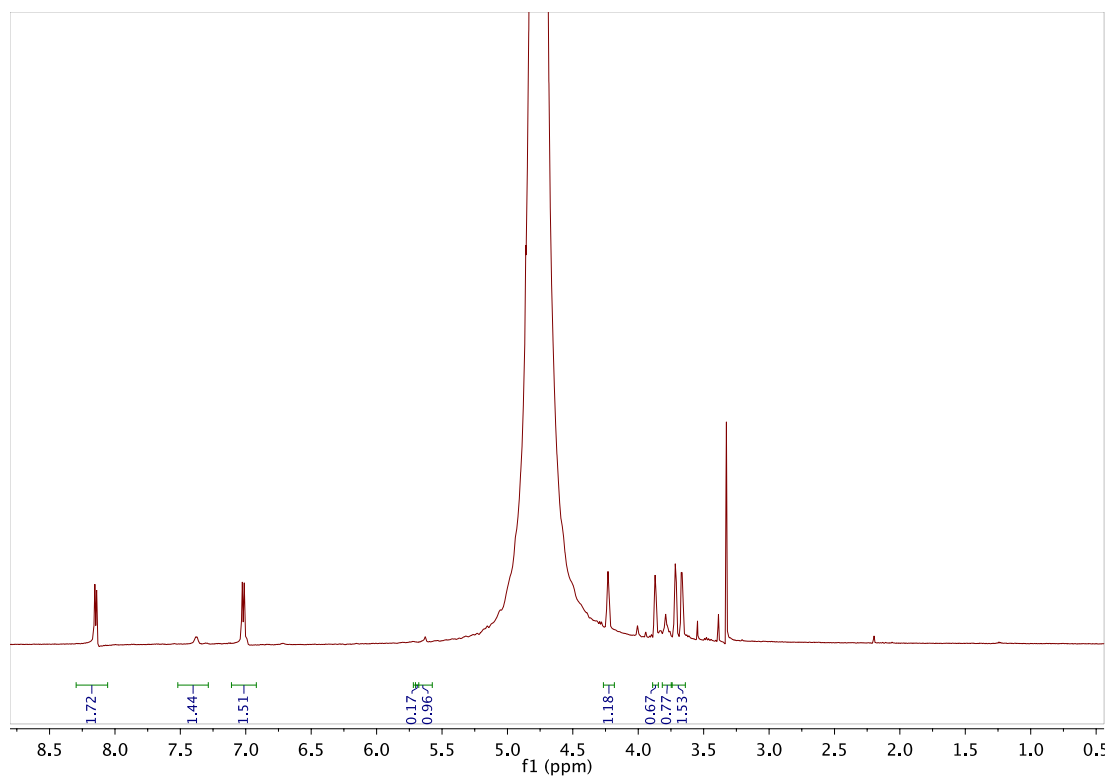
Tetraacetyl mono-galactosyl Yariv **72** – ¹H NMR



Tetraacetyl mono-galactosyl Yariv **72** – ¹³C NMR



Mono-galactosyl Yariv **68** – ¹H NMR (DMSO *d*₆)



Mono-galactosyl Yariv **68** – ¹H NMR (D₂O)

5.7 APPENDIX VII – Dynamic light scattering intensity and correlogram reports

DLS Data Summary

Yariv	Solvent	Temp. (°C)	Size (nm - largest peak)	Count rate (kcps)
α Gal	Water	10	209.6	19.4
α Gal	Water	60	146.3	18.8
α Gal	25% (v/v) MeOH	10 (hyst run 1)	1300	269.1
α Gal	25% (v/v) MeOH	60 (run 2)	46.59	13.9
α Gal	25% (v/v) MeOH	10 (run 3)	1262	177.7
α Gal	25% (v/v) MeOH	60 (run 4)	55.23	14.4
α Gal	25% (v/v) MeOH	10 (run 5)	1376	189.7
α Gal	5% (v/v) MeOH (X = 0.02)	10	223.9	24.9
α Gal	15% (v/v) MeOH (X = 0.07)	10	340.9	428.1
α Gal	25% (v/v) MeOH (X = 0.13)	10	692.1	168.0
α Gal	30% (v/v) MeOH (X = 0.16)	10	687.2	216.2
α Gal	35% (v/v) MeOH (X = 0.19)	10	1004	145.3
α Gal	50% (v/v) MeOH (X = 0.31)	10	635.5	131.1
α Gal	5% (v/v) EtOH (X = 0.02)	10	276.6	23.5
α Gal	10% (v/v) EtOH (X = 0.03)	10	272.5	44.1
α Gal	15% (v/v) EtOH (X = 0.05)	10	686.8	291.2
α Gal	20% (v/v) EtOH (X = 0.07)	10	690.9	278.4
α Gal	25% (v/v) EtOH (X = 0.09)	10	663.5	132.3
α Gal	50% (v/v) EtOH (X = 0.24)	10	1200	341.6
α Gal	5% (v/v) iPrOH (X = 0.01)	10	252.9	26.9
α Gal	7.5% (v/v) iPrOH (X = 0.02)	10	252.5	29.8
α Gal	10% (v/v) iPrOH (X = 0.03)	10	578.5	144.9
α Gal	15% (v/v) iPrOH (X = 0.04)	10	884.6	152.5

αGal	25% (v/v) iPrOH (X = 0.07)	10	1134	128.6
αGal	60% (v/v) iPrOH (X = 0.26)	10	420.9	106.3
αGal	75% (v/v) iPrOH (X = 0.41)	10	1271	260.9
βGlc	Water	10	335.5	18.8
βGlc	Water	60	108.5	30.5
βGlc	25% (v/v) MeOH	10 (hyst run 1)	921.2	213.7
βGlc	25% (v/v) MeOH	60 (run 2)	97.32	8.6
βGlc	25% (v/v) MeOH	10 (run 3)	1525	203.4
βGlc	25% (v/v) MeOH	60 (run 4)	86.69	8.6
βGlc	25% (v/v) MeOH	10 (run 5)	726.5	193.9
βGlc	5% (v/v) MeOH (X = 0.02)	10	274.1	94.1
βGlc	15% (v/v) MeOH (X = 0.07)	10	989.4	177.3
βGlc	25% (v/v) MeOH (X = 0.13)	10	4107	86.7
βGlc	30% (v/v) MeOH (X = 0.16)	10	714.8	257.1
βGlc	35% (v/v) MeOH (X = 0.19)	10	3192	134.9
βGlc	50% (v/v) MeOH (X = 0.31)	10	580.4	300.1

αGal Yariv in water at 10 °C

Size Distribution Report by Intensity

v2.2



Sample Details

Sample Name: BL-aGal-0.3mM-10c-1 1

SOP Name: mansettings.nano

General Notes:

File Name: Example Results.dts	Dispersant Name: Water
Record Number: 157	Dispersant RI: 1.330
Material RI: 1.45	Viscosity (cP): 1.3153
Material Absorbtion: 0.001	Measurement Date and Time: Friday, October 21, 2016 3:1...

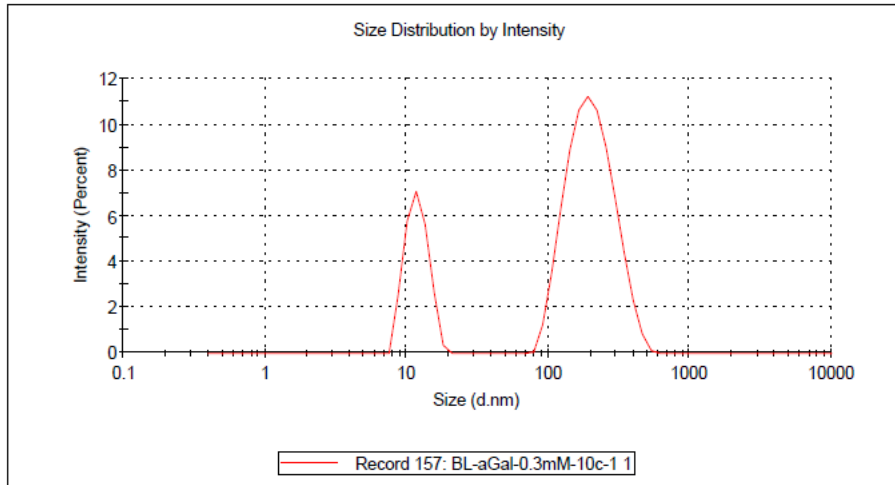
System

Temperature (°C): 9.9	Duration Used (s): 220
Count Rate (kcps): 19.4	Measurement Position (mm): 4.65
Cell Description: Glass cuvette with square apert...	Attenuator: 11

Results

	Size (d.nm):	% Intensity:	St Dev (d.n...
Z-Average (d.nm): 45.38	Peak 1: 209.6	76.0	78.35
PdI: 1.000	Peak 2: 11.97	24.0	2.162
Intercept: 0.670	Peak 3: 0.000	0.0	0.000

Result quality : **Refer to quality report**



Correlogram Report

v2.0



Malvern Instruments Ltd - © Copyright 2008

Sample Details

Sample Name: BL-aGal-0.3mM-10c-1 1

SOP Name: mansettings.nano

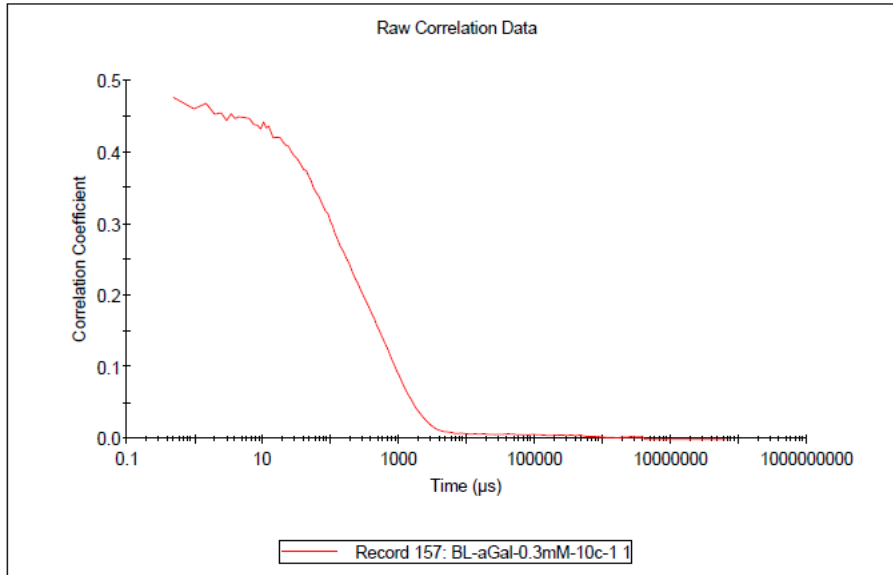
General Notes:

File Name: Example Results.dts	Dispersant Name: Water
Record Number: 157	Dispersant RI: 1.330
Material RI: 1.45	Viscosity (cP): 1.3153
Material Absorbtion: 0.001	Measurement Date and Time: Friday, October 21, 2016 3:...

System

Temperature (°C): 9.9	Duration Used (s): 220
Count Rate (kcps): 19.4	Measurement Position (mm): 4.65
Cell Description: Glass cuvette with square...	Attenuator: 11

Results



αGal Yariv in water at 60 °C

Size Distribution Report by Intensity

v2.2



Sample Details

Sample Name: 120216agal300uM60Cfit1

SOP Name: mansettings.nano

General Notes:

File Name: Example Results.dts	Dispersant Name: Water
Record Number: 217	Dispersant RI: 1.330
Material RI: 1.45	Viscosity (cP): 0.4712
Material Absorption: 0.001	Measurement Date and Time: Friday, December 02, 2016 3:...

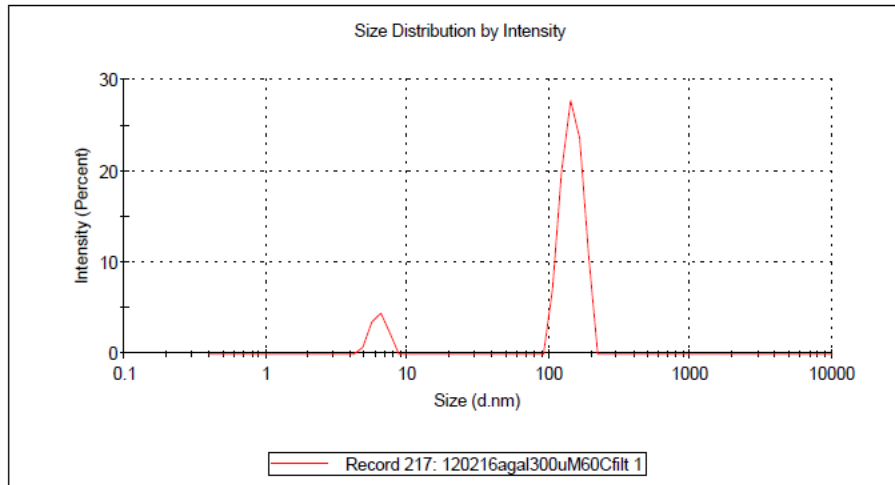
System

Temperature (°C): 60.0	Duration Used (s): 290
Count Rate (kcps): 18.8	Measurement Position (mm): 4.65
Cell Description: Glass cuvette with square apert...	Attenuator: 11

Results

	Size (d.nm):	% Intensity:	St Dev (d.n...)
Z-Average (d.nm): 278.5	Peak 1: 146.3	88.9	24.11
Pdl: 0.303	Peak 2: 6.323	11.1	0.7904
Intercept: 0.724	Peak 3: 0.000	0.0	0.000

Result quality : **Refer to quality report**



Correlogram Report

v2.0



Malvern Instruments Ltd - © Copyright 2008

Sample Details

Sample Name: 120216agal300uM60Cfilt 1

SOP Name: mansettings.nano

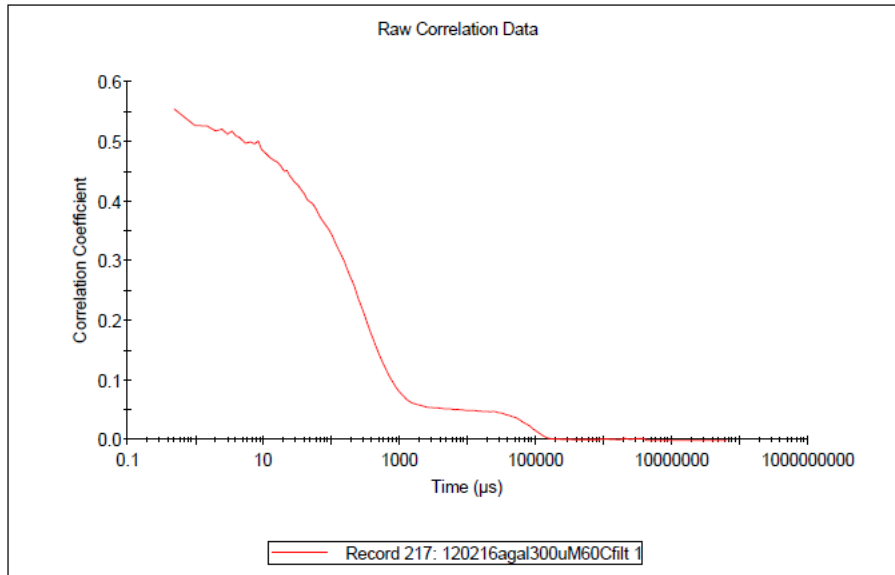
General Notes:

File Name: Example Results.dts	Dispersant Name: Water
Record Number: 217	Dispersant RI: 1.330
Material RI: 1.45	Viscosity (cP): 0.4712
Material Absorbtion: 0.001	Measurement Date and Time: Friday, December 02, 2016...

System

Temperature (°C): 60.0	Duration Used (s): 290
Count Rate (kcps): 18.8	Measurement Position (mm): 4.65
Cell Description: Glass cuvette with square...	Attenuator: 11

Results



α Gal Yariv in 25% (v/v) MeOH at 10 °C (run 1)

Size Distribution Report by Intensity

v2.2



Sample Details

Sample Name: BL-aGal-0.3mM25%meoh-10c-1 1

SOP Name: mansettings.nano

General Notes:

File Name:	Example Results.dts	Dispersant Name:	Water MeOH 25%
Record Number:	159	Dispersant RI:	1.338
Material RI:	1.45	Viscosity (cP):	2.1408
Material Absorbtion:	0.001	Measurement Date and Time:	Friday, October 21, 2016 3:3...

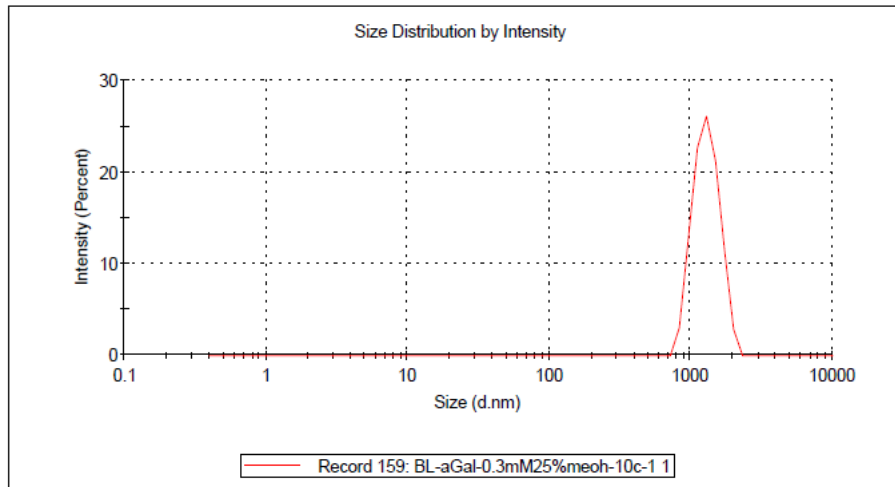
System

Temperature (°C):	10.0	Duration Used (s):	60
Count Rate (kcps):	269.1	Measurement Position (mm):	4.65
Cell Description:	Glass cuvette with square apert...	Attenuator:	10

Results

	Size (d.nm):	% Intensity:	St Dev (d.n...)
Z-Average (d.nm): 1254	Peak 1: 1300	100.0	267.4
Pdl: 0.008	Peak 2: 0.000	0.0	0.000
Intercept: 0.761	Peak 3: 0.000	0.0	0.000

Result quality : **Good**



Correlogram Report

v2.0



Malvern Instruments Ltd - © Copyright 2008

Sample Details

Sample Name: BL-aGal-0.3mM25%meoh-10c-1 1

SOP Name: mansettings.nano

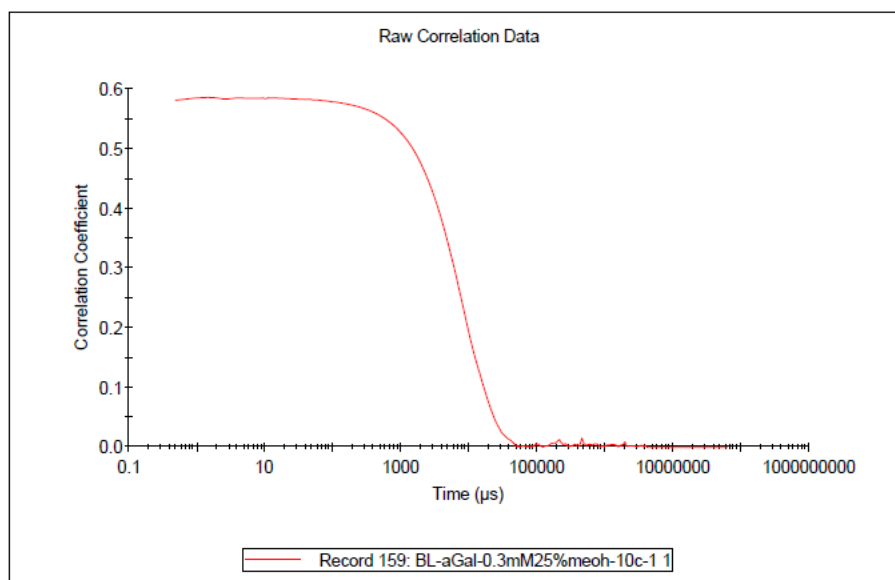
General Notes:

File Name: Example Results.dts	Dispersant Name: Water MeOH 25%
Record Number: 159	Dispersant RI: 1.338
Material RI: 1.45	Viscosity (cP): 2.1408
Material Absorbtion: 0.001	Measurement Date and Time: Friday, October 21, 2016 3:...

System

Temperature (°C): 10.0	Duration Used (s): 60
Count Rate (kcps): 269.1	Measurement Position (mm): 4.65
Cell Description: Glass cuvette with square...	Attenuator: 10

Results



αGal Yariv in 25% (v/v) MeOH at 60 °C (run 2)

Size Distribution Report by Intensity

v2.2



Sample Details

Sample Name: BL-aGal-0.3mM25%meoh-60c-1 1

SOP Name: mansettings.nano

General Notes:

File Name:	Example Results.dts	Dispersant Name:	Water MeOH 25%
Record Number:	162	Dispersant RI:	1.338
Material RI:	1.45	Viscosity (cP):	1.2967
Material Absorbtion:	0.001	Measurement Date and Time:	Monday, October 24, 2016 2:...

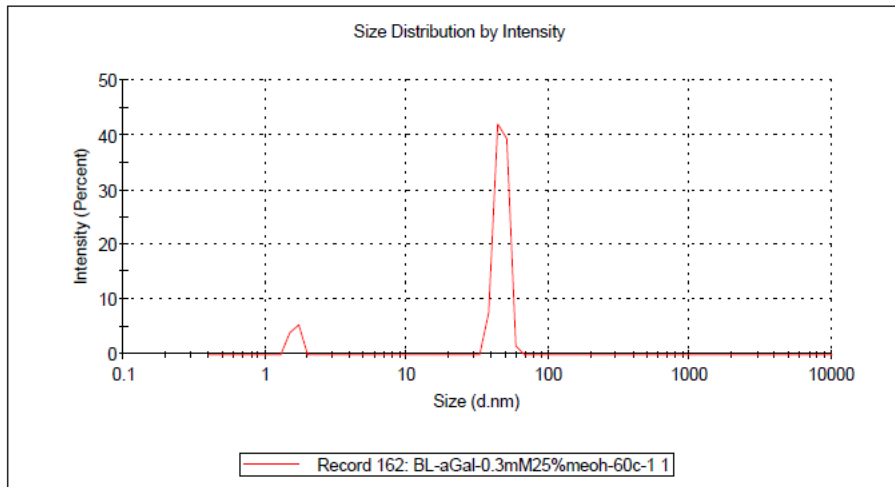
System

Temperature (°C):	60.0	Duration Used (s):	330
Count Rate (kcps):	13.9	Measurement Position (mm):	4.65
Cell Description:	Glass cuvette with square apert...	Attenuator:	11

Results

	Size (d.nm):	% Intensity:	St Dev (d.n...)
Z-Average (d.nm): 522.8	Peak 1: 46.59	90.5	4.494
PdI: 1.000	Peak 2: 1.636	9.5	0.1170
Intercept: 0.871	Peak 3: 0.000	0.0	0.000

Result quality : **Refer to quality report**



Correlogram Report

v2.0



Malvern Instruments Ltd - © Copyright 2008

Sample Details

Sample Name: BL-aGal-0.3mM25%meoh-60c-1 1

SOP Name: mansettings.nano

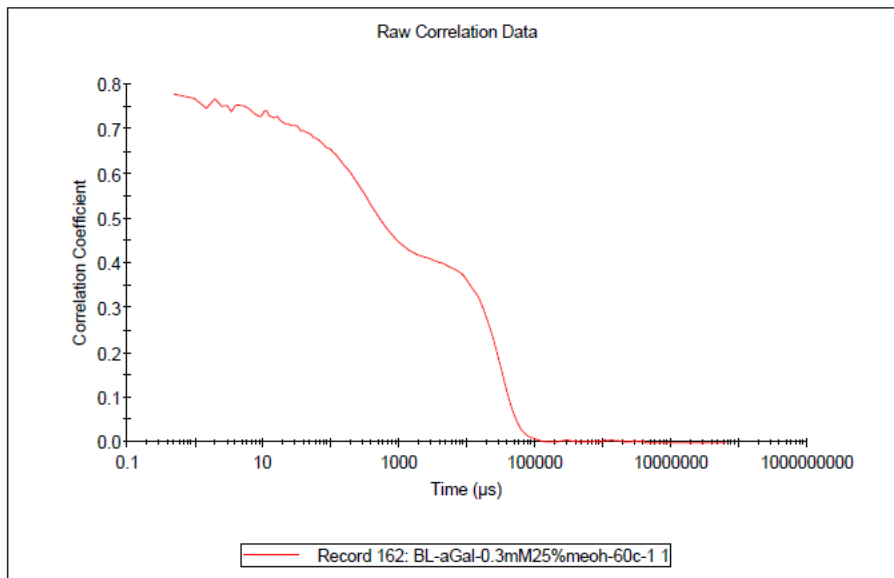
General Notes:

File Name: Example Results.dts	Dispersant Name: Water MeOH 25%
Record Number: 162	Dispersant RI: 1.338
Material RI: 1.45	Viscosity (cP): 1.2967
Material Absorbtion: 0.001	Measurement Date and Time: Monday, October 24, 2016 ...

System

Temperature (°C): 60.0	Duration Used (s): 330
Count Rate (kcps): 13.9	Measurement Position (mm): 4.65
Cell Description: Glass cuvette with square...	Attenuator: 11

Results



α Gal Yariv in 25% (v/v) MeOH at 10 °C (run 3)

Size Distribution Report by Intensity

v2.2



Sample Details

Sample Name: BL-aGal-0.3mM25%meoh-10c-postheat1 1

SOP Name: mansettings.nano

General Notes:

File Name: Example Results.dts

Dispersant Name: Water MeOH 25%

Record Number: 163

Dispersant RI: 1.338

Material RI: 1.45

Viscosity (cP): 2.1408

Material Absorbtion: 0.001

Measurement Date and Time: Monday, October 24, 2016 2:...

System

Temperature (°C): 10.0

Duration Used (s): 70

Count Rate (kcps): 177.7

Measurement Position (mm): 4.65

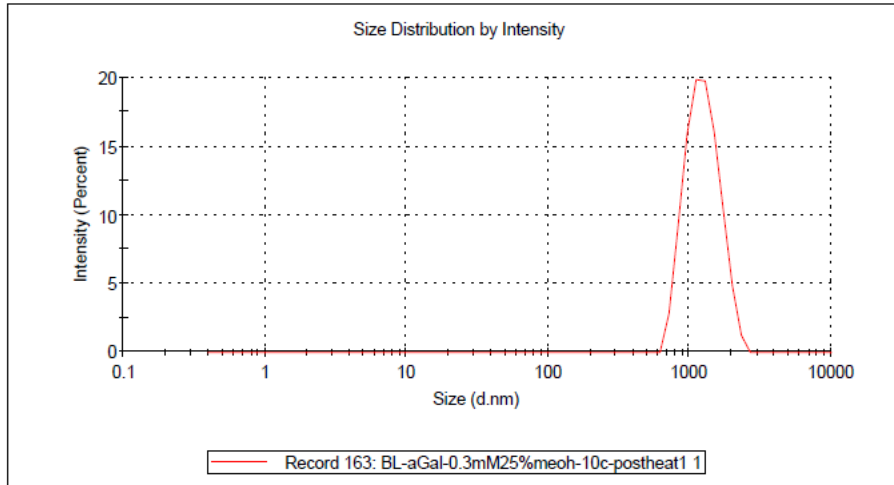
Cell Description: Glass cuvette with square apert...

Attenuator: 9

Results

	Size (d.nm):	% Intensity:	St Dev (d.n...)
Z-Average (d.nm): 1224	Peak 1: 1262	100.0	339.0
PdI: 0.180	Peak 2: 0.000	0.0	0.000
Intercept: 0.837	Peak 3: 0.000	0.0	0.000

Result quality : **Refer to quality report**



Correlogram Report

v2.0



Malvern Instruments Ltd - © Copyright 2008

Sample Details

Sample Name: BL-aGal-0.3mM25%meoh-10c-postheat1 1

SOP Name: mansettings.nano

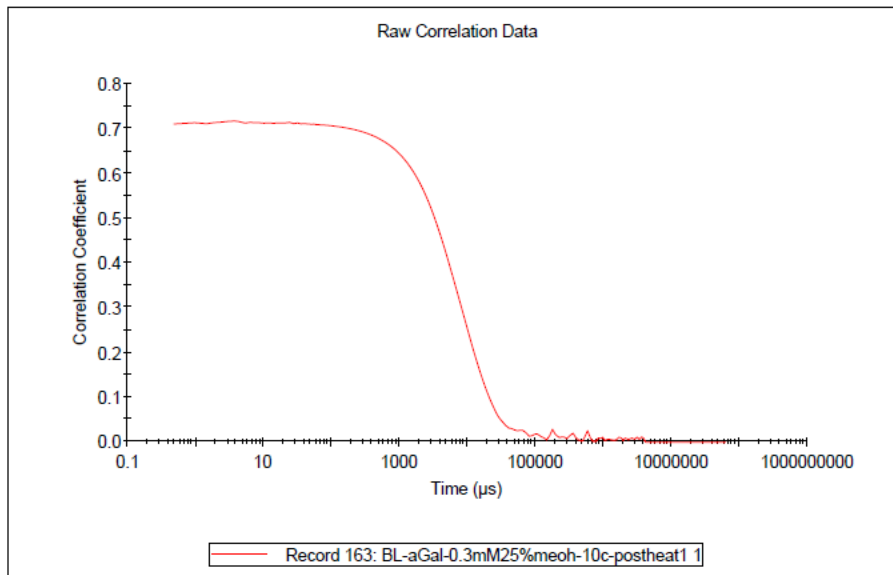
General Notes:

File Name: Example Results.dts	Dispersant Name: Water MeOH 25%
Record Number: 163	Dispersant RI: 1.338
Material RI: 1.45	Viscosity (cP): 2.1408
Material Absorbtion: 0.001	Measurement Date and Time: Monday, October 24, 2016 ...

System

Temperature (°C): 10.0	Duration Used (s): 70
Count Rate (kcps): 177.7	Measurement Position (mm): 4.65
Cell Description: Glass cuvette with square...	Attenuator: 9

Results



α Gal Yariv in 25% (v/v) MeOH at 60 °C (run 4)

Size Distribution Report by Intensity

v2.2



Sample Details

Sample Name: BL-aGal-0.3mM25%meoh-60c-cycle2 1

SOP Name: mansettings.nano

General Notes:

File Name: Example Results.dts	Dispersant Name: Water MeOH 25%
Record Number: 164	Dispersant RI: 1.338
Material RI: 1.45	Viscosity (cP): 1.2967
Material Absorbtion: 0.001	Measurement Date and Time: Monday, October 24, 2016 2:...

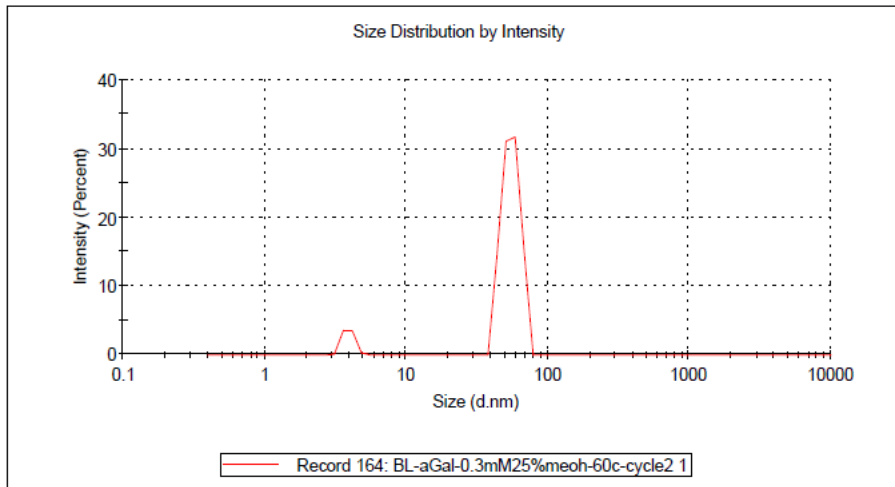
System

Temperature (°C): 60.0	Duration Used (s): 240
Count Rate (kcps): 14.4	Measurement Position (mm): 4.65
Cell Description: Glass cuvette with square apert...	Attenuator: 11

Results

	Size (d.nm):	% Intensity:	St Dev (d.n...)
Z-Average (d.nm): 328.6	Peak 1: 55.23	92.5	7.646
Pdi: 1.000	Peak 2: 3.929	7.5	0.3543
Intercept: 0.861	Peak 3: 0.000	0.0	0.000

Result quality : Refer to quality report



Correlogram Report

v2.0



Malvern Instruments Ltd - © Copyright 2008

Sample Details

Sample Name: BL-aGal-0.3mM25%meoh-60c-cycle2 1

SOP Name: mansettings.nano

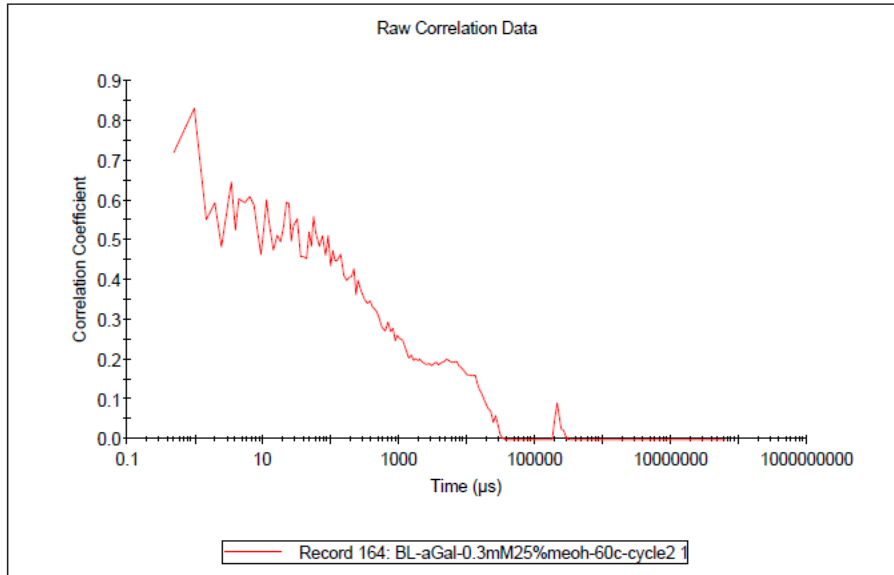
General Notes:

File Name: Example Results.dts	Dispersant Name: Water MeOH 25%
Record Number: 164	Dispersant RI: 1.338
Material RI: 1.45	Viscosity (cP): 1.2967
Material Absorbtion: 0.001	Measurement Date and Time: Monday, October 24, 2016 ...

System

Temperature (°C): 60.0	Duration Used (s): 240
Count Rate (kcps): 14.4	Measurement Position (mm): 4.65
Cell Description: Glass cuvette with square...	Attenuator: 11

Results



αGal Yariv in 25% (v/v) MeOH at 10 °C (run 5)

Size Distribution Report by Intensity

v2.2



Sample Details

Sample Name: BL-aGal-0.3mM25%meoh-10c-cycle2 1

SOP Name: mansettings.nano

General Notes:

File Name:	Example Results.dts	Dispersant Name:	Water MeOH 25%
Record Number:	165	Dispersant RI:	1.338
Material RI:	1.45	Viscosity (cP):	2.1408
Material Absorption:	0.001	Measurement Date and Time:	Monday, October 24, 2016 2:...

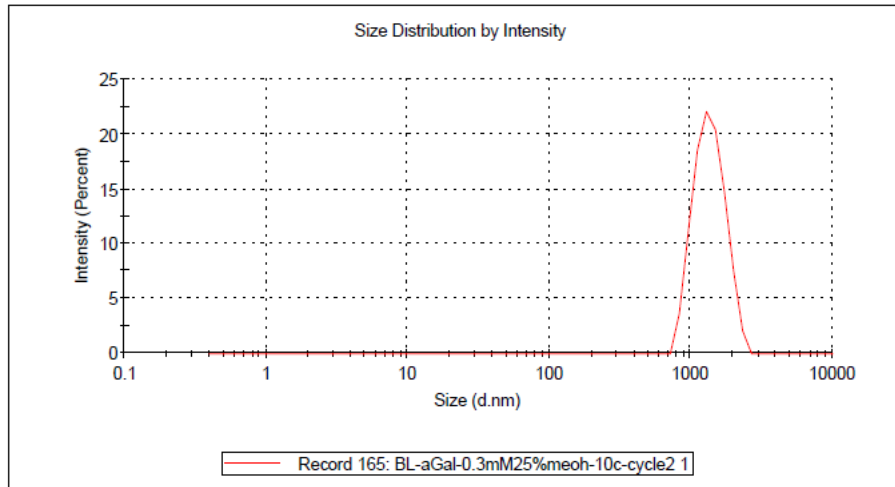
System

Temperature (°C):	10.0	Duration Used (s):	70
Count Rate (kcps):	189.7	Measurement Position (mm):	4.65
Cell Description:	Glass cuvette with square apert...	Attenuator:	9

Results

	Size (d.nm):	% Intensity:	St Dev (d.n...)
Z-Average (d.nm): 1282	Peak 1: 1376	100.0	335.2
Pdl: 0.105	Peak 2: 0.000	0.0	0.000
Intercept: 0.855	Peak 3: 0.000	0.0	0.000

Result quality : **Good**



Correlogram Report

v2.0



Malvern Instruments Ltd - © Copyright 2008

Sample Details

Sample Name: BL-aGal-0.3mM25%meoh-10c-cycle2 1

SOP Name: mansettings.nano

General Notes:

File Name: Example Results.dts

Dispersant Name: Water MeOH 25%

Record Number: 165

Dispersant RI: 1.338

Material RI: 1.45

Viscosity (cP): 2.1408

Material Absorbtion: 0.001

Measurement Date and Time: Monday, October 24, 2016 ...

System

Temperature (°C): 10.0

Duration Used (s): 70

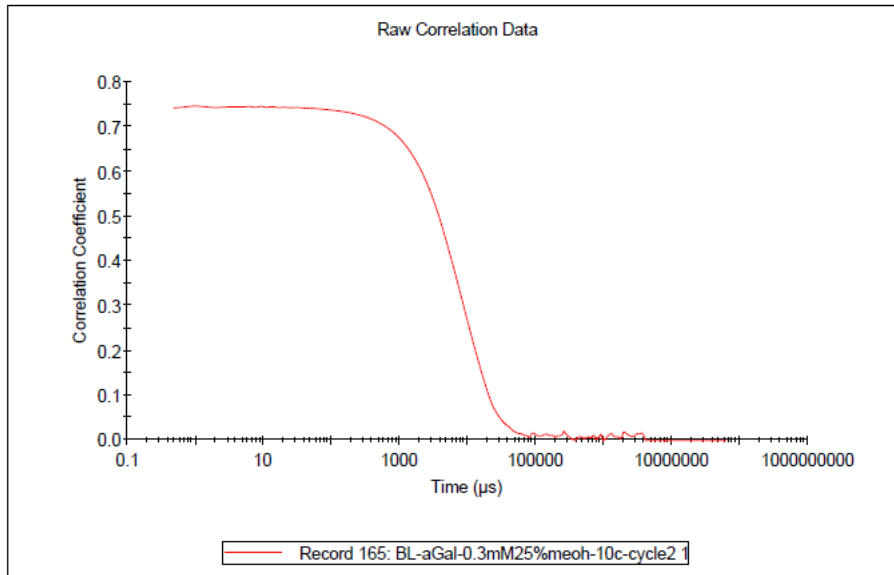
Count Rate (kcps): 189.7

Measurement Position (mm): 4.65

Cell Description: Glass cuvette with square...

Attenuator: 9

Results



α Gal Yariv in 5% (v/v) MeOH at 10 °C ($X = 0.02$)

Size Distribution Report by Intensity

v2.2



Sample Details

Sample Name: 052317aGal5% 1

SOP Name: mansettings.nano

General Notes:

File Name: bl.dts

Dispersant Name: Water-MeOH5%

Record Number: 7

Dispersant RI: 1.331

Material RI: 1.45

Viscosity (cP): 1.4468

Material Absorbtion: 0.001

Measurement Date and Time: Tuesday, May 23, 2017 3:21:...

System

Temperature (°C): 9.9

Duration Used (s): 250

Count Rate (kcps): 24.9

Measurement Position (mm): 4.65

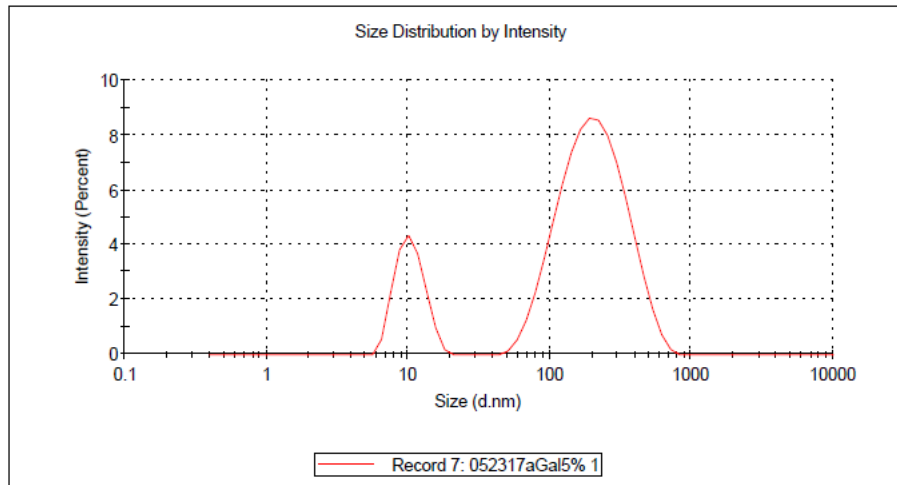
Cell Description: Glass cuvette with square apert...

Attenuator: 11

Results

	Size (d.nm):	% Intensity:	St Dev (d.n...)
Z-Average (d.nm): 53.51	Peak 1: 223.9	81.9	116.1
PdI: 1.000	Peak 2: 10.54	18.1	2.420
Intercept: 0.737	Peak 3: 0.000	0.0	0.000

Result quality : **Refer to quality report**



Correlogram Report

v2.0



Malvern Instruments Ltd - © Copyright 2008

Sample Details

Sample Name: 052317aGal5% 1

SOP Name: mansettings.nano

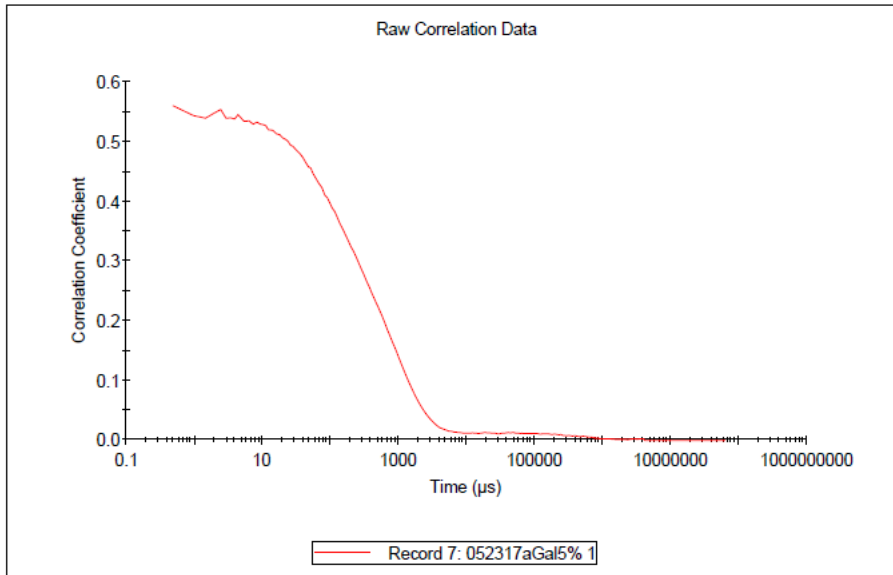
General Notes:

File Name:	bl.dts	Dispersant Name:	Water-MeOH5%
Record Number:	7	Dispersant RI:	1.331
Material RI:	1.45	Viscosity (cP):	1.4468
Material Absorbtion:	0.001	Measurement Date and Time:	Tuesday, May 23, 2017 3:2...

System

Temperature (°C):	9.9	Duration Used (s):	250
Count Rate (kcps):	24.9	Measurement Position (mm):	4.65
Cell Description:	Glass cuvette with square...	Attenuator:	11

Results



α Gal Yariv in 15% (v/v) MeOH at 10 °C ($X = 0.07$)

Size Distribution Report by Intensity

v2.2



Sample Details

Sample Name: 052317aGal15% 1

SOP Name: mansettings.nano

General Notes:

File Name:	bl.dts	Dispersant Name:	15% MeOH
Record Number:	8	Dispersant RI:	1.333
Material RI:	1.45	Viscosity (cP):	1.7042
Material Absorbtion:	0.001	Measurement Date and Time:	Tuesday, May 23, 2017 3:34:...

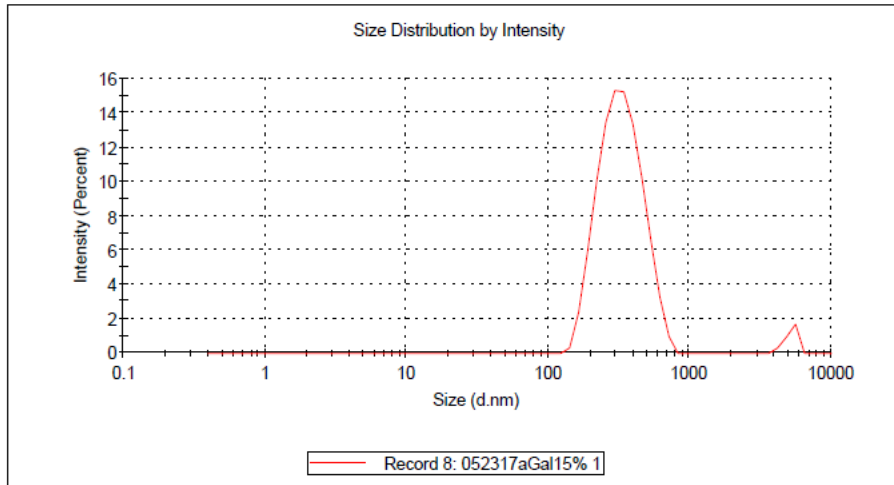
System

Temperature (°C):	9.9	Duration Used (s):	210
Count Rate (kcps):	428.1	Measurement Position (mm):	4.65
Cell Description:	Glass cuvette with square apert...	Attenuator:	11

Results

	Size (d.nm):	% Intensity:	St Dev (d.n...)
Z-Average (d.nm): 311.1	Peak 1: 340.9	97.0	115.8
PdI: 0.302	Peak 2: 5163	3.0	493.5
Intercept: 0.779	Peak 3: 0.000	0.0	0.000

Result quality : **Refer to quality report**



Correlogram Report

v2.0



Malvern Instruments Ltd - © Copyright 2008

Sample Details

Sample Name: 052317aGal15% 1

SOP Name: mansettings.nano

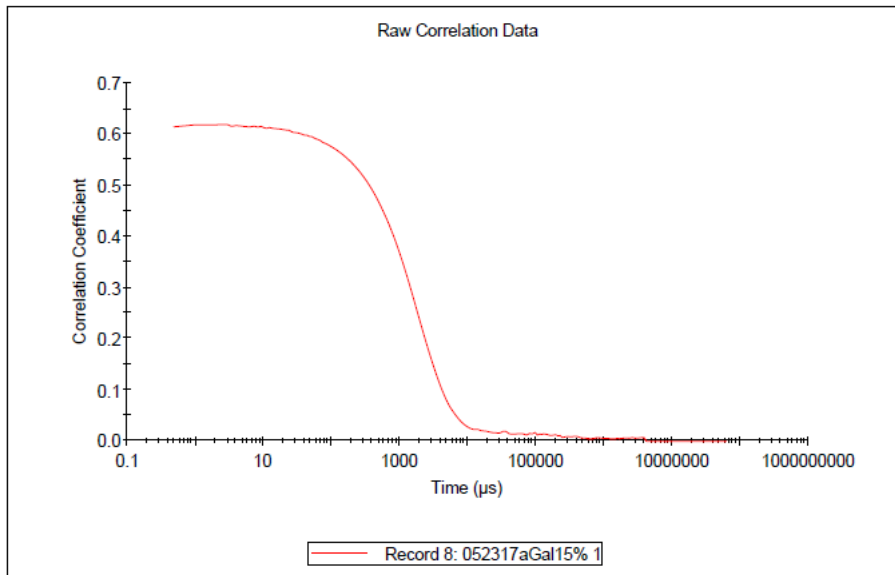
General Notes:

File Name: bl.dts	Dispersant Name: 15% MeOH
Record Number: 8	Dispersant RI: 1.333
Material RI: 1.45	Viscosity (cP): 1.7042
Material Absorbtion: 0.001	Measurement Date and Time: Tuesday, May 23, 2017 3:3...

System

Temperature (°C): 9.9	Duration Used (s): 210
Count Rate (kcps): 428.1	Measurement Position (mm): 4.65
Cell Description: Glass cuvette with square...	Attenuator: 11

Results



α Gal Yariv in 25% (v/v) MeOH at 10 °C ($X = 0.13$)

Size Distribution Report by Intensity

v2.2



Sample Details

Sample Name: 052317aGal25% 1

SOP Name: mansettings.nano

General Notes:

File Name: bl.dts	Dispersant Name: Water MeOH 25%
Record Number: 9	Dispersant RI: 1.338
Material RI: 1.45	Viscosity (cP): 2.1408
Material Absorbtion: 0.001	Measurement Date and Time: Tuesday, May 23, 2017 3:42:...

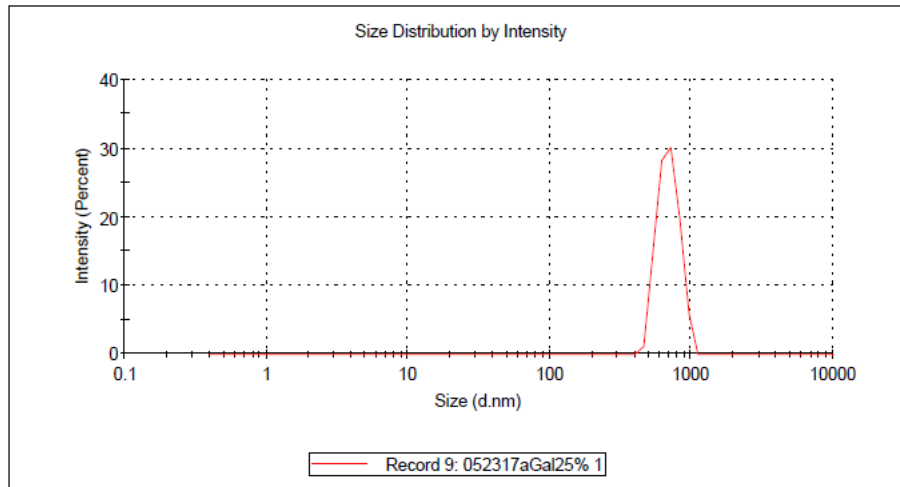
System

Temperature (°C): 10.0	Duration Used (s): 70
Count Rate (kcps): 168.0	Measurement Position (mm): 4.65
Cell Description: Glass cuvette with square apert...	Attenuator: 10

Results

	Size (d.nm):	% Intensity:	St Dev (d.n...)
Z-Average (d.nm): 712.2	Peak 1: 692.1	100.0	118.0
PdI: 0.391	Peak 2: 0.000	0.0	0.000
Intercept: 0.726	Peak 3: 0.000	0.0	0.000

Result quality : **Refer to quality report**



Correlogram Report

v2.0



Malvern Instruments Ltd - © Copyright 2008

Sample Details

Sample Name: 052317aGal25% 1

SOP Name: mansettings.nano

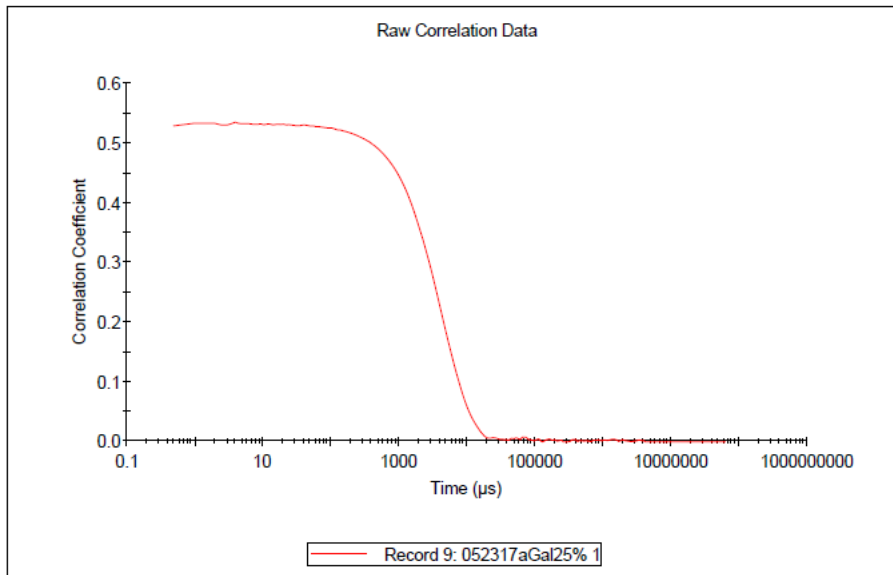
General Notes:

File Name: bl.dts	Dispersant Name: Water MeOH 25%
Record Number: 9	Dispersant RI: 1.338
Material RI: 1.45	Viscosity (cP): 2.1408
Material Absorbtion: 0.001	Measurement Date and Time: Tuesday, May 23, 2017 3:4...

System

Temperature (°C): 10.0	Duration Used (s): 70
Count Rate (kcps): 168.0	Measurement Position (mm): 4.65
Cell Description: Glass cuvette with square...	Attenuator: 10

Results



α Gal Yariv in 30% (v/v) MeOH at 10 °C ($X = 0.16$)

Size Distribution Report by Intensity

v2.2



Sample Details

Sample Name: 052317aGal30% 1

SOP Name: mansettings.nano

General Notes:

File Name:	bl.dts	Dispersant Name:	30%MeOH
Record Number:	10	Dispersant RI:	1.336
Material RI:	1.45	Viscosity (cP):	2.0237
Material Absorbtion:	0.001	Measurement Date and Time:	Tuesday, May 23, 2017 3:49:...

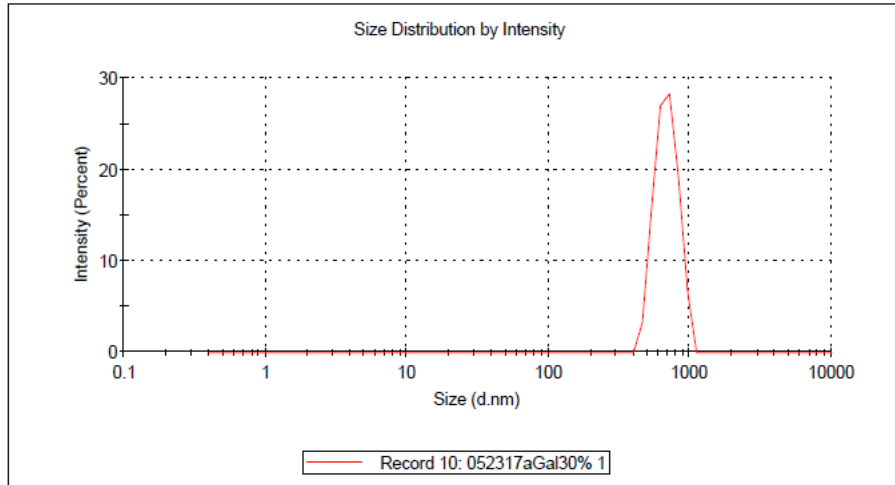
System

Temperature (°C):	10.0	Duration Used (s):	60
Count Rate (kcps):	216.2	Measurement Position (mm):	4.65
Cell Description:	Glass cuvette with square apert...	Attenuator:	10

Results

	Size (d.nm):	% Intensity:	St Dev (d.n...)
Z-Average (d.nm): 674.0	Peak 1: 687.2	100.0	124.9
PdI: 0.082	Peak 2: 0.000	0.0	0.000
Intercept: 0.763	Peak 3: 0.000	0.0	0.000

Result quality : **Good**



Correlogram Report

v2.0



Malvern Instruments Ltd - © Copyright 2008

Sample Details

Sample Name: 052317aGal30% 1

SOP Name: mansettings.nano

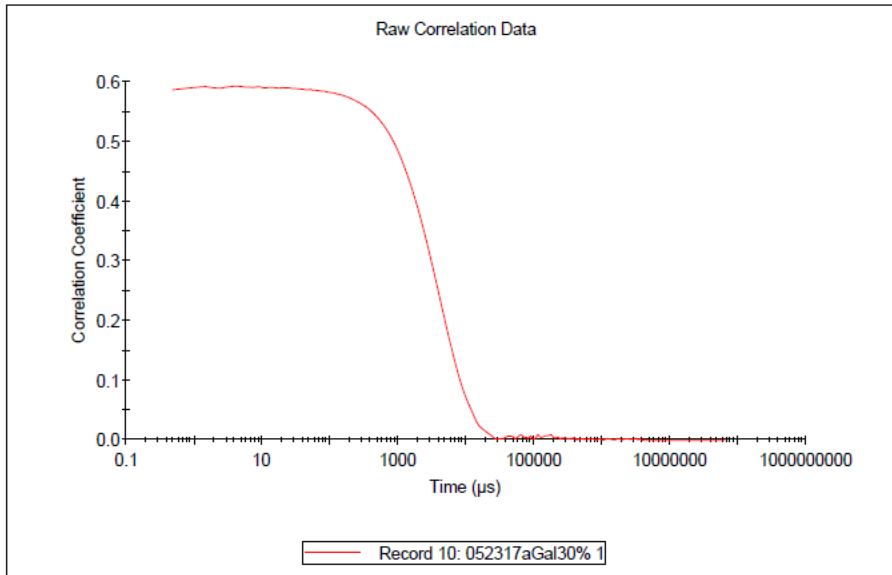
General Notes:

File Name: bl.dts	Dispersant Name: 30%MeOH
Record Number: 10	Dispersant RI: 1.336
Material RI: 1.45	Viscosity (cP): 2.0237
Material Absorbtion: 0.001	Measurement Date and Time: Tuesday, May 23, 2017 3:4...

System

Temperature (°C): 10.0	Duration Used (s): 60
Count Rate (kcps): 216.2	Measurement Position (mm): 4.65
Cell Description: Glass cuvette with square...	Attenuator: 10

Results



α Gal Yariv in 35% (v/v) MeOH at 10 °C ($X = 0.19$)

Size Distribution Report by Intensity

v2.2



Sample Details

Sample Name: 052317aGal35% 1

SOP Name: mansettings.nano

General Notes:

File Name:	bl.dts	Dispersant Name:	35% MeOH
Record Number:	11	Dispersant RI:	1.337
Material RI:	1.45	Viscosity (cP):	2.0952
Material Absorption:	0.001	Measurement Date and Time:	Tuesday, May 23, 2017 3:57:...

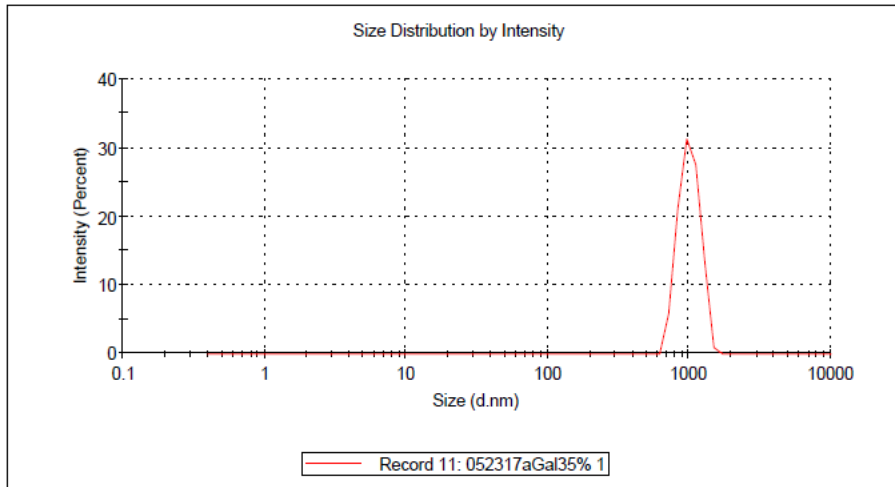
System

Temperature (°C):	10.0	Duration Used (s):	70
Count Rate (kcps):	145.3	Measurement Position (mm):	4.65
Cell Description:	Glass cuvette with square apert...	Attenuator:	10

Results

	Size (d.nm):	% Intensity:	St Dev (d.n...)
Z-Average (d.nm): 1112	Peak 1: 1004	100.0	166.8
PdI: 1.000	Peak 2: 0.000	0.0	0.000
Intercept: 0.694	Peak 3: 0.000	0.0	0.000

Result quality : **Refer to quality report**



Correlogram Report

v2.0



Malvern Instruments Ltd - © Copyright 2008

Sample Details

Sample Name: 052317aGal35% 1

SOP Name: mansettings.nano

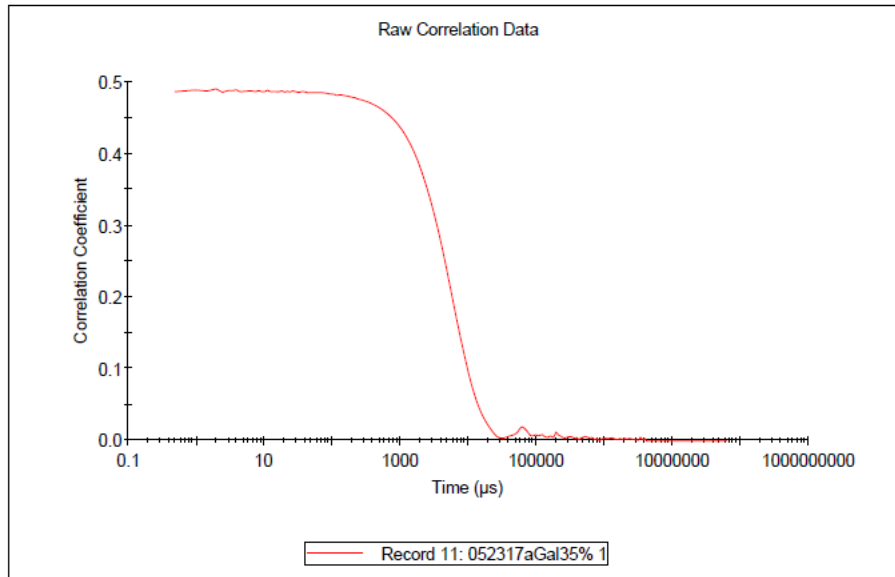
General Notes:

File Name: bl.dts	Dispersant Name: 35% MeOH
Record Number: 11	Dispersant RI: 1.337
Material RI: 1.45	Viscosity (cP): 2.0952
Material Absorbion: 0.001	Measurement Date and Time: Tuesday, May 23, 2017 3:5...

System

Temperature (°C): 10.0	Duration Used (s): 70
Count Rate (kcps): 145.3	Measurement Position (mm): 4.65
Cell Description: Glass cuvette with square...	Attenuator: 10

Results



α Gal Yariv in 50% (v/v) MeOH at 10 °C ($X = 0.31$)

Size Distribution Report by Intensity

v2.2



Sample Details

Sample Name: 052317aGal50% 1

SOP Name: mansettings.nano

General Notes:

File Name:	bl.dts	Dispersant Name:	50%MeOH
Record Number:	12	Dispersant RI:	1.340
Material RI:	1.45	Viscosity (cP):	2.1437
Material Absorbtion:	0.001	Measurement Date and Time:	Tuesday, May 23, 2017 4:05:...

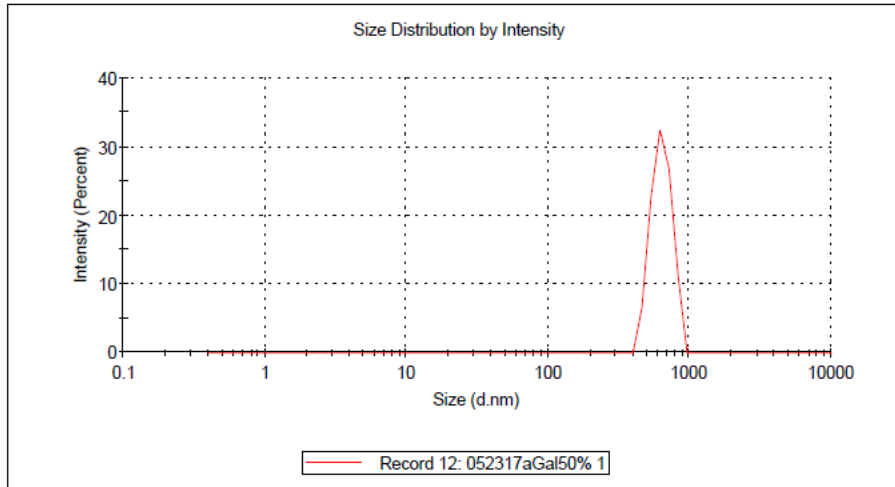
System

Temperature (°C):	10.0	Duration Used (s):	80
Count Rate (kcps):	131.1	Measurement Position (mm):	4.65
Cell Description:	Glass cuvette with square apert...	Attenuator:	10

Results

	Size (d.nm):	% Intensity:	St Dev (d.n...)
Z-Average (d.nm): 708.3	Peak 1: 635.5	100.0	101.7
Pdl: 1.000	Peak 2: 0.000	0.0	0.000
Intercept: 0.715	Peak 3: 0.000	0.0	0.000

Result quality : **Refer to quality report**



Correlogram Report

v2.0



Malvern Instruments Ltd - © Copyright 2008

Sample Details

Sample Name: 052317aGal50% 1

SOP Name: mansettings.nano

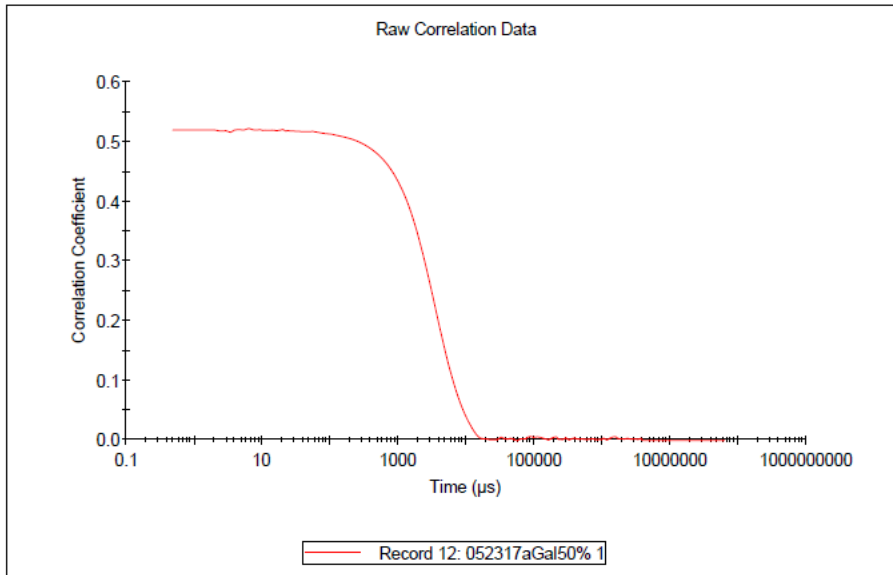
General Notes:

File Name:	bl.dts	Dispersant Name:	50%MeOH
Record Number:	12	Dispersant RI:	1.340
Material RI:	1.45	Viscosity (cP):	2.1437
Material Absorbtion:	0.001	Measurement Date and Time:	Tuesday, May 23, 2017 4:0...

System

Temperature (°C):	10.0	Duration Used (s):	80
Count Rate (kcps):	131.1	Measurement Position (mm):	4.65
Cell Description:	Glass cuvette with square...	Attenuator:	10

Results



α Gal Yariv in 5% (v/v) EtOH at 10 °C ($X = 0.02$)

Size Distribution Report by Intensity

v2.2



Sample Details

Sample Name: 052317aGal5%EtOH 1

SOP Name: mansettings.nano

General Notes:

File Name:	bl.dts	Dispersant Name:	5% EtOH
Record Number:	13	Dispersant RI:	1.332
Material RI:	1.45	Viscosity (cP):	1.4888
Material Absorbtion:	0.001	Measurement Date and Time:	Friday, June 02, 2017 11:28:...

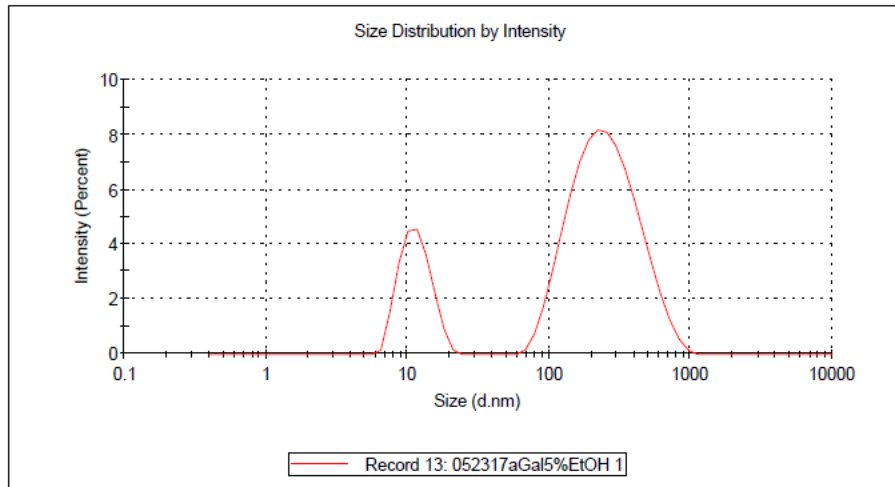
System

Temperature (°C):	10.0	Duration Used (s):	280
Count Rate (kcps):	23.5	Measurement Position (mm):	4.65
Cell Description:	Glass cuvette with square apert...	Attenuator:	11

Results

	Size (d.nm):	% Intensity:	St Dev (d.n...)
Z-Average (d.nm): 53.81	Peak 1: 276.6	79.0	150.3
Pd: 1.000	Peak 2: 11.64	21.0	2.872
Intercept: 0.690	Peak 3: 0.000	0.0	0.000

Result quality : **Refer to quality report**



Correlogram Report

v2.0



Malvern Instruments Ltd - © Copyright 2008

Sample Details

Sample Name: 052317aGal5%EtOH 1

SOP Name: mansettings.nano

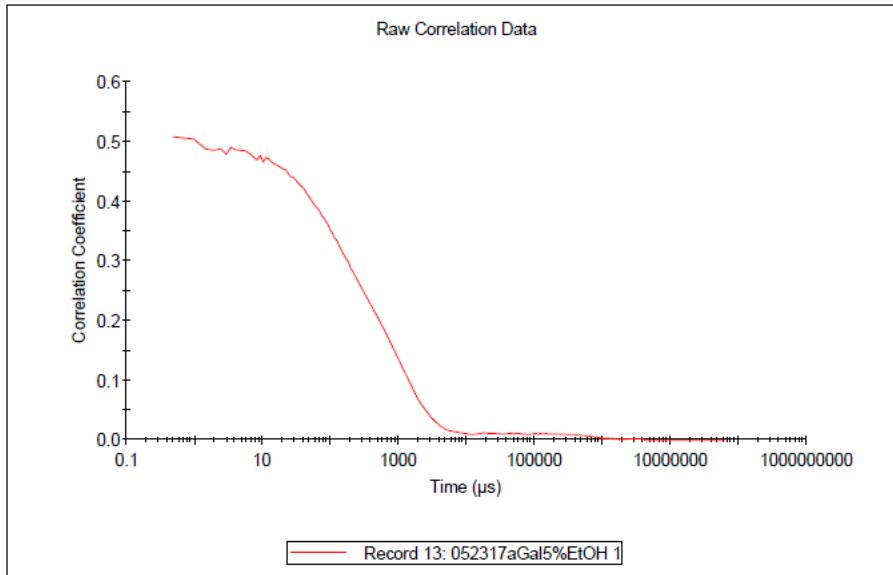
General Notes:

File Name: bl.dts	Dispersant Name: 5% EtOH
Record Number: 13	Dispersant RI: 1.332
Material RI: 1.45	Viscosity (cP): 1.4888
Material Absorbtion: 0.001	Measurement Date and Time: Friday, June 02, 2017 11:2...

System

Temperature (°C): 10.0	Duration Used (s): 280
Count Rate (kcps): 23.5	Measurement Position (mm): 4.65
Cell Description: Glass cuvette with square...	Attenuator: 11

Results



α Gal Yariv in 10% (v/v) EtOH at 10 °C ($X = 0.03$)

Size Distribution Report by Intensity

v2.2



Sample Details

Sample Name: 052317aGal10%EtOH 1

SOP Name: mansettings.nano

General Notes:

File Name:	bl.dts	Dispersant Name:	10%EtOH
Record Number:	14	Dispersant RI:	1.335
Material RI:	1.45	Viscosity (cP):	1.7019
Material Absorbtion:	0.001	Measurement Date and Time:	Friday, June 02, 2017 11:43:...

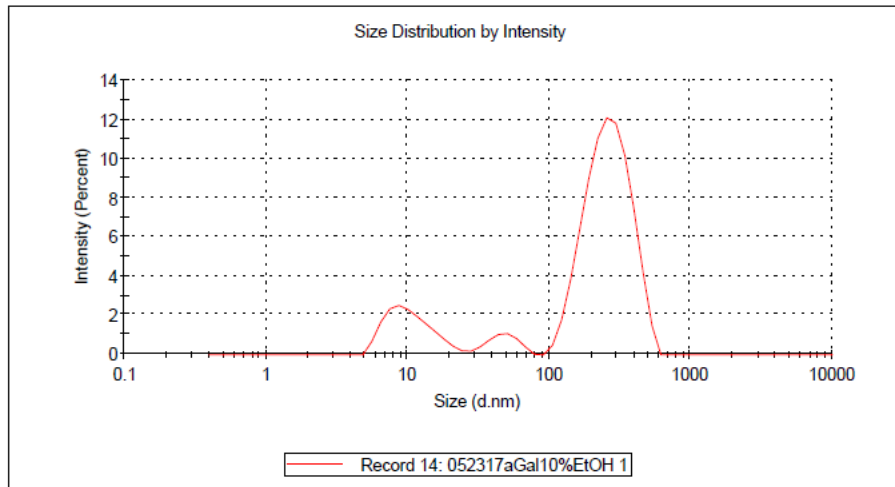
System

Temperature (°C):	10.0	Duration Used (s):	210
Count Rate (kcps):	44.1	Measurement Position (mm):	4.65
Cell Description:	Glass cuvette with square apert...	Attenuator:	11

Results

	Size (d.nm):	% Intensity:	St Dev (d.n...)
Z-Average (d.nm): 303.7	Peak 1: 272.5	79.4	93.98
Pd: 0.813	Peak 2: 11.01	15.9	4.447
Intercept: 0.817	Peak 3: 47.80	4.7	10.94

Result quality : **Refer to quality report**



Correlogram Report

v2.0



Malvern Instruments Ltd - © Copyright 2008

Sample Details

Sample Name: 052317aGal10%EtOH 1

SOP Name: mansettings.nano

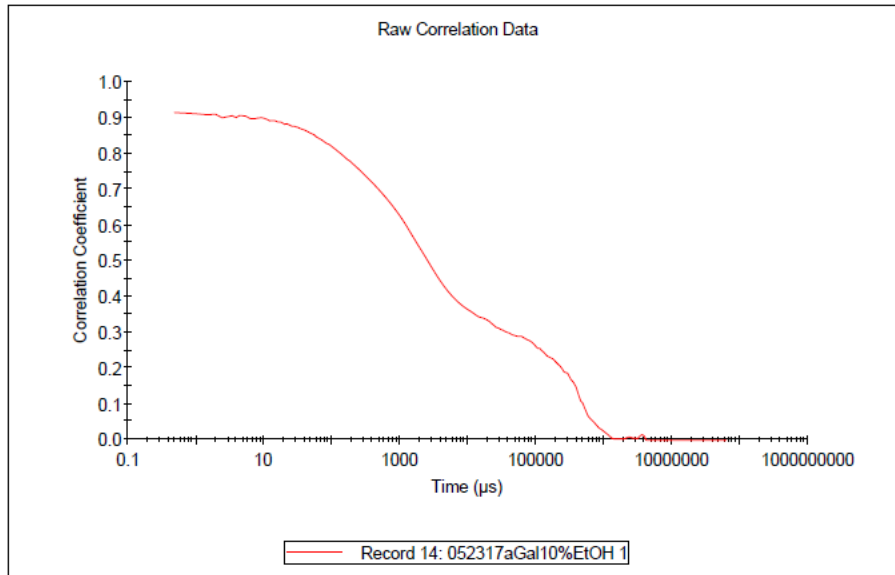
General Notes:

File Name: bl.dts	Dispersant Name: 10%EtOH
Record Number: 14	Dispersant RI: 1.335
Material RI: 1.45	Viscosity (cP): 1.7019
Material Absorbtion: 0.001	Measurement Date and Time: Friday, June 02, 2017 11:4...

System

Temperature (°C): 10.0	Duration Used (s): 210
Count Rate (kcps): 44.1	Measurement Position (mm): 4.65
Cell Description: Glass cuvette with square...	Attenuator: 11

Results



α Gal Yariv in 15% (v/v) EtOH at 10 °C ($X = 0.05$)

Size Distribution Report by Intensity

v2.2



Sample Details

Sample Name: 052317aGal15%EtOH 1

SOP Name: mansettings.nano

General Notes:

File Name:	bl.dts	Dispersant Name:	15% EtOH
Record Number:	15	Dispersant RI:	1.338
Material RI:	1.45	Viscosity (cP):	1.9505
Material Absorption:	0.001	Measurement Date and Time:	Friday, June 02, 2017 11:51:...

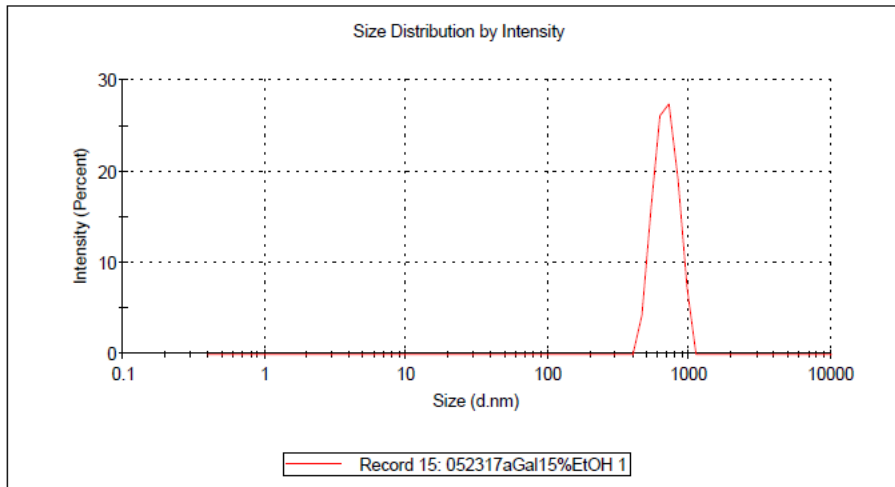
System

Temperature (°C):	10.0	Duration Used (s):	60
Count Rate (kcps):	291.2	Measurement Position (mm):	4.65
Cell Description:	Glass cuvette with square apert...	Attenuator:	10

Results

	Size (d.nm):	% Intensity:	St Dev (d.n...)
Z-Average (d.nm): 686.7	Peak 1: 686.8	100.0	128.6
PdI: 0.182	Peak 2: 0.000	0.0	0.000
Intercept: 0.761	Peak 3: 0.000	0.0	0.000

Result quality : **Good**



Correlogram Report

v2.0



Malvern Instruments Ltd - © Copyright 2008

Sample Details

Sample Name: 052317aGal15%EtOH 1

SOP Name: mansettings.nano

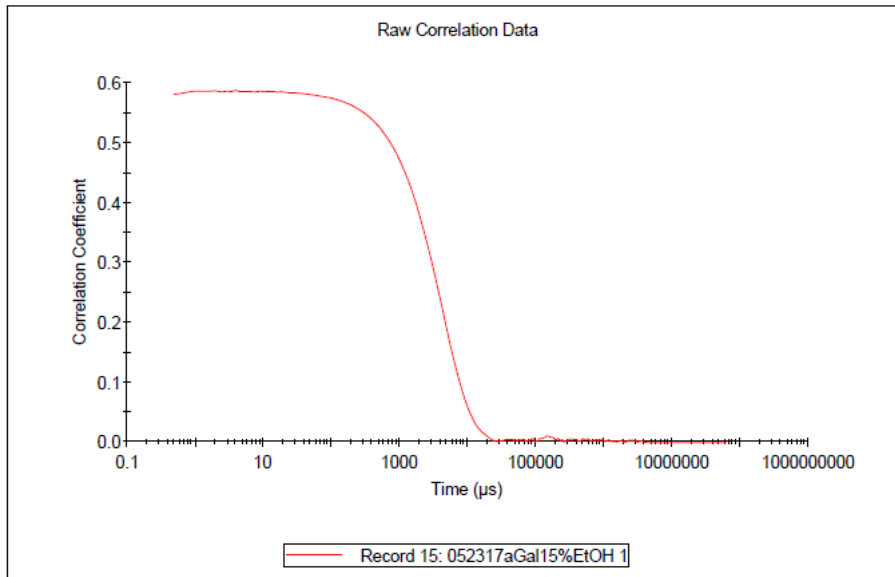
General Notes:

File Name: bl.dts	Dispersant Name: 15% EtOH
Record Number: 15	Dispersant RI: 1.338
Material RI: 1.45	Viscosity (cP): 1.9505
Material Absorbtion: 0.001	Measurement Date and Time: Friday, June 02, 2017 11:5...

System

Temperature (°C): 10.0	Duration Used (s): 60
Count Rate (kcps): 291.2	Measurement Position (mm): 4.65
Cell Description: Glass cuvette with square...	Attenuator: 10

Results



α Gal Yariv in 20% (v/v) EtOH at 10 °C ($X = 0.07$)

Size Distribution Report by Intensity

v2.2



Sample Details

Sample Name: 052317aGal20%EtOH 1

SOP Name: mansettings.nano

General Notes:

File Name:	bl.dts	Dispersant Name:	20% EtOH
Record Number:	16	Dispersant RI:	1.341
Material RI:	1.45	Viscosity (cP):	2.2158
Material Absorption:	0.001	Measurement Date and Time:	Friday, June 02, 2017 11:59:...

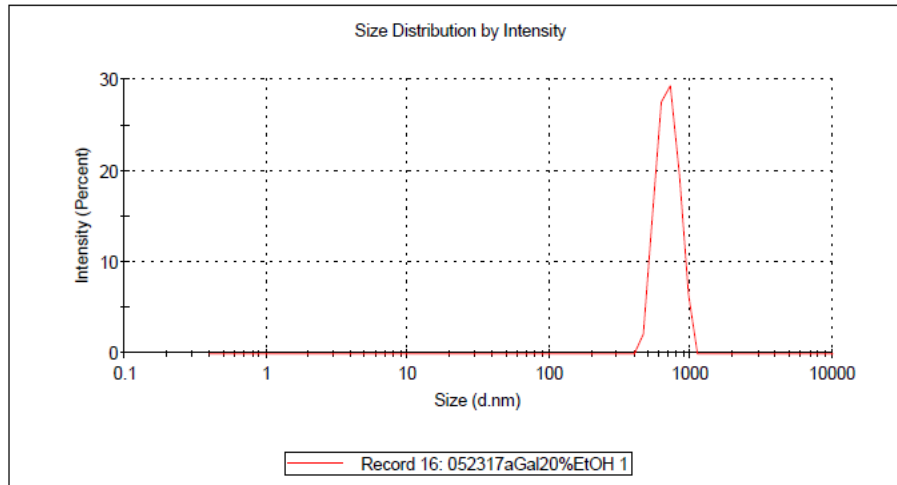
System

Temperature (°C):	10.0	Duration Used (s):	60
Count Rate (kcps):	278.4	Measurement Position (mm):	4.65
Cell Description:	Glass cuvette with square apert...	Attenuator:	10

Results

	Size (d.nm):	% Intensity:	St Dev (d.n...)
Z-Average (d.nm): 687.7	Peak 1: 690.9	100.0	121.6
PdI: 0.171	Peak 2: 0.000	0.0	0.000
Intercept: 0.773	Peak 3: 0.000	0.0	0.000

Result quality : **Good**



Correlogram Report

v2.0



Malvern Instruments Ltd - © Copyright 2008

Sample Details

Sample Name: 052317aGal20%EtOH 1

SOP Name: mansettings.nano

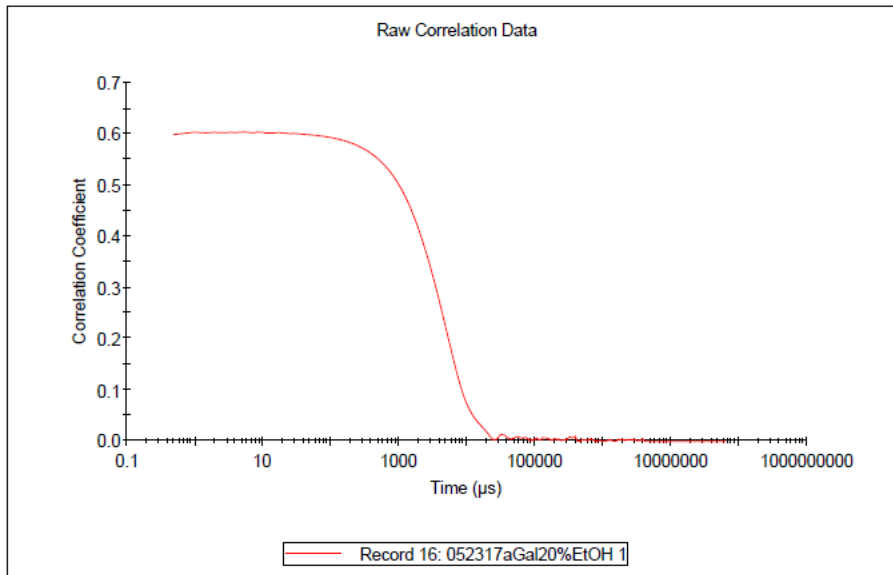
General Notes:

File Name: bl.dts	Dispersant Name: 20% EtOH
Record Number: 16	Dispersant RI: 1.341
Material RI: 1.45	Viscosity (cP): 2.2158
Material Absorbtion: 0.001	Measurement Date and Time: Friday, June 02, 2017 11:5...

System

Temperature (°C): 10.0	Duration Used (s): 60
Count Rate (kcps): 278.4	Measurement Position (mm): 4.65
Cell Description: Glass cuvette with square...	Attenuator: 10

Results



α Gal Yariv in 25% (v/v) EtOH at 10 °C ($X = 0.09$)

Size Distribution Report by Intensity

v2.2



Sample Details

Sample Name: 052317aGal25%EtOH 1

SOP Name: mansettings.nano

General Notes:

File Name:	bl.dts	Dispersant Name:	EtOH25%
Record Number:	17	Dispersant RI:	1.344
Material RI:	1.45	Viscosity (cP):	2.4791
Material Absorption:	0.001	Measurement Date and Time:	Friday, June 02, 2017 12:07:...

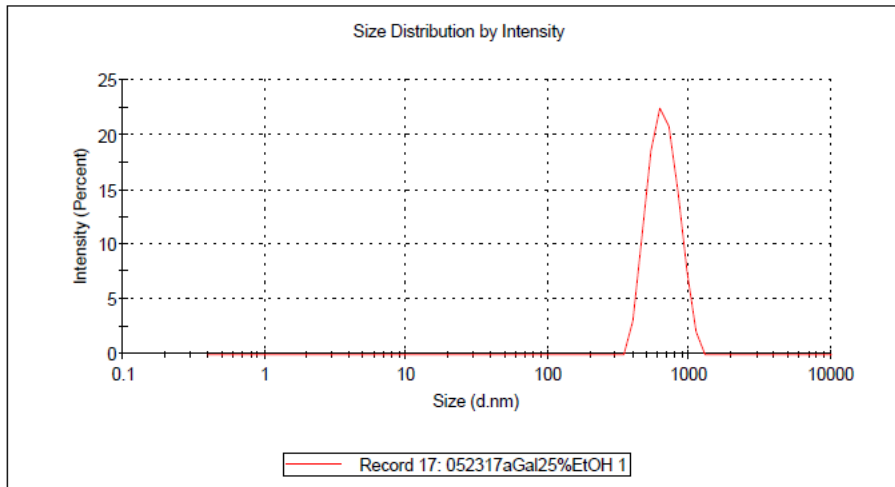
System

Temperature (°C):	10.0	Duration Used (s):	70
Count Rate (kcps):	132.3	Measurement Position (mm):	4.65
Cell Description:	Glass cuvette with square apert...	Attenuator:	9

Results

	Size (d.nm):	% Intensity:	St Dev (d.n...)
Z-Average (d.nm): 667.6	Peak 1: 663.5	100.0	159.5
PdI: 0.244	Peak 2: 0.000	0.0	0.000
Intercept: 0.784	Peak 3: 0.000	0.0	0.000

Result quality : **Good**



Correlogram Report

v2.0



Malvern Instruments Ltd - © Copyright 2008

Sample Details

Sample Name: 052317aGal25%EtOH 1

SOP Name: mansettings.nano

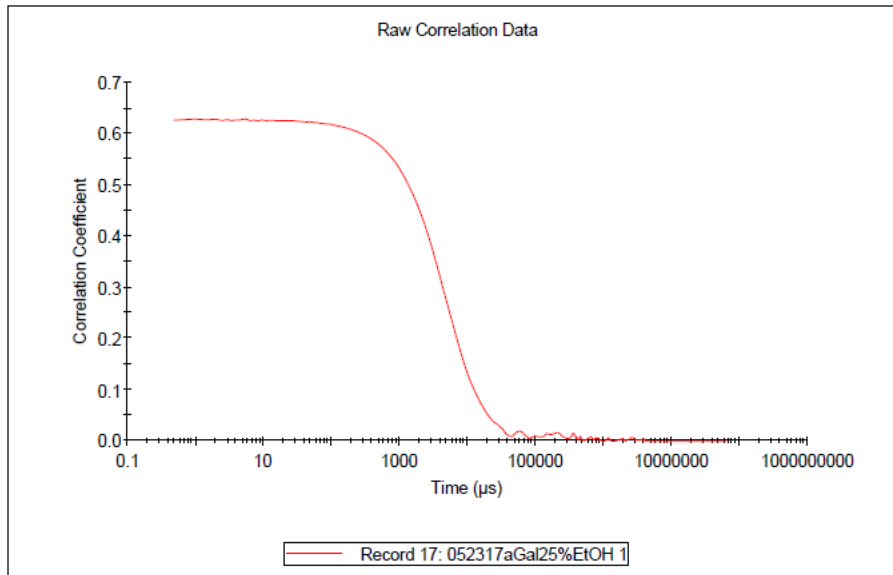
General Notes:

File Name:	bl.dts	Dispersant Name:	EtOH25%
Record Number:	17	Dispersant RI:	1.344
Material RI:	1.45	Viscosity (cP):	2.4791
Material Absorbtion:	0.001	Measurement Date and Time:	Friday, June 02, 2017 12:0...

System

Temperature (°C):	10.0	Duration Used (s):	70
Count Rate (kcps):	132.3	Measurement Position (mm):	4.65
Cell Description:	Glass cuvette with square...	Attenuator:	9

Results



α Gal Yariv in 50% (v/v) EtOH at 10 °C ($X = 0.24$)

Size Distribution Report by Intensity

v2.2



Sample Details

Sample Name: 052317aGal50%EtOH 1

SOP Name: mansettings.nano

General Notes:

File Name: bl.dts	Dispersant Name: 50% EtOH
Record Number: 18	Dispersant RI: 1.356
Material RI: 1.45	Viscosity (cP): 3.1131
Material Absorption: 0.001	Measurement Date and Time: Friday, June 02, 2017 12:15:...

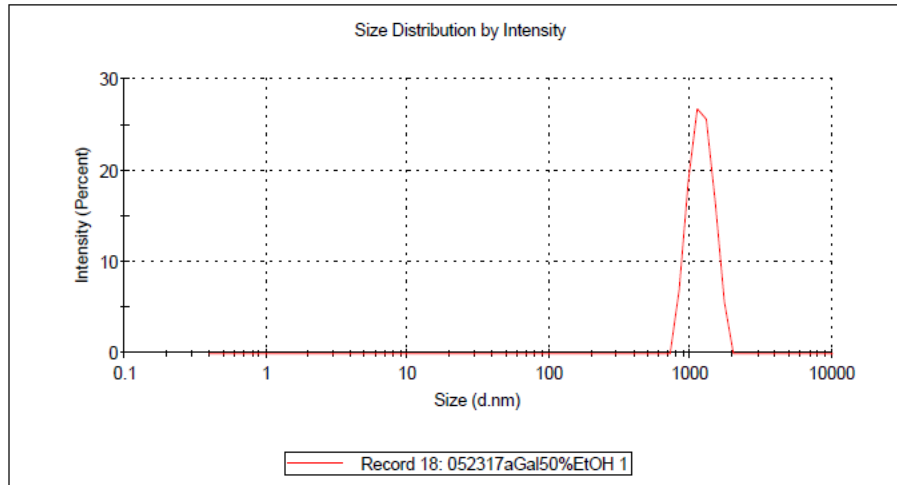
System

Temperature (°C): 10.0	Duration Used (s): 60
Count Rate (kcps): 341.6	Measurement Position (mm): 4.65
Cell Description: Glass cuvette with square apert...	Attenuator: 10

Results

	Size (d.nm):	% Intensity:	St Dev (d.n...)
Z-Average (d.nm): 1174	Peak 1: 1200	100.0	231.2
PdI: 0.062	Peak 2: 0.000	0.0	0.000
Intercept: 0.795	Peak 3: 0.000	0.0	0.000

Result quality : **Refer to quality report**



Correlogram Report

v2.0



Malvern Instruments Ltd - © Copyright 2008

Sample Details

Sample Name: 052317aGal50%EtOH 1

SOP Name: mansettings.nano

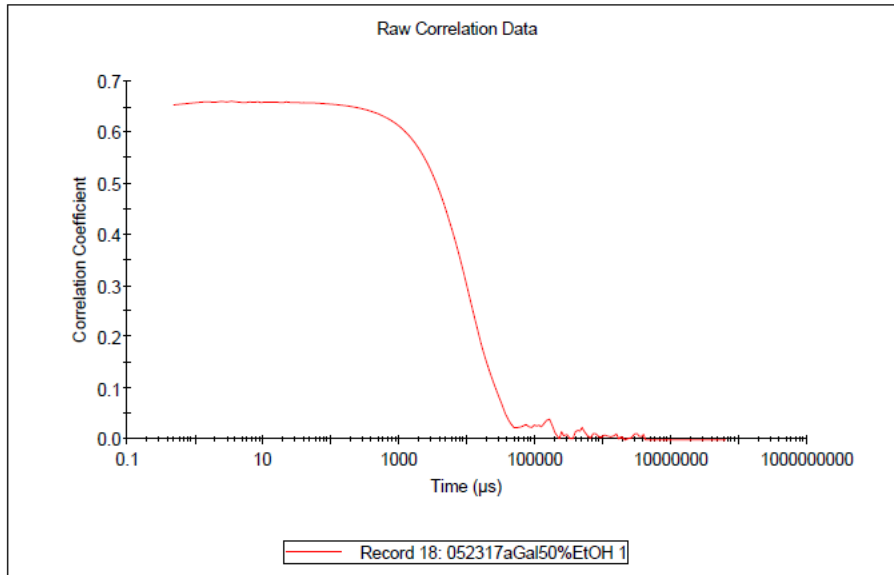
General Notes:

File Name: bl.dts	Dispersant Name: 50% EtOH
Record Number: 18	Dispersant RI: 1.356
Material RI: 1.45	Viscosity (cP): 3.1131
Material Absorbtion: 0.001	Measurement Date and Time: Friday, June 02, 2017 12:1...

System

Temperature (°C): 10.0	Duration Used (s): 60
Count Rate (kcps): 341.6	Measurement Position (mm): 4.65
Cell Description: Glass cuvette with square...	Attenuator: 10

Results



α Gal Yariv in 5% (v/v) iPrOH at 10 °C ($X = 0.01$)

Size Distribution Report by Intensity

v2.2



Sample Details

Sample Name: aGal5%IPA 1

SOP Name: mansettings.nano

General Notes:

File Name:	bl.dts	Dispersant Name:	5% IPA
Record Number:	19	Dispersant RI:	1.333
Material RI:	1.45	Viscosity (cP):	1.5248
Material Absorbtion:	0.001	Measurement Date and Time:	Tuesday, June 06, 2017 4:08:...

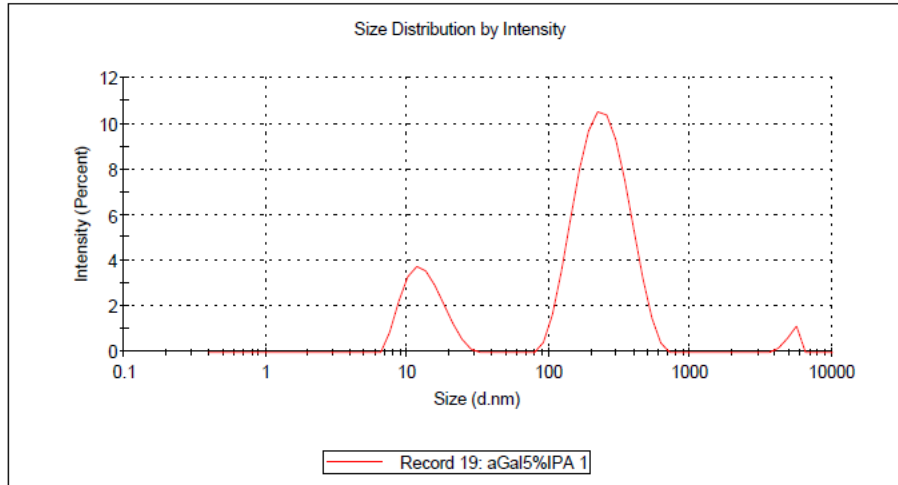
System

Temperature (°C):	9.9	Duration Used (s):	220
Count Rate (kcps):	26.9	Measurement Position (mm):	4.65
Cell Description:	Glass cuvette with square apert...	Attenuator:	11

Results

	Size (d.nm):	% Intensity:	St Dev (d.n...)
Z-Average (d.nm): 75.14	Peak 1: 252.9	77.3	100.8
Pdl: 0.996	Peak 2: 13.52	20.8	4.199
Intercept: 0.727	Peak 3: 5183	2.0	483.8

Result quality : **Refer to quality report**



Correlogram Report

v2.0



Malvern Instruments Ltd - © Copyright 2008

Sample Details

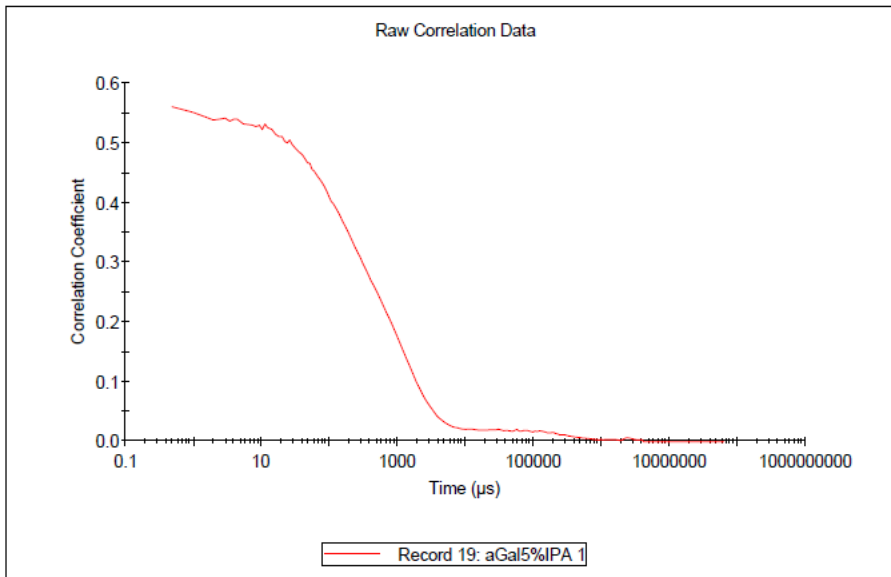
Sample Name: aGal5%IPA 1
SOP Name: mansettings.nano
General Notes:

File Name: bl.dts	Dispersant Name: 5% IPA
Record Number: 19	Dispersant RI: 1.333
Material RI: 1.45	Viscosity (cP): 1.5248
Material Absorbtion: 0.001	Measurement Date and Time: Tuesday, June 06, 2017 4:...

System

Temperature (°C): 9.9	Duration Used (s): 220
Count Rate (kcps): 26.9	Measurement Position (mm): 4.65
Cell Description: Glass cuvette with square...	Attenuator: 11

Results



α Gal Yariv in 7.5% (v/v) iPrOH at 10 °C ($X = 0.02$)

Size Distribution Report by Intensity

v2.2



Sample Details

Sample Name: aGal7.5%IPA 1
SOP Name: mansettings.nano
General Notes:

File Name: bl.dts	Dispersant Name: 7.5% IPA
Record Number: 20	Dispersant RI: 1.335
Material RI: 1.45	Viscosity (cP): 1.6530
Material Absorbtion: 0.001	Measurement Date and Time: Tuesday, June 06, 2017 4:23:...

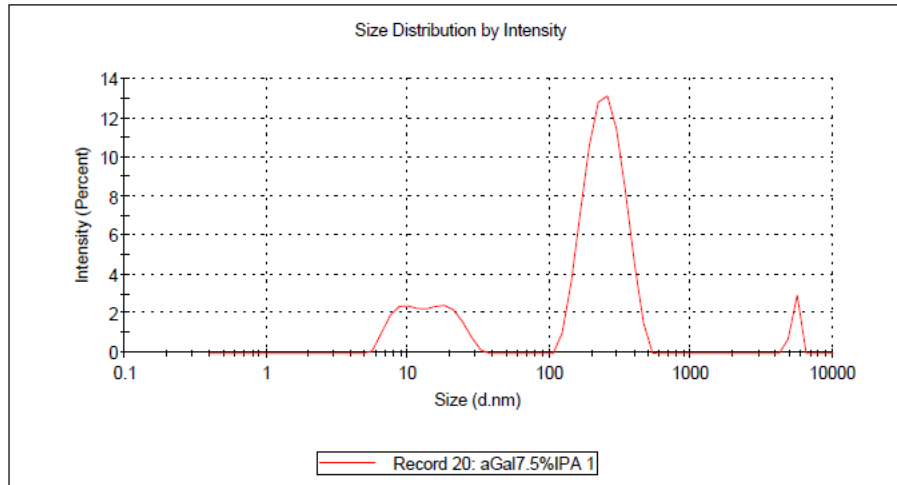
System

Temperature (°C): 10.0	Duration Used (s): 220
Count Rate (kcps): 29.8	Measurement Position (mm): 4.65
Cell Description: Glass cuvette with square apert...	Attenuator: 11

Results

	Size (d.nm):	% Intensity:	St Dev (d.n...
Z-Average (d.nm): 149.8	Peak 1: 252.5	72.4	75.36
PdI: 0.642	Peak 2: 10.00	12.2	2.306
Intercept: 0.744	Peak 3: 19.07	11.7	4.621

Result quality : **Refer to quality report**



Correlogram Report

v2.0



Malvern Instruments Ltd - © Copyright 2008

Sample Details

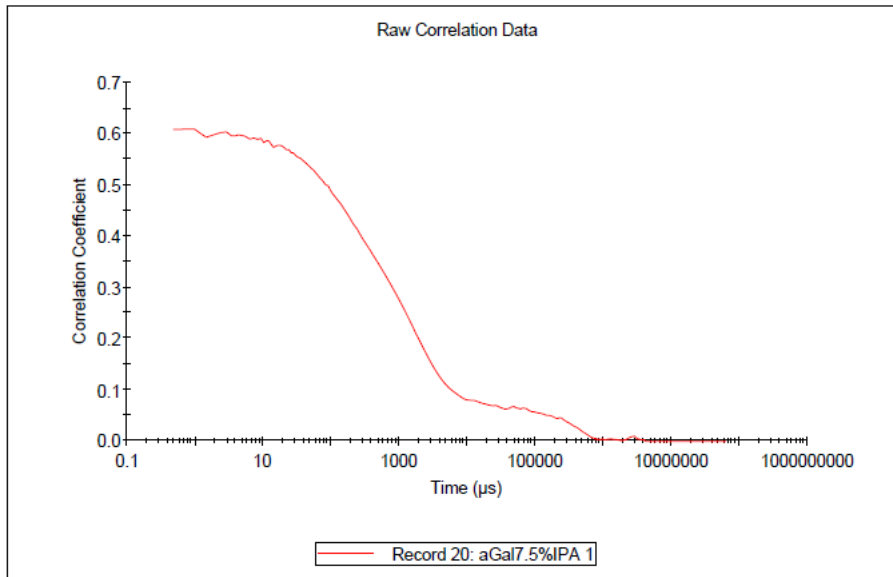
Sample Name: aGal7.5%IPA 1
SOP Name: mansettings.nano
General Notes:

File Name: bl.dts	Dispersant Name: 7.5% IPA
Record Number: 20	Dispersant RI: 1.335
Material RI: 1.45	Viscosity (cP): 1.6530
Material Absorbtion: 0.001	Measurement Date and Time: Tuesday, June 06, 2017 4:...

System

Temperature (°C): 10.0	Duration Used (s): 220
Count Rate (kcps): 29.8	Measurement Position (mm): 4.65
Cell Description: Glass cuvette with square...	Attenuator: 11

Results



α Gal Yariv in 10% (v/v) iPrOH at 10 °C ($X = 0.03$)

Size Distribution Report by Intensity

v2.2



Sample Details

Sample Name: aGal10%IPA 1

SOP Name: mansettings.nano

General Notes:

File Name:	bl.dts	Dispersant Name:	10% IPA
Record Number:	21	Dispersant RI:	1.337
Material RI:	1.45	Viscosity (cP):	1.7985
Material Absorbtion:	0.001	Measurement Date and Time:	Tuesday, June 06, 2017 4:31:...

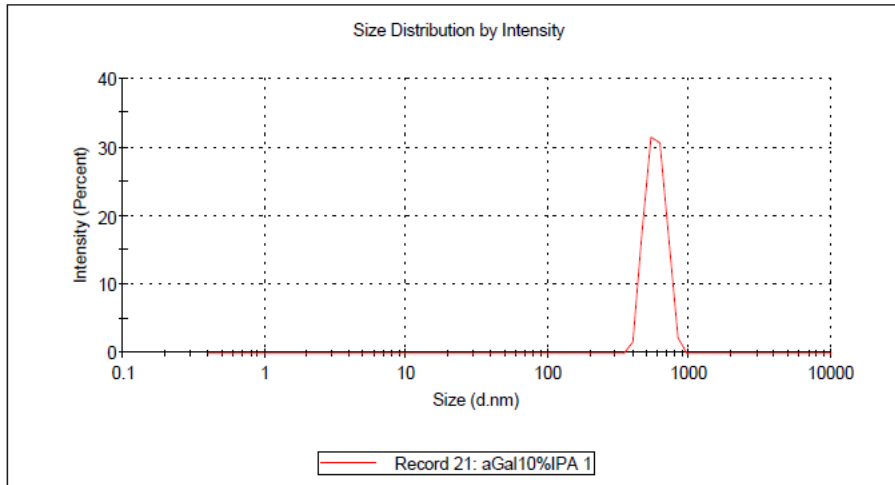
System

Temperature (°C):	10.0	Duration Used (s):	70
Count Rate (kcps):	144.9	Measurement Position (mm):	4.65
Cell Description:	Glass cuvette with square apert...	Attenuator:	10

Results

	Size (d.nm):	% Intensity:	St Dev (d.n...)
Z-Average (d.nm): 627.5	Peak 1: 578.5	100.0	92.32
Pdl: 0.829	Peak 2: 0.000	0.0	0.000
Intercept: 0.739	Peak 3: 0.000	0.0	0.000

Result quality : **Refer to quality report**



Correlogram Report

v2.0



Malvern Instruments Ltd - © Copyright 2008

Sample Details

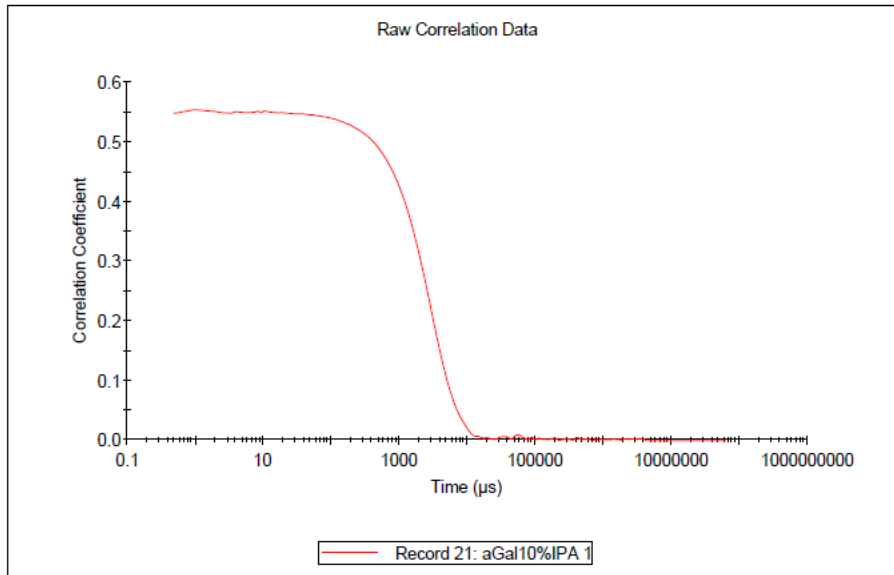
Sample Name: aGal10%IPA 1
SOP Name: mansettings.nano
General Notes:

File Name: bl.dts	Dispersant Name: 10% IPA
Record Number: 21	Dispersant RI: 1.337
Material RI: 1.45	Viscosity (cP): 1.7985
Material Absorbtion: 0.001	Measurement Date and Time: Tuesday, June 06, 2017 4:...

System

Temperature (°C): 10.0	Duration Used (s): 70
Count Rate (kcps): 144.9	Measurement Position (mm): 4.65
Cell Description: Glass cuvette with square...	Attenuator: 10

Results



α Gal Yariv in 15% (v/v) iPrOH at 10 °C ($X = 0.04$)

Size Distribution Report by Intensity

v2.2



Sample Details

Sample Name: aGal15%IPA 1
SOP Name: mansettings.nano
General Notes:

File Name: bl.dts Dispersant Name: 15% IPA
Record Number: 22 Dispersant RI: 1.341
Material RI: 1.45 Viscosity (cP): 2.1288
Material Absorbtion: 0.001 Measurement Date and Time: Tuesday, June 06, 2017 4:40:...

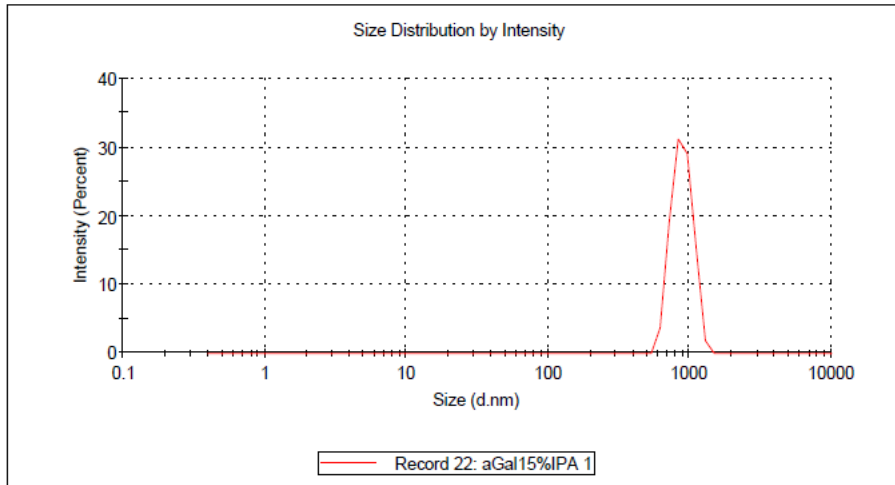
System

Temperature (°C): 10.0 Duration Used (s): 80
Count Rate (kcps): 152.5 Measurement Position (mm): 4.65
Cell Description: Glass cuvette with square apert... Attenuator: 10

Results

	Size (d.nm):	% Intensity:	St Dev (d.n...)
Z-Average (d.nm): 908.8	Peak 1: 884.6	100.0	145.9
Pdl: 0.524	Peak 2: 0.000	0.0	0.000
Intercept: 0.711	Peak 3: 0.000	0.0	0.000

Result quality : **Refer to quality report**



Correlogram Report

v2.0



Malvern Instruments Ltd - © Copyright 2008

Sample Details

Sample Name: aGal15%IPA 1

SOP Name: mansettings.nano

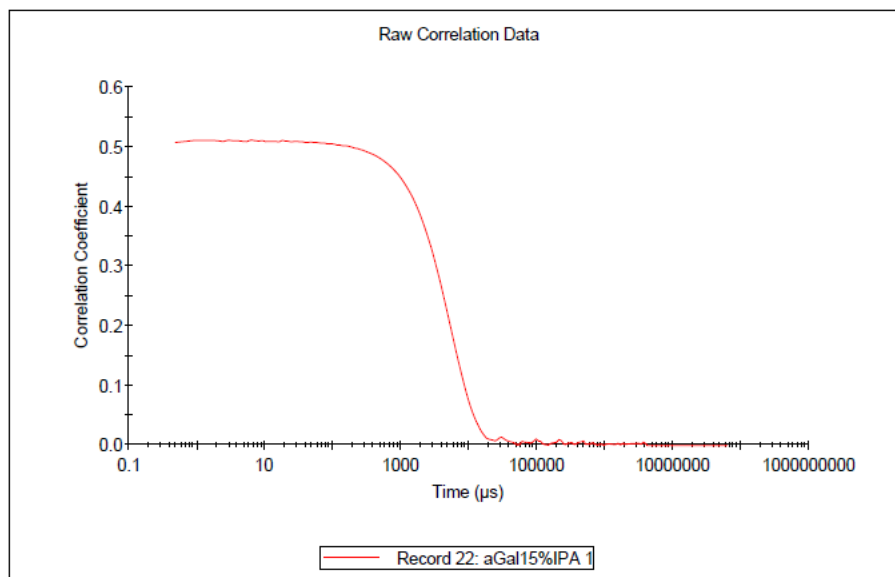
General Notes:

File Name: bl.dts	Dispersant Name: 15% IPA
Record Number: 22	Dispersant RI: 1.341
Material RI: 1.45	Viscosity (cP): 2.1288
Material Absorbtion: 0.001	Measurement Date and Time: Tuesday, June 06, 2017 4:...

System

Temperature (°C): 10.0	Duration Used (s): 80
Count Rate (kcps): 152.5	Measurement Position (mm): 4.65
Cell Description: Glass cuvette with square...	Attenuator: 10

Results



α Gal Yariv in 25% (v/v) iPrOH at 10 °C ($X = 0.07$)

Size Distribution Report by Intensity

v2.2



Sample Details

Sample Name: aGal25%IPA 1
SOP Name: mansettings.nano
General Notes:

File Name:	bl.dts	Dispersant Name:	25% IPA
Record Number:	23	Dispersant RI:	1.349
Material RI:	1.45	Viscosity (cP):	2.8551
Material Absorbtion:	0.001	Measurement Date and Time:	Tuesday, June 06, 2017 4:47:...

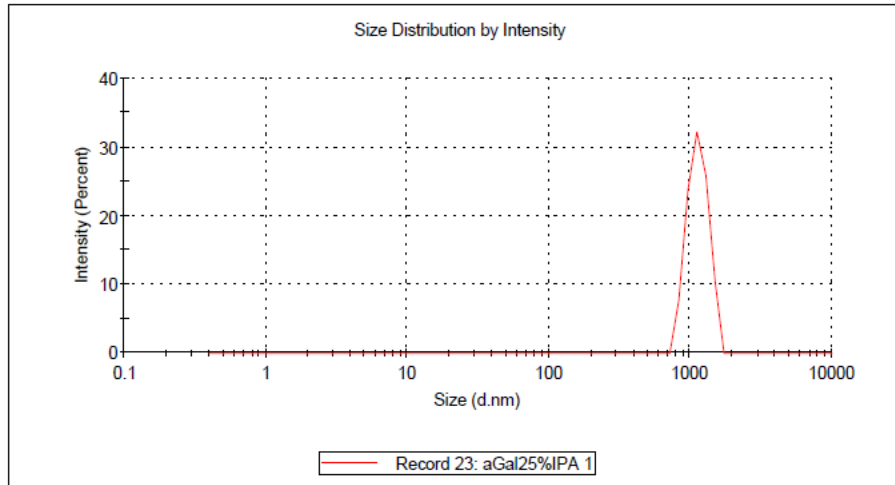
System

Temperature (°C):	10.0	Duration Used (s):	80
Count Rate (kcps):	128.6	Measurement Position (mm):	4.65
Cell Description:	Glass cuvette with square apert...	Attenuator:	10

Results

	Size (d.nm):	% Intensity:	St Dev (d.n...)		
Z-Average (d.nm):	1344	Peak 1:	1134	100.0	183.7
Pd:	1.000	Peak 2:	0.000	0.0	0.000
Intercept:	0.692	Peak 3:	0.000	0.0	0.000

Result quality : Refer to quality report



Correlogram Report

v2.0



Malvern Instruments Ltd - © Copyright 2008

Sample Details

Sample Name: aGal25%IPA 1

SOP Name: mansettings.nano

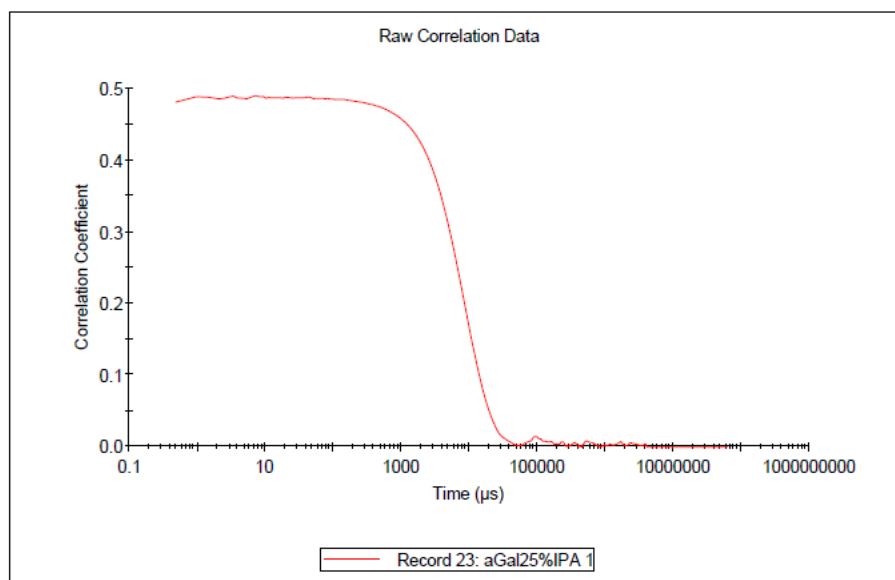
General Notes:

File Name: bl.dts	Dispersant Name: 25% IPA
Record Number: 23	Dispersant RI: 1.349
Material RI: 1.45	Viscosity (cP): 2.8551
Material Absorbtion: 0.001	Measurement Date and Time: Tuesday, June 06, 2017 4:...

System

Temperature (°C): 10.0	Duration Used (s): 80
Count Rate (kcps): 128.6	Measurement Position (mm): 4.65
Cell Description: Glass cuvette with square...	Attenuator: 10

Results



α Gal Yariv in 60% (v/v) iPrOH at 10 °C ($X = 0.26$)

Size Distribution Report by Intensity

v2.2



Sample Details

Sample Name: aGal60%IPA 1

SOP Name: mansettings.nano

General Notes:

File Name:	bl.dts	Dispersant Name:	60% IPA
Record Number:	24	Dispersant RI:	1.361
Material RI:	1.45	Viscosity (cP):	3.3687
Material Absorbtion:	0.001	Measurement Date and Time:	Tuesday, June 06, 2017 4:58:...

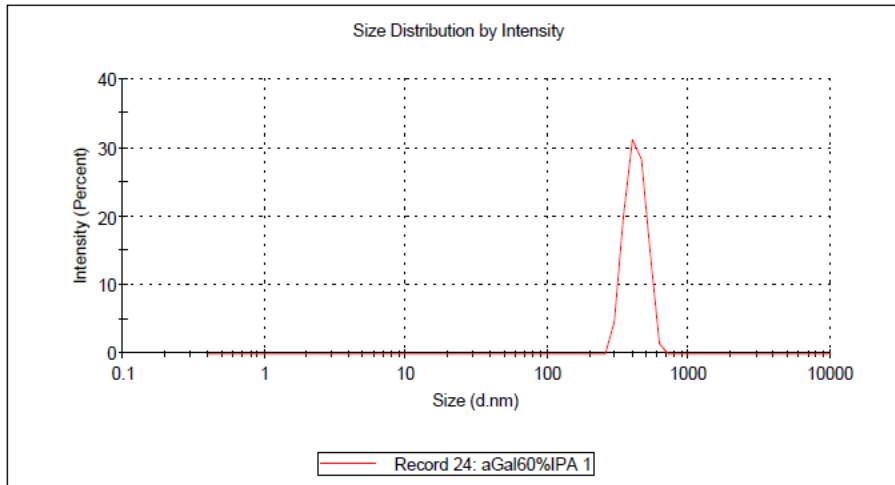
System

Temperature (°C):	9.9	Duration Used (s):	80
Count Rate (kcps):	106.3	Measurement Position (mm):	4.65
Cell Description:	Glass cuvette with square apert...	Attenuator:	10

Results

	Size (d.nm):	% Intensity:	St Dev (d.n...)
Z-Average (d.nm): 413.0	Peak 1: 420.9	100.0	69.95
Pdl: 0.123	Peak 2: 0.000	0.0	0.000
Intercept: 0.765	Peak 3: 0.000	0.0	0.000

Result quality : **Refer to quality report**



Correlogram Report

v2.0



Malvern Instruments Ltd - © Copyright 2008

Sample Details

Sample Name: aGal60%IPA 1

SOP Name: mansettings.nano

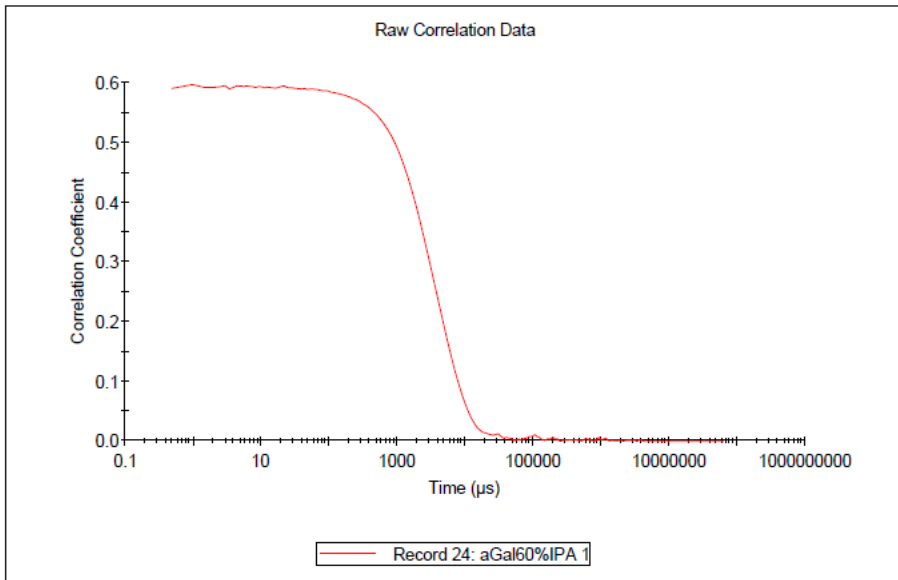
General Notes:

File Name: bl.dts	Dispersant Name: 60% IPA
Record Number: 24	Dispersant RI: 1.361
Material RI: 1.45	Viscosity (cP): 3.3687
Material Absorbtion: 0.001	Measurement Date and Time: Tuesday, June 06, 2017 4:...

System

Temperature (°C): 9.9	Duration Used (s): 80
Count Rate (kcps): 106.3	Measurement Position (mm): 4.65
Cell Description: Glass cuvette with square...	Attenuator: 10

Results



α Gal Yariv in 75% (v/v) iPrOH at 10 °C ($X = 0.41$)

Size Distribution Report by Intensity

v2.2



Sample Details

Sample Name: aGal75%IPA 1
SOP Name: mansettings.nano
General Notes:

File Name: bl.dts Dispersant Name: 75% IPA
Record Number: 25 Dispersant RI: 1.351
Material RI: 1.45 Viscosity (cP): 1.0683
Material Absorption: 0.001 Measurement Date and Time: Tuesday, June 06, 2017 5:06:...

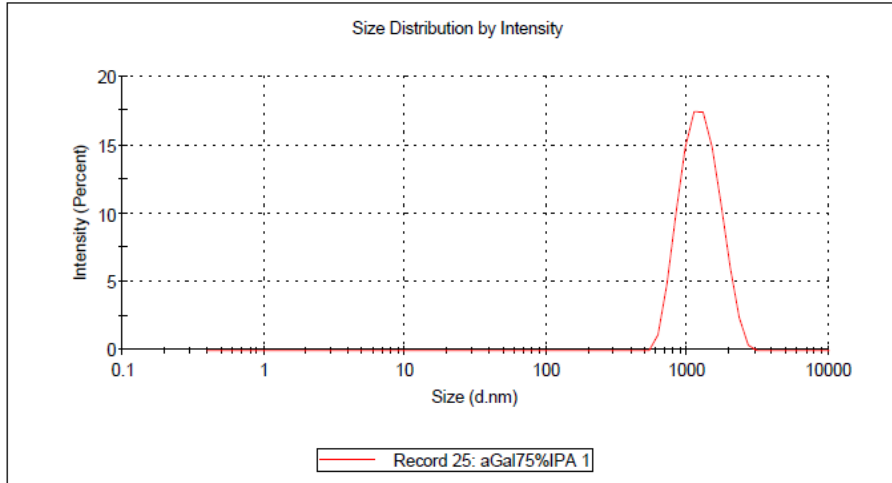
System

Temperature (°C): 10.0 Duration Used (s): 70
Count Rate (kcps): 260.9 Measurement Position (mm): 4.65
Cell Description: Glass cuvette with square apert... Attenuator: 10

Results

	Size (d.nm):	% Intensity:	St Dev (d.n...)
Z-Average (d.nm): 1150	Peak 1: 1271	100.0	390.7
PdI: 0.120	Peak 2: 0.000	0.0	0.000
Intercept: 0.837	Peak 3: 0.000	0.0	0.000

Result quality : **Good**



Correlogram Report

v2.0



Malvern Instruments Ltd - © Copyright 2008

Sample Details

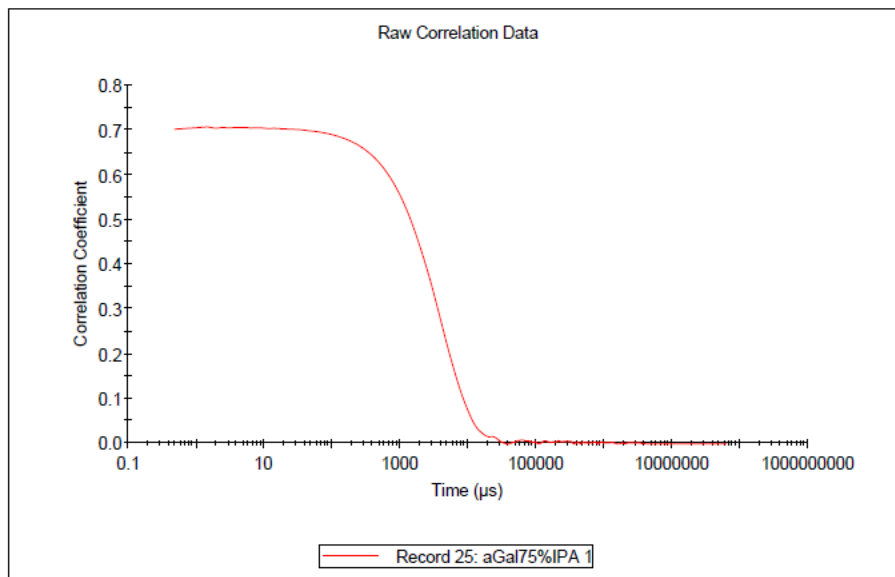
Sample Name: aGal75%IPA 1
SOP Name: mansettings.nano
General Notes:

File Name: bl.dts	Dispersant Name: 75% IPA
Record Number: 25	Dispersant RI: 1.351
Material RI: 1.45	Viscosity (cP): 1.0683
Material Absorbtion: 0.001	Measurement Date and Time: Tuesday, June 06, 2017 5:...

System

Temperature (°C): 10.0	Duration Used (s): 70
Count Rate (kcps): 260.9	Measurement Position (mm): 4.65
Cell Description: Glass cuvette with square...	Attenuator: 10

Results



βGlc Yariv in water at 10 °C

Size Distribution Report by Intensity

v2.2



Sample Details

Sample Name: BL-BGlc300u10c 1

SOP Name: mansettings.nano

General Notes:

File Name: Example Results.dts	Dispersant Name: Water
Record Number: 222	Dispersant RI: 1.330
Material RI: 1.45	Viscosity (cP): 1.3153
Material Absorbtion: 0.001	Measurement Date and Time: Tuesday, November 21, 2017...

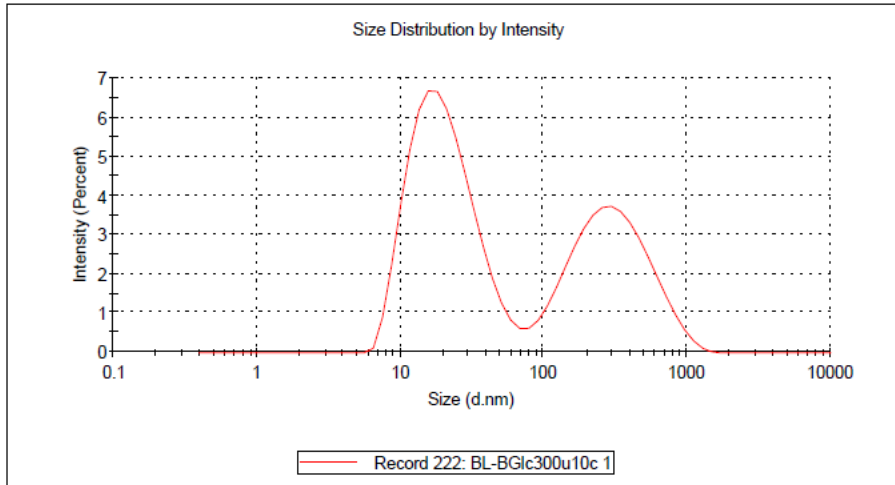
System

Temperature (°C): 10.0	Duration Used (s): 270
Count Rate (kcps): 18.8	Measurement Position (mm): 4.65
Cell Description: Glass cuvette with square apert...	Attenuator: 11

Results

	Size (d.nm):	% Intensity:	St Dev (d.n...)
Z-Average (d.nm): 27.33	Peak 1: 21.86	58.6	11.81
PdI: 0.678	Peak 2: 335.5	41.4	211.3
Intercept: 0.699	Peak 3: 0.000	0.0	0.000

Result quality : **Refer to quality report**



Correlogram Report

v2.0



Malvern Instruments Ltd - © Copyright 2008

Sample Details

Sample Name: BL-BGlc300u10c 1

SOP Name: mansettings.nano

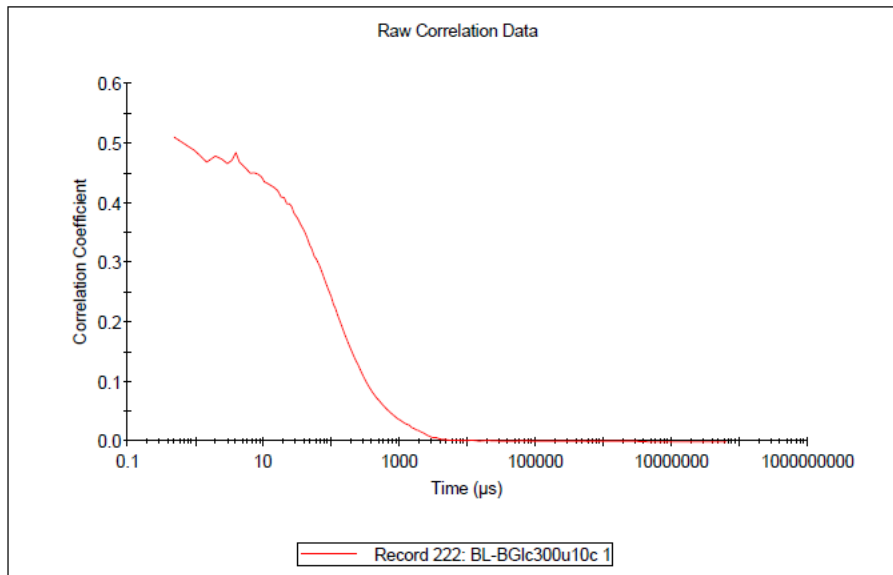
General Notes:

File Name: Example Results.dts	Dispersant Name: Water
Record Number: 222	Dispersant RI: 1.330
Material RI: 1.45	Viscosity (cP): 1.3153
Material Absorbtion: 0.001	Measurement Date and Time: Tuesday, November 21, 20...

System

Temperature (°C): 10.0	Duration Used (s): 270
Count Rate (kcps): 18.8	Measurement Position (mm): 4.65
Cell Description: Glass cuvette with square...	Attenuator: 11

Results



βGlc Yariv in water at 60 °C

Size Distribution Report by Intensity

v2.2



Sample Details

Sample Name: 120216BGlc300uM60Cfilt 1

SOP Name: mansettings.nano

General Notes:

File Name: Example Results.dts Dispersant Name: Water
Record Number: 221 Dispersant RI: 1.330
Material RI: 1.45 Viscosity (cP): 0.4712
Material Absorption: 0.001 Measurement Date and Time: Friday, December 02, 2016 3:...

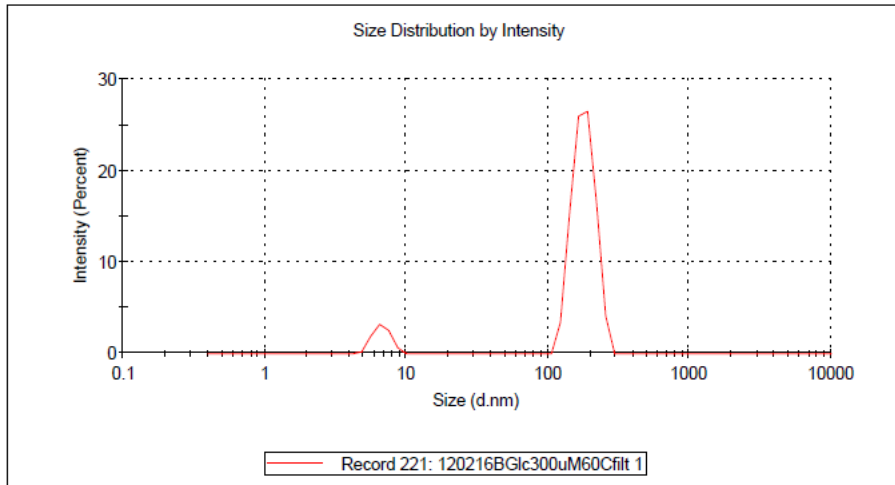
System

Temperature (°C): 60.0 Duration Used (s): 190
Count Rate (kcps): 30.5 Measurement Position (mm): 4.65
Cell Description: Glass cuvette with square apert... Attenuator: 11

Results

	Size (d.nm):	% Intensity:	St Dev (d.n...)
Z-Average (d.nm): 266.2	Peak 1: 180.5	91.5	31.79
PdI: 0.397	Peak 2: 6.746	8.5	0.9394
Intercept: 0.846	Peak 3: 0.000	0.0	0.000

Result quality : **Refer to quality report**



Correlogram Report

v2.0



Malvern Instruments Ltd - © Copyright 2008

Sample Details

Sample Name: 120216BGlc300uM60Cfilt 1

SOP Name: mansettings.nano

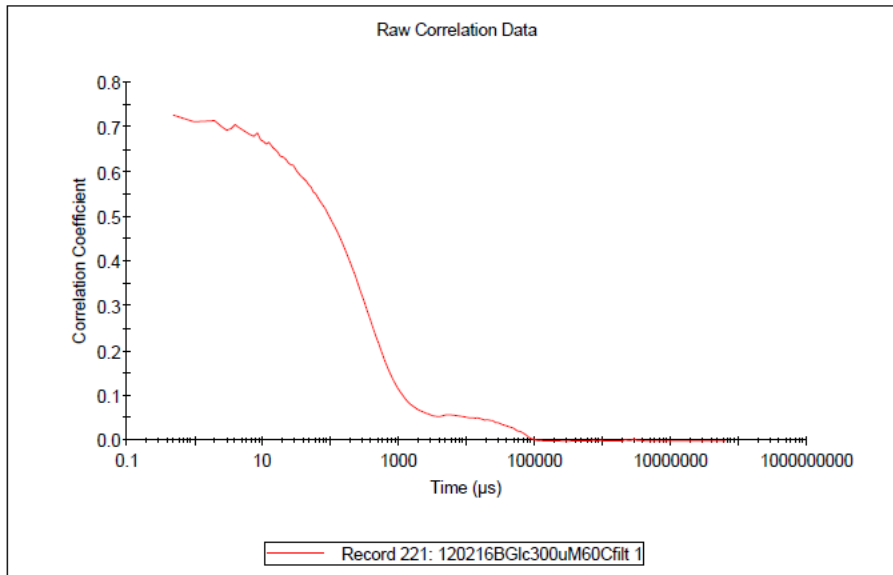
General Notes:

File Name: Example Results.dts	Dispersant Name: Water
Record Number: 221	Dispersant RI: 1.330
Material RI: 1.45	Viscosity (cP): 0.4712
Material Absorbtion: 0.001	Measurement Date and Time: Friday, December 02, 2016...

System

Temperature (°C): 60.0	Duration Used (s): 190
Count Rate (kcps): 30.5	Measurement Position (mm): 4.65
Cell Description: Glass cuvette with square...	Attenuator: 11

Results



βGlc Yariv in 25% (v/v) MeOH at 10 °C (run 1)

Size Distribution Report by Intensity

v2.2



Sample Details

Sample Name: BL-BGlc-0.3mM10c25%meoh-3 1

SOP Name: mansettings.nano

General Notes:

File Name: Example Results.dts	Dispersant Name: Water MeOH 25%
Record Number: 169	Dispersant RI: 1.338
Material RI: 1.45	Viscosity (cP): 2.1408
Material Absorbtion: 0.001	Measurement Date and Time: Monday, October 24, 2016 3:...

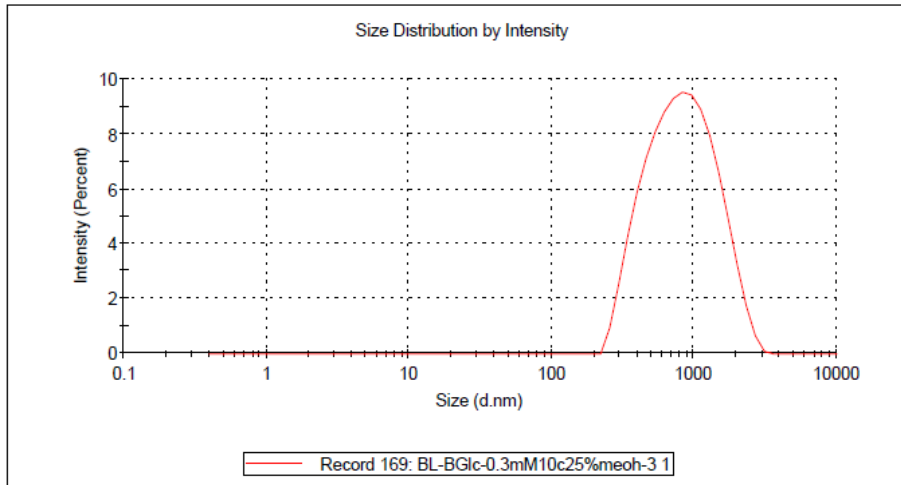
System

Temperature (°C): 10.0	Duration Used (s): 60
Count Rate (kcps): 213.7	Measurement Position (mm): 4.65
Cell Description: Glass cuvette with square apert...	Attenuator: 8

Results

	Size (d.nm):	% Intensity:	St Dev (d.n...)
Z-Average (d.nm): 708.7	Peak 1: 921.2	100.0	497.4
Pdl: 0.199	Peak 2: 0.000	0.0	0.000
Intercept: 0.878	Peak 3: 0.000	0.0	0.000

Result quality : **Good**



Correlogram Report

v2.0



Malvern Instruments Ltd - © Copyright 2008

Sample Details

Sample Name: BL-BGlc-0.3mM10c25%meoh-3 1

SOP Name: mansettings.nano

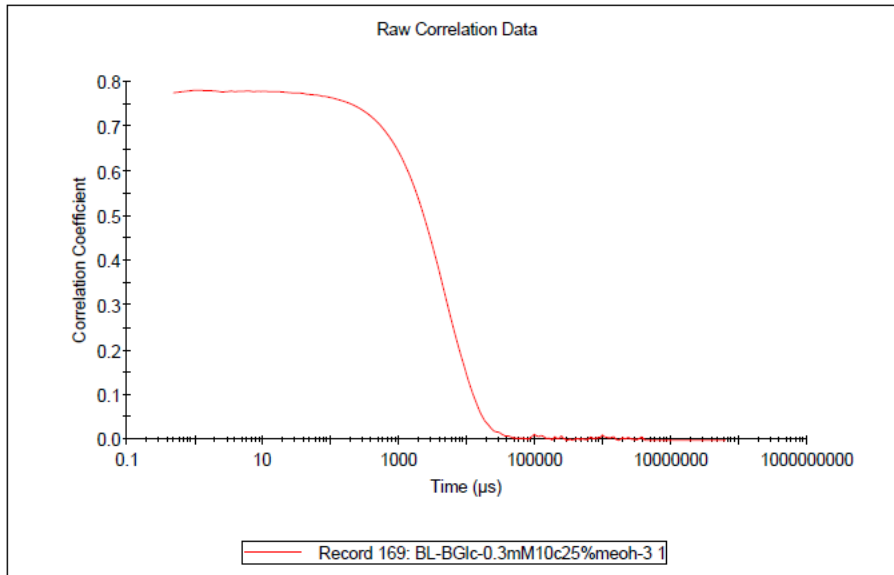
General Notes:

File Name: Example Results.dts	Dispersant Name: Water MeOH 25%
Record Number: 169	Dispersant RI: 1.338
Material RI: 1.45	Viscosity (cP): 2.1408
Material Absorbtion: 0.001	Measurement Date and Time: Monday, October 24, 2016 ...

System

Temperature (°C): 10.0	Duration Used (s): 60
Count Rate (kcps): 213.7	Measurement Position (mm): 4.65
Cell Description: Glass cuvette with square...	Attenuator: 8

Results



βGlc Yariv in 25% (v/v) MeOH at 60 °C (run 2)

Size Distribution Report by Intensity

v2.2



Sample Details

Sample Name: BL-BGlc-0.3mM60c25%meoh-3 1

SOP Name: mansettings.nano

General Notes:

File Name:	Example Results.dts	Dispersant Name:	Water MeOH 25%
Record Number:	170	Dispersant RI:	1.338
Material RI:	1.45	Viscosity (cP):	1.2967
Material Absorbtion:	0.001	Measurement Date and Time:	Monday, October 24, 2016 3:...

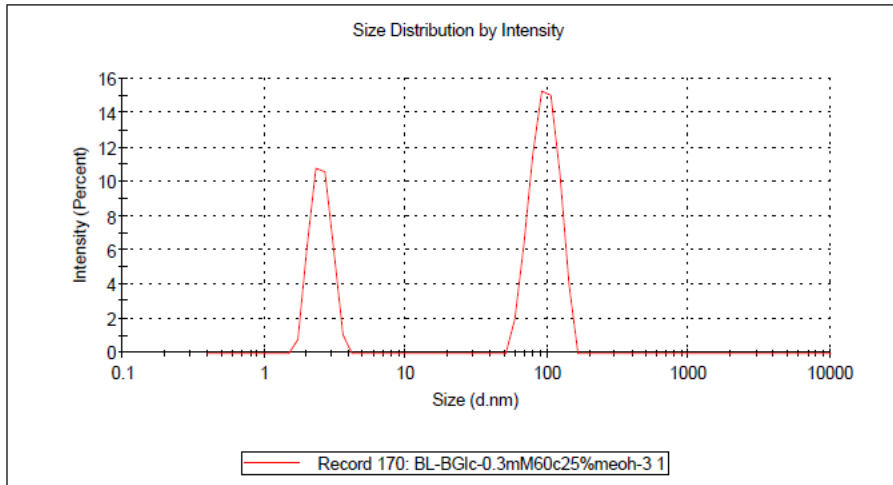
System

Temperature (°C):	60.0	Duration Used (s):	500
Count Rate (kcps):	8.6	Measurement Position (mm):	4.65
Cell Description:	Glass cuvette with square apert...	Attenuator:	11

Results

	Size (d.nm):	% Intensity:	St Dev (d.n...)
Z-Average (d.nm): 546.0	Peak 1: 97.32	64.7	21.01
Pdl: 0.944	Peak 2: 2.542	35.3	0.4205
Intercept: 0.556	Peak 3: 0.000	0.0	0.000

Result quality : **Refer to quality report**



Correlogram Report

v2.0



Malvern Instruments Ltd - © Copyright 2008

Sample Details

Sample Name: BL-BGlc-0.3mM60c25%meoh-3 1

SOP Name: mansettings.nano

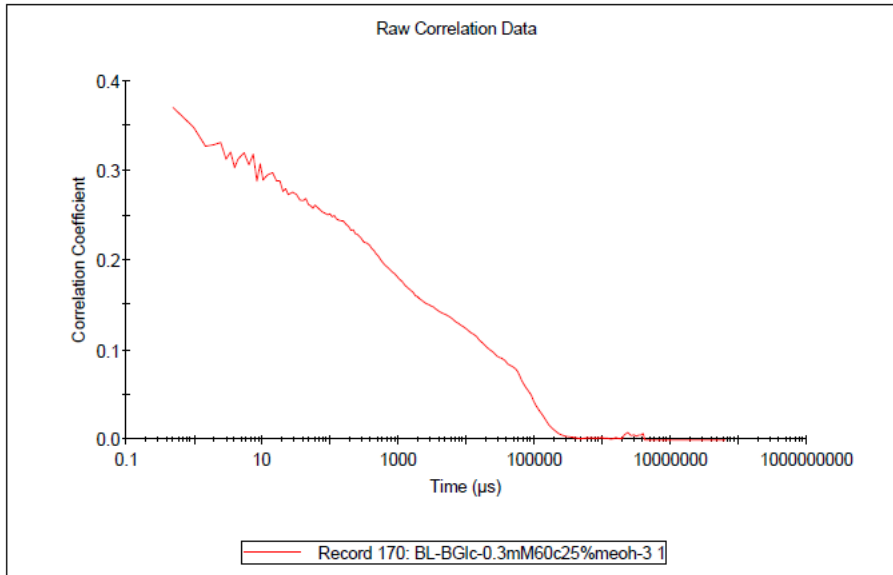
General Notes:

File Name: Example Results.dts	Dispersant Name: Water MeOH 25%
Record Number: 170	Dispersant RI: 1.338
Material RI: 1.45	Viscosity (cP): 1.2967
Material Absorbtion: 0.001	Measurement Date and Time: Monday, October 24, 2016 ...

System

Temperature (°C): 60.0	Duration Used (s): 500
Count Rate (kcps): 8.6	Measurement Position (mm): 4.65
Cell Description: Glass cuvette with square...	Attenuator: 11

Results



βGlc Yariv in 25% (v/v) MeOH at 10 °C (run 3)

Size Distribution Report by Intensity

v2.2



Sample Details

Sample Name: BL-BGlc-0.3mM10c25%meoh-afterheating 1

SOP Name: mansettings.nano

General Notes:

File Name: Example Results.dts Dispersant Name: Water MeOH 25%
Record Number: 171 Dispersant RI: 1.338
Material RI: 1.45 Viscosity (cP): 2.1408
Material Absorption: 0.001 Measurement Date and Time: Monday, October 24, 2016 4:...

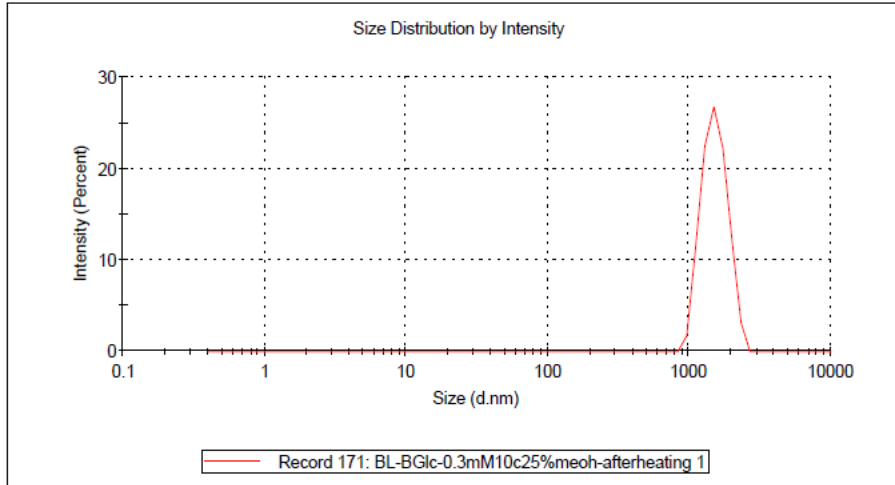
System

Temperature (°C): 10.0 Duration Used (s): 60
Count Rate (kcps): 203.4 Measurement Position (mm): 4.65
Cell Description: Glass cuvette with square apert... Attenuator: 9

Results

	Size (d.nm):	% Intensity:	St Dev (d.n...)
Z-Average (d.nm): 1427	Peak 1: 1525	100.0	306.1
PdI: 0.127	Peak 2: 0.000	0.0	0.000
Intercept: 0.810	Peak 3: 0.000	0.0	0.000

Result quality : **Good**



Correlogram Report

v2.0



Malvern Instruments Ltd - © Copyright 2008

Sample Details

Sample Name: BL-BGlc-0.3mM10c25%meoh-afterheating 1

SOP Name: mansettings.nano

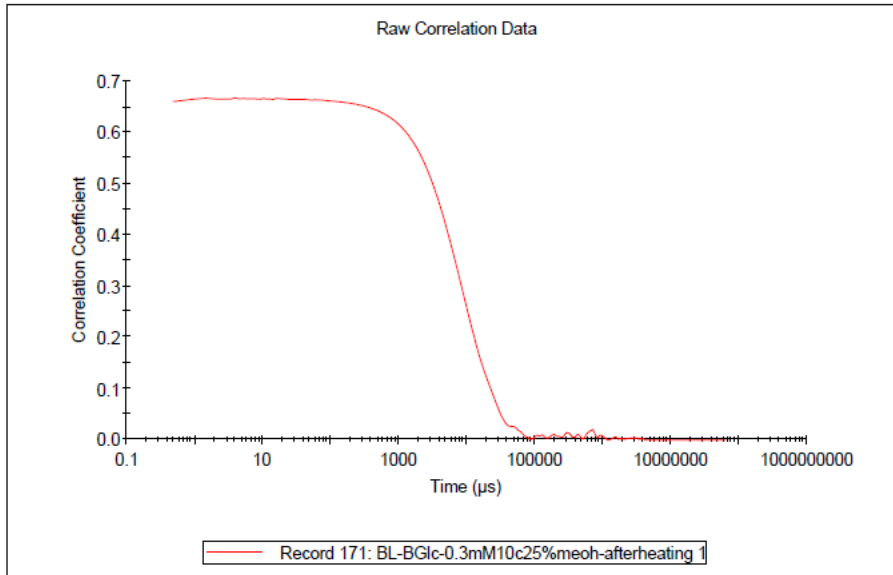
General Notes:

File Name: Example Results.dts	Dispersant Name: Water MeOH 25%
Record Number: 171	Dispersant RI: 1.338
Material RI: 1.45	Viscosity (cP): 2.1408
Material Absorbtion: 0.001	Measurement Date and Time: Monday, October 24, 2016 ...

System

Temperature (°C): 10.0	Duration Used (s): 60
Count Rate (kcps): 203.4	Measurement Position (mm): 4.65
Cell Description: Glass cuvette with square...	Attenuator: 9

Results



βGlc Yariv in 25% (v/v) MeOH at 60 °C (run 4)

Size Distribution Report by Intensity

v2.2



Sample Details

Sample Name: BL-BGlc-0.3mM60c25%meoh-cycle2 1

SOP Name: mansettings.nano

General Notes:

File Name:	Example Results.dts	Dispersant Name:	Water MeOH 25%
Record Number:	172	Dispersant RI:	1.338
Material RI:	1.45	Viscosity (cP):	1.2967
Material Absorbtion:	0.001	Measurement Date and Time:	Monday, October 24, 2016 4:...

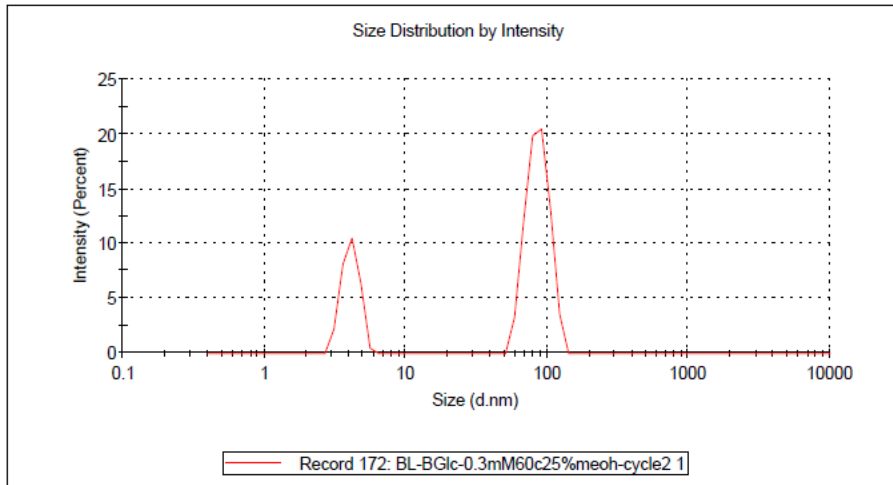
System

Temperature (°C):	60.0	Duration Used (s):	500
Count Rate (kcps):	8.6	Measurement Position (mm):	4.65
Cell Description:	Glass cuvette with square apert...	Attenuator:	11

Results

	Size (d.nm):	% Intensity:	St Dev (d.n...
Z-Average (d.nm): 505.7	Peak 1: 86.69	72.3	15.68
Pdi: 1.000	Peak 2: 4.110	27.7	0.5635
Intercept: 0.594	Peak 3: 0.000	0.0	0.000

Result quality : **Refer to quality report**



Correlogram Report

v2.0



Malvern Instruments Ltd - © Copyright 2008

Sample Details

Sample Name: BL-BGlc-0.3mM60c25%meoh-cycle2 1

SOP Name: mansettings.nano

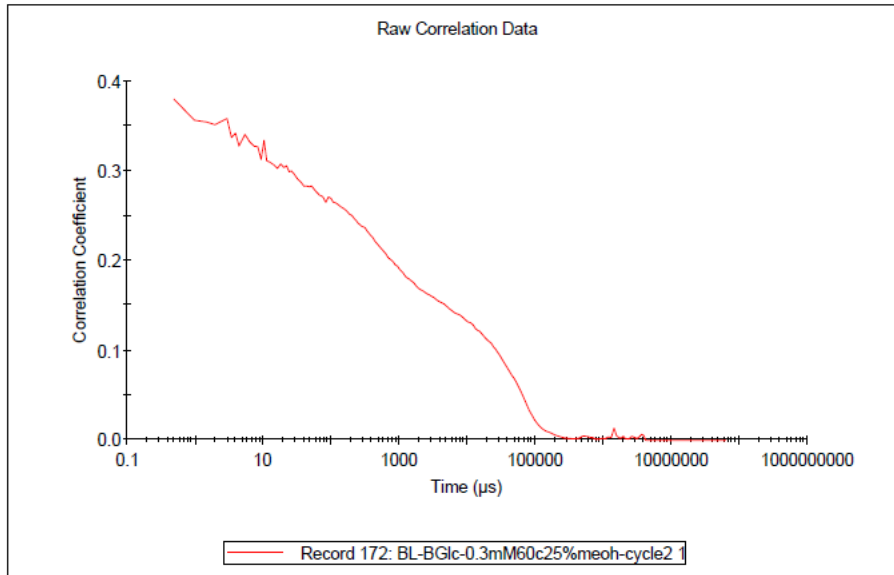
General Notes:

File Name: Example Results.dts	Dispersant Name: Water MeOH 25%
Record Number: 172	Dispersant RI: 1.338
Material RI: 1.45	Viscosity (cP): 1.2967
Material Absorbion: 0.001	Measurement Date and Time: Monday, October 24, 2016 ...

System

Temperature (°C): 60.0	Duration Used (s): 500
Count Rate (kcps): 8.6	Measurement Position (mm): 4.65
Cell Description: Glass cuvette with square...	Attenuator: 11

Results



βGlc Yariv in 25% (v/v) MeOH at 10 °C (run 5)

Size Distribution Report by Intensity

v2.2



Sample Details

Sample Name: BL-BGlc-0.3mM10c25%meoh-cycle2 1

SOP Name: mansettings.nano

General Notes:

File Name: Example Results.dts	Dispersant Name: Water MeOH 25%
Record Number: 173	Dispersant RI: 1.338
Material RI: 1.45	Viscosity (cP): 2.1408
Material Absorption: 0.001	Measurement Date and Time: Monday, October 24, 2016 4:...

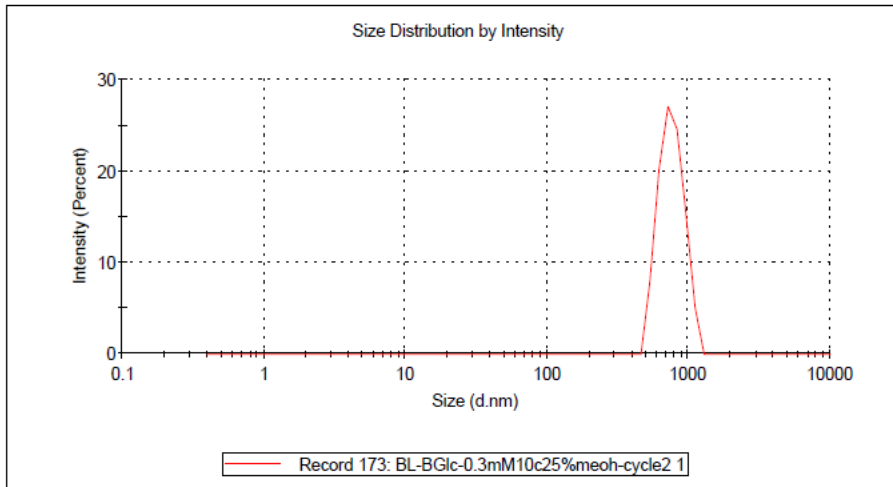
System

Temperature (°C): 10.0	Duration Used (s): 70
Count Rate (kcps): 193.9	Measurement Position (mm): 4.65
Cell Description: Glass cuvette with square aper...	Attenuator: 9

Results

	Size (d.nm):	% Intensity:	St Dev (d.n...)
Z-Average (d.nm): 890.4	Peak 1: 762.5	100.0	148.3
Pd: 0.379	Peak 2: 0.000	0.0	0.000
Intercept: 0.809	Peak 3: 0.000	0.0	0.000

Result quality : **Good**



Correlogram Report

v2.0



Malvern Instruments Ltd - © Copyright 2008

Sample Details

Sample Name: BL-BGlc-0.3mM10c25%meoh-cycle2 1

SOP Name: mansettings.nano

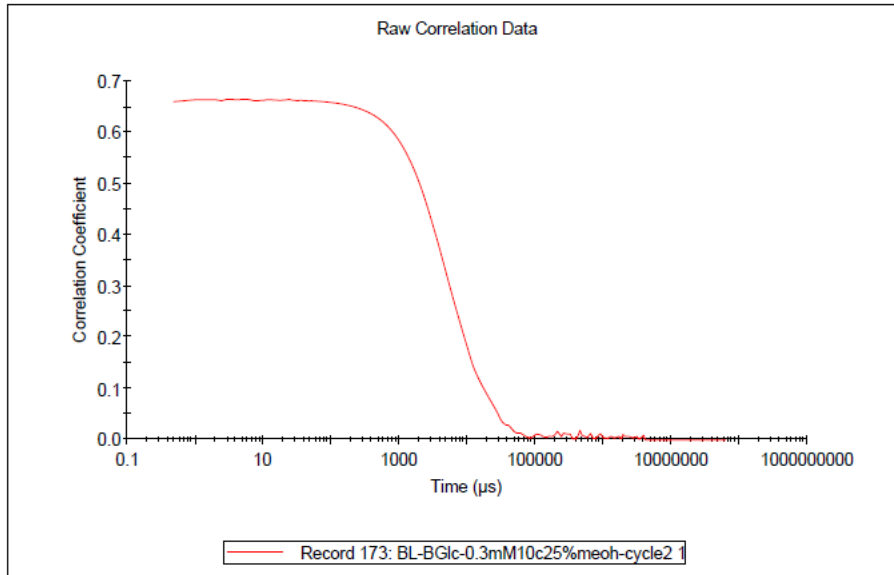
General Notes:

File Name: Example Results.dts	Dispersant Name: Water MeOH 25%
Record Number: 173	Dispersant RI: 1.338
Material RI: 1.45	Viscosity (cP): 2.1408
Material Absorbtion: 0.001	Measurement Date and Time: Monday, October 24, 2016 ...

System

Temperature (°C): 10.0	Duration Used (s): 70
Count Rate (kcps): 193.9	Measurement Position (mm): 4.65
Cell Description: Glass cuvette with square...	Attenuator: 9

Results



βGlc Yariv in 5% (v/v) MeOH at 10 °C (X = 0.02)

Size Distribution Report by Intensity

v2.2



Sample Details

Sample Name: 051917BGlc5% 1

SOP Name: mansettings.nano

General Notes:

File Name:	bl.dts	Dispersant Name:	Water-MeOH5%
Record Number:	1	Dispersant RI:	1.331
Material RI:	1.45	Viscosity (cP):	1.4468
Material Absorbtion:	0.001	Measurement Date and Time:	Friday, May 19, 2017 4:09:45 ...

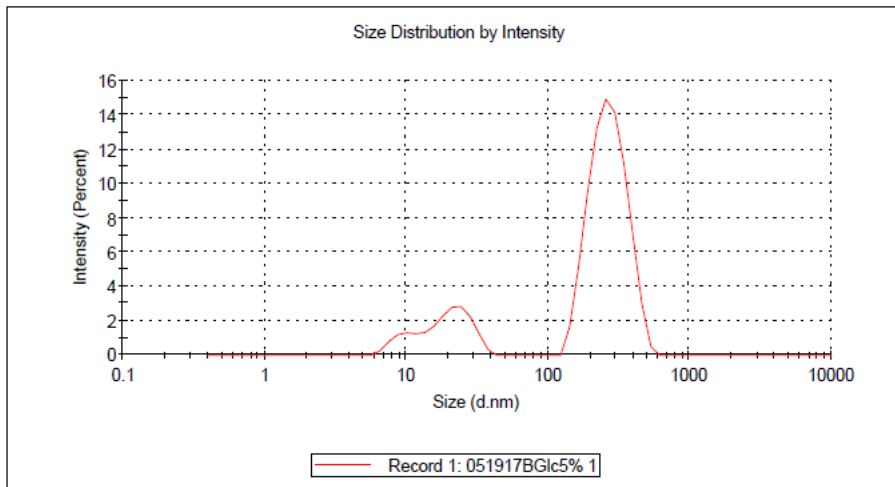
System

Temperature (°C):	9.8	Duration Used (s):	230
Count Rate (kcps):	94.1	Measurement Position (mm):	4.65
Cell Description:	Glass cuvette with square apert...	Attenuator:	11

Results

	Size (d.nm):	% Intensity:	St Dev (d.n...)
Z-Average (d.nm): 209.7	Peak 1: 274.1	79.2	78.86
PdI: 0.726	Peak 2: 21.58	16.0	6.427
Intercept: 0.873	Peak 3: 9.555	4.8	1.622

Result quality : **Refer to quality report**



Correlogram Report

v2.0



Malvern Instruments Ltd - © Copyright 2008

Sample Details

Sample Name: 051917BGlc5% 1

SOP Name: mansettings.nano

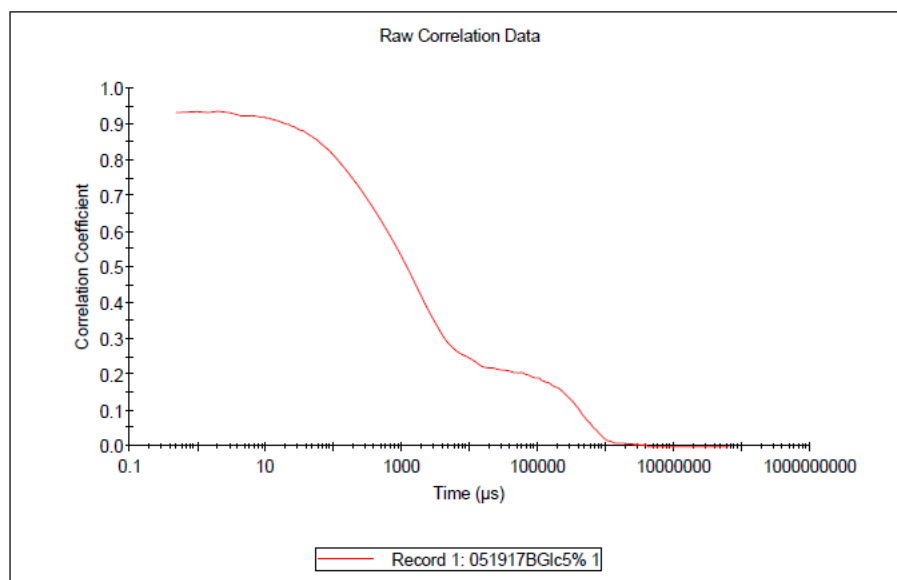
General Notes:

File Name: bl.dts	Dispersant Name: Water-MeOH5%
Record Number: 1	Dispersant RI: 1.331
Material RI: 1.45	Viscosity (cP): 1.4468
Material Absorbtion: 0.001	Measurement Date and Time: Friday, May 19, 2017 4:09:...

System

Temperature (°C): 9.8	Duration Used (s): 230
Count Rate (kcps): 94.1	Measurement Position (mm): 4.65
Cell Description: Glass cuvette with square...	Attenuator: 11

Results



βGlc Yariv in 15% (v/v) MeOH at 10 °C (X = 0.07)

Size Distribution Report by Intensity

v2.2



Sample Details

Sample Name: 051917BGlc15% 1

SOP Name: mansettings.nano

General Notes:

File Name:	bl.dts	Dispersant Name:	15% MeOH
Record Number:	2	Dispersant RI:	1.333
Material RI:	1.45	Viscosity (cP):	1.7042
Material Absorbtion:	0.001	Measurement Date and Time:	Friday, May 19, 2017 4:20:07 ...

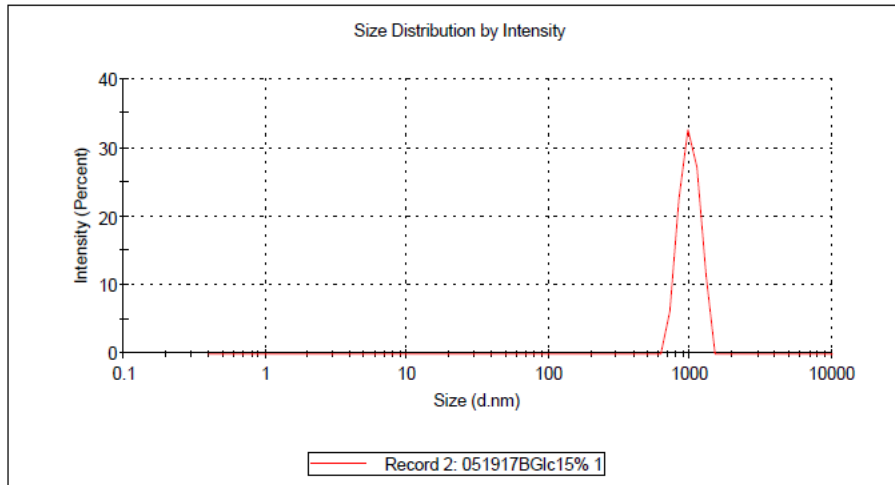
System

Temperature (°C):	9.7	Duration Used (s):	60
Count Rate (kcps):	177.3	Measurement Position (mm):	4.65
Cell Description:	Glass cuvette with square apert...	Attenuator:	10

Results

	Size (d.nm):	% Intensity:	St Dev (d.n...)
Z-Average (d.nm): 1059	Peak 1: 989.4	100.0	157.3
Pdl: 0.958	Peak 2: 0.000	0.0	0.000
Intercept: 0.694	Peak 3: 0.000	0.0	0.000

Result quality : **Refer to quality report**



Correlogram Report

v2.0



Malvern Instruments Ltd - © Copyright 2008

Sample Details

Sample Name: 051917BGlc15% 1

SOP Name: mansettings.nano

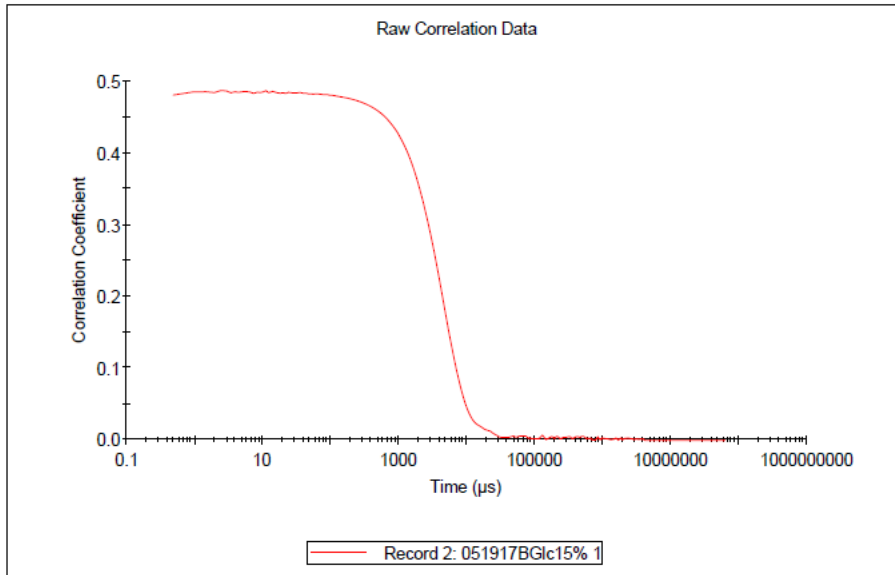
General Notes:

File Name: bl.dts	Dispersant Name: 15% MeOH
Record Number: 2	Dispersant RI: 1.333
Material RI: 1.45	Viscosity (cP): 1.7042
Material Absorbtion: 0.001	Measurement Date and Time: Friday, May 19, 2017 4:20:...

System

Temperature (°C): 9.7	Duration Used (s): 60
Count Rate (kcps): 177.3	Measurement Position (mm): 4.65
Cell Description: Glass cuvette with square...	Attenuator: 10

Results



βGlc Yariv in 25% (v/v) MeOH at 10 °C (X = 0.13)

Size Distribution Report by Intensity

v2.2



Sample Details

Sample Name: 051917BGlc25% 1

SOP Name: mansettings.nano

General Notes:

File Name: bl.dts	Dispersant Name: Water MeOH 25%
Record Number: 6	Dispersant RI: 1.338
Material RI: 1.45	Viscosity (cP): 2.1408
Material Absorbtion: 0.001	Measurement Date and Time: Sunday, May 21, 2017 1:58:5...

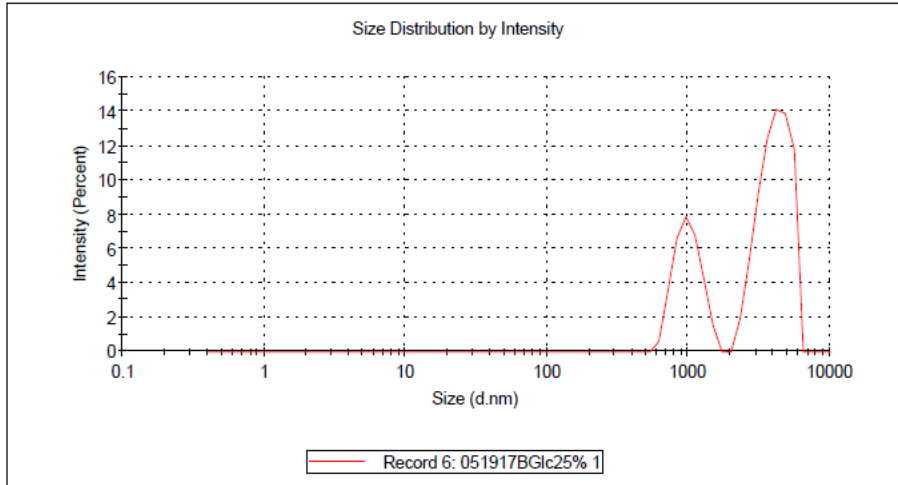
System

Temperature (°C): 10.0	Duration Used (s): 70
Count Rate (kcps): 86.7	Measurement Position (mm): 4.65
Cell Description: Glass cuvette with square apert...	Attenuator: 9

Results

	Size (d.nm):	% Intensity:	St Dev (d.n...
Z-Average (d.nm): 2362	Peak 1: 4107	68.8	951.1
Pdl: 0.345	Peak 2: 996.4	31.2	210.0
Intercept: 0.819	Peak 3: 0.000	0.0	0.000

Result quality : **Refer to quality report**



Correlogram Report

v2.0



Malvern Instruments Ltd - © Copyright 2008

Sample Details

Sample Name: 051917BGlc25% 1

SOP Name: mansettings.nano

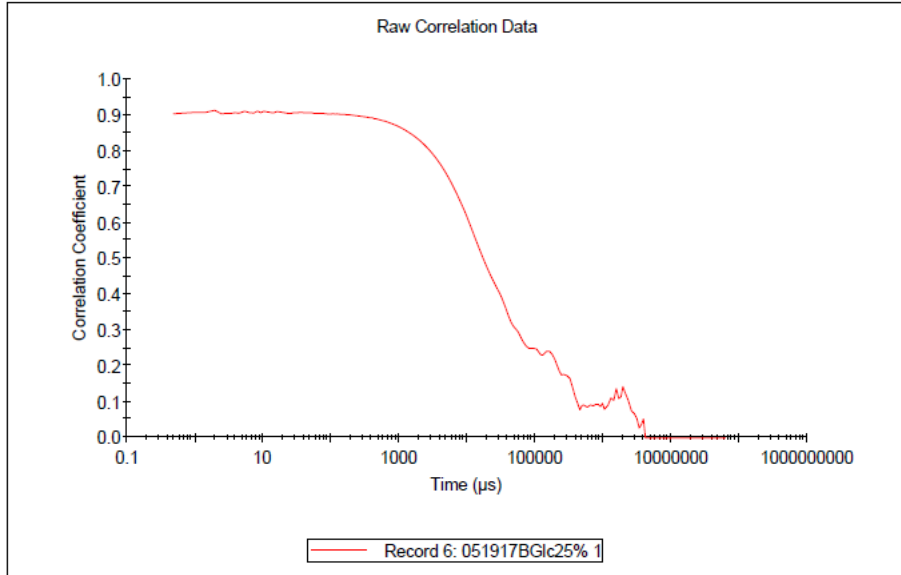
General Notes:

File Name: bl.dts	Dispersant Name: Water MeOH 25%
Record Number: 6	Dispersant RI: 1.338
Material RI: 1.45	Viscosity (cP): 2.1408
Material Absorbtion: 0.001	Measurement Date and Time: Sunday, May 21, 2017 1:58...

System

Temperature (°C): 10.0	Duration Used (s): 70
Count Rate (kcps): 86.7	Measurement Position (mm): 4.65
Cell Description: Glass cuvette with square...	Attenuator: 9

Results



βGlc Yariv in 30% (v/v) MeOH at 10 °C (X = 0.16)

Size Distribution Report by Intensity

v2.2



Sample Details

Sample Name: 051917BGlc30% 1

SOP Name: mansettings.nano

General Notes:

File Name: bl.dts	Dispersant Name: 30%MeOH
Record Number: 5	Dispersant RI: 1.336
Material RI: 1.45	Viscosity (cP): 2.0237
Material Absorbtion: 0.001	Measurement Date and Time: Sunday, May 21, 2017 1:51:5...

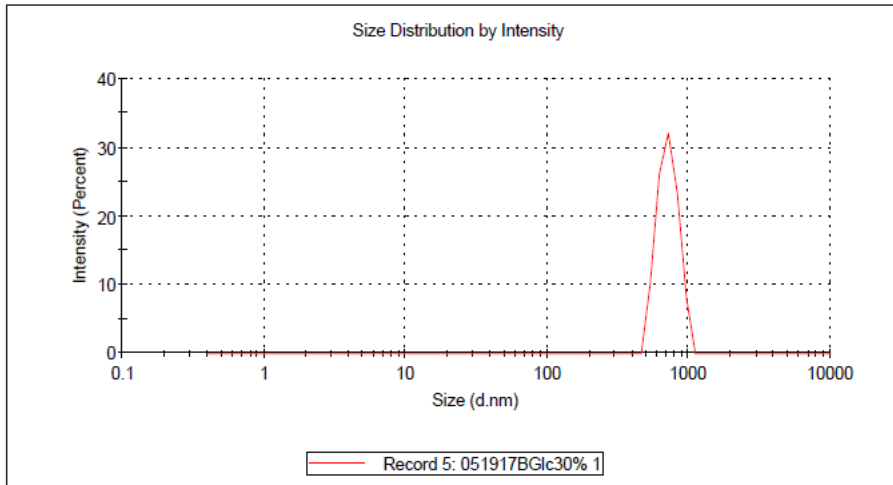
System

Temperature (°C): 10.0	Duration Used (s): 60
Count Rate (kcps): 257.1	Measurement Position (mm): 4.65
Cell Description: Glass cuvette with square apert...	Attenuator: 10

Results

	Size (d.nm):	% Intensity:	St Dev (d.n...)
Z-Average (d.nm): 795.9	Peak 1: 714.8	100.0	116.8
PdI: 1.000	Peak 2: 0.000	0.0	0.000
Intercept: 0.720	Peak 3: 0.000	0.0	0.000

Result quality : **Refer to quality report**



Correlogram Report

v2.0



Malvern Instruments Ltd - © Copyright 2008

Sample Details

Sample Name: 051917BGlc30% 1

SOP Name: mansettings.nano

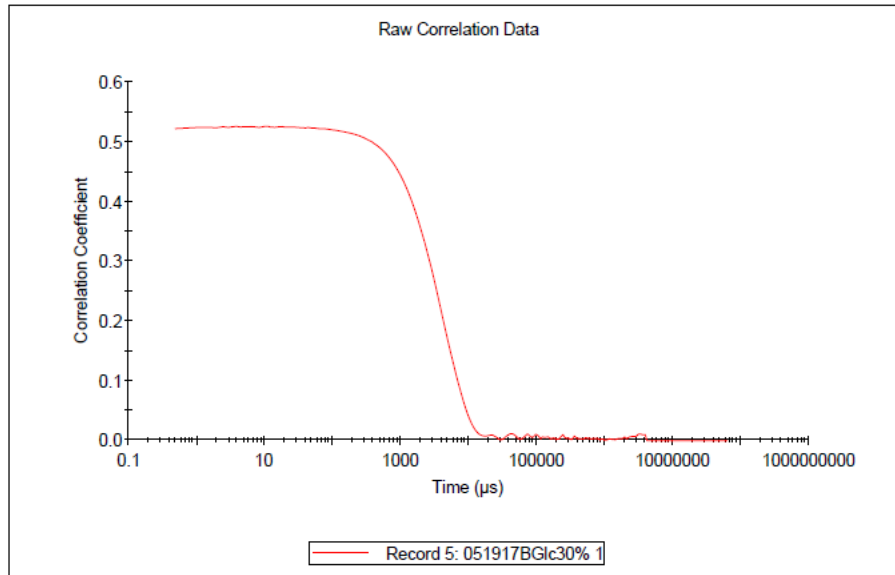
General Notes:

File Name:	bl.dts	Dispersant Name:	30%MeOH
Record Number:	5	Dispersant RI:	1.336
Material RI:	1.45	Viscosity (cP):	2.0237
Material Absorbion:	0.001	Measurement Date and Time:	Sunday, May 21, 2017 1:51...

System

Temperature (°C):	10.0	Duration Used (s):	60
Count Rate (kcps):	257.1	Measurement Position (mm):	4.65
Cell Description:	Glass cuvette with square...	Attenuator:	10

Results



βGlc Yariv in 35% (v/v) MeOH at 10 °C (X = 0.19)

Size Distribution Report by Intensity

v2.2



Sample Details

Sample Name: 051917BGlc35% 1

SOP Name: mansettings.nano

General Notes:

File Name: bl.dts	Dispersant Name: 35% MeOH
Record Number: 3	Dispersant RI: 1.337
Material RI: 1.45	Viscosity (cP): 2.0952
Material Absorbtion: 0.001	Measurement Date and Time: Friday, May 19, 2017 4:33:10 ...

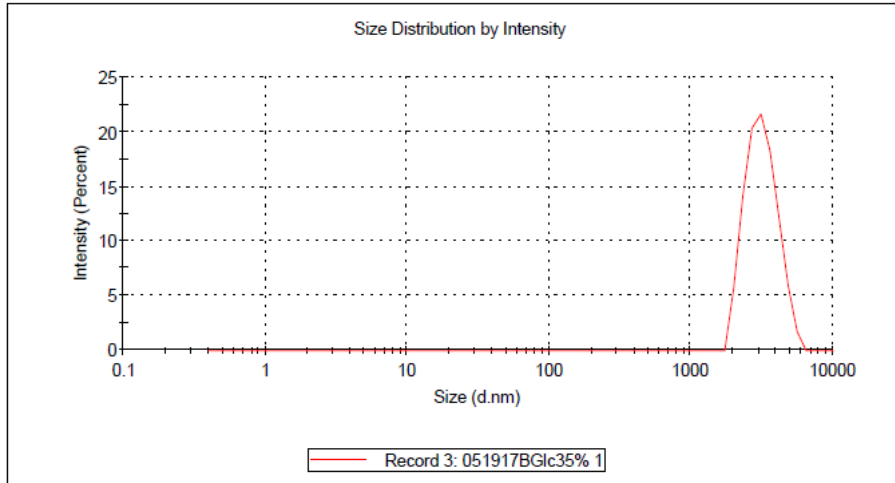
System

Temperature (°C): 10.0	Duration Used (s): 70
Count Rate (kcps): 134.9	Measurement Position (mm): 4.65
Cell Description: Glass cuvette with square apert...	Attenuator: 9

Results

	Size (d.nm):	% Intensity:	St Dev (d.n...)
Z-Average (d.nm): 3026	Peak 1: 3192	100.0	802.3
Pdl: 0.225	Peak 2: 0.000	0.0	0.000
Intercept: 0.729	Peak 3: 0.000	0.0	0.000

Result quality : **Refer to quality report**



Correlogram Report

v2.0



Malvern Instruments Ltd - © Copyright 2008

Sample Details

Sample Name: 051917BGlc35% 1

SOP Name: mansettings.nano

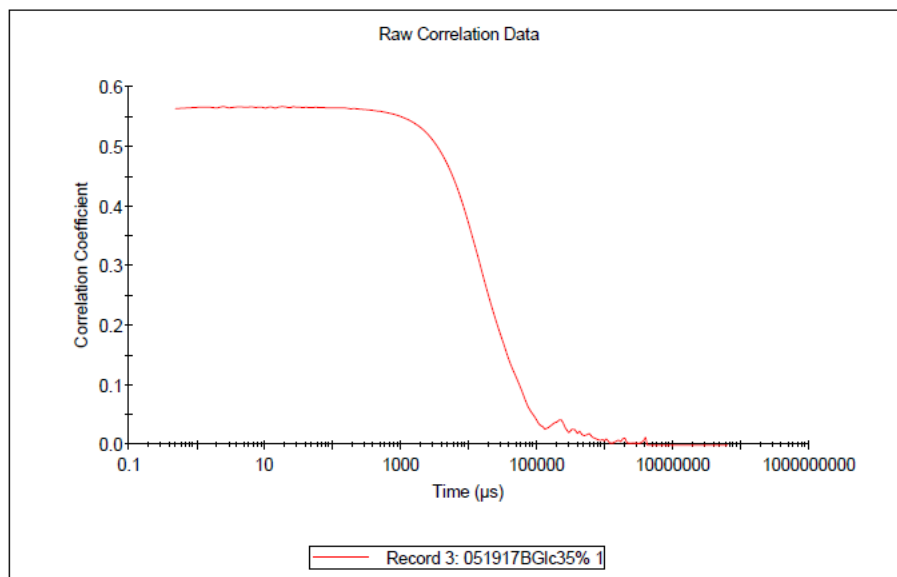
General Notes:

File Name: bl.dts	Dispersant Name: 35% MeOH
Record Number: 3	Dispersant RI: 1.337
Material RI: 1.45	Viscosity (cP): 2.0952
Material Absorbtion: 0.001	Measurement Date and Time: Friday, May 19, 2017 4:33:...

System

Temperature (°C): 10.0	Duration Used (s): 70
Count Rate (kcps): 134.9	Measurement Position (mm): 4.65
Cell Description: Glass cuvette with square...	Attenuator: 9

Results



βGlc Yariv in 50% (v/v) MeOH at 10 °C (X = 0.31)

Size Distribution Report by Intensity

v2.2



Sample Details

Sample Name: 051917BGlc50% 1

SOP Name: mansettings.nano

General Notes:

File Name: bl.dts	Dispersant Name: 50%MeOH
Record Number: 4	Dispersant RI: 1.340
Material RI: 1.45	Viscosity (cP): 2.1437
Material Absorption: 0.001	Measurement Date and Time: Friday, May 19, 2017 4:41:36 ...

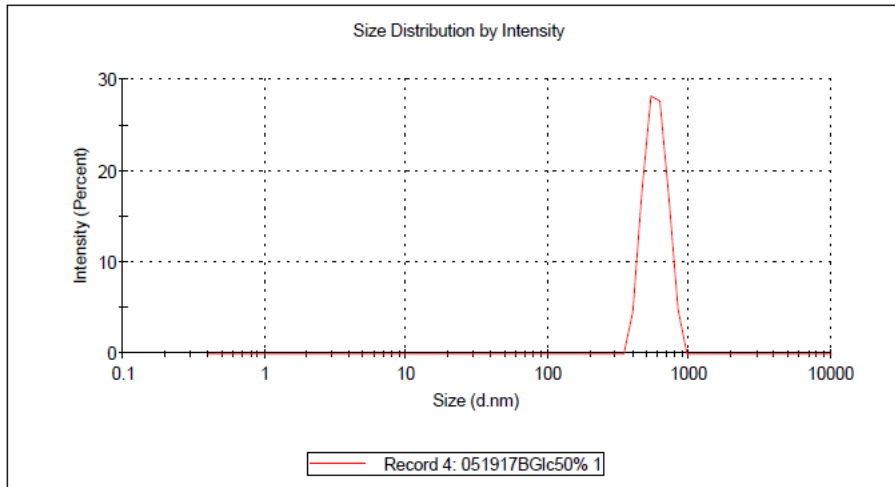
System

Temperature (°C): 10.0	Duration Used (s): 60
Count Rate (kcps): 300.1	Measurement Position (mm): 4.65
Cell Description: Glass cuvette with square apert...	Attenuator: 10

Results

	Size (d.nm):	% Intensity:	St Dev (d.n...)
Z-Average (d.nm): 564.1	Peak 1: 580.4	100.0	105.5
PdI: 0.029	Peak 2: 0.000	0.0	0.000
Intercept: 0.829	Peak 3: 0.000	0.0	0.000

Result quality : **Good**



Correlogram Report

v2.0



Malvern Instruments Ltd - © Copyright 2008

Sample Details

Sample Name: 051917BGlc50% 1

SOP Name: mansettings.nano

General Notes:

File Name: bl.dts	Dispersant Name: 50%MeOH
Record Number: 4	Dispersant RI: 1.340
Material RI: 1.45	Viscosity (cP): 2.1437
Material Absorbtion: 0.001	Measurement Date and Time: Friday, May 19, 2017 4:41:...

System

Temperature (°C): 10.0	Duration Used (s): 60
Count Rate (kcps): 300.1	Measurement Position (mm): 4.65
Cell Description: Glass cuvette with square...	Attenuator: 10

Results

